Unsaturated Silicon Species with Peripheral Functionality – from Multiple Bonding to Siliconoid Clusters

Dissertation

zur Erlangung des Grades

des Doktors der Naturwissenschaften

der Naturwissenschaftlich-Technischen Fakultät III

Chemie, Pharmazie, Bio- und Werkstoffwissenschaften

der Universität des Saarlandes

Vorgelegt von

M. Sc. Philipp Willmes

aus Saarbrücken

Saarbrücken

09/2016

Tag des Kolloquiums:	16. 12. 2016
Dekan:	Prof. Dr. Guido Kickelbick
Berichterstatter:	Prof. Dr. David Scheschkewitz
	Prof. Dr. Rolf Hempelmann
	Prof. Dr. Matthias Driess
Vorsitz:	Prof. Dr. Guido Kickelbick
Akad. Mitarbeiter	Dr. André Schäfer

The work described in this thesis was carried out from April 2013 until September 2016 at Saarland University, Naturwissenschaftlich-Technische Fakultät III Chemie, Pharmazie, Bio- und Werkstoffwissenschaften, Fachrichtung 8.1 Chemie, Krupp-Chair of General and Inorganic Chemistry under supervision of Prof. Dr. David Scheschkewitz.

Abstract

Functional groups are a prerequisite for the application of unsaturated heavier main group species, e.g. as building blocks of extended systems. The thesis deals with the introduction and transformation of functionality in the periphery of "classical" multiply bonded species and of unsaturated clusters of silicon (siliconoids).

A *P*-amino functionalized phosphasilene is shown to be a suitable reagent for the electrophilic transfer of the P=Si unit. Depending on the solvent polarity, it reacts with anionic nucleophiles either under substitution of the NMe_2 group or in an unprecedented metal-amino exchange.

In the context of the doping of Si=Si systems at the molecular scale, disilenes and heteronuclear silicon rings with boron and phosphorus functionalities were prepared from an anionic Si=Si reagent. Disilenes featuring remote sulfur-based anchors (designed for the grafting of Si=Si to gold surfaces) were obtained by a similar route.

The reduction of siliconoids affords the first anionic silicon clusters with additional "naked" vertices. With these results, the missing link between silicon-based Zintl anions and neutral unsaturated silicon clusters was established. Proof-of-principle for the high potential for the transfer of the intact unsaturated cluster skeleton was demonstrated by reactions with representative electrophiles of Groups 13, 14 and 15. A broad variety of functionalized siliconoids is now readily accessible.

Zusammenfassung

Funktionelle Gruppen sind eine Voraussetzung für die Anwendung ungesättigter schwerer Hauptgruppenspezies, z. B. als Bausteine für erweiterte Systeme. Die Arbeit behandelt die Einführung und Umwandlung von Funktionalität in der Peripherie „klassischer“ mehrfach gebundener Spezies und ungesättigter Cluster des Siliciums (Silicoide).

Ein *P*-Amino funktionalisiertes Phosphasilen erweist sich als geeignetes Reagenz zur elektrophilen Übertragung der P=Si-Einheit. Abhängig von der Lösemittelpolarität reagiert es mit anionischen Nukleophilen entweder unter Substitution der NMe_2-Gruppe oder in einem neuartigen Metall-Amino-Austausch.

Im Kontext der Dotierung von Si=Si-Systemen auf molekularer Ebene wurden Disilene und heteroatomare Siliciumringe mit Bor- und Phosphorfunktionalitäten aus einem anionischen Si=Si-Reagenz hergestellt. Disilene mit schwefelbasierenden Ankern (konzipiert für das Aufbringen von Si=Si auf Goldoberflächen) wurden auf gleichem Wege erhalten. Die Reduktion von Silicoiden lieferte die ersten anionischen Cluster mit zusätzlichen „nackten“ Gerüstatomen. Mit diesen Ergebnissen wurde das fehlende Bindeglied zwischen siliciumbasierenden Zintl-Anionen und neutralen Siliciumclustern etabliert. Das hohe Potential für den Transfer des intakten, ungesättigten Clustergerüstes wurde durch Reaktionen mit typischen Elektrophilen der Gruppen 13, 14 und 15 grundsätzlich demonstriert. Damit ist jetzt eine breite Vielfalt an funktionalisierten Silicoiden zugänglich.

Annotation

This thesis has been published in parts in:

- P. Willmes, M. C. Cowley, M. Hartmann, M. Zimmer, V. Huch, D. Scheschkewitz*,* Von Disilen (Si=Si) über Phosphasilen (Si=P) zum Phosphakumulen (P=C=N)*, Angew. Chem.* **2014**, *126*, 2248–2252; From Disilene (Si=Si) to Phosphasilene (Si=P) and Phosphacumulene (P=C=N), *Angew. Chem. Int. Ed.* **2014**, *53*, 2216–2220.

- P. Willmes, K. Leszczyńska, Y. Heider, K. Abersfelder, M. Zimmer, V Huch, D. Scheschkewitz, Isolierung und vielseitige Derivatisierung eines ungesättigten anionischen Siliciumclusters (Silicoid), *Angew. Chem.* **2016**, *128*, 2959–2963; Isolation and Versatile Derivatization of an Unsaturated Anionic Silicon Cluster (Siliconoid), *Angew. Chem. Int. Ed.* **2016**, 55, 8, 2907 –2910.

- P. Willmes, L. Junk, V. Huch, C. B. Yildiz, D. Scheschkewitz, Vielseitige Reaktivität eines elektrophilen Phosphasilens gegenüber anionischen Nukleophilen: Substitution oder Metall-Amino-Austausch, *Angew. Chem.* **2016**, *128*, 11074–11078; Diverse Reactivity of an Electrophilic Phosphasilene towards Anionic Nucleophiles: Substitution or Metal–Amino Exchange, *Angew. Chem. Int. Ed.* **2016,** *55,* 10913–10917.

“Everything that happens is a small part of our journey. We can choose to be passive or we can be proactive and overcome our fears, set our own goals and do the best to reach them. For better or for worse, we always have a choice.”

- ***Giorgio Pautrie***

Cited in Forbes, 10th of July, 2016
Quote of The Day

Meiner Familie

Acknowledgements/Danksagung

An erster Stelle möchte ich **Prof. Dr. David Scheschkewitz** ganz herzlich danken, für die Möglichkeit dieses spannende Projekt in seiner Gruppe zu bearbeiten, für das fortwährende Interesse an meiner Arbeit und die Freiheit, die er mir bei der Durchführung gelassen hat. Besonders möchte ich ihm aufrichtig danken für seine vorbehaltlose Unterstützung in allen Situationen auf die ich mich während meiner gesamten Tätigkeit in der Gruppe immer verlassen konnte. Außerdem danke ich ihm für die Möglichkeit zahlreiche Konferenzen zu besuchen und die sehr lustigen Abende dort!

Weiterhin möchte ich **Prof. Dr. Rolf Hempelmann** herzlich danken, dass er sich bereit erklärt hat, das Zweitgutachten zu übernehmen und für die Zusammenarbeit im Rahmen des Oberflächenprojektes.

Vielen Dank an **Prof. Dr. Matthias Drieß**, dass er mir die Ehre erwiesen hat, das Drittgutachten zu übernehmen.

Special thanks to **Dr. Michael Cowley** for his invaluable support at the beginning of my thesis.

Meinem Vertiefer **Lukas Junk** und Bachelorstudenten **Thomas „Mr. AFM“ Büttner** danke ich für die tatkräftige Unterstützung und die gute Zusammenarbeit.

Many thanks to my good friend from Turkey, **Dr. Cem B. Yildiz** for all the effort he has put into the DFT-calculations. Also during his stay in Saarbrücken, I enjoyed to work with him very much.

Einen großen Dank schulde ich meinem talentierten ACF-/Bachelor-/Vertiefungsstudenten/Kollegen/guten Freund **Yannic Heider**, der mir mit seinem Enthusiasmus und Fleiß eine große Hilfe war.

Nicht verzagen, Carsten fragen – ein ganz besonderer Dank gebührt **Dr. Carsten Präsang**. Sein Humor und seine fachliche Unterstützung waren für mich von unschätzbarem Wert, und er ist ein guter Freund.

Der besten Sekretärin der Welt, **Bianca Iannuzzi**, danke ich für ihre Unterstützung bei allen möglichen bürokratischen Angelegenheiten und die freundliche Zusammenarbeit.

Many thanks also to all other former and current group members **Dr. Jonathan Jeck**, **Dr. Kai Abersfelder**, **Dr. Moumita Majumdar**, **Dr. Anukul Jana**, **Dr. Antje Meltzer**, **Dr. Prasenjit Bag**, **Hui Zhao**, **Naim M. Obeid**, **Isabell Omlor**, **Nadine Poitiers**, **Marcel Lambert**, **Dr. Kinga Leszczyńska**, **Lukas Klemmer**, **Yvonne Kaiser**, **Dr. Andreas Rammo**, **Ramona Cullmann**, **Evelyne Altmeyer**, **Andreas Adolf**, **Bettina Piro** and **Günther Berlin** for all their support, the friendly working atmosphere and the great time that I had in this group.

Vielen Dank an **Susanne Harling** für die Messung der Elementaranalysen.

Bei **Dr. Volker Huch** möchte ich mich recht herzlich bedanken für die Kristallstrukturanalytik.

Herzlichen Dank an **Dr. Michael Zimmer** für das Durchführen der VT-NMR-Experimente und die Hilfe bei NMR-spektroskopischen Problemen.

Ein ganz besonderer Dank gebührt **David Nieder**, einem der korrektesten Menschen die ich kenne. Schon während des Studiums hatten wir eine gute Zusammenarbeit, und als Labornachbar waren seine Begeisterung für diese Chemie, sein Interesse auch an meiner Forschung und seine Ideen und Ratschläge ebenso unersetzlich für diese Arbeit wie die Feierabend-Biere.

Bei **Safwan** und **Christian Mardini** möchte ich mich für nunmehr jahrzehnte lange Freundschaft bedanken und dafür, dass ich immer auf sie zählen kann.

Herzliches Dankeschön an meine Schwiegereltern in Spe **Susi** und **Michael D´Haise** dafür, dass sie immer hinter mir stehen und für Hilfe bei computertechnischen Problemen.

Meinem Onkel **Peter Lang** danke ich ganz herzlich für seine Unterstützung während meines gesamten Studiums und sein wohltuendes Interesse an meiner Arbeit.

Von ganzem Herzen Danke ich meinen Eltern **Margarete** und **Dr. Arnold Willmes** für den ständigen Rückhalt in allen Lebenslagen und für alles was ich von Ihnen lernen durfte. Ich weiß sehr zu schätzen, dass Ihr mir mein Studium in dieser Form ermöglicht habt und was Ihr mein Leben lang alles für mich getan habt. Vielen Dank dafür!
Meinem Vater sei hier auch für wertvolle fachliche Unterstützung gedankt!

Vielen Dank Dir, **Kim D´Haise**, dass Du mir mein ganzes Studium zur Seite gestanden hast, für Deine ständige Geduld und dein Verständnis. Ich danke Dir aus tiefstem Herzen für die gemeinsame Zeit die wir hatten und noch haben werden.

Content

List of Abbreviations

Å	**A**ngström
AFM	**A**tomic **F**orce **M**icroscopy
Ar	**Ar**omatic substituent
Bbi	$Si(^{i}Pr)(C(H)(SiMe_3)_2))_2$
Bbt	$2,6\text{-}[(Me_3Si)_2CH]_2\text{-}4\text{-}[(Me_3Si)_3C]\text{-}C_6H_2)$
B3LYP	**B**ecke hybrid-**3**-parameter functional and the correlation functional of **L**ee, **Y**ang and **P**arr
C	**C**elsius
CGMT	**C**arter-**G**oddard-**M**alrieu-**T**rinquier
Cp	**C**yclo**p**entadienyl $\eta^5\text{-}C_5H_5$
Cp*	Pentamethyl**c**yclo**p**entadienyl $\eta^5\text{-}C_5Me_5$
CPCM	**C**onductor-like **P**olarizable **C**ontinuum **M**odel
CVD	**C**hemical **V**apor **D**eposition
Cy	**Cy**clohexyl
DBU	1,8-**D**iaza**b**icyclo[5.4.0]**u**ndec-7-ene
Dec.	**Dec**omposition
DFT	**D**ensity **F**unctional **T**heorie
Dip	2,6-**Di**isopropyl**p**henyl
DMAP	**Dim**ethyl**a**mino**p**yridine
dme	1,2-**d**i**m**ethoxy**e**thane
dppe	1,2-bis(**d**i**p**henyl**p**hosphino)**e**thane
Dur	**Dur**yl, 2,3,5,6-tetrametylphenyl
Dsi	$C(H)(SiMe_3)_2)$
EMind	1,1,3,3,7,7-Hexaethyl-5,5-dimethyl-s-hydrindacen-4-yl
equ	**equ**ivalent
Et	**Et**hyl, $\text{-}C_2H_5$
EV	**E**lectron **V**olt
GIAO	**G**auge **I**ndependent **A**tomic **O**rbital
HF	**H**artree-**F**ock
h	**h**our
HOMO	**H**ighest **O**ccupied **M**olecular **O**rbital

^{i}Pr	***iso*-Propyl, -C_3H_7**
IR	**I**nfra**r**ed
LDA	**L**ithium **D**iisopropyl**a**mide
LUMO	**L**owest **U**noccupied **M**olecular **O**rbital
M	**M**olar
Me	**M**ethyl, -CH_3
Mes	2,4,6-Trimethylphenyl
Mes*	2,4,6-Tri-*tert*.-butylphenyl
MO	**M**olecular **O**rbital
M. p.	**M**elting **p**oint
MS	**M**ass **S**pectrometry
Naph	**Naph**thalene
NBO	**N**atural **B**ond **O**rbital
NHC	**N**-**H**eterocyclic **C**arbene
NICS	**N**ucleus **I**ndependent **C**hemical **S**hifts
NMR	**N**uclear **M**agnetic **R**esonance
Ph	**Ph**enyl
rt	**r**oom **t**emperature
SAM	**S**elf-**A**ssembled **M**onolayer
Tbt	2,4,6-**T**ris[**b**is(**t**rimethylsilyl)methyl]phenyl
^{t}Bu	***tert*.-Butyl, -C_4H_9**
TD	**T**ime **D**ependent
thf	**t**etra**h**ydro**f**urane
Tip	2,4,6-**T**ri**i**sopropyl**p**henyl
tmeda	N,N,N',N'-**t**etra**m**ethyl**e**thylene**d**i**a**mine
UV	**U**ltra**v**iolet
vis	**vis**ible
VT	**V**ariable **T**emperature
WBI	**W**iberg **B**ond **I**ndices
Xyl	**Xyl**yl, 2,6-dimethylphenyl

List of Figures

List of Schemes

List of Tables

Foreword

Carbon can be regarded as the central element of biology; the scaffold of all organisms is based on carbon and its chemical variety makes it a key element of life. Compounds based on silicon, carbon's heavier congener, feature entirely different structural properties making it a key element of civilization.[1] Building materials such as concrete,[2] ceramics[3] and glass[4] are based on silicon dioxide and/or silicates. Silicones, polymers with alternating silicon and oxygen atoms, are widely used sealants, adhesives and lubricants.[5] In addition, silicon in its elemental form is the semiconductor par excellence and thus ubiquitous in modern electronics.[6]

Silicon is the second most abundant element in the Earth´s crust, constituting 27.7% measured by mass.[7] The first name proposed for the element was “silicium” (from Latin silex for flint, and “-ium” because of its metalloid character) and goes back to Sir Davy, who attempted to isolate silicon in 1808.[8] Its present name was coined a decade later by Thomson. He referred to the ending “-on” because he thought silicon to be rather similar to boron and carbon than to a metal.[9] In 1824, Berzelius was finally able to produce pure silicon by reducing silicon tetrafluoride with elemental potassium and he is thus usually given the credit of discovery.[10]

The first silicon based semiconducting device was patented as early as 1905[11] and the production of high purity silicon *via* the floating zone process in 1954 was responsible for the breakthrough of silicon in semiconductor industry in the second half of the 20th century.[6] To selectively modulate properties of the materials, silicon materials are doped[12] by incorporating small amounts of electron acceptors, *e. g.* boron[13] (p-type doping),[14] or electron donors, *e. g.* phosphorus[15] (n-type doping).[16]

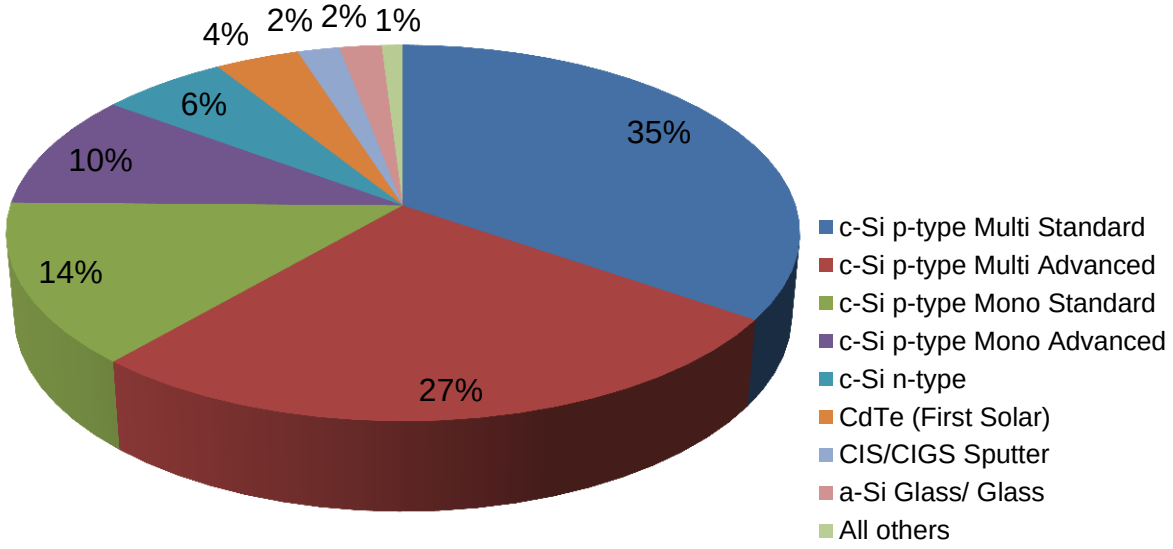

Figure 1. 2014 solar PV module production by technology (modified from: NPD Solarbuzz PV Equipment Quaterly).[17]

Today, silicon is omnipresent in semiconducting devices such as light emitting diodes or solar cells (Figure 1).[17] The amazing progress in microprocessor performance of the last decades would be difficult to imagine without silicon. It has already been predicted that our epoch subsequent to the Stone, Iron and Bronze Age will be referred to as the Silicon Age in future historiography.[18]

The progress made in electronics is due largely to the scaling down of devices over microelectronics to nanoelectronics in the deep sub-100-nm regime and has already been described as “smaller is better”.[19] To further improve performance of silicon-based devices soon novel methods for its production such as bottom-up approaches to control properties of materials on a sub-nano (molecular) level will have to be established.[20]

Preface

The indefinite variety of compounds known in organic chemistry is a result of the ability of carbon to form multiple bonds and the simultaneous presence of functional groups attached to the (unsaturated) carbon centers.

Heavier analogs of low-valent organic compounds attracted chemists early on, however, attempts to synthesize these molecules failed for more than a century.[21] These findings resulted in the so-called “double-bond rule” alleging that compounds with multiple bonds to main group elements heavier than the second row were non-existent.[22]

Three important breakthroughs were reported in 1981: isolation of the first silene (Si=C) by Brook,[23] disilene (Si=Si) by West[24] and diphosphene (P=P) by Yoshifuji,[25] all three stabilized by bulky substituents. These pioneering findings prompted a large body of research concerning chemistry of low-valent main group elements in general[26] and silicon in particular.[27] To date, dozens of homo- and heteronuclear examples have been reported employing the concept of steric protection to overcome kinetic instability. Even isolable disilynes, the silicon analogs of alkynes, have been reported.[28,29]

While the phenomenon of aromaticity in organic chemistry has gathered much attention since the discovery of benzene,[30] soon aromatic systems involving heavy main group elements moved into focus. The incorporation of heavier Group 14 elements into organic aromatic structures such as benzene, as well as all-metalla aromatics have been reported.[31]

Main group elements in lower oxidation states feature chemical and physical properties entirely different from their carbon analogs turning them into promising precursors for catalytic processes or material chemistry. Their ability to activate small molecules such as dihydrogen has recently been demonstrated.[32] Furthermore, the unsaturated moieties show a large variety of colors even in the absence of additional chromophores. Recently, Tamao *et al.* provided the first example for electroluminescence in a disilene and its application in an organic light emitting device.[33]

Similar to synthetic organic chemistry, a prerequisite for further manipulations on the heavy low-valent Group 14 systems is the presence of functional groups attached to the unsaturated atoms. It is crucial for the incorporation of unsaturated moieties into

more extended systems such as polymers. Heavier Group 14 compounds with novel structural motifs unknown for their carbon analogs become accessible by taking advantage of the reactivity of functional groups attached to the low-valent centers. The study of peripherally functionalized unsaturated molecules may be an instrumental factor in fully awakening the potential of Group 14 chemistry for applications.[34]

1. Introduction

1.1. Multiple Bonding in Heavier Main Group Compounds

1.1.1. Pioneering Works

The first heavier analogues of alkenes, digermene **1** and distannene **2** (Scheme 1)[35] were isolated in 1976 by Lappert *et al*. In solution both compounds dissociate into the corresponding tetrylene fragments, but in crystalline state the dimeric double bond structure is observed.

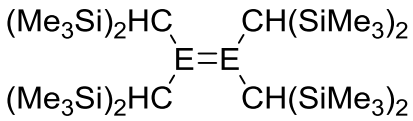

1: E = Ge, **2**: E = Sn

Scheme 1. The first stable heavy alkene analogues, digermene **1** and distannene **2** reported by Lappert.[35]

The first plausible evidence for the transient existence of a disilene was provided in 1973 by Roark and Peddle.[36] They generated a tetramethyl disilene *via* a retro-Diels-Alder process and subsequently trapped the product in a Diels-Alder reaction with anthracene. A mass spectrometric study further supported the intermediacy of the proposed product.[36]

In 1981, the first stable compound containing a Si=Si bond was reported by West.[24] Irradiation of hexamethyltrisilane **3** afforded tetramesityl disilene **4** as yellow-orange crystals (Scheme 2).[24] Protected by sterically demanding mesityl substitutents, disilene **4** is stable at room temperature in the absence of air and moisture and it was finally possible to fully characterize the first disilene.

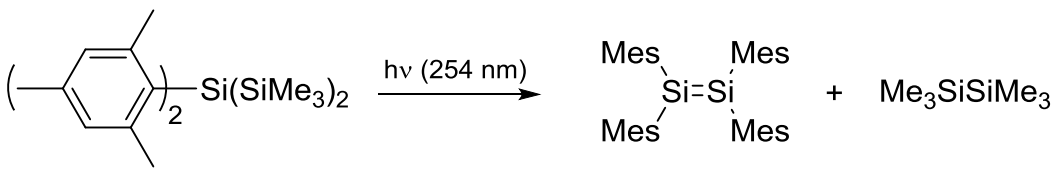

3 **4**

Scheme 2. Synthesis of the first isolable disilene **4** reported by West (Mes = mesityl, 2,4,6-trimethylphenyl).[24]

A compound featuring a P-P double bond was initially observed as early as 1966. Fluck and Issleib generated diphenyl diphosphene from molten poly phenylphosphorus and were able to detect the compound by ^{31}P NMR spectroscopy.[37]

The first isolation of a persistent diphosphene that could be structurally characterized goes back to the year 1981.[25] Yoshifuji *et al.* coupled dihalo phosphane Mes*PCl_2 (Mes* = 2,4,6-tri-*tert.*-butylphenyl) reductively with elemental magnesium to diphosphene **5** (Scheme 3).

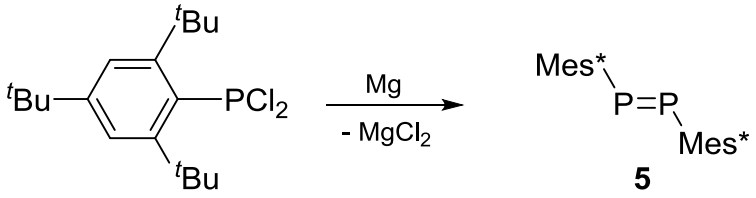

Scheme 3. Yoshifuji´s synthesis of the first diphosphene **5** (Mes* = 2,4,6-tri-*tert*.-butylphenyl).[25]

After these pioneering works concerning E=E bonds (E = main group element heavier than the second row) to date numerous of examples for compounds featuring unsaturated heavy main group elements have been reported.[26,27] In the following, special structural features of these compounds will be discussed briefly. Furthermore, selected published examples will be illustrated with focus on silicon in low coordination as well as its heteronuclear combinations with phosphorus.

1.1.2. Theory

1.1.2.1. Bonding

A first explanation for the less pronounced tendency of carbon's heavier congeners to form multiple bonds was given as early as 1948 by Pitzer. He referred to the “inner shell repulsion” between one atom and the core electrons of its bonding partner that plays an important role in the stability of the bonds formed.[38] Later Mullikan pointed out, that ongoing from carbon to heavier Group 14 elements the σ_{pp} interaction is getting stronger whereas the π_{pp} bond strength decreases.[39]

A major structural difference between C=C and E=E bonds (E = Group 14 element heavier than the second row) is apparent in the conformation of the double bonds. While alkenes feature a rigid planar arrangement, for the heavier homologues a distinct deviation from planarity is observed in most cases.

These distortions are described by two geometric parameters. The *trans*-bent angle θ (or cis-bent angle θ´) represents the angle between the R_2Si planes and the Si=Si vector and thus the degree of pyramidalization at the silicon centers. The angle between the planes defined by the two silicon atoms and the bonds to their respective substituents is quantified by the twist angle τ (Figure 2).

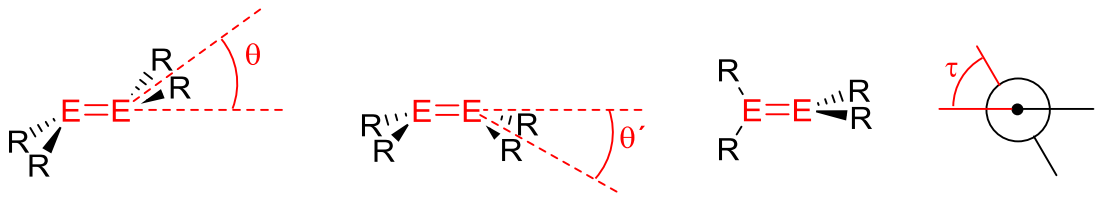

Figure 2. Selected parameters for the characterization of E=E bonds (E = Group 14 element heavier than the second row): *trans*-bent angle θ, *cis*-bent angle θ´ and twist angle τ.

While the twisting around the double bonds occurs in order to minimize steric repulsion between very bulky substituents, the phenomenon of a *trans*-bent conformation of heavy Group 14 double bonds is inherent to heavier main group elements and can be explained with the Carter-Goddard-Malrieu-Trinquier (CGMT) model (Figure 3).[40]

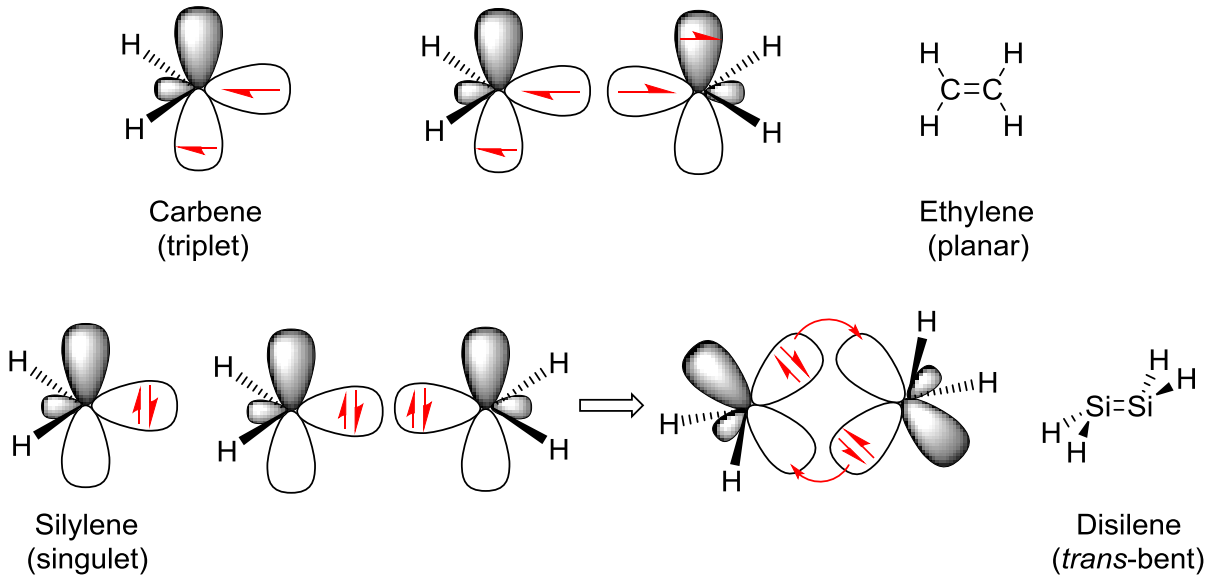

Figure 3. Effect of the nature of the ground state of the tetrylene fragment on the geometry of the double according to the CGMT-model demonstrated using the example of parent methylene (ethylene) and silylene (silene).

In the CGMT model, the double bond is considered to be formed by the interaction of the two corresponding tetrylene fragments (Figure 3).

While in :ER_2 species (E = heavier Group 14 element) the singlet state accomodates two electrons in an orbital of σ-symmetry, these electrons are unpaired in the triplet state and one of the electrons now resides in the p-orbital. For carbenes, the isoelectronic lightest congener, the triplet is usually the ground state (*e. g.* for methylene the singlet is 9.0 kcal/mol higher in energy).[41] The combination of two of such fragments results in the classical planar C-C double bond (Figure 2). However, for the heavier homologues the singlet becomes significantly more favorable.[42] Since a direct interaction between two singlet fragments is not possible on grounds of Coulomb repulsion, the doubly occupied, formally sp^2-hybridized orbital of each of the two fragments forms a donor-acceptor bond to the empty p_z-orbital of the other (Figure 3). This interaction leads to the *trans*-bent structure known for the heavier alkene analogues.

Indeed, for the parent disilene $H_2Si=SiH_2$, a *trans*-bent arrangement has been calculated (θ = 12.9°).[43] Generally, disilenes show a pronounced conformational flexibility depending on the substituents. The first systematic ab initio study concerning the substituent effects on the geometry of disilenes was reported in 1990 by Karni and Apeloig.[43] Electropositive substituents (*e. g.* Li, BeH, BH_2 and SiH_3) promote a planar arrangement, while electronegative as well as π-donating groups (F, OH and NH_2) induce large deviations from planarity.[43] The potential energy surface for the conformation of disilenes is generally very flat. Not only the substituents, but also the co-crystallized solvent can have a distinct effect. In case of disilene **4**, three different conformations were observed depending on the solvate (toluene: τ = 12°, θ = 18°;[44] thf: τ = 13°, no bending;[45] solvent free: τ = 3°, θ = 14°).[46]

1.1.2.2. UV/vis Spectroscopy

In contrast to their carbon homologues, disilenes (and unsaturated heavy main group compounds in general) absorb in the visible region of the electromagnetic spectrum as a result of the significantly smaller HOMO-LUMO gap of disilenes compared to alkenes. For the parent systems, $H_2C=CH_2$ and $H_2Si=SiH_2$, the HOMO-LUMO gap

has been contrasted in a computational study by Kira and Iwamoto and they found twice the splitting in ethylene compared to disilene (Figure 4).[47]

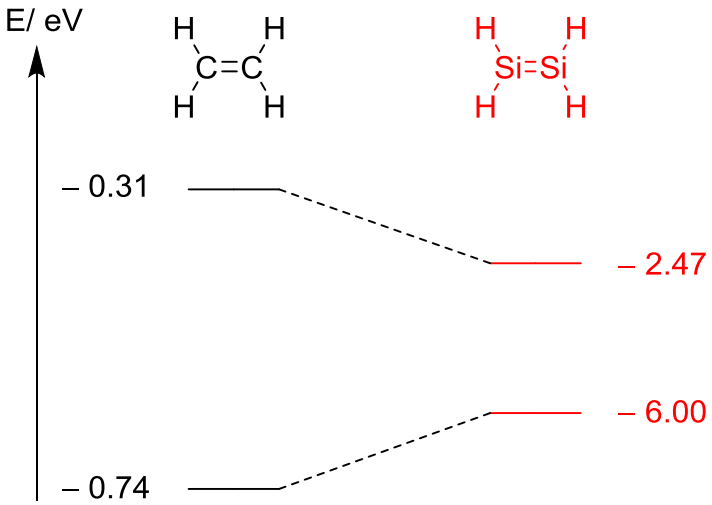

Figure 4. π-orbitals (HOMO) and π*-orbitals (LUMO) of ethylene compared to disilene.[47]

The size of the HOMO-LUMO gap in disilenes is strongly dependent on the conformation of the silicon-silicon double bond. Hence, a variety of colors is observed for disilenes bearing different substituents (*cf.* Chapter 1.1.2.1). As rationalized in Figure 5,[48] a more pronounced bending or twisting of the substituents results in decreased overlap of the orbitals.

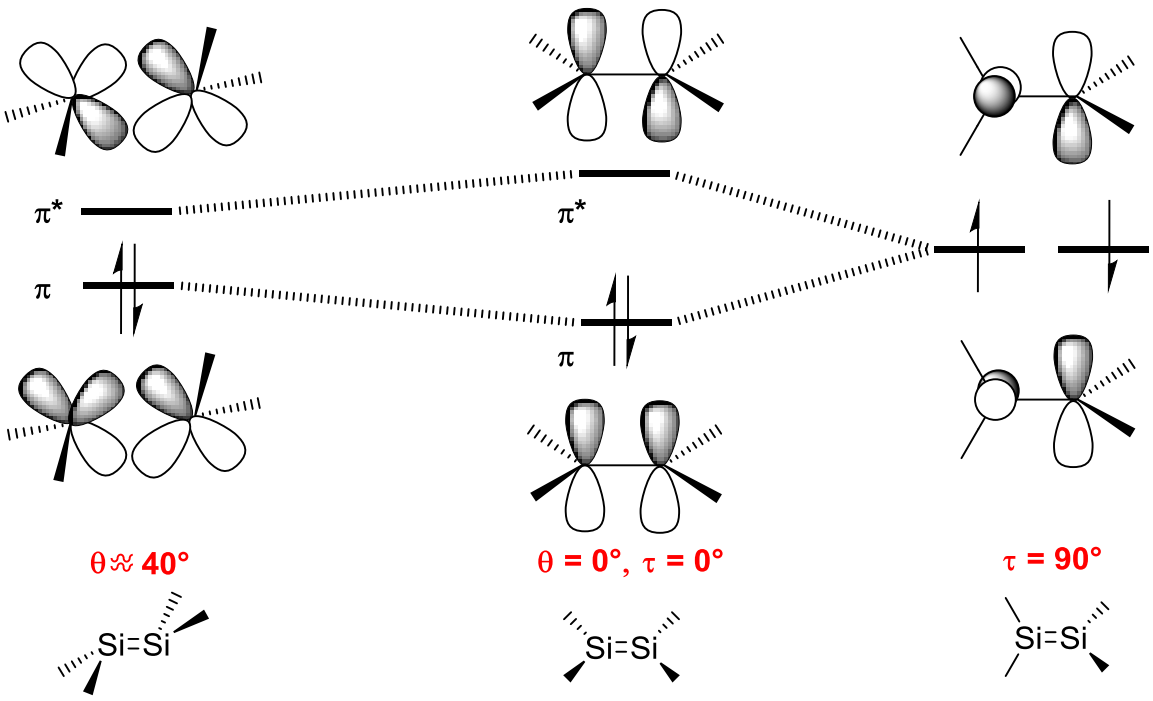

Figure 5. Effect of bending and twisting of disilenes on the HOMO-LUMO gap (figure reproduced from literature).[48]

Consequently, the π-orbital is raised in energy as the π*-orbital is lowered. The influence of the substituent on the HOMO-LUMO gap of Si=Si bonds is confirmed by experimental findings. For example, tetramesityldisilene **4** is yellow to orange in color (depending on the solvate),[44-46] whereas the silyl substituted disilene ((^{t}Bu$_2$Me)Si)$_2$Si=Si((^{t}Bu$_2$Me)Si)$_2$ reported by Sekiguchi *et al.*, the hitherto most twisted derivative (τ = 54.5°), was isolated as intense blue crystals.[49]

1.1.3. Syntheses of Disilenes

After the synthesis of the first disilene **4** by irradiation of linear trisilane **3**, the concept of photolytic generation of Si=Si bonds was successfully applied to cyclotrisilane **6** as precursor by Masamune.[50] The mechanism involves an initial formation of disilene **7** and a silylene that subsequently dimerizes to **7**. This mechanism was later confirmed by Weidenbruch through the trapping of both silylene and disilene intermediates with methanol during the photolysis of hexakis(*tert.*-butyl)cyclotrisilane.[51] Kira reported the synthesis of tetrasilyl substituted disilene **8** by a similar methodology (Scheme 4).[52]

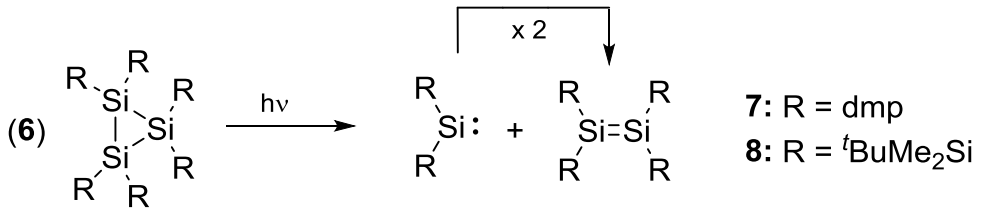

Scheme 4. Synthesis of disilenes **7** and **8** by irradiation of cyclotrisilanes reported by Masamune and Kira, respectively.[50,52]

The reductive coupling of bulky 1,1-dihalosilanes as novel synthetic route to disilenes was developed in 1987. Watanabe succeeded in the isolation of disilene **9** from the reaction of Tip$_2$SiCl$_2$ with two equivalents of lithium/naphthalene.[53] In the same year, Masamune applied this strategy to synthesize disilyl(alkyl) substituted disilene **10** (Scheme 5).[54]

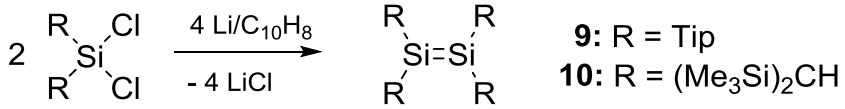

Scheme 5. Examples for the syntheses of disilenes *via* reductive coupling of dihalo silanes reported by Watanabe (**9**)[53] and Masamune[54] (**10**) (Tip = 2,4,6-triisopropylphenyl).

A more sophisticated reductive technique to synthesize disilenes is the dehalogenation of 1,2-dihalodisilanes. Notably, unsymmetrically substituted disilenes become accessible *via* this method. Reduction of 1,2-dibromo-disilanes **11a,b** allowed for the characterization of disilenes of the $A_2Si{=}SiB_2$ type (**12a,b**) by an X-ray structure study for the first time (Scheme 6).[55]

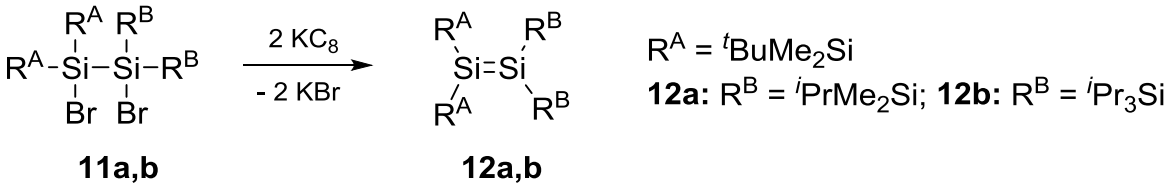

Scheme 6. Reductive dehalogenation of 1,2-dibromo disilanes **11a,b** to afford unsymmetrically substituted disilenes **12a,b** reported by Kira.[55]

An alternative synthetic route to unsymmetrically substituted disilenes of the type $A_2Si{=}SiB_2$ was reported by the group of Sekiguchi. Reduction of persila-substituted silacyclopropenes **13a,b** with lithium metal yields dilithiosilanes **14a,b**[56] that can be reacted with dihalo silanes as difunctional electrophiles to afford the corresponding disilenes **15a-d** in excellent yields (Scheme 7).[57]

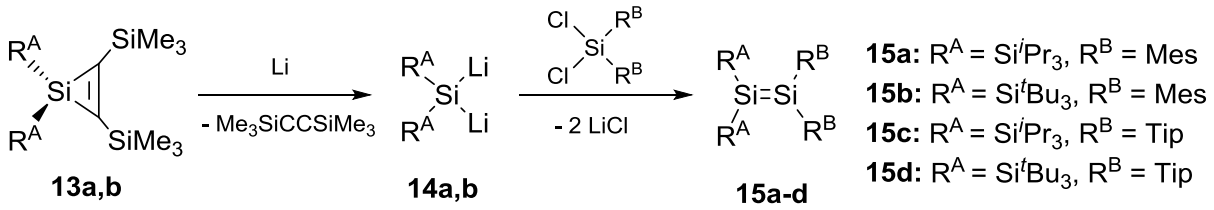

Scheme 7. Reduction of silirenes **13a,b** to afford dilithiosilanes **14a,b**[56] and subsequent conversion to unsymmetrically substituted disilenes **15a-d** communicated by Sekiguchi.[57]

1.1.4. Peripherally Functionalized Disilenes

1.1.4.1. Synthesis of Disilenides – Disila Analogues of Vinyl Anions

Initial studies concerning the reactivity of disilenes were mainly focused on addition reactions across the double bonds.[58] Numerous functionalized silanes have been isolated from dipolar addition reactions of disilenes with *e. g.* water, hydrogen halides,[59] alcohols,[59,60] ammonia,[61] or halo alkanes[62] to name only a few. Disila

cycles are readily accessible from cycloadditions of the Si=Si bond to *e. g.* chalcogenes,[63] isonitriles[64] or alkenes.[65]

It has become a major target in low-valent main group chemistry not only to explore the reactivity under consumption of the heavy double bonds, but to also perform manipulations on the systems without loss of the unsaturated moiety. This is a crucial step regarding the synthesis of larger macro- or supramolecular systems incorporating heavier unsaturated building blocks.[34]

A fundamental aspect in synthetic organic chemistry is the presence of nucleophilic and electrophilic functionalities in the periphery of unsaturated carbon atoms. Total syntheses would be unimaginable without nucleophilic and electrophilic substitution reactions as key manipulations in the presence of unsaturated moieties. In a similar fashion, heavy double bonds substituted with functional groups that provide nucleophilic or electrophilic centers have become valuable synthons in low-valent main group chemistry. In case of disilenes both nucleophilic and electrophilic derivatives have been reported and their synthetic potential was demonstrated impressively.[34,48,66]

In 1998, Weidenbruch treated Watanabe´s disilene **9**[53] with two equivalents elemental lithium in order to generate lithium disilenide **16**, a disila analogue of vinyl lithium, *via* the reductive cleavage of one substitutent.[67] A similar reaction had been reported by Masamune for digermene $Tip_2Ge{=}GeTip_2$.[68]

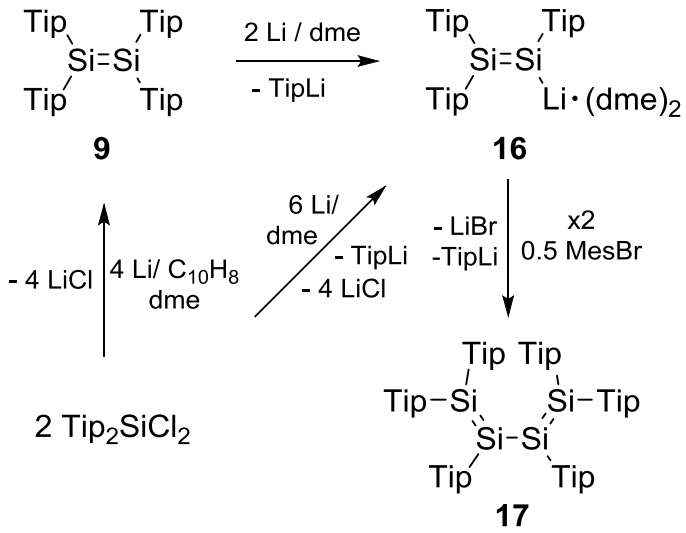

Scheme 8. Original synthesis of Watanabe's disilene **9**,[53] proposed intermediacy of disilenide **16** in Weidenbruch´s synthesis of tetrasilabutadiene **17**[67] as well as the direct synthesis of **16**[69] from Tip_2SiCl_2 (dme = dimethoxyethane, Tip = 2,4,6-triisopropylphenyl).

Even though Weidenbruch *et al.* were unable to isolate **16**, subsequent treatment of the product with half an equivalent of mesityl bromide afforded the first tetrasilabutadiene **17** and lend the intermediacy of **16** significant support (Scheme 8).[67] The similarity in reaction conditions between the synthesis of **9**, and its assumed reduction to **16**, prompted Scheschkewitz to attempt a direct reduction of Tip_2SiCl_2 with an excess of lithium powder. Indeed, from this reaction it was possible to isolate **16** and finally provide the first structural characterization of a disilenide (Scheme 8).[69]
Only shortly thereafter, Sekiguchi reported the synthesis of a different disilenide: reaction of tetrasilabutadiene **18** with ^{t}BuLi resulted in the formal cleavage of the central Si-Si bond to yield disilenide **19a** (Scheme 9).[70]

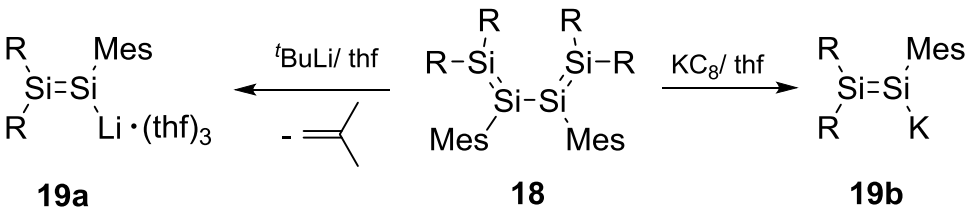

Scheme 9. Reduction of tetrasilabutadiene **18** to lithium disilenide **19a** and potassium disilenide **19b** both reported by Sekiguchi (R = ^{t}Bu$_2$MeSi, Mes = 2,4,6-trimethylphenyl).[70]

The mechanism of the formation of **19a** has not been elucidated yet. However, the detection of isobutene as the only formed by-product excludes an initial addition of ^{t}BuLi over the Si-Si single bond. After the pioneer works concerning disila analogs of vinyl alkaline metal compounds several disilenides have been published and their syntheses and reactivity has been the subject of review articles recently.[34,48,66]
Potassium disilenide **19b** was isolated as dme/diglyme solvate (diglyme = diethylenglycoldimethylether) from the reduction of **18** with potassium graphite in thf (Scheme 9).[71]
In 2001, the Sekiguchi group demonstrated that the reduction of tetrasilyldisilene **20** with $M/C_{10}H_8$ (M = Li, Na, K) affords the corresponding 1,2-dimetalla silanes **21a-c**. While **21a-c** are stable in thf, they readily undergo ^{t}Bu$_2$MeSiM elimination to yield alkaline metal disilenides **22a-c** upon solvent exchange for benzene (Scheme 10).[72]
As communicated by Iwamoto, reductive dehalogenation of 1,1,2-trichloro disilane **23** with potassium graphite affords the sole example of a trialkyl substituted disilenide **24**·$(thf)_2$.[73] Two examples for alkaline earth metal disilenides have been reported to date. Magnesium disilenide **25** is accessible from the transmetallation of lithium disilenide **16** with magnesium bromide.[74] From the reduction of dichlorosilyl

substituted disilene **26** with activated magnesium trisilen-1,3-diide **27** was obtained.[75] Notably, also a cyclic disilenide has been isolated. Upon sequestration of the lithium counter ion of trisilacyclopentadienide **28** with 12-crown-4 one silyl substituent migrates to the neighboring silicon atom to yield **29** (Scheme 10).[76]

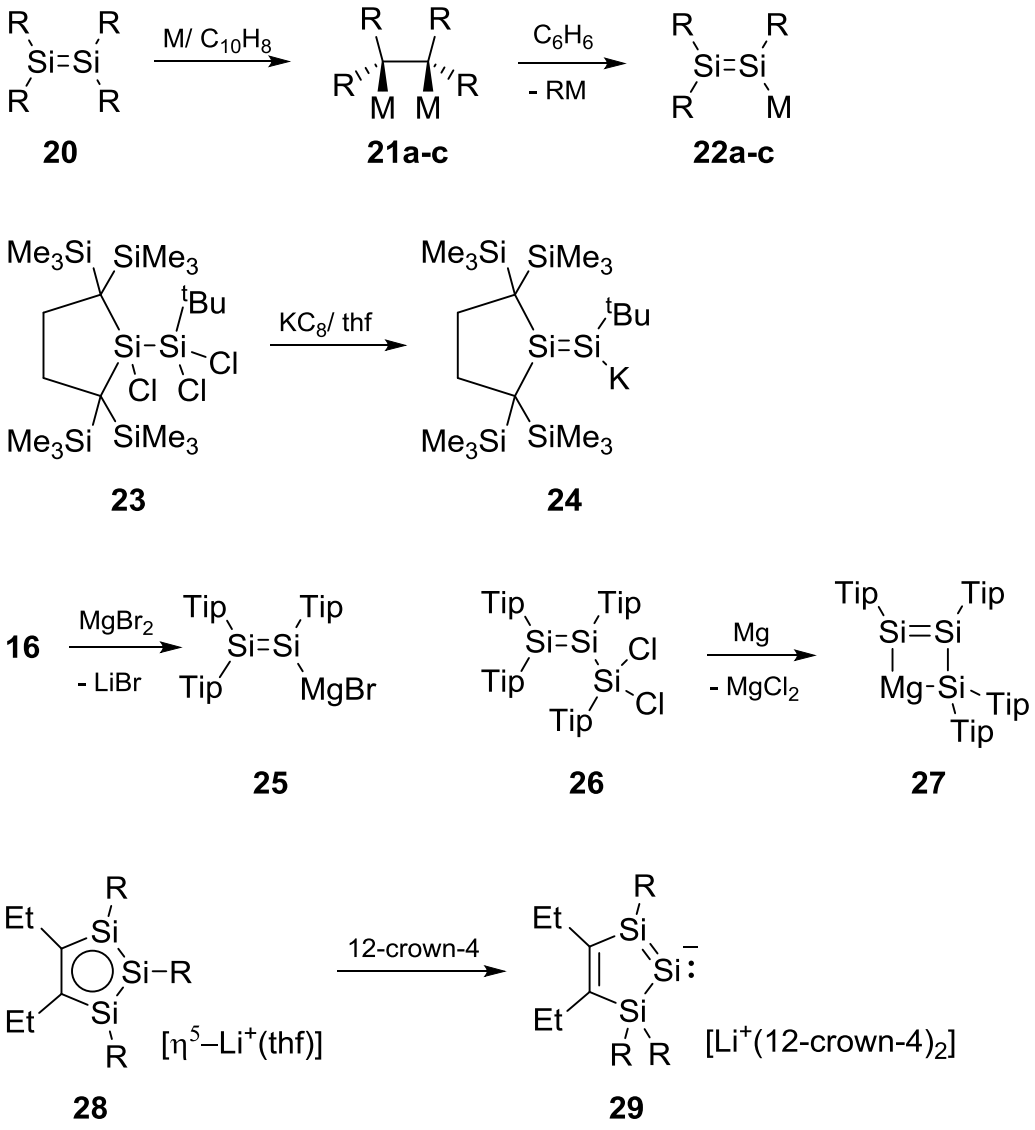

Scheme 10. Reduction of disilene **20** with metal/naphthalene to yield dianions **21a-c** and formation of disilenides **22a-c** *via* elimination of RM (M = Li, a; Na, b; K, c);[72] reductive dehalogenation of **23** to afford disilenide **24**;[73] synthesis of magnesium disilenide **25** and reduction of silyl disilene **26** to trisilendiide **27**;[75] rearrangement trisilacyclopentadienide **28** to cyclic disilenide **29** (R = $^{t}Bu_2MeSi$).[76]

1.1.4.2. Disilenides as Nucleophilic Si=Si Transfer Reagents

Soon after the isolation of the first disilenides their synthetic potential has been recognized. The anionic silicon atom provides a reactive site that allows for the nucleophilic transfer of the Si=Si moiety to a variety of organic and inorganic substrates.[34,48,66]

Disilenide **16** readily reacts with organic electrophiles such as iodoarenes. The reaction of **16** with phenyl iodide yields the corresponding phenyl substituted disilene **30**, an unsymmetrically substituted disilene of the $A_2Si{=}SiAB$ type. When **16** is treated with half an equivalent 1,4-diiodobenzene, *para*-phenylene-bridged tetrasiladiene **31** is obtained in good yields. The compound features two phenylene-conjugated Si-Si double bonds and shows significant conjugation of the π-system (Scheme 11).[77] It should be mentioned that this type of π-conjugated Si=Si systems is still difficult to obtain by classical reductive coupling techniques.[78] In subsequent work, Scheschkewitz *et al.* successfully employed **31** as precursor for σ-π-conjugated organosilicon hybrid polymers formed through regiospecific [2+2] cycloadditions of alkynes and the Si=Si moieties.[79]

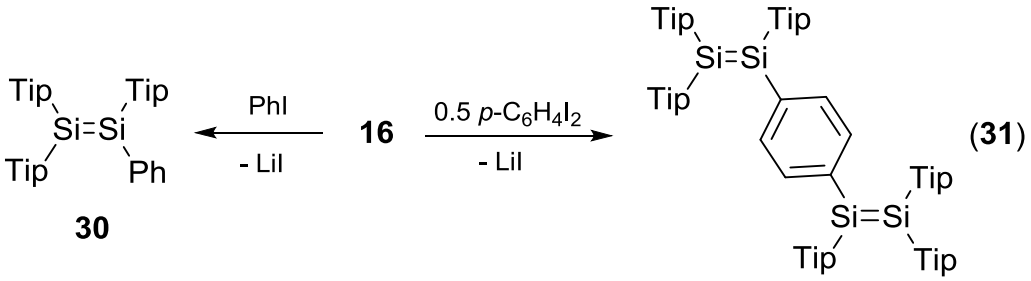

Scheme 11. Synthesis of phenyl disilene **30** and tetrasiladiene **31**.[77]

Heteroatom-substituted disilenes can be isolated from the reaction of disilenides with main group halides. Sekiguchi *et al.* reacted disilenide **22a** with boronic acid chlorides and were able to isolate the first boryl disilenes **32a,b** (Scheme 12).[80]

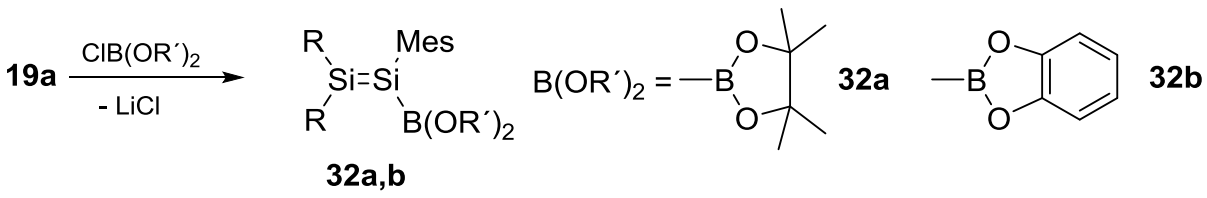

Scheme 12. Sekiguchi´s synthesis of boryl substituted disilenes **32a,b** (R = ^{t}Bu$_2$MeSi).[80]

Phosphino functionalization of disilenes *via* the reaction of **16** with dialkyl or diaryl chlorophosphines **33a-d** was reported by the Scheschkewitz group (Scheme 13).[81]

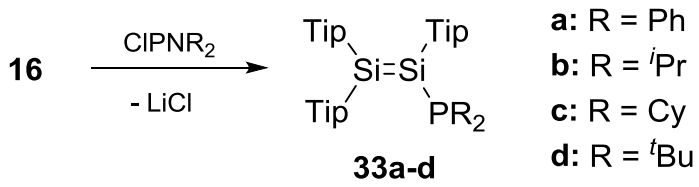

Scheme 13. Synthesis of phosphino disilenes **33a-d** (Cy = cyclohexyl).[81]

Transfer of the Si=Si unit to transition metals *via* the reaction of **16** with the corresponding transition metal chlorides has been reported. The products of these reactions can be regarded as coordination of the disilenide ligand to the transition metal center in η^1-fashion. Bis(disilenyl)zinc complex **34** was isolated from the reaction of two equivalents disilenide **16** with zinc dichloride. Treatment of CuI with two equivalents of **16** yielded the cuprate **35**.[82] The UV/vis spectra of both complexes **34** and **35** show a significant redshift of the longest wavelength absorption revealing an interaction between the two disilenyl moieties through the transition metal center. An intensely green disilenyl zirconocene complex **36** displaying a strong ligand-to-metal charge transfer transition was obtained from the reaction of disilenide **16** with Cp_2ZrCl_2 (Scheme 14).[83]

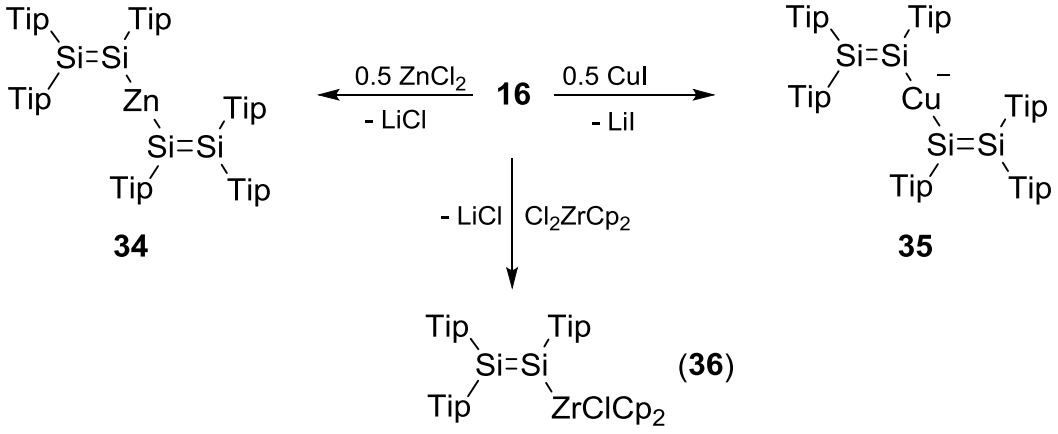

Scheme 14. Syntheses of η^1-disilenide zinc, copper and zirconocene complexes **34**, **35**[82] and **36** (cp = cyclopentadienyl).[83]

An interesting reactivity of disilenide **16** is observed when treated with Group 14 halides. The classic transfer of the Si=Si bond was reported for the treatment of **16** with mono chlorinated silanes or stannanes. By this means, tetrel functionalities in

vinylic position can be introduced to disilenes. Silyl substituted disilene **37** and the corresponding stannyl substituted derivatives **38a-d** became accessible (Scheme 15).[84,85] Conversely, if the Group 14 substituent features residual chloro functionality, cyclization under consumption of the double bonds was observed unless prevented by the steric demand, *e. g.* in case of **38d**. Disilastannirane **39** was isolated from the reaction of **16** with dichlorodimethyl stannane.[85] Similarly, chloro functionalized cyclotrisilanes **40a,b** were obtained from treatment of **16** with the corresponding dichloro silanes (Scheme 15).[84] Concerning the mechanism of the cyclization reaction, an intermediate disilanyl silylene that readily undergoes Si-Cl bond insertion has been proposed. The high synthetic potential of cyclotrisilanes featuring chlorine substituents will be elucidated in more detail in Chapter 1.2.

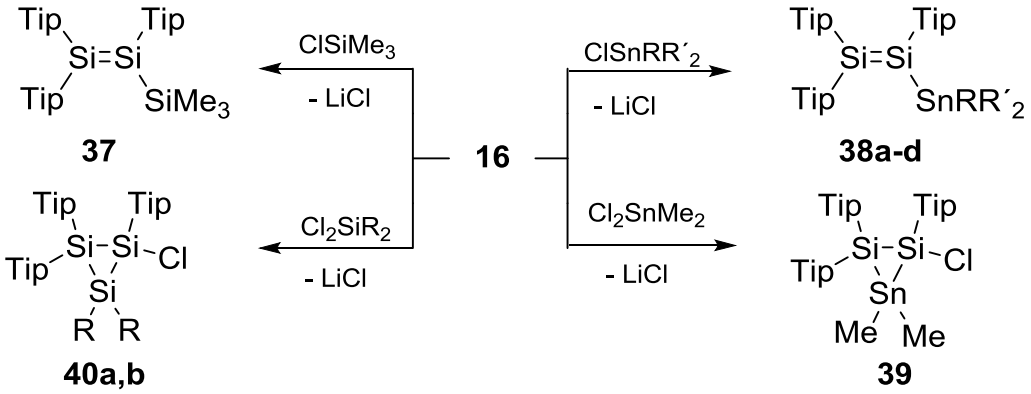

Scheme 15. Synthesis of trimethylsilyl substituted disilene **37**, stanyl substituted disilenes **38a-d**, chloro disilastanirane **39** and chloro cyclotrisilanes **40a,b** (**a:** R = R´ = Me, **b:** R = R´= Ph, **c:** R = R´ = ^{n}Bu, **d:** R = Cl, R´ = ^{t}Bu).[84,85]

Besides the aforementioned transfer of Si=Si motif under retention of the double bond and the formation of three-membered rings under consumption of the Si-Si double bond, a third reactivity has been reported: the transformation of the Si=Si bond into a heteronuclear silicon containing double bond. Sekiguchi and coworkers studied the reactivity of disilenide **22a** towards ketones and found the formation of anionic silenes **41** and **42**.[86,87] Depending on the steric bulk of the ketone moiety, the lithium counter cation is either coordinated in η^1-fashion to the silyl anion only (**41**)[86] or in η^3-fashion to an allyl anion (**42**,Scheme 16).[87]

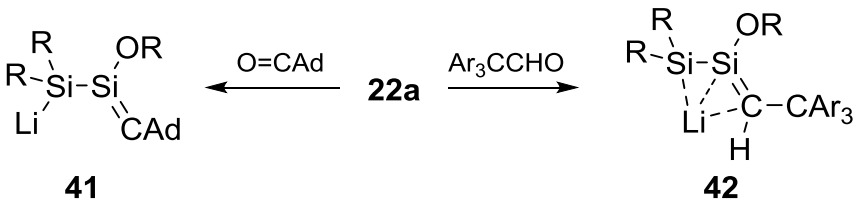

41 **42**

Scheme 16. Sekiguchi´s syntheses of anionc silenes **41** and **42** from the reaction of **22a** with ketones (R = SiMe^{t}Bu$_2$, Ad = adamantyl, Ar = 3,5-^{t}Bu$_2$C$_6$H$_3$).[86,87]

A similar reactivity has been reported in a collaborative work of the groups of Scheschkewitz and Sekiguchi for both disilenides **16** and **22a**. The reactions of **16** and **22a** with vinyl bromides afford four-membered cyclic silenes **43a-e**.[88] As mechanism for the formal transformation of the Si=Si bond into a Si=C bond an intermolecular [2+2] cycloaddition of an intermediate vinyl disilene was proposed. In analogy, cyclic Brook-type silenes **44a-c** could be isolated from the reactions of **16** and **22a** with carboxylic acid chlorides (Scheme 17).[89]

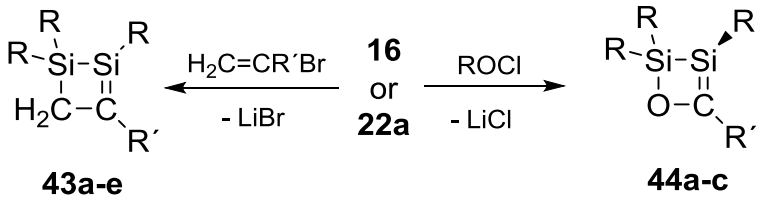

43a-e **44a-c**

Scheme 17. Reactions of disilenides **16** and **22a** with carboxylic acid chlorides and vinyl bromides (**43a**: R= Tip, R´ = Ph; **43b**: R = SiMe^{t}Bu$_2$, R´ = Ph; **43c**: R = Tip, R´ = SiMe$_3$; **43d**: R = SiMe^{t}Bu$_2$, R´ = SiMe$_3$; and **43e**: R = SiMe^{t}Bu$_2$, R´ = H; **44a**: R = Tip, R´ = 1-adamantlyl; **44b**: R = Tip, R´ = ^{t}Bu; **44c**: R= SiMe^{t}Bu$_2$, R´ = 1-adamantyl).[88,89]

Very recently, the Scheschkewitz group reported the transformation of the Si=Si bond into a Si=Ge bond. Treatment of **16** with the NHC$^{i\text{Pr2Me2}}$ adduct of germanium dichloride (NHC$^{i\text{Pr2Me2}}$ = 1,3-diisopropyl-4,5-dimethylimidazol-2-ylidene) afforded NHC coordinated silagermenylidene **45**, an isolable base adduct of a heavy vinylidene analogue.[90] The mechanism proposed for the formation involves a 1,3-shift of a chlorine atom in a disilenyl chloro germylene as unobserved, but plausible intermediate (Scheme 18). The degree of functionalization in **45** (double bond, NHC-coordination, lone pair at germanium, and chlorine substituent in β-position) is remarkable, and unsurprisingly further manipulations on this system already have been published.[91] This reaction is yet another striking example for the variety of structural motifs that are accessible from nucleophilic disilenes.

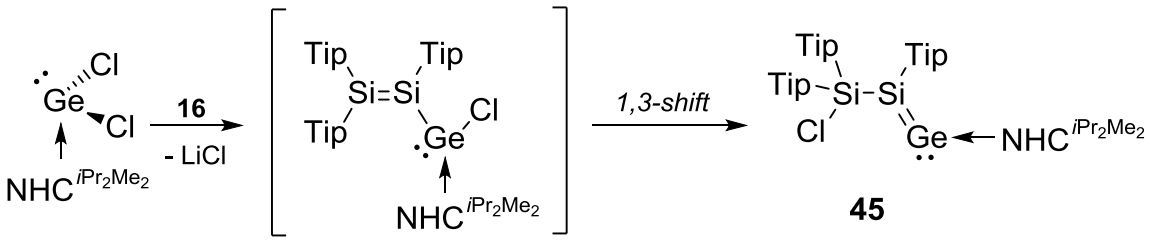

Scheme 18. Synthesis of NHC-coordinated silagermenylidene **45** (NHC^{i}Pr$_2$Me$_2$ = 1,3-diisopropyl-4,5-dimethyl-imidazol-2-ylidene).[90]

1.1.4.3. Halodisilenes: Electrophilic Disilenes

Halodisilenes that can formally be regarded as the electrophilic counterparts of disilenides (*vide supra*) should be equally useful building blocks. The lighter congeners, vinyl halides, are valuable synthons in organic chemistry.[92] The first stable dihalodisilene R(Cl)Si=Si(Cl)R (R = Si[CH(SiMe$_3$)$_2$]$_2$(^{i}Pr)) was reported as early as 2002 by Wiberg *et al.*, but turned out to be sterically too crowded to allow the attack of nucleophiles at the unsaturated silicon centers.[93] In 2008, Tokitoh *et al.* isolated dibromo disilene **46** stabilized by bulky Bbt-substituents (Bbt = 2,6-[(Me$_3$Si)$_2$CH]$_2$-4-[(Me$_3$Si)$_3$C]-C$_6$H$_2$) *via* reduction of tribromo Bbt-silane with two equivalents of lithium/naphthalene (Scheme 19).

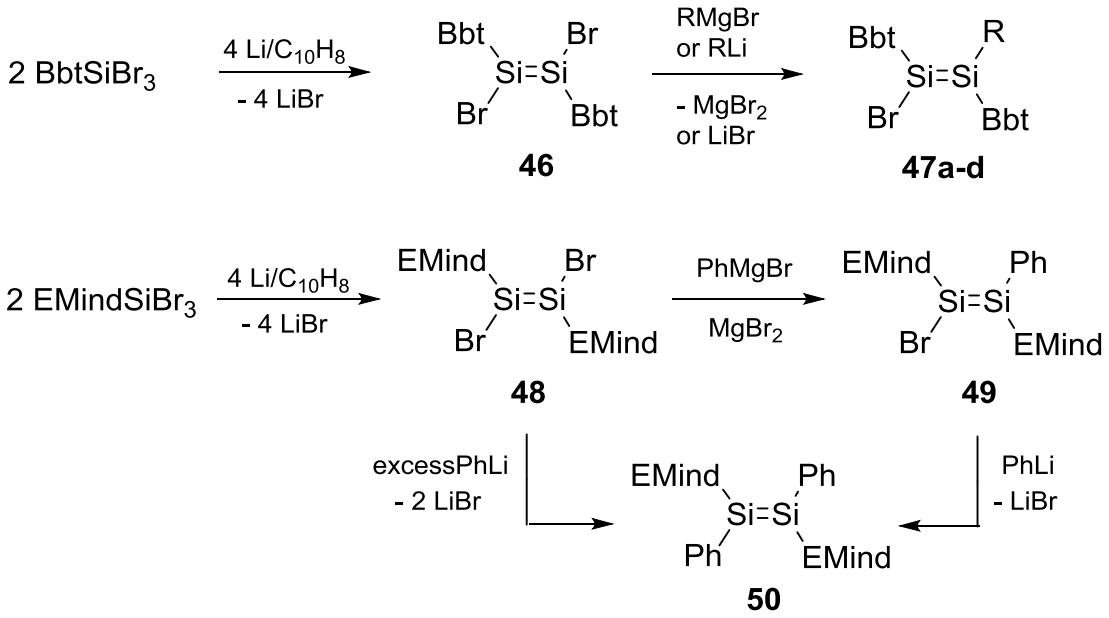

Scheme 19. Tokitoh´s synthesis of dibromo disilene **46** and monosubstitution products **47a-d** (Bbt = 2,6-[(Me$_3$Si)$_2$CH]$_2$-4-[(Me$_3$Si)$_3$C]-C$_6$H$_2$),[94] **a**: R = Me, **b**: R = Et, **c**: R = ^{n}Bu, **d**: R = Ph) and Tamao´s synthesis of dibromo disilene **48** and mono- and disubstitution products **49** and **50** (EMind = 1,1,3,3,7,7-hexaethyl-5,5-dimethyl-s-hydrindacen-4-yl).[95]

They demonstrated that treatment of **46** with one equivalent of various organo lithium and magnesium reagents indeed affords the corresponding substituted monobromo disilenes **47a-d**.[94] However, attempts to substitute both bromo functionalities failed, according to the authors due to a slightly higher LUMO energy of **47a-d** than that of **46**.

An analogous route was applied by Tamao *et al.* to synthesize dibromo disilene **48** with EMind-groups (EMind = 1,1,3,3,7,7-hexaethyl-5,5-dimethyl-s-hydrindacen-4-yl) in a more recent work. Notably, in the case of **48** mono- or disubstituted derivatives **49** and **50** are accessible from the reaction with one or two equivalents phenyl lithium/phenyl magnesiumbromide, respectively (Scheme 19).[95]

The synthesis of iodo disilene **51** *via* an umpolung strategy, namely the oxidation of disilenide **16** with elemental iodine, has been reported by the Scheschkewitz group. As outlined in Scheme 13, phosphino disilenes **33a-d** are accessible *via* the transfer of nucleophilic disilenide **16** to the corresponding phosphorus electrophiles. A proof-of-concept that **51** indeed represents the electrophilic counterpart of **16** was provided by the authors: as alternative synthetic route to **33a** the iodine functionality in **51** can be substituted with diphenyl phosphide as nucleophile (Scheme 20).[81]

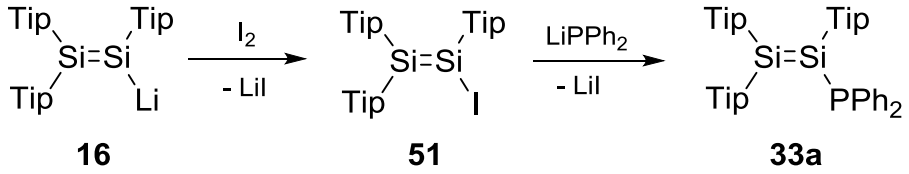

16 **51** **33a**

Scheme 20. Synthesis of iodo disilene **51** via umpolung strategy and its conversion to **33a** with lithium diphenyl phosphide.[81]

1.1.4.4. Disilynes – Disila Analogues of Alkynes

In 2000, the first heavier Group 14 analogue with a formal triple bond, a diplumbyne, was reported by the Power group.[96] Two years later, the same group succeeded in the synthesis of the first distannyne[97] and digermyne.[98] The series of heavier Group 14 analogues of alkynes was completed in 2004. The first relatively stable disilyne was prepared by Wiberg *et al.* and its constitution supported by high resolution mass spectrometry and NMR spectroscopy.[28]

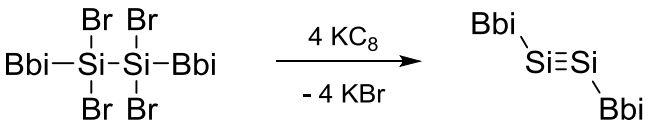

52 **53**

Scheme 21. Synthesis of the first structurally characterized disilene **53** communicated by Sekiguchi (Bbi = Si(^{i}Pr)(Dsi)$_2$, Dsi: C(H)(SiMe$_3$)$_2$).[29]

In the same year, Sekiguchi *et al.* provided the first X-ray diffraction study of a persistent disilyne. Reductive dehalogenation of 1,1,2,2-tetrabromo disilane **52** yields disilyne **53** protected by extremely bulky silyl groups (Scheme 21).[29] To date, some additional examples of stable Si≡Si bonds have been reported including a diaryl substituted disilyne (prepared by reduction of **46**)[94] as well as an unsymmetrically substituted derivative.[99] Recent developments have been subject to a review article published in 2012.[100]

Disilynes have been employed as precursors for functionalized disilenes. It has been demonstrated that disilynes are readily amenable to addition reactions over the triple bond due to the comparably small HOMO-LUMO gap of disilynes, which – as disilenes – show a *trans*-bent arrangement of substituents about the Si≡Si bond (*cf*. 1.1.2).[100]

Addition reactions across the silicon-silicon triple bond provided access to disilenes featuring a substitution pattern that is otherwise not accessible. Similar to alkynes, disilyne **53** undergoes hydroboration reactions with 9-BBN and catechol borane to yield 1-boryl-2-hydro-disilenes **54a,b**.[101,102] For **54b** a certain degree of delocalization of the π-electrons is apparent (**54b´**,Scheme 22).[102] As reported by Sekiguchi *et al*., **53** also reacts with a variety of primary and secondary amines to the 1,2-hydroamination products **55a-d**.[101,103] It should be noted that in contrast to hydroborations, uncatalyzed hydroamination reactions are unknown in organic chemistry. For **55a-d** certain contributions of zwitterionic structures **55'a-d** (Scheme 22) has been proposed by the authors.[101,103]

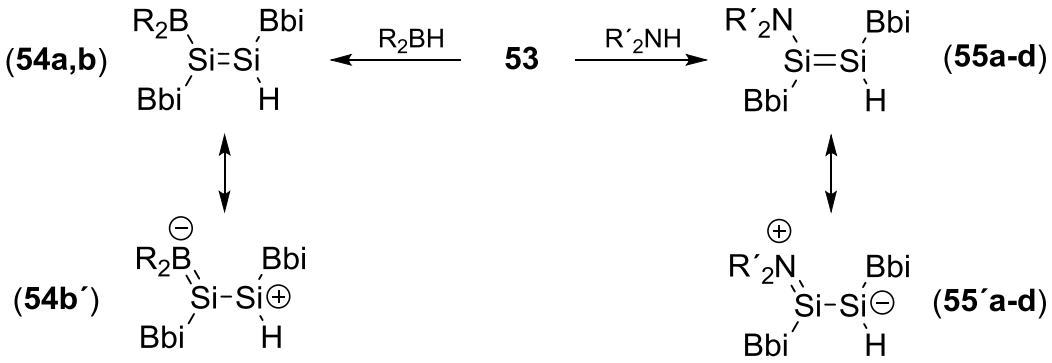

Scheme 22. Sekiguchi´s synthesis of boryl disilenes **54a,b** (**a**: R_2 = 9-BBN, **b**: catechol) and amino disilenes **55a-d** (**a**: R´ = Et, **b**: R´ = Ph, **c**: NR´$_2$ = NH^{t}Bu, **d**: R´ = -$(CH_2)_4$-) *via* addition reactions to **53**.[101-103]

1.1.5. Phosphasilenes

After the first successful isolations of compounds with homonuclear double bonds between heavier main group elements, soon also heteronuclear combinations moved into focus. Early on, the combination of silicon with its Group 15 neighbor was of interest. Compounds of the type E_{14}=E_{15} (E_{14}, E_{15} = Group 14, 15 element) generally display some characteristic features. The lone pair of electrons at E_{15} can be regarded as functionalization, since it provides a reactive site in the molecule. Furthermore, the double bond is inherently polarized due to the difference in electronegativity of the two centers (*e. g.* Si: 1.90 *vs* P: 2.19 on Pauling scale).

A little more than two dozen reports have been published on phosphasilene chemistry to date. In the 1980´s and beginning 1990´s, the focus was on developing synthetic methods of the preparation of Si=P bonds and stabilizing the skeletons. Also the reactivity under consumption of the silicon-phosphorus double bonds was studied extensively.[104] Afterwards, the reputed laboratory curiosities left center stage for more than a decade.

In the new millennium, the potential of heavier low-valent compounds for applications in material chemistry began to emerge. Considering the pivotal role of phosphorus in doping of silicon materials, the combination of these two elements is especially exciting. Arguably, in the last few years also phosphasilenes have experienced a renaissance. As in low-valent main group chemistry in general, focus has shifted on incorporating Si=P into extended systems. A prerequisite to build up larger units based on heavy double bonds is the presence of peripheral functionalization. Hence,

in recent reports on phosphasilene chemistry the introduction of functional groups to the low-valent silicon and/or phosphorus centers was investigated.

1.1.5.1. Classical Synthesis of Phosphasilenes

In 1984, Bickelhaupt reported the isolation of phosphino silane **56a** from the reaction of Mes*PH_2 (Mes* = 2,4,6-$^{t}Bu_3C_6H_2$) with dimesityl dichloro silane (mesityl = 2,4,6-$Me_3H_2C_6$) in the presence of ^{n}BuLi. Formal hydrogen chloride elimination afforded **57a**, the first spectroscopically characterized phosphasilene.[105] While **57a** shows only limited stability, the authors adapted the synthesis to four other, in some cases more stable phosphasilenes **57b-e** (Scheme 23).[106]

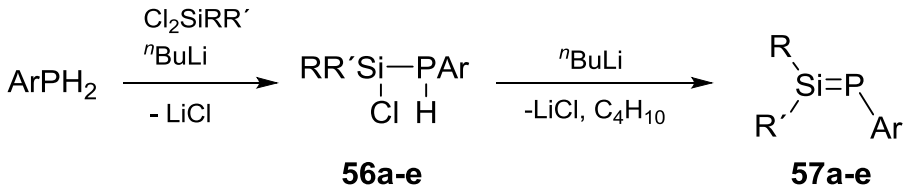

56a-e **57a-e**

Scheme 23. Bickelhaupt´s syntheses of phosphasilenes **57a-e** (Ar = Mes* = 2,4,6-$^{t}Bu_3H_2C_6$; **a**: R = R´ = Mes = 2,4,6-$Me_3C_6H_2$; **b**: R = R´ = Es = 2,4,6-$Et_3C_6H_2$; **c**: R = Ph, R´ = Tip = 2,4,6-$^{i}Pr_3C_6H_2$; **d**: R = Mes, R´ = Tip; **e**: R = ^{t}Bu, R´ = Tip).[105,106]

In 1991, Driess reported the synthesis of phosphasilenes *via* salt metathesis. Lithio phosphanes **58a-c** obtained from lithiation of the corresponding silylphosphanes undergo thermally induced lithium fluoride elimination and he was thus able to characterize *P*-silyl and *P*-phosphino substituted phosphasilenes **59a-c** by NMR spectroscopy (Scheme 24).[107]

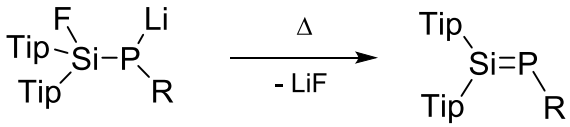

58a-c **59a-c**

Scheme 24. Syntheses of phosphasilenes **59a-c** (Tip = 2,4,6-$^{i}Pr_3H_2C_6$; **a**: R = Si$^{i}Pr_3$; **b**: R = $SiMe_2{}^{t}Bu$, **c**: R = $^{t}Bu_2P$) reported by Driess.[107]

The first X-ray diffraction study on a phosphasilene was realized in 1993. Niecke *et al.* showed that their previously reported lithium 1,3-phospha-2-silaallyl complex **60**[108]

can be derivatized with diphenylchloro phosphane as an electrophilic reagent. From this reaction, phosphasilene **61** was isolated as yellow crystals (Scheme 25).[109]

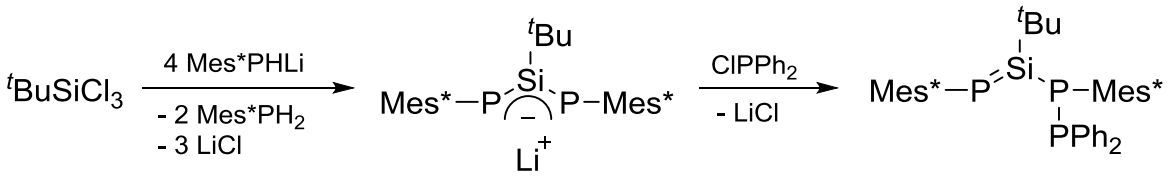

60 **61**

Scheme 25. Niecke´s synthesis of the first crystalline phosphasilene **61**.[109]

Two years later, a second crystalline derivative was obtained by the Driess group. The same strategy as reported for phophasilenes **59a-c** was applied to synthesize ^{t}Bu(Tip)Si=P-Si^{i}Pr$_3$, which was isolated as yellow single crystals and investigated by an X-ray diffraction study.[110]

1.1.5.2. Early Reactivity Studies

Similar to the initial studies concerning disilene reactivity, addition reactions across the Si=P bond were the primary focus of investigations. Already in the first reports of Bickelhaupt selective hydrolysis and methanolysis were investigated.[105,106] Later on, an impressive amount of silaphosphacycles was synthesized by the Driess group *via* addition of various substrates to the Si=P bond. In Scheme 26, a non-comprehensive overview of the reactivity of **59b** is displayed.[104]

The oxidation of phosphasilene **59b** with elemental sulfur or tellurium afforded the corresponding silaphosphacyclopropane analogues **62a,b**. A [2+3] cycloaddition reaction is observed with mesityl azide to furnish silaphosphatriazol **63**.

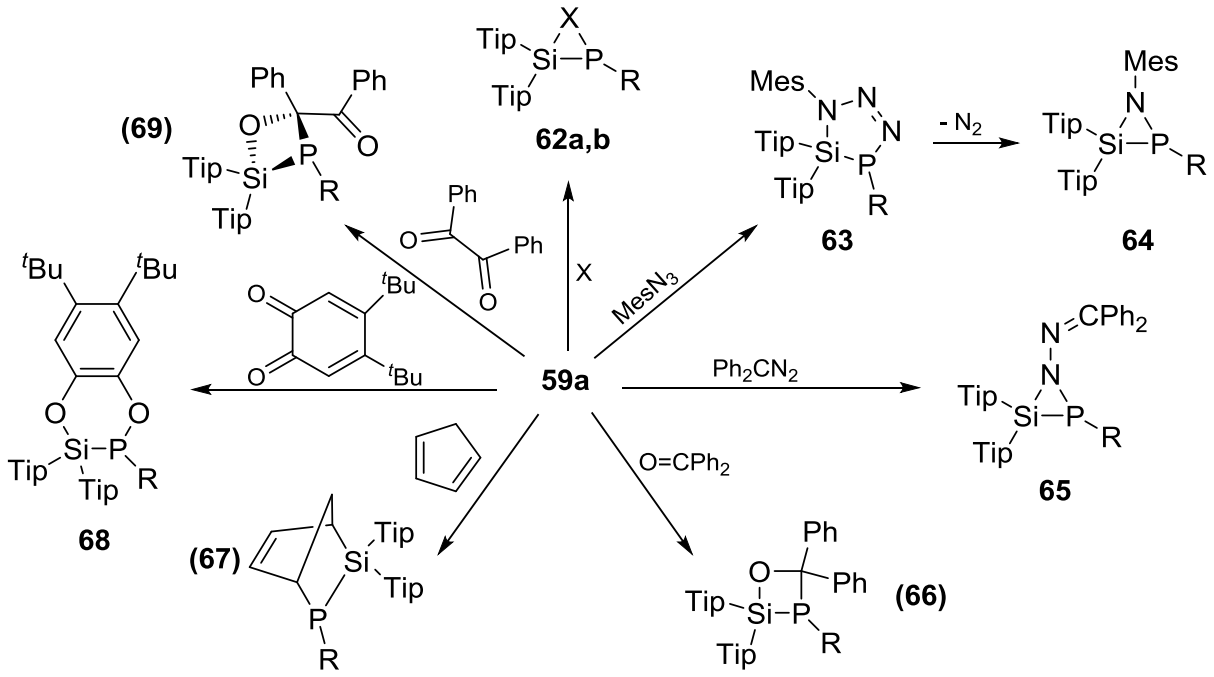

Scheme 26. Overview of phosphasilene **59a** reactivity towards selected compounds (R = Si^{i}Pr$_3$, **62a**: X = S, **62b:** X = Te).[104,111,112]

Upon heating the compound transforms into aziridine derivative **64** under loss of N_2.[111] In contrast, treatment of **59b** with diphenyl diazomethane yielded the [2+1] cycloaddition product **65**.[112] It was shown that heterocyclobutane **66** is accessible from the reaction of **59b** with benzophenone. Furthermore, **59b** can be applied as dienophile. From a Diels-Alder reaction with cyclopentadiene **67** was obtained. It was demonstrated that [2+4] cycloaddition reactions also occur with 1,2-diketones. The reaction of **59b** with 4,6-di-^{t}Bu-*o*-quinone afforded the benzo-condensed heterocycle **68**. Surprisingly, with 1,2-ethanedione the four-membered [2+2] cycloadduct **69** was obtained instead of the expected [4+2] adduct.[112]

1.1.5.3. Recent Advances in Phosphasilene Chemistry

After the successful isolation of compounds with Si=P bonds and reactivity studies under consumption of the double bond have been carried out, the functionalization and the incorporation of phosphasilenes into extended systems has become a central objective.

In 2009, Tamao established the synthesis of very sterically encumbered phosphasilenes by the classical route of base induced hydrogen halide elimination.

The bulky lithium phosphide EMindPHLi (EMind = 1,1,3,3,7,7-hexaethyl-5,5-dimethyl-s-hydrindacen-4-yl) was coupled with dibromosilanes to yield precursors **70a-c**. Subsequent HBr elimination with DBU (DBU = 1,8-diazabicyclo[5.4.0]undec-7-ene) afforded phosphasilenes **71a-c**.[113] Notably, this strategy also allowed for the synthesis of a molecule featuring two Si=P bonds connected by a phenylene linker. The precursor **72** is accessible from the reaction of EMindPHLi with 1,4-bis(dibromosilyl)benzene followed by DBU-promoted HBr elimination to yield 1,4-bis(phosphasilenyl)benzene **73** (Scheme 27).

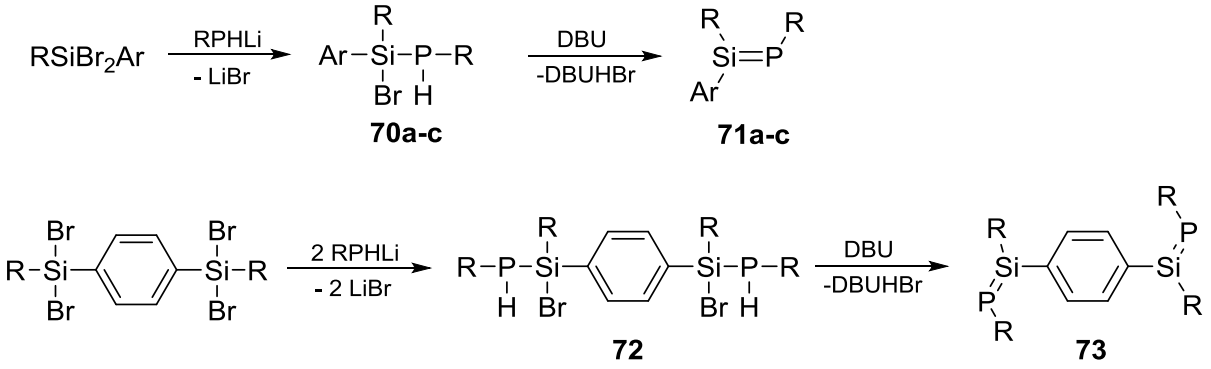

Scheme 27. Tamao´s synthesis of phosphasilenes **71a-c** and π-conjugated phosphasilene **73** (R = EMind = 1,1,3,3,7,7-hexaethyl-5,5-dimethyl-s-hydrindacen-4-yl); **a**: Ar = phenyl, **b**: Ar = naphtyl, **c**: Ar = anthracenyl; DBU = 1,8-diazabicyclo[5.4.0]undec-7-ene).[113]

An X-ray diffraction study of **73** revealed that the phenylene unit is entirely coplanar with the Si=P bonds, which is well-suited for $2p_\pi$−$3p_\pi$ conjugation. Efficient π-delocalization over the skeleton is further supported by the UV/vis spectrum exhibiting a bathochromic shift of the longest wavelength absorption compared to reported phosphasilenes.[113]

As mentioned above, the lone pair of electrons on phosphorus can be regarded as a functionalization attached to the Si=P bond. Indeed, Tamao demonstrated that phosphasilene **71a** can be transferred to a gold center by treatment with gold chloride to afford complex **74**.[114] Notably, the chlorine atom in **74** can be removed in the presence of another molecule of phosphasilene **71a** by the addition of $[Ph_3C][B(C_6F_5)_4]$ to produce the cationic complex **75** with two phosphasilene ligands (Scheme 28). Comparable to bisdisilenyl transition metal complexes **34** and **35** (*cf.* Chapter 1.1.4.2, Scheme 14),[82] conjugation between the two Si=P bonds through the Au atom is confirmed by a red-shift of the longest wavelength absorption in the UV/vis spectrum.[114]

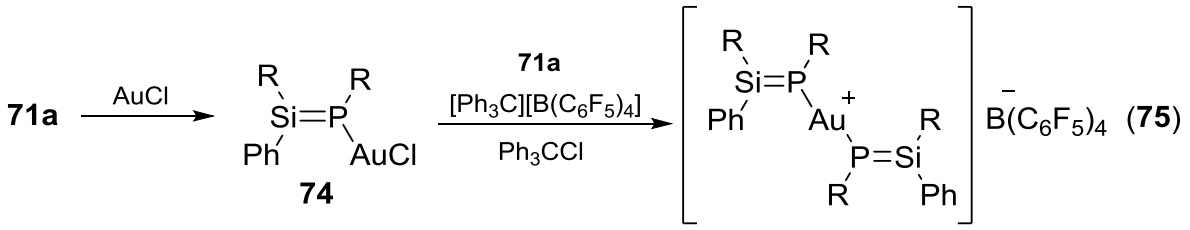

Scheme 28. Synthesis of neutral and cationic phosphasilene gold complexes **74** and **75** reported by Tamao (R = EMind).[114]

Some reports concerning the attachment of functional groups to the unsaturated phosphorus or silicon centers of phosphasilenes have been published. Considering the benefit of disilenides[34,48,66] for synthetic chemistry (*cf.* Chapter 1.1.4.2), *P*-metallo phosphasilenes are of current interest. The inherent nucleophilicity of the phosphorus end of the double bond should be increased significantly in such compounds. The first example was documented by Driess in 1998. *P*-ferrio phosphane **76** was synthesized in direct analogy to the reported procedures for **59a-c**. Deprotonation of phosphane **76** to **77** and subsequent LiF elimination was expected to afford *P*-ferryl substituted phosphasilene **78**. Attempts to lithiate **76**, however, failed, but the authors finally prepared phosphasilene **78** through transmetalation of *P*-ferrio-*P*-stanna phosphane **79** (Scheme 29).[115]

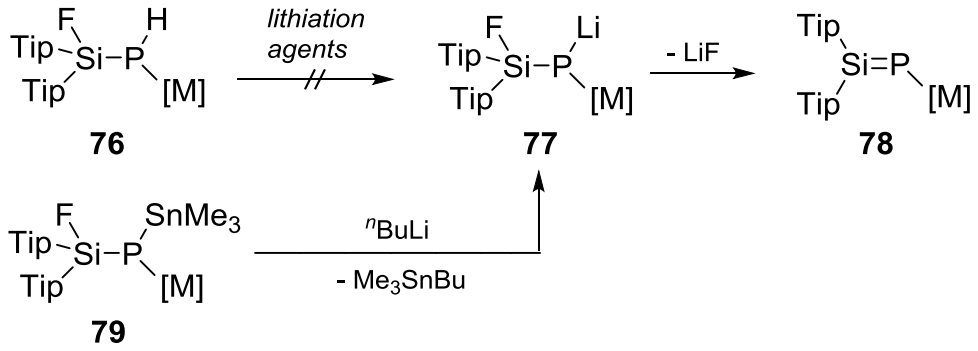

Scheme 29. Driess´ synthesis of *P*-ferrio phosphasilene **78** starting from ferryl stannyl substituted phosphane **79** (M = $(C_5H_5)(OC)_2Fe$).[115]

As demonstrated by the Driess group, (fluoro)silylphosphane **80** can be readily lithiated to afford "half-parent" phosphasilene **81a** *via* LiF elimination.[116] It should be noted that unlike in carbon chemistry, hydrogen atoms are generally regarded as functional groups in main group chemistry. For instance, the hydridic character of the hydrogen atoms bonded to heavier Group 14 atoms enables relatively facile hydrometalation reactions.[34] Unsaturated main group compounds typically require steric protection by bulky substituents and thus the study of compounds closer to the

parent systems is of particular interest. Finally, hydrogen-metal exchange reactions offer the possibility of further functionalization. Indeed, the PH moiety in **81a** can be metalated: *P*-zincio phosphasilene **81b** and *P*-plumbylenio phosphasilene **81c** were obtained from the reaction of **81a** with Me_2Zn/tmeda (tmeda = N,N,N',N'-tetramethylethylenediamine) and LPb[$N(SiMe_3)_2$] (L = *N,N*-Dip_2-2,4-dimethyl-β-diketiminate, Dip = 2,6-$^{i}Pr_2$-C_6H_3), respectively (Scheme 30).[116,117]

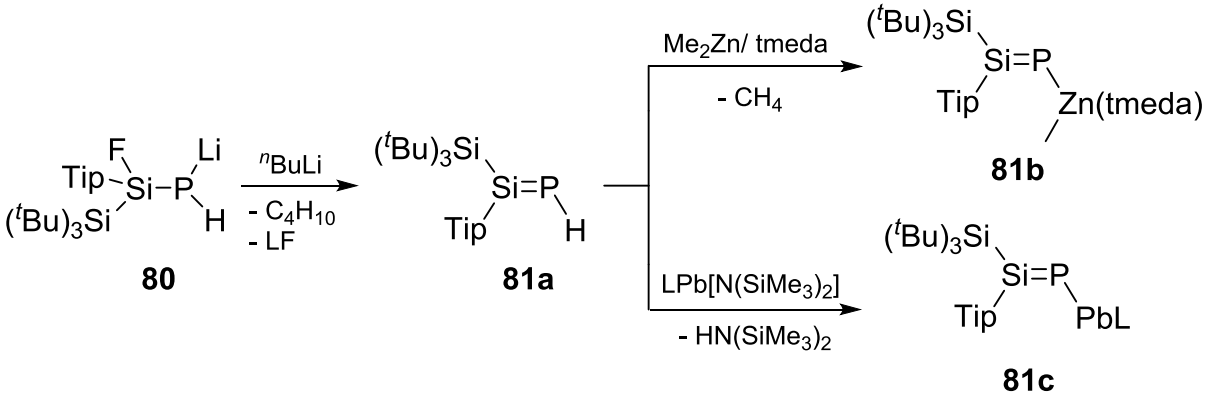

Scheme 30. Synthesis of "half-parent" phosphasilene **81a** and metalation to *P*-zincio phosphasilene **81b** and *P*-plumbylenio phosphasilene **81c** (tmeda = *N,N,N',N'*-tetramethylethylenediamine; L = *N,N*-Dip_2-2,4-dimethyl-β-diketiminate, Dip = 2,6-$^{i}Pr_2$-C_6H_3).[116,117]

So far, however, no nucleophilic reactivity of the *P*-metallo phosphasilenes has been published.

Coordination of Lewis-bases can stabilize low-valent main group compounds that are otherwise only fleeting intermediates. The concept of donor-stabilization has been employed extensively during the last years in particular in Group 13-15 chemistry. Recently, it has triggered a debate whether the description of dative bonding ("arrows") of the donors to stabilize unsaturated compounds is appropriate, or the structure is better described as an ylidic structure with formal charges.[118]

While the first report of a donor-stabilized Si=P bond goes back to Corriu as early as 1991,[119] this concept was widely studied in phosphasilene chemistry during the last years, in particular by the groups of Driess and Inoue. Although donor-coordinated phosphasilenes indeed exhibit double bond-reactivity, the polarity of the Si=P bond (δ^+ on Si and δ^- on P) is increased and thus they possess a zwitterionic character. The electronic structures may equally well be described by ylidic resonance forms without Si-P double bond. In the following, ylidic phosphasilenes will be largely represented without formal charges (as in the original publications) for reasons of clarity.

Reported examples feature nitrogen substituents in the periphery of the silicon atom and/or external donors, such as N-heterocyclic carbenes (Scheme 31).

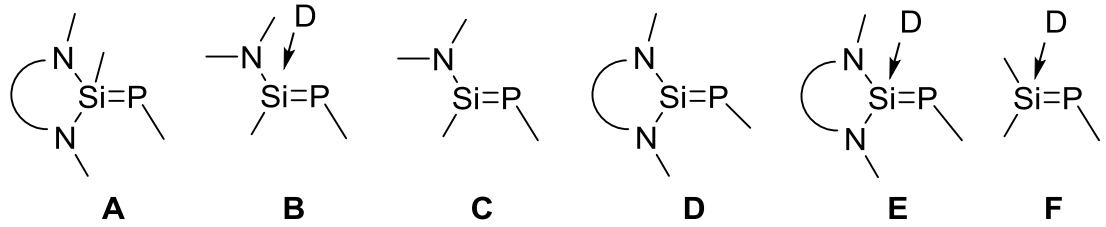

Scheme 31. Types of donor stabilized phosphasilenes (D = DMAP (4-(dimethylamino)-pyridine) or NHC).

The first example of a zwitterionic *N*-heterocyclic phosphasilene (type **A**, *cf.* Scheme 31) was reported in 2011 by Driess and Inoue. N-heterocyclic chlorosilylene can be phosphanylated to yield bis(trimethylsilyl)phosphino silylene **82**. Thermally induced 1,2-silyl migration afforded phosphasilene **83** (Scheme 32). NMR and UV/vis data clearly reveal a preference for the ylidic resonance form **83´**.[120]

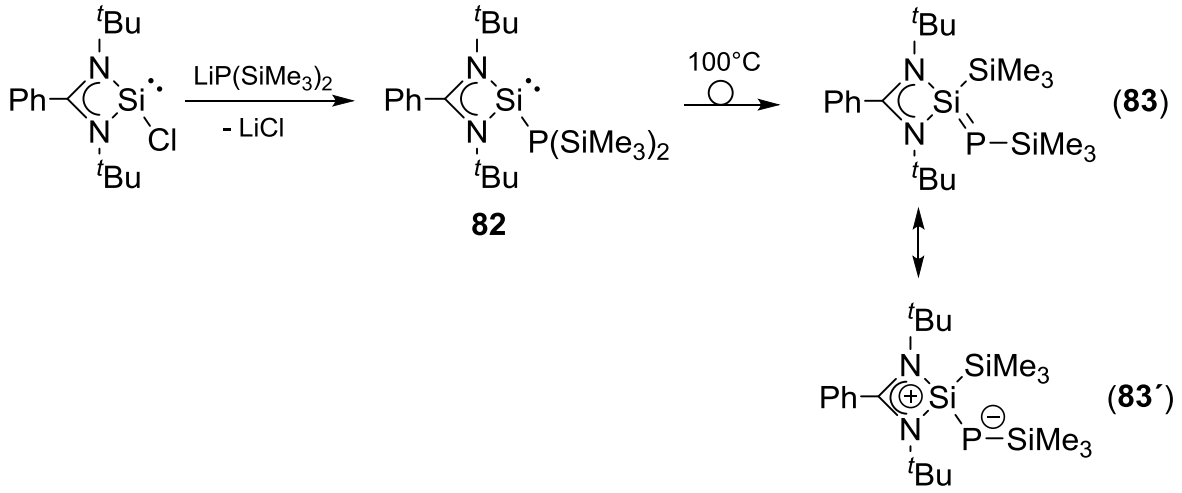

Scheme 32. Synthesis of the first *N*-heterocyclic phosphasilene **83** reported by Driess and Inuoe.[120]

As demonstrated by the Inoue group, **83** is an interesting ligand for transition metal complexes. Phosphasilene **83** reacts with $W(CO)_5 \cdot (thf)$ to afford complex **84**, in which the Si=P unit is coordinated in η^1-fashion to tungsten. Upon heating of **84**, the silyl group attached to the silicon atom migrates back to phosphorus yielding silylene complex **85**.[121]

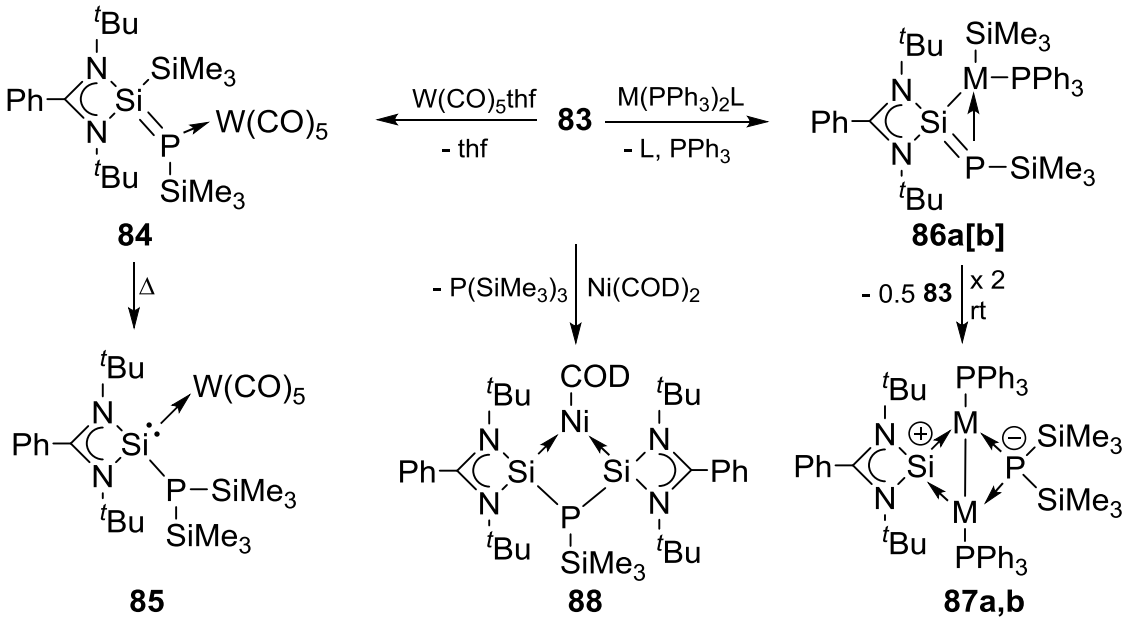

Scheme 33. Reactivity of zwitterionic phosphasilene **84** towards transition metal complexes (**a**: M = Pt, L = ethylene, **b**: M = Pd, L = $P(Ph_3)_2$; COD = cycloocta-1-5-diene).[121,122]

The reactivity of **83** with d^{10}-transition metal centers of Group 10 has been investigated by Inoue *et al*.[122] As confirmed by multinuclear NMR spectroscopy, treatment of **83** with bis(triphenylphosphine)platinum ethylene complex results in a coordination of the Si=P bond in η^2-fashion (**86a**). The initial product spontaneously rearranges to an isolable dinuclear platinum complex, which according to the authors is best described as silyliumylidene phosphide complex **87a**.[122] While from the reaction of **83** with tetrakis(triphenylphosphine) palladium no side-on coordination to form **86b** could be detected by NMR spectroscopy, its intermediacy was supported by DFT calculations and dinuclear palladium complex **87b** isolated as final product. In contrast, when **83** is reacted with half an equivalent $Ni(COD)_2$ (COD = cycloocta-1,5-diene), bis(silylene) complex **88** was obtained and tris(trimethylsilyl)phosphane formed as by-product (Scheme 33).[122]

The certain degree of lability of the trimethylsilyl group in both silylene **82** and phosphasilene complex **83** might have inspired Inoue *et al.* to investigate the reactivity of silylene **82** towards pivaloyl chloride. Indeed, trimethylsilyl chloride elimination was observed and compound **89** isolated, which according to the authors is best described as an acyl substituted phosphasilene and thus the first time a classical organic functionality has been introduced in the periphery of a phosphasilene (Scheme 34).[123]

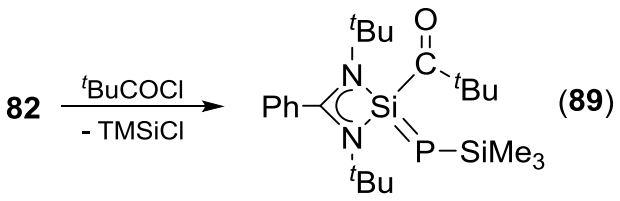

Scheme 34. Inoue´s synthesis of *Si*-acyl functionalized phosphasilene **89**.[123]

Cui *et al*. have shown that the chlorine functionality in aminochloro silylene **90** can be substituted with RPHLi (R = 2,6-Mes_2-C_6H_3) to afford aminophosphino silylene **91**. Subsequent 1,2-shift of the hydrogen atom from phosphorus to silicon yielded the NHC adduct of 2-hydro-2-amino phosphasilene **92** (Scheme 35, type **B**, *cf.* Scheme 31).[124] The authors demonstrated that the NHC can be removed by the addition of triphenylborane as Lewis-base and 2-hydro-2-amino phosphasilene **93** (type **C,** *cf.* Scheme 31) was isolated (Scheme 35).

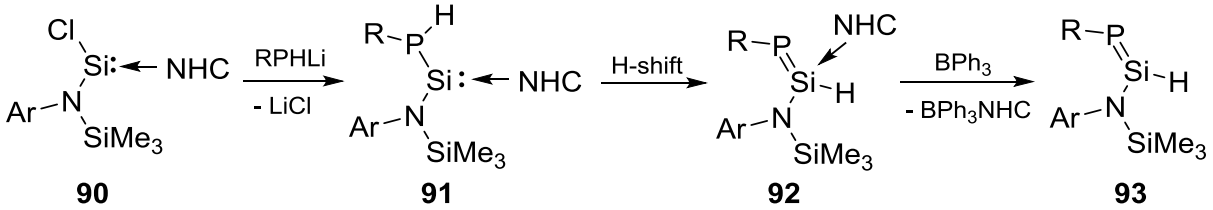

90 **91** **92** **93**

Scheme 35. Synthetic route to 2-hydro-2-amino phosphasilene **93** published by Cui (Ar = Dip; R = 2,6-Mes_2-C_6H_3; NHC = 1,3-diisopropyl-4,5-dimethyl-imidazol-2-ylidene) communicated by Cui.[124]

Both X-ray data and DFT calculations suggest that the amino group on silicon results in significant N-Si-P π conjugation.[124]

In 2013, the Driess group reported “half-parent” zwitterionic phosphasilene of the type **D** (*cf.* Scheme 31). Phosphino-chloro exchange in diphosphino silane **94** using HCl afforded product **95**. Subsequent treatment of **95** with lithium diisopropylamide (LDA) resulted in the base-assisted dehydrochlorination to yield the desired phosphasilene **96**, which shows only limited stability in solution (Scheme 36). Notably, **96** is capable of transferring the parent phosphinidene moiety :PH to an NHC to afford **97** with concomitant silylene elimination.[125] This reaction is certainly facilitated by the ylidic nature of the phosphasilene that is best described by resonance structure **96´** (Scheme 36).

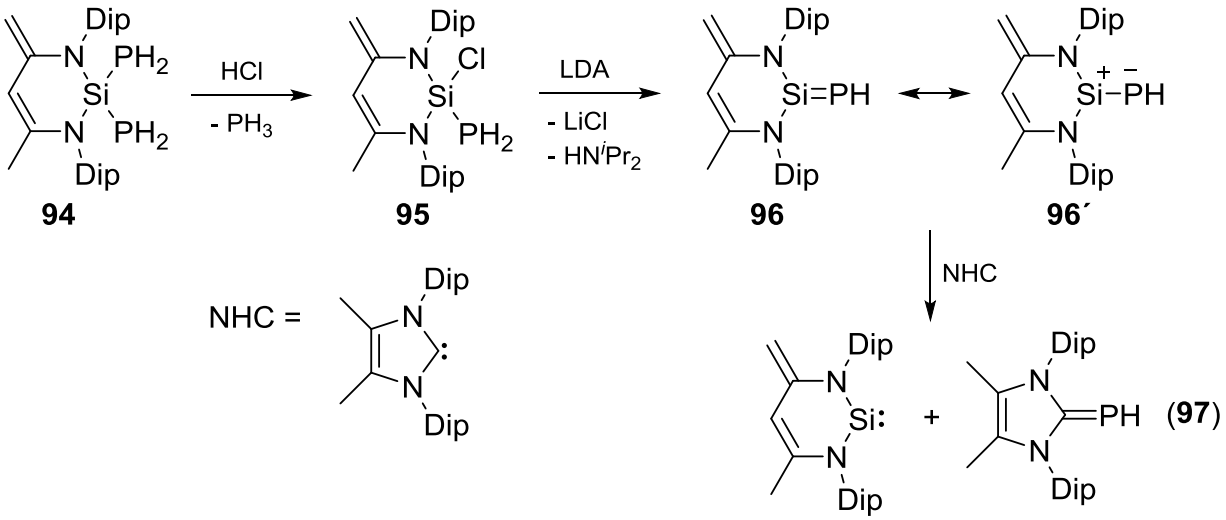

Scheme 36. Driess´ Synthesis of zwitterionic "half-parent" phosphasilene **96** and transfer of the :PH unit from **96** to NHC.[125]

In a subsequent publication it was demonstrated that upon addition of DMAP (dimethylaminopyridine) to **96** a much more stable phosphasilene **98** of type **E** (*cf.* Scheme 31) is obtained. Base-stabilized phosphasilene **98** shows a striking reactivity towards small molecules. 1,2-Aminophosphino silane **99** was obtained from the reaction of **98** with ammonia (Scheme 37). When **98** was treated with one equivalent H_2S gas, the first thiosilanoic phosphane derivative **100** could be isolated.[126]

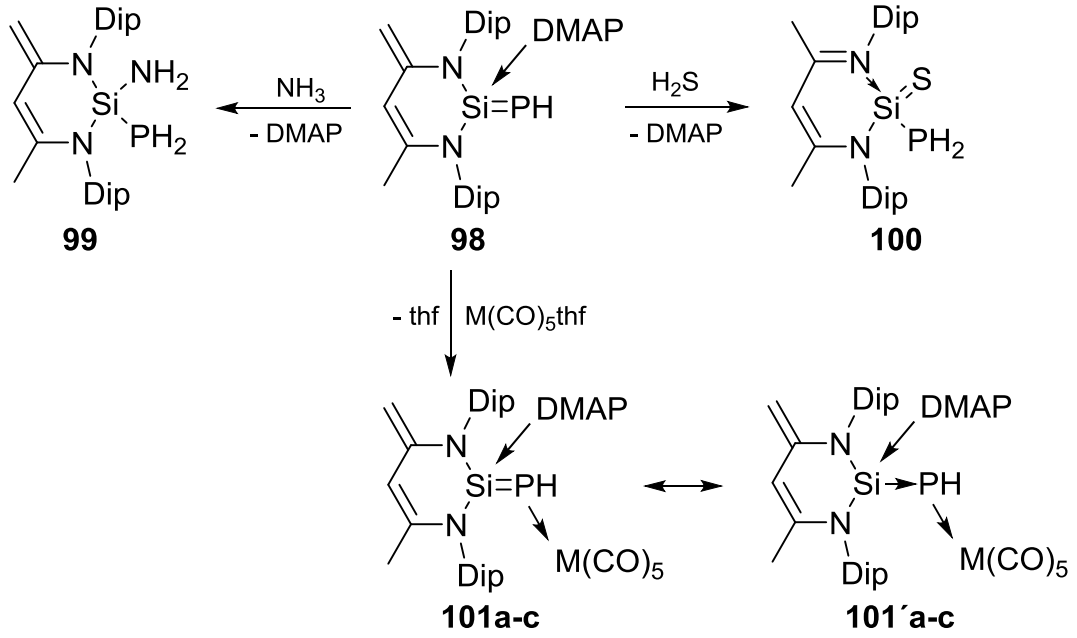

Scheme 37. Reactivity of base-stabilized phosphasilene **98** towards ammonia and H_2S and coordination of **98** to Group 6 transition metals reported by Driess (**a**: M = Cr, **b**: M = Mo, **c**: M = W).[126,127]

Furthermore, the coordination of **98** to Group 6 transition metals was reported. The reaction of **98** with $M(CO)_5$·thf afforded complexes **101a-c** that represent push-pull donor->silylene->phosphinidene->metal rather than Si=P->metal complexes according to DFT-computations (Scheme 37).[127]

In analogy to the procedures for the preparation of phosphasilenes **83** and **92**, Driess *et al.* developed the synthesis of a base adduct of a 1,2-dihydro phosphasilene (type **F**, *cf.* Scheme 31) starting from bulky NHC-coordinated chloro silylene **102**. The chlorine functionality in **102** was substituted with lithium phosphanide and subsequent 1,2-hydrogen migration afforded phosphasilene **103**.[128] Interestingly, the NHC in **103** seems to be relatively labile. Upon storing the compound in solution, the head-to-tail dimerization product **104** is formed under dissociation of the NHC from the molecule (Scheme 38).[128]

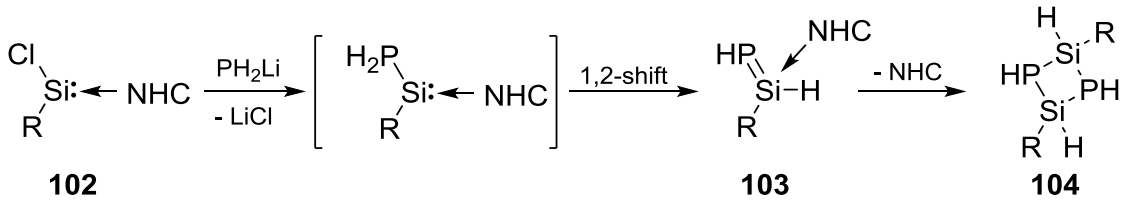

Scheme 38. Synthesis of NHC-stabilized 1,2-dihydro phosphasilene **103** by Driess and dimerization product **104** (R = 2,6-Tip-C_6H_3 , NHC = $(MeC)_2$-$(NMe)_2C$).[128]

The conceptual reversal of zwitterionic phosphasilenes was reported by the group of Sekiguchi preparing an inverse polarized phosphasilene. Silyl dianion **105** (*cf.* Chapter 1.1.3) was reacted with Mes*PCl_2 (Mes* = 2,4,6-^{t}Bu_3-H_2C_6) to yield phosphasilene **106**. In **106**, two σ-donating silyl groups are attached to the unsaturated silicon center, and the phosphorus atom is substituted with an electron withdrawing aryl group. According to the authors, this “push-pull” substitution pattern results in more negative polarization at Si and less electron density at phosphorus formally reversing the usual polarization (Scheme 39).[129]

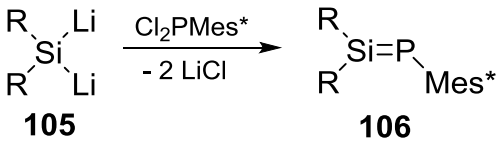

Scheme 39. Sekiguchi´s synthesis of inverse polarized phosphasilene **106** (R = ^{t}Bu_2MeSi, Mes* = 2,4,6-^{t}Bu_3-H_2C_6).[129]

As part of my master thesis, the reactivity of disilenide **16** towards bis(dialkylamino) chloro phosphanes $ClP(NR_2)_2$ was investigated.[130] For R = ^{i}Pr phosphino disilene **107** was obtained. Conversely, less bulky amino substituents (R = Me, Et) resulted in the formation of unprecedented *P*-amino functionalized phosphasilenes **108a,b** as *E/Z*-isomers. As mechanism for the formation of **108a,b** we propose a formal 1,3-shift of one amino substituent of intermediate phosphino disilenes (Scheme 40). Both crude products are reasonable pure, but only the methyl substituted derivative **108a** crystallizes in excellent yields.[130] Spectroscopic and structural features of **108a,b** indicate an inverse polarization of the Si=P bond which we attribute to the electronegative, π-donating amino substituent at phosphorus. DFT calculations of the Mulliken charges (performed by Dr. M. C. Cowley, Edinburgh University) indeed revealed a truly inverse polarization in this case (Si2: −0.095, P1: +0.169).

A preliminary reactivity study with **108a** revealed that the amino functionalization at phosphorus opens doors to further manipulations. Upon addition of ^{t}Bu-isonitrile the amino group is shifted to the neighboring silicon atom affording 1-aza-3-phosphaallene **109a**.[130]

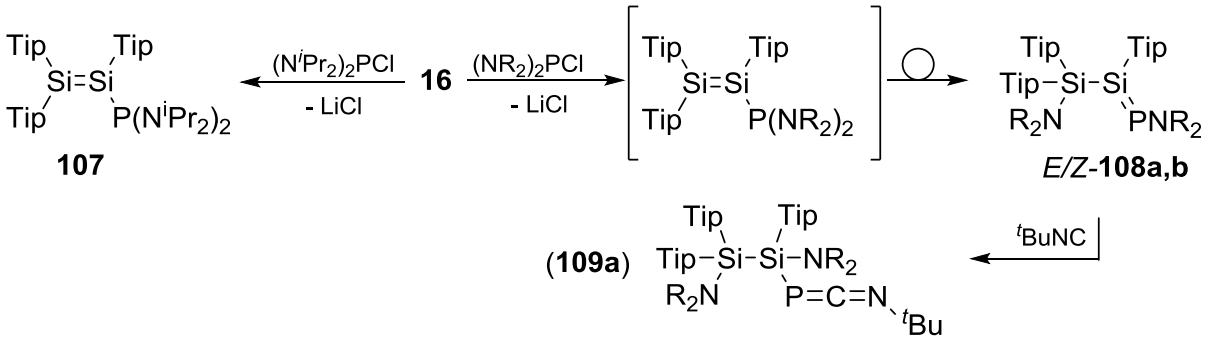

Scheme 40. Synthesis of phosphino disilene **107**, phosphasilenes ***E/Z*-108a,b** and conversion of **108a** into 1-aza-3-phosphaallene **109a** (**a**: R = Me, **b**: R = Et).[130]

As it is known that dimethylamino groups can be substituted by anionic nucleophiles in selected cases,[131] and the *P*-amino functionality in **108a** apparently features a certain degree of mobility, phosphasilene **108a** was going to be investigated as electrophilic reagent in this project. An electrophilic phosphasilene as Si=P analogue of halodisilenes (*cf.* Chapter 1.1.4.3) had not been known at the outset of this project.

1.2. Unsaturated Cluster Compounds

1.2.1. Relationship Between Soluble Zintl Anions, (Anionic) Cage Compounds and (Anionic) Metalloid Cluster Compounds of the Group 14

The chemistry of polyhedral Group 14 clusters is a major objective in main group chemistry since the first observation of an anionic Pb_9 species **110d** more than a century ago (Scheme 41).[132] Clusters of this type are nowadays known as Zintl ions named after Eduard Zintl whose pioneering works led to a basic understanding of these compounds.[133] Zintl clusters are to this day subject of active investigations. Novel protocols for their extraction from solid-state phases into polar solvents have been reported and recent advances have been reviewed.[134]

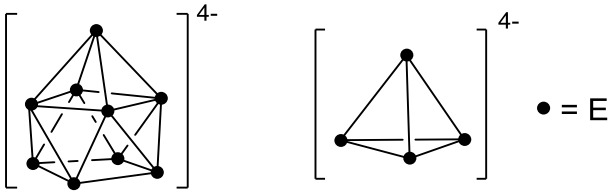

110a-d **111a-d**

Scheme 41. Structures of Group 14 Zintl anions E_9^{4-} **110a-d** and E_4^{4-} **111a-d** (**a**: E = Si, **b**: E = Ge, **c**: E = Sn, **d**: E = Pb).

In the vaguest sense, the multiple negative charges of Zintl anions can be considered as nucleophilic functionalities. Formal addition of substituents R^+ to Zintl anions can in principle (partially) compensate the negative charges. Addition of n R^+ to the smallest Zintl anions known (**111a-d**, Scheme 41) would basically afford anionic (n = 1 - 3) or neutral (n = 4) cage compounds, respectively. This “top-down” approach that is the experimental realization of the reaction of E_4^{4-} with n electrophiles R^+ to yield compounds of the type $E_4R_n^{(4-n)-}$ was not successful yet, presumably due to the strong reducing nature conferred by the multiple negative charges. In 1988, the first “bottom-up” synthesis of a cage compound, $Si_8(Si^tBuMe_2)_8$,[135] was reported by Matsumoto and after this breakthrough this new field developed rapidly.[136] Notably, also the formal (partial) compensation of negative charges in the Zintl ions **111a,b** has been achieved *via* the "bottom-up" method. Wiberg *et al.* succeeded in reducing **112a,b** to the corresponding Si_4- and Ge_4-tetrahedrons **113a,b**.[137,138] The Sekiguchi

group accomplished the reductive cleavage of one silyl substituent from tetrahedrane **113c** to yield tetrasilahedranide **114c** (Scheme 42). [139]

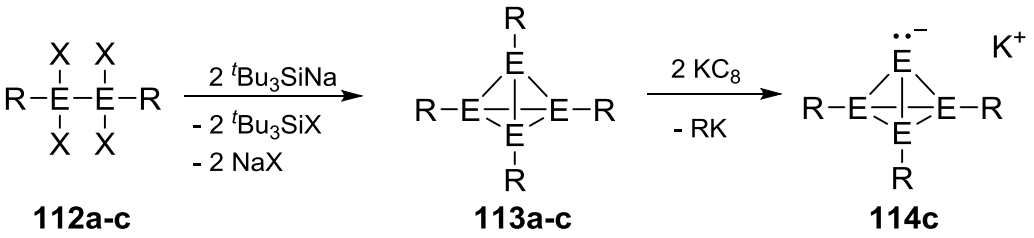

112a-c **113a-c** **114c**

Scheme 42. Synthesis of tetrahedron **113a-c**[137,138] and tertrasilahedranide **114c** (**a**: E = Si, X = Br, R = Si^{t}Bu$_3$; **b**: E = Ge, X =Cl, R = Si^{t}Bu$_3$; **c**: E = Si, X = Br, R = Dis$_2$MeSi, Dis = CH(SiMe$_3$)$_2$).[139]

More recently, a third class of Group 14 clusters, the metalloid cluster compounds, was established.[140] The term metalloid (also described as unsaturated) cluster compounds was introduced by Schnöckel in the context of Group 13 clusters.[141] According to Schnepf, in metalloid clusters of Group 14 "naked" as well as substituted metal atoms are present and they possess the general formulae E_nR_m with n>m leading to an average oxidation state between 0 and 1. These clusters can be seen as intermediates on the way from molecular precursors to the elemental metal.[140] As will be outlined in more detail in Chapter 1.2.2, Scheschkewitz *et al.* proposed a slightly different definition for E = Si.[142] In contrast to the definition by Schnepf, neither the average oxidation state of the cluster skeleton atoms nor the general formulae is considered. The presence of at least one unsubstituted ("naked") silicon vertex (that certainly requires a formal oxidation state of zero) in a neutral cluster with a three dimensional silicon backbone remains the sole criterion. This implies a hemispheroidal coordination environment for the silicon atom in question.

Metalloid cluster compounds of Group 14 elements heavier than silicon can be obtained experimentally from soluble Zintl anions of the type E_m^{x-} (m>x). In the case of E = Ge and Sn the partial compensation of negative charges in Zintl anions to afford anionic metalloid clusters has been reported.[134] Although the reactions suffer from low yields and poor selectivity, possibly because of the involvement of competing radical mechanisms, these findings prove that the anionic vertices in Zintl anions indeed allow for chemical transformations. Alkylation or vinylation of **110c** to the corresponding anionic metalloid tin cluster Sn_9R^{3-} (R = ^{i}Pr, ^{t}Bu, CH=CH$_2$, CH=CHPh) was communicated.[143] Mono- and divinylation of **110b** to afford Ge_9R^{3-}

and $Ge_9R_2^{2-}$ (R = $CH{=}CH_2$), respectively, was achieved.[144] In stark contrast, for soluble Zintl anions[134] of silicon the only rational chemical transformations reported so far result in the complexation of the silicide anions to transition-metal centers without any compensation of negative charges.[145]

The first bottom-up synthesis of a metalloid Group 14 cluster was achieved by Wiberg *et al*. Sn_8R_6 cluster **115** was prepared *via* thermally induced isomerization of the corresponding cyclotristannene.[146] Two years later Power reported the synthesis of Sn_8R_4-type cluster **116** by reducing [{Sn(η-Cl)(2,6-$Mes_2C_6H_3$)}$_2$] with elemental potassium (Scheme 43).[147]

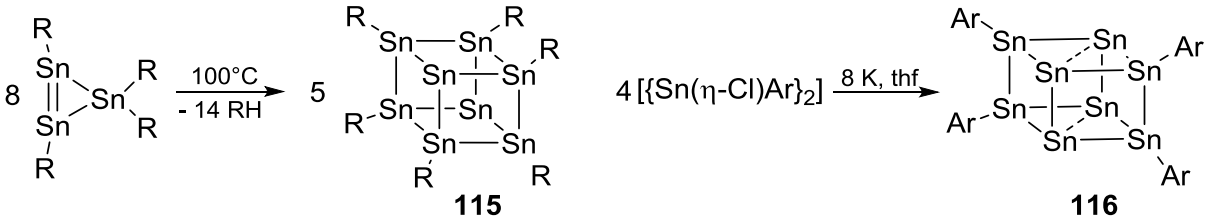

Scheme 43. Synthesis of the first metalloid cluster compounds **115** by Wiberg[146] and **116** by Power[147] (R = Si^{t}Bu$_3$, Ar = 2,6-Mes-H_3C_6, Mes = 2,6-Me-H_3C_6).

After these pioneering contributions several metalloid cluster compounds of germanium and tin have been synthesized and were subject to several comprehensive review articles.[140] The synthesis of metalloid silicon clusters, however, is still much less developed.

1.2.2. Unsaturated Silicon Cluster Compounds (Siliconoids)

Elemental silicon is ubiquitous in semiconducting devices. The understanding and manipulation of silicon surfaces[148] are key aspects to improve silicon-based technologies.[149] Silicon surfaces feature “dangling bonds”, *i. e.* unsubstituted (naked) silicon vertices with free valencies. These dangling bonds are the source of the pronounced chemical activity of silicon surfaces.[150] As the size of particles decreases, the surface-to-volume ratio increases. Consequentially, in silicon nanoparticles a large fraction of all the atoms in the particle are surface atoms and the surface contribution to the properties becomes progressively more significant as size decreases.[151] By definition, surface atoms of spherical particles will feature a

hemispheroidal coordination environment (*i. e.* all *used* valencies point into one half of a sphere). The characterization of nanoparticles, however, is still challenging partly due to the lack of suitable analytical techniques and on the other hand due to the low stability of pristine surfaces with unsaturated valencies.[152]

During the gas-phase processes typically employed for the production of amorphous silicon materials (a-Si), partially hydrogenated silicon clusters with unsaturated vertices have been proposed as transient intermediates.[153] Crucial properties of a-Si (such as its luminescence) depend on the incorporation of similar clusters into the bulk material.[154] On the basis of mass spectrometric studies supplemented by theoretical calculations, the involvement of hemispheroidally coordinated vertices in the structure of these clusters was proposed. At present, however, it is impossible to isolate unsaturated clusters from the bulk material.[155]

Isolable metalloid silicon clusters are therefore ideal model systems to study structural features of bulk and nano surfaces with the analytical techniques of molecular chemistry. The naked vertices (the unsaturated valencies) mimic dangling bonds of the silicon surface and confer the reactivity and properties of the transients in CVD processes to the stable molecular species.

The first metalloid silicon cluster fulfilling the criterions employed by Schnepf (*vide supra*, general formulae Si_nR_m with n>m, “naked” silicon atoms as well as ligand bound ones, average oxidation state between 0 and 1) was reported in 2000 by Kira. Upon reduction of $R_3Si\text{-}SiBr_2Cl$ with potassium graphite in thf spiropentadiene **117** was isolated in 3.5% yield (Scheme 44).[156]

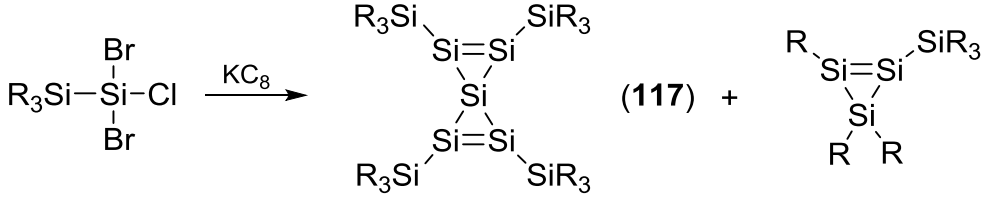

Scheme 44. Kira´s synthesis of the first metalloid silicon cluster **117** (R = ^{t}BuMe$_2$Si).[156]

It should be noted, however, that the bonding in **117** is clearly electron-precise: the *spiro*-silicon atom features a coordination environment of a distorted tetrahedron and lacks the hemispheroidal coordination environment encountered on pristine surfaces of the bulk and in the nano regime.

As a consequence, the description of **117** as a metalloid cluster compound exposes a deficit of the Schnepf definition. Following up on Schnöckel's original definition, Scheschkewitz thus coined the term “siliconoid” for a certain class of unsaturated silicon cluster compounds in order to account for their intermediacy between molecular precursors and elemental silicon. The presence of at least one naked silicon vertex with hemispheroidal coordination in a neutral molecule with a three dimensional silicon backbone is taken as sole criterion to define a siliconoid.[142]

The first siliconoid, a compound featuring a naked silicon vertex, was synthesized in 2005 by the Scheschkewitz group.[157] When disilenide **16** was treated with 0.25 equivalents $SiCl_4$, siliconoid **118** was isolated from the reaction in variable yields (22-37%). As systematically formed byproduct, tetrasilabutadiene **17**, the formal oxidation product of **16**, could be identified by NMR spectroscopy (Scheme 45). Interestingly, this reaction bridges the field between disilenes and siliconoids. Obviously, functionalized disilenes are potent precursors for unsaturated silicon clusters.

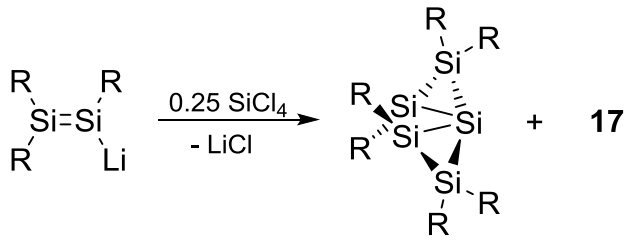

Scheme 45. Synthesis of the first siliconoid **118** reported by Scheschkewitz (R = Tip = 2,4,6-$^{i}Pr_3$-H_2C_6).[157]

A second siliconoid was published in the same year by Wiberg and Veith *et al*.[158] Complete reductive dehalogenation of a (pentaiodo)tetrasilabutane derivative afforded siliconoid **119** featuring two naked silicon vertices (Scheme 46).

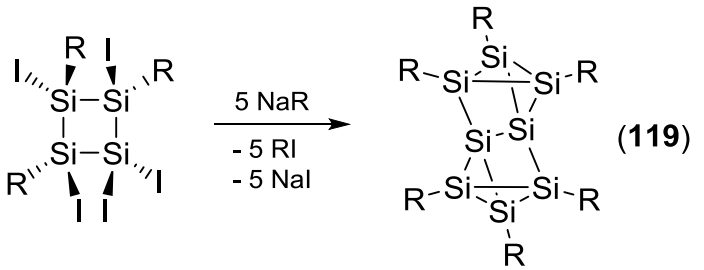

Scheme 46. Synthesis of Si_8R_6 -siliconoid **119** by Wiberg and Veith (R = $Si^{t}Bu_3$).[158]

In 2010, siliconoid **120**, a persilapropellane, was isolated by Breher *et al.* from the reduction of dimesityldichloro silane (mesityl = 2,4,6-Me_3-H_2C_6) and hexachloro disilane in a 3:1 ratio (Scheme 47).[159] The most striking structural feature of **120** is the bond between the two hemispheroidallly coordinated bridgehead silicon atoms that is about 13% longer than a normal Si-Si single bond. In the ^{29}Si NMR spectrum, the naked silicon vertices appear at very high field (δ = − 273.2 ppm) while the $SiMes_2$ bridges resonate in the typical area for tetracoordinate silicon atoms (δ = 25.5 ppm). The long bond between the bridge-head silicon atoms indicates a weak interaction between these particular atoms and the molecule might thus be described as diradical species. The authors calculated the bridgehead bond-strength to ~174 kJ mol^{-1}. This interaction is considerably weaker than the single bond of normal silanes (306-332 kJ mol^{-1}).[159] Investigations concerning the reactivity of **120** revealed that it shows both closed-shell and radical type of reactivity.

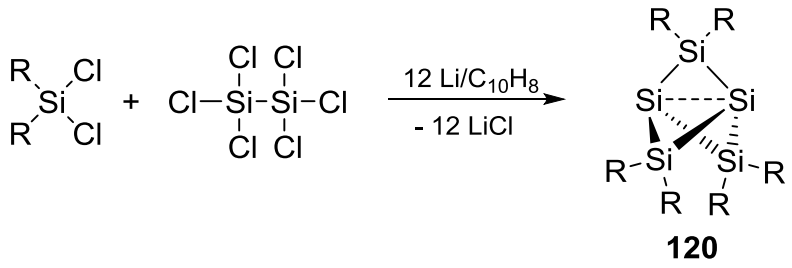

Scheme 47. Breher´s synthesis of propellane-like siliconoid **120** (R = Mes = 2,4,6-Me_3-H_2C_6).[159]

While compounds such as H_2O, PhSH, PhOH and Me_3SnH can be readily added over the bridgehead bond, treatment of **120** with 9,10-dihydroanthracene which is a typical reagent for radical-type reactivity indeed afforded the dihydrogen adduct.[159]

In 2010, Scheschkewitz *et al.* succeeded in synthesizing the first aromatic hexasilabenzene isomer. Addition of an excess silicon tetrachloride to disilenide **16** does not afford siliconoid **117** but rather 1,1,2-trichlorocyclotrisilane **121** in analogy to cyclization reactions described in Chapter 1.1.4.2. Complete reductive dehalogenation of **121** with three equivalents lithium/naphthalene induces dimerization to afford siliconoid **122** comprising silicon atoms with two, one and no directly attached Tip-substituents (Scheme 48).[160] The structure of **122** features a rhomboid Si_4-ring in the center and two $SiTip_2$ bridges that point up- and downwards to the Si_4-plane.

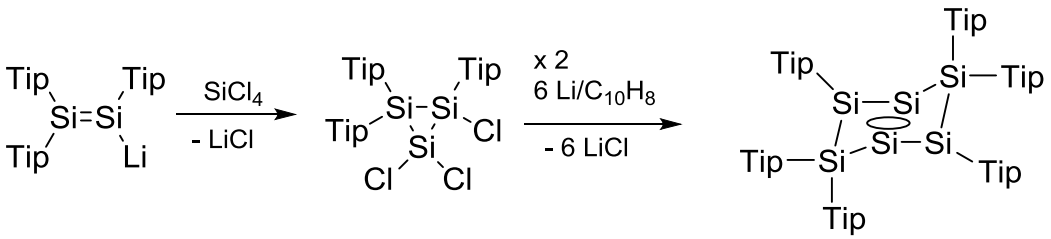

16 **121** **122**

Scheme 48. Synthesis of 1,1,2-trichloro cyclotrisilane **121** and hexasilabenzene isomer **122**.[160]

The intense green color as well as the wide distribution of ^{29}Si NMR chemical shifts (SiTip: δ = 124.6, $SiTip_2$: δ = −84.8, Si: δ = −89.3 ppm) observed for **122** speak against an electron precise, saturated system. Its electronic structure is best described by cyclic delocalization of two π, two σ, and two nonbonding orbitals over the Si_4-skeleton formally interrupted by the two $SiTip_2$-bridges (**122A,B**; Scheme 49). Nucleus-independent chemical shift (NICS) calculations indicate a significant degree of aromaticity in **122**, which was further supported by a subsequent work involving experimental charge density investigations.[161]

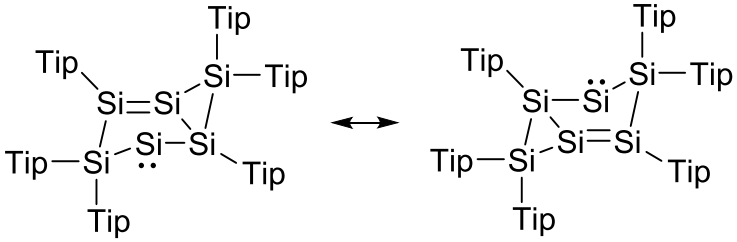

122A **122B**

Scheme 49. Resonance formulae **122A,B** for dismutational hexasilabenzene isomer.[160]

The general formalism leading to this type of aromaticity is a twofold 1,2-shift in the classical Hückel-aromatic compound. As opposed to the uniform oxidation state of +1 in hexasilabenzenes, the formal oxidation states in **122** are +2 ($SiTip_2$), +1 (SiTip) and 0 (Si). Scheschkewitz and Rzepa suggested the term “dismutational aromaticity” for this novel type of aromaticity.[160,161]

An alternative synthetic route to dismutational isomer **122** was provided by a collaborative work of the groups of Scheschkewitz and Jutzi. The Cp^*Si^+ cation **123**[162] acts as a stoichiometric source of silicon in the reaction with disilenide **16** affording cyclotrisilene **124**.[163] The Cp* ligand in **124** can be cleaved in a one

electron reduction and the presumably occurring transient cyclotrisilenyl radical dimerizes to yield siliconoid **122** (Scheme 50).[164]

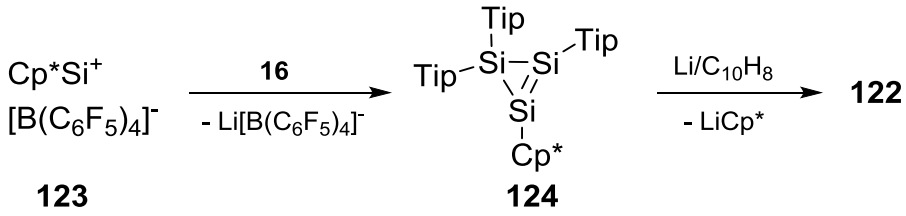

Scheme 50. Synthesis of dismutational isomer **122** from the reaction of disilenide **16** with Cp^*Si^+ cation **123**.[163,164]

In 2011 Scheschkewitz *et al*. reported that dismutational hexasilabenzene isomer **122** can be isomerized either thermally or photolytically to the bridged propellane structure **125**, the first stable derivative of the assumed global minimum on the Si_6H_6 potential energy surface (Scheme 51).[165]

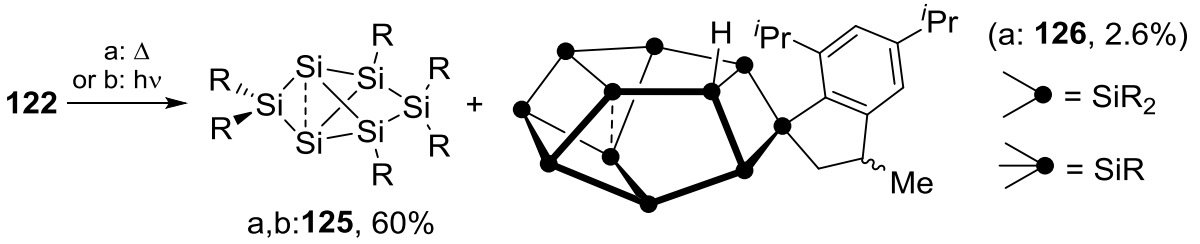

Scheme 51. Synthesis of bridged hexasilapropellane **125** by thermally or photolytically induced rearrangement of **122**; byproduct Si_{11}-siliconoid **126** isolated from the thermal rearrangement of **122** (R = Tip).[165,142]

In comparison to Breher´s propellane **120**, in **125** two "propeller blades" are bridged by an additional Tip_2Si unit. The bond distance between the two naked silicon atoms in **125** (2.7076(8) Å) is even longer than what was reported for **120** (2.636 Å). As observed for **120** the two naked silicon atoms show pronounced shielding in the ^{29}Si NMR spectrum (δ = −274.2 ppm). The neighboring $SiTip_2$ unit in **125**, however, is observed at very atypically low-field for a tetracoordinate silicon atom (δ = 174.6 ppm). This until then unprecedented wide distribution of chemical shifts is regarded as a manifestitation of an extreme electronic anisotropy in **125** and was explained by magnetically induced current density vectors obtained from DFT calculations. The "naked" silicon vertices of **125** are included into a diatropic current loop, which induces a magnetic shielding effect by back-induction. The flanking $SiTip_2$-unit,

however, is not included in this loop but surrounded by a paratropic current vortex, leading to the strong deshielding of this particular silicon atom.[165]

As a byproduct from the thermal isomerization of **122** to **125**, core-expanded siliconoid **126** was isolated.[142] While cluster expansion is a pivotal process during the gas-phase deposition of silicon based materials, this was the first observation of such a process in the condensed phase.

Initial studies concerning the reactivity of both isomers **122** and **125** have been carried out by the Scheschkewitz group. Treatment of **125** with elemental bromine or iodine, respectively, yielded the corresponding 1,5-dihalogenated species **127a,b** demonstrating high reactivity of the bridgehead silicon atoms.[165] In contrast, the reaction of **122** with an excess of iodine resulted in a cluster contraction to afford the first 1,2,3,4-tetraaryl-substituted cyclopentasilane **128** (Scheme 52).[142]

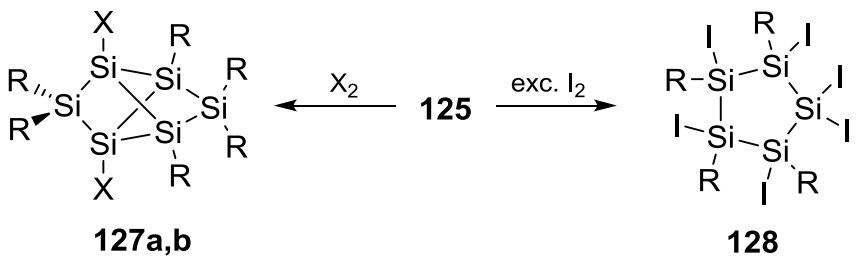

Scheme 52. Halogenation of bridged propellane **125** (R = Tip; **127a**: X = Br, **127b**: X = I).[142,165]

The isolation of three different chlorinated species from the reaction of dismutational isomer **122** with $BiCl_3$ was reported by the Scheschkewitz group. 1,2-Dichloro isomer **129a** resembling more the global minimum structure than the dismutational isomer is formed as main product. As by-products, the twofold chlorinated species **129b** as well as the chlorination product across the bridgehead silicon atoms **126c** were isolated (Scheme 53).[142]

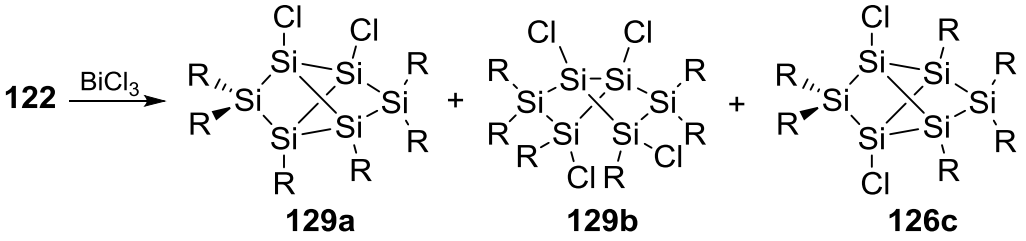

Scheme 53. Isolated products from the reaction of dismutational isomer **122** with $BiCl_3$ reported by Scheschkewitz (R = Tip).[142]

Very recently, the Scheschkewitz group succeeded in the formal replacement of silicon atoms in **122** and **125** by germanium and tin *via* the reduction of suitable low-valent precursors. Reaction of disilenide **18** with $GeCl_2$·dioxane or $SnCl_2$·dioxane, respectively, afforded the unobserved but plausible disilenyl chloro tetrylenes **130a,b** as intermediates. Reduction with one equivalent of lithium/naphthalene for the germanium species yielded the dismutational digermatetrasila benzene isomer **131a**. Upon heating at 65°C in thf for 12 h the compound isomerizes to bridged propellane **132a** featuring germanium atoms on the bridgehead positions. In contrast, in the tin case the dismutational isomer **131b** is not observed, but rather direct isomerization to the assumed global minimum structure **132b** (Scheme 54).[166]

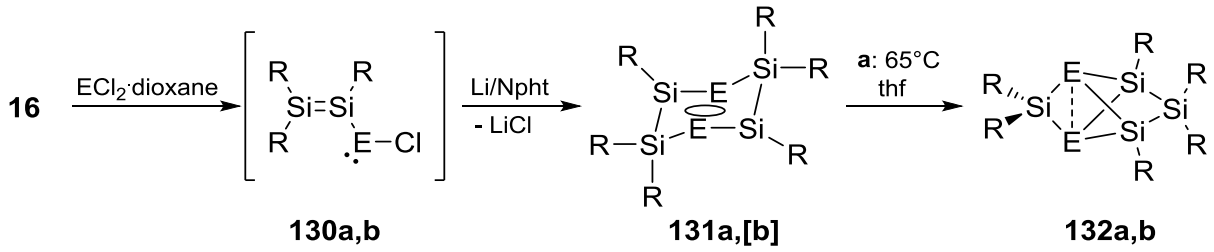

Scheme 54. Synthesis of unsaturated silicon clusters labeled with heavier Group 14 elements (R = Tip; **a**: E = Ge, **b**: E = Sn).[166]

Regarding the pivotal role unsaturated silicon cluster compounds play in the production and for the properties of silicon based materials, the incorporation of hetero atoms from other groups of the periodic table is of particular interest, especially dopants such as boron or phosphorus. Structure and properties of small silicon clusters doped with phosphorus have been studied theoretically and were predicted to lead to dramatic alterations in in the optoelectronic properties.[167]

In analogy to the reports for **131a,b** and **132a,b**, appropriately functionalized low-valent silicon-boron or silicon-phosphorus compounds might turn out to be suitable precursors, but have yet to be synthesized. Alternatively, the functionalization of intact siliconoids, *e. g.* with hetero atoms, can be seen as a first step in expanding the cluster core. Evidently, functionalized vertices are also a prerequisite for the embedding of siliconoids into extended supramolecular assemblies. Promising properties of siliconoids, such as the pronounced electronic anisotropy, would be an attractive feature for the construction of structures at the nanoscale. Only unfunctionalized siliconoids have been reported so far, however, severely limiting further developments in both regards.

„Das Wesentliche an jeder Erfindung tut der Zufall,
aber den meisten begegnet er nicht.
Was er Zufall nennt, ist in Warheit der Einfall,
und der begegnet jedem, der für ihn wach und bereit ist!“

- Friedrich Nietzsche (1844 – 1900)
In Morgenröthe, 1881.

2. Aims and Scope

The central objective of this project was the targeted synthesis of novel functionalized unsaturated silicon compounds. Subsequently, it was going to be investigated whether the introduced functionalization indeed can be utilized for further manipulations in the presence of the unsaturated scaffold.

For organic systems, the simultaneous presence of unsaturated moieties and electrophilic and nucleophilic centers is the key to the variety of transformations known. In disilene chemistry, both nucleophilic (type **I**) and electrophilic (type **II**) disilenes have been reported and turned out to be valuable synthons.[34] For Si=P bonds only derivatives of the type **III** with a formally increased nucleophilictiy on phosphorus are known (Scheme 55).[115-117]

Lithium disilenide **16**, the disila analogue of a vinyl anion, is a useful reagent to transfer the Si=Si bond to various electrophiles.[48,66] As outlined in Chapter 1.1.5.3, we demonstrated that the reaction of **16** with $ClP(NMe_2)_2$ affords the first *P*-amino substituted phosphasilenes *E/Z*-**108a,b** (Scheme 40). Proof for a certain degree of mobility of the amino substituent on phosphorus was provided by the reaction with *tert.*-butylisonitrile.[130] One major target of this work was therefore to investigate the suitability of **108a** as electrophile of type **IV**. In this regard, the leaving group character of the amino functionality at phosphorus was going to be investigated by the reactions of **108a** with several nucleophiles. Phosphasilenes that react with anionic nucleophiles under substitution are to date unknown, but should in principle allow for the synthesis of novel silicon-phosphorus motifs (Scheme 55).

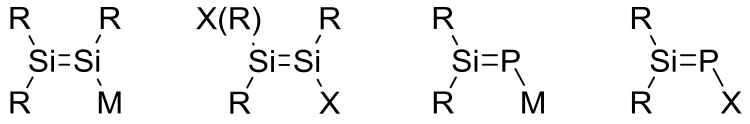

I **II** **III** **IV**

Scheme 55. Nucleophilic and electrophilic disilenes **I** and **II**,[31] nucleophilic phosphasilenes **III**[115-117] and potentially electrophilic phosphasilenes **IV** (M = metal, X = anionic leaving group, R = alkyl, aryl or silyl).

As described in the introduction, disilenide **16** provides access to siliconoids, unsaturated silicon cluster compounds. Complete reductive dehalogenation of 1,1,2-trichlorocyclotrisilane **121** obtained from the reaction of **16** with $SiCl_4$ affords

siliconoid **122** (Scheme 48).[160] Suitable reduction precursors to unsaturated silicon clusters labeled with germanium or tin (**131a,[b]** and **132a,b**) are accessible *via* treatment of **16** with the corresponding element(II)chlorides as dioxane adducts (Scheme 54).[166] Considering the possibility of a reductive cleavage of the amino groups in **108a**, investigations into the the reactivity of phosphasilene **108a** towards reducing agents will be described in the present work.

Furthermore, the reactivity of disilenide **16** towards various phosphorus or boron containing electrophiles X_nER_{3-n} (X = halogen or hydrogen; E = P or B; R = hydrogen, alkyl, aryl or amino; n = 1-3) was studied. A prime focus was the rentention of functionality on the thus obtained (unsaturated) silicon-phosphorus or silicon-boron containing species (Scheme 56).

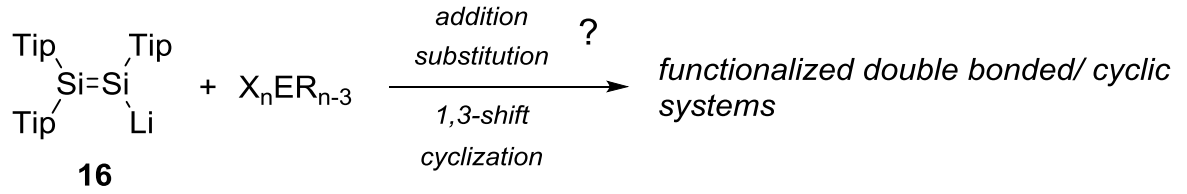

Scheme 56. Proposed reactivity of disilenide **16** towards phosphorus or boron containing electrophiles, respectively (X = halogen or hydrogen; E = P or B; R = hydrogen, alkyl, aryl or amino; n = 1-3).

In the reaction with **16**, Cp^*Si^+ **123** acts as stoichiometric source of silicon to afford cycotrisilene **124**.[163] Analogous phosphorus species are unknown but would be desirable precursors *e. g.* for unsaturated silicon clusters doped with phosphorus. Consequently, the reactivity of **16** towards formal P(I) cations was going to be explored during this project.

In preliminary studies in the Scheschkewitz group, the formation of anionic siliconoid **133** was observed upon reduction of **122** with an excess of lithium/naphthalene.[168] Apparently, in addition to the chlorine functionalities a Tip-substituent is cleaved to yield the bridged propellanide **133**, the first example of an anionic siliconoid.[169] Cluster **133** closes the conceptual gap between silicon based Zintl-anions and siliconoids and represents the first functionalized siliconoid. With its anionic (and thus nucleophilic) silicon vertex, **133** should be a valuable synthon for the further functionalization of the cluster-scaffold. As proof-of concept for this reactivity, a trichlorosilyl substituted siliconoid was isolated from the reaction of **133** with silicon tetrachloride.[168] Another central objective of this project was the in-depth

investigation of the reduction chemistry of siliconoids **122** and **125** in order to reproduce the synthesis of **133** and explore the possibility to obtain different anionic siliconoids. In a next step, the universality of the concept of the nucleophilic transfer of anionic siliconoids should be tested during this project by reactions with various electrophiles (Scheme 57).

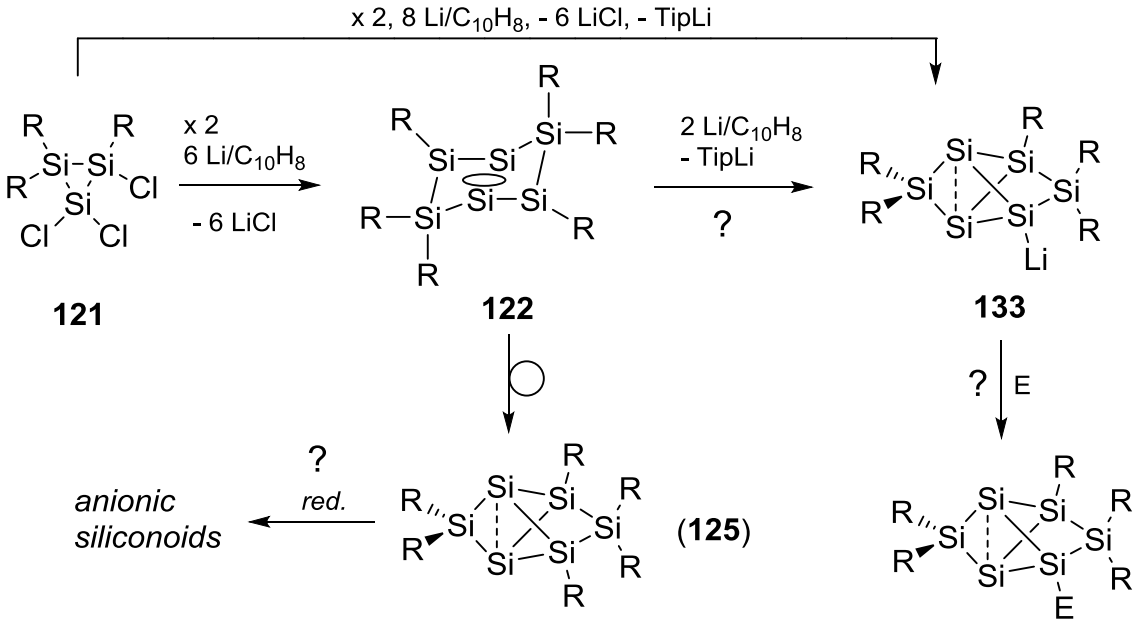

Scheme 57. Proposed synthesis and reactivity of anionic siliconoids (R = Tip).

As mentioned before, the efficient transfer of intact unsaturated clusters is a prerequisite for the preparation of larger units. Furthermore, the linking of heteroatoms to the cluster skeleton can be seen as a first step in expanding the cluster. Consequently, functionalization with dopant atoms such as phosphorus or boron is of special interest.

Disilenes and digermenes have been applied as mimics for silicon and germanium surfaces.[170] The grafting of low-valent main group compounds to surfaces, however, is to the best of our knowledge unknown, even though interesting electronic properties of these compounds make it a potentially rewarding challenge. The final objective of the present work was therefore to functionalize disilenes with anchoring groups that would in principle allow for the linking of the Si=Si unit to gold surfaces. Linking of saturated silicon-based precursors on gold surfaces *via* thio-functionalized substrates has been reported.[171] By reaction of disilenide **16** with different halogenated methylsulfides Br-(LU)-SMe and disulfides Br-(LU)-S-S-(LU)-Br (LU = aromatic or aliphatic linking unit) it was to be probed whether the residual

sulfide/disulfide functionality is tolerated by the highly reactive Si=Si moiety (Scheme 58).

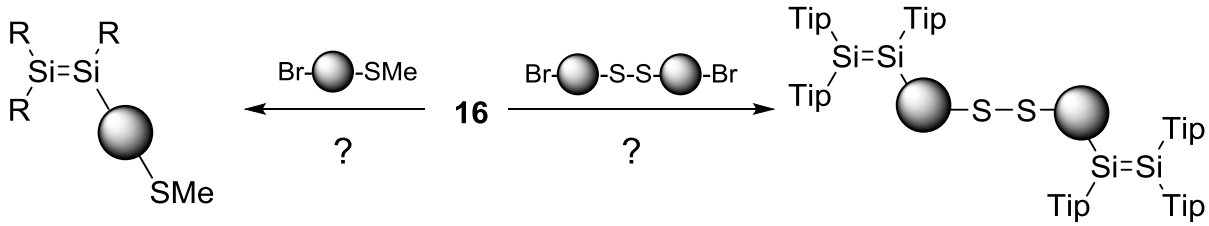

Scheme 58. Proposed reactivity of disilenide **16** towards bromo sulfides and disulfides
● =aromatic or aliphatic linking unit.

3. Results and Discussion

3.1. *P*-Amino Substituted Phosphasilenes

3.1.1. Determination of Activation Parameters for *Cis*/*Trans* Isomerization of *E/Z*-108b

The treatment of disilenide **16** with $ClP(NR_2)_2$ (R = Me, Et) results in the formation of *P*-amino substituted phosphasilenes **108a,b** presumably upon 1,3-migration of one amino substituent of intermediate phosphino disilenes (Scheme 59).[130]

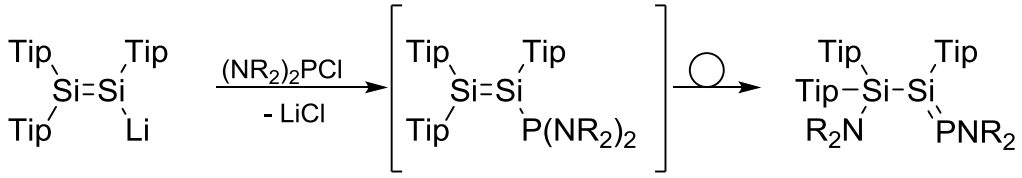

16 *E/Z*-**108a,b**

Scheme 59. Synthesis of *P*-amino substituted phosphasilenes *E*/*Z*-**108a,b** (Tip = 2,4,6-$^{i}Pr_3C_6H_2$, **a**: R = Me, **b**: R = Et).[130]

Both *P*-amino substituted phosphasilenes **108a,b** exist as *E/Z*-mixture in solution. The determination of the isomerization barrier is of current interest since it is strongly related to the strength of the P-Si π bond. Even though the Driess group already reported *E/Z*-isomerism for an unsymmetrically substituted phosphasilene, the barrier was too high to detect coalescence within an observable window (<120°C).[172]
In case of **108a,b**, for both compounds the exchange is sufficiently fast. We decided to determine the activation parameters of the *E/Z*-isomerization to provide an estimate of the P-Si π bond energy on the basis of experimental data for the first time. Owing to the more favorable ratio of *E/Z*-isomers (**108a**: 95:5, **108b**: 70:30) our study was restricted to **108b**. The activation parameters for the isomerization of *E*/*Z*-**108b** (
Scheme 60) were determined by two methods, *via* a pulse-selective ^{31}P 1D-NOESY NMR experiment and with the coalescence temperature. [173]

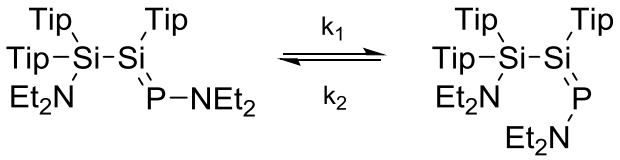

***E*-108b** ***Z*-108b**

Scheme 60. *E*/*Z*-Equilibrium of **108b.**

During the pulse selective NMR experiment, the phosphorus nucleus in the *E*-isomer *E*-**108b** was excited with a selective pulse, essentially 'labelling' the *E*-**108b** component of the equilibrium mixture of two isomers. By inserting a delay, the mixing time *d8*, between excitation and signal acquisition, the rate of isomerization of *E*-**108b** to *Z*-**108b** can be determined. The population of labeled spins present in *Z*-**108b** increases with longer mixing times d8, until the equilibrium population is reached (Figure 6).

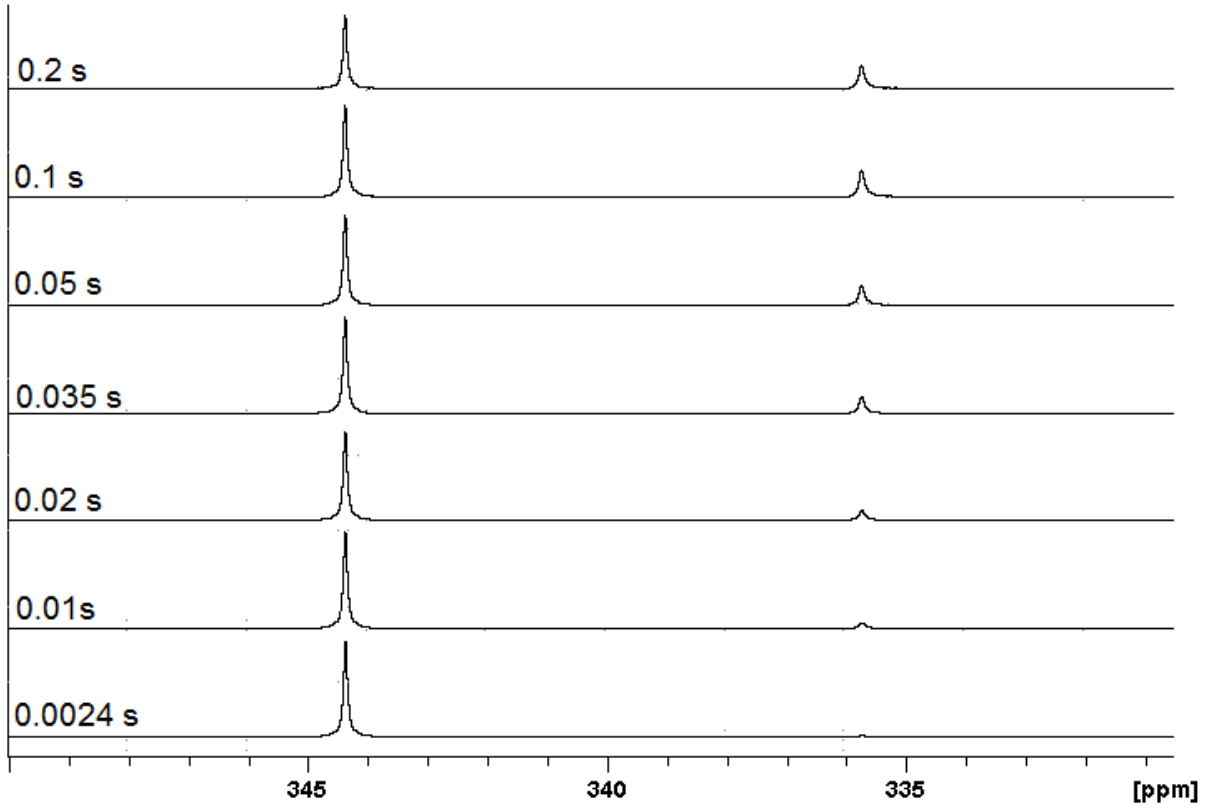

Figure 6. $^{31}P\{^{1}H\}$-NMR spectra of **108b** after selective excitation of *E*-**108b** at seven different mixing times (0.0024-0.2 s) at 280 K.

Using the mixing time d8 and the corresponding populations to model the exchange allows determination of k_2 and k_1 (Figure 7).[174]

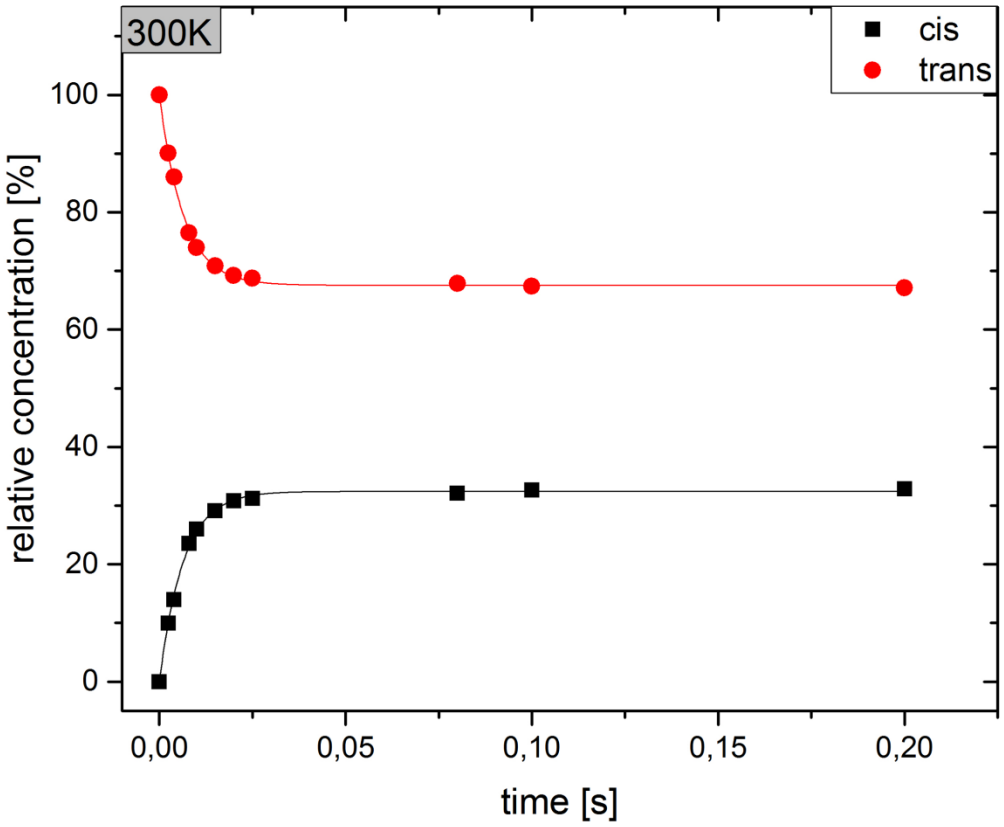

Figure 7. Example for a plot of population of *E*/*Z*-**108b** against mixing time d8 (300 K).[174]

The experiment is repeated for four additional temperatures (290 – 260 K); lower temperatures lead to slower exchange requiring longer mixing times d8 to reach the equilibrium population. Tables with the values for d8 and the corresponding mixing times for all temperatures investigated (300 – 260 K, Table 4-Table 8) as well the plots for the remaining temperatures (290 – 260 K, Figure 101-Figure 104) are shown in the appendix (Chapter 7.1.1)

With the thus obtained values for k_1 and k_2, $\Delta H^{\#}$ and $\Delta S^{\#}$ of each isomer were determined *via* Eyring Plot (see Chapter 7.1.1, Table 9-Table 11, Figure 105, Figure 106). Applying the Gibb´s equation, $\Delta G^{\#} = \Delta H^{\#} - T^* \Delta S^{\#}$ can be calculated ($\Delta G^{\#} = \Delta H^{\#} - T^* \Delta S^{\#}$) for both isomerization steps (300 K):

E-**108b**: $\Delta G^{\#} = 59.535 \pm 0.844$ kJ/mol,

Z-**108b**: $\Delta G^{\#} = 55.488 \pm 2.08$ kJ/mol

The difference in $\Delta G^{\#}$ represents $\Delta\Delta G^0$ between the two isomers:

$\Delta\Delta G^0_{(E/Z)} = 4.050 \pm 1.12$ kJ/mol.

b) Coalescence Temperature

To confirm the range of the values determined by the pulse selective ^{31}P NMR 1D-NOESY experiment, we applied a second approach. The determination of the coalescence temperature of the *E*/*Z* exchange allows calculation of a weighted average for $\Delta G^{\#}$ of both isomers *via* the Eyring equation (Figure 8).

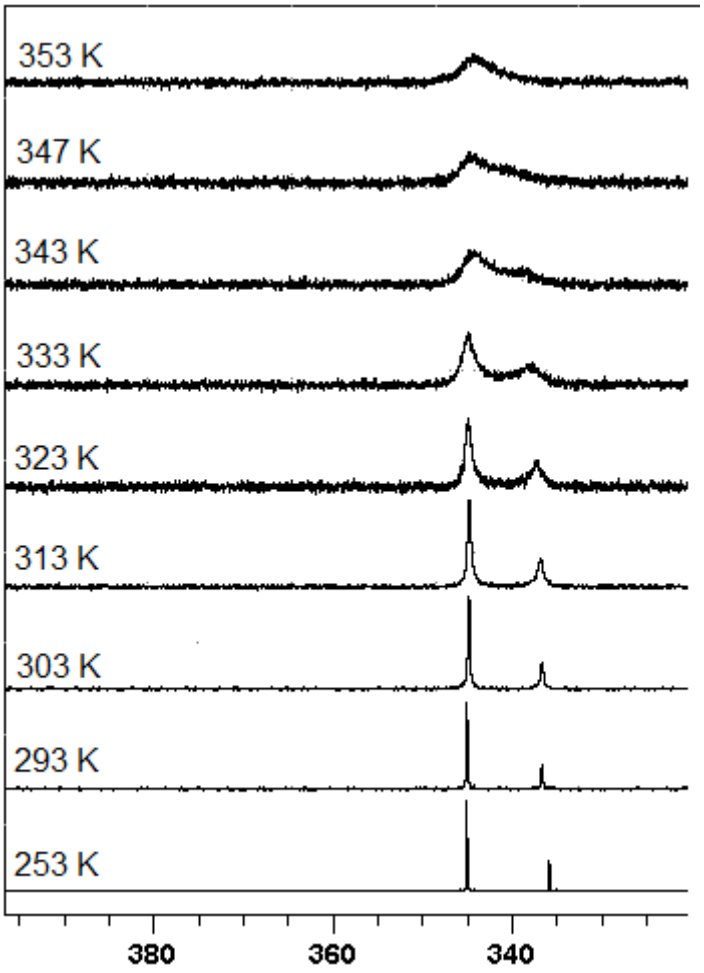

Figure 8. ^{31}P{^{1}H}-NMR spectra of **108b** at different temperatures (253 K – 353 K).

Eyring –equation: $\Delta G^{\neq} = \frac{\mathrm{R}\cdot T_c\cdot\sqrt{2}}{\pi\cdot N_A\cdot h\cdot|\nu_a-\nu_b|}$

$T_c \cong$ 347 K – 353 K

The ^{31}P NMR chemical shifts of both isomers are temperature dependent. Even in the temperature range where both resonances are sharp, the chemical shifts drift with temperature. This drift was determined and extrapolated in order to obtain values for $|\nu_a - \nu_b|$ at the coalescence temperature.

$|\nu_a - \nu_b|$ at 253 K: 1118.98 Hz

$|\nu_{a-\nu_b}|$ at 263 K: 1092.93 Hz
$|\nu_{a-\nu_b}|$ at 273 K: 1066.20 Hz
$|\nu_{a-\nu_b}|$ at 283 K: 1040.77 Hz
Extrapolation for 347 K: 871.77 Hz
353 K: 858.77 Hz
Error in T: ±0.5 K

⇨ $\Delta G^{\neq}_{(347\ K)}$ = 63.594 ± 0.096 kJ/mol
$\Delta G^{\neq}_{(353\ K)}$ = 64.771 kJ ± 0.095 kJ/mol

The values obtained from the coalescence temperature confirm those determined *via* the pulse selective NMR study. The values are close to what was recently calculated for the Si=P π bond energy of ylidic phosphasilene **96** (*cf.* Chapter 1.1.5.3) by Driess and Inoue (47.3 kJ/mol).[125] Notably, for **96** a certain contribution of zwitterionic structure **96´** to the bonding situation was proposed by the authors (Scheme 61).

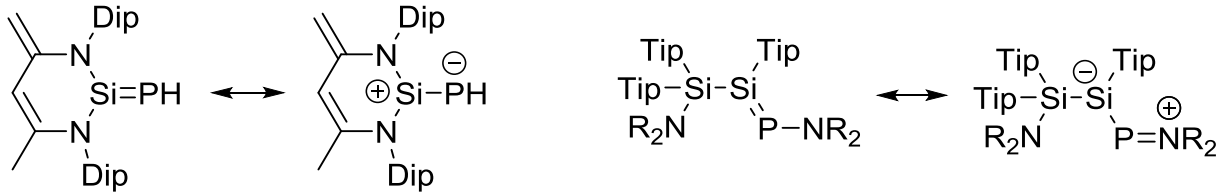

96 **96´** *E/Z*-**108a,b** *E/Z*-**108a,b´**

Scheme 61. Polarized phosphasilene **96**[125] reported by Driess and inverse polarized phosphasilenes **108a,b**[130] and the corresponding resonance formulae **96´** and **108a,b´** with single bonds between silicon and phosphorus (Dip = 2,6-$^{i}Pr_2C_6H_3$, Tip = 2,4,6-$^{i}Pr_3C_6H_2$, **108a**: R = Me, **108b**: R = Et).

Consequently, the π-bond is less predominant in this compound. The WBI (1.68) of **96** indeed revealed relatively low double bond character between silicon and phosphorus.[125] As outlined previously (*cf.* Chapter 1.1.5.3) for **108b** inverse polarization was confirmed experimentally and by computations. This is attributed to the nitrogen donor-substituent at phosphorus. Consequently, resonance formulae **108a,b´** without double bond between silicon and phosphorus can be drawn for the molecule. In the NMR spectra, the contribution of these resonance structures manifests in an unusually strong deshielding of the phosphorus nuclei in *E/Z*-**108a,b** (344.8/336.2 and 344.8/336.7 ppm). Furthermore, it is highlighted by the relatively long Si-P bond (2.1187(7) Å) and the slightly pyramidalized tricoordinated silicon atom (358.858°). A red-shift observed for the longest wavelength absorption in the UV/vis spectra of **108a,b** (λ_{max} = 410 and 421 nm) is in accord with the delocalization

of the nitrogen lone-pair into P=Si antibonding orbitals.[130] We reason that the considerable weakening of the double bond lowers the rotation energy and thus allowed for its determination. Roughly one year after the report of our pioneering studies concerning experimental investigations of *E/Z*-isomerization of a phosphasilene the Inoue group was equally able to determine the rotation energy around the formal Si=P bond in **83** (59.4 kJ/mol).[121] However, in their case derivatization to tungsten complex **84** was necessary to sufficiently weaken the Si=P bond (Scheme 33).

3.1.2. Reactivity Studies of *P*-Amino Substituted Phosphasilene 108a

3.1.2.1. Reactivity of 108a towards Aryl Substituted Isonitriles

Upon addition of *tert.*-butylisonitrile to phosphasilene **108a**, the amino group on phosphorus is shifted to the neighboring silicon atom affording 1-aza-3-phosphaallene **109a** in good yields without any detectable side- or by-products (Scheme 62).[130] Usually this type of phosphacumulene is difficult to prepare and had previously been synthesized *via* Peterson type reactions of bulky silyl anions with carbodiimides.[175]

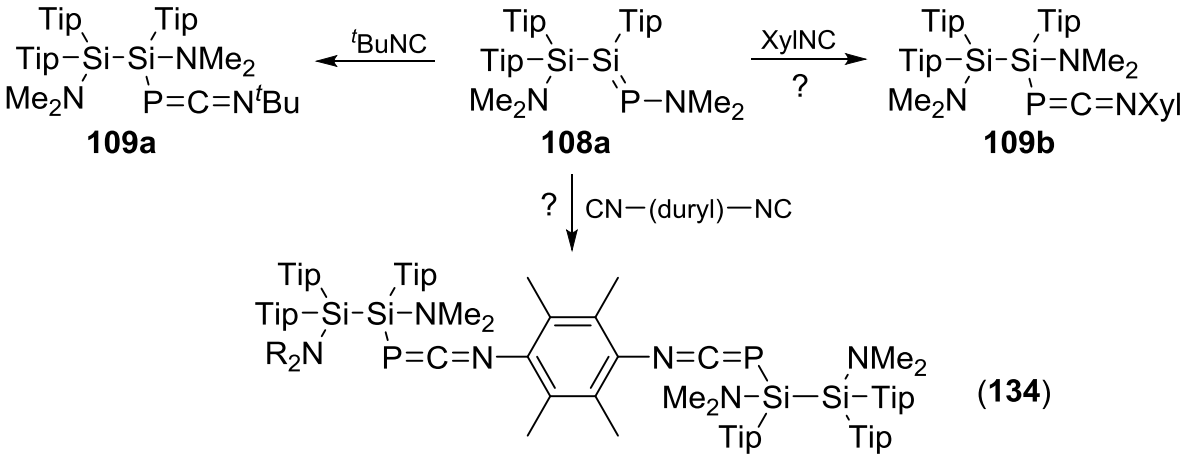

Scheme 62. Synthesis of ^{t}Bu-substituted 1-aza-3-phosphaallene **109a**,[130] presumed reactivity of phosphasilene **108a** towards xylyl-isonitrile and duryl bridged bisisonitrile (xyl = xylyl = 2,6-Me-C_6H_3, duryl = 2,3,5,6-methylphenyl).

With the straightforward synthesis of **109a** in hands, we considered the synthesis of an unprecedented system **110** with two π-conjugated P=C=N-moieties by the reaction of **108a** with *para*-phenylene-bridged bis(isonitriles) (Scheme 62).

Before employing a phenylene bridged bis(isonitrile), however, the reactivity of **108a** towards 2,6-xylyl isonitrile was probed. One equivalent 2,6-xylyl isonitrile was thus added at room temperature to **108a** (Scheme 62) upon which the yellow solution turned orange rapidly.

Monitoring the reaction by ^{31}P NMR spectroscopy revealed slow conversion at room temperature directly after addition of xylyl-isonitrile to **108a** while the reaction of **108a** with *tert.*-butylisonitrile required elevated temperatures (55°C). Two new resonances appear in the ^{31}P NMR spectrum at δ = 141.6 ($^{1}J_{Si-P}$ = 27 Hz) and 136.8 ($^{1}J_{Si-P}$ = 42 Hz) ppm. The intensity of both signals (ratio ~ 1:2) increases uniformly with time hinting towards the formation of stereo isomers (Figure 9). The ^{31}P NMR chemical shifts at downfield are very different form the highfield shifts of the *tert.*-butyl-substituted 1-aza-3-phosphaallene **109a**: (δ = −194.4 and −214.5 ppm). In the ^{29}Si NMR spectrum two sets of signals are observed in the ratio 1:2 at δ = − 7.0, −80.6 (d, $^{1}J_{Si-P}$ = 27 Hz) and δ = −10.6, −81.4 ($^{1}J_{Si-P}$ = 42 Hz) ppm, which provides further evidence against the formation of phosphacumulene **109b** (**109a**: δ = 4.7 ($^{1}J_{Si-P}$ = 100.4 Hz) −2.3 ($^{1}J_{Si-P}$ = 91.3 Hz), −6.8 ($^{2}J_{Si-P}$ = 45.28 Hz), −8.5 ($^{2}J_{Si-P}$ = 33.5 Hz) ppm, Table 1).[130] The Driess group investigated the reactivity of phosphasilene **59b** towards isionitriles and they proposed the initial [2+1] addition of the isonitriles over the Si=P bond to afford **[135a,b]**.[176] According to the authors, **[135a,b]** isomerize to phosphaalkenes **[136a,b]** that readily react with a second equivalent isonitrile so that **137a,b** could be isolated as final products (Scheme 63).

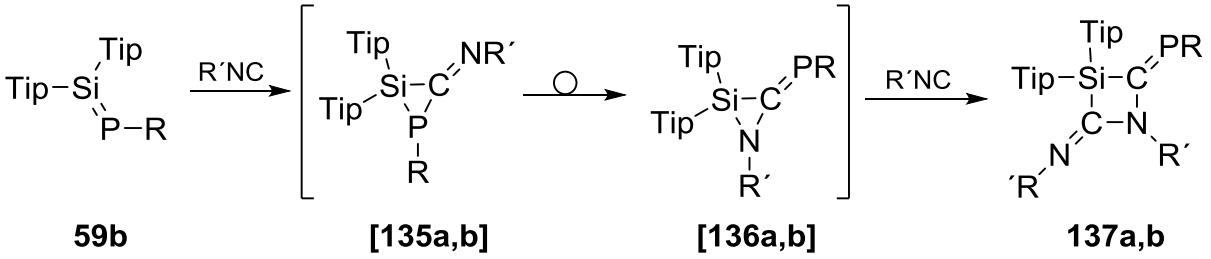

59b **[135a,b]** **[136a,b]** **137a,b**

Scheme 63. Synthesis of phospaalkenes **137a,b** with proposed intermediacy of **[135a,b]** and **[136a,b]** reported by Driess (R = $^{i}Pr_3Si$, **a**: R´ = cyclohexyl, **b**: R = mesityl = 2,4,6-$Me_3C_6H_2$).[176]

We propose that upon treatment of **108a** with xylyl isonitrile a [2+1] cycloadduct **[138]** is formed initially. The NMR data of the initially detected product (*vide supra*) are consistent with the rearrangement to **139** (Scheme 64) as a mixture of *E*/*Z*-isomers in analogy to the report by Driess. The shielded ^{29}Si NMR doublets due to ^{31}P coupling as well as the characteristically small coupling constants are diagnostic for three-membered Si-P-rings.[177,178,] On the other hand, the deshielding of the ^{31}P nuclei is consistent with the presence of a C=P double bond.[176,179] The ^{29}Si singulets at δ = −7.0 and −10.6 ppm are in accord with the exocyclic amino silyl moieties in *E/Z*-**139**.

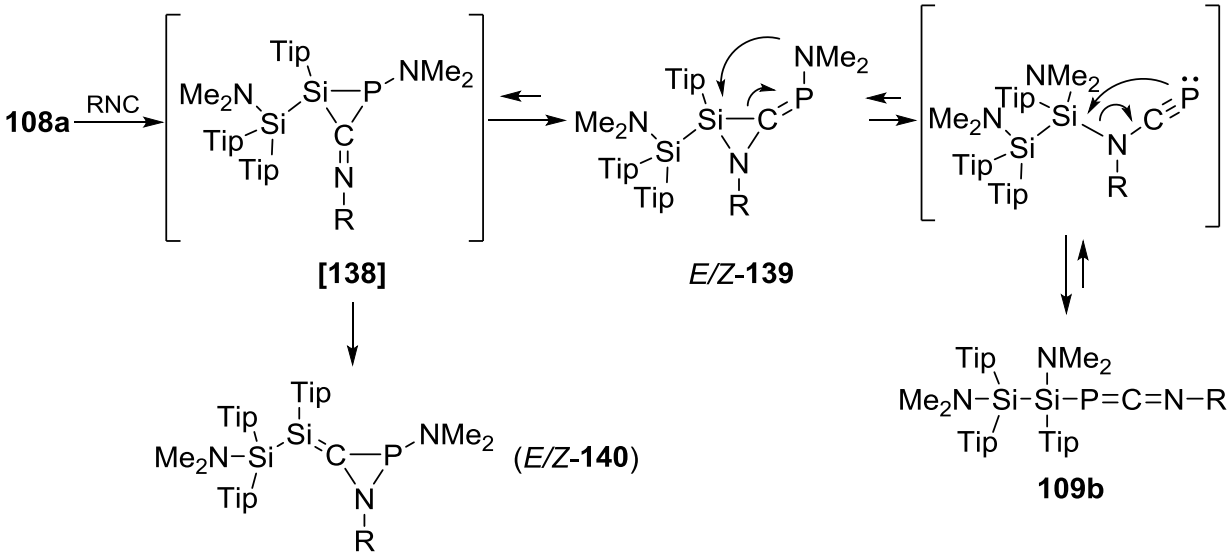

Scheme 64. Proposed products from the reaction of phosphasilene **108a** with xylyl isonitril (R = xylyl = 2,6-dimethylphenyl).

The initial product **139** evolves to a secondary product even before full conversion of **108a**. After two hours (ratio **108a** : **139** = 70:30) the red color of the solution intensified and a third set of signals starts to grow in at the expense of those of **139**. The NMR spectroscopic data suggest the formation of phosphacummulene **109b**, the compound analogous to **109a**. As to be expected, the ^{31}P NMR spectrum once more indicates the presence of two stereoisomers, observed at δ = −212.0 and −226.5 ppm (ratio 6:94). In case of **109a**, two stereoisomers were observed in comparable ratio (5:95). In the ^{29}Si NMR spectrum, only the major isomer could be detected due to the lower natural abundance of ^{29}Si with doublets at δ = −2.0 ($^{1}J_{Si-P}$ = 89.5 Hz) and −8.2 ($^{2}J_{Si-P}$ = 34.5 Hz) ppm (Table 1). The chemical shifts in the ^{31}P as well as in the ^{29}Si NMR spectrum and the magnitude of the coupling constants are very similar to those observed for **109a** (Table 1).

NMR	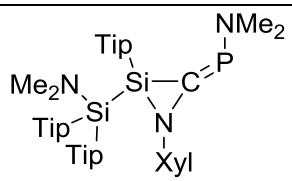 *E/Z*-**139**	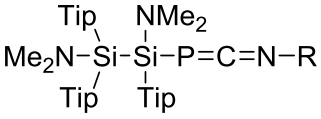 **109a,b**	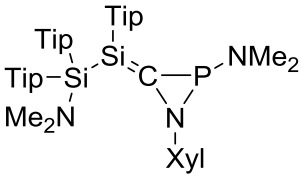 *E/Z*-**140**
δ^{29}Si [ppm]	−7.0, −80.6 −10.6, −81.4	**a**: 4.7, −6.8 −2.3, −8.5 **b**: −2.2, −8.2	39.6, −2.9 11.1, −4.7
δ^{31}P [ppm]	141.6 136.8	**a**: −194.4, −214.5 **b**: −212.0, −226.5	−50.8 −64.8

Table 1. Comparison of the ^{29}Si and ^{31}P NMR chemical shifts of **109a,b**, *E/Z*-**139** and *E/Z*-**140** (**a**: R = ^{t}Bu, **b**: R = Xylyl).

For the generation of **109b** an intermediate phosphaalkyne is proposed that can readily isomerize to the cumulene structure (Scheme 64). After 16h at rt, a third product is starting to appear as evidenced by two new ^{31}P resonances at $\delta = -50.8$ and −64.8 ppm (ratio 63 : 37) again indicating the formation of two stereo isomers. As confirmed by ^{31}P NMR spectroscopy, after heating to 40°C for two hours, phosphasilene **108a**, the assumed initial product **139**, 1-aza-3-phosphaallene **109a** and the third product are present in an approximate equimolar ratio (Figure 9).

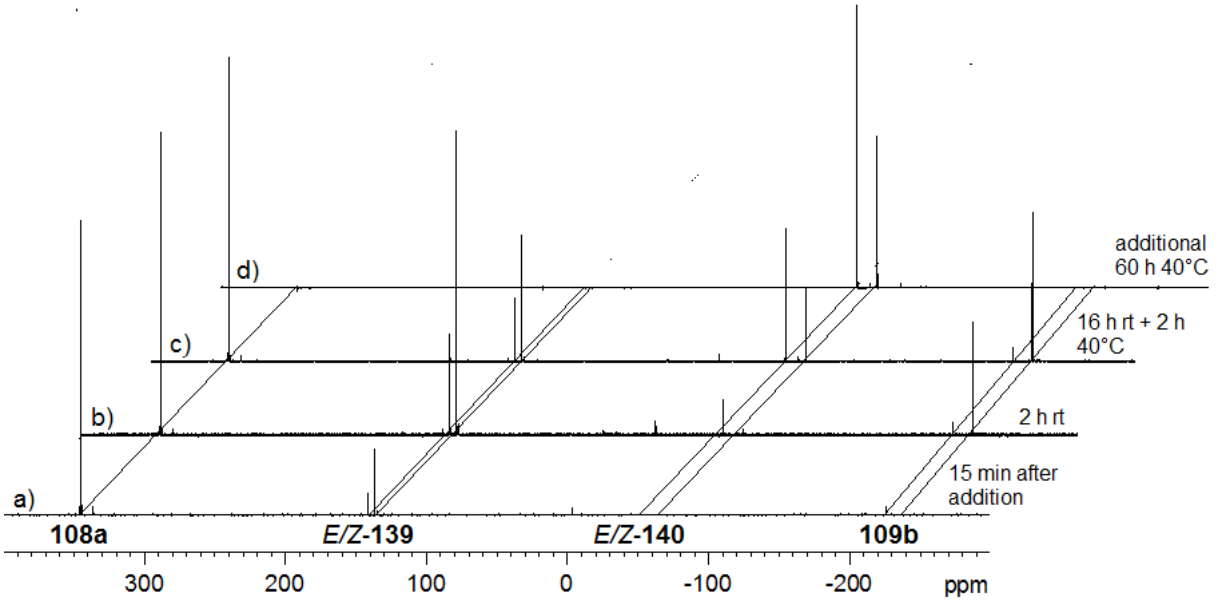

Figure 9. Stacked plot of ^{31}P{^{1}H} NMR spectra from the reaction of xylyl isonitrile with phosphasilene **108a**; a) 15 min after addition, b) additional 2 h rt, c) additional 16 h rt and 2 h 40°C, d) additional 60 h 40°C.

Upon heating to 40°C for additional 58 h complete conversion to the third product was accomplished. The ^{29}Si NMR spectrum (Figure 10) shows two pairs of doublets with ^{31}P coupling at δ = 39.6 ($^{2}J_{Si-P}$ = 66.9 Hz), −2.9 ($^{3}J_{Si-P}$ = 11.6 Hz) ppm and δ = 11.1 ($^{2}J_{Si-P}$ = 51.2 Hz), −4.7 ($^{3}J_{Si-P}$ = 57.0 Hz) ppm (Table 1).

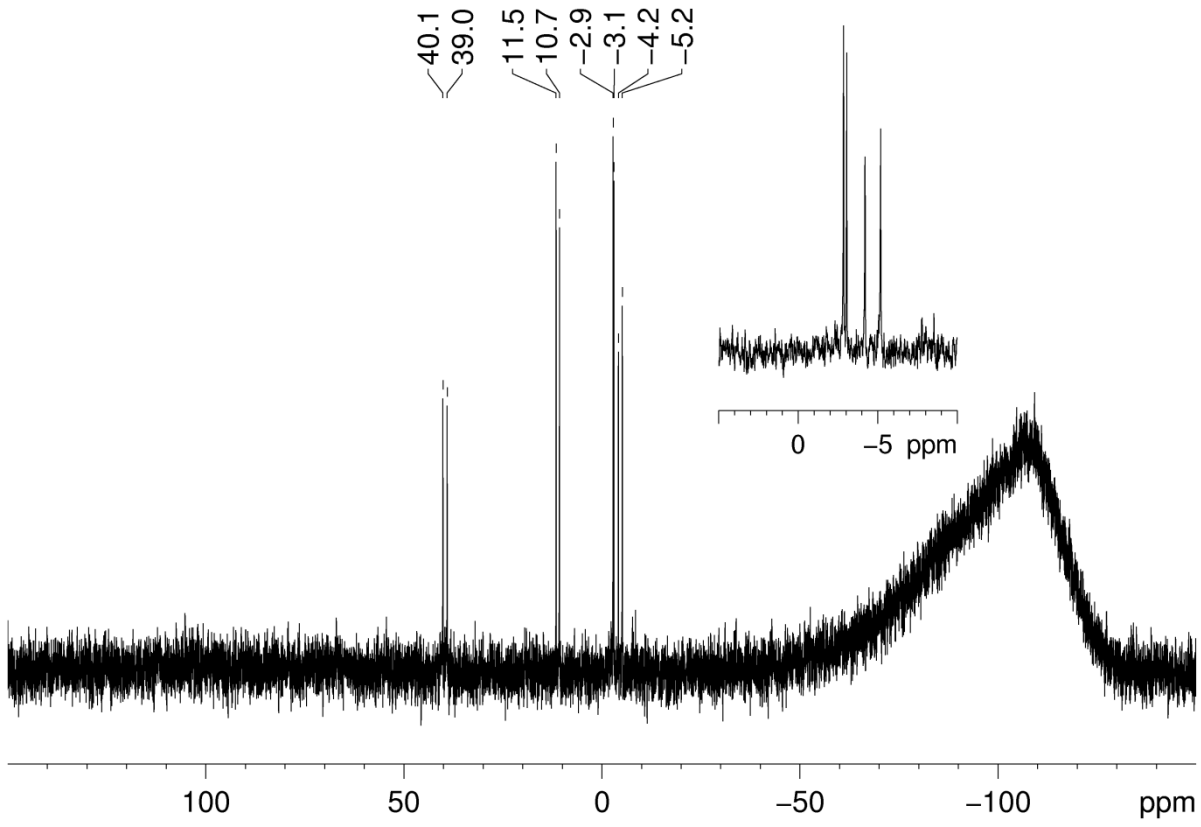

Figure 10. ^{29}Si{^{1}H} NMR spectrum of proposed product *E/Z*-**140**.

The two low-field shifted resonances indicate a double bonded silicon atom. Furthermore, two deshielded signals coupling to phosphorus appear in the ^{13}C NMR spectrum at δ = 202.5 ($^{2}J_{C-P}$ = 65.7 Hz) and 175.1 ($^{1}J_{Si-P}$ = 54.4 Hz) ppm. Recently, the formation of silaaziridines with exocyclic Si=C bonds from the reaction of unsymmetrically substituted disilenes with isonitriles has been reported by our group.[180] The NMR data for the second rearrangement product is in line with formation of the analogous compound, phosphaaziridine **140** as *E/Z*-mixture. The significantly smaller value for the ^{3}J coupling constant observed for the ^{29}Si resonance at δ = −2.9 ppm can be readily explained by the *cis*-relationship of the phosphorus and silicon nuclei in this case (Scheme 65).

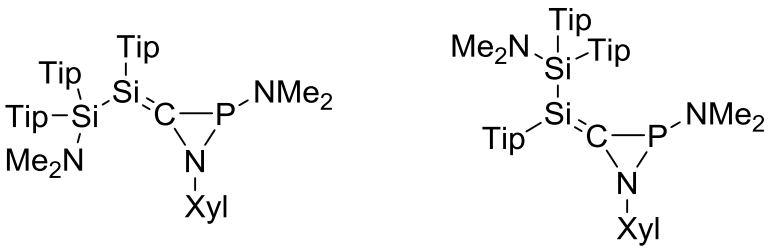

E-**140** *Z*-**140**

Scheme 65. Silaaziridines *E*-**140** and *Z*-**140**.

In analogy to what was reported for the reaction of unsymmetrically substituted disilenes with isonitriles,[180] silene **140** can be generated in one step from the [2+1] cycloaddtition product **138** (Scheme 64). Presumably, phosphaalkene **139** and 1-aza-3-phosphaallene **109a** are kinetic products and thus in equilibrium with **138** and **135** is the thermodynamic product. The higher thermodynamic stability of **109a** might be due to the pronounced +I-effect of the ^{t}Bu-moiety. For the **109a** (Table 1) a certain degree of ylidic character is apparent. Thus, the positive charge on nitrogen is stabilized by the electron donating ^{t}Bu-group. Furthermore, steric effects that favor the cyclic structure in the xylyl-case cannot be excluded. Efforts to obtain single crystals suitable for an X-Ray diffraction study were as yet unsuccessful, and thus no further proof for the constitution of any of the products can be provided.

With the before mentioned findings in mind, **108a** was treated with 0.5 equivalents of 1,4-durylbisisonitrile. It has to be considered that in principle four isomers for each product can be expected.

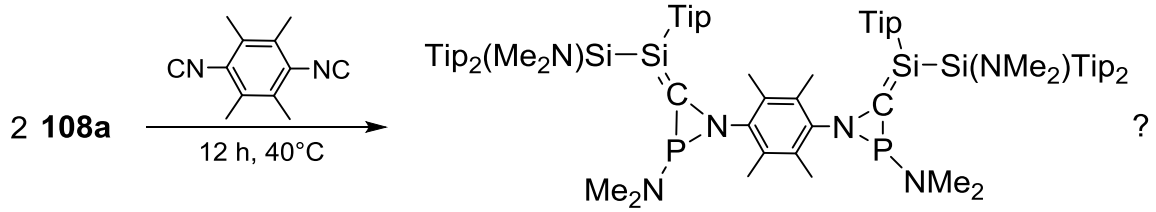

141

Scheme 66. Proposed reactivity of phosphasilene **108a** towards duryl bisisonitrile.

While no reaction was observed at rt, after 30 min at 40°C besides approximately 82% starting material indeed conversion to an analoguous mixture as in case of the xylyl-isonitrile was observed by ^{31}P NMR spectroscopy. Three main signals appear at δ = 145.5, 137.2 and −227.4 ppm. Upon heating for another 12 h at 40°C two additional major resonances arise in the ^{31}P NMR spectrum at δ = −49.0 and −66.8

ppm which are comparable to those of the final product from treatment of phosphasilene **108a** with xylyl-isonitrile (Figure 11) and thus might be assigned to **141** (Scheme 66).

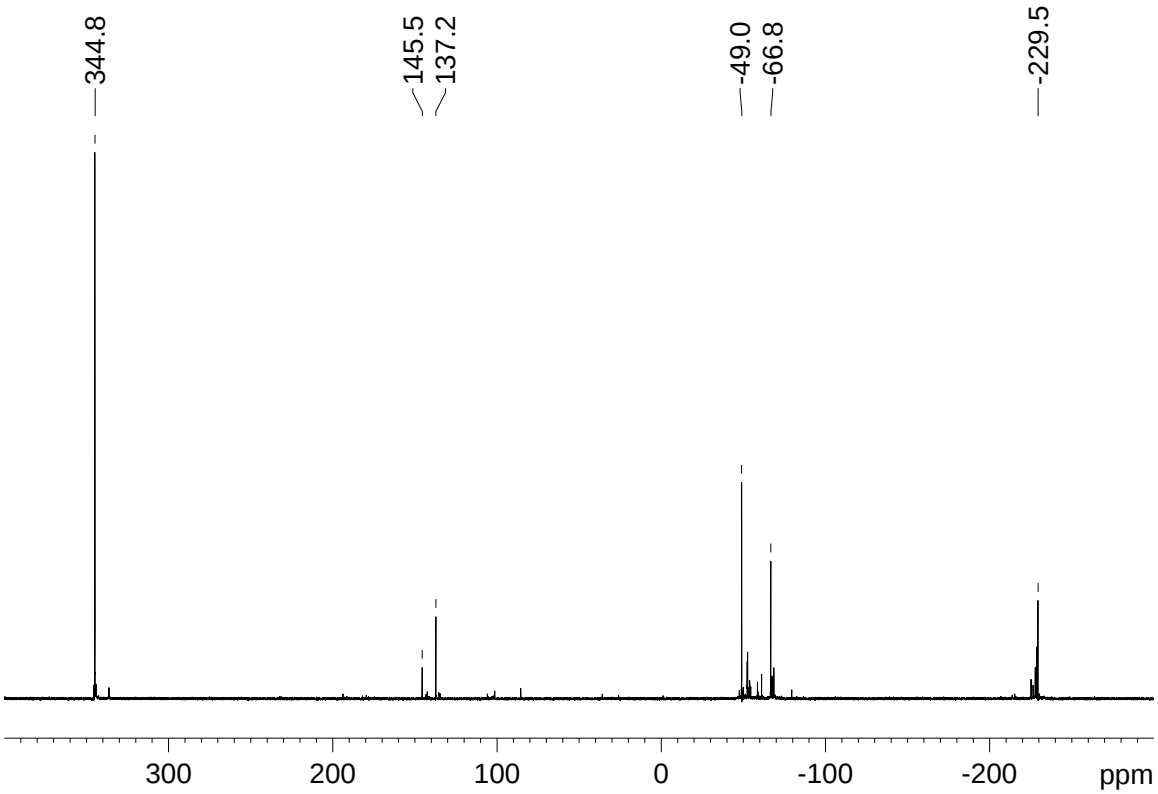

Figure 11. $^{31}P\{^{1}H\}$ NMR spectrum from the reaction of phosphasilene **108a** with 1,4-durylbisisonitrile after 12h at 40°C.

However, the reaction is less uniform and upon further heating to 40°C slow decomposition to a complex mixture was observed by NMR spectroscopy. Consequently, no product could be isolated and the reaction was not investigated any further.

3.1.2.2. Reactivity of 108a towards Anionic Nucleophiles

Nucleophilic and electrophilic substitution reactions are key manipulations in synthetic organic chemistry. Similarly, in main group chemistry unsaturated compounds with reactive nucleophilic or electrophilic centers have become useful building blocks.[34] In disilene chemistry nucleophilic[48,66] (*cf.* Chapter 1.1.4.1 and 1.1.4.2) and electrophilic derivatives[81,93-95] (*cf.* Chapter 1.1.4.3) **I** and **II** have been

reported and their use as disilene transfer agents is documented (Scheme 67). For Si=P bonds with *P*-metalla phosphasilenes formally nucleophilic congeners are available, however, to the best of our knowledge no nucleophilic reactivity under retention of the Si=P bond has been published (Scheme 67).[48,115-117] The grafting of typical anionic leaving groups would in principle allow for nucleophilic substitution reactions at the P=Si double bond (Scheme 67).

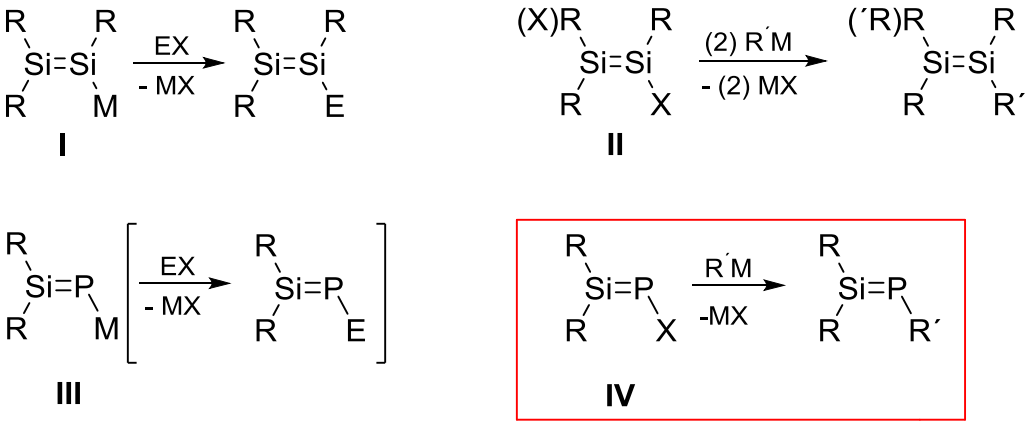

Scheme 67. Nucleophilic[48,66] and electrophilic[81,93-95] disilenes **I** and **II**, and their reactivity towards electrophiles and nucleophiles, respectively; nucleophilic[48,115-117] and potentially electrophilic phosphasilenes **III** and **IV** and their presumed reactivity towards electrophiles and nucleophiles, respectively (M = metal, X = anionic leaving group, R = alkyl, aryl or silyl).

The amino functionality in phosphasilene **108a** in principle provides a leaving group at phosphorus for substitution reactions. Dimethylamides are known to react as leaving groups with anionic nucleophiles (*e. g.* carboxylic acid amides with silyl lithiums).[131] A certain degree of mobility of the amino functionality at phosphorus is in fact indicated by the reactions of **108a** with isonitriles.[130]

Consequently, we decided to investigate the reactivity of **108a** towards several anionic nucleophiles in order to substitute the amino group at phosphorus. In a first attempt, **108a** was treated with one equivalent of methyl lithium in benzene (Scheme 68).

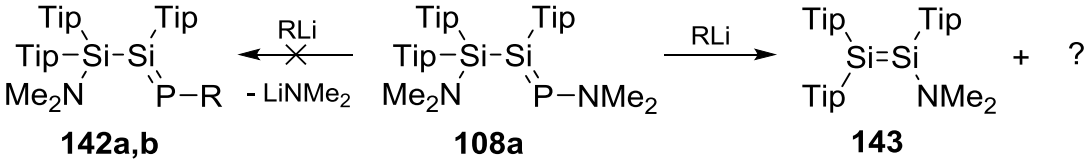

Scheme 68. Attempts to substitute the amino group in **108a** with alkyl lithium species (**142a**: R = Me, **142b**: R = ^{t}Bu).

Subsequently, the yellow solution turned deep red. The ^{31}P NMR spectrum of the mixture recorded immediately after addition revealed resonances at δ = 224.1, 206.2, −104.9 (q, $^{1}J_{P\text{-}Li}$ = 60.3 Hz), −106.5 ($^{1}J_{P\text{-}Si}$ = 33.3 Hz) and −161.0 ppm besides 50% of starting material (Figure 12).

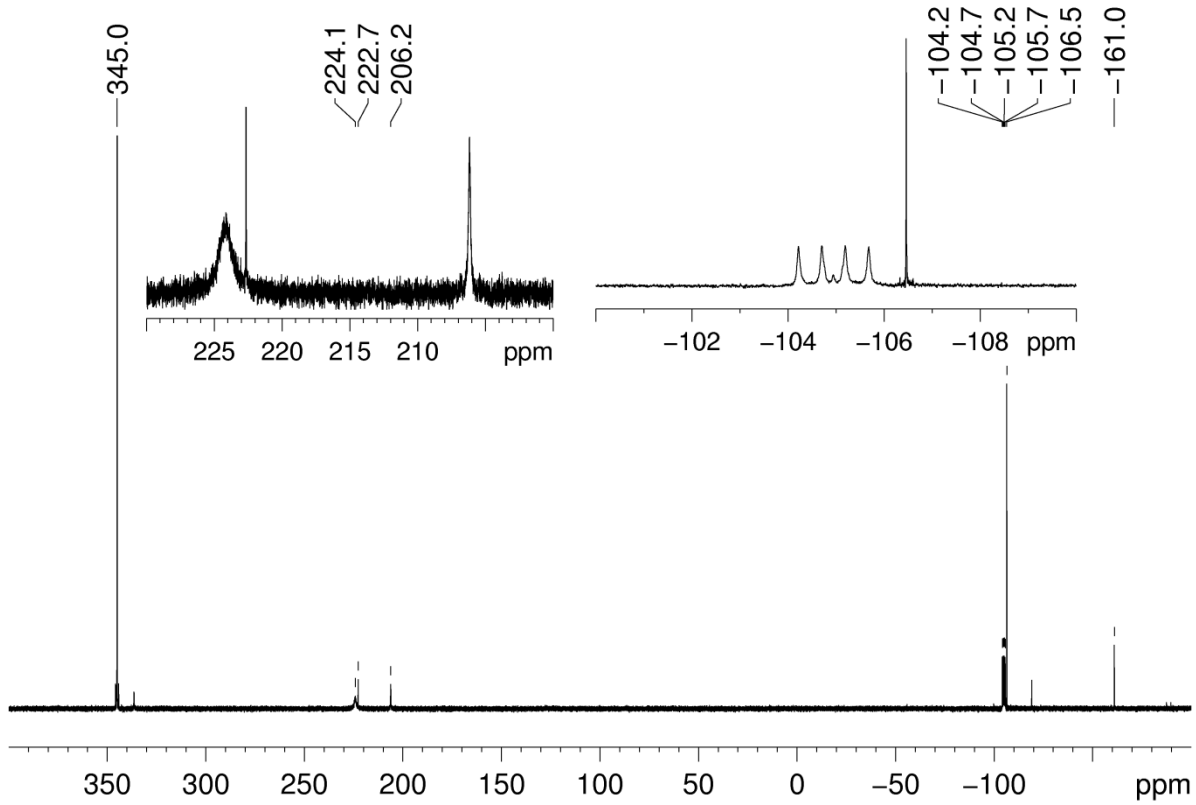

Figure 12. ^{31}P{^{1}H} NMR spectrum from the reaction of phosphasilene **108a** with methyl lithium recorded 15 min after addition.

The signals at δ = 224.1 and 206.2 ppm are in accord with the formation of **142a** (Scheme 68) as *E/Z*-isomers, [104-117] however, no silicon satellites could be detected. For the low-field resonance, this is attributed to a pronounced broadening of the peak (half width 133 Hz). In contrast, the signal at δ = 206.2 ppm is significantly sharper (half width 28 Hz) and consequently the absence of silicon satellites speaks against formation of **142a**. The intensity of the resonance at −106.5 increases with time under consumption of the remaining resonances and after 12 h at room temperature and 2 h at 60°C this signal is observed exclusively in the ^{31}P NMR spectrum besides minor amounts of starting material. Obviously, the Si=P bond is consumed in the course of the reaction.

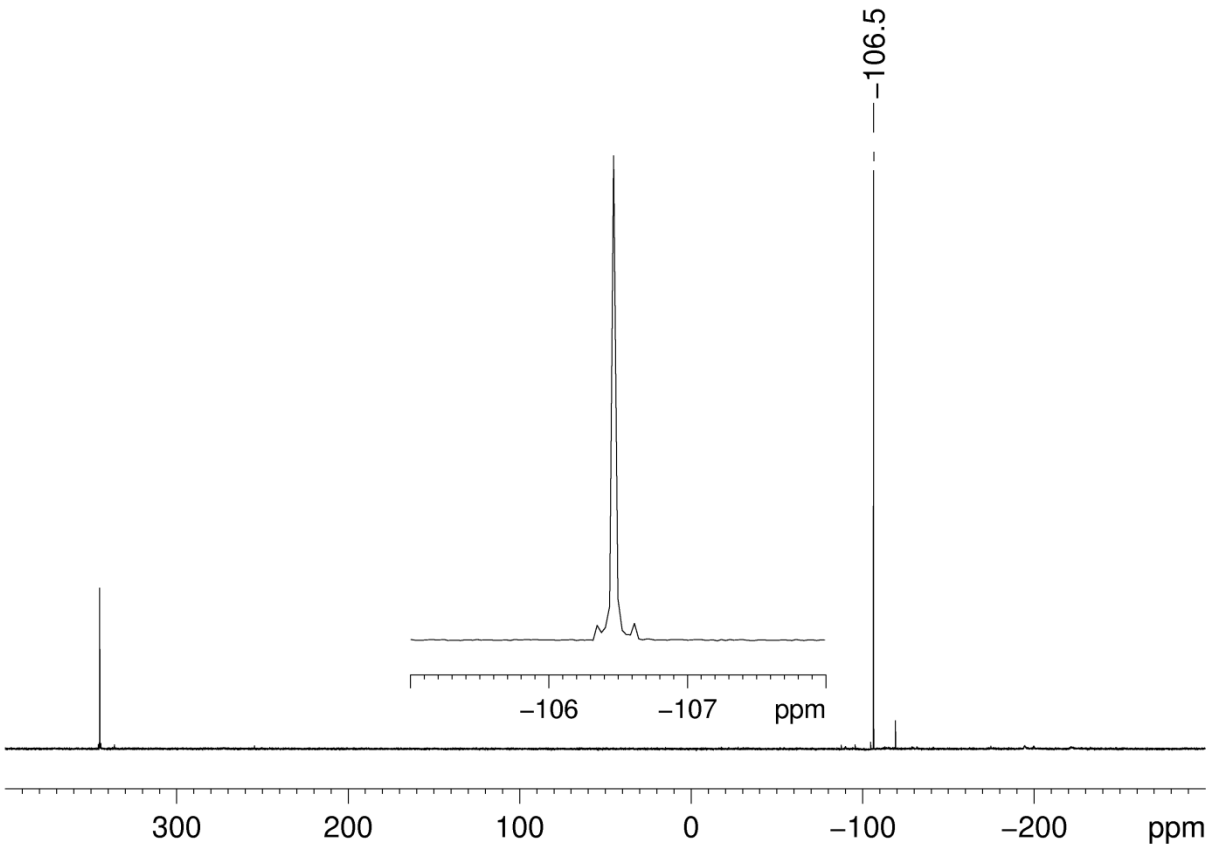

Figure 13. $^{31}P\{^{1}H\}$ NMR spectrum from the reaction of phosphasilene **108a** with methyl lithium recorded after 12 h at rt and 2 h at 60°C.

The corresponding ^{29}Si NMR spectrum reveals resonances at δ = 95.5, 26.3, −0.5 (d, $^{1}J_{P\text{-}Si}$ = 33.3 Hz), −24.5, −25.1 ppm (Figure 14). While the chemical shift of the signal with phosphorus coupling further supports the formation of a saturated silicon-phosphorus species, the two low-field shifted resonances indicate formation of an unsymmetrically substituted disilene.[27] In a subsequent experiment these resonances were unambiguously assigned to amino disilene **143** (*cf*. Chapter 3.1.2.5). The generation of **143** during the reaction of **108a** with methyl lithium, however, remains obscure at this point. We assumed that an initially formed phosphasilene might be unstable due to insufficient steric protection at the phosphorus end of the double bond. Consequently, we decided to employ a sterically more demanding alkyl lithium species. One equivalent *tert.*-butyl lithium was added to **108a** and subsequently the reaction was monitored by NMR spectroscopy (Scheme 68). After 3 h at rt, full conversion was reached: as in the previous reaction with methyl lithium, two low-field resonances without silicon coupling were detected in the ^{31}P NMR spectrum at δ = 294.6 and 282.2 ppm. Two additional signals of significantly lower intensity appear at δ = 19.5 and 11.9 ppm. However, the product attributed to the deshielded

resonances is stable in this case since no rearrangement could be detected at rt. Surprisingly, the ^{29}Si NMR spectrum is very similar to what was observed during the reaction of **108a** with methyl lithium since the same four resonances at δ = 95.5, 26.2, −21.5 (lower in intensity) and −25.1 ppm are observed in both cases (Figure 14).

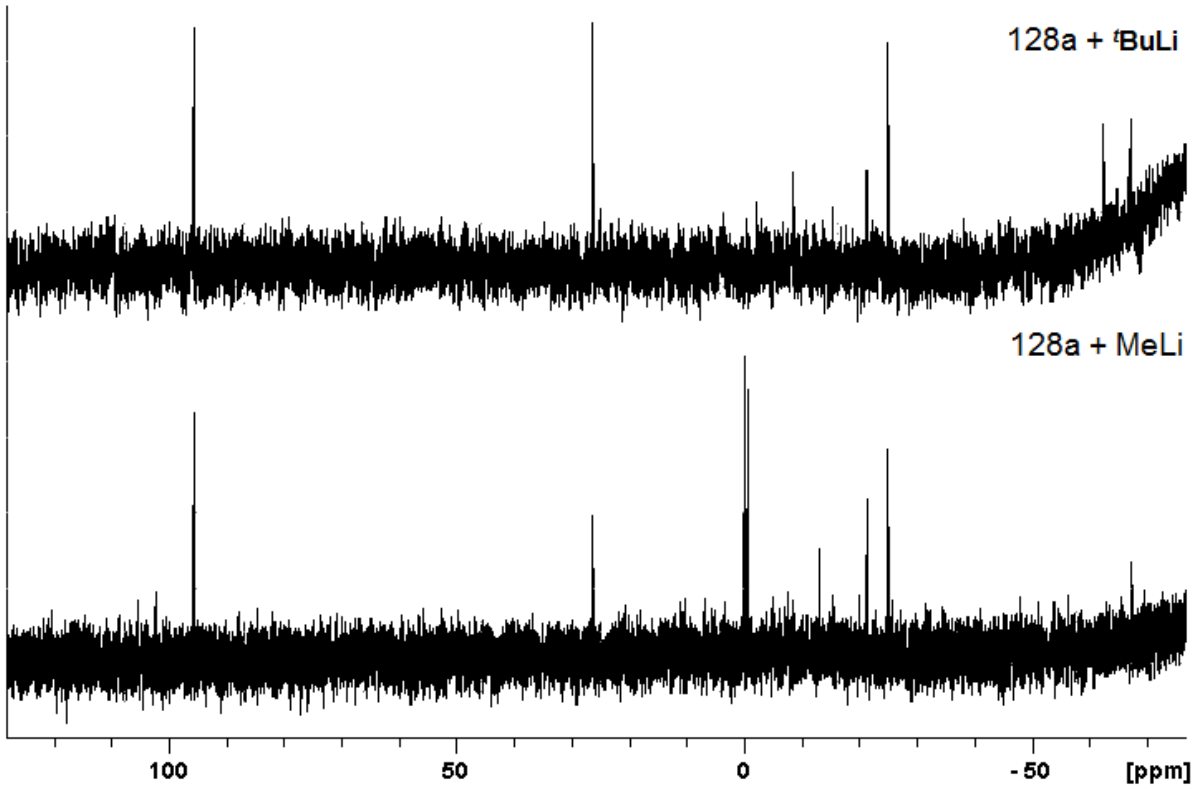

Figure 14. ^{29}Si{^{1}H} NMR spectra from the reaction of MeLi and ^{t}BuLi with phosphasilene **108a**.

No signal with discernible ^{31}P-coupling could be identified. From neither of the reactions of **108a** with methyl lithium or with *tert.*-butyl lithium a uniform product was isolated.

In a next attempt we considered the use of mesityl lithium as nucleophile. The steric demand of the mesityl moiety is comparable to *tert.*-butyl but the electronic situation is entirely different. While alkyl groups have a strong +I-effect, aryl substituents are more electron withdrawing. Phosphasilene **108a** and mesityl lithium were thus combined in toluene. No reaction occurred at room temperature, but after heating to 60°C for 60 h indeed quantitative substitution of the amino group was confirmed by multinuclear NMR spectroscopy yielding *P*-mesityl substituted phosphasilene **144** as *E/Z*-mixture (Scheme 69). The ^{31}P NMR resonances of both isomers at δ = 234.4 and

217.9 ppm (*E/Z*-ratio: 84:16) are in the typical range for Si=P bonds and both signals feature silicon satellites with characteristically large coupling constants (*E*-**144**:$^{1}J_{P\text{-}Si}$ = 193.9 Hz, $^{2}J_{P\text{-}Si}$ = 46.6 Hz and *Z*-**144**:$^{1}J_{P\text{-}Si}$ = 189.0 Hz $^{2}J_{P\text{-}Si}$ = 25 Hz).[104-117]

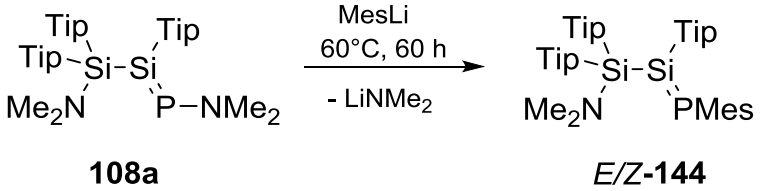

108a *E/Z*-**144**

Scheme 69. Synthesis of *P*-mesityl substituted phosphasilene **144** *via* the reaction of **108a** with mesityl lithium (Mes = mesityl = 2,4,6-trimethylphenyl).

The significantly larger value for the $^{2}J_{P\text{-}Si}$ coupling of the in the ^{29}Si signal at δ = 234.4 ppm is attributed to the *cis*-relationship between the lone pair on phosphorus and the β-silicon atom and thus allows for the assignment of the major isomer *E*-**144**.[181] Notably, the ^{31}P nuclei in *E/Z*-**144** exhibit a considerably stronger shielding than in *E/Z*-**108a**: (*E*-**108a**: 344.8 ; *Z*-**108a**: 336.2 ppm)[130] and in Sekiguchi´s "push-pull" phosphasilene **106** (389.3 ppm),[129] for both of which a certain degree of inverse polarization has been suggested. This shielding can be clearly assigned to a higher electron density at the phosphorus end of the double bond and is thus in line with a more "normal" polarization in mesityl-substituted **144**. Consequently, the inverse trend is observed by ^{29}Si NMR spectroscopy: The resonance assigned to the unsaturated silicon atom in *E*-**144** (δ = 192.3 ppm) is roughly shifted 100 ppm downfield compared to *E*-**108a** (δ = 103.5 ppm) indicating more positive polarization at the silicon atom. The saturated silicon atom in **144** is observed at δ = −6.6 (d, $^{2}J_{Si\text{-}P}$ = 46.6 Hz) ppm and as expected barely affected by the substitution of the amino functionality at phosphorus by a mesityl group (**108a**: δ = −8.1 ($^{2}J_{Si\text{-}P}$ = 40.8 Hz) ppm). Single crystals of the major isomer *E*-**144** were obtained from hexane (Mp 208°C, dec.) in 64% yield. An X-ray diffraction study confirmed the structural assumptions made on the basis of NMR spectroscopy (Figure 15). For **108a**, a relatively long Si=P bond (2.1187(7) Å) and a slightly pyramidalized unsaturated silicon atom (358.85°) is found, which can be attributed to delocalization of the nitrogen lone-pair into Si=P antibonding orbitals. Indeed, the double bond in *P*-mesityl substituted phosphasilene **144** (Si2-P1 2.0923(6) Å) is shortened compared to **108a** (2.1187(7) Å) and thus in the typical range for phosphasilenes.[109-117] Furthermore, the coordination

environment of Si2 is perfectly planar (Σ of angles at Si2: 360.0°). Consequently, the longest wavelength absorption in the UV/vis spectrum of **144** (λ_{max} = 374 nm, ε = 7700 $M^{-1}cm^{-1}$) is assigned to the π-π*-transition and is blue-shifted in comparison with **108a** (λ_{max} = 410 nm)[130] due to the absence of the *P*-amino group with its delocalized lone-pair. A further absorption band is observed at 270 nm (ε = 24100 $M^{-1}cm^{-1}$, Figure 107-Figure 109).

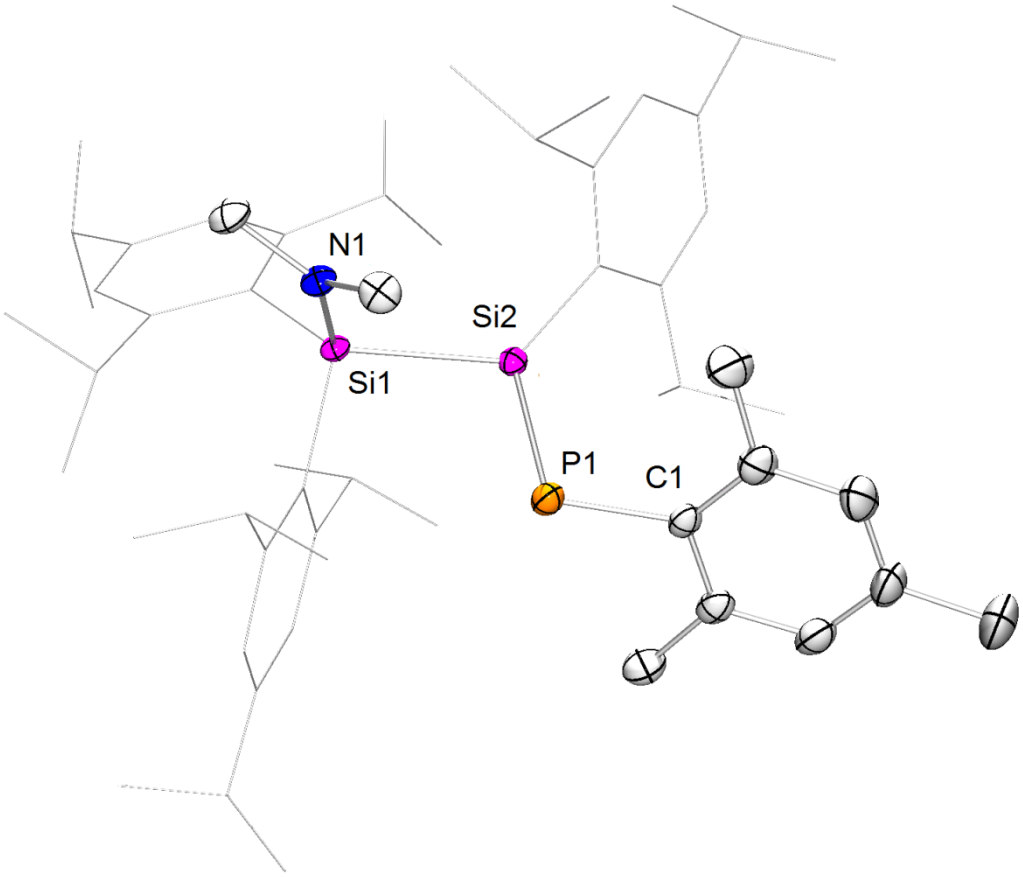

Figure 15. Molecular structure of *E*-**144** in the solid state (thermal ellipsoids at 50%, H atoms and disordered ^{i}Pr-groups omitted for clarity). Selected bond lengths [Å]: Si2-P1 2.0923(6), Si1-Si2 2.4174(6), Si1-N1 1.7357(3), P1-C1 1.847(17).

3.1.2.3. Synthesis of Trisilaphospha[1.1.0]bicyclobutane Derivative 146

Encouraged by the finding that we are indeed able to perform nucleophilic substitution reactions at the Si=P bond for the first time, we decided to investigate the reactivity of **108a** towards a more elaborate nucleophile, namely disilenide **16**. As possible products of this reaction trisilaphosphabutadiene **145** (Scheme 70) or one of its valence isomers was anticipated. For the homonuclear Si_4R_6-series the 1,3-

butadiene analogue[67] as well as the valence isomeric tetrasila[1.1.0]bicyclobutane,[182] tetrasilacyclobutene[183,184] and silylcyclotrisilene[184] are known. In case of the partially phosphorus-substituted systems, a 1,3-diphospha-2,4-disilabicyclo[1.1.0]butane[185] reported by West *et al.* and two 1,2,3-triphospha-4-silabicyclo [1.1.0]butanes[107] synthesized in the Driess group remain the sole examples.

Disilenide **16** and phosphasilene **108a** were combined in toluene. While no reaction occurred at room temperature, after heating to 65°C for 3h the mixture turned red and complete conversion to a new product with a ^{31}P NMR resonance at δ = −212.3 ppm was observed. The strong shielding of the phosphorus nucleus is indicative for the absence of an unsaturated phosphorus atom. Notably, in the ^{29}Si NMR spectrum only three of the expected four signals are observed. The multiplicity of the signals as doublets at δ = −5.1 ($^1J_{Si-P}$ = 84.7 Hz), −39.5 ($^1J_{Si-P}$ = 84.7 Hz) and −119.8 ($^1J_{Si-P}$ = 5.2 Hz) ppm is well in line with the formation of a phosphatrisila[1.1.0]butane, although the value of the coupling constants in polycyclic systems is additive and consequently to be treated with caution.

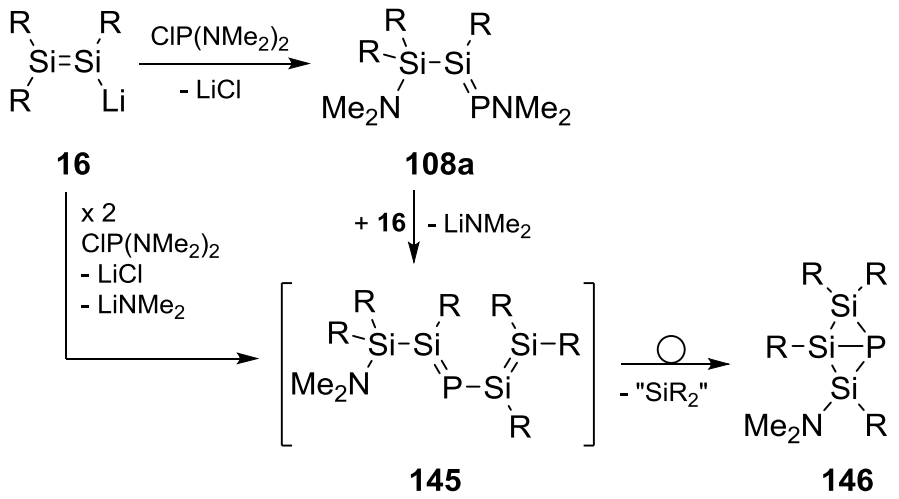

Scheme 70. Synthesis of phosphatrisila[1.1.0]bicyclobutane derivative **146** with proposed intermediacy of butadiene analogue **[145]** (R = Tip = 2,4,6-^{i}PrC$_6$H$_2$).

While the two resonances at δ = −5.1 and −39.5 can be assigned to the flanking silicon atoms, the strong shielding and the small value of the J_{Si-P} coupling constant (J = 5.2 Hz) for the high-field resonance are in good agreement with a bridgehead silicon atom.[108,182,185,186] On the basis of a two-dimensional ^{1}H/^{29}Si correlation experiment the resonance at δ = −4.9 ppm was assigned to the amino substituted silicon atom. The signals at δ = −39.4 and −119.8 ppm should thus arise from the

$SiTip_2$ and SiTip units, respectively. Colorless single crystals (Mp > 220°C) were obtained from a concentrated pentane solution in 34% yield.

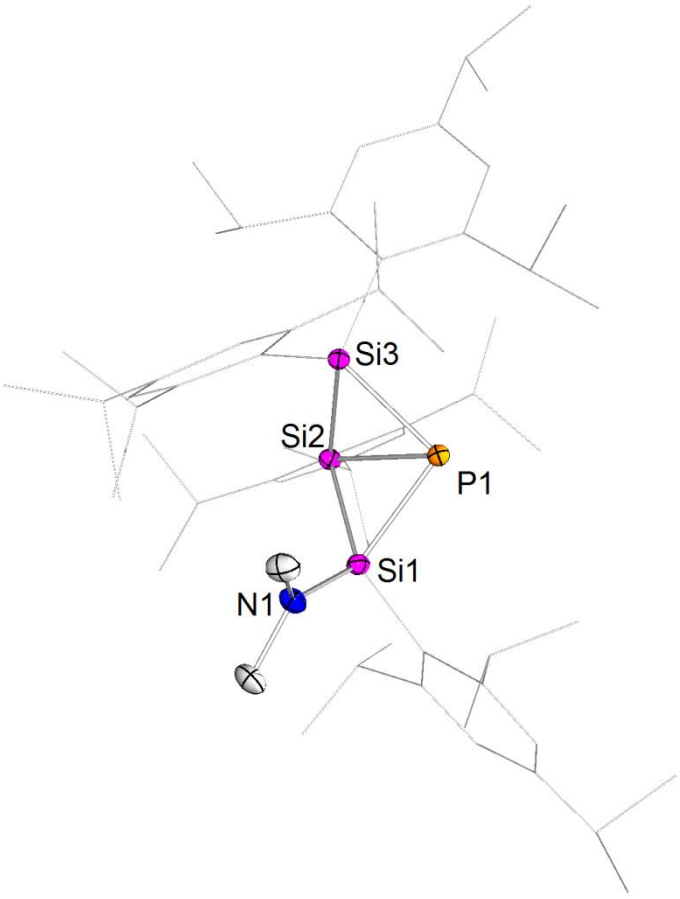

Figure 16. Molecular structure of **146** in the solid state (thermal ellipsoids at 50%, H atoms and disordered ^{i}Pr groups omitted). Selected bond lengths [Å] and angles [°]: Si1-P1 2.2217(8), Si2-P1 2.4273(8), Si3-P1 2.2566(8), Si1-Si2 2.2899(8), Si2-Si3 2.2915(8), Si1-N1 1.7105(19), P1-Si1-Si2 65.08(3), Si1-Si2-Si3 94.58(3) P1-Si3-Si2 64.51(3).

An X-ray diffraction study confirmed the constitution as phosphatrisilabicyclo[1.1.0]-butane derivative **146** (Figure 16, Scheme 70). The structural features elucidated by multinuclear NMR spectroscopy can be readily retrieved in the solid state. The Si-P bridgehead bond (Si2-P1 2.4273(8) Å) is markedly elongated compared to single bonds for reported cyclic silicon phosphorus species.[177] While the Si3-P1 bond and all Si-Si bonds are in the fairly normal range, the Si1-P1 bond of 2.2217(8) Å is markedly shortened (for comparison $CH(SiMe_3)_2SiMe_2PPh_2$ 2.295 Å),[187] which is line with planarization of the amino group on Si1 by an apparent electron donation of the lone pair to the adjacent silicon atom (Σ of angles N1: 359.21°). The phosphorus atom in **146** is constrained to extreme pyramidalization by the bridgehead position (Σ of angles P1: 214°). Despite this apparent strain, **146** is an extremely stable

compound. It is not sensitive towards air or moisture and shows no indications of decomposition when it is kept at 400°C in an argon atmosphere for several minutes. It is worth mentioning that due to similarity in reaction conditions it is also possible to synthesize bicycle **146** in a convenient one pot reaction starting from disilenide **16** without isolating phosphasilene **108a** (Scheme 70). Half an equivalent of bis(dimethylamino)chlorophosophane was added to a solution of disilenide **16** in toluene at −80°C. The reaction mixture was allowed to warm to room temperature and afterwards it was kept at 65°C for three hours. Thus, the additional equivalent of **16** reacts with intermediate formed phosphasilene **108a** and it is possible to crystallize **146** in comparable yield (28%).

In order to gain more insight into the bonding situation in **146**, DFT-calculations were performed by Cem B. Yildiz (Aksaray University, Turkey). The geometry of the slightly truncated model system **146-Dip** was optimized at the B3LYP/6-31+G(d,p) level of theory (Tip replaced by Dip = 2,6-diisopropylphenyl). The ^{29}Si NMR chemical shifts for **146-Dip** are calculated at δ = −5.3, −34.1, and −102.9 ppm in good agreement the experimental results for **146** (δ = −5.1, −39.5 and −119.8 ppm). Equally, the calculated ^{31}P NMR chemical shift of δ = −207.4 is consistent with the experimental findings. The Wiberg bond index (WBI) of the Si2-P1 bond in **146-Dip** is with 0.821 somewhat smaller than for the other endocyclic bonds of the bicyclobutane scaffold (calculated WBIs: 0.903-0.942). The pyramidalization of P1 calculated for **146-Dip** (Σ of angles P1: 217°) is in good agreement with the experimental value. The frontier molecular orbitals calculations of **146-Dip** depict that the highest occupied molecular orbitals HOMO, HOMO-1, and HOMO-2 are mainly localized on the Si-Si and Si-P σ bonds of the Si_3P ring and unpaired electrons of the phosphorus atom (Figure 17). Moreover, the LUMO consists of the σ^* orbital of the Si-Si bonds, slightly mixed with the anti-bonding orbital at the P atom.

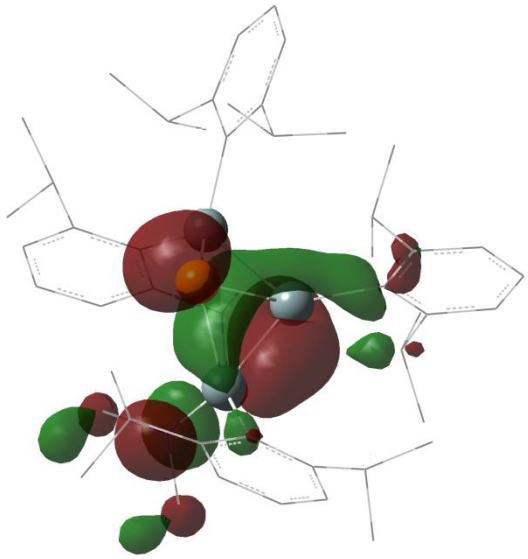

HOMO

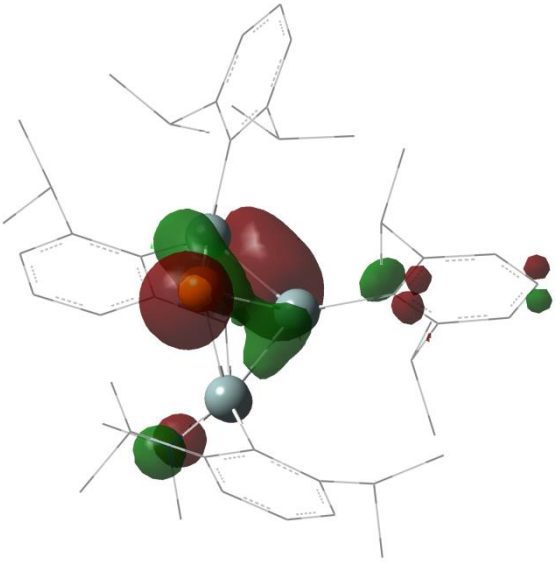

HOMO-1

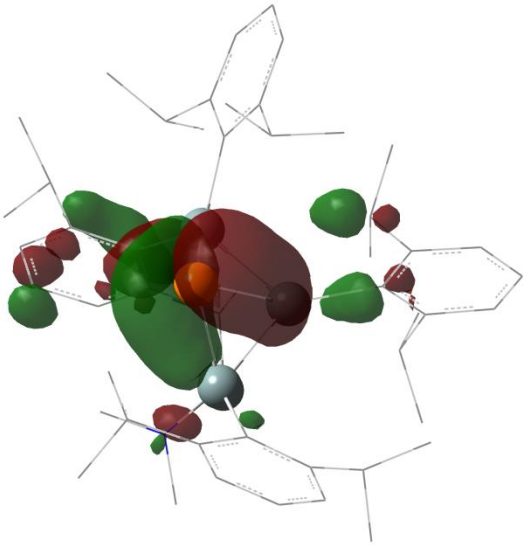

HOMO-2

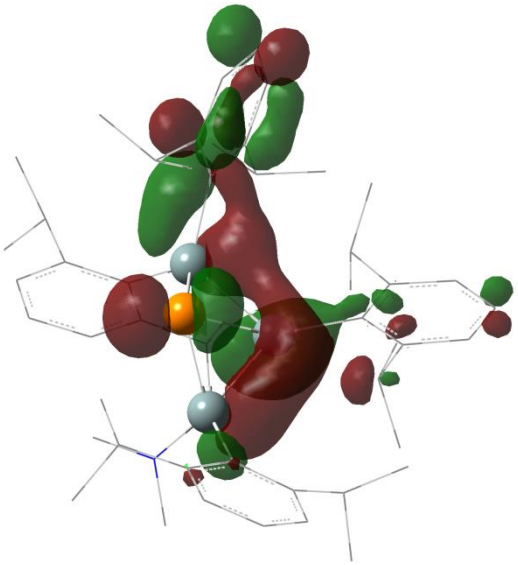

LUMO

Figure 17. Frontier molecular orbitals of model **146**-Dip at an *iso*density *value* of 0.035 au (figures courtesy of Cem B. Yildiz, Aksaray University, Turkey).

The formation mechanism of **146** plausibly proceeds *via* the initial substitution product, tetrasilabutadiene derivative **[145]**, even though it was not observed by NMR spectroscopy (Scheme 71).

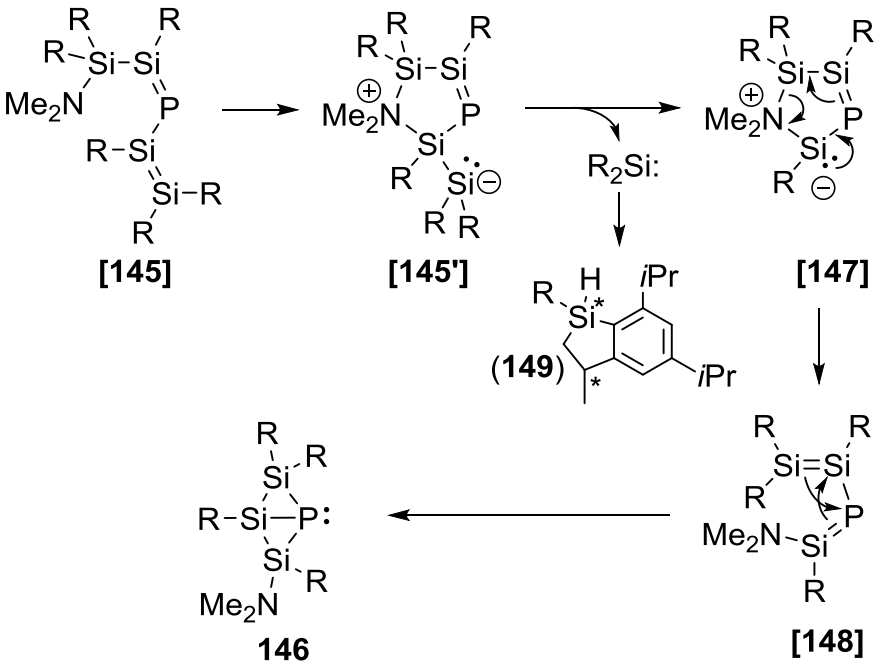

Scheme 71. Plausible mechanism for the formation of **146** and proposed byproduct **149** (R = Tip = 2,4,6-triisopropylphenyl).

DFT calculations at the B3LYP/6-31+G(d,p) level of theory on a simplified model **[145]-Me** (methyl instead of Tip-groups, NH_2 instead of NMe_2) were performed by Cem B. Yildiz (Aksaray University, Turkey) to substantiate mechanistic speculations. As initial step the intramolecular coordination of the amino group to the newly introduced Si=Si moiety is proposed to afford cyclic **[145´]-Me** (Figure 18).

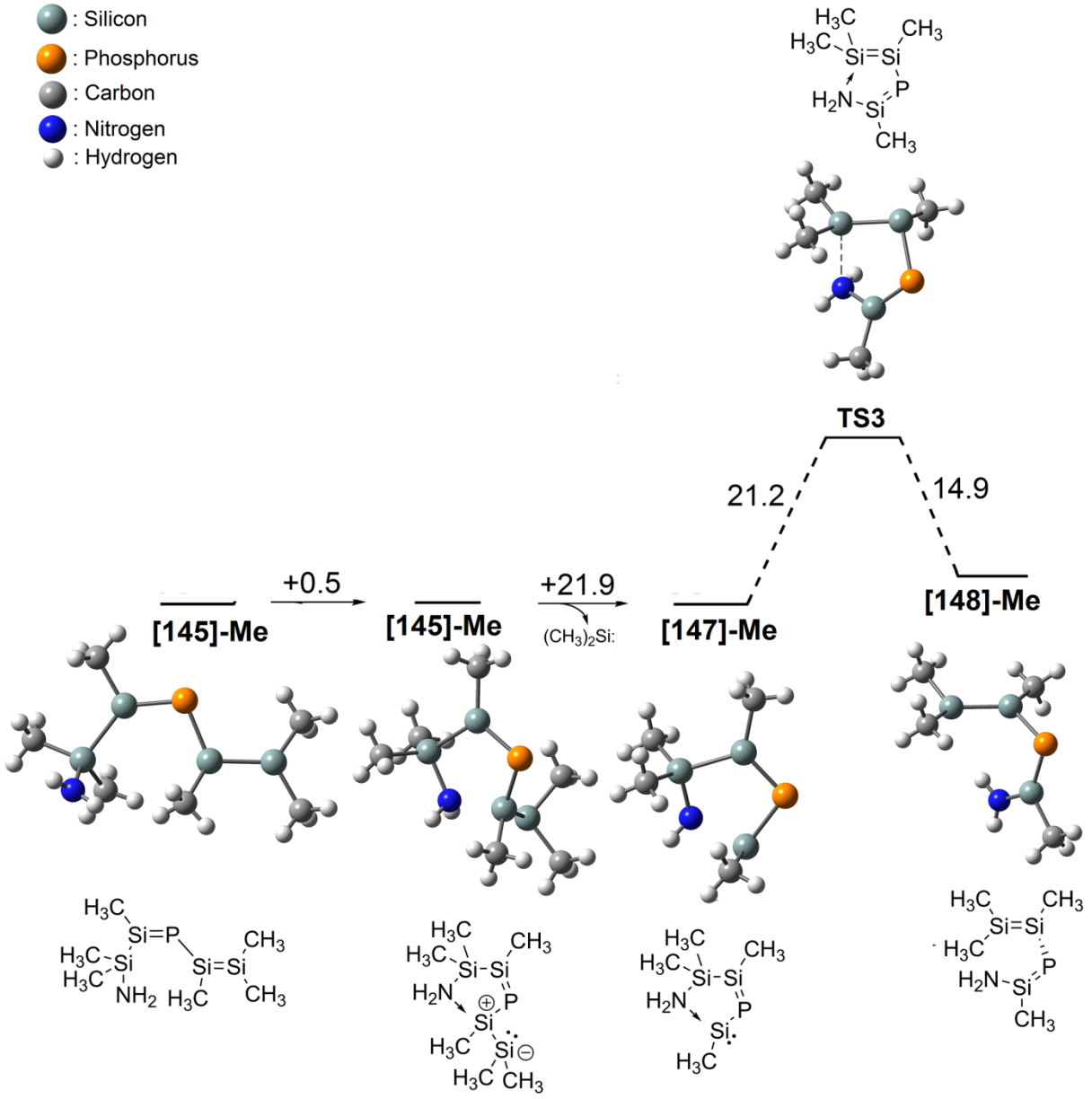

Figure 18. Proposed mechanism and intermediates for the formation of **[147]**-Me using simplified model system with methyl groups instead of Tip-substituents at B3LYP/6-31+G(d,p) level of theory. ΔG energy values at 298 K are given in kcal mol^{-1} (figure courtesy of Cem B. Yildiz, Aksaray University, Turkey).

This step is only mildly endergonic with ΔG = 0.5 kcal mol^{-1} and a negligible barrier. The reversible coordination of Lewis bases to Si=Si bonds has been demonstrated recently in a collaboration with the Jutzi group.[163] The extrusion of SiR_2 from the five-membered ring **[145´]-Me** with an exocyclic SiR_2 moiety is strongly endergonic with ΔG = +21.9 kcal mol^{-1}. Although this value is still compatible with the reaction conditions, it could be reduced further significantly in the experimental case due to much more severe steric congestion imposed by the Tip-substituents. As shown by Okazaki, Tokitoh and co-workers, steric strain can indeed lead to the dissociation of

Si-Si double bonds into two silylene fragments either with or without the trapping by coordination of an external base.[95,188] Surprisingly, the ring opening of the resulting ylide **[147]-Me** to give an unstable 1-phospha-1,3,4-trisilabutadiene **[148]-Me** is endergonic by ΔG = +6.6 kcal mol^{-1} with a substantial barrier of $\Delta G^{\neq}$ = +21.2 kcal mol^{-1}.

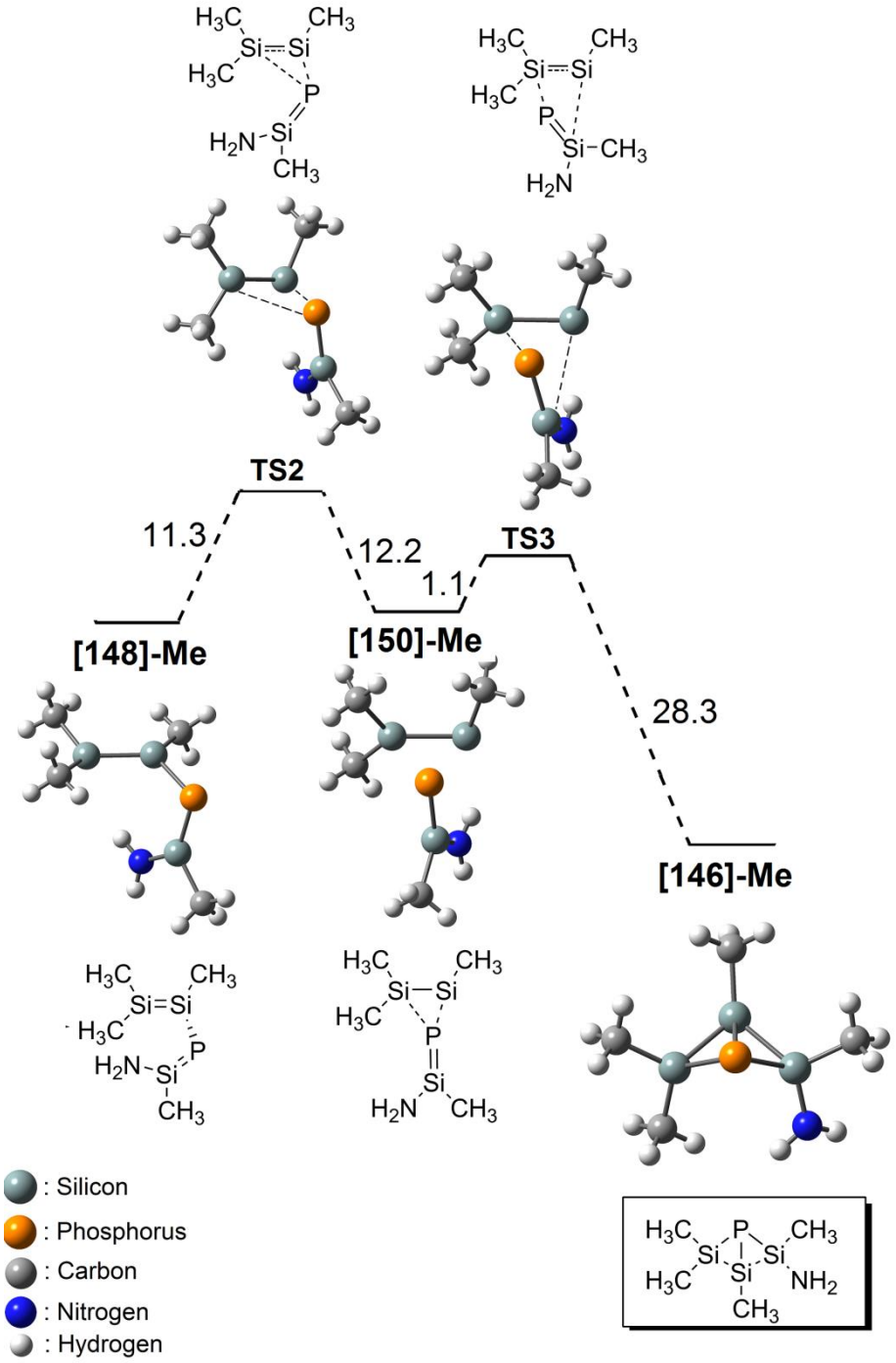

Figure 19. Proposed mechanism and intermediates for the formation of **146-Me** from **[148]-Me** using simplified model system with methyl groups instead of Tip-substituents at B3LYP/6-31+G(d,p) level of theory. ΔG energy values at 298 K are given in kcal mol^{-1} (figure courtesy of Cem B. Yildiz, Aksaray University, Turkey).

The final step of the pathway to the bicyclo[1.1.0]butane analogue **146-Me**, easily overcompensates for this in being exergonic by $\Delta G = -27.5$ kcal mol^{-1}, which is in accordance with reported 1,3-butadiene – bicycle[1.1.0]butane isomerizations of 3rd row systems (Figure 19).[189]

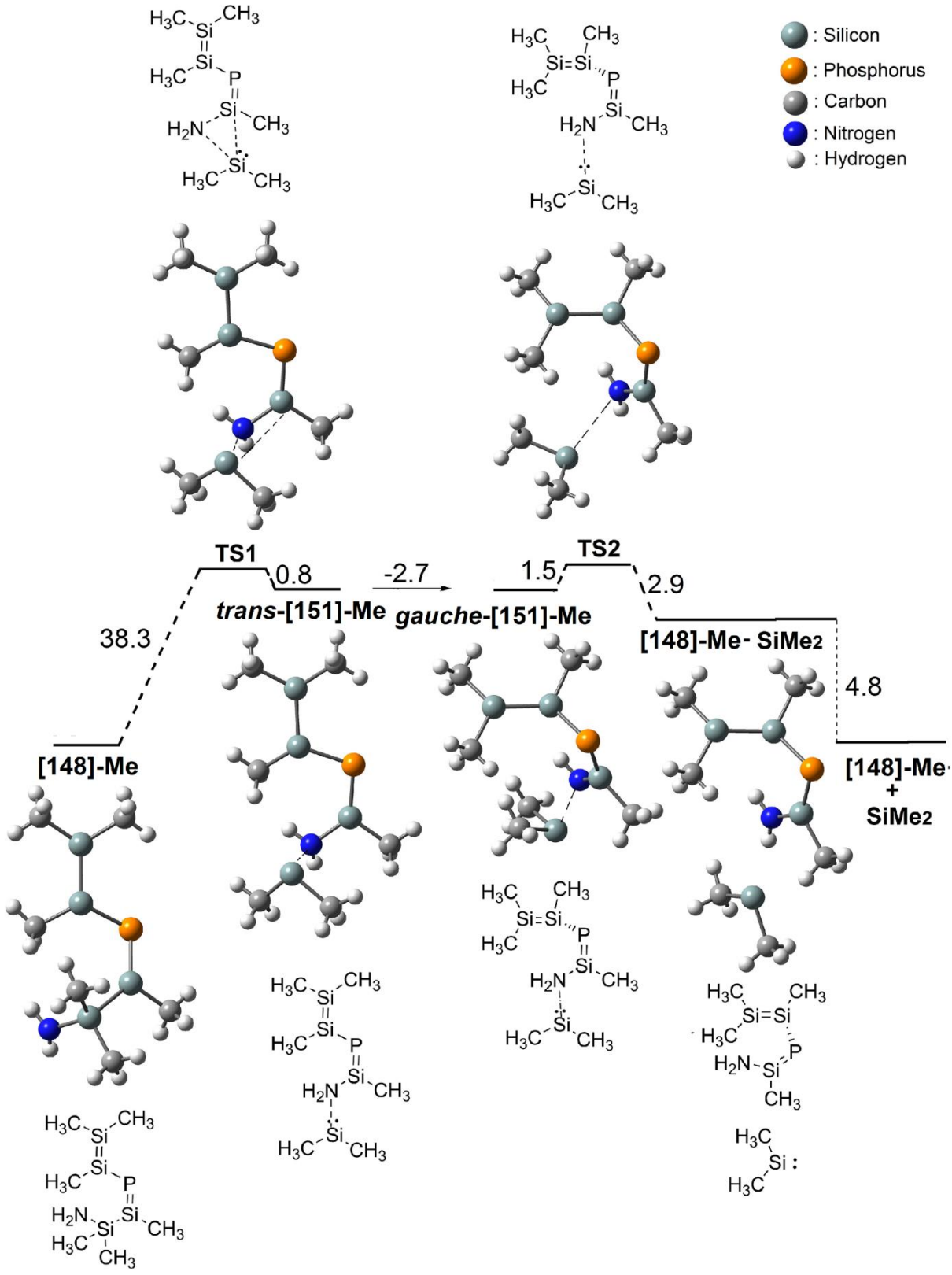

Figure 20. Alternate mechanism and intermediates for the formation of **[148]-Me** using simplified model system with methyl groups instead of Tip-substituents at B3LYP/6-31+G(d,p) level of theory. ΔG energy values at 298 K are given in kcal mol^{-1} (figure courtesy of Cem B. Yildiz, Aksaray University, Turkey).

An alternative mechanism for the formation of **148-Me** *via* direct extrusion of the SiR_2-moiety from **[145]-Me** was also considered. However, based on the much more substantial barrier of $\Delta G^{\neq}$ = +38.3 kcal mol^{-1} this pathway appears unlikely (Figure 20).

The $SiTip_2$ silylene liberated in the experimental case is likely undergoing insertion into a methyl group of the substituent: in addition to the signals of the product **146**, the crude reaction mixture shows a two additional ^{29}Si NMR signals at δ = −21.5 and −25.1 ppm in a 2:3 ratio which we assign to the diastereomeric mixture of **149**. A two-dimensional $^{29}Si,^{1}H$-correlation experiment shows cross peaks to ^{1}H resonances in the typical Si-H region (δ = 6.05 ppm, $^{1}J_{Si-H}$ = 295.8 Hz and δ = 5.77 ppm, $^{1}J_{Si-H}$ = 213.3 Hz). Silylenes (as well as germylenes) typically undergo intramolecular C,H-insertion reactions, especially when generated at elevated temperatures.[84,190]

3.1.2.4. Trisilaphospha[1.1.0]bicyclobutane Derivative 146 as Ligand for Transition Metal Complexes

Some of the experiments discussed in this chapter were carried out together with Lukas Junk during his research lab course and are also described in his report.[191] The inherent strong pyramidalization of the phosphorus center should confer excellent σ-donor properties to **146** and we decided to investigate its potential as ligand for transition metal complexes. Since rhodium based complexes are of current interest for catalytic applications,[192] we probed the reactivity of **146** towards rhodium containing reagents. While with $[RhCl(COD)]_2$ (COD = 1,5-cycloocatdiene) no reaction occurred, with $[RhCl(CO)_2]_2$ a mixture was obtained even at low temperatures (Scheme 72).

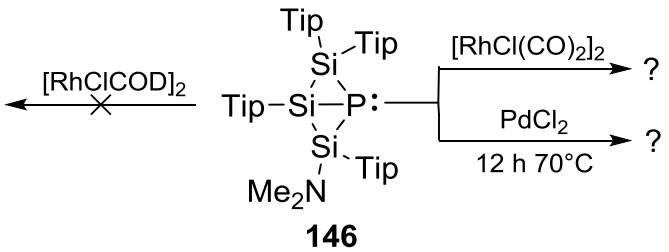

146

Scheme 72. Treatment of trisilaphospha[1.1.0]bicyclobutane **146** with $[RhCl(COD)]_2$, $[RhCl(CO)_2]_2$ and $PdCl_2$, respectively (Tip = 2,4,6-$^{i}Pr_3C_6H_2$, COD = 1,5-cyclooctadiene).

Palladium is equally attractive in catalytic chemistry.[193] One equivalent $PdCl_2$ was added to a solution of **146** in benzene (Scheme 72). No reaction could be detected at room temperature and after 3h at 60°C. Upon heating the mixture to 70°C overnight formation of a metallic mirror was observed. Subsequent filtration and investigation of the filtrate by ^{31}P NMR spectroscopy revealed 80% conversion to a mixture with three main products featuring resonances at δ = −142.3 (br), −168.4 ($^1J_{P\text{-}Si}$ = 45.2, 31.8 Hz), −179.0 (br) ppm (ration1:2:1). A separation of the mixture by crystallization in order to identify any of the products has not been achieved as yet.

Subsequently, the possibility of the coordination of **146** to a copper center was investigated. Phosphane copper complexes are *inter alia* applied as hydroboration catalysts.[194] Even at elevated temperatures no reaction occurred in thf with CuCl or CuI, respectively (Scheme 73). Due to the significantly higher solubility in organic solvents we decided to employ CuBr dimethyl sulfide adduct as source of Cu(I). One equivalent CuBr dimethyl sulfide adduct was combined with **146** in benzene.

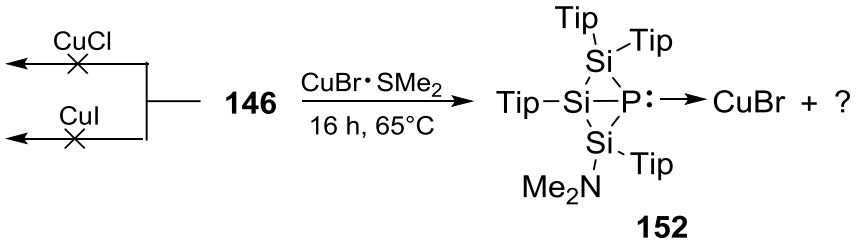

Scheme 73. Treatment of **146** with CuCl and CuI, respectively; proposed formation of **152** from the reaction of **146** with $CuBr{\cdot}SMe_2$.

Upon heating to 65°C indeed conversion to two new products with ^{31}P NMR signals at δ = −222.8 (br) and −230.4 ($^1J_{P\text{-}Si}$ = 100.7, 76.5 Hz) ppm was observed by NMR spectroscopy. After continued heating to 65°C for 16h only marginally amounts of the starting material **146** could be detected (Figure 21).

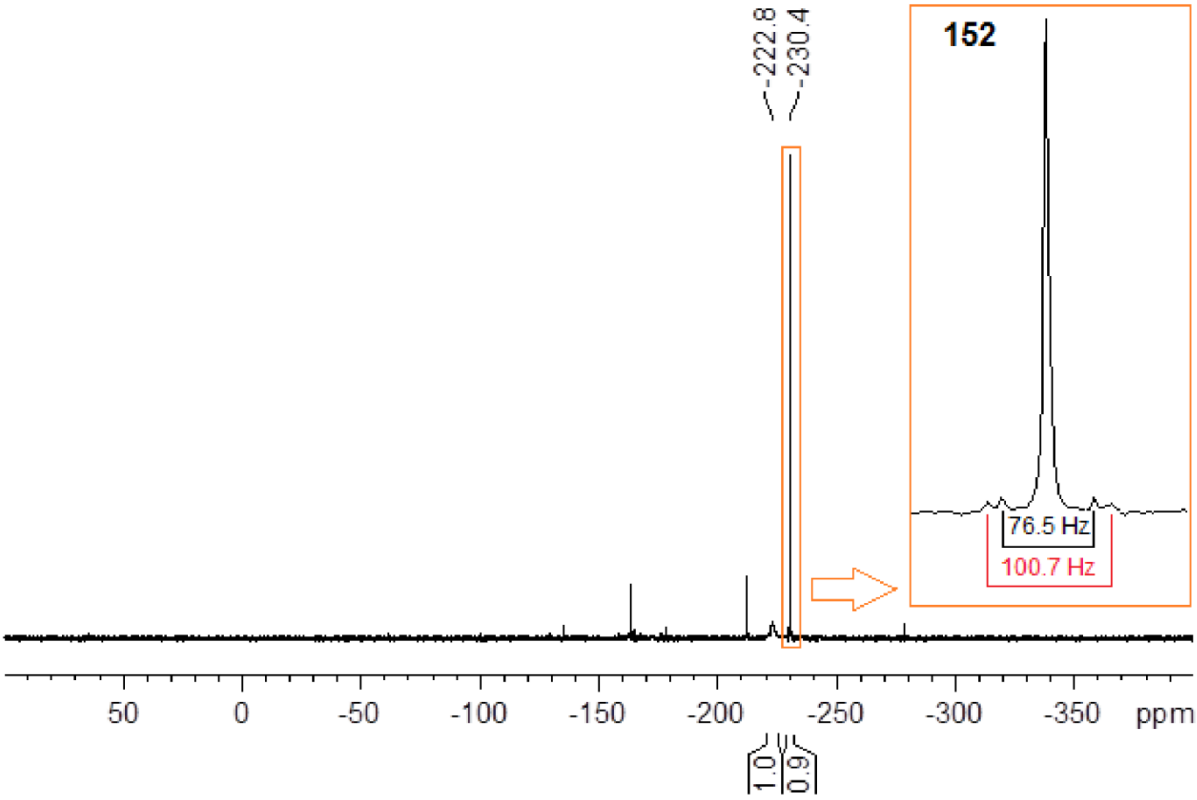

Figure 21. $^{31}P\{^{1}H\}$ NMR spectrum from the reaction of **146** with $CuBr{\cdot}SMe_2$ after 16h at 65°C; the resonance at −230.4 ppm (orange box) is assigned to **152**.

Four doublets were observed by ^{29}Si NMR spectroscopy at δ = −6.9 ($^{1}J_{P\text{-}Si}$ = 100.7 Hz), −6.8 ($^{1}J_{P\text{-}Si}$ = 27.5 Hz), −39.8 ($^{1}J_{P\text{-}Si}$ = 76.5 Hz) and -125.3 ($^{1}J_{P\text{-}Si}$ = 3.3 Hz) ppm. Additionally, two strongly broadened resonances appear at δ = −1.4 and −162.4 ppm and three sharp singlets at δ = −14.8, −18.3 and −26.8 ppm (Figure 22). The ^{29}Si signals at δ = −6.9, −39.8 and −125.3 and the ^{31}P resonance at δ = −230.4 ppm are consistent with a coordination of **146** to the copper center to afford **152**. Unfortunately, the mixture could not be separated by crystallization so no further assertions can be made concerning structural details of any of the products.

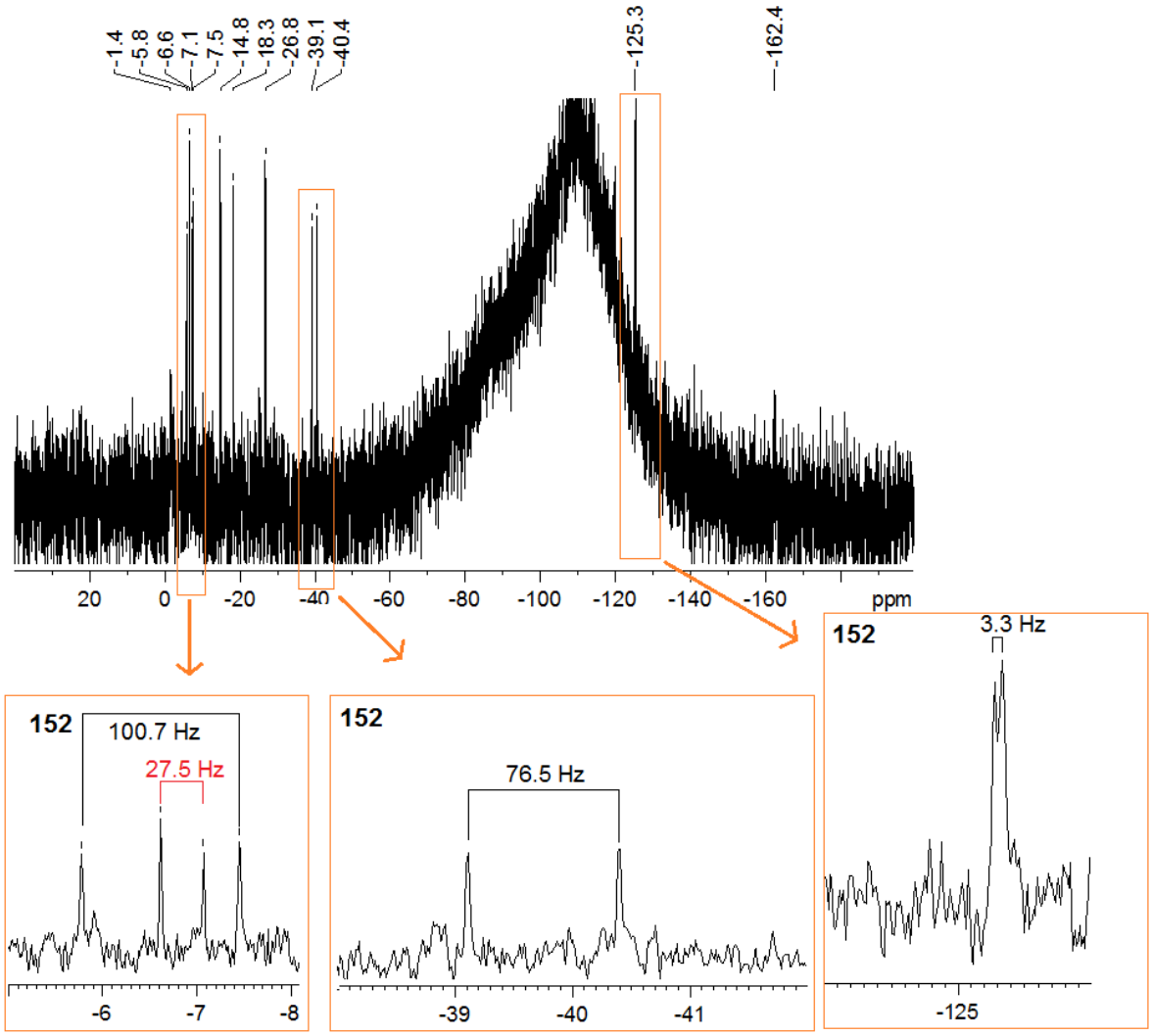

Figure 22. $^{29}Si\{^{1}H\}$ NMR spectrum from the reaction of **146** with $CuBr{\cdot}SMe_2$ after 16 h at 65°C; the resonances where the Si-P coupling constants are indicated with black brackets are assigned to **152**.

Finally, we considered the reaction of **146** with an excess of diiron nonacarbonyl in thf as source of the highly reactive $Fe(CO)_4$-fragment. After adding four equivalents $Fe_2(CO)_9$ to a solution of **146** in thf, the solution turned deep red. Indeed, quantitative conversion to the corresponding tetracarbonyl iron complex **153** was confirmed by multinuclear NMR spectroscopy (Scheme 74).

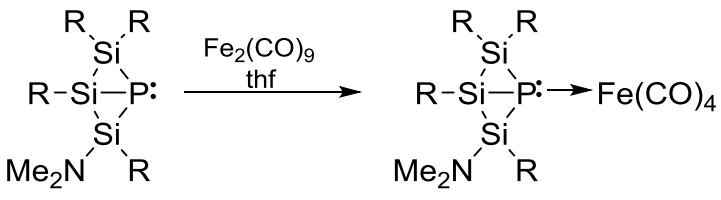

146 **153**

Scheme 74. Reaction of **146** with $Fe_2(CO)_9$ to afford **153** (R = Tip).

The resonance in the ^{31}P NMR spectrum of **153** is observed at –92.5 ppm and this upfield shift in comparison with **146** is consistent with the coordination of the phosphorus atom to the electropositive iron center. While the chemical shifts of the signals found in the ^{29}Si NMR spectrum at δ = −20.7 ($^{1}J_{Si\text{-}P}$ = 85.9 Hz), −68.8 ($^{1}J_{Si\text{-}P}$ = 37.4 Hz) and −118.2 ($^{1}J_{Si\text{-}P}$ = 45.8 Hz) ppm are similar to those of **146** and the assumed CuBr complex, significant changes are observed in the coupling pattern giving a first indication for alterations of the bonding situation in the bicyclic ligand upon coordination.

The strong increase in the $^{1}J_{P\text{-}Si}$ coupling constant to the bridgehead silicon atom suggests a significant strengthening of the transannular bond upon coordination. In the ^{13}C NMR of **153**, the downfield resonance at δ = 214.6 ppm with a characteristic phosphorus coupling[195] across the iron center ($^{2}J_{C\text{-}P}$ = 14.3 Hz) was assigned to the carbonyl ligands attached to the Fe-atom. Single crystals of **153** (M. p. 93°C, dec.) were obtained as orange blocks from a concentrated pentane solution (Figure 23) and an X-ray diffraction study expectedly revealed the iron center in a trigonal bipyramidal coordination sphere with an almost linear P-Fe-C66 axes (179.12(4)°). Presumably due to the steric congestion around the phosphorus atom, the P-Fe bond distance (2.3181(3) Å) is significantly larger than those reported for phosphane iron complexes (2.08-2.211 Å).[196] As already indicated by NMR spectroscopy, the bonding situation of the bicyclic ligand in **153** has considerably changed compared to free **146**. While the bridgehead bond is significantly shortened (**146**: 2.4273(8); **153**: Si2-P 2.3418(3) Å), the bond length between phosphorus and the amino substituted silicon atom is more than 0.15 Å longer (Si1-P 2.3764(3) Å).

A very broad and featureless shoulder was observed in the UV/vis absorption spectrum of **153** approximately from 450 to 300 nm (Figure 110).

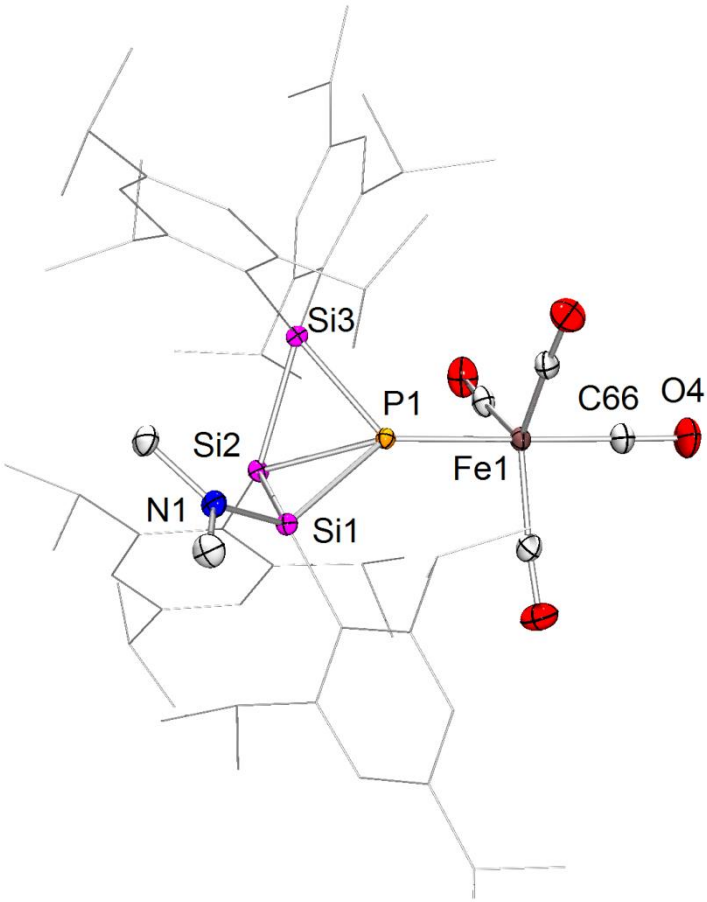

Figure 23. Molecular structure of **153** in the solid state (thermal ellipsoids at 50%, H atoms and disordered *i*Pr groups omitted). Selected bond lengths [Å] and angles [°]:Si1-P1 2.3764(3), Si2-P1 2.3418(3), Si3-P1 2.2609(3), Si1-Si22.2736(3), Si2-Si3 2.3447(3), Si1-N1 1.7079(7), P1-Fe1 2.3182(3), P1-Si1-Si2 60.432(10), Si1-Si2-Si3 96.446(11), P1-Si3-Si2 61.091(10).

Also for $Fe(CO)_4$-complex **153** the geometry of the slightly truncated model system **153-Dip** has been optimized at the B3LYP/6-31+G(d,p) level of theory (all DFT calculations in this chapter by Cem B. Yildiz, Aksaray University, Turkey). The calculated ^{29}Si chemical shifts (δ = −20.2, −72.0 and −125.7) are in good agreement with the experimental findings. The calculated ^{31}P NMR chemical shift of δ = −66.9 ppm is in satisfactory agreement with the experimental value (δ = −92.5 ppm) and confirms the trend of a certain deshielding of the phosphorus nucleus upon coordination. The strengthening of the Si1-P bond is reflected in an increased WBI for the computational model **153-Dip** (WBI = 0.933) compared to **146-Dip** (0.821). On the other hand, the Si2-P bond of **153**-**Dip** has a stronger covalent bonding interaction (WBI = 0.860) than that of **146**-**Dip.**

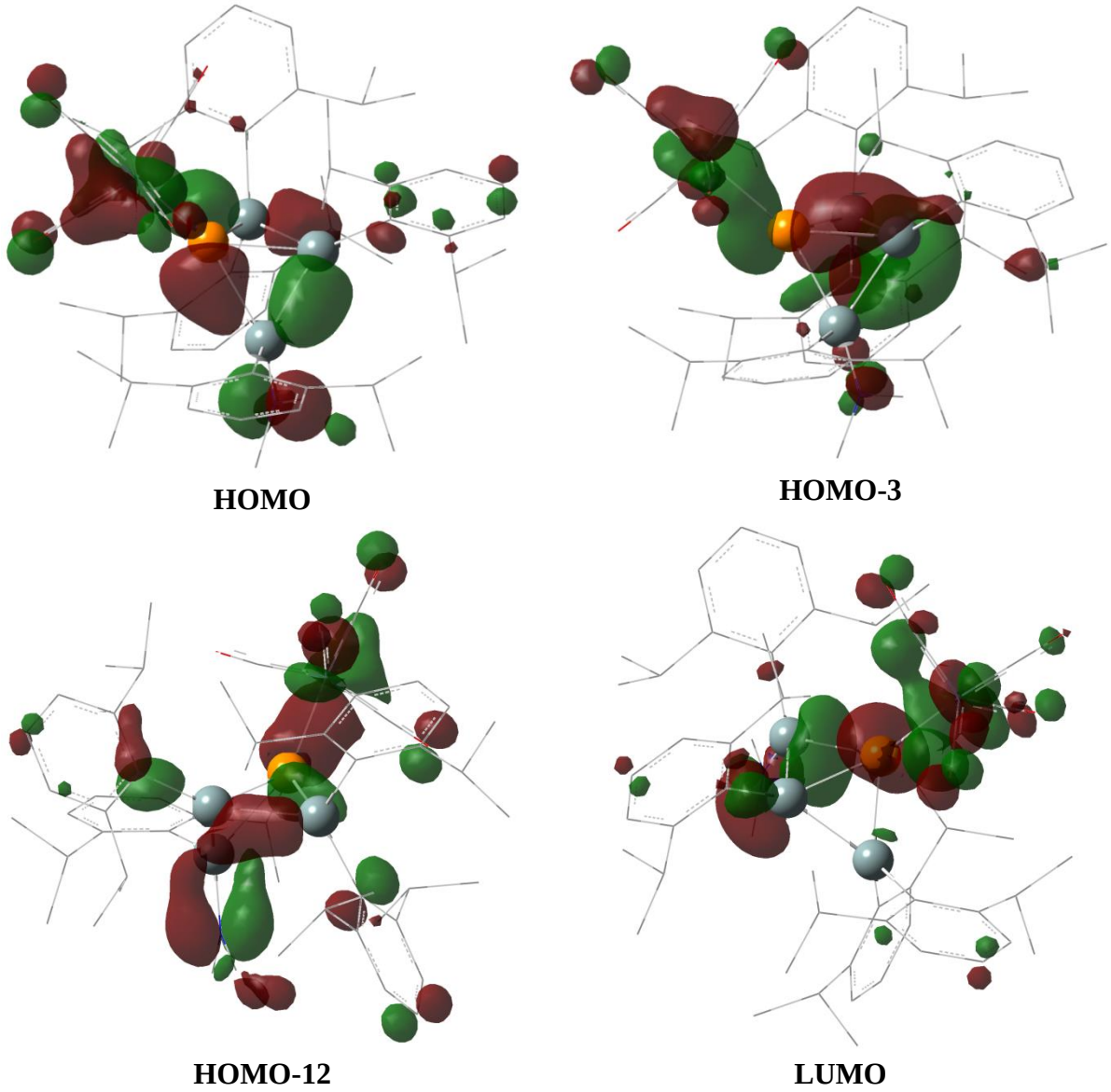

Figure 24. Frontier molecular orbitals of model **153**-Dip at an *iso*density *value* of 0.035 au; figures courtesy of Cem B. Yildiz, Aksaray University, Turkey.

According to frontier molecular orbital calculations of **153-Dip** the strengthening of the bridgehead bond is mainly due to a constructive interaction of the iron center along the bridgehead Si-P vector in the HOMO−3. The HOMO is primarily populated on the Si-Si and Si-P σ bonds in **153**-**Dip**. The Si1-N1 bonding can be seen from HOMO-12. Furthermore, the lowest unoccupied MO (LUMO) of **153-Dip** is a mixture of the σ* orbital of Si-Si and Si-P bonds (Figure 24)

The absorption spectrum was predicted using the optimized geometry at time-dependent density functional theory (TD-DFT) method in and is in good agreement

with the experimental findings (Figure 111). A broad shoulder is observed between λ = 450 and 250 nm (highest intensity at λ = 303 nm).

The σ-donor strength of ligands in metal carbonyl complexes can be estimated by IR spectroscopy. Stronger σ-donation causes increased backbonding of the metal into CO antibonding orbitals and thus smaller stretching frequencies observed for the carbonyl ligands. In the IR spectrum, the carbonyl stretching bands of **153** are observed at ν = 2036, 1959, 1941, 1926 cm^{-1} (Figure 25). Apparently, **153** indeed is a somewhat stronger σ-donor than common phosphanes and donating with a similar strength as for instance the N-heterocyclic carbene NHC^{Dip} ($NHC^{Dip}Fe(CO)_4$: σ = 2035, 1947, 1928, 1919 cm^{-1}) (NHC^{Dip} = C{N(Ar)CH}$_2$, Ar = 2,6-diisopropylphenyl).[197]

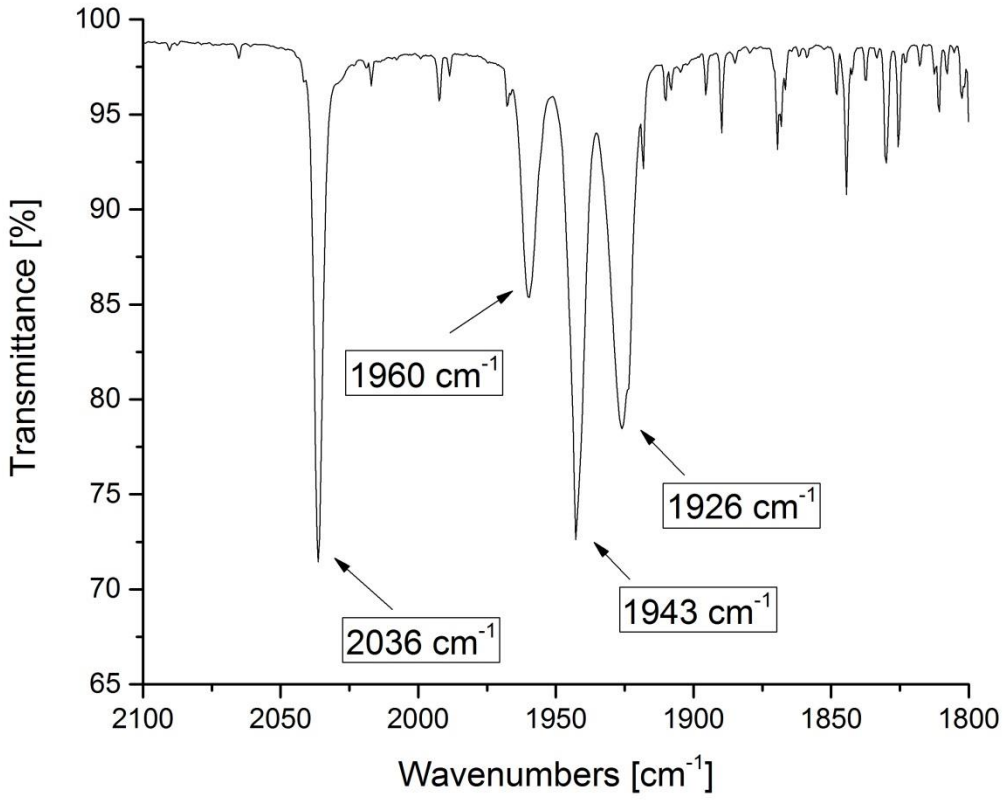

Figure 25. IR spectrum of **153**.

3.1.2.5. Synthesis of Disilaphosphiranide 155a

From the reaction of disilenide **16** with **108a** in toluene at 65°C we isolated trisilaphospha[1.1.0]bicyclobutane **146**. The formation mechanism of **146** plausibly proceeds *via* the initial substitution product **[145]**, even though it could not be observed by NMR spectroscopy. We anticipated that a more polar solvent could facilitate the initial substitution reaction of **16** with **108a** to occur under milder reaction conditions and thus allow for the detection of **[145]** by NMR spectroscopy.

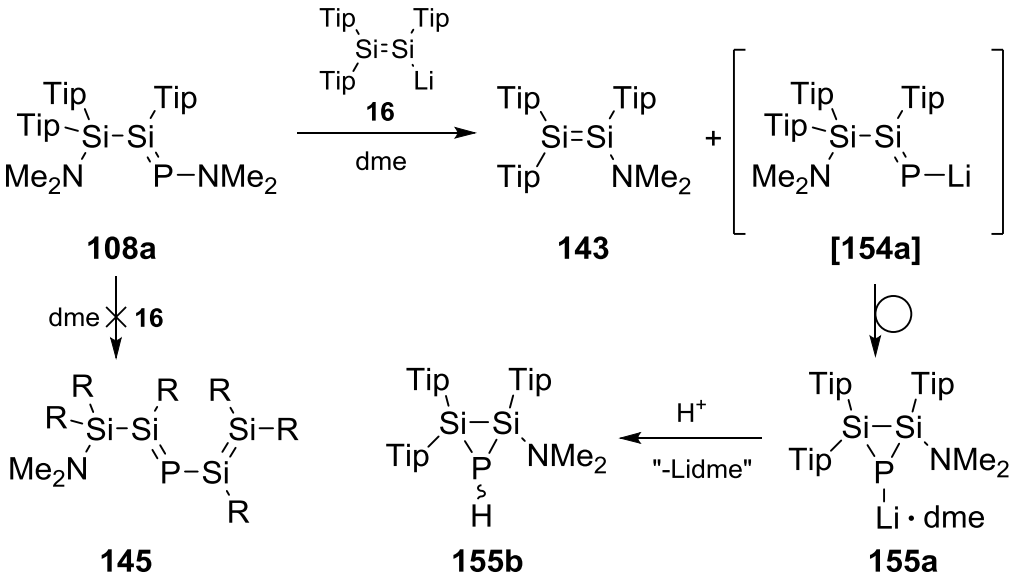

Scheme 75. Synthesis of disilaphosphiranide **155a** with proposed intermediacy of **[155a]** and plausible by-product **143**, protonation of **155a** to disilaphosphirane **155b**.

Disilenide **16** was combined with **108a** in dme at room temperature and an immediate color change from orange to deep red was observed. The ^{31}P NMR spectrum in dme of the reaction mixture revealed uniform formation of a new product showing a sharp resonance at δ = −245.9 ppm. After two days at rt, the reaction is complete according to ^{31}P NMR spectroscopy (Figure 26). Notably, the phosphorus nucleus in the product is even more shielded than that of **146** (δ = −212.3 ppm) ruling out the presence of an unsaturated phosphorus atom. In the ^{31}P NMR spectrum in benzene a broad resonance at similar field (δ = −248.0 ppm) is found as main signal. The broadening of the ^{31}P NMR resonance could be attributed to the formation of a contact ion pair of a phosphide anion to a quadrupolar ^{7}Li nucleus in various coordination environments. Indeed, the ^{7}Li NMR spectrum reveals a broad resonance at −0.19 ppm. As a consequence, the sharp signal in dme could be explained by the exclusive presence of the solvent separated ion pair. This was confirmed by adding

an excess of dme to the sample in C_6D_6 which indeed leads to a significant sharpening of the resonance (Figure 26).

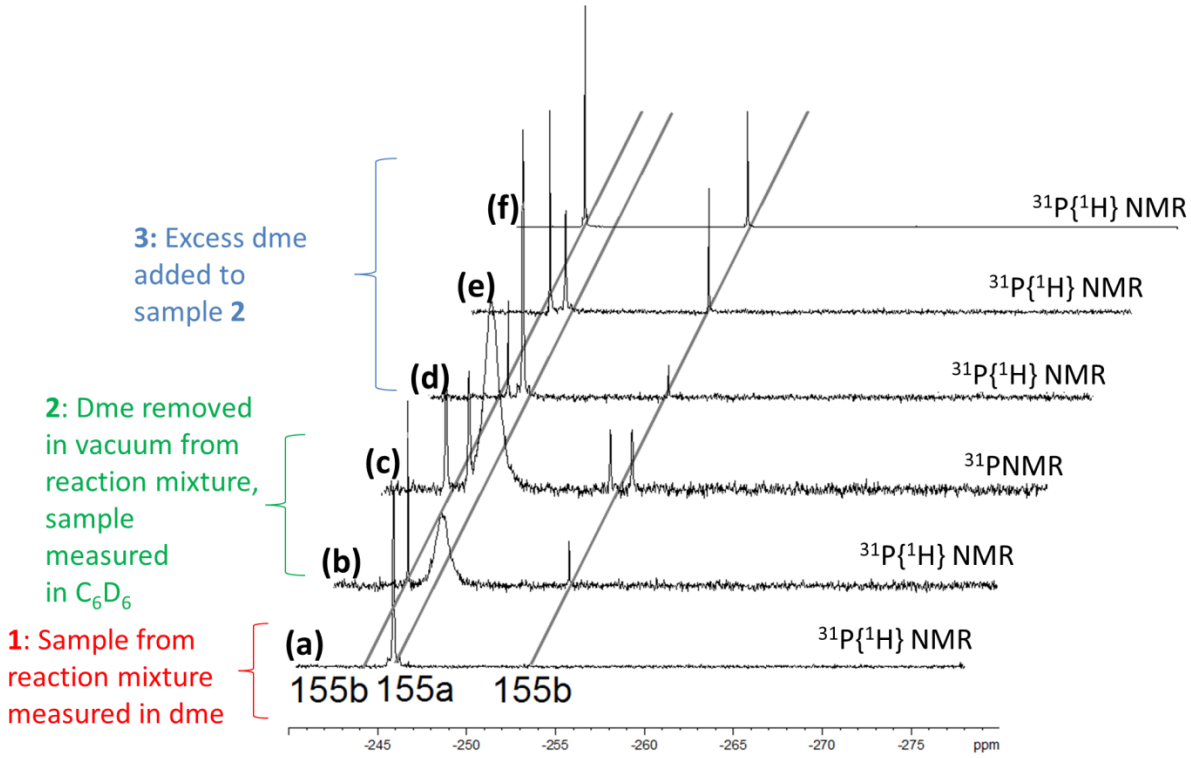

Figure 26. Stacked plot of $^{31}P\{^1H\}$ NMR/^{31}P NMR spectra from the reaction of disilenide **16** with phosphasilene **108a**; (a): sample from reaction mixture recorded in dme; (b): dme removed in vacuum, recorded in C_6D_6; (c): same sample, proton coupled, measured in C_6D_6; (d): same sample, 0.2 mL dme added; (e): same sample, one week at rt; (f): sample after three weeks at rt.

In the $^{31}P\{^1H\}$ NMR spectrum in C_6D_6, two signals of minor intensity appear at δ = −246.1 (10%) and −252.2 (4%) ppm (Figure 26). While the main resonance remains unchanged in the proton-coupled ^{31}P NMR, the two minor signals are split into doublets ($^1J_{P\text{-}H}$ = 157.1 and 145.7 Hz) proving beyond doubt the presence of a P-H unit (Figure 26). Apparently, during work-up of the reaction mixture an initially formed phosphide product is partially protonated, presumably upon the removal of dme in vacuum. After leaving the sample containing the product mixture from the reaction of **16** with **108a** with an excess dme at room temperature for one week, it indeed showed significantly larger amounts of the protonated products (36% and 19%, Figure 26). In the ^{29}Si NMR spectrum of the reaction mixture after drying two broadened doublets are observed at δ = −33.8 and −68.1 ppm showing relatively small coupling constants ($^1J_{P\text{-}Si}$ = 74.2 Hz and $^1J_{P\text{-}Si}$ = 67.4 Hz), which is indeed in accordance with the formation of the disilaphosphiranide **155a** (Scheme 75). To date,

three Si_2P-ring systems have been reported.[177,178] The ^{29}Si NMR chemical shifts (−32.8 to –47.5 ppm) as well as the magnitude of the $^{1}J_{P\text{-}Si}$ coupling constants (36 - 70.5 Hz) are comparable to those of **156a**, as are the characteristic high-field shifts in the ^{31}P NMR spectrum (−241.4 to −325 ppm). As reported by Driess *et al.* the disilaphosphiranide **156a** is readily protonated to **156b**.[177] In their case, the anionic species **[156a]** could not be detected, let alone isolated and only **156b** was unambiguously characterized. The authors suggested coordinated thf as only reasonable proton source.

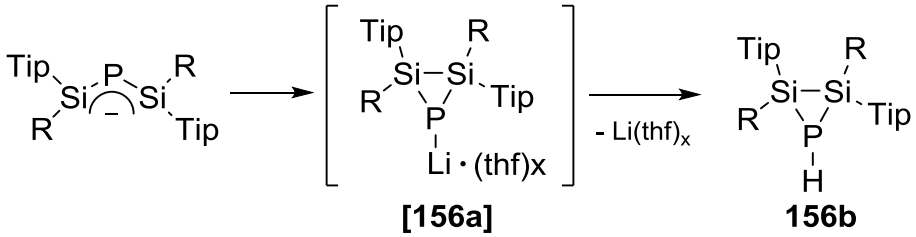

[156a] **156b**

Scheme 76. Driess´ synthesis of disilaphosphirane **156b** with proposed intermediacy of **156a** (R = ^{t}Bu).[178]

The formation of **155a** can only be explained by a lithium-amino group exchange which implies the concomitant formation of an amino-substituted disilene. Whereas the halogen-metal exchange is a textbook reaction,[198] an amino-metal exchange reaction is unknown, but in line with the apparent pronounced leaving group characteristics of the amino functionality of **108a**. Indeed, two additional signals at δ = 95.5 and 26.2 ppm are detected in the ^{29}Si NMR spectrum of the product mixture in accordance with dimethylamino-substituted disilene **143**. (Scheme 75) In case the reaction of **108a** with **16** is carried out in dme, the donor solvent presumably provokes a stronger separation of the lithium disilenide lone-pair and allows for the coordination of the phosphorus lone-pair to lithium. Subsequently the dimethyl amino group is transferred to the silylene-like silicon of **16** to afford amino-substituted disilene **143**. Mechanistically, the strong solvent effect on the reaction of **108a** with **16** could be explained by a stronger separation of the ion pair of lithium disilenide **16**, which should facilitate the coordination of the phosphorus lone-pair in phosphasilene **108a** to the lithium cation. The transfer of the dimethylamino group to the silylene-like silicon atom in **16** could occur *via* a four-membered transition state not unlike that of the classical metal-halogen exchange reaction (Scheme 77).

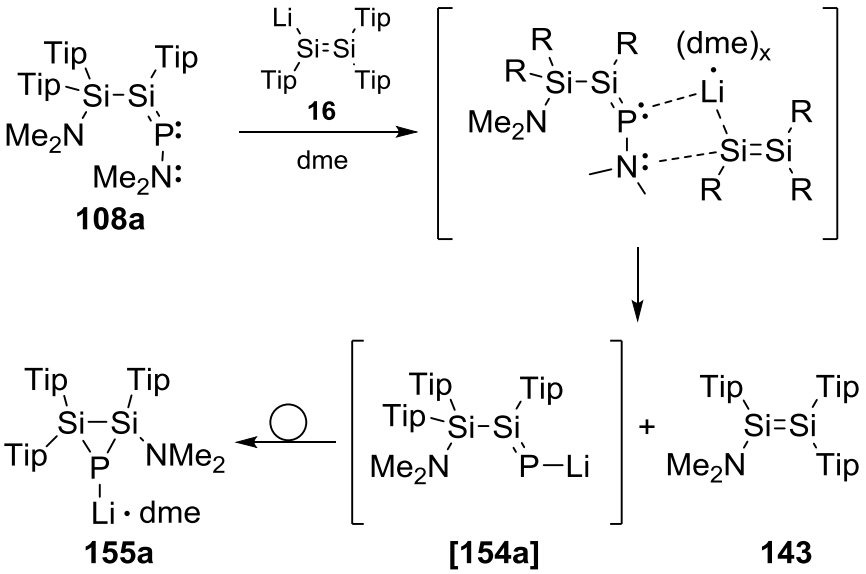

Scheme 77. Proposed mechanism for the formation of **143** and **155a** from the reaction of disilenide **16** with phosphasilene **108a** in dme (R = Tip).

Colorless crystals of **155a** (M. p. 151°C, dec.) suitable for X-ray diffraction analysis were obtained in 22% yield by crystallization from pentane.

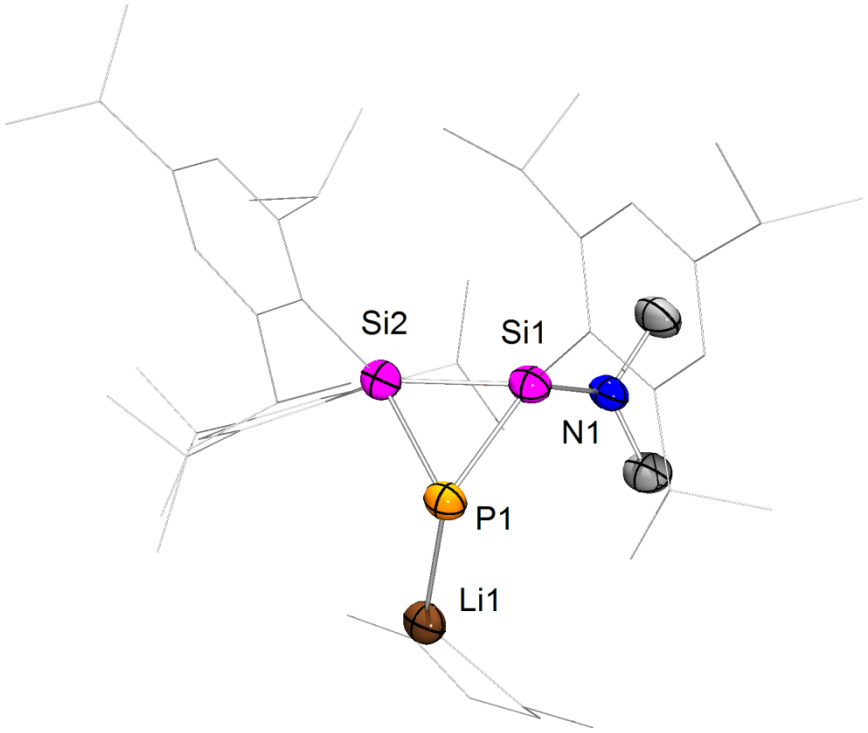

Figure 27. Molecular structure of **155a** in the solid state (thermal ellipsoids at 50%, H atoms and disordered ^{i}Pr groups omitted). Selected bond lengths [Å] and angles [°]: Si2-P1 2.2312(7), Si1-P1 2.1720(7) Si1-Si2 2.2958(7), Si1-N1 1.7405(15), P1-Li1 2.464(3), Si1-P1-Si2 62.84(2), P1-Si1-Si2 59.84(2), P1-Si2-Si1) 57.32(2).

The structure of **155a** in the solid state confirms the constitution as three-membered lithium disilaphospiranide (Figure 27).

Two molecules of **155a** form a dimeric species bridged by the lithium cations coordinated by one dme molecule each. Although Driess et al. have reported the solid state structure of an Si_2P-ring, their data was tainted by co-crystallized oxidation product and therefore the bonding parameters not discussed.[178] In **155a**, all endocyclic bonds are relatively short (Si1-Si2 2.2958(7) Å; Si1-P1 2.1720(7) Å; Si2-P1 2.2312(7) Å). For open chained disilyl phosphides shortened Si-P bonds (2.203-2.234 Å) have been reported which was attributed to additional electrostatic attractions between the negatively charged phosphorus and the positively polarized silicon atoms.[199] In the case of **155a**, however, the shortening is more likely due to back-donation by the anionic phosphorus into σ*-orbitals at silicon. Similar shortening had been observed for a homonuclear cyclotrisilanide.[84] Especially conspicuous is the shortening of the Si1-P1 bond in **155a**. The presence of the electronegative aminogroup at Si1 could facilitate backdonation of non-bonding electron density to Si1. Indeed, there is also some donation from the nitrogen lonepair as a certain degree of planarization is apparent for N1 (∑ of angles N1: 357.4°). The P1-Li1 bond distance (P1-Li1 2.464(3) Å) is at the short end of reported values for silylated lithium phsophides (2.449-2.642 Å) indicating a strong contact ion pair.[199]

Even though the single crystals obtained for **155a** were of good quality, it proved difficult to obtain NMR spectra completely free of impurities due to the high sensitivity of **155a** towards protonation (Scheme 75). However, the crystals grown at −25°C contained only small quantities of **155b** (7% and 2%) as determined by ^{31}P NMR (Figure 28). In the ^{29}Si NMR spectrum (Figure 29) **155a** is observed exclusively due to the lower natural abundance of ^{29}Si.

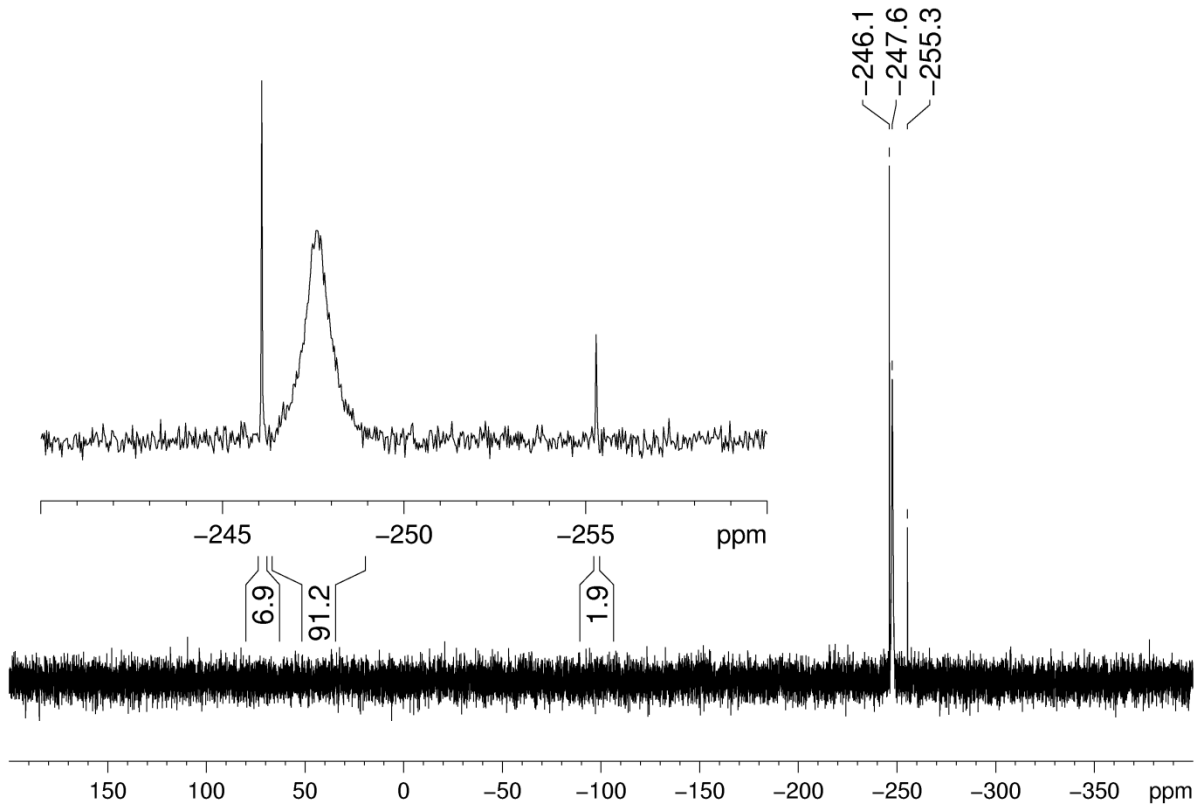

Figure 28. $^{31}P\{^{1}H\}$ NMR spectrum of disilaphosphiranide **155a** containing 9% of the protonated species **155b**.

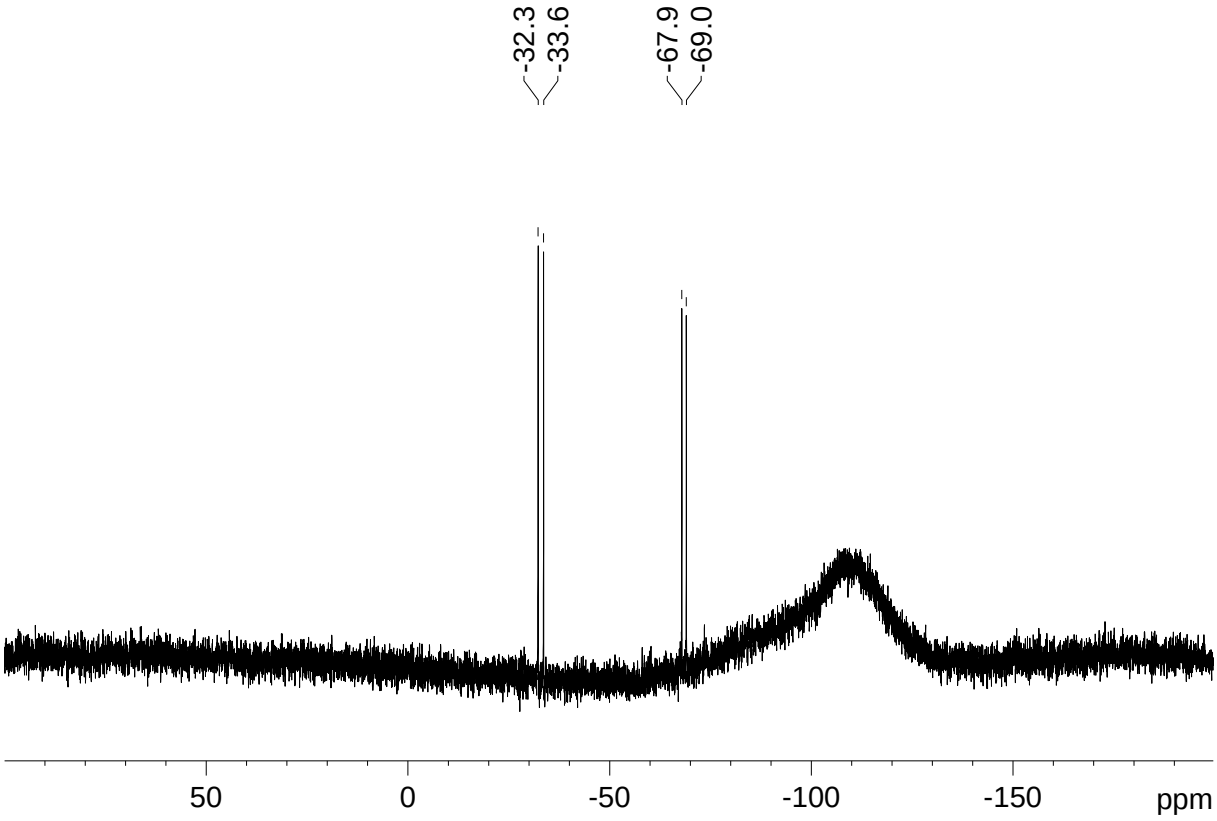

Figure 29. $^{29}Si\{^{1}H\}$ NMR spectrum of crude **155a**.

Single crystals of protonated **155b** could not be obtained yet, but after several weeks in a concentrated pentane solution complete conversion of **155a** to **155b** was achieved. In the ^{31}P NMR spectrum only two resonances at δ = −246.1 and −252.2 ppm in a ratio of 2:1 remain (Figure 26). The ^{29}Si NMR spectrum of this sample revealed two doublets at $\delta = -42.1$ ($^{1}J_{Si\text{-}P}$ = 30.9 Hz, Tip*Si*NMe$_2$) and −74.1 ($^{1}J_{Si\text{-}P}$ = 25.1 Hz, SiTip$_2$) for the major isomer and at $\delta = -35.9$ (d, $^{1}J_{Si\text{-}P}$ = 38.4 Hz, Tip*Si*NMe$_2$), −67.7 ($^{1}J_{Si\text{-}P}$ = 30.9 Hz, *Si*Tip$_2$) for the minor isomer (Figure 30). The amino functionalities of both isomers can be readily identified in the ^{1}H (2.61 and 2.39 ppm, ratio 1:2) and ^{13}C NMR spectra (40.6 and 40.4 ppm, ratio 1:2).

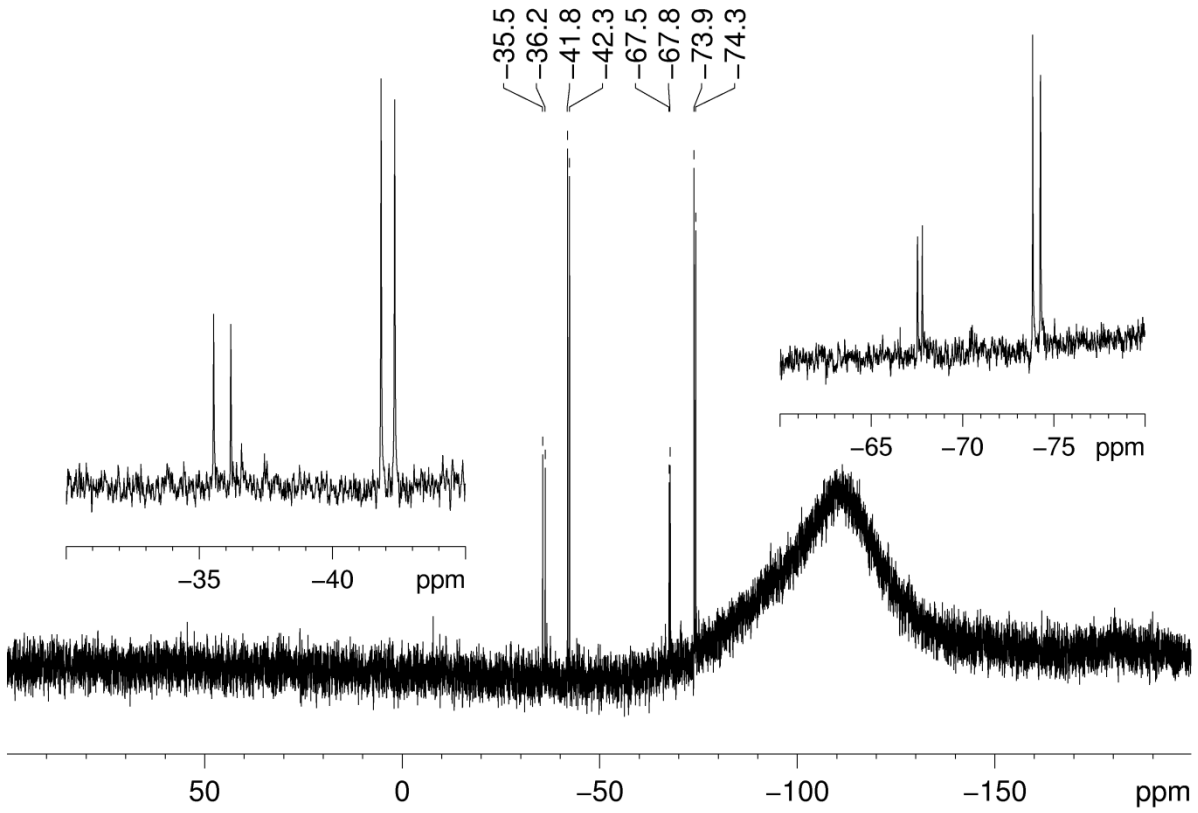

Figure 30. ^{29}Si{^{1}H} NMR spectrum of the two diastereomers of **155b**.

The mother liquor from the crystallization of **155a** contains amino-substituted disilene **143** in near spectroscopic purity. The relatively wide distribution of the ^{29}Si NMR resonances (Figure 31) is in accord with what has been reported for 1-amino-2-hydrodisilenes **55a-d** due to polarization of the double bond by the donor substituent.[101,103]

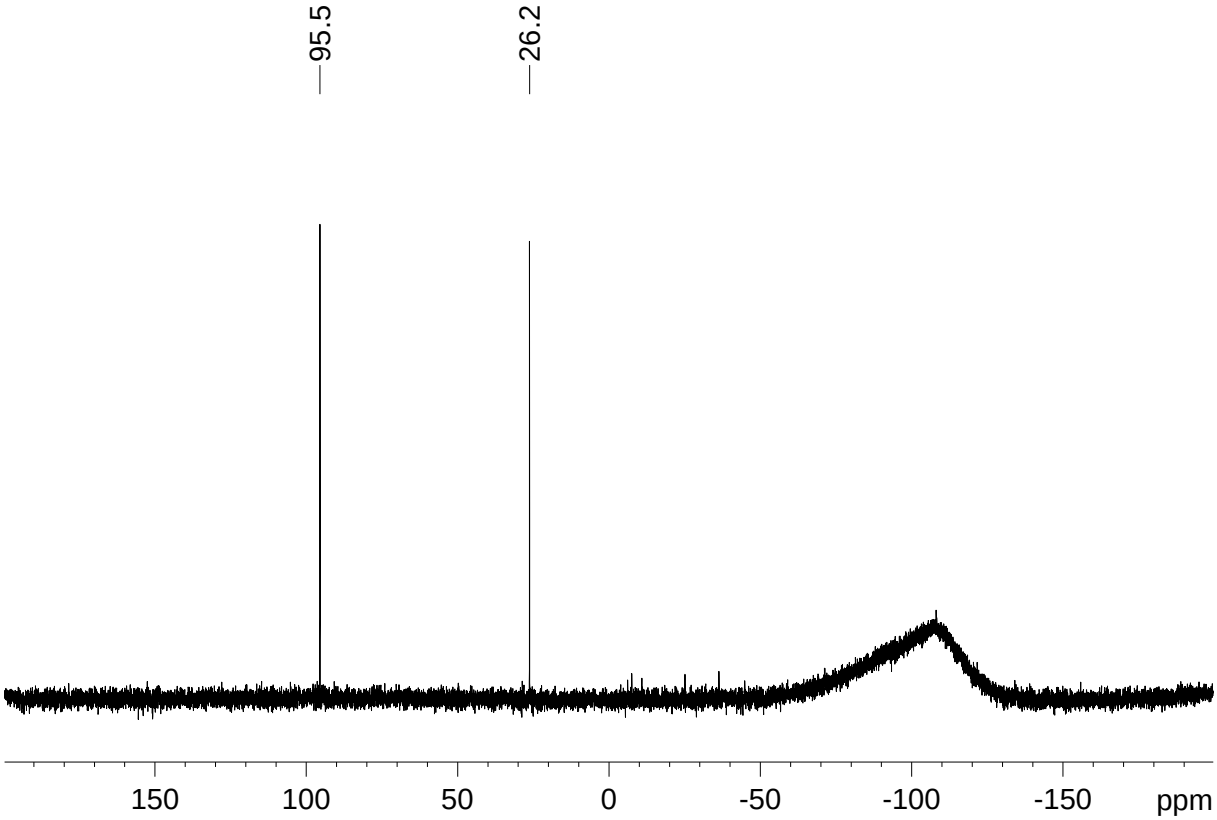

Figure 31. $^{29}Si\{^{1}H\}$ NMR spectrum of the motherliquor from the reaction of disilenide **16** with phosphasilene **108a** in dme.

The protons of the amino group are found at δ = 2.03 ppm in the ^{1}H NMR spectrum. The 2D Si-H correlation NMR spectrum shows cross peaks of this particular resonance to both unsaturated silicon atoms. The silicon atom directly attached to the amino functionality is positively polarized, which is in accordance with a more intense cross peak observed to the lowfield signal at δ = 95.5 (Figure 32).

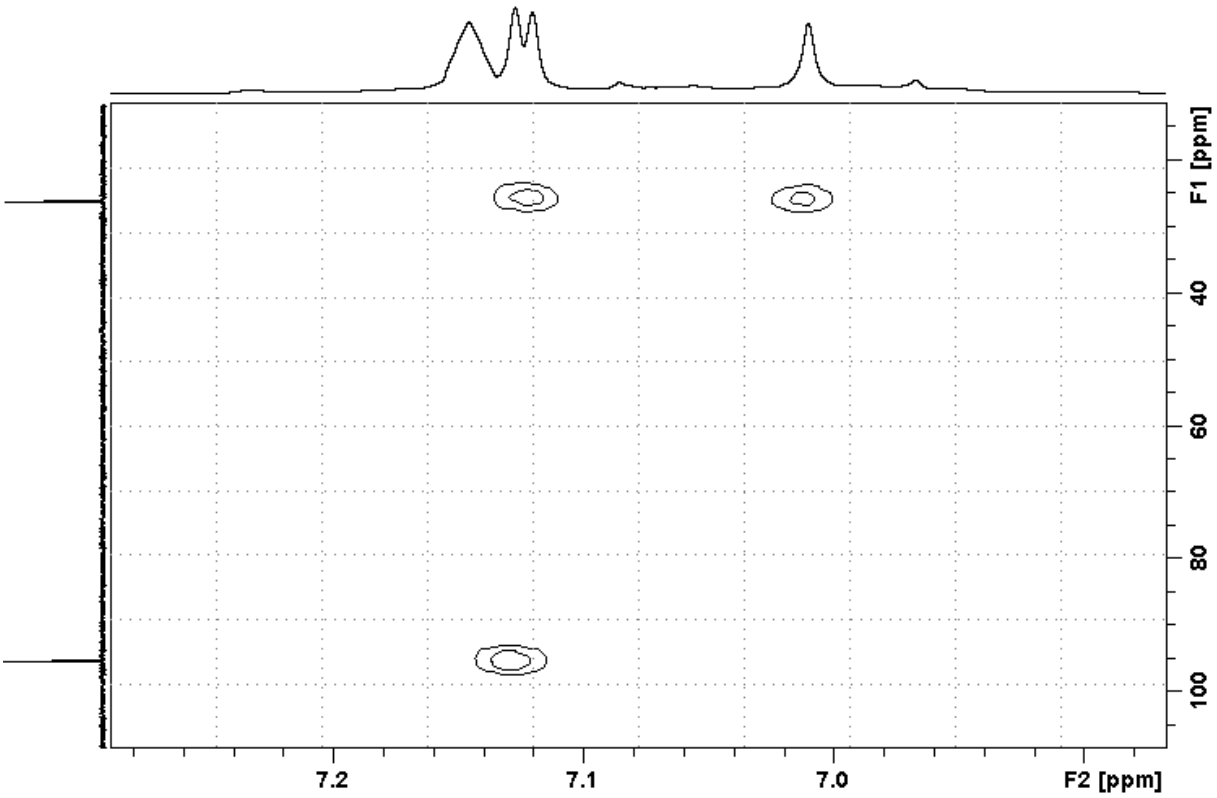

Figure 32. Selected area of the 2D ^{1}H-^{29}Si correlation NMR spectrum of amino disilene **143**.

As usual for disilenes of this type, three resonances appear in the ^{1}H NMR spectrum for the aromatic Tip-protons due to free rotation of the Tip-substituents. While the more shielded resonance shows equally intense cross peaks to two Tip-moieties, for the low-field resonance only one cross peak of comparable intensity is observed (Figure 32). Unfortunately, single crystalline material in order to finally confirm the constitution of **143** by an X-ray structure analysis was not obtained as yet.

In order to test their possible transient occurrence during the formation of bicycle **146** in a non-donor solvent, a mixture of **155a** and **143** in C_6D_6 was heated to 65°C for three hours (Scheme 78), but apart from a certain amount of protonation to **155b** no significant conversion was detected by NMR, ruling out the intermediacy of **155a** during the formation of **146** in toluene (Figure 33).

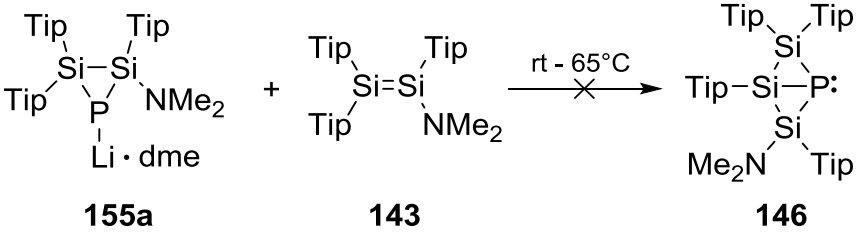

155a **143** **146**

Scheme 78. Attempted synthesis of **146** from disilaphosphiranide **155a** and amino disilene **143**.

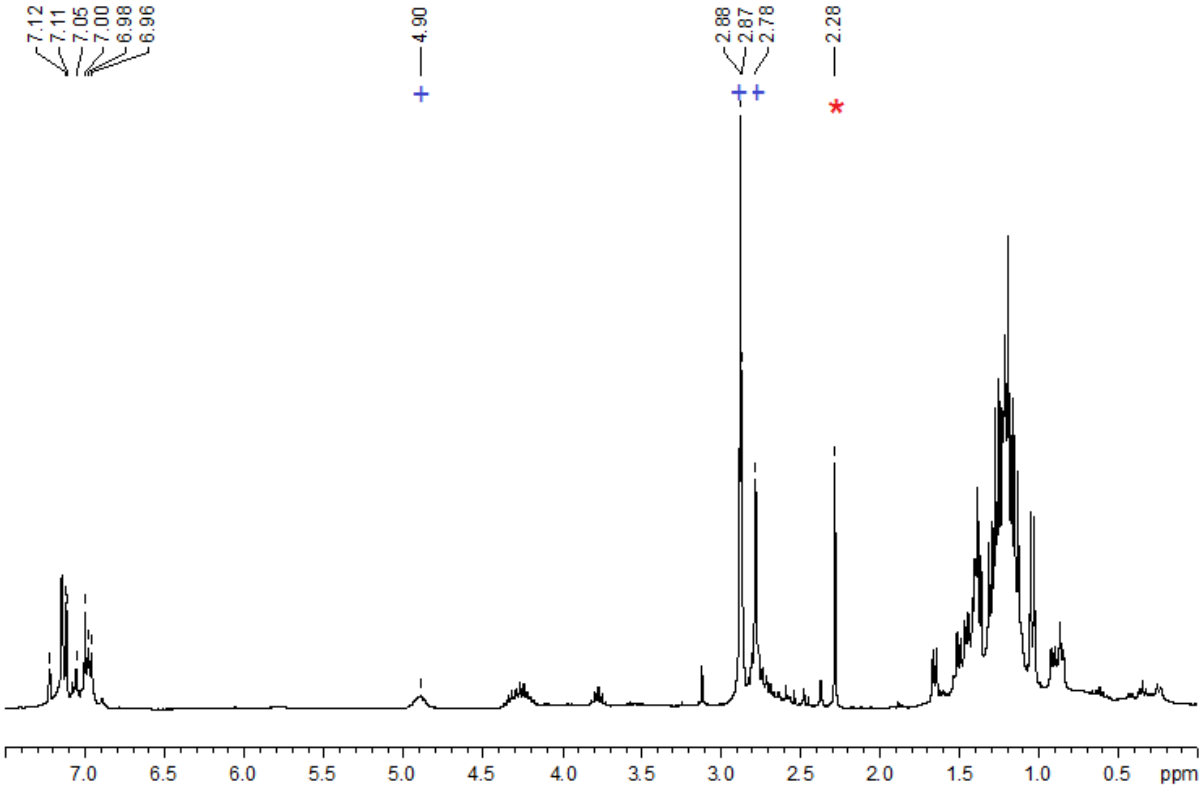

Figure 33. ^{1}H NMR spectrum of a mixture of disilaphosphiranide **155a** and amino disilene **143**(+ selected signals of **155a**, * selected signals of **143**).

With the isolation of **155a** the first distinct structural evidence for a Si_2P-three-membered ring was provided. Previously, a disilaphosphiranide had not even been observed by NMR spectroscopy, but was only proposed as highly reactive intermediate.[178] The anionic functionality of the Si_2P skeleton of **155a** should be interesting for further manipulations of the system, *e. g.* the derivatization with electrophiles. With the amino group, **155a** also contains a potential anionic leaving group, offering the principal possibility of conversion of **155a** into an unsaturated three-membered ring by elimination of $LiNMe_2$. As demonstrated in Chapter 2.1.2.2, lithium dimethylamide can indeed be eliminated under appropriate conditions.

3.1.2.6. Reduction Attempts of Phosphasilene 108a

In the preceding chapters, it was demonstrated that the amino functionality at phosphorus in **108a** exhibits a certain pseudo-halogenide behavior. The NMe_2-group can be substituted with nucleophiles under lithium dimethyl amide elimination and undergoes an unprecedented amino-metal exchange in the reaction of

phosphasilene **108a** with disilenide **16**. For halogenated species metal-exchange reactions are widely applied. Another benefit of halogen functionalities, especially in main group chemistry is that they can be cleaved with reducing agents (*cf.* Chapter 1). Investigations of the reactivity of phosphasilene **108a** towards reducing agents were thus considered the logical next step. To begin with, a more straightforward synthetic route to **155a** without concomitant formation of amino disilene **143** as by-product would be desirable. Furthermore, the second amino group located at the β-silicon atom of **108a** might act as a leaving group equally well. The reductive cleavage of both amino groups at phosphorus and silicon could provide a viable synthetic strategy to obtain the unsaturated heavier cyclopropene analogue **157** that would presumably dimerize to **158** (Scheme 79).

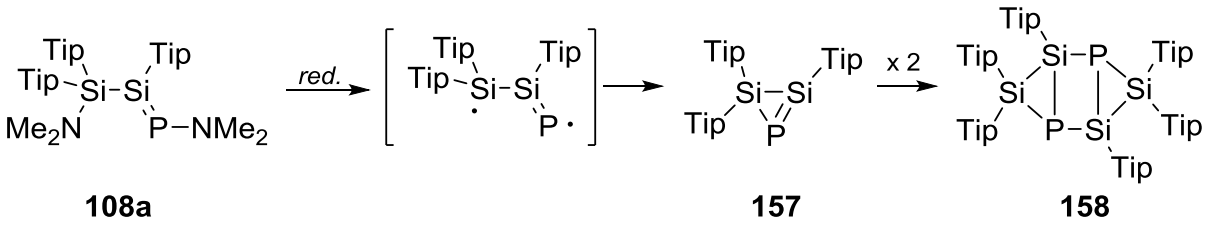

Scheme 79. Possible reaction pathway for the reduction of **108a** with two equivalents reducing agent.

In order to achieve complete reduction, phosphasilene **108a** was reacted with an excess of lithium powder at rt in dme. The reaction mixture spontaneously turns deep brown-red. The ^{31}P NMR spectrum shows several high-field resonances indicating a complex mixture. However, a small amount of orange single crystals grew from a concentrated pentane solution. An X-ray diffraction study revealed the structure of the 1,3-disila-2,4-diphosphabutadiene radical anion **159** (Scheme 80, Figure 34).

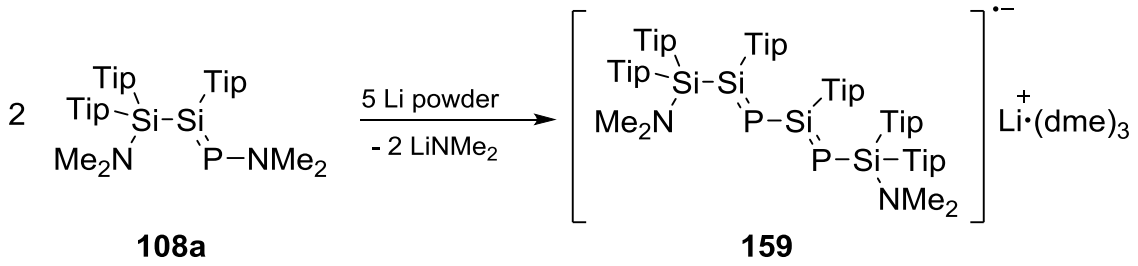

Scheme 80. Unreproducible synthesis of 1,3-disila-2,4-diphosphabutadiene radical anion **159**.

While for tetrasilabutadiene **17** a *cis*-arrangement was reported,[67] the radical anion **159** adopts a transoid structure. The lithium counter cation is fully sequestered by three dme molecules. On the one hand, the Si2-P2 double bond (2.128(5) Å) is only slightly longer than reported silicon-phosphorus double bonds (2.06 - 2.1114 Å).[109-117]

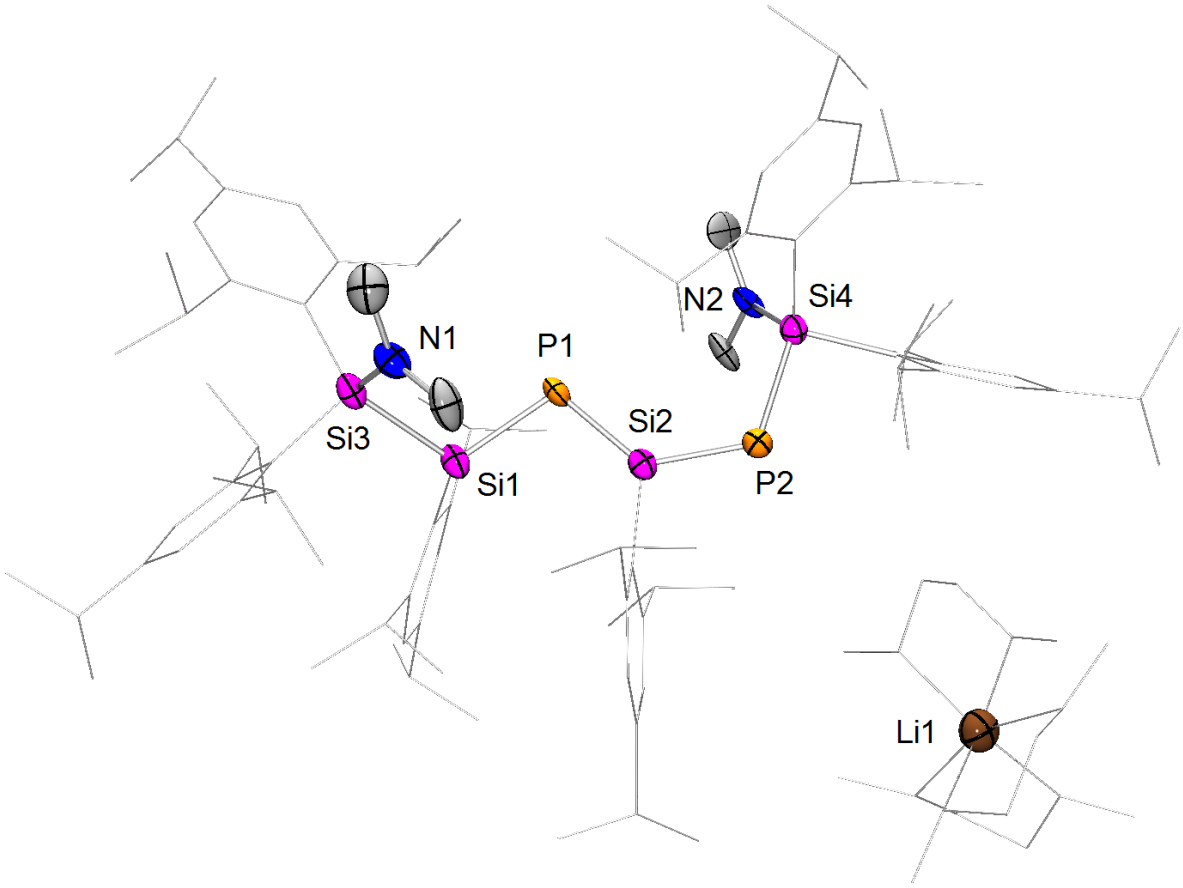

Figure 34. Molecular Structure of **159** in the solid state (thermal ellipsoids at 50%, H atoms and disordered ^{i}Pr groups omitted). Selected bond lengths [Å]: Si3-Si1 2.445(5), Si1-P1 2.227(5), P1-Si2 2.130(5), Si2-P2 2.128(5), P2-Si4 2.229(5), Si3-N1 1.739(11), Si4-N2 1.728(9).

On the other hand, the Si1-P1 bond length (2.227(5) Å) is close to what was reported for silicon-phosphorus single bonds (*e. g.* phosphino disilene **33c** 2.2367(12) Å).[81] Consequently, the Si2 atom is in perfectly planar geometry (Σ of angles Si2: 360.0°) while the Si1 atom is pyramidalized (Σ of angles S1: 347.2°). The central formal single bond length (P1-Si2 (2.130(5) Å) is close to what was found for Si2-P2 (2.128(5) Å), indicating efficient conjugation of the double bonds. A reason for the allegedly lower bond order of the Si1=P1 bond might be due to higher spin density in the π* orbital at Si1 and P1. The dihedral angle Si3-Si1-P1-Si2 is with 45.1(2)°

significantly wider than P1-Si2-P2-Si4 (7.2(2)°) lending further support to this assumption. In order to clarify this question EPR spectroscopic studies would have been desirable, which, however, were impossible due to a lack of material.

The mechanism for the formation of **159** remains unclear at present. Importantly, the amino group at phosphorus in phosphasilene **108a** was obviously cleaved reductively prior to an additional one electron reduction event. During the synthesis of disilaphosphiranide **155a** from **108a** and disilenide **16**, **155a** and **108a** exist simultaneously in solution under similar conditions. Consequently, an initial reaction of **108a** with **155a** during the formation of radical monoanion **159** is ruled out (Scheme 81). Presumably, an intermediate *P*-lithio phosphasilene **154a** initially reacts with **108a** under substitution. Following, a rearrangement under alteration of the Si-P sequence occurs either prior or subsequent to the additional reduction step.

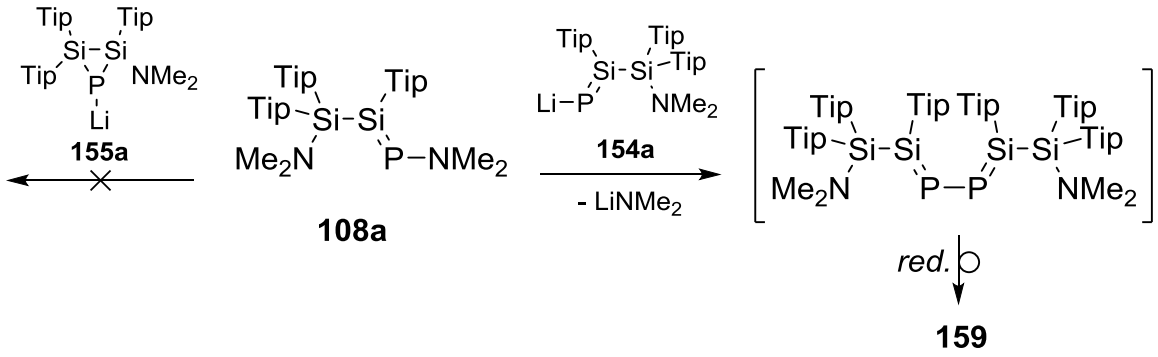

Scheme 81. Proposed mechanism for the formation of radical monoanion **159**.

Unfortunately all attempts to reproduce the synthesis of the radical monoanion **159** for full characterization were unsuccessful. Upon repeating the reaction different complex mixtures were obtained from which **159** could not be isolated. Repetition with exactly two equivalents of lithium powder at low temperatures equally afforded mixtures according to NMR spectroscopy. Curiously, one attempt under these conditions led to the isolation of a different product as single crystalline material from a concentrated pentane solution at room temperature. The X-ray diffraction study revealed the unexpected constitution of the four-membered diphosphide **160** (Scheme 82, Figure 35).

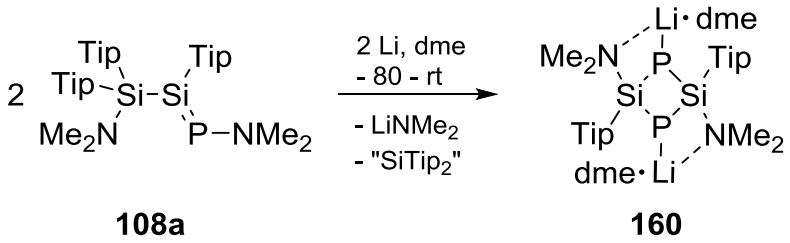

108a **160**

Scheme 82. Unreproducible synthesis of diphosphide **160.**

Once again, the amino functionality at phosphorus is cleaved reductively. The dilithio salt **160** is the formal [2+2]-head-to-tail addition product of a *P*-lithio phosphasilene, formally derived by the elimination of a "$SiTip_2$" unit in the course of the reaction.

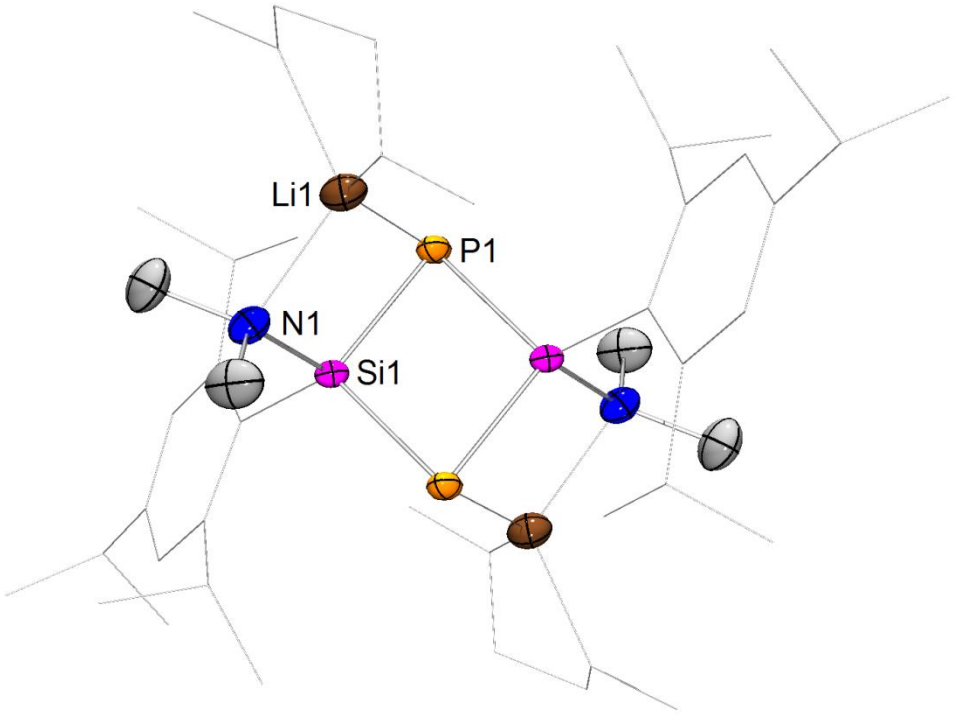

Figure 35. Molecular Structure of **160** in the solid state (thermal ellipsoids at 50%, H atoms and disordered ^{i}Pr groups omitted). Selected bond lengths [Å]: Si1-P1 2.2124(5) Å, N1-Si1 1.8112(13), P1-Li1 2.524(3), N1-Li1 2.095(3).

The lithium countercations of **160** are coordinated to the phosphide units, the amino groups are attached to the adjacent silicon atoms in *trans*-fashion. The Si1-P1 bond length (2.2124(5) Å) is slightly shortened and thus comparable to what was found for cyclic silyl phosphide **156a** (2.226 and 2.173 Å). As in the case of **156a**, this shortening could be attributed to electrostatic attractions between the phosphide unit and the silicon atom,[199] but is more likely a consequence of back-donation from the anionic phosphorus to σ*-orbitals at silicon (*cf*. Chapter 3.1.2.5, disilaphosphiranide

155a). Both anionic species, **159** and **160**, represent highly functionalized silicon-phosphorus compounds with a large synthetic potential, but unfortunately a preparative access is at present not available. The isolation of these compounds, however, suggested further investigations concerning the reduction of **108a** under different conditions. Lithium powder in dme may be too harsh a reducing agent and therefore milder reductive conditions were considered. Neither exposure of **108a** to lithium granules nor to lithium powder in any other solvent than dme led to appreciable conversion, not even at elevated temperatures.

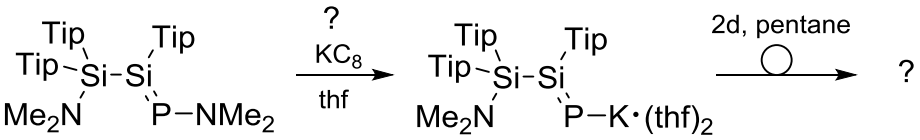

108a **154b**

Scheme 83. Proposed reactivity of phosphasilene **108a** towards potassium graphite.

In contrast, when phosphasilene **108a** is treated with two equivalents of potassium graphite (Scheme 83) the yellow solution turns red immediately and the formation of a black precipitate, presumably graphite, is observed.

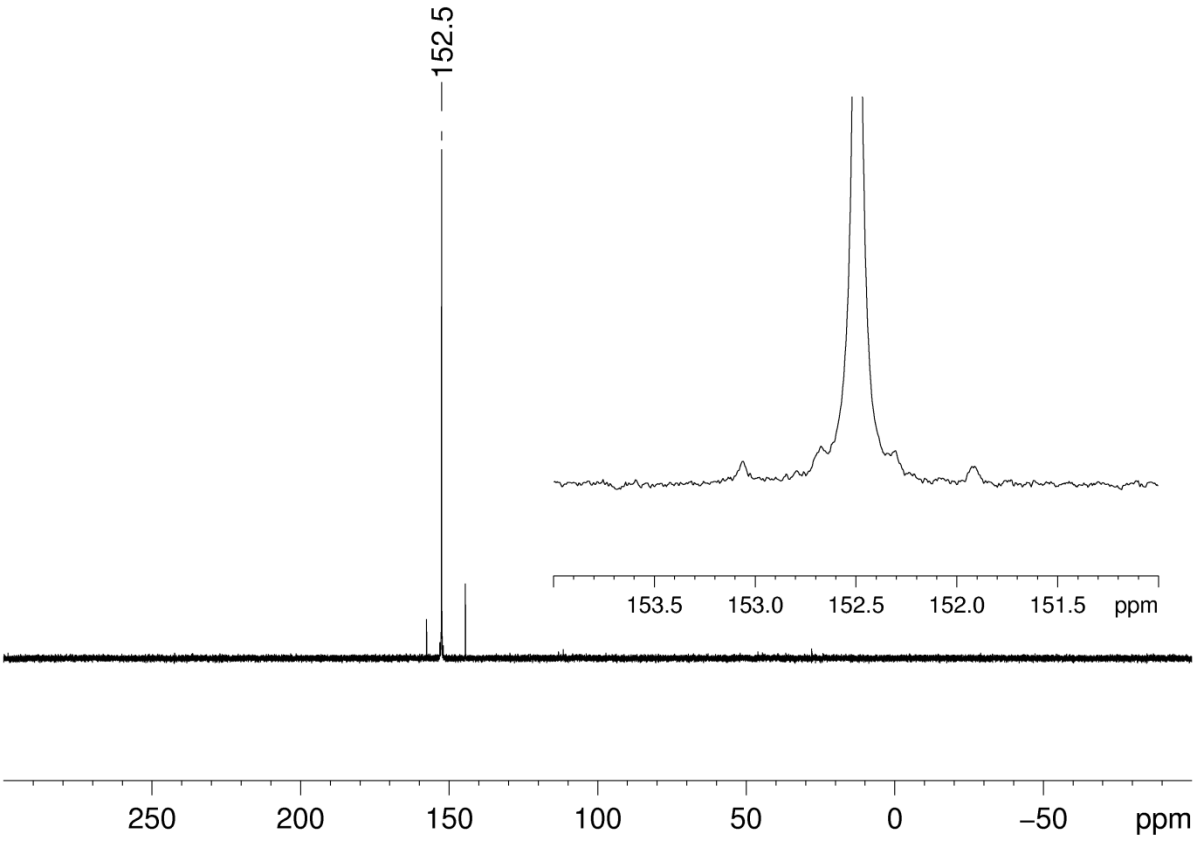

Figure 36. $^{31}P\{^{1}H\}$ NMR spectrum from the reaction of **108a** with two equivalents potassium graphite.

In contrast, two doublets in the ^{29}Si NMR appear at comparatively high field (δ = 1.1 ($^{2}J_{P\text{-}Si}$ = 44.7 Hz) and −56.2 ($^{1}J_{P\text{-}Si}$ = 139.8 Hz) ppm), thus reiterating the coupling constants derived from the ^{31}P NMR spectrum (Figure 37). In addition, an equally intense singlet at δ = −25.1 ppm is observed. Due to the absence of phosphorus coupling the latter signal is tentatively attributed to an unidentified side product. Strongly shielded ^{29}Si signals in Si-P doubly bonded compounds are not entirely unusual, but typically observed between 80 and 200 ppm.[104-117] Based on the ^{31}P NMR signal at low field and the large ^{29}Si-^{31}P coupling constant – that indicates a high s-character of the silicon-phosphorus bond – we nonetheless tentatively suggest the constituton of *P*-potassio phosphasilene **154b** for the major product of this reaction (Scheme 83).

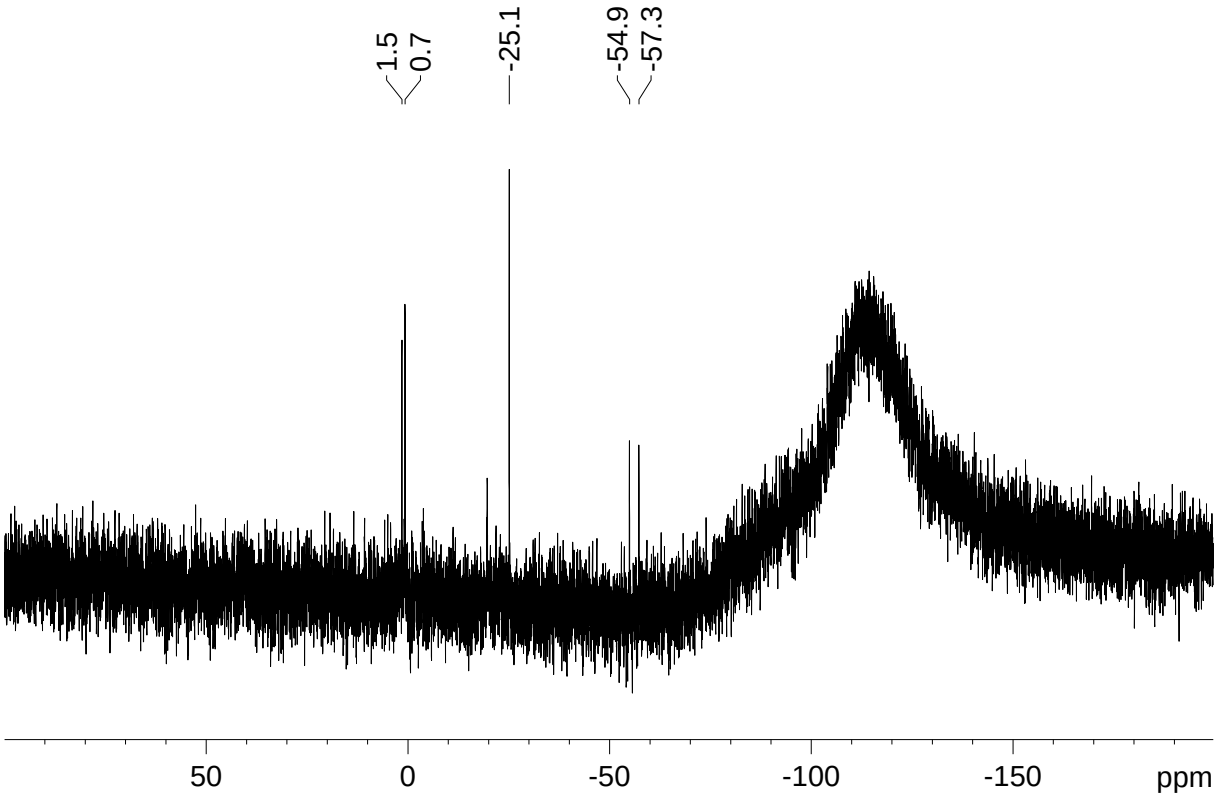

Figure 37. ^{29}Si{^{1}H} NMR spectrum from the reaction of **108a** with two equivalents potassium graphite.

A phosphasilene with an alkaline metal substituent at phosphorus has not been reported to date. The *P*-lithio substituted **154a** phosphasilene was proposed as undetected intermediate during the synthesis of **156a** (*cf.* Chapter 3.1.2.5); a *P*-potassio substituted derivative **154b** may well be sufficiently stable for isolation. As for the unusually shielded ^{29}Si NMR signals, it cannot be excluded that a strongly

electropositive substituent at phosphorus results in the localization of negative charge at silicon and thus pronounced pyramidalization. It should be mentioned, however, that *P*-metalla phosphasilenes typically show ^{29}Si NMR resonances at much lower field (*cf.* Chapter 1.1.5.3).[116,117]

The presence of coordinated thf in the molecule is proven by broad signals at 3.63 and 1.78 ppm in the ^{1}H NMR spectrum. Further support for the proposed constitution of **154b** is derived from the absence of P-coupling in the signal of the one remaining dimethylamino group at 2.63 ppm. Careful comparison of the phosphorus-coupled and decoupled ^{1}H NMR of the product gave no indications for any protons with phosphorus coupling.

While the initial product from the reaction of phosphasilene **108a** with potassium graphite is stable in thf, the compound undergoes a uniform rearrangement in apolar solvents. Even though neither a significant change in color nor formation of precipitate was observed, the ^{31}P NMR spectrum after three days in pentane revealed a new resonance at δ = 106.9 ($^{1}J_{P\text{-}Si}$ = 74.6 Hz, $^{1\text{ or }2}J_{P\text{-}Si}$ = 33.0 Hz) ppm (Figure 38).

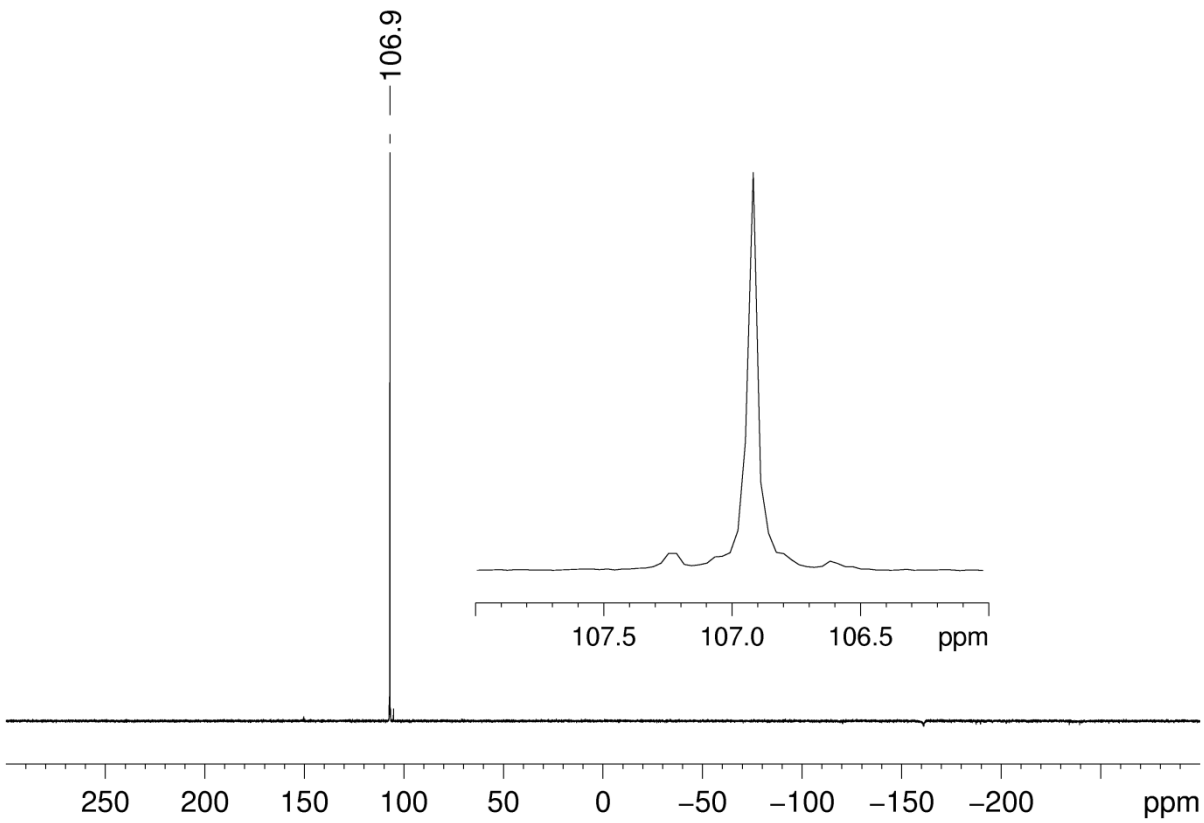

Figure 38. ^{31}P{^{1}H} NMR spectrum from the reaction of **108a** with two equivalents potassium graphite after the initial product was kept in pentane for three days.

The ^{29}Si NMR spectrum of the rearrangement product (Figure 39) shows two doublets at δ = −8.3 ($^{1\text{ or }2}J_{P\text{-}Si}$ = 33.0 Hz) and −59.5 ($^{1}J_{P\text{-}Si}$ = 74.6 Hz) ppm. The singlet at δ = −8.3 ppm remains unchanged providing corroboration for the assertion that it is due to an unrelated side-product. While the ^{31}P NMR chemical shift of the rearranged product is still compatible with a Si=P bond, the decrease in the size of the coupling constants (initial product: $^{1}J_{P\text{-}Si}$ = 139.8 Hz and $^{2}J_{P\text{-}Si}$ = 44.7 Hz), especially the ^{1}J-coupling (ΔJ = 65.2 Hz) is remarkable and hints towards a cyclisation step. Notably, as confirmed by recording phosphorus coupled and decoupled spectra, two resonances in the ^{1}H NMR spectrum in the typical range for dimethylamino groups at δ = 2.57 and 2.41 ppm (ratio 1:1) now do show coupling to a phosphorus nucleus. The size of the coupling constants ($^{3}J_{P\text{-}H}$ = 9.4 and 9.6 Hz) is in line with reported $^{3}J_{P\text{-}H}$ coupling constants. Furthermore, the intensity of each signal is roughly in accord with three methyl protons. Presumably, a shift of the NMe_2-functionality from silicon to phosphorus takes place during the rearrangement and both methyl groups are chemically inequivalent. These finding are further support by ^{13}C NMR spectroscopy.

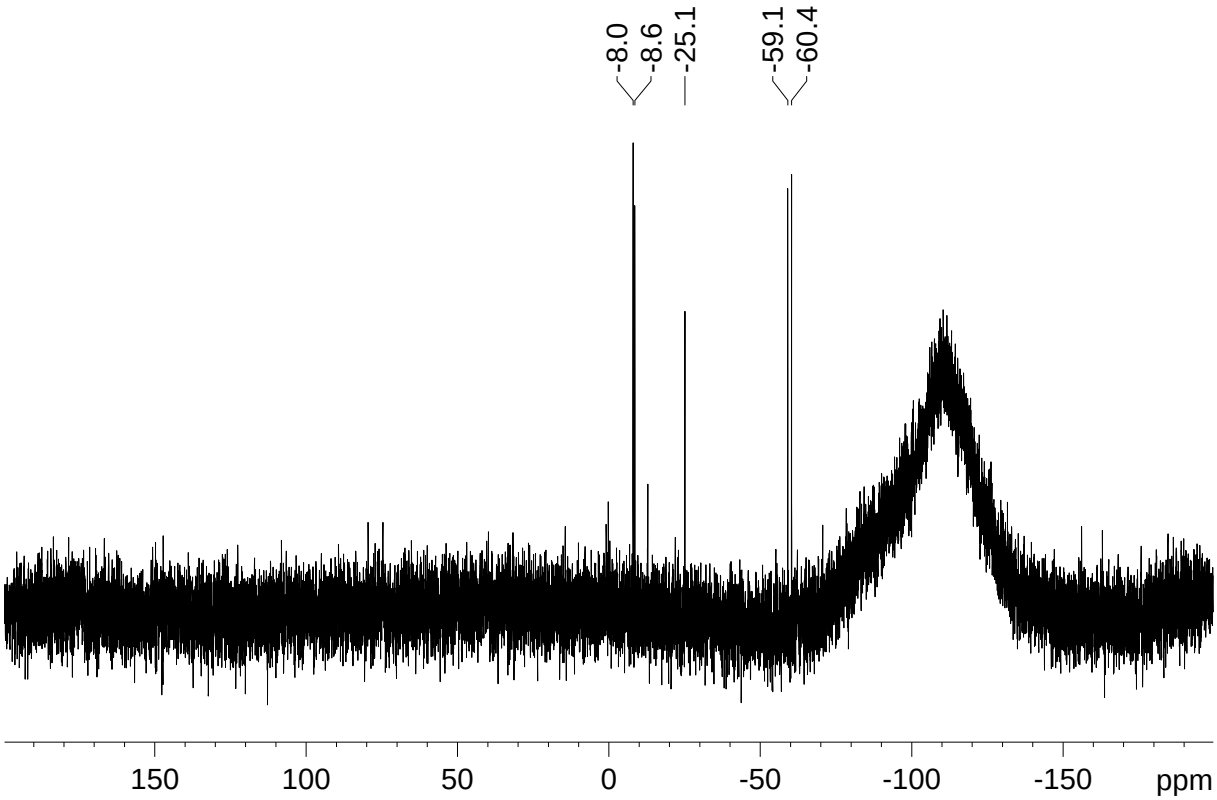

Figure 39. ^{29}Si{^{1}H} NMR spectrum from the reaction of **108a** with two equivalents potassium graphite after the initial product was kept in pentane for three days.

Two resonances in the area of dialkyl amines featuring characteristic coupling constants are observed at δ = 46.3 ($^2J_{P-C}$ = 13.2 Hz) and 45.6 ($^2J_{P-C}$ = 10.5 Hz) ppm. Coordinated thf is not present according to ^{1}H and ^{13}C NMR spectroscopy. Single crystals suitable for X-ray diffraction could neither be obtained of the initial or the rearranged product so that all assertions regarding their constitution remain speculative at present.

3.1.3. Reactivity of Disilenide 16 towards Cl_2PNPh_2

The findings described in the previous sections of Chapter 3.1 demonstrate that the amino functionality at phosphorus is responsible for the high reactivity of **108a** since it can be substituted or cleaved reductively. Conversely, the amino group bonded to the saturated silicon atom seems to be rather inert, at least for the initial reaction steps. In contrast, Si-Cl functionalities usually constitute highly reactive reaction sites even in the presence of several bulky Tip substituents (*cf.* Chapter 1). For instance, all three chlorine atoms in 1,1,2-trichloro cyclotrisilane **121** can be cleaved reductively to afford hexasilabenzene isomer **122** (Scheme 48).[160] Similarly, it was demonstrated that the β–chlorine functionality in silagermenylidene **45** opens the door to several further preparative manipulations of the system.[90,91] Therefore a β-chloro functionalized phosphasilene was considered as an attractive target. In analogy to the synthesis of the β-amino substituted phosphasilene **108a** – obtained from the reaction of disilenide **16** with $ClP(NMe_2)_2$ (Scheme 40)[130] – the combination of **16** with phosphorus electrophiles with two or even three halogen functionalities seemed to be the obvious approach. In a previous study, however, it was found that the reaction of **16** with PCl_3 or Cl_2PNMe_2 results in complex mixtures, presumably due to chlorination of the double bond.[130,200] A bulkier electrophile was employed in anticipation of an improved selectivity: we envisaged that the reaction of disilenide **16** with $Cl_2P(NPh_2)$ could result in a 1,3-chlorine shift (Scheme 84, path a) in analogy to the formation of silagermenylidene **45** (Scheme 18)[90] and phosphasilenes **108a,b** (Scheme 40).[130] Alternatively, a cyclization reaction (Scheme 84, path b) in a similar manner as during the reaction of **16** with multiply chlorinated silanes- or stannanes (Scheme 15 and Scheme 48) had to be considered.[84,85]

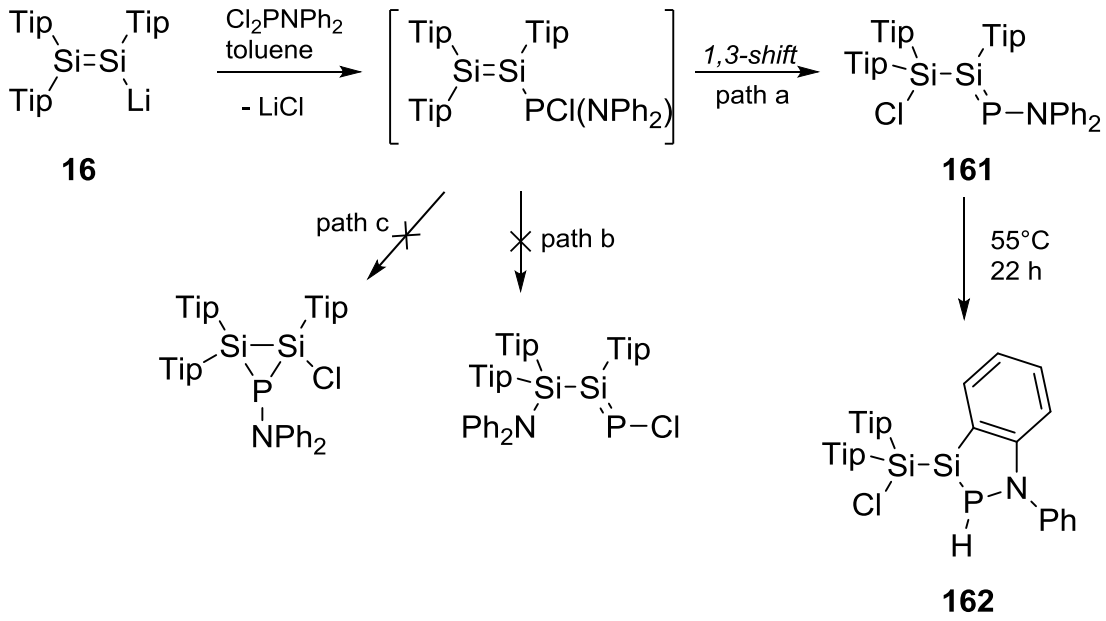

Scheme 84. Synthesis of β-chloro *P*-amino substituted phosphasilene **161** and rearrangement to silaphospha indoline derivative **162.**

Indeed, when disilenide **16** was treated with one equivalent $Cl_2P(NPh_2)$ uniform conversion to a new product was observed by NMR spectroscopy. The ^{31}P NMR spectrum shows a slightly broadened resonance at δ = 315.6 ppm. The *P*-amino substituted derivative **108a** exhibits a ^{31}P NMR signal at similar field (δ = 344.8 ppm), which was attributed to a certain degree of inverse polarization of the Si=P bond induced by the donor-substituent at phosphorus.[130] In the ^{29}Si NMR spectrum two resonances appear at δ = 204.4 ppm ($^1J_{P\text{-}Si}$ = 217.3 Hz) and δ = −5.7 ppm ($^2J_{P\text{-}Si}$ = 23.0 Hz, Figure 40). The strong deshielding of the unsaturated silicon atom is more in line with a more normally polarized phosphasilene (*e. g.* **144**: δ = 192.3 ppm *vs*. **108a**: 103.5 ppm).

These findings strongly suggest the formation of a Si=P bond and thus the *P*-amino substituted phosphasilene **161**.

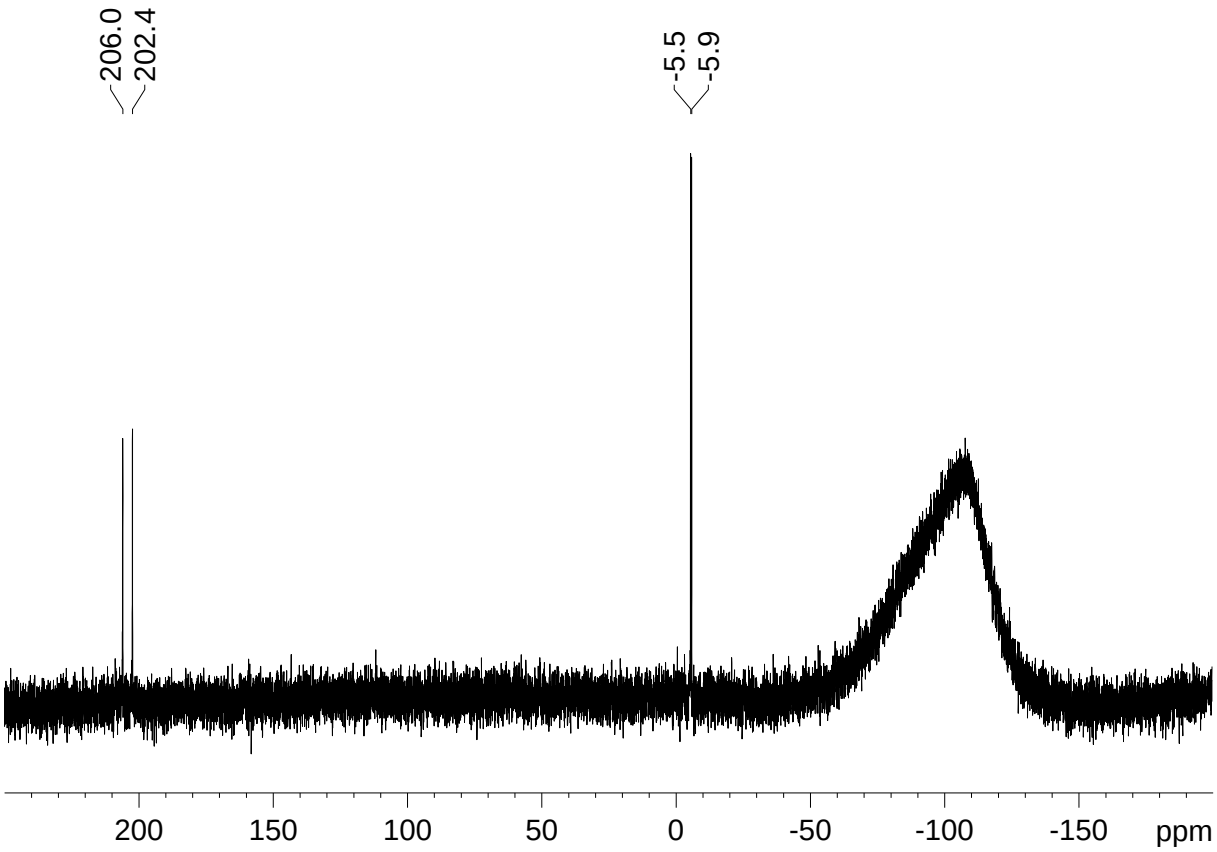

Figure 40. $^{29}Si\{^{1}H\}$ NMR spectrum of phosphasilene **161**.

On the basis of these NMR spectroscopic finding a migration of the NPh_2 moiety instead of a chlorine atom to afford a *P*-chloro phosphasilene cannot be fully excluded, even though it appears unlikely due to the certainly higher steric demand of NPh_2 (Scheme 84, path c).

After several hours at room temperature, the beginning rearrangement of **161** can be detected by NMR spectroscopy. The process can be accelerated by heating to 55°C; after 22 h full conversion was achieved. In the ^{31}P NMR spectrum of the rearranged product, a signal at δ = −29.1 ppm ($^{1}J_{P\text{-}Si}$ = 30.0 Hz) indicates a saturated phosphorus atom. In the ^{29}Si NMR spectrum, two resonances are observed at δ = −0.5 (s) and −21.0 (d, $^{1}J_{P\text{-}Si}$ = 30.0 Hz) ppm are similarly in line with saturated ^{29}Si nuclei. The characteristically small value observed for the P-Si coupling constant suggests the formation of a cyclic system. A doublet in the ^{1}H NMR spectrum at δ = 6.38 ($^{1}J_{P\text{-}H}$ = 158.7 Hz) ppm is diagnostic for the presence of a P-H moiety. These NMR spectroscopic findings argue for the insertion of Si=P bond into the *ortho*-CH-bond of one phenyl substituent at nitrogen to form the azaphosphasila indane derivative **162**. C-H insertion reactions of silicon double bonds are not unusual.[81,83] An X-ray analysis on single crystals obtained by crystallization from a concentrated pentane solution at

room temperature confirms the constitution of **162** as a silaphospha indoline (Figure 41).

Furthermore, the assumption of β-chloro *P*-amino phosphasilene **161** as initial product is substantiated by these findings even though attempts to grow single crystals at low temperatures were so far unsuccessful in that case (Scheme 84).

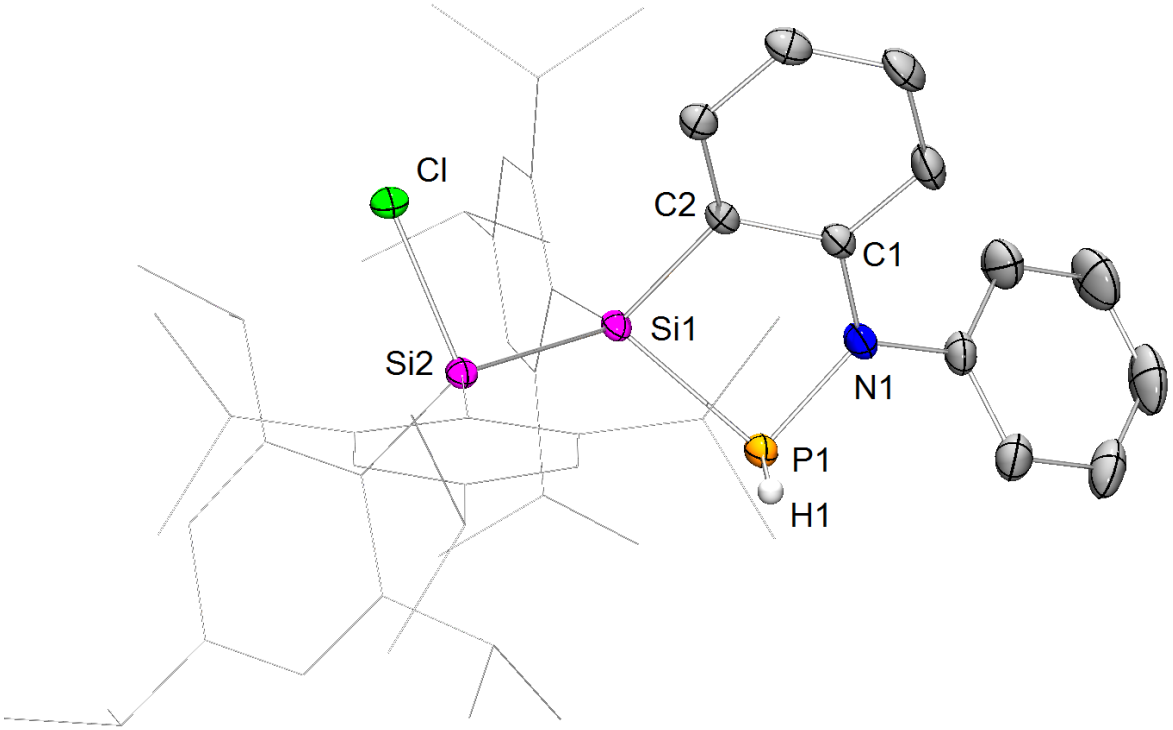

Figure 41. Molecular structure of silaphsopha indoline derivative **162** in the solid state (thermal ellipsoids at 50%, H atoms omitted). Selected bond lengths [Å]: Si1-P1 2.2770(5), P1-N1 1.7351(13), N1-C1 1.4149(19), Si1-Si2 2.3854(5).

With the PH-moiety and the chlorine substituent at the exocyclic silicon atom **162** still features an interesting functionality that could in principle allow for further manipulations of the system in future studies.

The endocyclic bond lengths (Si1-P1 2.2770(5), P1-N1 1.7351(13), N1-C1 1.4149(19) Å) and the distance of the exocyclic Si1-Si2 bond (Si1-Si2 2.3854(5) Å) are in the normal range for single bonds. While N1, C1, C2 and Si1 show an almost planar arrangement (distance from the C1, C2, Si1 plane to N1 is 0.046 Å), P1 is significantly distorted out of this plane (distance from the C1, C2, Si1 plane to P1 is 0.617 Å).

While the experiments described in Chapter 2.1.2.4 confirm that amino groups at the low-valent phosphorus center can be cleaved reductively, the chloro functionality at the saturated silicon atom in **161** might be equally useful in this regard. In an initial

attempt phosphasilene **161** was generated and subsequently two equivalents of lithium/naphthalene added at low-temperatures. Subsequent NMR spectroscopic investigation of the reaction mixture, however, revealed formation of **162** exclusively (Scheme 85).

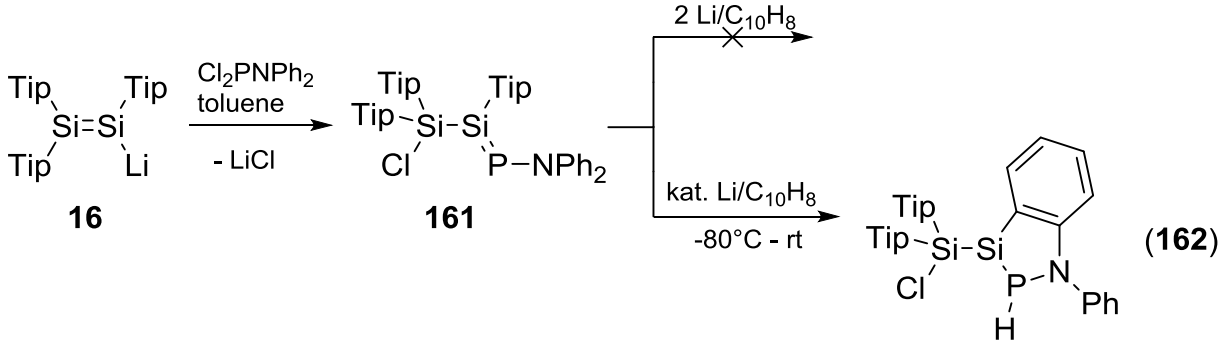

Scheme 85. Attempted reduction of postulated phosphasilene **161**.

Obviously, the rearrangement is catalyzed by addition of the reducing agent. Due to a shift in priorities further investigations concerning the reactivity of **161** or **162**, respectively, have been postponed.

3.2. An NHC-stabilized Cyclic Phosphasilene

3.2.1. Reactivity of Disilenide 16 towards P^I-Cations

As outlined in previous chapters, reports on three-membered Si_2P-rings are rare.[177,178] In general, the synthesis of functionalized derivatives is a particular, albeit worthwhile, challenge. For instance, the homonuclear 1,1,2-trichloro cyclotrisilane **121** shows intriguing reactivity: it serves as precursor for the targeted synthesis of hexasilabenzene isomer **122** (Scheme 48).[160] However, an analogous synthetic protocol to small rings with silicon and phosphorus is not applicable, because the reaction of disilenide **16** with phosphorus trichloride is rather unselective.[200]

In a collaboration of our group with the Jutzi group it was demonstrated that the reaction of silylium type cation Cp^*Si^+ **123**[162] with disilenide **16** affords Cp^* - functionalized cyclotrisilene **124** (Scheme 50).[163] Notably, the Cp*-ligand can be cleaved in a one electron reduction providing access to hexasilabenzene isomer **122** *via* an alternative synthetic strategy.[164] As the silicon(II) cation **123** acts as a

stoichiometric source of silicon during this reaction, lowvalent electrophilic phosphorus reagents were considered as alternative entry to the P_2Si_4 chemisty.

Recently, Macdonald *et al.* reported base-stabilized phosphorus(I) cations **163**[X] (Scheme 86).[201,202] Subsequently, they demonstrated that the dppe ligand can be replaced by the addition of two equivalents N-heterocyclic carbene (NHC) to afford NHC-adducts of P(I)-cations.[203] Strong σ-donors such as phosphanes and N-hetrocyclic carbenes have gathered increased attention as dative ligands for the stabilization of low-valent main group reagents.[204] For the application as transfer reagents of the lowvalent element the possibility of subsequent cleavage of the stabilizing base is of crucial importance. In light of the current discussion whether these compounds are better described as Lewis-acid-base complexes or ylidic structures,[118] we argued that in fact reversible coordination is a strong indication, if not even prerequisite, for dative bonding.[91,205] It should be mentioned that even though stabilized by coordination of strong donors, a remarkable reactivity is observed for base-adducts of low-valent main goup compounds rendering them useful precursors for the synthesis of novel structural motifs.

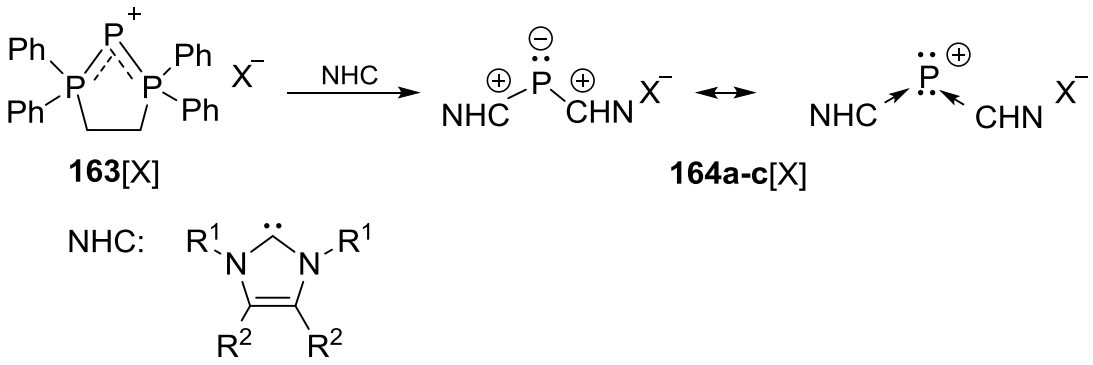

Scheme 86. Macdonalds synthesis of stabilized phosphorus(I) cations **163**[X] and **164a-c**[X] (**a**: R^1 = Et, R^2 = Me; **b**: R^1 = ^{i}Pr, R^2 = Me; **c**: R^1 = Mes, R^2 = H, X= Cl, Br, I, BPh_4).[201-203]

We anticipated that in analogy to the formation of cyclotrisilene **124** (Scheme 50),[163] a phosphorus(I) cation of the type **163** might equally serve as a stoichiometric source of phosphorus in the reaction with disilenide **16** and thus provide access to **157** or **158** (Scheme 87)**.**

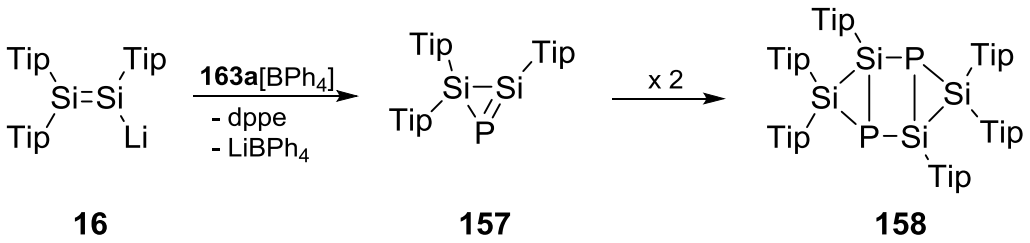

16 **157** **158**

Scheme 87. Anticipated reaction of disilenide **16** with **163a**[BPh_4].

While in our hands the isolation of **163**[I] from the reaction of dppe with PI_3 proved impossible, we were able to isolate very pure **163**[Br] employing a different protocol in the presence of cyclohexene as halogen-scavenger.[202] Due to the insolubility of **163**[Br] in common solvents other than chlorocarbons, the bromide anion was exchanged for tetraphenylborate by the reaction with $NaBPh_4$ according to the procedure reported by the Macdonald group.[203] The salt **163**[BPh_4] shows adequate solubility in thf and the solution was treated with one equivalent **16** at −80°C. The orange solution turned very intense green immediately. While the formation of free dppe as well as lithium tetraphenylborate as expected by-products was indeed confirmed by NMR spectroscopy, no other phosphorus or silicon containing species could be detected. The formation of paramagnetic species cannot be excluded. Consequently, we considered the use of cations of the type **164a-c** as alternative source of phosphorus in the reaction with **16**. According to the procedure published by Macdonald *et al.,* phosphenium salt **163**[BPh_4] was reacted with two equivalents of dimethyldiisopropylcarbene and **164b**[BPh_4] was isolated as yellow powder.[203]
After treatment of **164b**[BPh_4] with one equivalent disilenide **16** in thf a complete and uniform reaction is confirmed by NMR spectroscopy (Scheme 88).

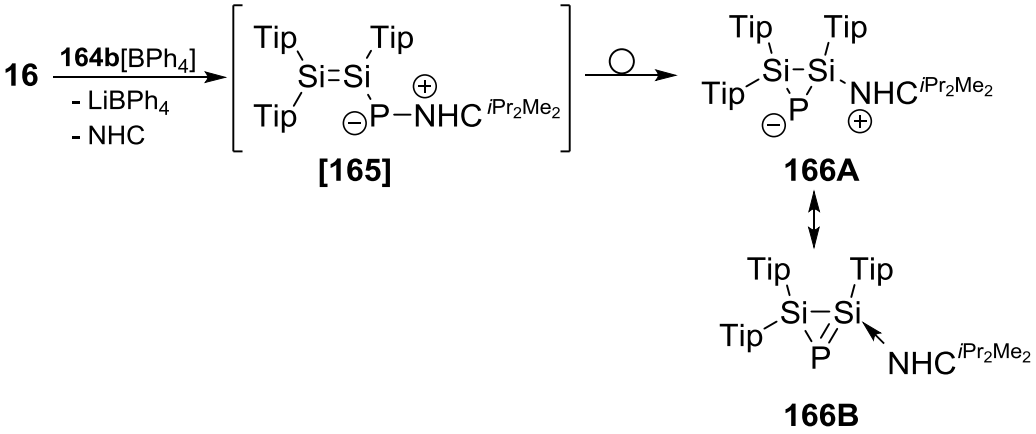

Scheme 88. Synthesis of the first NHC adduct of a cyclic phosphasilene (shown as two resonance formulas **166A** and **166B**) with proposed intermediacy of **[165]** ($NHC^{iPr_2Me_2}$ = 1,3-diisopropyl-4,5-dimethylimidazol-2-ylidene).

Two resonances are observed in the ^{31}P NMR spectrum at δ = −252.2 and −267.9 ppm (ratio 10 : 9). In the ^{29}Si NMR four doublets are found at δ = −68.7 ($^1J_{P\text{-}Si}$ = 91.8 Hz), −68.91 ($^1J_{P\text{-}Si}$ = 107.4 Hz), −69.9 ($^1J_{P\text{-}Si}$ = 105.3 Hz) and −73.6 ($^1J_{P\text{-}Si}$ = 97.4Hz) ppm (Figure 42).

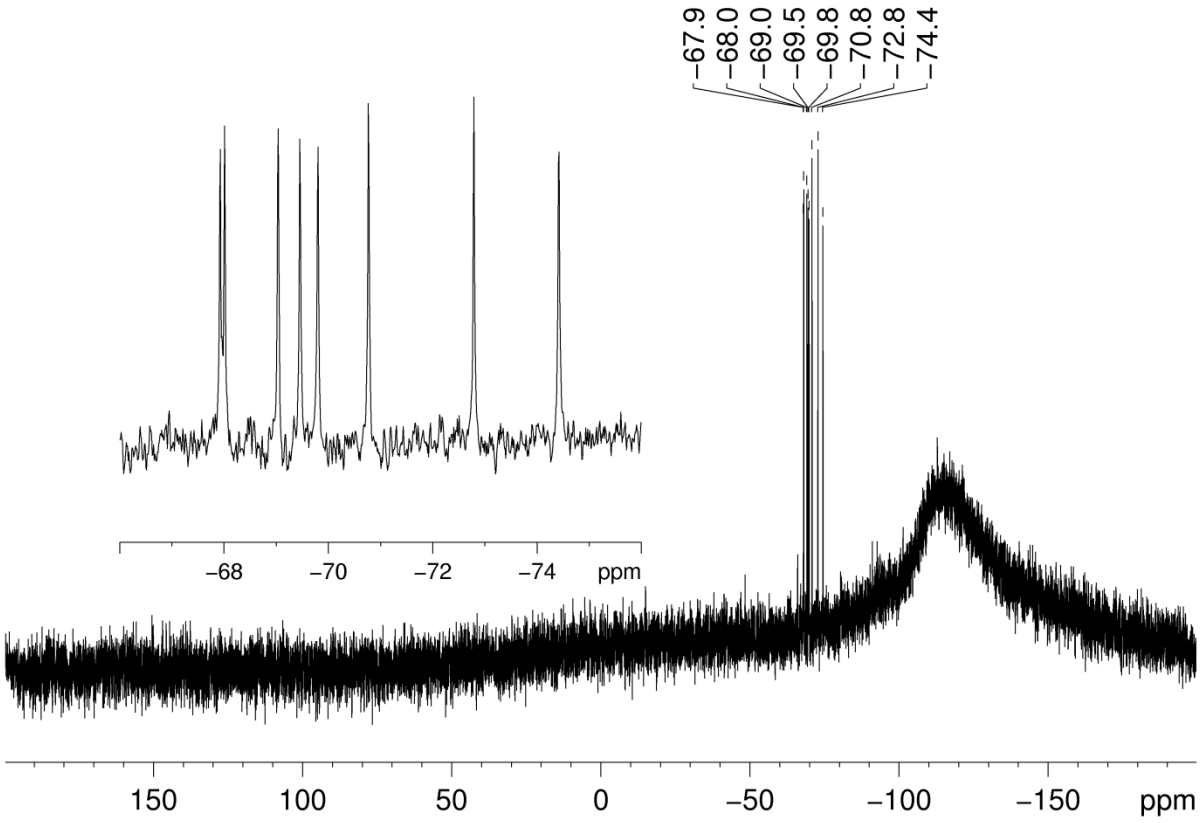

Figure 42. $^{29}Si\{^1H\}$ spectrum of **166.**

While the high-field resonances in both spectra are in accordance with formation of two three-membered Si_2P-ring species, the magnitude of the $^1J_{P\text{-}Si}$-coupling constants is on the greater end for reported chemical shifts of small silicon-phosphorus rings[177,178] (*cf.* also Chapter 3.1.2.5). The similarity in the range of the NMR chemical shifts and the coupling constants hints towards the formation of stereoisomers during the reaction of disilenide **16** with P(I) species **164b**[BPh_4]. Importantly, the ^1H and ^{13}C NMR spectra indicate the liberation of one equivalent NHC in the course of the reaction. The second equivalent NHC is confirmed to be coordinated to the product on the basis of ^1H and ^{13}C NMR spectroscopy. The fact that all isopropyl protons are chemically inequivalent reveals significantly hindered rotation of the NHC ligand.
Notably, the absence of a resonance with direct phosphorus coupling in the ^{31}C NMR spectrum supports the coordination of NHC to a silicon rather than phosphorus atom in the product.
We propose that initially one equivalent NHC is substituted in **164b** during the reaction with disilenide **16** to yield NHC-coordinated disilenyl phosphinidene **165**. In a subsequent cyclization step the NHC is shifted to the neighboring silicon atom affording a three-membered Si_2P-ring that can either be described as zwitterionic disilaphosphirane **166A** or an NHC-stabilized cyclic phosphasilene **166B** (Scheme 88). It should be mentioned that the strong shielding observed in the ^{31}P and ^{29}Si NMR spectra is more in line with the ylidic structure **166A**. The two isomers can be assigned to rotamers of **166** in analogy to what has reported by Baines *et al.* for coordinated NHCs with hindered rotation.[206] Yellow-orange single crystals (M. p. 200-205°C, dec.) were obtained from a concentrated pentane solution in very good yield (89 %) and an X-ray diffraction study confirmed the constitution of **166** (Figure 43).
The Si1-Si2 bond length of 2.3082(6) Å is on the short end of reported values for Si-Si single bonds. Both the Si1-P1 (2.1718(6) Å) and Si(2)-P(1) (2.1938(6) Å) are significantly shortened compared to normal silicon phosphorus single bonds.[187] Similar to the bonding situation in cyclic phosphides **156a** and **160** (*cf.* Chapter 3.1.2.5 and 3.1.2.6), these findings are ascribed to back-donation by the anionic phosphorus into σ^*-orbitals at silicon. Interactions between the formal phosphide vertex in **166** and the electropositive silicon atoms might also play a role.[199] As an essentially equivalent rationalization, the more pronounced shortening of the Si1-P1 bond could be due to a certain double bond character and a dative bonding

interaction of the NHC with Si1 (resonance formulae **166B**). The bond between the carbenic carbon (C1) and silicon (Si1) is 1.9569(17) Å, which is in the normal range for NHC-silicon adducts (1.9271-1.9843 Å).[207]

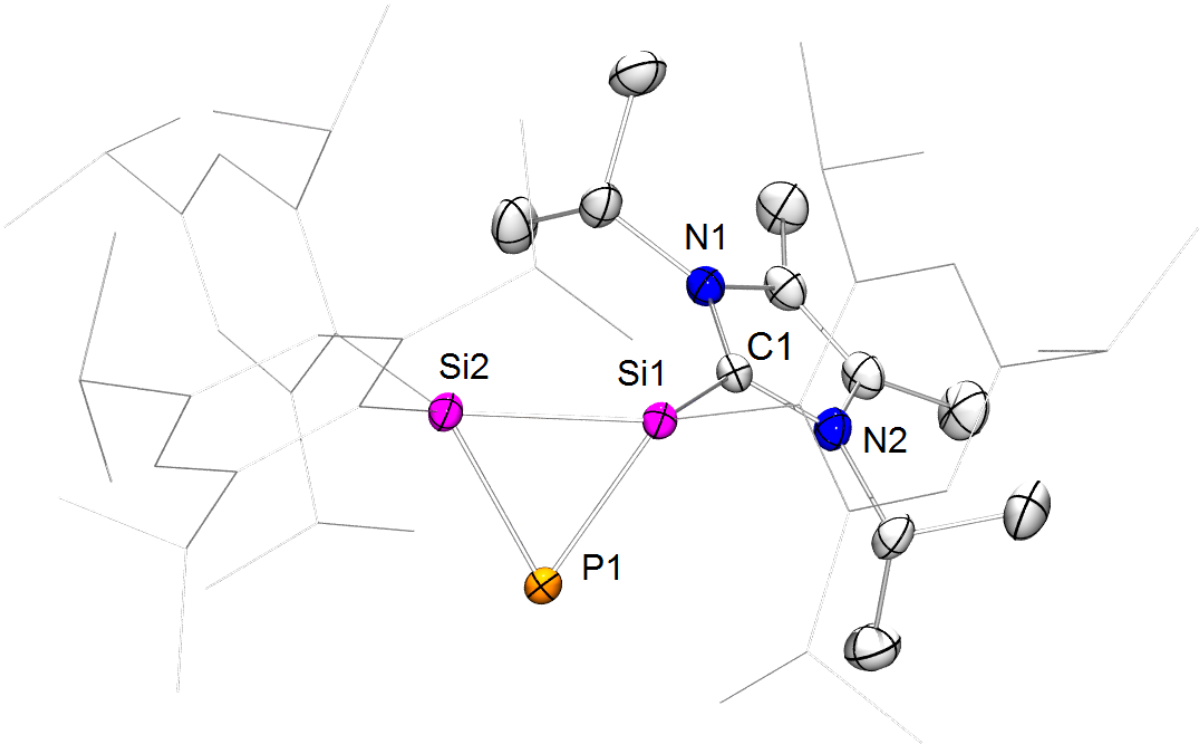

Figure 43. Molecular Structure of **166** in the solid state (thermal ellipsoids at 50%, H atoms and co-crystallized solvent omitted). Selected bond lengths [Å] and angles [°]: Si(1)-Si(2) 2.3082(6), Si(1)-C(1) 1.9569(17), Si(1)-P(1) 2.1718(6), Si(2)-P(1) 2.1938(6), Si1-P1-Si2 63.84(2).

In the UV/vis absorption spectrum of **166** a broad shoulder is detected (460-370 nm, Figure 112). A second absorption band is observed at λ = 334 nm (ε = 8700 $M^{-1}cm^{-1}$, Figure 112, Figure 113).

In order to confirm that the two sets of signals detected in the NMR spectra of **166** can be assigned to two species in equilibrium, the compound was investigated by a variable temperature ^{31}P NMR study. Indeed, a linear change in the ratio of the two isomers can be observed. Even though it was not possible to detect coalescence within the observable temperature window of toluene-d_8, a significant broadening well as an approaching of the resonances is apparent and higher temperatures (Figure 44).

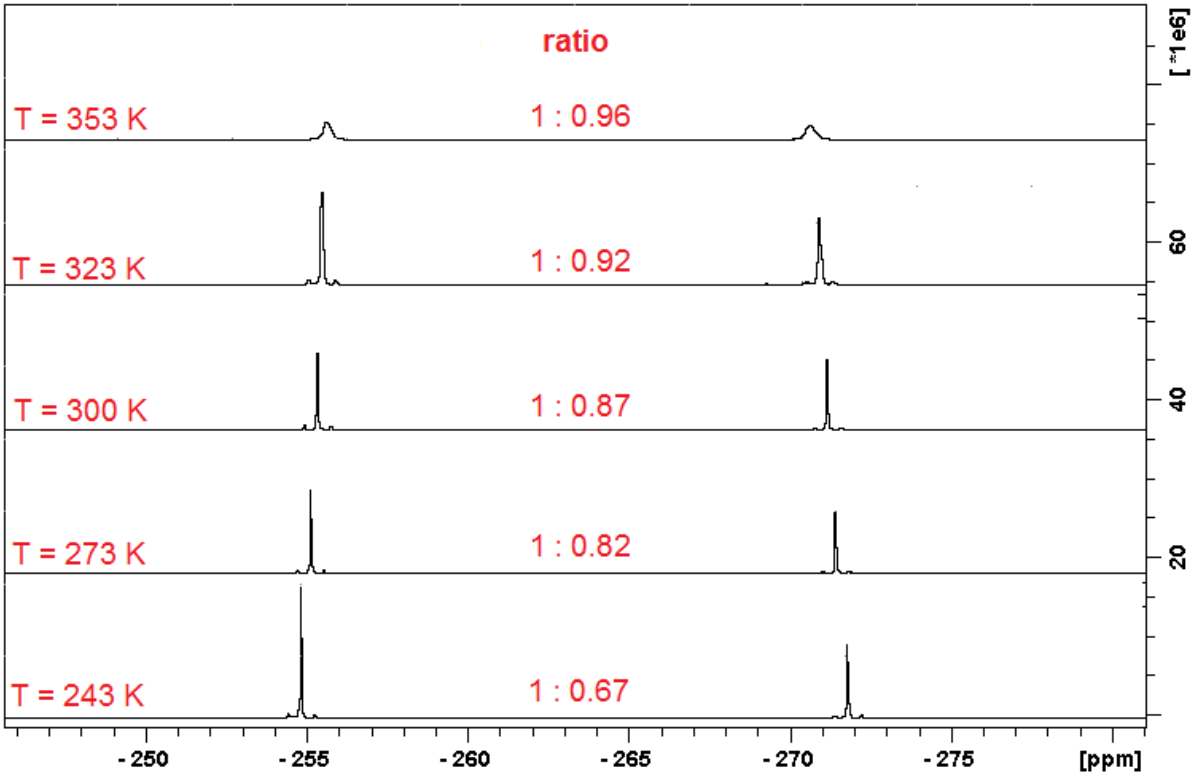

Figure 44. $^{31}P\{^{1}H\}$ NMR spectra of **166** at five different temperatures (T = 243 – 353 K), numbers represent ratio of the intensity of the signals to each other.

A solid state ^{31}P NMR spectrum of **166** revealed that the compound also exists as two stereo isomers in the solid state even though in a slightly different ratio. Two resonances could be observed (δ = −255.8 and −270.5 ppm, (ratio 5 : 3, Figure 45). As commonly observed for small rings of heavier maingroup elements,[208] the chemical shift anisotropy (CSA) of the ^{31}P signals of **166** is significant as shown by the intensity of the rotational side bands caused by the spinning of the sample at 10 kHz. A detailed analysis of the CSA, however, is beyond the scope of this discussion.

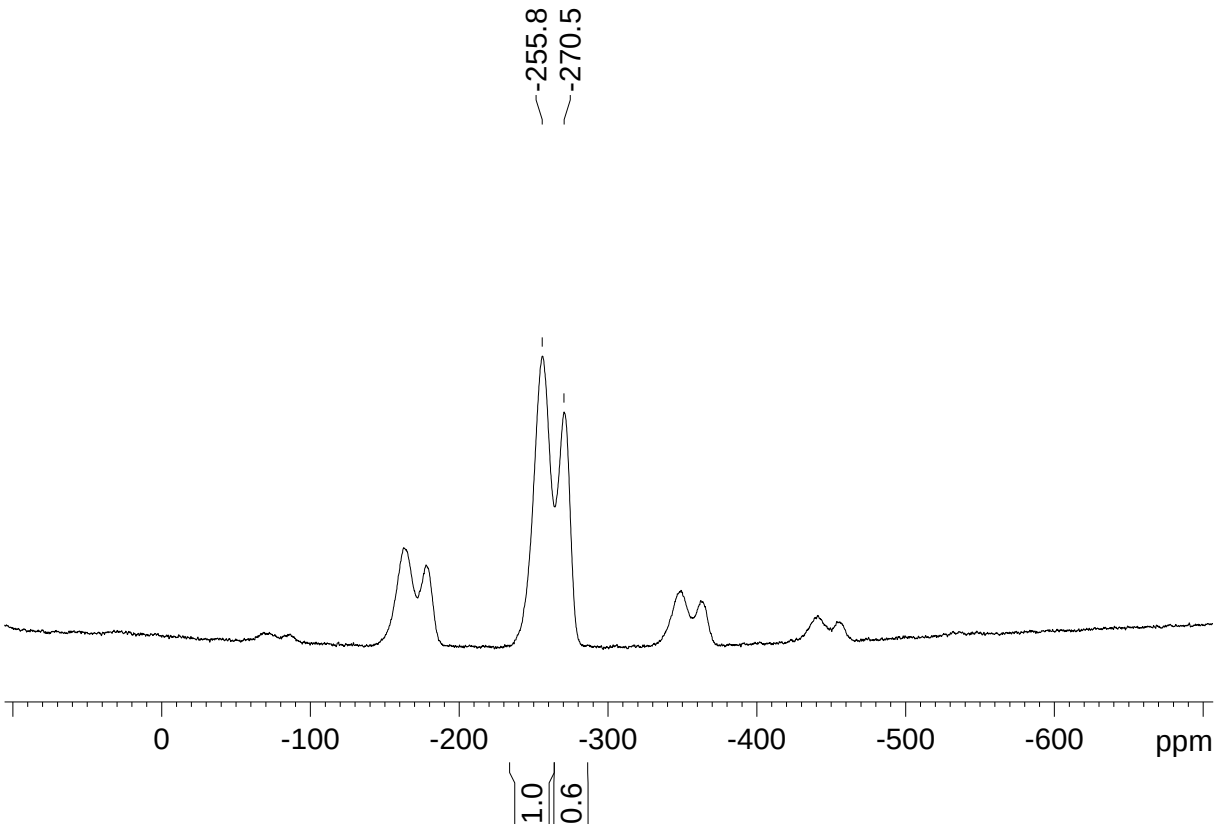

Figure 45. CP-MAS solid state $^{31}P\{^{1}H\}$ NMR spectrum of **166** (rotational frequency: 10 kHz).

MacDonald *et al.* reported that an inseparable mixture of **164**[Cl] and 2-chloro-1,3-diisopropyl-4,5-dimethylimidazolium chloride is accessible by the treatment of PCl_3 with three equivalents of the corresponding *N*-heterocyclic carbene (Scheme 89).[203]

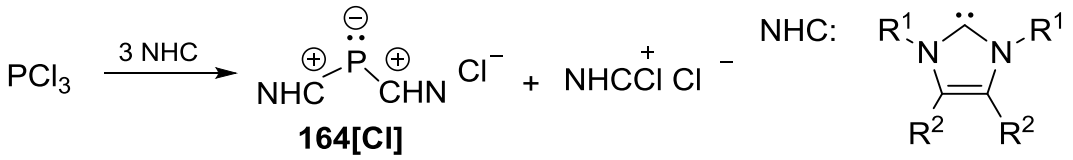

164[Cl]

Scheme 89. Synthesis of an inseparable mixture of **164**[Cl] and 2-chloro-1,3-diisopropyl-4,5-dimethylimidazolium chloride reported by Mcdonald.[203]

We anticipated that the direct addition of disilenide **16** might provide an easier synthetic access to **166** without the necessity of isolation of the P(I) starting material. Therefore, we treated the mixture of **164b**[Cl] and 2-chloro-1,3-diisopropyl-4,5-dimethylimidazolium chloride with one equivalent **16** in thf.

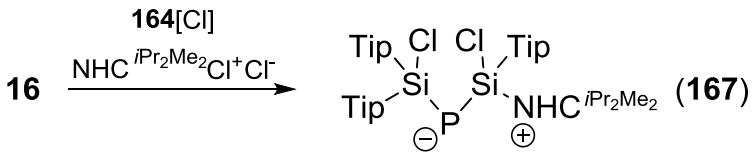

Scheme 90. Synthesis of **167** *via* addition of disilenide to a mixture of **164**[Cl] and 2-chloro-1,3-diisopropyl-4,5-dimethylimidazolium chloride (NHC^{iPr_2Me_2} = 1,3-diisopropyl-4,5-dimethyl-imidazol-2-ylidene).

^{31}P NMR spectroscopy of the reaction mixture revealed only small quantities of **166** (5 %). Instead a very broad resonance at δ = −203.3 ppm appeared that is in agreement with a strongly negatively polarized phosphorus atom. Two very broad resonances at δ = 10.1 and 7.7 ppm were observed in the ^{29}Si NMR spectrum. This considerable deshielding compared to **166** indicates the formation of an open chained system rather than a cyclic species. The chemical shifts are comparable to the range reported for halo silanes.[209] Crystalline material of very low crystal quality was obtained from a pentane solution. Despite the low quality it was possible to determine the constitution as ylide **158** (Scheme 90, Figure 46).

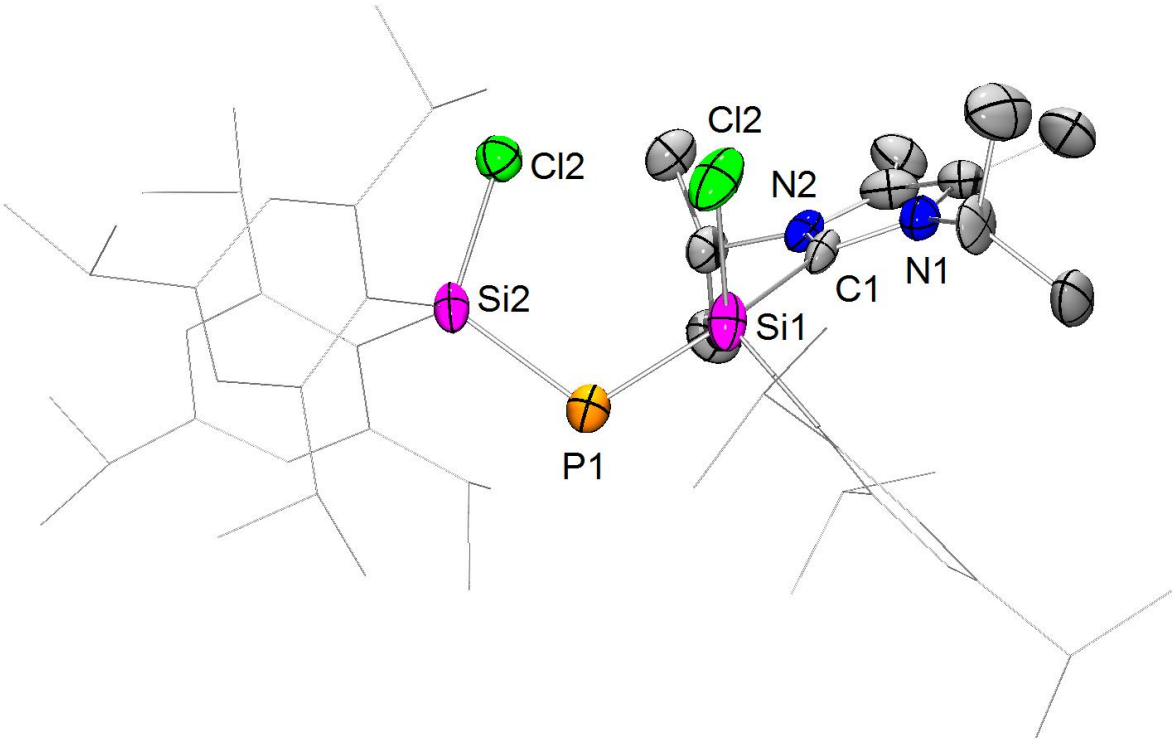

Figure 46. Molecular structure of **167** in the solid state (thermal ellipsoids at 50%, H atoms and co-crystallized solvent omitted).

The formation of **167** can be rationalized by the chlorination of the Si-Si σ-bond in **166**, presumably by 2-chloro-1,3-diisopropyl-4,5-dimethylimidazolium chloride. Since

a satisfactory refinement was not possible on the basis of the obtained data, a detailed discussion of bond length and angles would be meaningless.

3.2.2. Synthesis of Tetracarbonyliron Complex 168

The NHC-coordinated phosphadisilirene **166** is accessible in very good yields and it was of therefore of interest to study the reactivity of this unprecedented type of silicon-phosphorus species. The formation of **167** indicates a high reactivity of the Si-Si bond. However, attempts to add isonitriles or alkynes over this particular bond in **166** were unsuccessful. No reaction of **166** was observed with xylyl isonitrile, *tert.*-butyl isonitril or phenylacetylene even after keeping the mixtures at 60°C or 80°C, respectively, for more than 12 h.

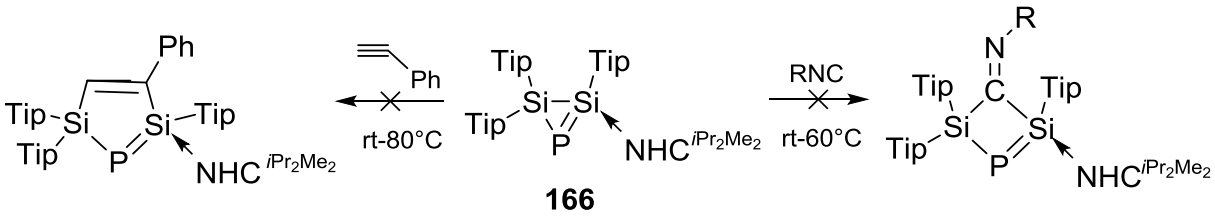

Scheme 91. Unsuccessful attempts to react **166** with isonitriles or phenylacetylene (R = Xylyl, *tert.*-butyl).

The NHC coordinated to silicon in principle provides another reactive side in **166**. Cui *et al.* reported the successful abstraction of the NHC ligand from silicon in base-stabilized phosphasilene **92** by the addition of triphenylborane as Lewis-acid .[124]

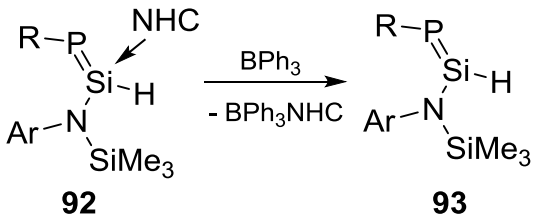

Scheme 92. NHC-abstraction from base-stabilized phosphasilene **92** by the addition of triphenylborane reported by Cui.[124]

Recently, it was demonstrated by our group that the same strategy provides excess to digermenes starting from NHC stabilized germylenes.[205] Unfortunately, in case of **166** it was not possible to remove the NHC by the addition of BPh_3 to obtain **157** or **158**, respectively. Also the exchange of the NHC for the corresponding smaller tetramethyl substituted carbene in analogy to what was reported by our group[207] for silagermenylidene **45** (Scheme 18) was not possible (Scheme 93). In both cases no reaction was observed and upon heating at 80°C slow unselective decomposition occurred.

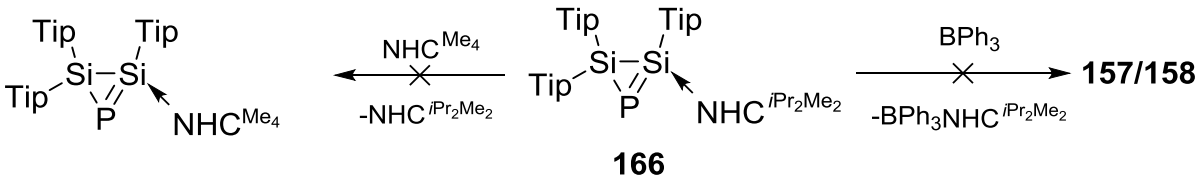

Scheme 93. Unsuccessful attempts to exchange the carbene in **166** for the smaller Tetramethyl derivative and remove the carbene with BPh_3, respectively ($NHC^{iPr2Me2}$ = 1,3-diisopropyl-4,5-dimethylimidazol-2-ylidene, NHC^{Me4} = 1,3,4,5-tetramethylimidazol-2-ylidene).

The formal phosphide functionality in **166** in principle allows for the coordination to metal centers and we decided to investigate the suitability of **166** as novel ligand for transition metal complexes. After treatment of **166** with one equivalent diiron nonacarbonyl indeed quantitative and uniform conversion to a new product was confirmed by NMR spectroscopy. The chemical shifts are fairly comparable to those of **166** (δ = −252.2 and −267.9 ppm) and indicate an intact Si_2P-moitety. In the ^{31}P NMR spectrum again two isomers are observed at δ = −245.9 and −267.7 ppm even though the ratio has changed significantly (89:11, **166**: 100:90). Due to the lower natural abundance of ^{29}Si only the major isomer can be detected in the ^{29}Si NMR spectrum with signals at δ = −59.5 ($^1J_{P\text{-}Si}$ = 74.9 Hz) and −62.2 ($^1J_{P\text{-}Si}$ = 62.0 Hz) ppm. Compared to **166** a significant decrease in the magnitude of the coupling constants is observed (**166**: 91.8-107.4 Hz) indicating a lower s-character of the endocyclic bonds. For the carbonyl moieties a low-field doublet is observed at δ = 221.8 ppm. The size of the $J_{C\text{-}P}$ couling constant (11.5 Hz) is consistent with a ^2J-coupling[195] and confirms the coordination of the phosphide vertex to the iron center (Scheme 94). Orange single crystals (M. p. 153°C, dec.) were grown from toluene in excellent yields (91%) and revealed the constitution of complex **168** (Figure 47).

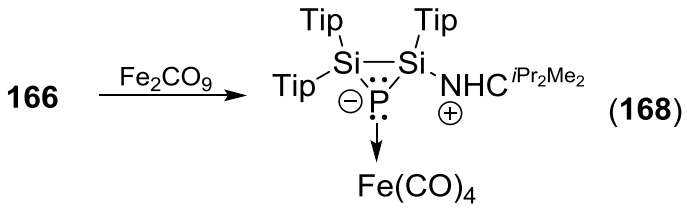

Scheme 94. Synthesis of tetracarbonyl iron complex **168** (NHC^{iPr_2Me_2} = 1,3-diisopropyl-4,5-dimethylimidazol-2-ylidene).

The P1-Fe1 distance (2.2874(4) Å) is longer than usually observed phosphane-iron complexes,(2.08-2.211 Å),[196] which can be attributed to the high steric congestion about the coordinating phosphorus center. While the bond of the carbenic carbon to silicon (Si(1)-C(1) 1.9542(13) Å) is very similar to that in **166** (1.9569(17) Å), the Si1-Si2 bond length (Si(1)-Si(2) 2.3755(5) Å) has increased significantly (**166**: 2.3082(6) Å). On the other hand, the P1-Si1 and P1-Si2 bonds in **168** are shortened (Si(1)-P(1) 2.1635(5) and Si(2)-P(1) 2.1838(5) Å) compared to those in **166** (2.1718(6) and 2.1938(6) Å).

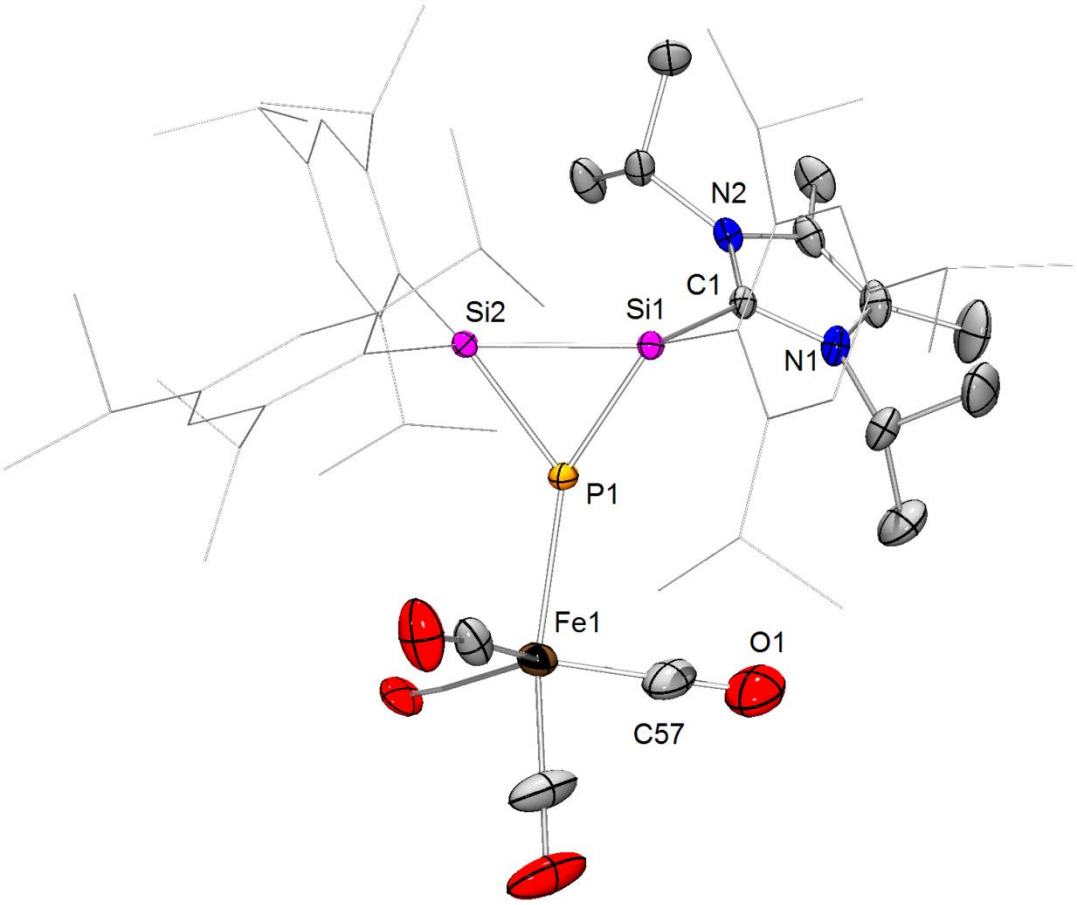

Figure 47. Molecular structure of **168** in the solid state (thermal ellipsoids at 50%, H atoms and co-crystallized solvent, disordered ^{i}Pr-groups and iron carbonyl moiety omitted). Selected bond lengths [Å] and angles [°]: P-Fe1 2.422, Si(1)-Si(2) 2.3755(5), Si(1)-C(1) 1.9542(13), Si(1)-P(1) 2.1635(5), Si(2)-P(1) 2.1838(5), Si1-P1-Si2 66.243(16).

As a consequence, a widening of the Si1-P1-Si2 angle (66.243(16)°) in **168** is observed (**166**: 63.84(2)°).

The UV/vis spectrum of **168** revealed a broad absorption band at λ = 460-340 nm (Figure 114). In the IR spectrum, the most intense carbonyl stretching bands of **168** are observed at 2025, 1930, 1907 and 1890 cm^{-1}. Apparently, **168** is a somewhat stronger σ-donor than for instance the N-herocyclic carbene NHC^{Dip} ($NHC^{Dip}Fe(CO)_4$: v = 2035, 1947, 1928, 1919 cm^{-1}) (NHC^{Dip} = $C\{N(Ar)CH\}_2$, Ar = 2,6-diisopropylphenyl).[197]

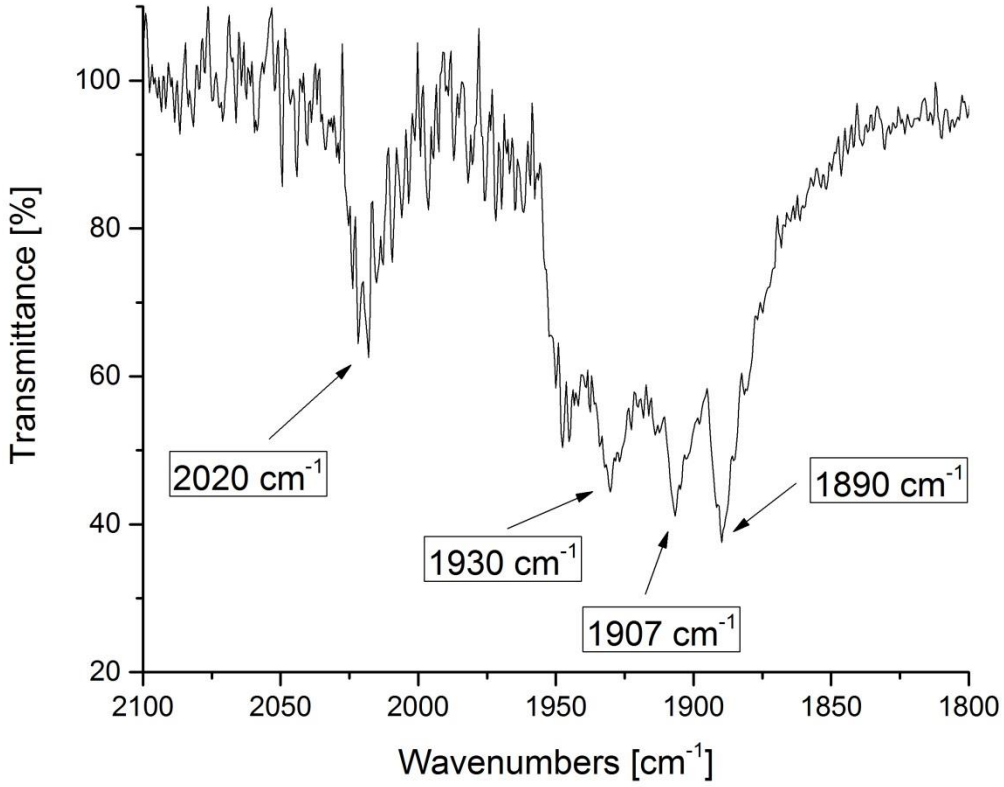

Figure 48. IR spectrum of **168**.

3.2.3. Rearrangement of 168 to Bicyclobutane Analogue 169

We anticipated that **168** can thermally rearrange to one of its constitutional isomers. Indeed, after 17 h at 80°C complete and uniform conversion of **168** to a new product was observed by NMR spectroscopy. Notably, in the ^{13}C NMR spectrum a singlet was observed for the carbonyl resonance at δ = 219.2 ppm. The absence of ^{31}P

coupling gives a first indication that the iron center is not directly coordinated by phosphorus. Both silicon nuclei are with δ = 30.8 (br d, $^1J_{P\text{-}Si}$ = 113.6 Hz) and 26.4 (d, $^1J_{P\text{-}Si}$ = 138.8 Hz) ppm considerably deshielded compared to **166** (δ = −68.7, −68.91, −69.9 and −73.6 ppm) and **168** (δ = −59.5 and −62.2 ppm), which is in accordance with coordination to the electropositive ironcarbonyl moiety.[90] Conversely, the ^{31}P NMR resonance is observed at very high field at δ = −378.6 ppm indicating a free phosphide moiety. While only one set of signals was observed in this case, a pronounced broadening of the resonances still hints towards hindered rotation in the molecule. The NMR spectroscopic findings support the formation of a bicyclo[1.1.0]butane structure **168** (Scheme 95).

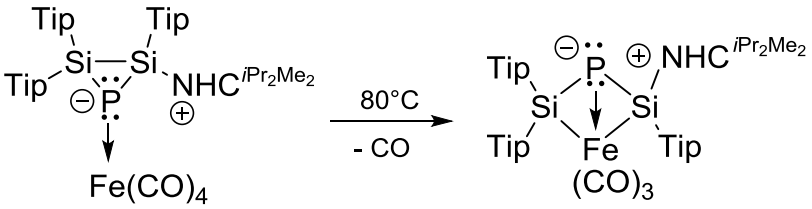

168 **169**

Scheme 95. Rearrangement of tetracarbonyl iron complex **168** to butterfly structure **169** (NHC$^{i\text{Pr}_2\text{Me}_2}$ =1,3-diisopropyl-4,5-dimethylimidazol-2-ylidene)**.**

An analogous compound has recently been reported by Scheschkewitz *et al*. At room temperature silagermenylidene tetracarbonyl iron complex *Z*-**170** isomerizes slowly to *E*-**170**. The authors demonstrated that in case the isomerization is carried out at 65°C, formation of bicyclo[1.1.0]butane like structure **171** with iron and germanium in the bridgehead positions is formed as side product (14 %).[90]

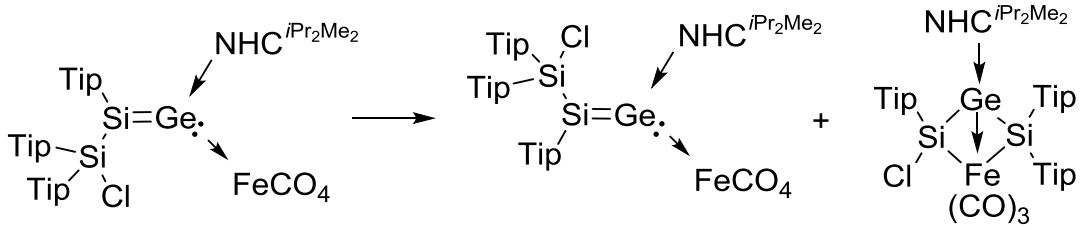

Z-**170** *E*-**170** **171**

76% (25°C) 0% (25°C)
56% (65°C) 14% (65°C)

Scheme 96. Rearrangement of iron complexes *Z*-**168** to *E*-**168** and **169** reported by Scheschkewitz *et al.* (NHC$^{i\text{Pr}_2\text{Me}_2}$ = 1,3-diisopropyl-4,5-dimethylimidazol-2-ylidene).[90]

The constitution of the butterfly structure **169** was confirmed by an X-ray diffraction study on orange single crystals (M. p. 163°C, dec.) obtained in acceptable yields (48 %) from a toluene solution at room temperature. The iron atom (Fe1) and the phosphide unit (P1) are in the bridgehead positions and the iron center is coordinated in a distorted octahedral fashion by one $SiTip_2$, one Tip-Si-NHC moiety and three carbonyl ligands.

The Si1-Fe1 bond length is with 2.3344(9) Å significantly shorter than the Si2-Fe1 bonds distance (2.3946(9) Å). Equally, the Si1-P1 bond (2.1725(12) Å) is shorter than Si2-P1 (2.2139(11) Å). These findings are tentatively attributed to the NHC-coordination to Si1 inducing a higher bond order in the Si1-P1 and Si1-Fe1 bond. The P1-Fe1 distance is unusually long (2.4970(8) Å) indicating very weak interactions between the phosphide unit and the iron center. This is in accordance with the absence of a detectable coupling between the phosphorus nucleus and the carbonyl ligands in the ^{13}C NMR spectrum.

The UV/vis spectrum of **169** shows a broad absorption band at λ = 500-350 nm (Figure 115) comparable to what was found for **168** (λ = 460-340 nm).

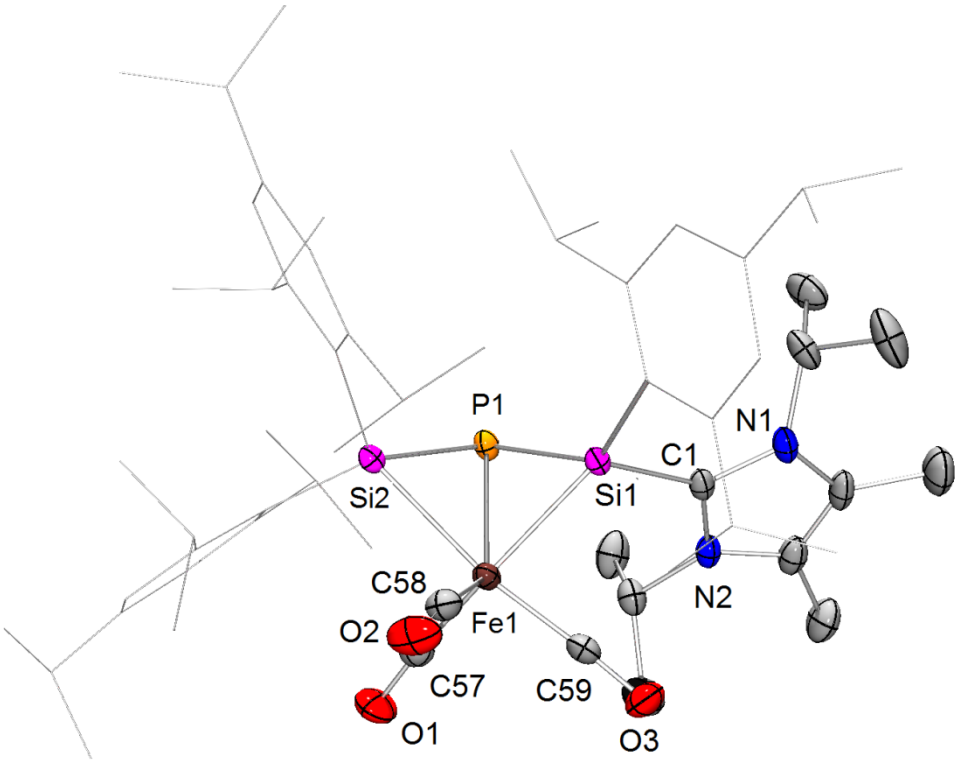

Figure 49. Molecular structure of **169** in the solid state (thermal ellipsoids at 50%, H atoms omitted). Selected bond lengths [Å] and angles [°]: Si1-Fe1 2.3344(9), Si2-Fe1 2.3946(9), P1-Fe1 2.4970(8), Si1-C1 1.990(3), Si1-P1 2.1725(12), Si2 P1 2.2139(11), Si2-P1-Si2 97.09(4).

3.3. Reactivity of Disilenide 16 towards Boron Containing Electrophiles

Low-valent silicon compounds feature unique chemical and physical properties and have thus moved into focus as promising precursors for material chemistry applications. A prerequisite for further manipulations on the unsaturated silicon systems and their incorporation into extended systems is the presence of residual functionality.[34] Phosphorus is the most important n-type dopant for silicon materials[15] and consequently its combination with unsaturated silicon moieties is of significant interest, also on a molecular level. In Chapter 3.1 and 3.2 it was demonstrated that reactions of disilenide **16** with appropriate phosphorus electrophiles yield novel functionalized unsaturated or cyclic silicon-phosphorus species. Proof-of-concept that these systems indeed retain a high reactivity was provided in the previous chapters.
Boron is the key element for p-type doping of silicon based materials.[13] Reports on silicon-boron containing molecules are generally relatively rare, presumably due to the weakness of the Si-B-bond. In case of boryl-substituted unsaturated silicon compounds, boryl disilenes **28a,b** and **54a,b** so far remain the sole examples.[80,101,102] However, the sterically very demanding, electron-donating substituents at boron in these compounds presumably result in a decreased reactivity and therefore prevent further manipulations. We anticipated that reactions of disilenide **16** with appropriate boron electrophiles might provide excess to Si-B compounds with valuable residual functionality.

3.3.1. Synthesis of Methylisilene 172

When disilenide **16** was reacted with neat BCl_3, a complex mixture was obtained.[200] Treatment of **16** with one equivalent $BCl_3 \cdot SMe_2$ resulted in a complex mixture as well.[210]
During this project, **16** was reacted with one equivalent of $BF_3 \cdot Et_2O$ at −80°C. Upon warming to room temperature, the orange reaction mixture turned dark yellow and complete and uniform conversion to a new product was observed by ^{29}Si NMR spectroscopy. Two resonances appear at δ = 77.2 and 54.1 ppm. While these values

clearly indicate formation of a disilene, the absence of a characteristically broadened signal rules out the presence of a silicon-boron bond.

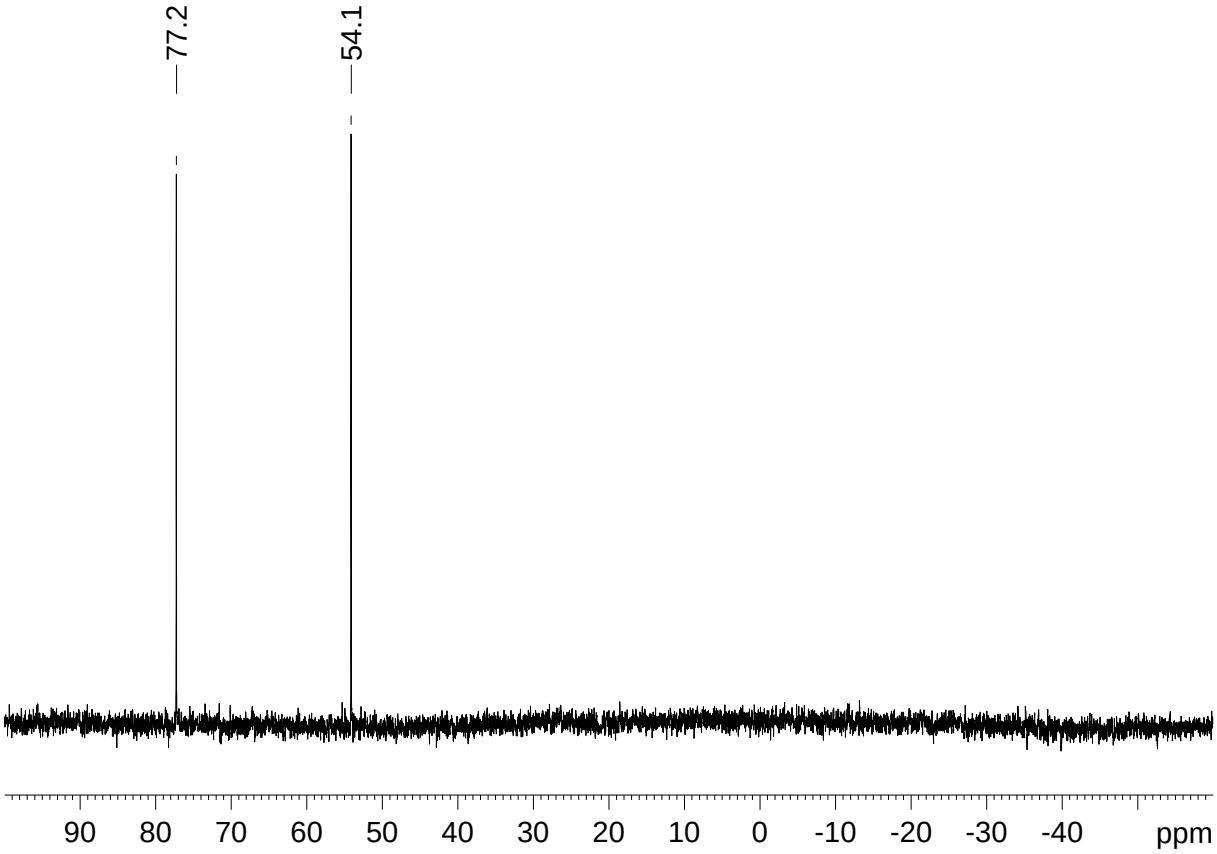

Figure 50. $^{29}Si\{^{1}H\}$ NMR spectrum of methyl substituted disilene **173**.

In the ^{11}B spectrum of the reaction mixture, a resonance at δ = −5.3 ppm can be observed, which is in line with reported values for lithium boron trifluoromethoxyethanolate **172**.[211] The formation of **172** is confirmed by a resonance at δ = −156.7 ppm in the ^{19}F NMR spectrum. We reason that a Lewis-acid induced ether cleavage occurs to methylate **16** and unsymmetrically substituted disilene **173** is obtained (Scheme 97)**.**

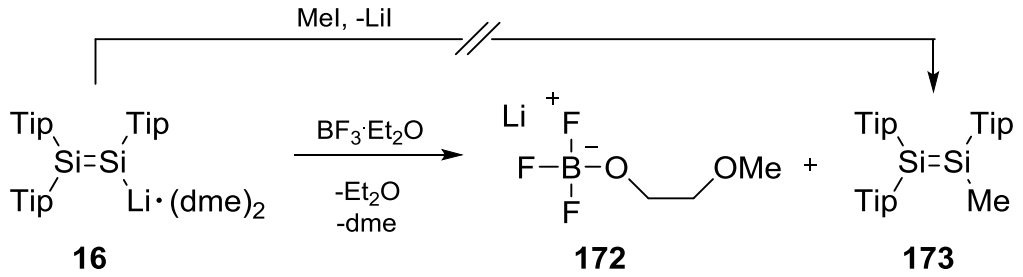

Scheme 97. Synthesis of methyl substituted disilene **173** and proposed by-product **172**.

The use of dme as methylation agent for silanes has been reported by West and coworkers.[212] It was possible to grow yellow single crystals of the silicon containing product in pentane at 0°C and an X-ray diffraction study confirmed the constitution of methyl substituted disilene **173** (Figure 51).

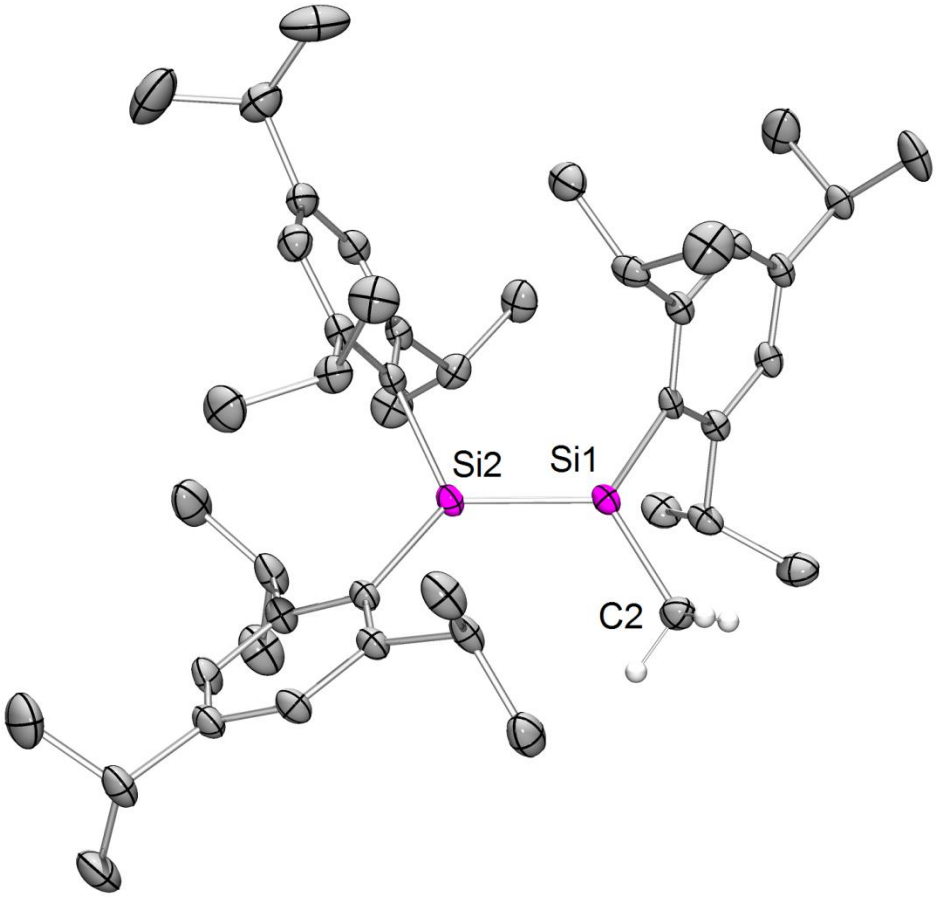

Figure 51. Molecular structure of **173** in the solid state (thermal ellipsoids at 50%, H atoms omitted). Selected bond lengths [Å]: Si1-Si2 2.1533(6).

The length of the Si-Si double bond in **173** is with 2.1533(6) Å at the short end of typical values of disilenes.[27] As a consequence the two slicon atoms of the Si=Si moiety are only slightly pyramidal (Σ of angles around Si1 358.15°, Si2 356.27°). The Si=Si bond is slightly twisted: the twist angle was determined to τ = 6.612°. In the UV/vis spectrum the longest wave length absorption is observed at λ_{max} = 426 nm (ε = 2900 $M^{-1}cm^{-1}$), which in normal range for disilenes with small deviations from planarity.[27]

As outlined in Chapter 1.1.4.2, unsymmetrically substituted disilenes of the type $A_2Si=SiAB$ are accessible *via* the reaction of **16** with the corresponding aryl halides.

It was investigated whether methyl substituted disilene **173** can also be synthesized *via* a direct nucleophilic substitution reaction of disilenide **16** and methyl iodide (Scheme 97). After one equivalent MeI was added to **16** at 0°C, a decolorization of the mixture from orange to pale yellow was observed. Subsequent NMR spectroscopic investigation revealed a mixture of products without indications for the formation of **173**. The resonances observed in the ^{29}Si NMR spectrum are in the typical range for saturated silicon species (δ = 6.1 to −61.9 ppm). Additionally, characteristic Si-*H* resonances are found in the ^{1}H NMR spectrum (δ = 6.24 (d, *J* = 4.6 Hz), 6.17 (d, *J* = 8.1 Hz), 5.77 (d, *J* = 4.6 Hz), 5.7 (s), 5.63 (d, *J* = 8.1 Hz). Obviously, the reaction of disilenide **16** with $BF_3{\cdot}Et_2O$ provides access to unsymmetrically substituted disilenes with one sterically unencumbered side that cannot be synthesized *via* the standard substitution strategy.

3.3.2. Synthesis of *B*-functionalized Boryl Disilenes

The reaction of disilenide **16** with bis(dimethyl)aminochlorophosphane yields phosphasilenes **108a,b**, most likely *via* a 1,3-shift of one amino group in intermediate phosphino disilenes (*cf.* Chapter 1.1.5.3). In case **16** is reacted with Cl_2PNPh_2, chlorine migration to afford the corresponding phoshasilene **161** takes place (*cf*. Chapter 3.1.3).

The reaction of disilenide **16** with analogous boron electrophiles is of distinct interest. Even though a functional group migration from boron to silicon under Si=B bond[213] formation appears less likely due to the electron deficiency at boron, it cannot be excluded from the outset. Furthermore, boryl disilenes with small and reactive substituents on boron are to date unknown and of equal interest.

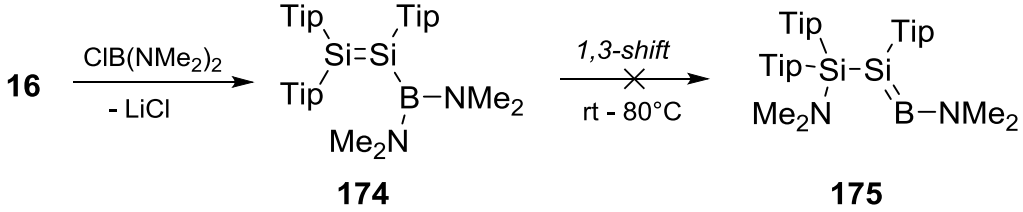

174 **175**

Scheme 98. Synthesis of boryl dsilene **174**.

Disilenide **16** was treated with one equivalent bis(dimethylamino)chloro borane. Clean formation of the corresponding boryl disilene **174** (Scheme 98) was observed by ^{29}Si NMR spectroscopy. Two resonances at δ = 85.8 and 51.3 ppm are in the typical range reported for disilenes.[27] For the signal at δ = 51.3 ppm a characteristic broadening is apparent, which is due to the coupling of this silicon atom to the quadrupolar ^{11}B nucleus. The ^{11}B NMR spectrum revealed a very broad resonance at δ = 38.2 ppm. In the ^{1}H NMR spectrum two signals at δ = 2.63 and 2.57 ppm are attributed to two chemically inequivalent dimethylamino substituents at boron. Even though the reaction is uniform and well reproducible, no single crystals of **174** were obtained to date. Attempts to induce a migration of one amino group to afford silaborene **175** by heating were so far unsuccessful (Scheme 98).

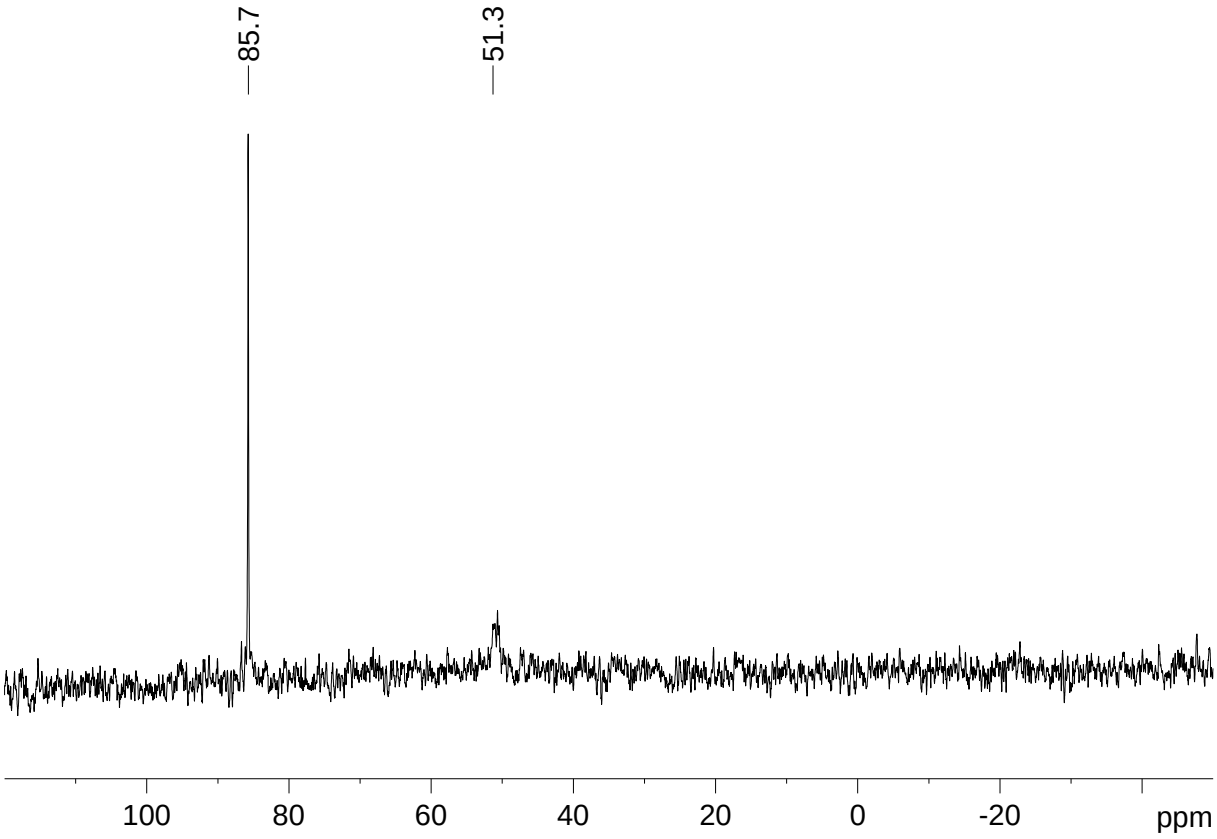

Figure 52. ^{29}Si{^{1}H} NMR spectrum of boryl disilene **174**.

Subsequently, the reaction with dichlorinated boron electrophiles was considered. Residual chlorine functionalization on boron would certainly provide a reactive side in the molecule. Furthermore, it was speculated that a chlorine migration from boron might occur more readily compared to the π-donating amino substituents.

In analogy to the synthesis of **174**, disilenide was treated with one equivalent Cl_2BNPh_2 in toluene (Scheme 99). The ^{29}Si NMR spectrum of the reaction mixture revealed three resonances in the typical area for disilenes at δ = 101.8, 71.2 and 47.7 ppm.[27] While the two low-field resonances (ratio 3:1 according to ^{29}Si NMR spectroscopy) are only slightly broadened, the latter is markedly broader and thus assigned to the boron-bonded silicon atom. In the ^{11}B NMR spectrum no resonance could be observed, which might be due pronounced broadening of the signal. Orange single crystals (M. p. 123-128°C) were obtained in good yields (81%) and investigated by X-ray diffraction which revealed the constitution of boryl disilene **176** (Figure 53).

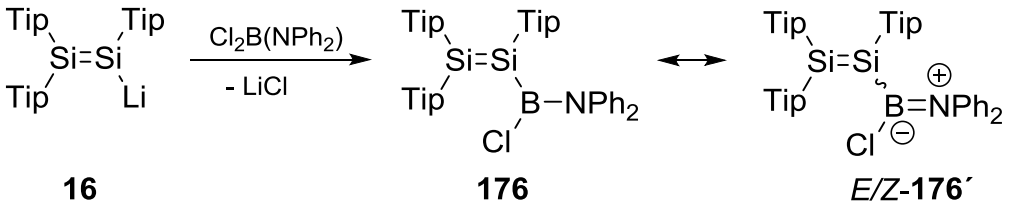

16 **176** *E/Z*-**176´**

Scheme 99. Synthesis of boryl disilene **176** and mesomeric resonance structure *E/Z*-**176´**.

For boryl disilenes **28a,b**[80] and **54a,b**[101,102] published by Sekiguchi two different structural findings were observed. In **28a,b** and **54b** an efficient π-conjugation between the Si=Si-bond and the vacant 2p orbital at boron is not possible due to large dihedral angles between the Si=Si-unit and the boryl group plane (**28b**: 85.4°, **54b**: 52°).[214] In contrast, for **54a** a nearly coplanar arrangement of the Si=Si-bond and the boryl substituent (dihedral angle 17°) is reported. The conjugation between the silicon-silicon double bond and the vacant orbital at boron is in this case confirmed by a significant redshift in the UV/vis absorption spectrum.[101,102]

For **176**, a butadiene-like structure *E/Z*-**176´** is likely due to the π-donating nitrogen substituent. In contrast to tetrasilabutadiene **17**, a *transoid*-conformation is observed for the two formal double bonds. Expectedly, the boron and the nitrogen center are in a perfectly planar geometry (Σ angles 360°) and the N1-B1 bond length (N1-B1 1.400(2) Å) is closer to what has been reported for nitrogen-boron double bonds (1.379-1.391 Å) than to N-B single bonds (1.629-1.698 Å).[215] Both unsaturated silicon centers show only slight deviations from planarity (Σ angles Si1 355.6°, Si2 359.4°). The Si=Si bond is relatively long (Si1-Si2 2.1703(6) Å), which can be taken as an indication for conjugation between the Si=Si- and the formal B=N-bond. For instance,

the length of the Si-Si double bond in phenyl disilene **30** (217.54(11) Å) is comparable, even though **30** shows pronounced *trans*-bending (*trans*-bent angle: θ = Si1 23.6(3)8 and Si2 22.3(3)8°).[77]

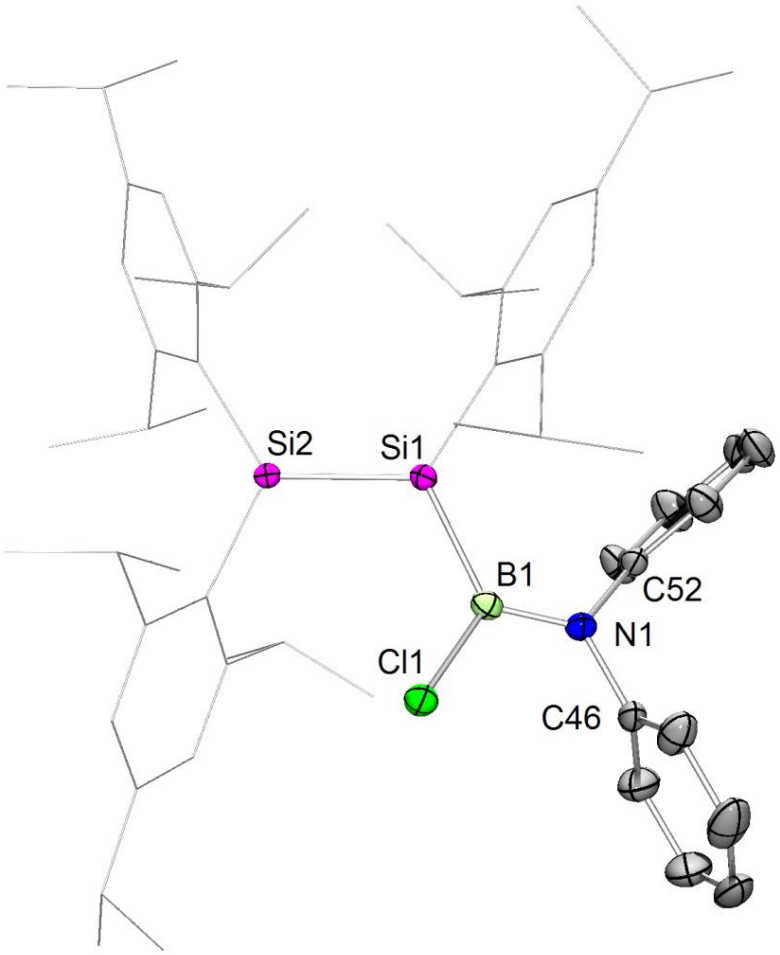

Figure 53. Molecular Structure of **176** in the solid state (thermal ellipsoids at 50%, H atoms omitted). Selected bond lengths [Å]: Si1-Si2 2.1703(6), N1-B1 1.400(2), Si2-B1 2.0043(18).

The torsion angle for Si2-Si1-B1-N1 of 25.270(81)° would indeed allow for a fair amount of conjugation between the two π-bonds. Furthermore, the Si2-B1 bond length is with 2.0043(18) Å slightly shorter than in boryl disilene **28b** (2.022(8) Å) and in the same range as that of **54a** (2.002(4) Å).[80,101,102]

UV/vis spectroscopy shows the longest wavelength absorption of **176** at λ_{max} = 457 nm (Figure 54, Figure 119) which is significantly red-shifted compared to reported nearly planar disilenes (385-430 nm) and a hallmark of conjugation. The longest wavelength absorption in the UV/vis absorption spectra of boryl disilenes **28a,b** and **54b** (λ_{max} = 393, 395 and 411 nm), for which isolated Si=Si-bonds have been confirmed, are hypsochromically shifted compared to **176**. The longest wavelength absorption of **54b**, however, is slightly red-shifted (λ_{max} = 479 nm) compared to **176**.

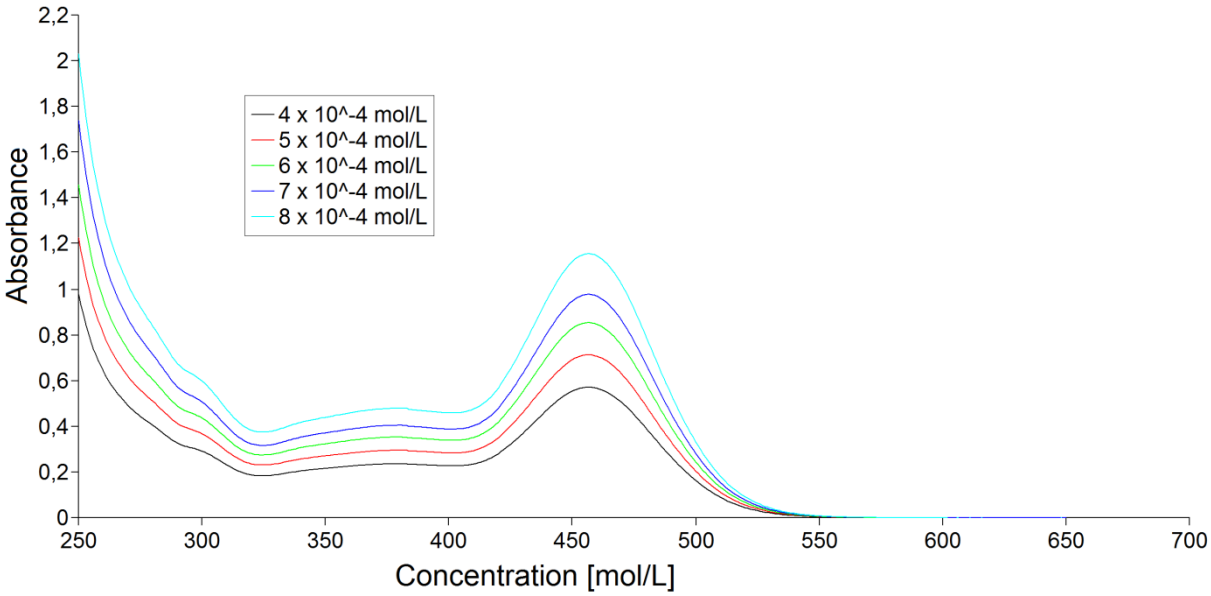

Figure 54. UV/vis spectra of **176** in hexane at different concentrations ($4 \cdot 10^{-4}$ - $8 \cdot 10^{-4}$ mol/L).

When single crystalline material of **176** is dissolved and investigated by NMR spectroscopy at room temperature, two relatively sharp resonances are observed in the ^{29}Si NMR spectrum at δ = 101.8 and 71.2 ppm as well as a very broad signal at 47.7 ppm. Consequently, we anticipated the presence of two isomers in equilibrium, presumably *E/Z*-isomerism of butadiene structure **176´**. While even at 223 K no ^{11}B NMR resonance could be detected, the signals in the ^{29}Si NMR spectrum indeed significantly sharpened (Figure 55). Furthermore, the very broad resonance at δ = 47.7 ppm splits in two resonances (δ = 48.1 and 46.4 ppm) indeed confirming a dynamic process in solution. Remaining broadening of this signal is tentatively attributed to the coupling to the quadrupolar boron nucleus. The resonances of the major isomer in the ^{29}Si NMR spectrum at δ = 101.4 and 46.4 ppm are indeed in line with a conjugated butadiene analogue: in the resonance formulae **176´´** (Scheme 100) the positive polarization of the Si2-atom becomes apparent and we therefore assign the low field resonance at δ = 101.4 ppm to this silicon atom.

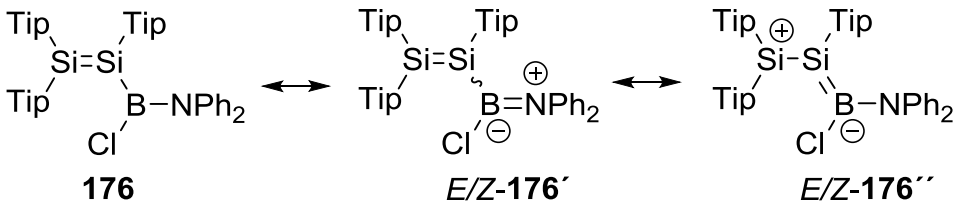

Scheme 100. Resonance formulae of bory disilene **176**.

In case of **54b** a signal at even lower field was reported for the silicon atom in β-position to the boryl substituent due to the electropositive silyl substituents (δ = 150.5 ppm).[101,102] The resonances found for the minor isomer of **176** (δ = 69.6 and 48.1 ppm) show much less wide distribution of chemical shifts which strongly suggests the absence of conjugation between the two formal double bonds. Single crystals of the minor isomer *E*-**176** in order to confirm the absence of conjugation by X-ray structure analysis could not be not obtained.

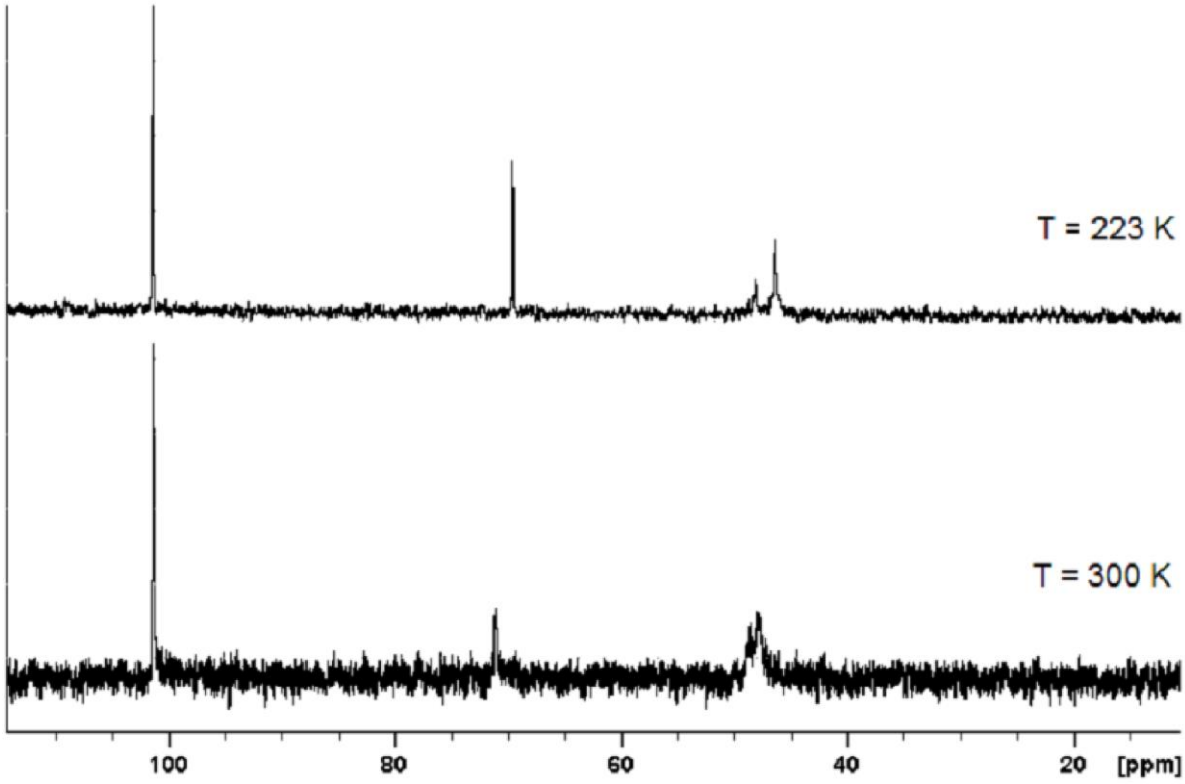

Figure 55. $^{29}Si\{^{1}H\}$ NMR spectra of *E/Z*-**176** at T = 300 K (red) and T = 223 K (blue).

The residual chlorine functionalization in **176** should in principle allow for further manipulations of the system and initial studies in this respect were carried out. Attempts to cleave the chlorine functionality reductively with KC_8 or lithium/naphthalene, however, were unsuccessful so far, resulting in complex, inseparable mixtures. Equally, upon treatment of **176** with $NHC^{iPr_2Me_2}$ no uniform conversion was achieved.

3.3.3. Synthesis of Disilaboriranide 178

The experiments discussed in Chapter 3.3.3-3.3.5 were carried out together with Yannic Heider during his Bachelor project.[210] As already alluded to in the introduction, hydrogen atoms are valuable functional groups in main group chemistry. Especially B-H functionalities are of considerable interest. Hydroboration reactions are renowned as the paragon for hydrometallations as they typically occur under mild conditions without catalysts.[216] Compounds of the type R-BH_2 (R = silyl) are usually prepared by the reaction of silyllithium species with two equivalents $BH_3{\cdot}SMe_2$. In the course of these reactions, the second equivalent $BH_3{\cdot}SMe_2$ typically abstracts one hydrogen atom from the intermediately occuring borates, R-BH_3Li, thus liberating the desired primary borane. The abstraction step is generally rapid compared to the initial addition reaction and the corresponding silyl borates can only be isolated from the reaction of silylanions with $BH_3{\cdot}NEt_3$, which exhibits a significantly reduced Lewis-acidity.[217]

When disilenide **16** was combined with two equivalents $BH_3{\cdot}SMe_2$ in toluene, a complex mixture of products was formed according to NMR spectroscopy. In contrast, the treatment of **16** with one equivalent $BH_3{\cdot}SMe_2$ resulted in a very clean reaction.

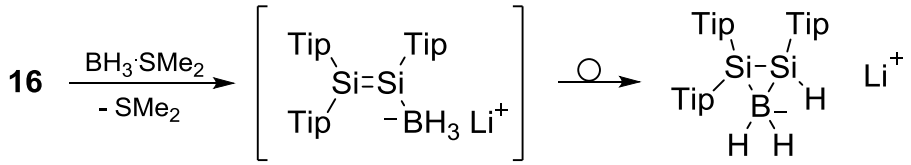

Scheme 101. Synthesis of **178** with proposed intermediacy of disilenyl borate **[177]**.

In the ^{11}B NMR, a triplet is observed at δ = −38.4 ($^1J_{B\text{-}H}$ = 96.1 Hz) ppm in accordance with a four-coordinate boron center coupling to two protons (Figure 56). In the ^{7}Li NMR, the lithium counter cation is found at δ = −0.2 ppm.

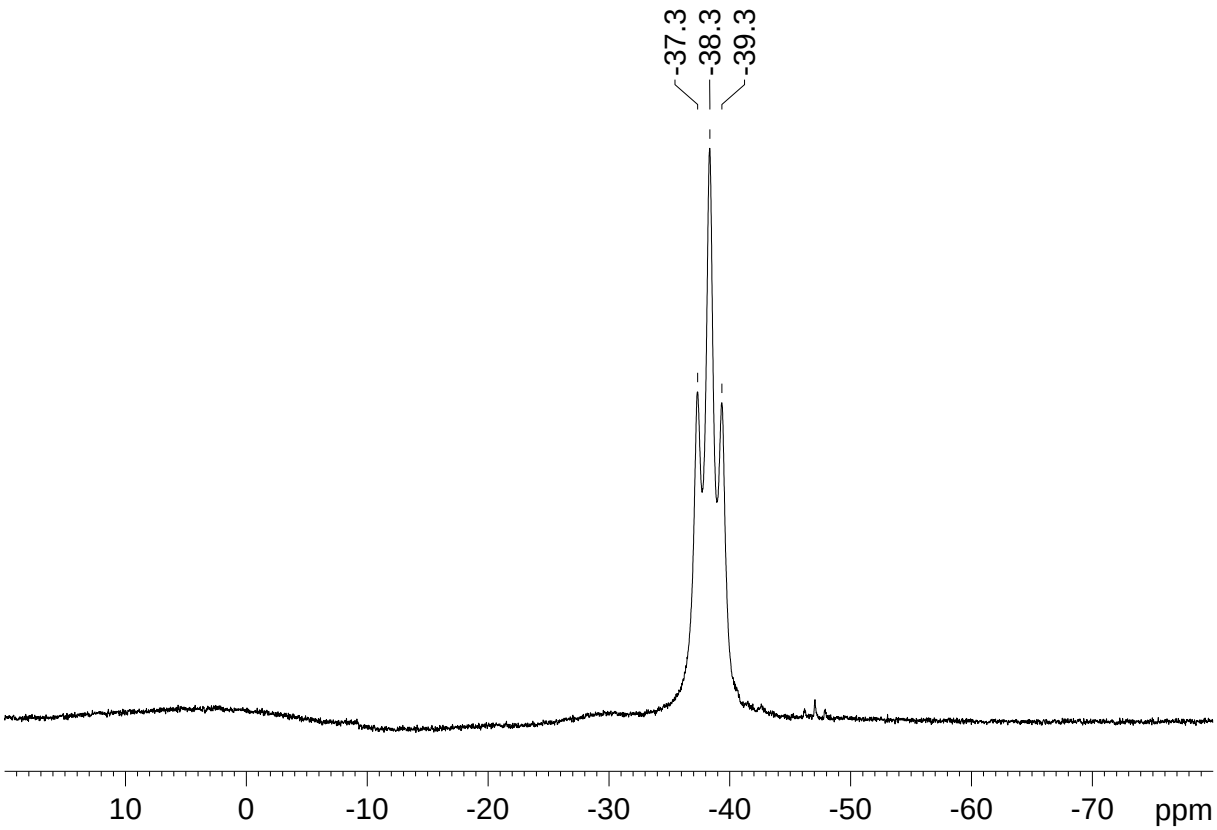

Figure 56. ^{11}B NMR spectrum of disilaboriranide **178**.

Two characteristically broadened resonances in the ^{29}Si NMR spectrum at δ = −81.5 and −99.3 ppm (Figure 57) indicate that both silicon atoms are coupling to the quadrupolar boron nucleus. Consequently, cyclization of an intermediate disilenyl borate **[177]** to afford borate **178** is proposed in analogy to the reported rearrangements of stannyl and silyl disilenes to disilastanniranes **39** and cyclotrisilanes **40a,b**,[84,85] respectively (Scheme 101). Obviously, in case of sp^2-type silyl anions, the hydride abstraction step is considerably slower than the initial addition of the nucleophile to the borane unit. On the basis of two dimensional Si-H correlation NMR spectroscopy, a signal in the ^{1}H NMR at δ = 3.97 ppm was attributed to Si-H resonance further supporting the proposed formation of **178**. The BH_2-unit gives rise to a broadened peak at δ = 1.17 ppm in the ^{1}H NMR spectrum. Unexpectedly, three sharp signals are detected for the aromatic Tip-protons. For comparable cyclic systems, either six sharp signals or broadened resonances are typical in due to the strongly hindered rotation of the bulky Tip groups.[84,85]

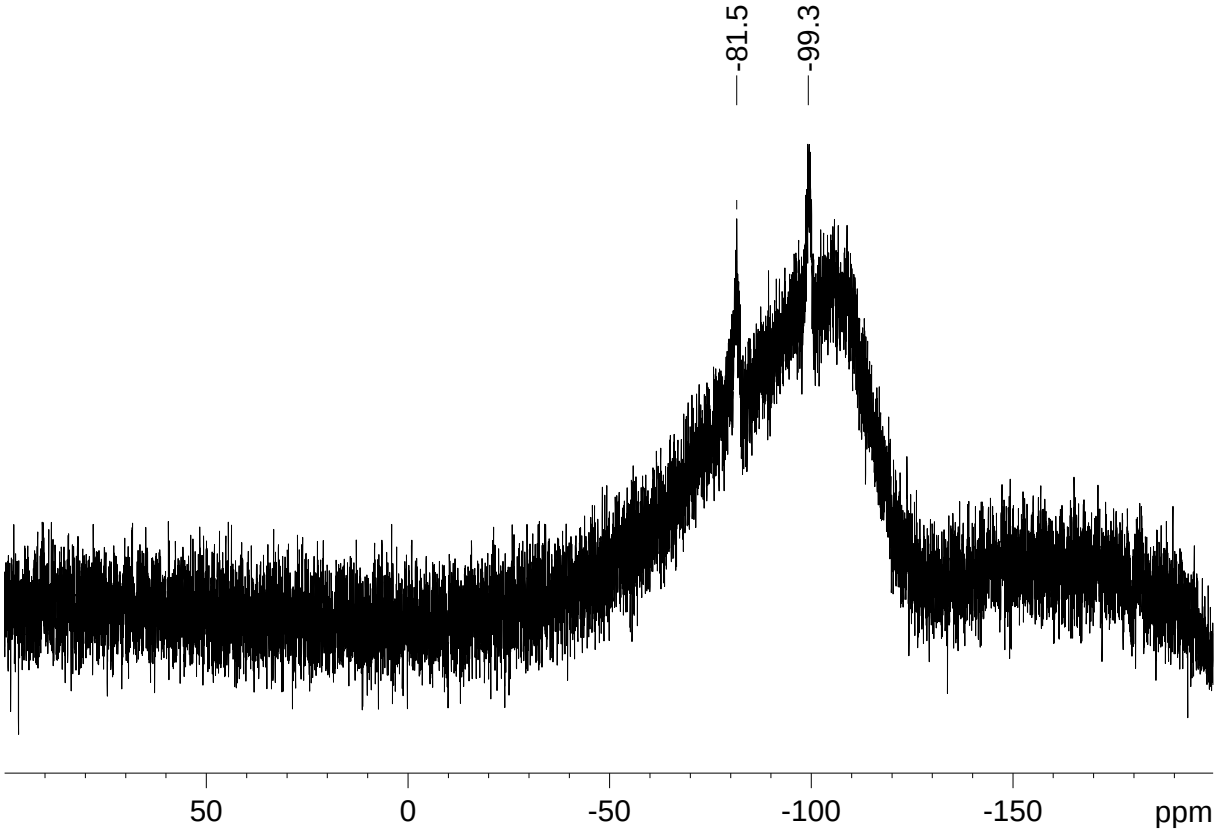

Figure 57. $^{29}Si\{^{1}H\}$ NMR spectrum of disilaboriranide **178**.

Unfortunately, all attempts to grow single crystals of disilaboriranide **178** to finally confirm the molecular constitution by an X-ray structure analysis were unsuccessful. The compound shows limited stability in concentrated solutions in apolar solvents. Upon leaving a pentane solution for several days, formation of an oily residue with a very broad resonance in the ^{11}B NMR spectrum at δ = −40 ppm is observed even at low temperatures. Efforts to obtain a solvent-separated ion pair by application of sequestering agents such as dme, TMEDA (tetramethylethylene diamine), 12-crown-4 or [2.2.1]-cryptand resulted in decomposition of **178**. A cation exchange reaction with *n*-butyltriethylammonium chloride led to the same result.

3.3.4. Hydride Abstraction Attempts from Disilaboriranide 178

The hydrogen abstraction reaction from disilaboriranide **178** to give a neutral borane derivative is interesting with respect to the potential use of the neutral target product in hydroboration reactions. Furthermore, according to theoretical calculations by Skancke and Liebman, in the parent Si_2BH_5 system the boryl silylene **179a** is the

global minimum structure.[218] In 2003, Jemmis *et al.* reported further calculations on the Si_2BH_5 system: cyclic disilaborirane **179a´** containing a pyramidal tricoordinate boron center was found as minimum structure and significantly lower in energy than the conventional planar geometry in **179a´´** (Scheme 102).[219]

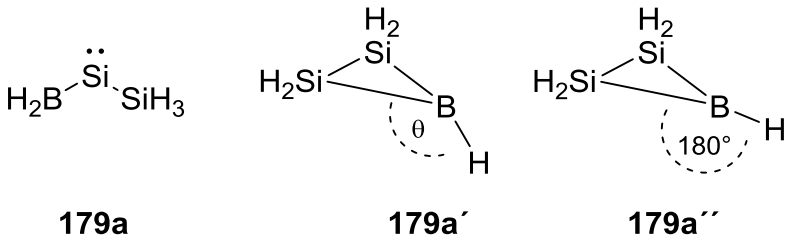

179a **179a´** **179a´´**

Scheme 102. Calculated global minimum isomers of the Si_2BH_5 system: boryl silylene **179a** (Skancke/ Liebmann) and cyclic disilaborirane **179a´** showing pyramidalization (θ) at the boron center (Jemmis *et. al.*) in contrast to conventional planar geometry (**179a´´**).[218,219]

Even though the straight forward method to $Si_2BTip_3H_2$-derivatives *via* the reaction of disilenide **16** with two equivalents $BH_3{\cdot}SMe_2$ was not successful, the reported computational studies encouraged us to further investigate hydride abstraction reactions from crude disilaboriranide **178** as a possible access to **179b** or one of its constitutional isomers such as **179b´**. Several reagents are known to effectively abstract hydrogen atoms from borates.[220-222] For the attempted hydrogen abstraction reactions described in the following **178** was prepared according the procedure outlined above and used without further purifications.

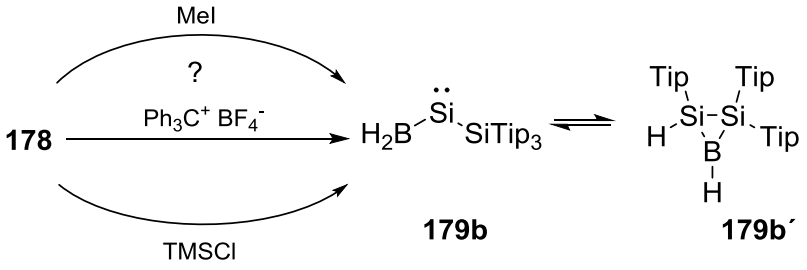

179b **179b´**

Scheme 103. Presumed reactivity of disilaboriranide **178** towards hydrogen abstraction reagents.

Reactions of borates with methyl iodide yield beside the corresponding boranes only lithium iodide and methane as by-products, which are easy to separate from the reaction mixture.[220] An equimolar amount of methyl iodide was added to a solution of disilaboriranide **178** in benzene. The ^{11}B NMR spectrum of the reaction mixture

revealed two very broad multiplet resonances from δ = −38.2 to −46.6 and from δ = −30.9 to −33.1 ppm. In the ^{29}Si NMR spectrum three major signals are observed at δ = −50.5, −75.0 and −78.5 ppm. Three minor resonances appear at δ = −61.8, −65.9 and −73.5 (Figure 58).

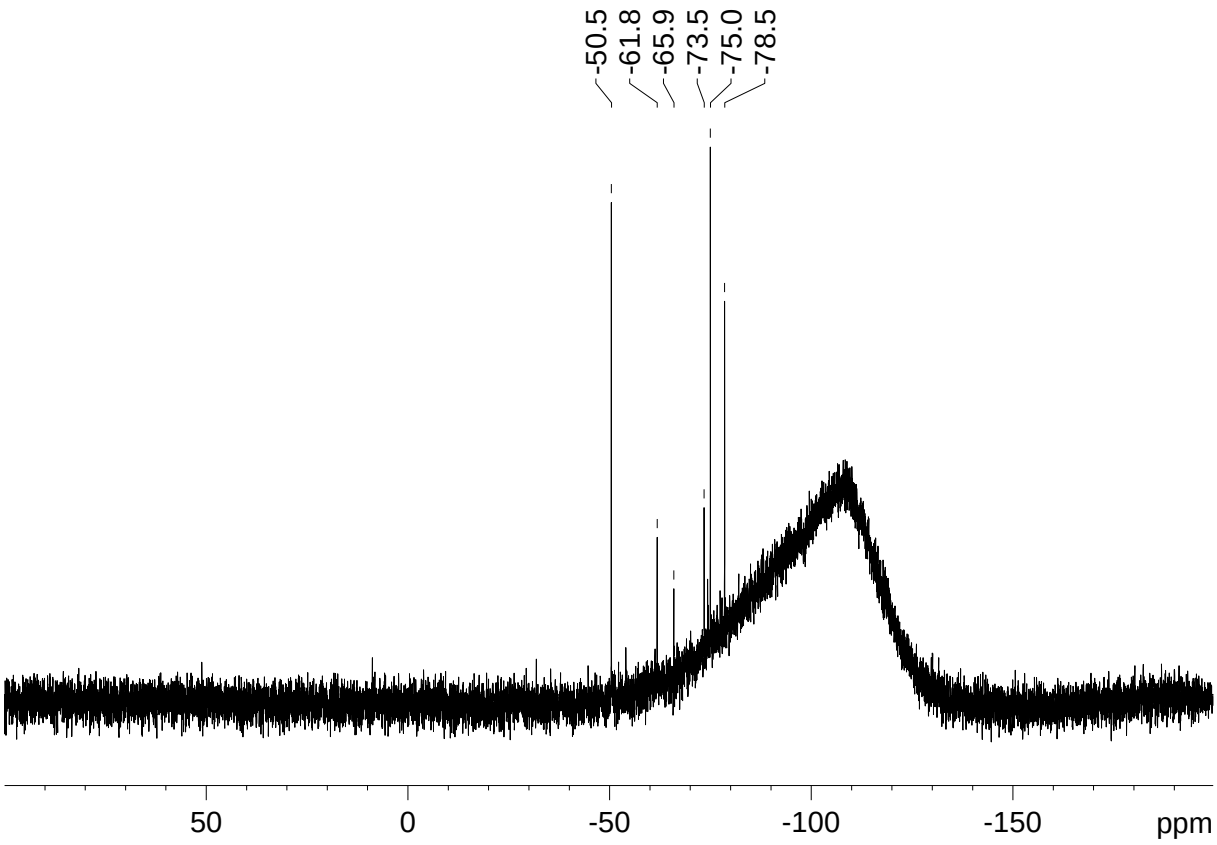

Figure 58. ^{29}Si{^{1}H} NMR spectrum from the reaction of crude disilaboriranide **178** with methyl iodide.

While the sharpness of the ^{29}Si NMR resonances hints towards the absence of intact Si-B bonds, the range of the chemical shifts of the signals speak for the formation of saturated cyclic silicon species. Neither product could be isolated.

In a next attempt, disilaboriranide **178** was treated with one equivalent trityl tetrafluoroborate as hydride abstraction reagent.[221] The ^{29}Si NMR spectrum of the product shows two major signals at δ = −65.9 and −78.5 ppm and a second set of minor intense resonances at δ = −61.8 and −73.6 ppm (Figure 59). Notably, these signals were already observed in the ^{29}Si NMR spectrum from the reaction of **178** with methyl iodide even though in a different ratio (*vide supra*).

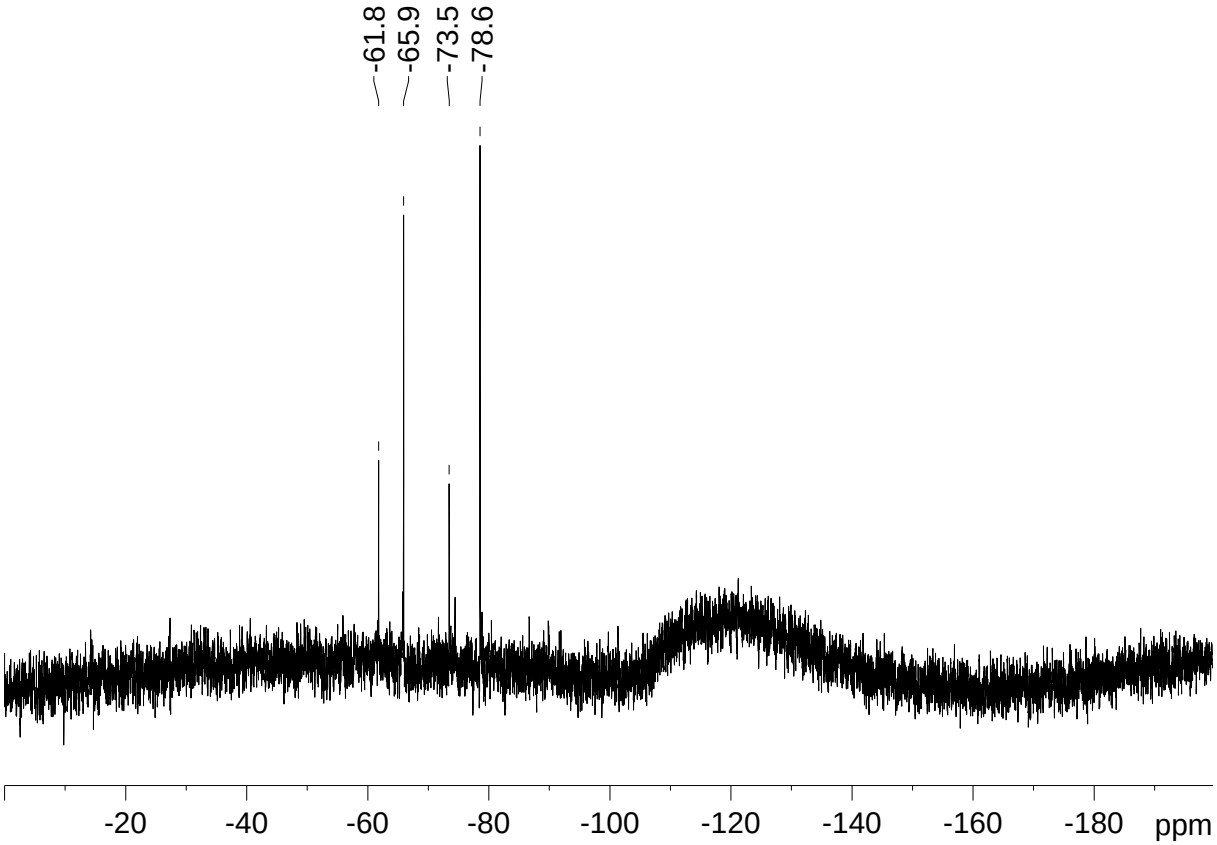

Figure 59. $^{29}Si\{^{1}H\}$ NMR spectrum from the reaction of crude **178** with $Ph_3C^+BF_4^-$.

In the ^{11}B NMR spectrum a broad signal at δ = −25.2 ppm as well as three triplet resonances at δ = −33.2 ppm ($^{1}J_{B\text{-}H}$ = 74.7 Hz), −40.5 ppm ($^{1}J_{B\text{-}H}$ = 85.6 Hz) and −45.2 ($^{1}J_{B\text{-}H}$ = 85.6 Hz) ppm are observed. Apparently, also in this case Si-B bond cleavage occurs and a cyclic silane is formed.

The use of trimethylchlorosilane as another hydride scavenger has been reported.[222] In a last attempt to abstract hydride from disilaboriranide **178**, it was combined with one equivalent of Me_3SiCl. The color of the reaction mixture changed from yellowish to deep red. Curiously, no resonance could be detected in the ^{11}B NMR spectrum. In the ^{29}Si NMR spectrum three sharp signals were found in the range of cyclic, saturated silicon species at δ = −12.4 ppm, −76.6 ppm and −79.2 ppm (Figure 60) again speaking against the presence of a Si-B bond. On the basis of Si/H correlation 2D NMR spectroscopy, the ^{29}Si resonance at δ = −12.4 ppm can be assigned to the trimethylsilyl unit. The corresponding C*H*$_3$-protons are identified at δ = 0.3 ppm in the ^{1}H NMR spectrum. Interestingly, the SiC*H*$_3$ unit shows an additional cross peak in the Si/H correlation NMR spectrum to the resonances at δ = −79.2 ppm and −76.6 ppm (Figure 61). These findings unambiguously proof the incorporation of the $SiMe_3$ moiety into the final product.

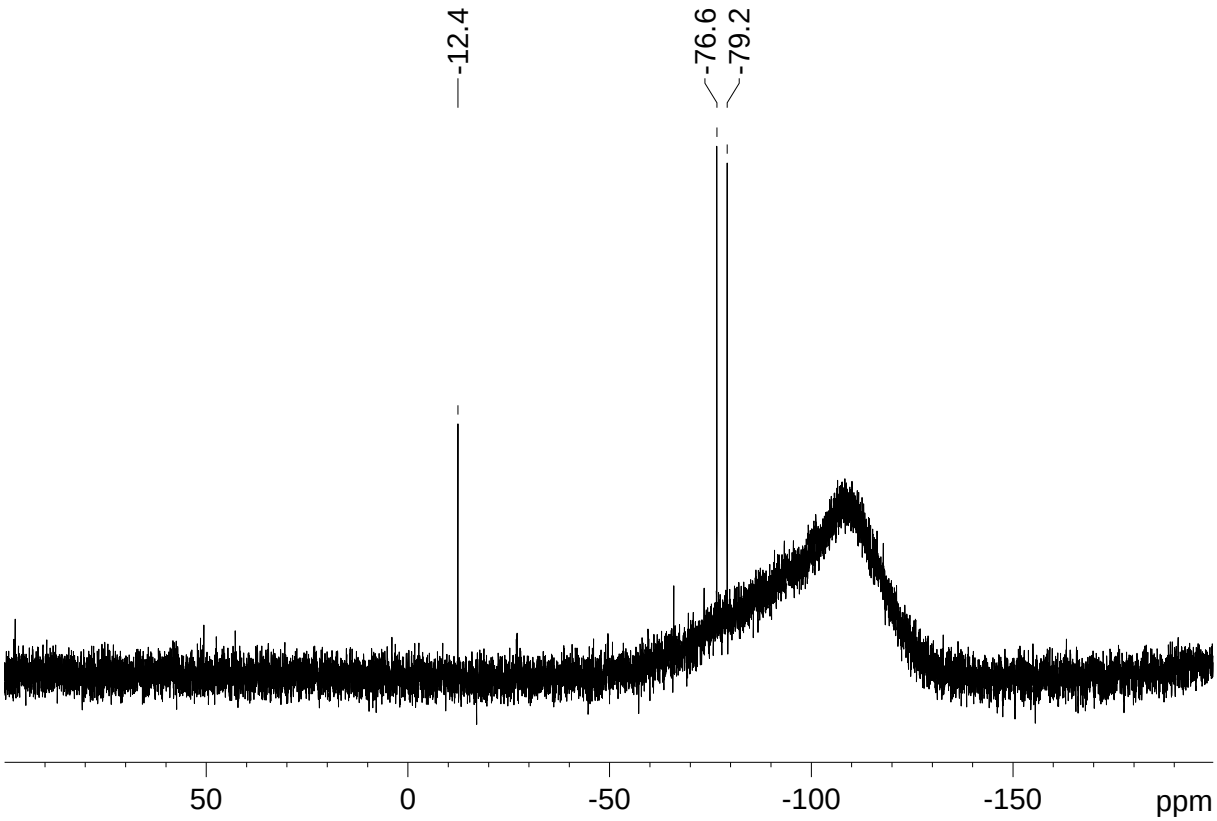

Figure 60. $^{29}Si\{^{1}H\}$ NMR spectrum from the reaction of crude **178** with Me_3SiCl.

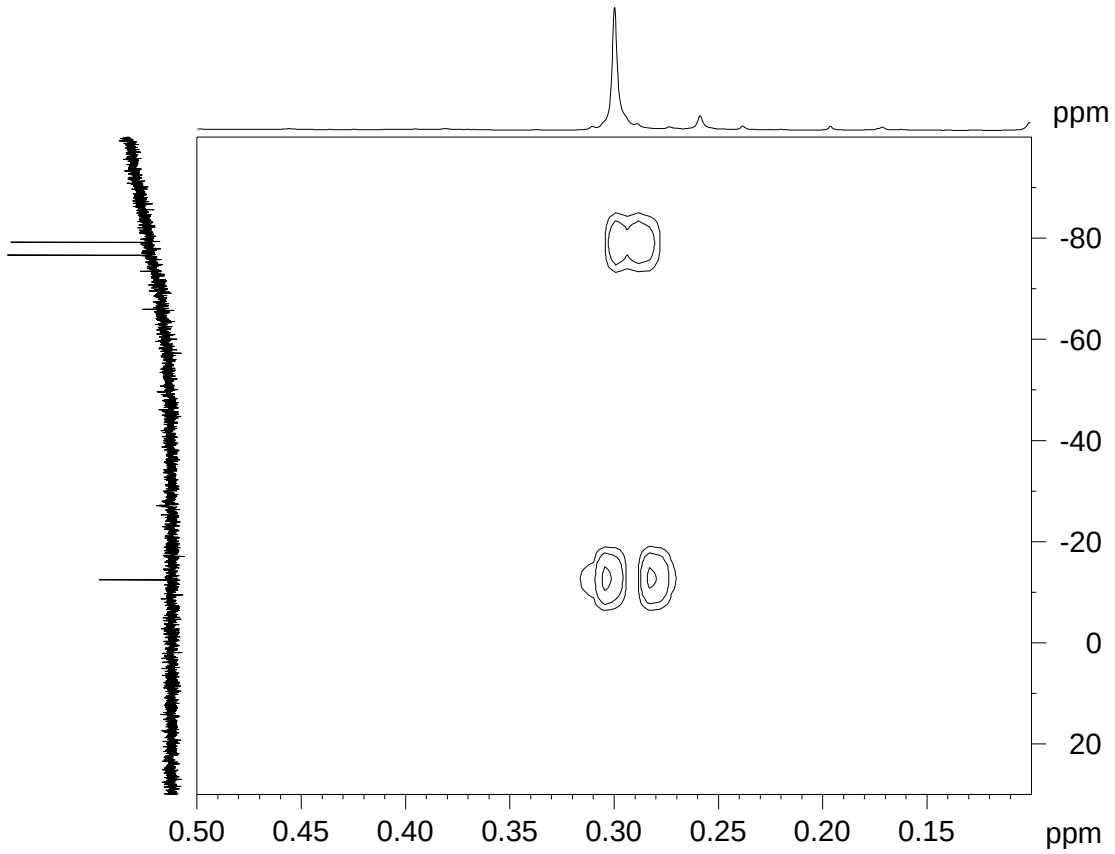

Figure 61. Selected section of the Si/H correlation 2D NMR spectrum from the reaction of crude **178** with Me_3SiCl.

Unfortunately, hitherto no crystal structure of any of the products was obtained from the hydride abstraction attempts from disilaboriranide **178** was obtained and so no further assertions can be made concerning structural details. Equally, the mechanism of the Si-B bond cleavage as well as the incorporation of the trimethylsilyl moiety into the molecule remains at present obscure.

The initial formation of a neutral species of the type **179** during the hydride abstraction attempts cannot be excluded even though no indications were found by NMR spectroscopy. Performing a hydrogen abstraction reaction in the presence of an alkyne could trap possible transient intermediates featuring B-H functionality *via* hydroboration. However, the borate **178** itself readily reacts with phenyl acetylene to a complex mixture, so that further investigations in this regard were abandoned.

3.3.5. Synthesis of Disilenyl Borate 180

A major problem in obtaining single crystals of disilaboriranide **178** is the aforementioned instability of the compound in concentrated solution. A sterically demanding substituent at boron might overcome this instability and it was therefore decided to study the reactivity of **16** towards *tert.*-butyl borane. It has to be taken into account that the increased bulk at boron might prevent cyclization in analogy to what had been reported for (chloro)stanyl disilene **28d**.[85]

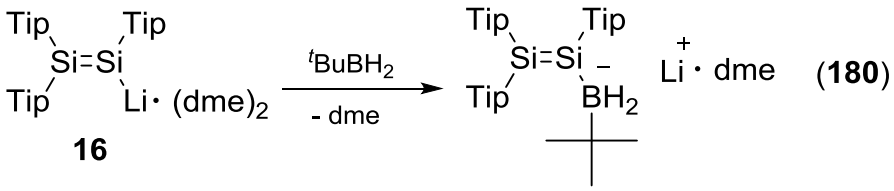

Scheme 104. Synthesis of disilenyl borate **180**.

Tert.-Butylborane was synthesized starting from lithium *tert.*-butyltrihydroborate and hydrogen chloride and due to its limited stability directly reacted with an equimolar amount of disilenide **16**. In the ^{11}B-NMR spectrum of the product a triplet resonance is observed at δ **=** −19.9 ppm which is in line with an anionic BH_2 moiety indicating an open chained system **180**.

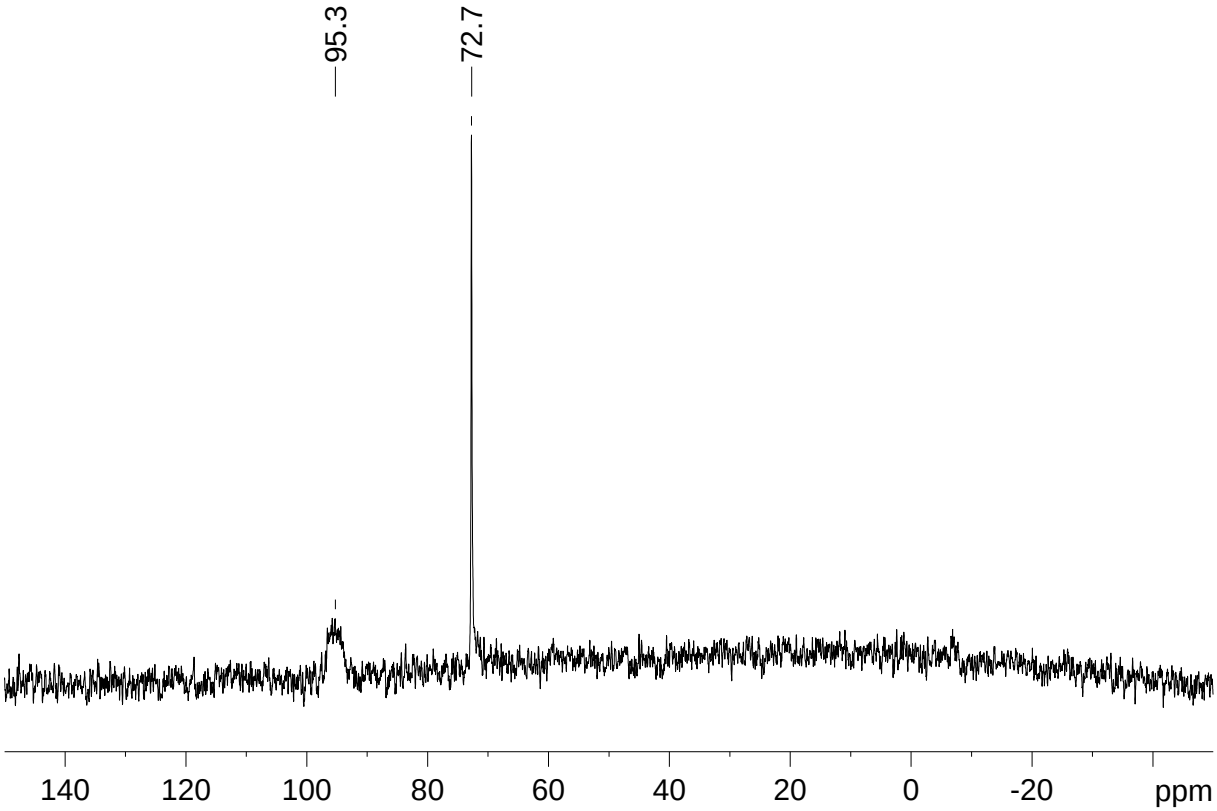

Figure 62. $^{29}Si\{^{1}H\}$ NMR spectrum of disilenyl borate **180**.

The lithium counter cation is observed by ^{7}Li NMR spectroscopy at δ = −0.79 ppm and the resonances at δ = 2.52 ppm and 2.86 ppm in the ^{1}H-NMR spectrum are assigned to coordinated dme. The ^{29}Si NMR spectrum revealed two resonances at δ = 95.3 and 72.7 ppm (Figure 62). For the low-field resonance a very strong broadening is apparent and consequently this signal is assigned to a Si-B unit. Both ^{29}Si NMR resonances are in the typical range for disilenes further supporting the constitution of disilenyl borate **180**. Yellow single crystals (M. p. 151°C) were obtained at room temperature from a concentrated hexane solution in 58% yield. X-ray analysis confirmed the NMR spectroscopic findings and revealed the structure of the first isolated disilenyl borate **180** (Figure 63).

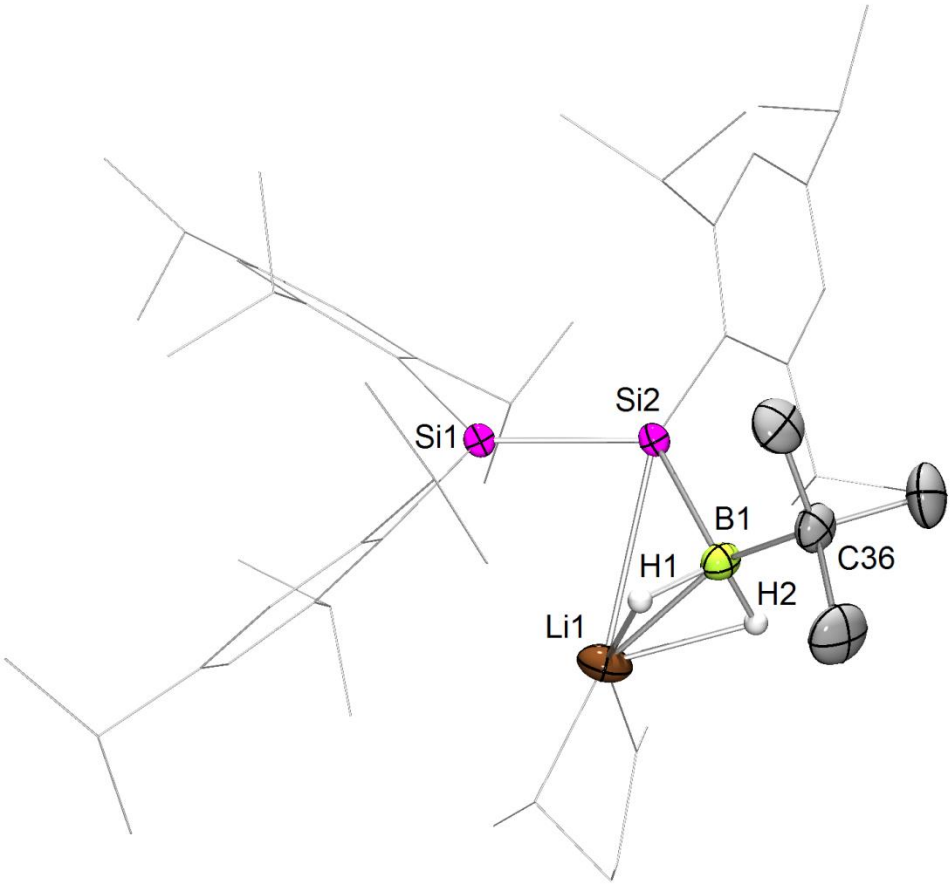

Figure 63. Molecular structure of **180** in the solid state (thermal ellipsoids at 50%, H atoms omitted). Selected bond lengths [Å]: Si1-Si2 2.1802(5), Si2-B1 2.0435(16), Si2-Li1 2.834(3), Li1-B1 2.296(3).

Both unsaturated silicon atoms show a nearly planar geometry (Si1 359.97°, Si2 359.81°) which is in line with theoretical predictions by Apeloig *et al.* that have demonstrated the influence of electropositive substituents such as boron (and thus a borate in particular) on the conformation of the Si=Si bond.[43] The length of the Si=Si-bond (2.1802(5) Å) is larger compared to what was reported for planar disilenes and even longer than in phenyl disilene **30** (2.1754(11) Å) showing pronounced *trans*-bending (23.6(3)8 and 22.3(3)°).[77] The silicon boron bond (Si2-B1 2.0435(16) Å) is longer than in silyl borates (RPh_2SiBH_3)Li (R = Ph, ^{t}Bu) (1.984-1.993 Å),[223] presumably to due larger steric congestion about the boron center. Furthermore the Si1-B1 distance is slightly longer than in boryl disilene **28b** (2.022(8) Å) featuring an isolated Si=Si-bond.[80]

The UV/vis spectrum of **180** (Figure 120) revealed the longest wavelength absorption at λ_{max} = 414 nm which is comparable to reported planar disilenes (385-430 nm). The extinction coefficient (ε = 3700 $M^{-1}cm^{-1}$, Figure 121), however, is lower than in

disilenes of comparable geometry (> 10000 $M^{-1}cm^{-1}$). For disilenide **16** an even smaller extinction coefficient has been reported (ε = 760 $M^{-1}cm^{-1}$).[69]

3.4. Functionalization and Transfer of Siliconoids

3.4.1. An Anionic Siliconoid

Siliconoids are unsaturated silicon cluster compounds with at least one naked silicon vertex in a neutral molecule with a three dimensional silicon backbone.[142] The naked vertices are reminiscent of the so called “dangling bonds” of silicon surfaces[150] making siliconoids suitable models to study surface properties on a molecular level. Furthermore, similar silicon clusters with unsubstituted vertices have been detected during CVD processes of silanes to produce amorphous silicon (a-Si).[153] The incorporation of unsaturated silicon clusters in the matrix of a-Si is to some degree determining its properties such as the band-gap.[154] Recently, the targeted synthesis of siliconoids has been achieved by ourselves[157,160,165] and by the groups of Wiberg and Veith[158] and Breher[159] (*cf.* Chapter 1.2.2). Interesting properties of these compounds such as a pronounced electronic anisotropy that is manifest in an unprecedented wide distribution of ^{29}Si NMR chemical shifts make them promising precursors for silicon based materials. As for low-valent main group compounds in general, the presence of functionalities is crucial in this regard. While for the introduction of functional groups to silicon containing double bonds several examples has been reported (*cf*. Chapter 1),[34] functionalized siliconoids were hitherto unknown. Dr. Kai Abersfelder found in studies related to his PhD thesis that the reduction of cyclotrisilane **121** with an excess of naphthalene/lithium (compared to the synthesis of dismutational hexasilabenzene isomer **122**) leads to the reductive cleavage of one aryl substituent to afford anionic siliconoid **133** (Scheme 105).

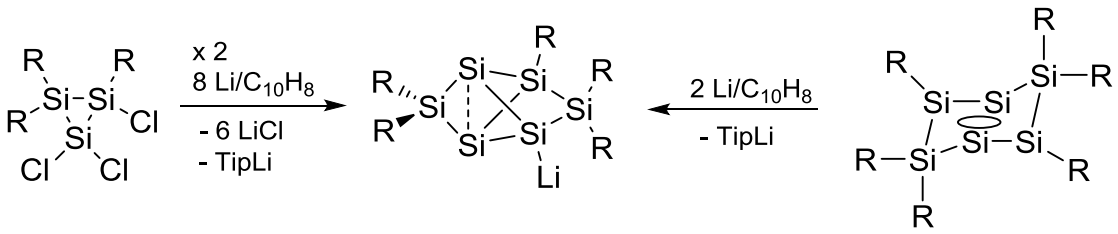

Scheme 105. Synthesis of anionic siliconoid **133** either from 1,1,2-trichlorocyclotrisilane **121** or from dismutational isomer **122** (R = Tip).

In this project, this synthetic route was reproduced and indeed **133** isolated in 62% yield as orange crystals (*cf.* Chapter 5.7.1, experimental). We reasoned that the dismutational hexasilabenzene isomer **122** must be the initial product of the reduction, followed by the cleavage of a Tip-substituent. The reductive cleavage of aryl substituents in silicon compounds is known to generate anionic species.[69,224] An undetected anionic intermediate would then isomerize to the isolated bridged propellanide **133** resembling the assumed global minimum structure **125**. To confirm this assumption, **122** was dissolved in diethyl ether and two equivalents of lithium/naphthalene solution in thf were added at −80°C. Upon warming to room temperature, the green solution turned dark orange. In the ^{29}Si NMR spectrum of the reaction mixture the clean formation of anionic siliconoid **133** can indeed be confirmed. Six resonances are observed with a large dispersion of chemical shifts similar to those reported for the global minimum isomer **125**.[165] The ^{29}Si NMR signal of one $SiTip_2$ moiety appears far downfield at δ = 159.6 ppm, while resonances for another $SiTip_2$ and a monosubstituted SiTip unit are found in the usual region at δ = 12.8 and 27.6 ppm, respectively (in **125**: δ = 174.6, 14.8 and 27.6 ppm). Notably, two upfield signals at δ = −237.3 and −238.2 ppm are detected that can be assigned to the “naked” silicon vertices (in **125**: δ = −274.2 ppm). A resonance at δ = −66.8 ppm is assigned to a lithium-bonded silicon atom on grounds of the apparent broadening through the coupling to the quadrupolar ^{7}Li nucleus.

The bridged propellanide crystallizes with two molecules of thf coordinated to the lithium as contact-ion pair **133**·$(thf)_2$ albeit with low quality data due to pronounced disorder. The lithium cation in **133** has been sequestered with 12-crown-4 by Dr. Kinga Leszczyńska and the structure of **133**·$(12\text{-crown-4})_2$ could be refined without major disorder problems.[225] The distance between the unsubstituted bridgehead atoms in **133** (Si1–Si2 2.5506(9) Å) is much shorter than in **125** (2.7076(8) Å)[165] or in

Breher´s pentasilapropellane **120** (2.636 Å, Mes = 2,4,6-trimethylphenyl),[159] which is tentatively attributed to delocalization of the lone pair of the anionic silicon atom into cluster bonding orbitals. While all other Si-Si bond lengths are comparable to those of the global minimum Si_6Tip_6 isomer **125**,[165] the release of steric strain by the elimination of one of the Tip-groups is reflected in a less-acute angle between the two bridged "propeller blades" in **133** (Si1-Si2-Si3/Si1-Si2-Si4: 107.618°) *versus* the corresponding angle in **125** (96.78°).[165]

Anionic siliconoid **133** closes the conceptual gap between siliconoids and silicon based Zintl anions. For Zintl anions of germanium and tin the partial compensation of negative charges *via* the reaction of Zintl anions with nucleophiles (top-down, *cf.* Chapter 1.2.1) has been reported. By this means, anionic metalloid clusters, intermediate species between metalloid germanium and tin clusters and the corresponding Zintl anions, are accessible.[134] In case of silicon, such an approach is unknown as yet. The bottom-up synthesis of electron precise tetrasilahedranide **114c** represents the sole example of formal partial compensation of negative charges in Zintl anions.[139] Notably, the anionic **133** represents the first example of a functionalized siliconoid: with its nucleophilic silicon vertex it should be a valuable synthon for further manipulations of the uncompromised Si_6R_5-scaffold. Based on the pronounced thermodynamic stability of **125** (the alleged global minimum on the Si_6Tip_6 potential-energy surface),[165] **133** can be regarded as the silicon analogue of phenyl lithium. A first proof that **133** is indeed a viable synthon to transfer the intact Si_6R_5-unit has been provided by Dr. Kai Abersfelder.[168] The reaction of **133** with silicon tetrachloride yielded trichlorosilyl substituted bridged propellane **181** (Scheme 106).

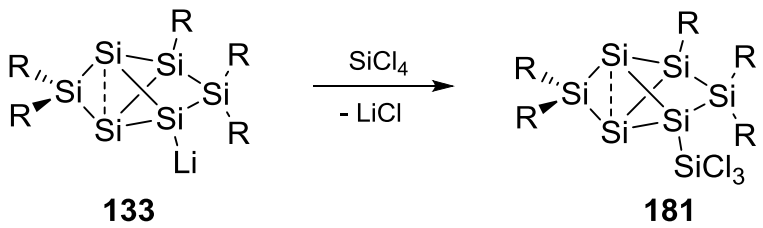

133 **181**

Scheme 106. Synthesis of silyl substituted siliconoid **181** (R = Tip) initially performed by Dr. Kai Abersfelder.

The unsaturated skeleton in **181** is perfectly intact and the usually highly reactive "naked" silicon vertices remain untouched. This is readily deduced from the characteristic wide distribution of ^{29}Si NMR chemical shifts. As observed for **125** and

133 the two unsubstituted silicon atoms of **181** appear at high-field (δ = −252.3 and −264.3 ppm), while the neighboring $SiTip_2$-unit is strongly deshielded (δ = 175.4 ppm, Figure 64). Surprisingly, despite chemical equivalence, the two naked vertices give rise to two different ^{29}Si NMR signals. These findings were tentatively attributed to hindered rotation of the substituents and/or the functional group. Indeed, the highfield resonances of **181** are considerably broadened at room temperature and we decided to investigate the compound by a VT-NMR study. Cooling to 223 K resulted in a significant sharpening of these particular resonances. Coalescence is observed at 315 K, finally leading to a still somewhat broadened signal at δ = −256.7 ppm at 343 K (Figure 64). By application of the Eyring equation, the barrier of rotation for the $SiCl_3$ group is estimated:

Eyring equation: $k = \frac{RT}{h*N_A}\, e^{-\frac{\Delta G^{\#}}{RT}}$

At coalescence temperature: $k_{T_c} = \frac{\pi}{\sqrt{2}} |\nu_A - \nu_B|$

⇨ $\Delta G^{\#} = RT_c \ln \frac{\sqrt{2} RT_c}{h\,|\nu_A - \nu_B|\pi\, N_A} = 57.9$ kJ

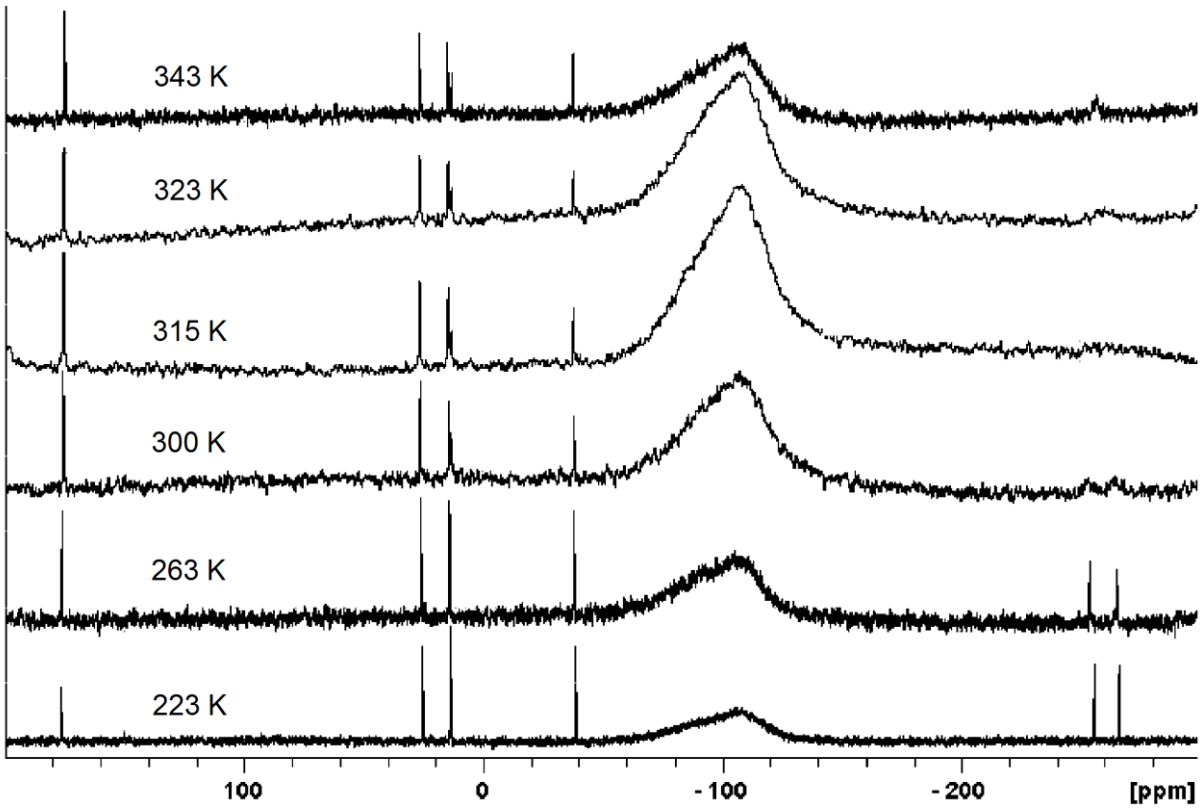

Figure 64. $^{29}Si\{^1H\}$ NMR spectrum of **181** at different temperatures (223 K-343 K).

3.4.2. Synthesis of Pivaloyl Substituted Siliconoid 182

The experiments discussed in this chapter were carried out together with Yannic Heider during his Bachelor studies.[210] The synthesis of silyl-substituted bridged propellane **181** from the reaction of anionic siliconoid **133** with silicon tetrachloride[168] gives a first indication that **133** is indeed a promising synthon for the nucleophilic transfer of the intact cluster core to electrophiles and by this means obtain functionalized siliconoids. Notably, residual chlorine functionalities are tolerated on the newly introduced substituent. Consequently further manipulations of the system should be possible.

During this project, the reactivity of anionic siliconoid **133** towards different electrophiles was investigated to demonstrate the general applicability of this concept to synthesize functionalized siliconoids. Generally, we focused on retaining functionality on the newly introduced substituent, available for further manipulations at a later stage.

To investigate whether the Si_6-core can be transferred to organic electrophiles, **133** was treated with one equivalent pivaloyl chloride. The dark orange solution turned deep red and quantitative conversion to a new product was observed by NMR spectroscopy. The characteristic distribution of chemical shifts in the ^{29}Si NMR spectrum confirms that the bridged propellane skeleton remains intact and pivaloyl substituted derivative **182** has been formed (Scheme 107).

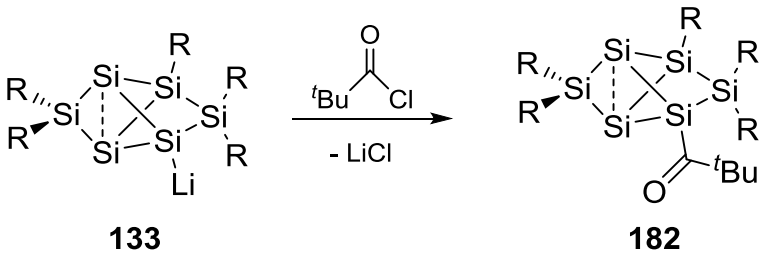

133 **182**

Scheme 107. Synthesis of ketone functionalized silconoid **182**.

One $SiTip_2$-unit is observed at very low field (δ = 171.8 ppm) while two highfield signals (δ = −264.7 and −271.1 ppm) unambiguously indicate that the unsubstituted silicon vertices are not comprised by the reaction. The fact that sharp resonances are observed for the “naked” silicon atoms is attributed to the higher steric demand of the

pivaloyl substituent compared to $SiCl_3$ and thus more hindered rotation. As expected for the bridged propellane motif[165] the remaining ^{29}Si NMR signals appear in a less conspicuous area: 13.6 (*Si*Tip$_2$), 10.1 (*Si*Tip), and −27.4 ppm for the carbonyl substituted silicon.

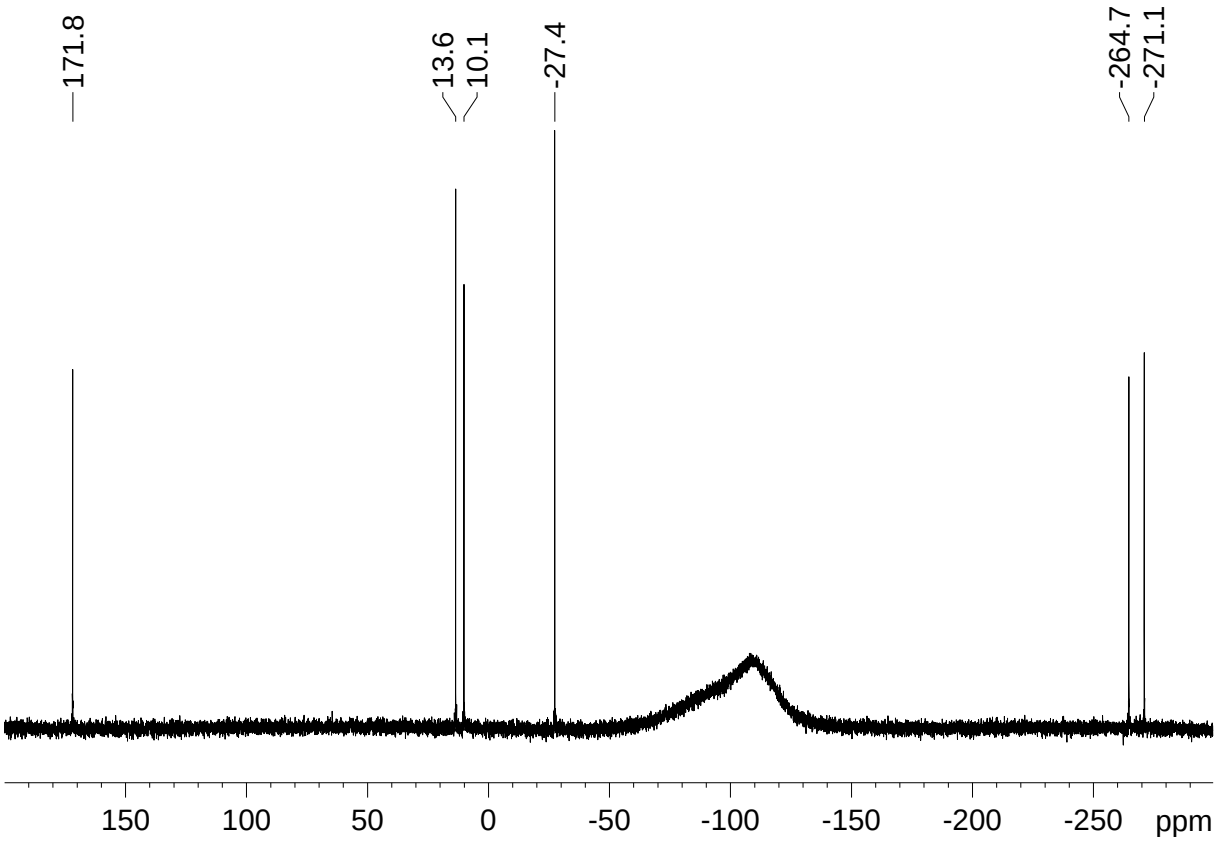

Scheme 108. ^{29}Si{^{1}H} NMR spectrum of ketone functionalized siliconoid **182**.

The ^{13}C shift of the carbonyl carbon of **182** is observed at δ = 239.0 ppm in the typical range for silyl-substituted ketones.[226] In line with reported CO stretching frequencies, the two characteristic absorptions in the infrared spectrum of **172** at ν = 1637 and 1602 cm^{-1} are assigned to the asymmetric and symmetric C=O stretches of the carbonyl moiety.[227]

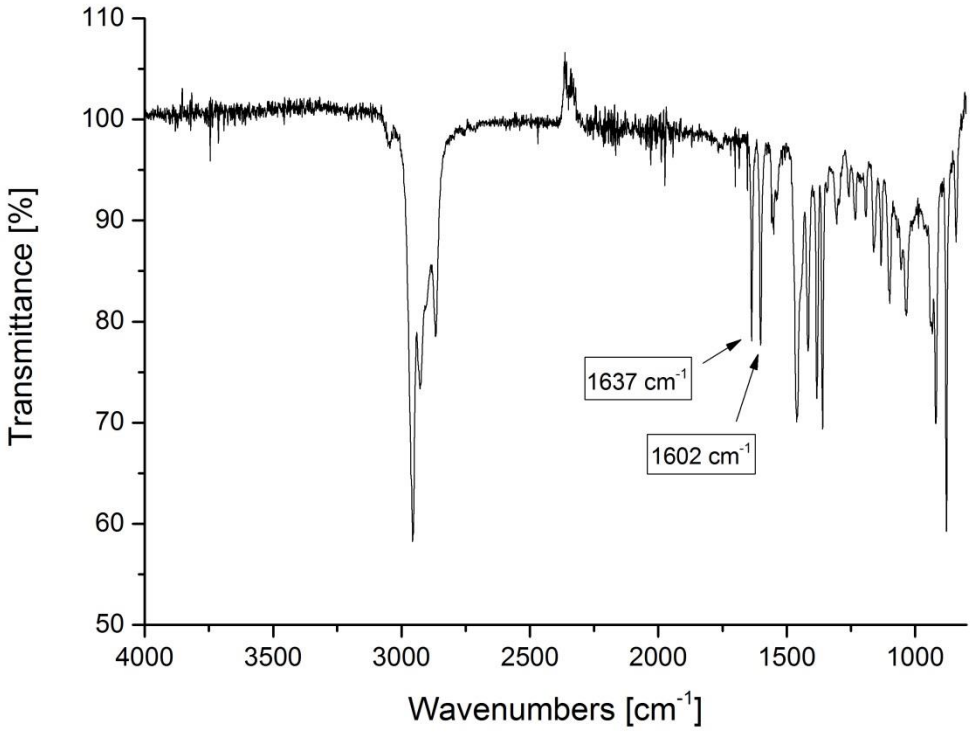

Figure 65. IR spectrum of pivaloyl substituted siliconoid **182**.

Orange single crystals of **182** (M. p. 187°C) were obtained in moderate yield (38%) from pentane. An X-ray structure study confirmed the presence of the intact bridged propellane skeleton functionalized with a pivaloyl substituent. The bridgehead bond length (Si1-Si2 2.6430(6) Å) in pivaloyl functionalized siliconoid **182** is significantly lengthened compared to anionic **133** (2.5506(9) Å) but slightly shorter than in all-Tip substituted propellane **125** (2.7076(8) Å).[165] The Si1-Si2 bond distance found in silyl substituted siliconoid **181** (2.635(1) Å) is comparable to **182**. All remaining endocyclic cluster bonds are in accord with what was reported for **125**.[165] Due to the high steric demand of the pivaloyl group, the angle between the two bridged “propeller blades” (Si1-Si2-Si3/Si1-Si2-Si4 = 96.960°) is significantly more-acute than in bridged propellanide **133** (107.618°) and close to the corresponding angle in **125** (96.78°).[165] The C1-O1 bond length (1.212(2) Å) is at the shorter end of C=O bonds (1.204 – 1.242 Å) and very similar to what was reported for an acyl substituted cyclohexasilane (1.213(2) Å).[228] The Si3-C1 bond distance in **182** (1.9550(17) Å) is slightly larger than the Si-Tip bond lengths (1.8927 – 1.931 Å), but shorter than what is reported for the aforementioned acyl substituted cyclohexasilane (1.970(1) Å).[228]

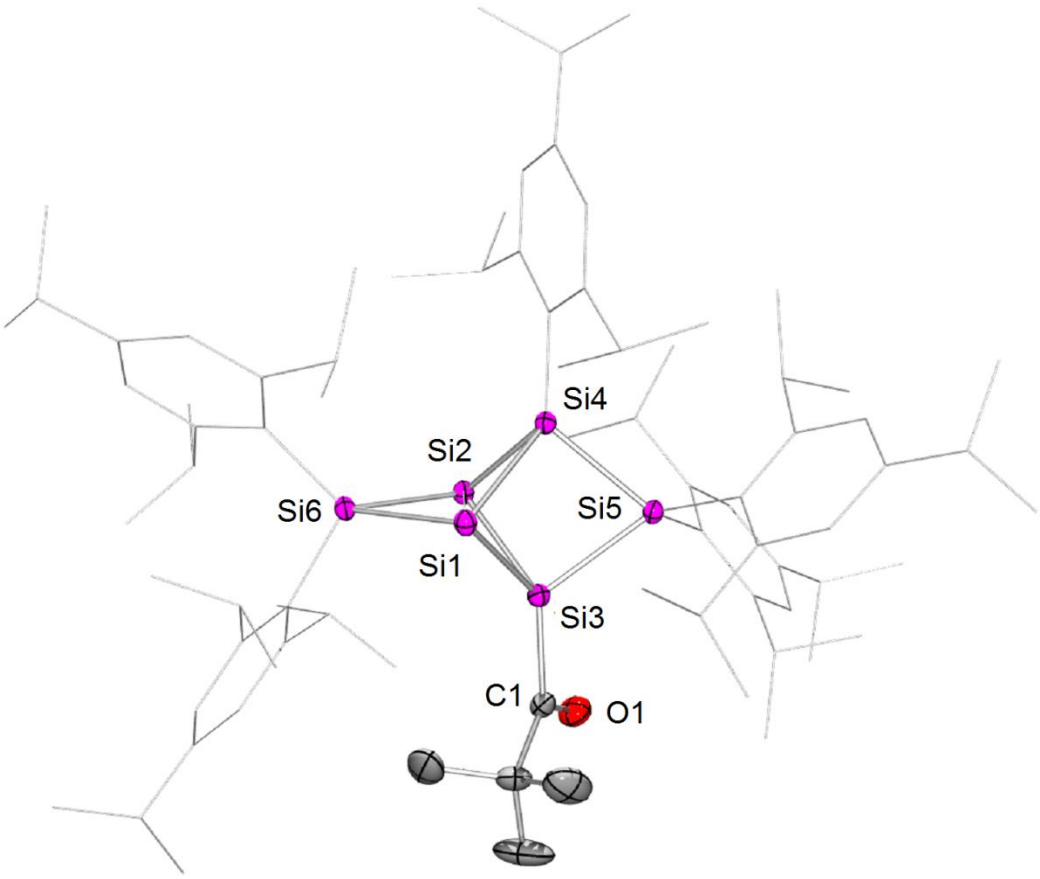

Figure 66. Molecular Structure of **182** in the solid state (thermal ellipsoids at 50%, H atoms and co-crystallized solvent molecules omitted). Selected bond lengths [Å] and angles [°]: Si1-Si2 2.6430(6), Si2-Si4 2.3818(6), Si2-Si3 2.3167(6), Si2-Si6 2.4125(6), Si4-Si5 2.3760(6), Si3-C1 1.9550(17), C1-O 1.212(2); Si4-Si2-Si6 97.90(2), Si3-Si2-Si4 76.498(19), Si3-Si5-Si4 75.845(19), Si1-Si6-Si2 67.473(18), Si3-Si1-Si2 54.707(17).

The longest wavelength absorption in the UV/vis spectrum of **182** (λ_{max} = 475 nm) is similar to that observed for all-Tip derivative **125** (473 nm) and thus assigned to the HOMO–LUMO vertical singlet excitation (Figure 122).[165] For **182** the intensity of this absorption (ε = 500 $M^{-1}cm^{-1}$, Figure 123) however, is somewhat smaller than in the global minimum isomer (**125**: ε = 700 $M^{-1}cm^{-1}$). As in **125**, a second absorption band is found at λ = 349 nm (ε = 9000 $M^{-1}cm^{-1}$, Figure 124).

Given that carbonyl functionalities are usually highly reactive towards unsaturated silicon compounds,[86-89] the fact that **182** is perfectly stable at room temperature in the absence of air and moisture is remarkable. In organic chemistry ketones are generally valuable synthons that allow for several functional group transformations. The Wittig-reaction is a textbook reaction to couple aldehydes or ketones to alkenes.[229] Consequently the residual carbonyl functionality offers several possibilities for further manipulations.

A first indication of the high reactivity of the carbonyl moiety is observed upon melting **182** (M. p. 187°C). The rearrangement to a major product showing six resonances in the ^{29}Si NMR spectrum at δ = 56.5, −6.4, −13.3, −66.6, −156.7 and −172.6 ppm is observed. In addition, a second set of six signals of minor intensity is detected at δ = 157.7, 106.4, 0.2, −35.8, −94.5 and −200.1 ppm.

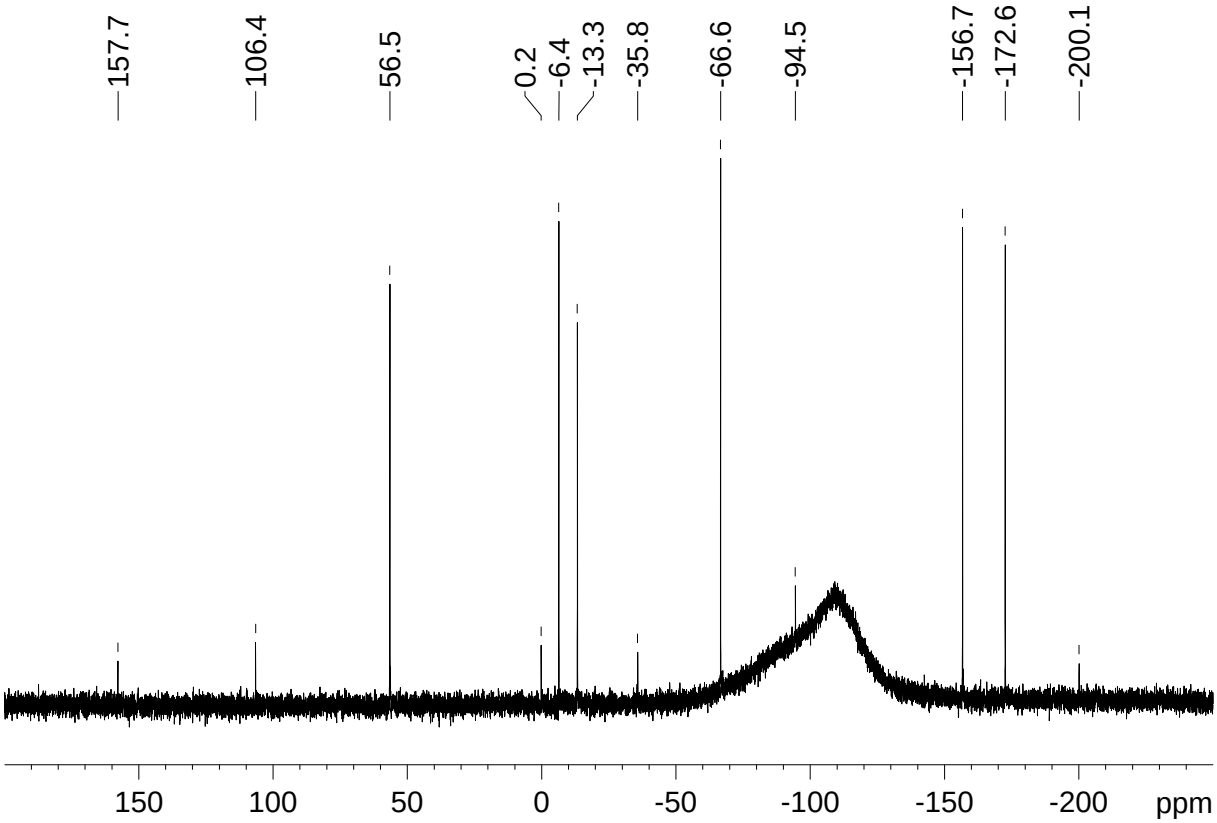

Figure 67. ^{29}Si{^{1}H} NMR spectrum of the rearrangement product of **182** upon melting.

For the major product, the low-field resonance is assigned to a SiTip-unit on the basis of Si/H correlation 2D NMR spectroscopy (Figure 68). While the signals at δ = −6.4 and −13.3 ppm both can be attributed to $SiTip_2$ moieties, the three silicon nuclei observed high-field apparently do not couple to Tip substituents.

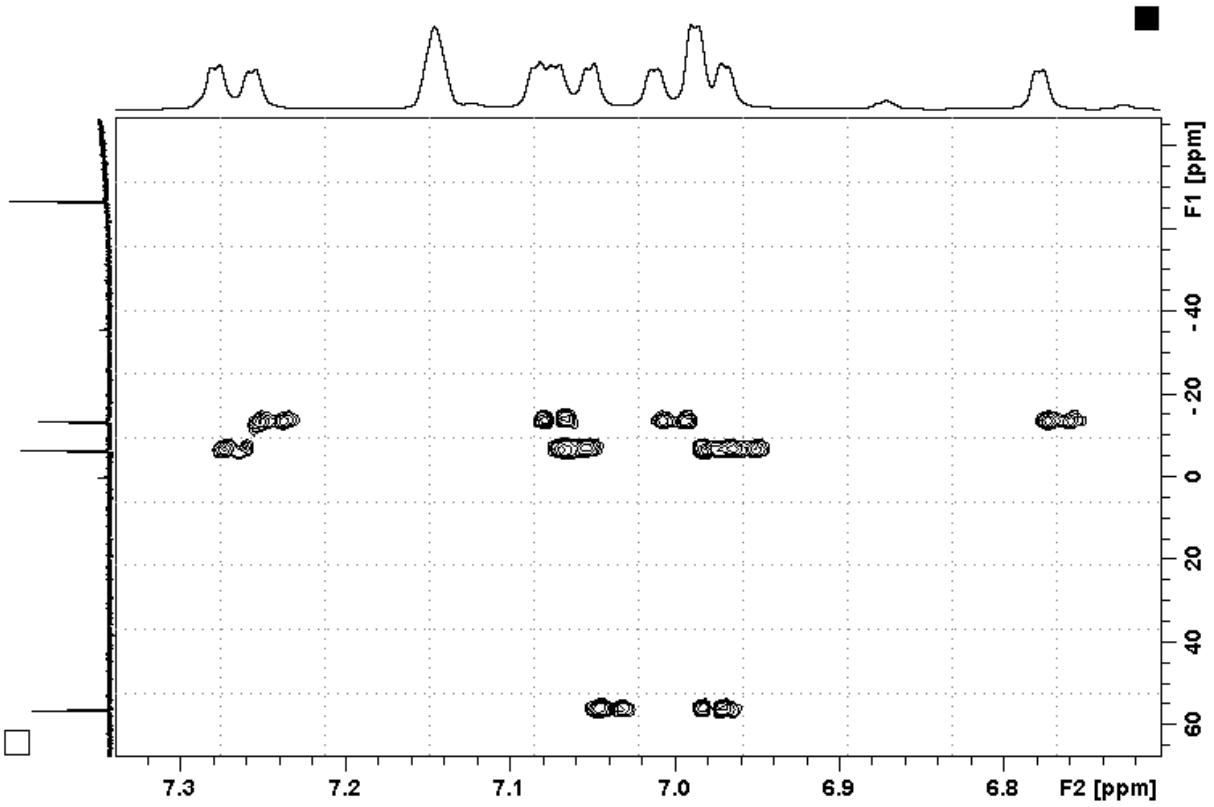

Figure 68. Selected area of the 2D ^{29}Si-^{1}H correlation NMR spectrum of the rearrangement product of **182** upon melting.

A rearrangement of pivaloyl substituted siliconoid **182** in analogy to what was reported for the reaction of disilenides **16** or **22a** with carboxylic acid chlorides can be proposed.[88,89] In this case, intermediate carbonyl substituted disilenes rearrange to cyclic brook-type silenes **44a-c** (Scheme 17). Upon melting, **182** might undergo a [2+2]-cycloaddition of the C=O-bond over an endocyclic cluster bond to yield *e. g.* cluster **183** or related isomeric species (Scheme 109).

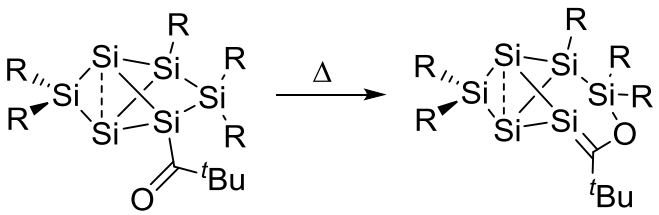

182 **183**

Scheme 109. Possible rearrangement of siliconoid **182** to **183** upon melting (R = Tip).

Indeed, a resonance observed at δ = 221.4 ppm in the ^{13}C NMR spectrum is in accordance with the presence of a donor-substituted Si=C bond.[89] However, no single crystals suitable for an X-ray structure analyses have been obtained yet and

consequently no proof for the constitution of the rearrangement product of **182** upon melting can be provided.

3.4.3. Reactivity of Bridged Propellanide 133 towards Chlorophosphanes

As outlined in previous sections, siliconoids are strongly related to unsaturated cluster compounds that play an important role in CVD processes of silanes (*cf*. Chapter 1.2.2). As a consequence, the combination of siliconoids and dopant atoms is of particular interest. Phosphorus is the most important n-type dopant for silicon materials.[15] The incorporation of phosphorus into silicon clusters has been studied theoretically and found to dramatically alter their optoelectronic properties.[167] The successful transfer the unperturbed bridged propellane skeleton by reaction of anionic siliconoid **133** with appropriate electrophiles inspired us attempt the synthesis of a phosphino substituted siliconoid. Since we demonstrated that dimethylamino groups on phosphorus turned out to be a valuable functionality for further manipulations (*cf*. Chapter 3.1.2), $ClP(NMe_2)_2$ was chosen as electrophilic phosphorus species.

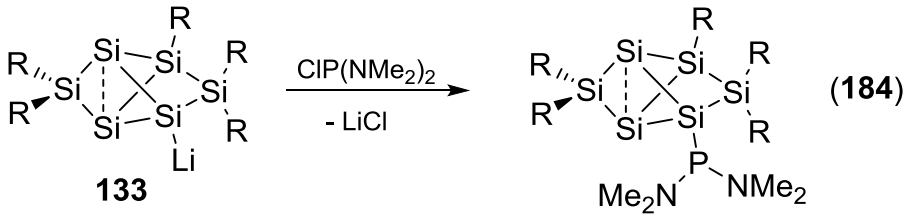

Scheme 110. Synthesis of phosphino substituted siliconoid **184** (R = Tip).

After addition of one equivalent bis(dimethylamino)chloro phosphane to a solution of **133** the color changed from orange to red. The ^{29}Si NMR spectrum (Figure 69) of the reaction mixture revealed uniform conversion to a new Si_6-species showing resonances at δ = 168.7 (s, Tip_2*Si*), 18.2 (d, $^2J_{Si\text{-}P}$ = 16.2 Hz, Tip_2*Si*), 14.4 (d, $^3J_{Si\text{-}P}$ = 14.0 Hz, Tip*Si*), −33.8 ($^1J_{Si\text{-}P}$ = 186.6 Hz, P-*Si*), −256.0 ($^2J_{Si\text{-}P}$ = 7.6 Hz, *Si*Si_3) and −261.4 ($^2J_{Si\text{-}P}$ = 7.6 Hz, *Si*Si_3).

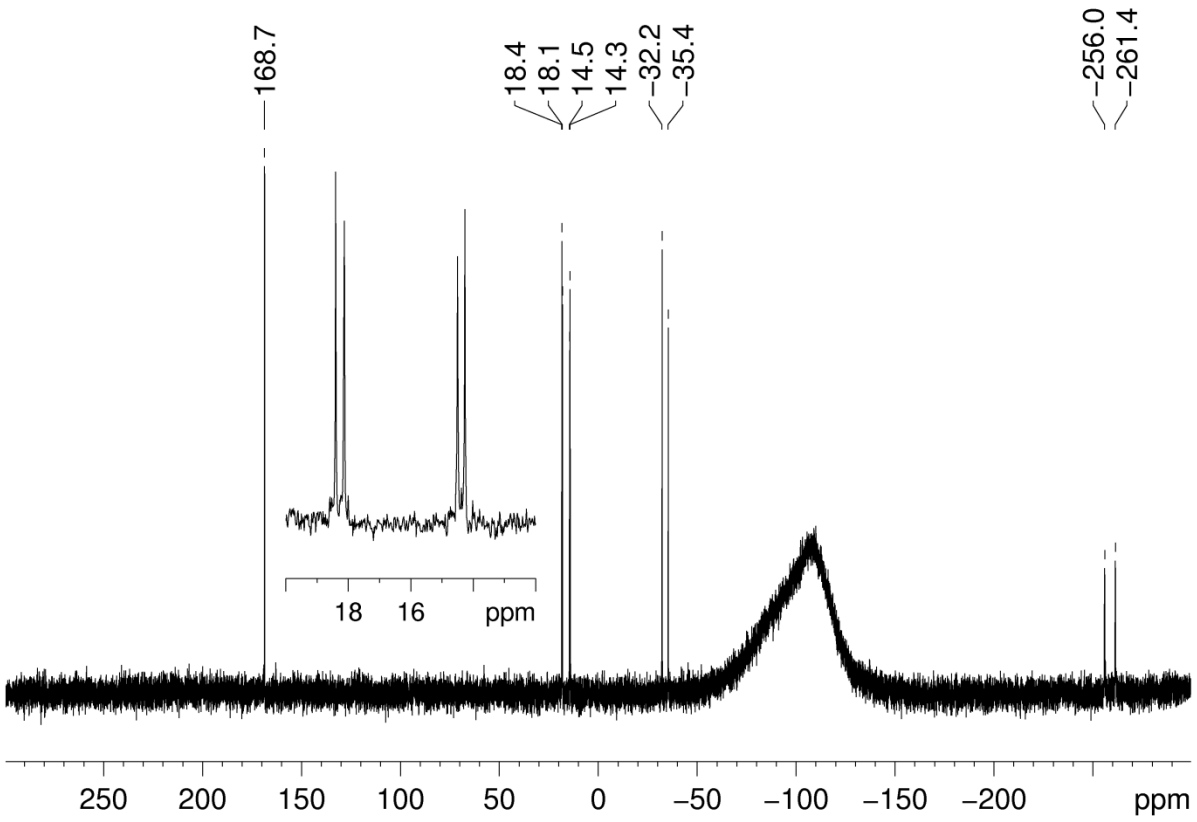

Figure 69. $^{29}Si\{^{1}H\}$ NMR spectrum of phosphino substituted siliconoid **184**.

The diagnostic distribution of ^{29}Si NMR chemical shifts in combination with the Si-P coupling constants unambiguously confirms formation of the phosphino substituted siliconoid **184** (Scheme 110). As observed for pivaloyl functionalied derivative **182**, the ^{29}Si NMR resonances of the naked silicon vertices are sharp, which is again attributed to the high steric demand of the newly introduced substituent.

The ^{31}P NMR chemical shift (δ = 148.0 ppm) is detected at surprisingly low field compared to usual diamino silyl phosphanes, which are generally observed by about 100 ppm more upfield.[230] We tentatively attribute this to the cluster current in **184** that is also responsible for the strong shielding of the bridgehead silicon atoms. Furthermore, the value observed for the $^{1}J_{Si\text{-}P}$ coupling constant (186.6 Hz) is rather large and even at the higher end of values known for Si=P bonds. This indicates a remarkably high s-character in this exocyclic bond. Single crystals (M. p. > 220°C, dec.) were obtained in excellent yield (91%) from a concentrated pentane solution and investigated by X-ray analysis.

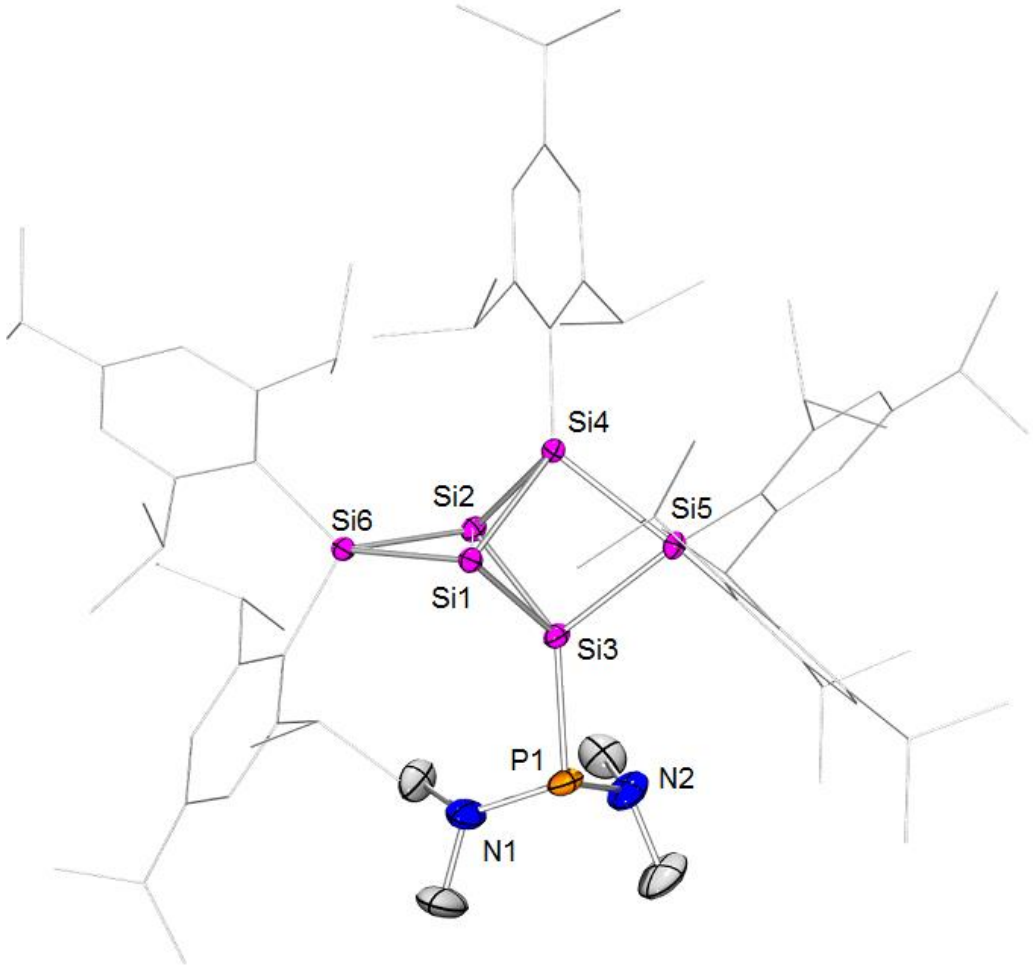

Figure 70. Molecular Structure of **184** in the solid state (thermal ellipsoids at 50%, H atoms and co-crystallized solvent molecules omitted). Selected bond lengths [Å] and angles [°]: Si1-Si2 2.6231(5), Si2-Si4 2.3124(5), Si2-Si3 2.3924(5), Si2-Si6 2.3384(5), Si4-Si5 2.3756(5), Si3-P1 2.2944(6), P1-N1 1.6853(16), P1-N2 1.7077(18); Si4-Si2-Si6 97.90(2), Si3-Si2-Si4 76.498(19), Si3-Si5-Si4 75.845(19), Si1-Si6-Si2 67.473(18), Si3-Si1-Si2 54.707(17).

The bond length between the two unsubstituted silicon vertices (Si1-Si2 2.6231(5) Å) in phosphino substituted siliconoid **184** is shorter than in the all-Tip substituted derivative **125** (2.7076(8) Å),[165] but expectably longer than in anionic **133** (2.5506(9) Å) and thus comparable to what was found in pivaloyl functionalized siliconoid **182** (2.6430(6) Å). Due to comparable steric demand of the $P(NMe_2)_2$-moiety the angle between the two bridged "propeller blades" in phosphino functionalized siliconoid **184** (Si1-Si2-Si3/Si1-Si2-Si4 = 97.798°) is much closer to that in pivaloyl substituted derivative **182** (96.960°) or all-Tip bridged propellane **125** (96.78),[165] respectively, than to that in anionic siliconoid **133** (107.618°). The silicon-phosphorus bond length in **184** (Si3-P1 2.2944(6) Å) is within the typical range for Si-P single bonds (2.23 – 2.31 Å). The phosphorus center shows a strongly pyramidal geometry (Σ of angles P1 315.21°).

UV/vis spectroscopy of **184** reveals the longest wavelength absorption at λ_{max} = 475 nm (Figure 125) which is very similar to the all-Tip derivative **125** and the pivaloyl substituted bridged propellane **182** (λ_{max} = 473 and 475nm) and thus assigned to the HOMO-LUMO vertical singlet excitation. While the extinction coefficient of this absorption of **182** (ε = 545 $M^{-1}cm^{-1}$) is smaller than that the corresponding absorption of **125** (ε = 700 $M^{-1}cm^{-1}$) the value observed for **184** (ε = 1200 $M^{-1}cm^{-1}$, Figure 126) is significantly larger. As in the previous cases, the second absorption band of **184** is found at λ = 354 nm (for **182**: 349 nm). Equally, this band is more intense in case of **184** (ε = 16500 $M^{-1}cm^{-1}$, Figure 127) compared to the corresponding absorption band in **182** (λ = 349 nm, ε = 9000 $M^{-1}cm^{-1}$).

Subsequently, we were interested in synthesizing phosphino substituted siliconoid **185** with residual chlorine functionality at phosphorus. For disilenide **16** a uniform reaction was observed with dichlorodiphenylamino phosphane (*cf.* Chapter 3.1.3). In a similar manner, bridged propellanide **133** was treated with one equivalent Cl_2PNPh_2 (Scheme 111). A ^{31}P NMR spectrum recorded ten minutes after addition revealed a main resonance at δ = 152.9 ($^1J_{P\text{-}Si}$ = 179.6 Hz) ppm.

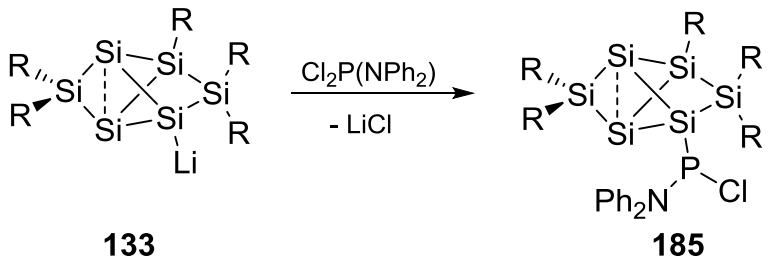

133 **185**

Scheme 111. Attempted synthesis of (chloro)phosphino substituted siliconoid **185** (R = Tip).

The chemical shift as well as the value of the P-Si coupling constant are very similar to the values for phosphino substituted siliconoid **184** (δ = 148.0 ($^1J_{P\text{-}Si}$ = 186.6 Hz)) and in line with formation of **185**. However, two additional signals are detected in the ^{31}P NMR spectrum at δ = 149.5 and 139.6 ppm (intensity: 69 and 38%). Monitoring the reaction mixture for several days indicated decomposition to a complex mixture.

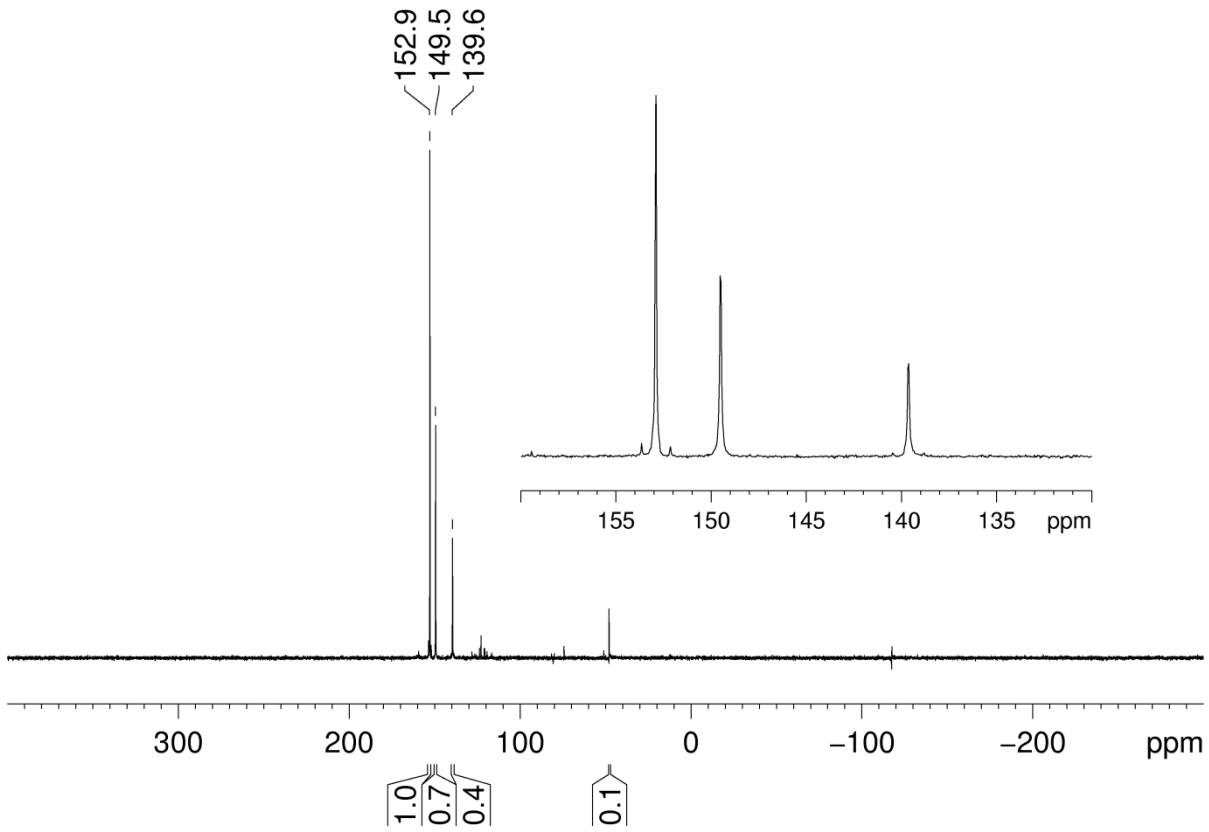

Figure 71. $^{31}P\{H\}$ NMR spectrum from the reaction of anionic siliconoid **133** with Cl_2PNPh_2 recorded ten minutes after addition.

3.4.4. Synthesis of NHC-stabilized Phosphinidenyl Substituted Siliconoid 186

In Chapter 3.2.1 it was demonstrated that one NHC ligand in P(I) cation **164b**[BPh_4] can be substituted by disilenide **16**. As initial product an unobserved but plausible NHC-stabilized disilenyl phosphinidene **[165]** was proposed that cyclizes to the finally isolated three-membered ring **166**. During this reaction, **164b**[BPh_4] formally acts as stoichiometric source of phosphorus. In view of the desired incorporation of the n-type dopant phosphorus into unsaturated silicon cluster compounds, we considered the substitution of one NHC-ligand in **164b**[BPh_4] with anionic siliconoid **133**. When **164b**[BPh_4] and **133** were combined in thf, no reaction occurred at room temperature. Upon heating the reaction mixture to 75°C for three hours, however, a color change from orange to deep green was observed. Complete and uniform conversion to a product with a broadened ^{31}P NMR resonance at δ = −163.8 ($^1J_{P\text{-}Si}$ = 223.7 Hz) ppm is achieved (Figure 72).

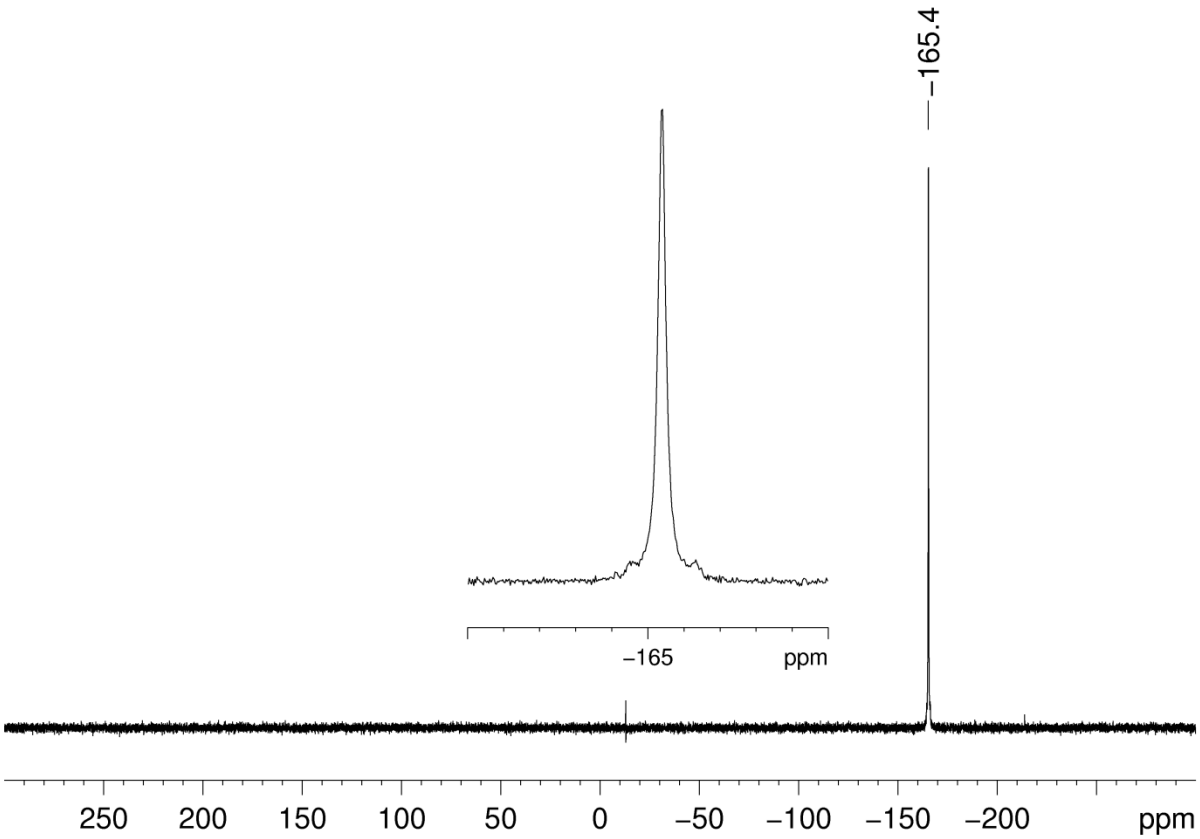

Figure 72. $^{31}P\{^{1}H\}$ NMR spectrum of NHC stabilized phosphinidenyl substituted siliconoid **186**.

The value of the coupling constant is surprisingly large and to the best of our knowledge it exceeds even all Si-P coupling constants reported for Si-P double bonds. While indeed liberation of one equivalent NHC is confirmed by ^{1}H NMR spectroscopy, the second equivalent remains coordinated in the molecule. A resonance in the ^{13}C NMR spectrum at δ = 166.7 ppm is assigned to the carbenic carbon of the coordinated NHC. The characteristically large $J_{C\text{-}P}$ value of 134.4 Hz indicates the direct coordination of the NHC to phosphorus. Apparently, one NHC ligand in **164b**[BPh_4] is substituted by anionic siliconoid **133** to result in the NHC-stabilized phosphinidene-substituted siliconoid **186**, unlike in case of the reaction of disilenide **16** with **164b**[BPh_4] without subsequent rearrangements (Scheme 112).

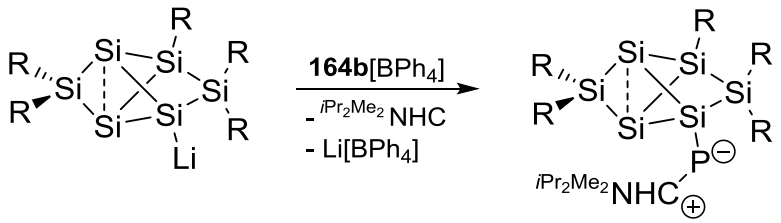

133 **186**

Scheme 112. Synthesis of NHC-stabilized phosphenidenyl substituted siliconoid **186** (R = Tip, NHC^{iPr2Me2} = 1,3-diisopropyl-4,5-dimethylimidazol-2-ylidene).

This is unambiguously confirmed by ^{29}Si NMR spectroscopy. The diagnostic distribution of the ^{29}Si NMR signals mirrors the intact bridged propellane scaffold of **186**. While one $SiTip_2$ unit is observed at δ = 167.7 ppm, the second $SiTip_2$ and the SiTip moieties are detected at δ = −9.3 (d, $^2J_{Si-P}$ = 25.6 Hz) and 8.5 (d, $^3J_{Si-P}$ = 16.0 Hz). The phosphorus bonded silicon atom appears at δ = 7.2 (d, $^1J_{Si-P}$ = 223.7 Hz) ppm. The signals of the unsubstituted silicon vertices show the usual shielding at δ = −252.5 and −261.4 ppm. As observed for silyl and pivaloyl substituted derivatives **181** and **182**, these resonances are slightly broadened which we attribute to hindered rotation.

Single crystals of **186** (M. p. 205°C, dec.) were obtained from hexane as deep green needles in satisfactory yield (50%) and an X-ray structure diffraction study confirmed the constitution of an NHC stabilized phosphinidene-substituted siliconoid **186** (Figure 73).

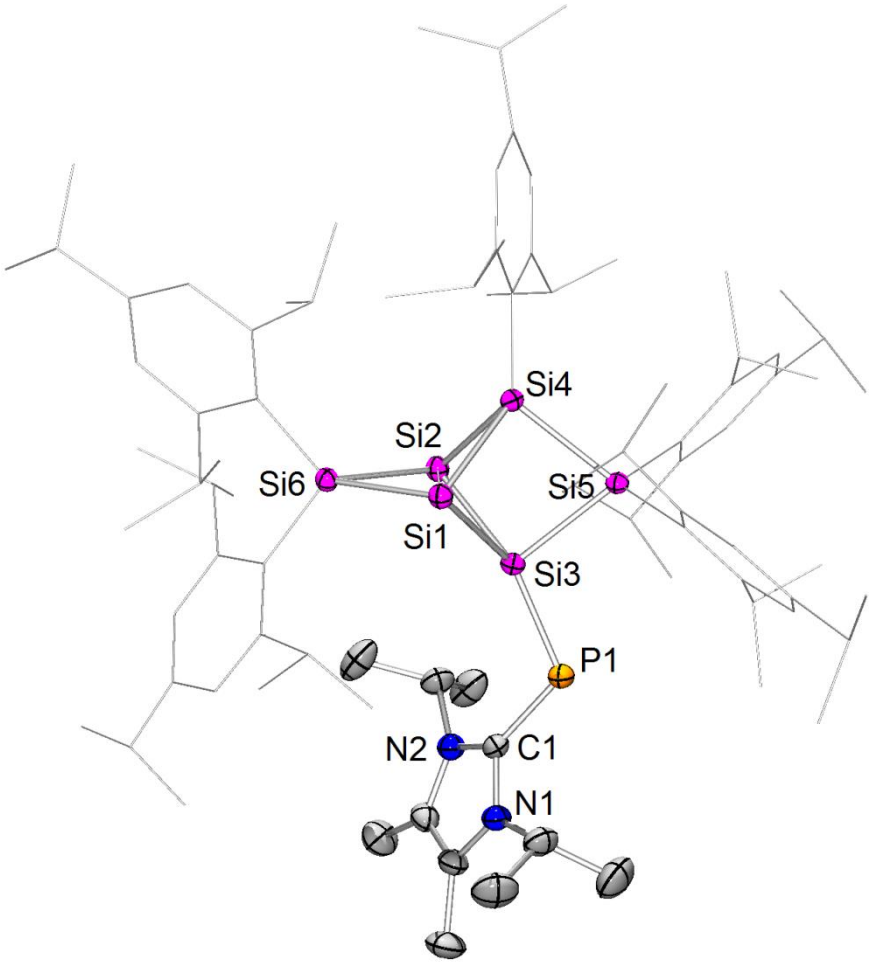

Figure 73. Molecular Structure of **186** in the solid state (thermal ellipsoids at 50%, H atoms and disordered Tip-^{i}Pr-groups omitted). Selected bond lengths [Å] and angles [°]: Si1-Si2 2.6412(6), Si2-Si4 2.3771(6)), Si2-Si3 2.3667(6), Si2-Si6 2.4084(6), Si4-Si5 2.3698(6), Si3-P1 2.1974(6), P1-C1 1.8054(17); Si4-Si2-Si6 96.09(2), Si3-Si2-Si4 77.54(2), Si3-Si5-Si4 77.445(19), Si1-Si6-Si2 67.271(19), Si3-Si1-Si2 55.691(17), C1-P1-Si3 115.24(5).

As already observed for pivaloyl and phosphino functionalized siliconoids **182** and **184**, the length of the bridgehead bond (Si1-Si2 2.6412(6) Å) in phosphinidene-substituted derivative **186** is in between that of all-Tip siliconoid **125** (2.7976(8) Å) and bridged propellanide **133** (2.5506(9) Å).[165] Likewise, the angle between the two bridged "propeller blades" (Si1-Si2-Si3/Si-Si2-Si4 97.697°) is much closer to the corresponding angles observed in **125** (96.78°), **182** (96.960°) and **184** (97.798°) than to those in in **133** (107.618°) due to comparable steric demand of the NHCP-unit. The silicon phosphorus bond (Si3-P1 2.1974(6) Å) is slightly shortened compared to reported Si-P single bonds (for comparison $CH(SiMe_3)_2SiMe_2PPh_2$: 2.295 Å[187]) presumably due to a certain degree of phosphide character of P1 and thus attractive interactions with the positively polarized Si3 atom.[199] The bond distance between the carbenic carbon and phosphorus (C1-P1 1.8054(17) Å) is

larger than what was reported for NHC stabilized phosphinidenes (1.743(2)-1.774(1) Å), which might indicate a looser bonding of the NHC ligand.[231] Steric repulsion between the NHC unit and the sterically demanding cluster skeleton could contribute to this lengthening of C1-P1 bond.

The UV/vis absorption spectrum of phosphinidene-substituted siliconoid **186** (Figure 74) revealed the longest wavelength absorption at λ_{max} = 589 nm (ε = 400 Mcm^{-1}), which is more than 100 nm red-shifted compared to that of the bridged propellane derivatives discussed before (*vide supra*, λ_{max} = 473-475 nm), but of comparable intensity (ε = 220-1200 Mcm^{-1}).

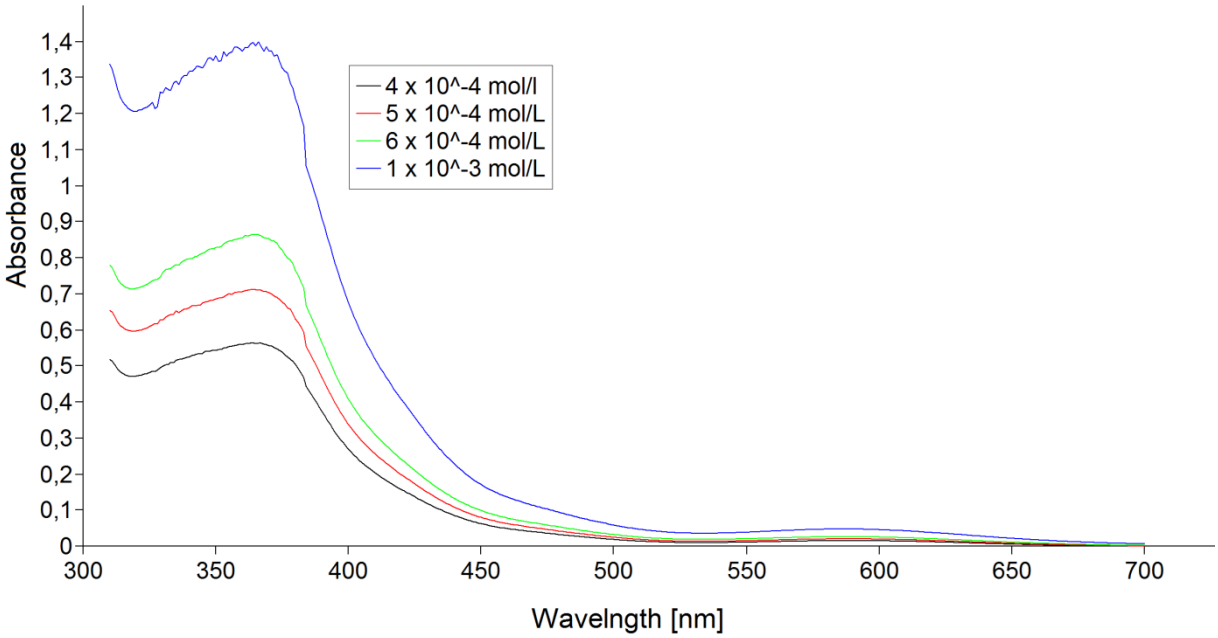

Figure 74. UV/vis spectra of **186** in hexane at different concentrations ($5 \cdot 10^{-4}$ - $9 \cdot 10^{-4}$ mol/L).

This bathochromic shift nicely explains the green color of **186** in contrast to the yellow to red in the other cases. A certain degree of double bond character between Si4 and P (as represented by resonance formula **186´**) would allow the admixture of $\pi_{Si=P}$-orbitals and thus potentially influence the energy of cluster orbitals. Stalke, Frenking and Roesky *et al.* discussed π-backbonding in ylidic Si-P species.[232] The very large Si-P coupling constant ($^1J_{P\text{-}Si}$ = 223.7 Hz) further supports high s-character in the Si4-P1 bond in line with above back-bonding scenario.

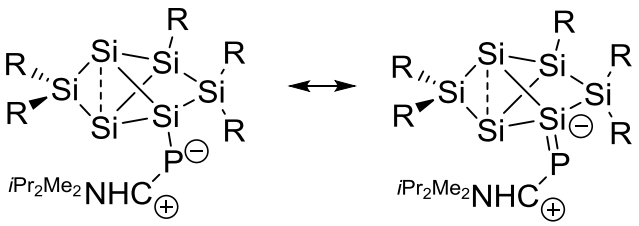

186 **186´**

Scheme 113. Phosphinidene substituted siliconoid **186** and resonance formula **186´** (R = Tip, NHC^{iPr_2Me_2} = 1,3-diisopropyl-4,5-dimethylimidazol-2-ylidene).

During her studies in our group, Dr. Kinga Leszczyńska reacted bridged propellanide **133** with siliconocene. A selective cluster expansion occurs presumably *via* an intermediate silylenyl substituted derivative **[187]**. The Si_7-siliconoid **188** featuring three “naked” vertices was isolated by Dr. K. Leszczyńska as the final product.

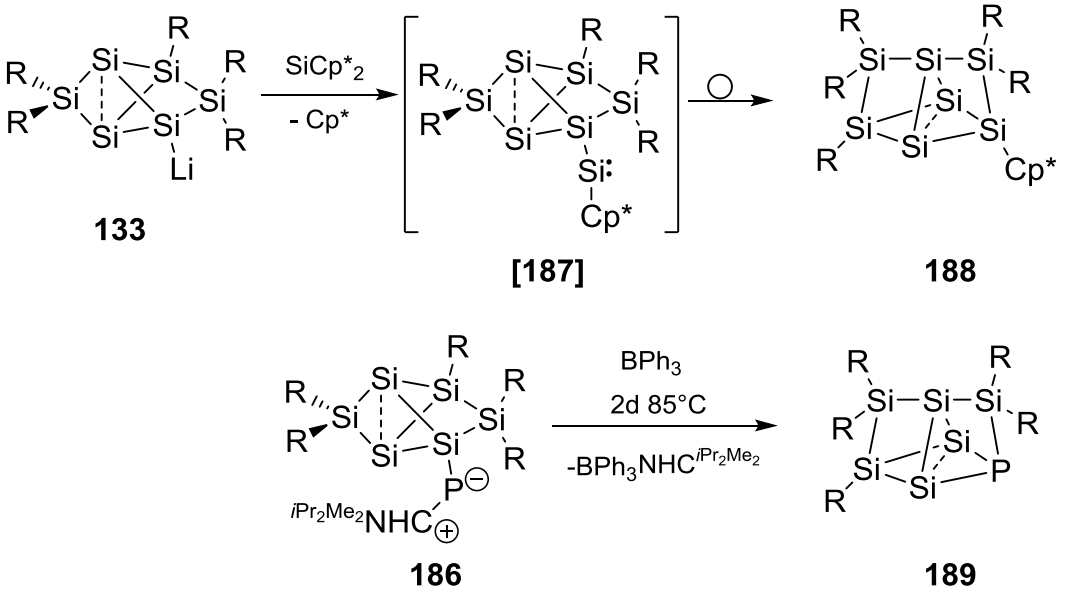

133 **[187]** **188**

186 **189**

Scheme 114. Synthesis of siliconoid **188** performed by Dr. Leszczyńska, presumed reactivity of phosphenidenyl substituted siliconoid **186** towards triphenyl borane (R = Tip, Cp* = η^5-C_5Me_5, NHC^{iPr_2Me_2} = 1,3-diisopropyl-4,5-dimethylimidazol-2-ylidene).

Siliconoid **186** closely resembles the proposed initial product **[187]** during the cluster expansion to **188**. Consequently, regarding the selective expansion of the unsaturated silicon cluster core with phosphorus, siliconoid **186** represents a promising precursor. The abstraction of *N*-heterocyclic carbenes from low-valent main group compounds by the addition of Lewis-acids such as triphenyl borane has been reported.[124, 205] As already mentioned (*cf.* Chapter 3.2.1), in our opinion this is a strong indication for the presence of a dative bonding of the NHC-ligand.[205] In case

the NHC-substituent in **176** can be removed from phosphorus with a Lewis acid, the unstabilized phosphinidene unit would presumably be incorporated into the unsaturated Si_6-core to yield **189** providing the first example for n-type doping of an unsaturated silicon cluster at the molecular level. An initial experiment in this regard was performed during this project. An excess (~2 two equivalents) triphenyl borane was added to a solution of **186** in benzene. After heating to 85°C, the green solution turned intense red and indeed the formation of the corresponding triphenylborane-NHC adduct was confirmed by ^{1}H and ^{11}B NMR spectroscopy. In the ^{31}P NMR spectrum a new resonance arises at δ = −278.9 ppm (Figure 75). After two days at 85°C only small amounts of the starting material (10 %) remain. Besides the main resonance at δ = −278.9 ppm two signals of minor intensity are observed in the ^{31}P NMR spectrum at δ = −160.9 and −162.2 ppm. Three pairs of silicon satellites (^{1}J = 120.4, 61.3 and and 48.3 Hz) are found for the main signal which is indeed in accord with formation of phosphorus doped siliconoid **189**.

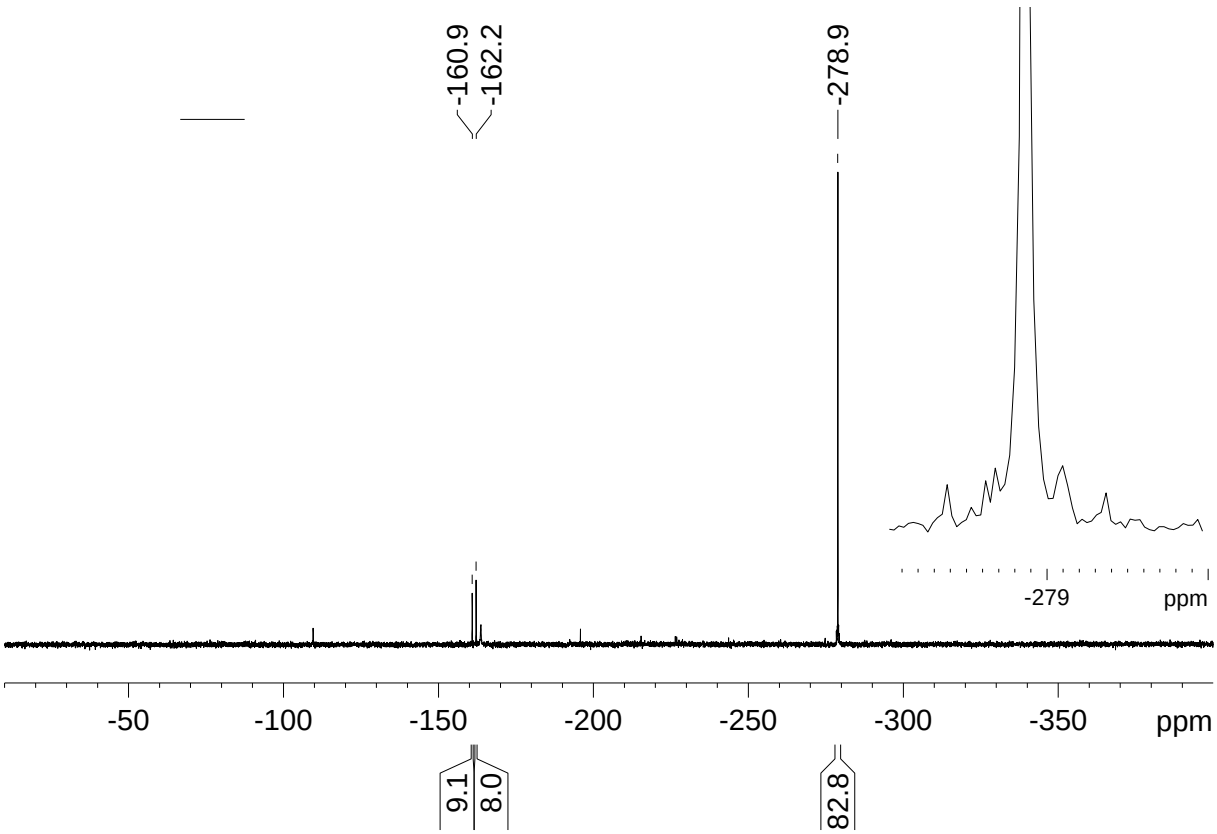

Figure 75. $^{31}P\{^{1}H\}$ NMR spectrum from the reaction of siliconoid **186** with triphenyl borane after three days at 85°C.

Unfortunately, not enough material to obtain ^{29}Si NMR data let alone single crystals was available. It the timeframe of this project it was not possible to repeat the reaction on a larger scale, but it is currently investigated in our laboratory.

3.4.5. Reactivity of Anionic Siliconoid 133 towards Chloroboranes

The experiments discussed in this and the following chapter (3.4.5 and 3.4.6) were partially carried out together with Yannic Heider during his Bachelor studies.[210]

In the preceding chapters it was demonstrated that bridged propellanide **133** is a suitable reagent to transfer the intact unsaturated silicon cluster motif to several electrophiles from Group 14 (carbonyl and silyl) as well as Group 15 (phosphino and phosphenidenyl). We decided to investigate the possibility of amending the list of functionalization to include Group 13 derivatives. Boron is the most important p-type dopant and thus the linking of a boron based substituent to siliconoids appeared an attractive challenge.

With the findings concerning the reactivity of disilenide **16** towards boron containing reagents in mind (*cf.* Chapter 3.3), aminochloro boranes seemed appropriate electrophiles. One equivalent bis(dimethylamino)chloro borane was added to a solution of **133** in benzene in order to synthesize boryl substituted siliconoid **190** (Scheme 115).

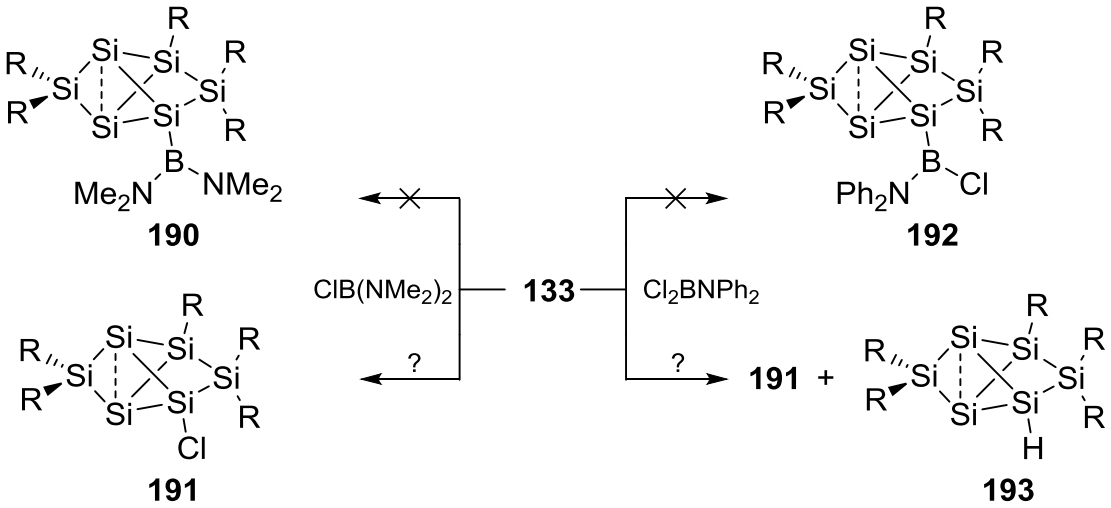

Scheme 115. Attempted synthesis of boryl substituted siliconoids **190** and **192** from the reactions of **133** with the corresponding boranes presumably affords **191** or **191** with minor amounts of **193**, respectively (R = Tip).

No reaction was observed at room temperature but upon heating to 50°C for 30 minutes, approximately 50% conversion to a new product was observed by NMR spectroscopy. In the ^{11}B NMR spectrum a resonance arises at δ = 25.3 ppm. While in the ^{29}Si NMR spectrum new six new signals were observed at δ = 169.2, 11.9, 5.9, 3.7, −266.1 and −278.0 ppm indicating an intact bridged propellane structure. The absence of broadened resonances (as typically observed due to the quadrupolar moment of ^{11}B) appears to rule out the presence of a silicon-bonded boryl group. Alternatively, the lithio silane might be chlorinated by the borane to afford chloro siliconoid **191** (Scheme 115). Given that the linking of a boryl unit to the cluster core was of major interest during this study, this reaction was not investigated in more detail.

The reaction of **133** with $ClB(NMe_2)_2$ required relatively harsh conditions and consequently in a next attempt **133** was treated with dichloro(diphenylamino)borane. It was anticipated that the reaction with this more electrophilic species might yield boryl substituted siliconoid **192** (Scheme 115).

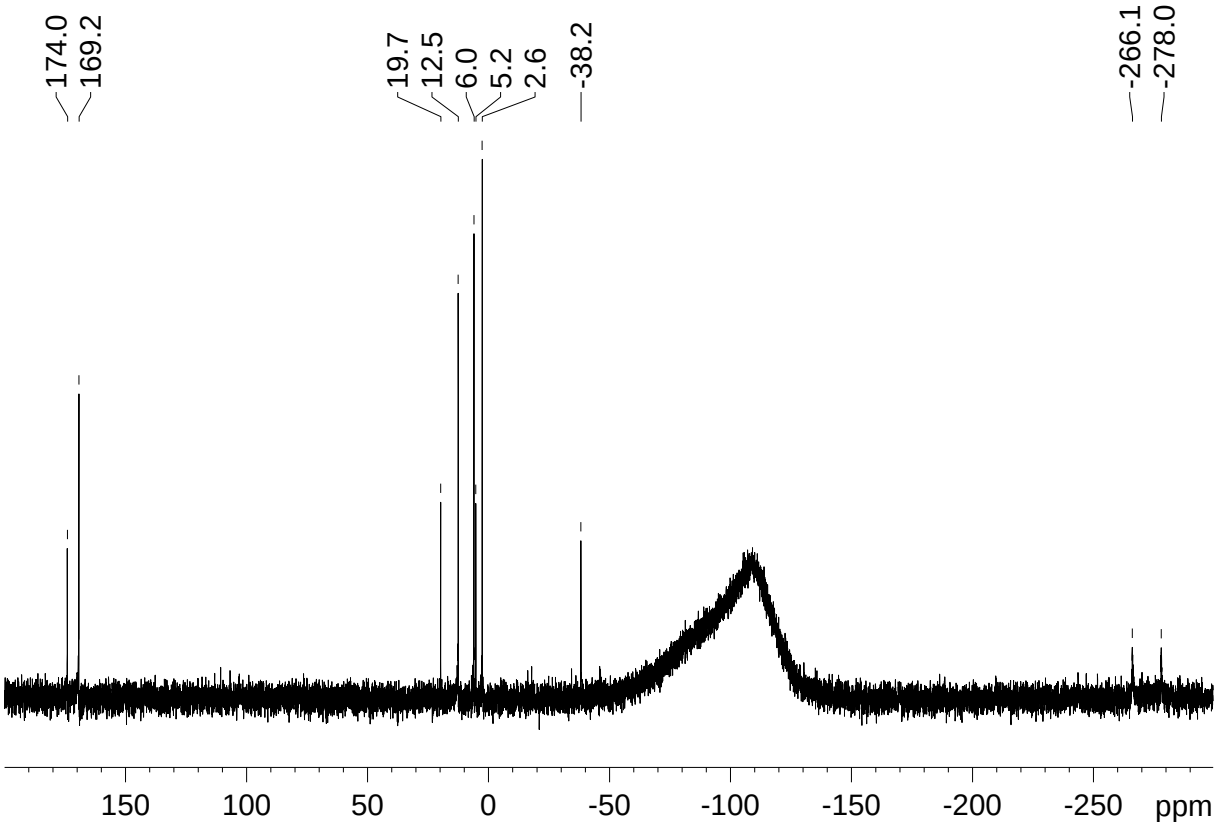

Figure 76. ^{29}Si{^{1}H} NMR spectrum from the reaction of anionic siliconoid **133** with dichlorodiphenylamino borane.

In this case, already at room temperature complete rapid consumption of the starting materials was observed. In the ^{29}Si NMR spectrum of the reaction mixture six major resonances are detected at δ = 169.2, 12.5, 6.0, 2.6, −266.1 and −278.0 ppm (Figure 76). These values are very similar to what was found for the reaction with $ClB(NMe_2)_2$ and thus equally assigned to the chlorinated species **191**. Additional four resonances of minor intensity appear in the ^{29}Si NMR spectrum at δ = 174.0, 19.7, 5.2 and −38.2 ppm. These minor resonances are in accordance with the ^{29}Si NMR signals observed for protonated siliconoid **193** (Scheme 115).[233] It should be mentioned that the ^{29}Si NMR resonances of the "naked" silicon vertices of **193** were found to be broadened. Accordingly, due to the minor amounts of **193** present in the reaction mixture, these high field resonances were left undetected in the ^{29}Si NMR spectrum.

As yet, no single crystals suitable for an X-ray diffraction study from any of the products were obtained and thus no further assumptions concerning structural details can be made.

3.4.6. Synthesis of Borate Substituted Siliconoid 194

Apparently, the reaction of anionic siliconoid **133** with chlorinated boranes is unsuitable for the introduction of a boron functionality to the siliconoid cluster motif. Chlorination of the anionic silicon vertex appears to occur as main reaction path and consequently hydroboranes were considered a promising alternative. Clean reactions are observed in case disilenide **16** is treated with $BH_3{\cdot}SMe_2$ or ^{t}BuBH$_2$ (*cf.* Chapter 3.3.2).

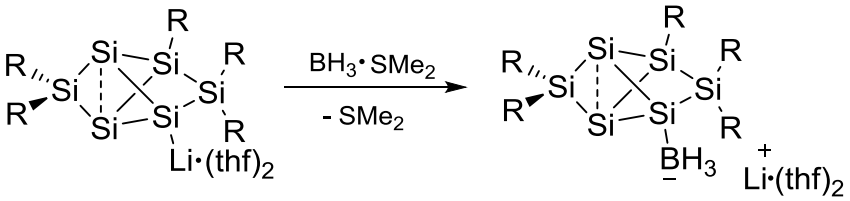

133 **194**

Scheme 116. Synthesis of borate substituted siliconoid **194** (R = Tip).

When anionic siliconoid **133** was treated with one equivalent $BH_3{\cdot}SMe_2$, the orange solution turned yellow instantly (Scheme 116). Subsequent NMR spectroscopic investigation of the reaction mixture revealed complete and absolutely uniform conversion to a new Si_6-species. Three resonances are observed in the ^{29}Si NMR

spectrum in the diagnostic areas of the intact bridged propellane (δ = 161.2 (s, *Si*Tip$_2$), −257.3 and −265.0 (*Si*Si$_3$) ppm, Figure 77).

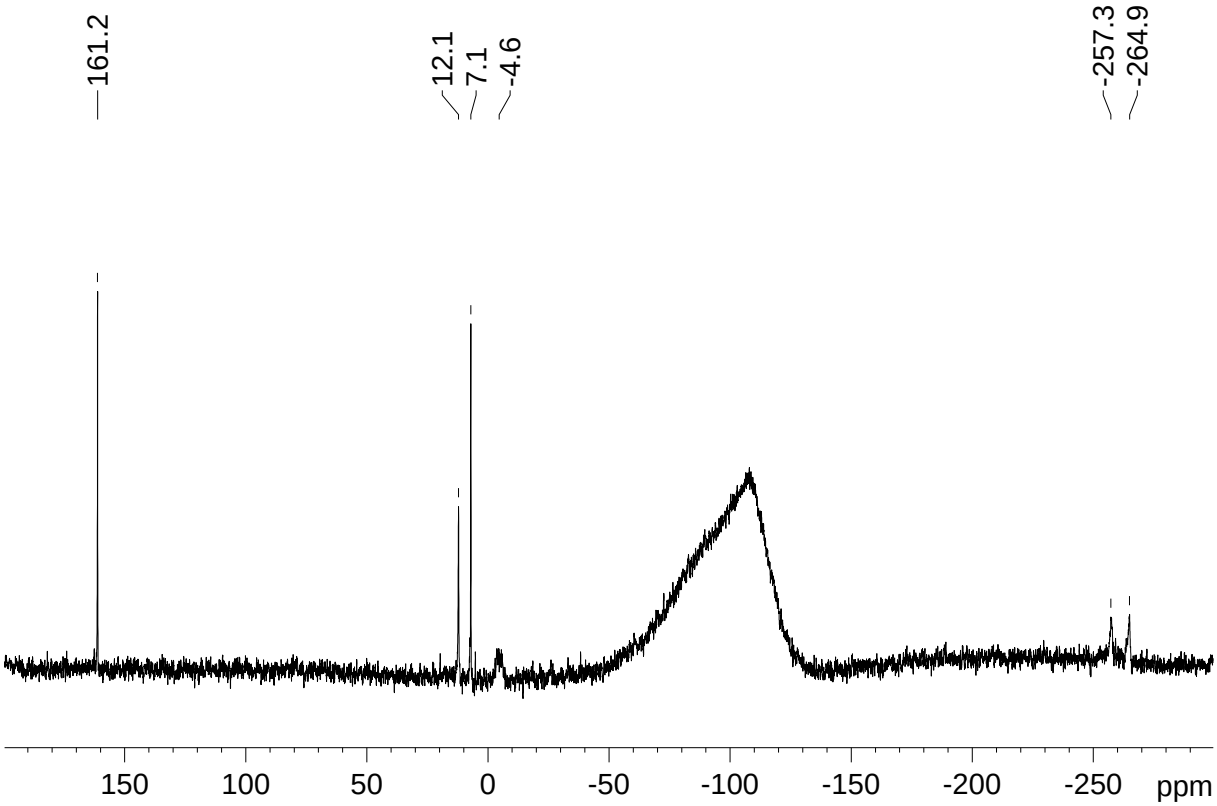

Figure 77. ^{29}Si{^{1}H} NMR spectrum of borate substituted siliconoid **194**.

Three additional signals appear in the ^{29}Si NMR spectrum at δ = 12.2, 7.1 and −4.8 ppm.

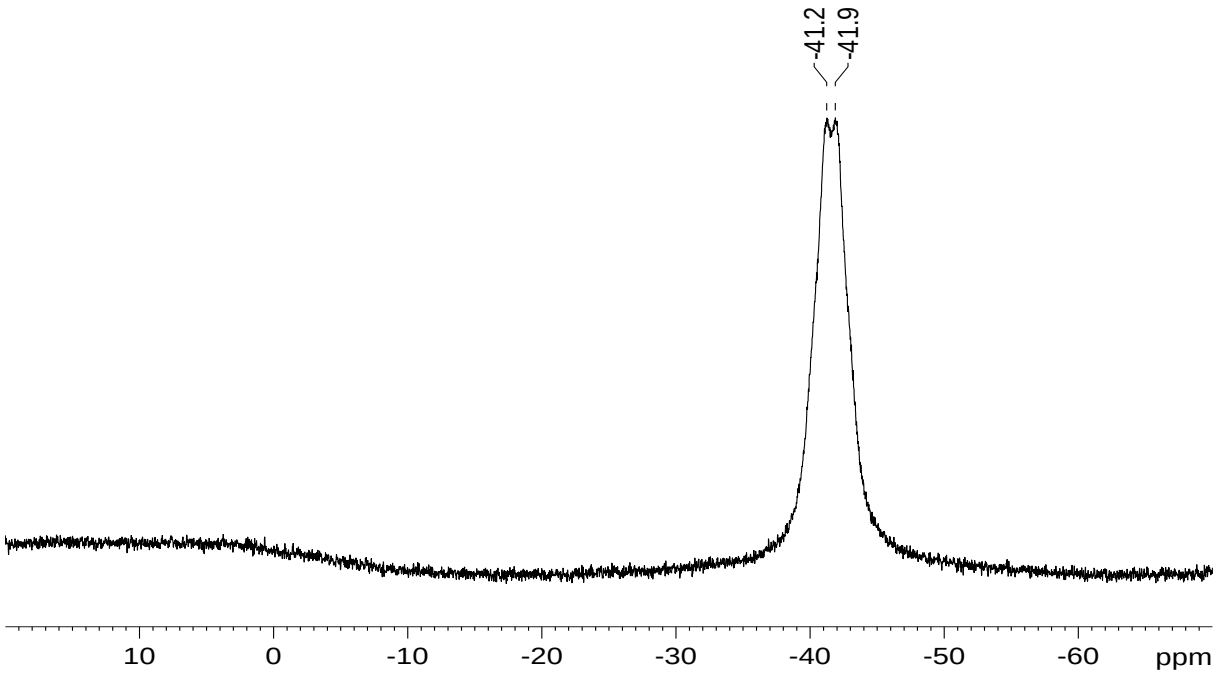

Figure 78. ^{11}B NMR spectrum of borate substituted siliconoid **194**.

For the resonance at δ = −4.8 ppm a significant broadening is apparent and thus this resonance can be assigned to a silicon atom coupling to the quadrupolar ^{11}B nucleus (Figure 77).

In the ^{11}B NMR spectrum (Figure 78) a broadened quartet resonance is observed at δ = −41.27 (q, $^{1}J_{B\text{-}H}$ = 75 Hz) in accordance with an anionic BH_3-moitiety, which further confirms the formation of borate substituted siliconoid **194** (Scheme 116).

The resonances observed for the naked silicon vertices are slightly broadened. Comparable to for the case of silyl substituted siliconoid **181**, these findings are attributed to less hindered rotation of the BH_3-unit compared to the pivaloyl or phosphino substituent in **182** or **184**, respectively. The lithium counter cation is detected at δ = −0.66 ppm in the ^{7}Li NMR spectrum. As witnessed by ^{1}H NMR spectroscopy, two molecules thf are coordinated to the lithium cationic lithium atom (δ = 3.35 and 1.38 ppm).

Yellow single crystals (M .p. > 220°C, dec) were obtained in good yield (60%) from a concentrated toluene solution. An X-ray diffraction study confirms the constitution of borate substituted bridged propellane **194** (Figure 79).

The bridgehead bond distance in **194** (Si1-Si2 2.6199(10) Å) is longer than in anionic **133** (2.5506(9) Å), but shorter than in the other substituted bridged propellanes (*cf.* **182**-**186**, 2.6231(5)-2.6430(6) Å) and the all-Tip derivative **125** (2.7076(8) Å).[165] It can be reasoned that electronegativity as well as steric demand of the substituents affect the bridgehead bond distance in the bridged propellane motifs: While small electropositive substituents induce a shortening of the bond (Li, BH_3^-), relatively long bridgehead bonds are observed for bulky electron-withdrawing substituents (pivaloyl, Tip).

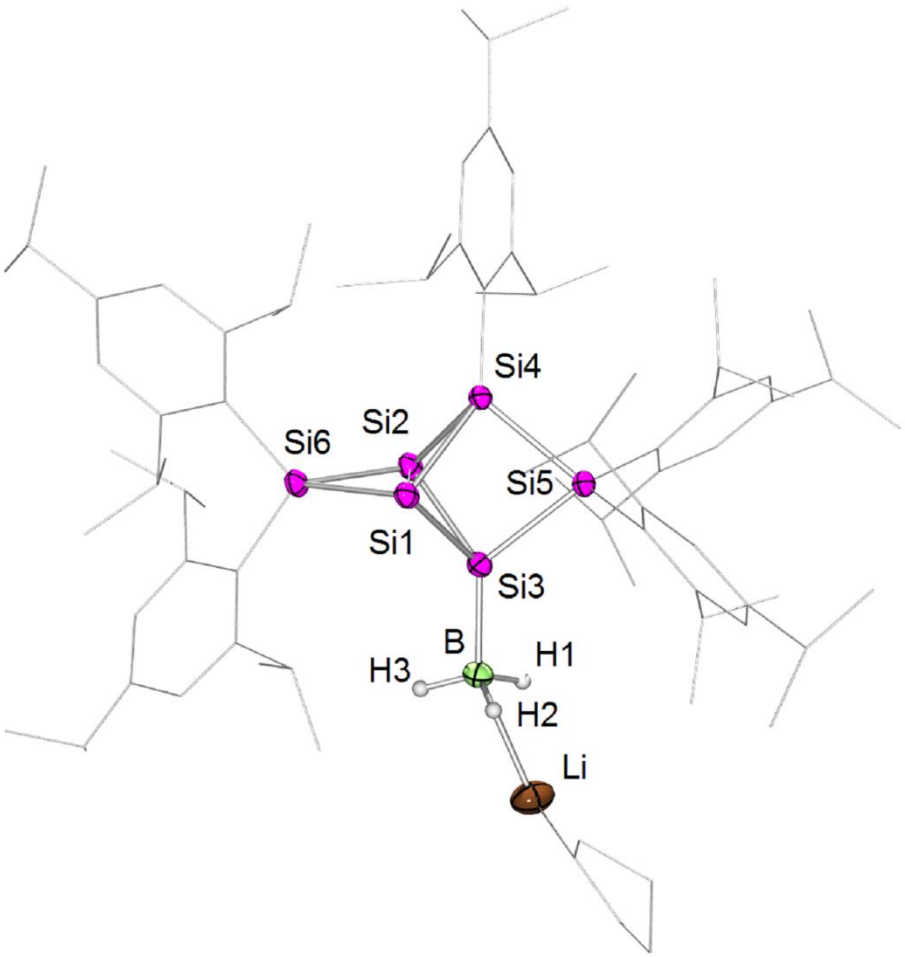

Figure 79. Molecular structure of **194** in the solid state (thermal ellipsoids at 50%, H atoms and disordered ^{i}Pr-groups omitted). Selected bond lengths [Å] and angles [°]: Si1-Si2 2.6199(10), Si2-Si4 2.3546(10), Si2-Si3 2.3667(6), Si2-Si6 2.3784(10), Si4-Si5 2.3605(9), Si3-B1 2.009(3), B1-Li1 2.384(6); Si4-Si2-Si6 97.89(3), Si3-Si2-Si4 79.45(3), Si3-Si5-Si4 78.87(3), Si1-Si6-Si2 67.33(3), Si3-Si1-Si2 55.56(3).

The comparable small steric strain in borate functionalized siliconoid **194** is manifest in a less-acute angle between the two bridged "propeller blades" (Si1-Si2-Si3/Si1-Si2-Si4 100.333°) *versus* the corresponding angles in **182**-**186** (96.960-97.798°). Expectably, this angle in anionic **133** (107.618°) is still significantly less acute than in **194**.

The longest wavelength absorption in the UV/vis spectrum of **194** is observed at λ_{max} = 475 nm (Figure 130) is very similar to that of the functionalized bridged propellanes discussed before (**182** and **184**: 475 nm) and **125** (473 nm) and hence equally assigned to the HOMO-LUMO vertical singlet excitation.[165] The intensity of this absorption (ε = 200 $M^{-1}cm^{-1}$, Figure 131), however, is less intense than the corresponding bands in **182** (ε = 500 $M^{-1}cm^{-1}$) and **184** (ε = 1200 $M^{-1}cm^{-1}$). A second absorption band in the UV/vis spectrum of **194** (Figure 130) is observed at λ

= 357 nm (**182**: λ = 349 nm, **184**: λ = 354 nm). Equally, the intensity of this absorption (ε = 4000 $M^{-1}cm^{-1}$, Figure 132) is smaller than those of the comparable absorption bands of the previously discussed derivatives (**182**: ε = 9000 $M^{-1}cm^{-1}$, **184**: 16500 $M^{-1}cm^{-1}$). Apparently, borate substitution generally causes a decreased intensity of absorption. Also for borate functionalized disilene **180** a weak UV/vis absorption was observed in comparison with other disilenes (*cf.* Chapter 3.3.2).

3.4.7. Summary: Functionalization of Bridged Propellanes at Si3

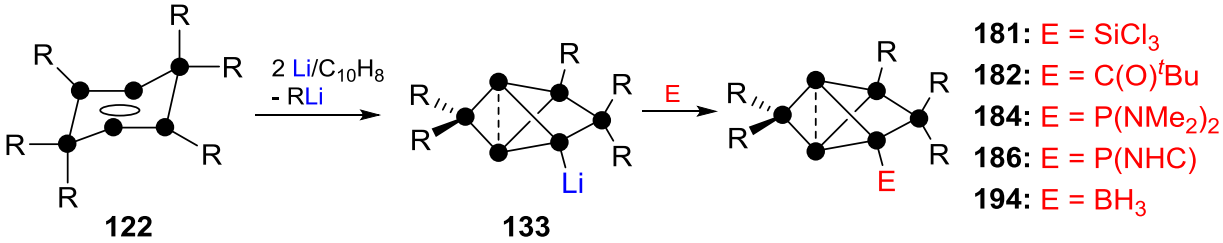

Scheme 117. Synthesis of anionic siliconoid **133** and rectivity of **133** towards electrophiles; a: **181**, E= $SiCl_4$, b: **182**, E= $ClC(O)^tBu$, c: **184**, E= $ClP(NMe_2)_2$, d: **186**, E= $P(NHC)_2$, NHC= 1,3-diisopropyl-4,5-dimethylimidazol-2-ylidene, e: **194**, E= $BH_3{\cdot}SMe_2$; R= Tip.

Reduction of dismutational hexasilabenzene isomer **122** affords anionic siliconoid **133**, the first example of a functionalized siliconoid and an intermediate species between siliconoids and silicon based Zintl anions (Scheme 117).

Subsequently it was demonstrated that **133** is valuable synthon to transfer the unperturbed bridged propellane skeleton to electrophiles from Group 13 (Chapter 3.4.6), Group 14 (Chapter 3.4.1.and 3.4.2) and Group 15 (Chapter 3.4.3 and 3.4.4, Scheme 117).

For all derivatives a characteristic wide distribution of ^{29}Si NMR chemical shifts was observed that has also been reported for the all-Tip substituted bridged propellane **125** (Table 2).[165]

	Functional Group	**^{29}Si Si1/Si2** [ppm]	**^{29}Si Si6** [ppm]	**Si1-Si2** [Å]	**Si1-Si2-Si3/ Si1-Si2-Si4** [°]	**λ_{max} (ε)** [nm (M^{-1} cm^{-1})]
133	Li	−230.9 −232.6	152.2	2.5506(9)	107.618	364 (7400)
181	$SiCl_3$	−252.3 −264.2	175.4	2.635(1)	96.241	460 (800)
182	C(O)^{t}Bu	−264.7 −271.1	171.8	2.6430(6)	96.960	475 (500)
184	$P(NMe_2)_2$	−256.0 −261.4	168.7	2.6231(5)	97.798	475 (1200)
186	P(NHC)	−252.5, −261.4	167.7	2.6412(6)	97.697	589 (400)
194	BH_3	−257.3 −265.0	161.2	2.620(1)	100.333	475 (220)
125	Tip[a]	−274.2[a]	174.6[a]	2.7076(8)[a]	96.78[a]	473 (700)

Table 2. Pertinent analytical data of siliconoids functionalized at Si4 (data for homoleptic siliconoid **125**[165] included for comparison); NHC = 1,3-diisopropyl-4,5-dimethylimidazol-2-ylidene; [a] atom numbering differing in **125**.

While the “naked” silicon vertices are strongly shielded, the neighboring $SiTip_2$-moiety is found a long way downfield. The substituent at Si3 does not dramatically affect the ^{29}Si NMR chemical shifts since all values found are very similar (Table 2).

The steric demand of substituents has a distinct effect on the angle between the two bridged “propeller blades” (Si1-Si2-Si3/Si1-Si2-Si4): the release of steric strain caused by smaller substituents (Li, BH_3) results in a less acute angle (Table 2). The Si1-Si2 bond distance in anionic siliconoid **133** (2.5506(9) Å) is 0.157 Å shorter than in **125** (2.7076(8) Å), which is tentatively attributed to delocalization of the lone-pair on silicon into cluster bonding orbitals. Generally, the trend continues that electropositive substituents induce a shortening of the bridgehead bond. While for the borate substituted derivative **194** also a relatively short Si1-Si2 bond is found (2.6231(5) Å), this particular bond in ketonyl substituted bridged proprellane **182** (2.6430(6) Å) is closest to what has been reported for **125** (2.7076(8) Å, Table 2).[165] The longest wavelength absorptions in the UV/vis spectra of most of the functionalized derivatives (λ_{max} = 460-475 nm) are in good agreement with that observed for the homoleptic species **125** (λ_{max} = 473 nm) and are thus assigned to the HOMO-LUMO vertical singlet excitation. The longest wavelength absorption of phosphinidene substituted siliconoid **186**, however, was found significantly red-shifted (λ_{max} = 589 nm) what we assign to a certain degree of double bond character

between Si and P. For anionic siliconoid **133** an absorption band in this area could not be detected, presumably due to a too low intensity of this particular band (**133**: λ_{max} = 364 nm). The intensity of the longest wavelength absorptions of the neutral functionalized siliconoids varies with the type of substituent linked to the Si_6-backbone (ε = 220 to 1200 M^{-1} cm^{-1}).

3.4.8. Functionalization of Siliconoids at Si6

With the isolation of bridged propellanide **133** the first example of an anionic siliconoid, formally an intermediate species between siliconoids and silicon based Zintl anions, was provided. In the previous chapters it was demonstrated that the anionic silicon vertex in **133** provides a nucleophilic reaction side. Various functionalized siliconoids are accessible from the reactions of **133** with electrophiles from Group 13-15.

As the anionic scaffold of **133** is formed upon reductive cleavage of one Tip-substituent in dismutational hexasilabenzene isomer **122**, the question arose at which point on the reaction coordinate the rearrangement to the global minimum scaffold would occur. We therefore investigated whether the reduction of **125** under similar conditions would also afford the same anionic cluster **133** (Scheme 118).

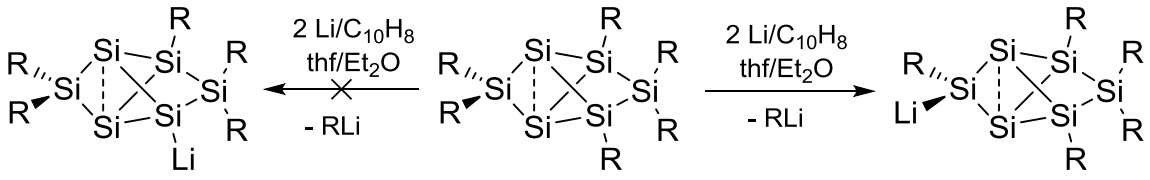

Scheme 118. Reduction of the global minimum isomer **125** does not afford bridged propellanide **133** but novel anionic siliconoid **195** functionalized at a different position (R = Tip).

Bridged propellane **125** was dissolved in diethyl ether and two equivalents of a solution of lithium/naphthalene in tetrahydrofurane were added at −80°C. While warming to room temperature, the orange solution turned red. Subsequent NMR spectroscopic investigation of the mixture revealed complete and absolutely uniform conversion to a new product, clearly differing from **133** and thus unambiguously

excluding the interemidiacy of **125** in the formation of **133**. While ^{1}H and ^{7}Li NMR spectroscopy indeed indicate the formation of TipLi as by-product and hence the reductive cleavage of one Tip-substituent, this cleavage must necessarily occur in a different position of the Si_6 cluster. In the ^{29}Si NMR spectrum, the six resonances of the new species are observed at δ = 267.9, 100.2, 15.3, −43.8, −222.2 and −231.4 ppm (Figure 80).

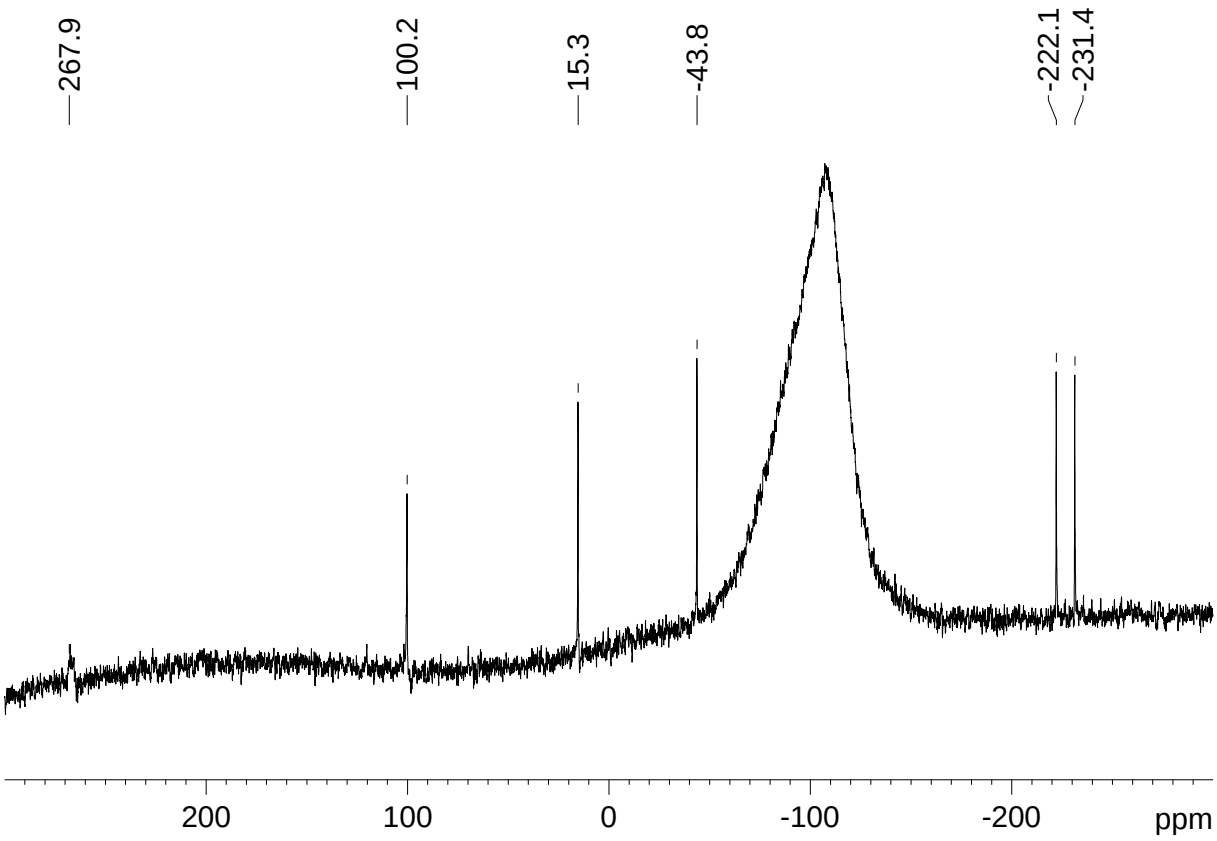

Figure 80. ^{29}Si{^{1}H} NMR spectrum of anionic siliconoid **195**.

The wide distribution of ^{29}Si NMR chemical shifts can be attributed to a distinct cluster current in the product and suggests an intact siliconoid backbone. In analogy to the previously discussed bridged propellanes, the two high-field resonances (δ = −222.2 and −231.4 ppm) are assigned to “naked” silicon vertices. Strikingly, the low-field resonance usually observed for the neighboring $SiTip_2$-unit is even dramatically more deshielded than in the previously described derivatives (δ = 175.4-152.2 ppm). The characteristic broadening of this particular resonance is in accord with a direct coupling to the quadrupolar lithium nucleus. These NMR spectroscopic findings make the reductive cleavage of one of the Tip-substituents from the $SiTip_2$-moiety flanking the unsubstituted vertices to afford anionic siliconoid **195** plausible (Scheme 118).

This is further confirmed by a two-dimensional Si/H correlation NMR experiment (due to the wide distribution of ^{29}Si NMR chemical shifts, two spectra had to be recorded, Figure 81).

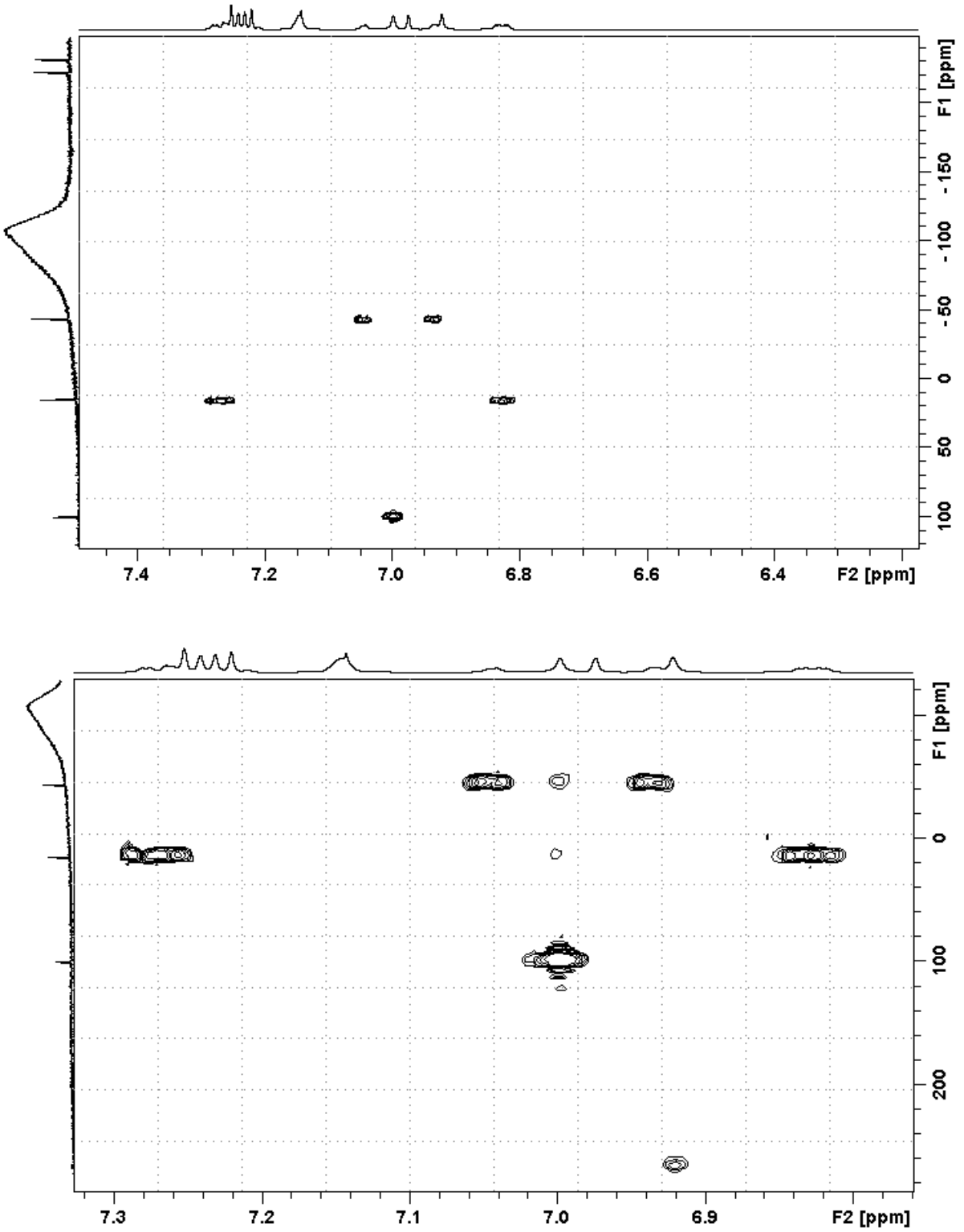

Figure 81. Selected area of the Si/H correlation 2D NMR spectra of anionic siliconoid **195** (two experiments had to be performed due to the wide distribution of chemical shifts).

While the broadened low-field signal shows a cross peak to one Tip-ligand, the two strongly shielded ^{29}Si NMR resonances do not couple to Tip-substituents. The remaining signals can be attributed to SiTip-units (δ = 100.2 and −43.8 ppm) and a $SiTip_2$-silicon (δ = 15.3 ppm). It should be mentioned that a formally four-coordinate silyl anion as in **195** with such a dramatic deshielding is astonishing and to the best of our knowledge completely without precedence. Notably, even donor-free tricoordinate silylium cations resonate at significantly higher field (*e. g.* $Mes_3Si^+B(C_6F_5)_4$ in C_6D_6: δ = 225.5 ppm).[234] The anionic charge at this particular position obviously has a distinct effect on the cluster current as also suggested by a considerable deshielding of one of the remaining SiTip-units (δ = 100.2 ppm) in **195**. Usually, these resonances were observed in a fairly inconspicuous area in the ^{29}Si NMR spectrum (27.6-7.2 ppm, *cf.* Chapter 3.4.7). The range of ^{29}Si NMR chemical shifts in **195** is even larger than in the other bridged propellane derivatives and has reached 500 ppm.

Anionic siliconoid **195** is only sparingly soluble in hexane and we were therefore able to obtain very pure **195**·$(thf)_2$ in acceptable yield (31%) by washing the crude product with hexane to remove TipLi and naphthalene (Figure 82). [235]

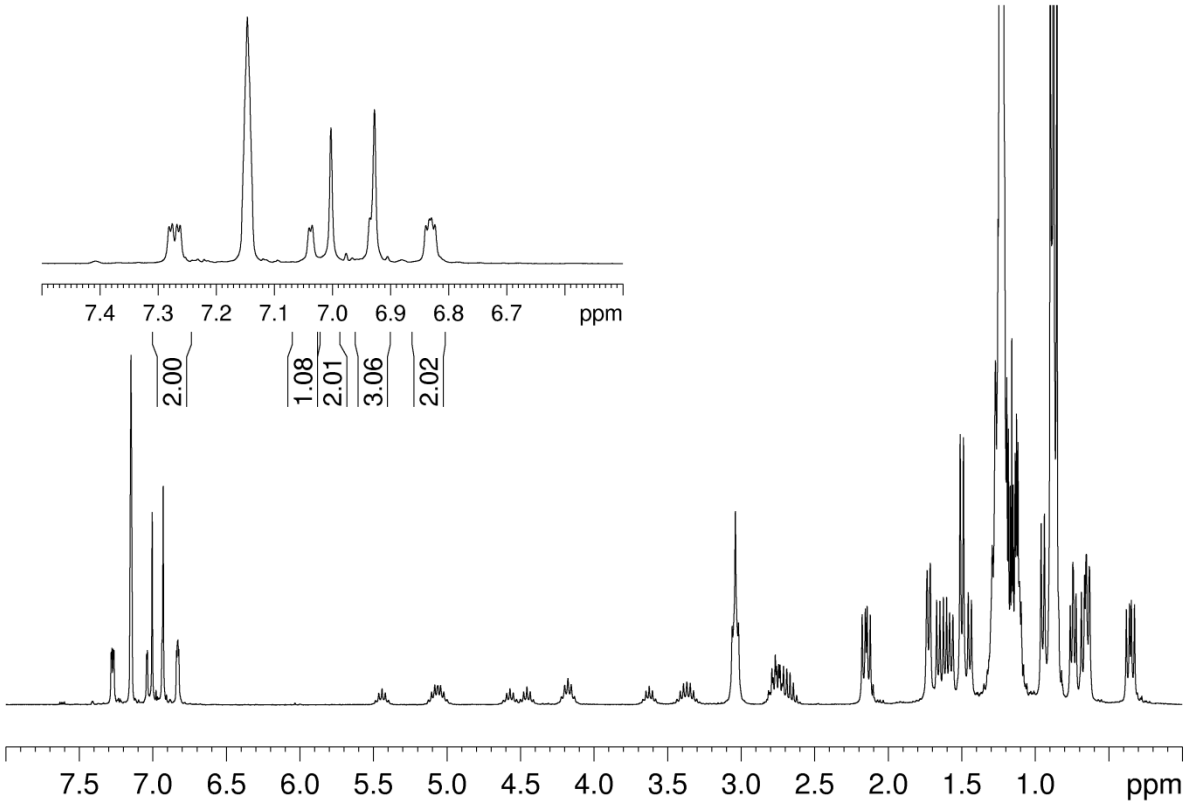

Figure 82: ^{1}H NMR spectrum of anionic siliconoid **195**·$(thf)_2$.

Orange single crystals of **195** (M. p. 208-212°C, rearrangement) suitable for X-ray diffraction analyses were obtained from a toluene/thf mixture as **195**·$(thf)_3$ and the constitution of a bridged propellane motif bearing the anionic charge at Si6 was unequivocally confirmed (Figure 83).

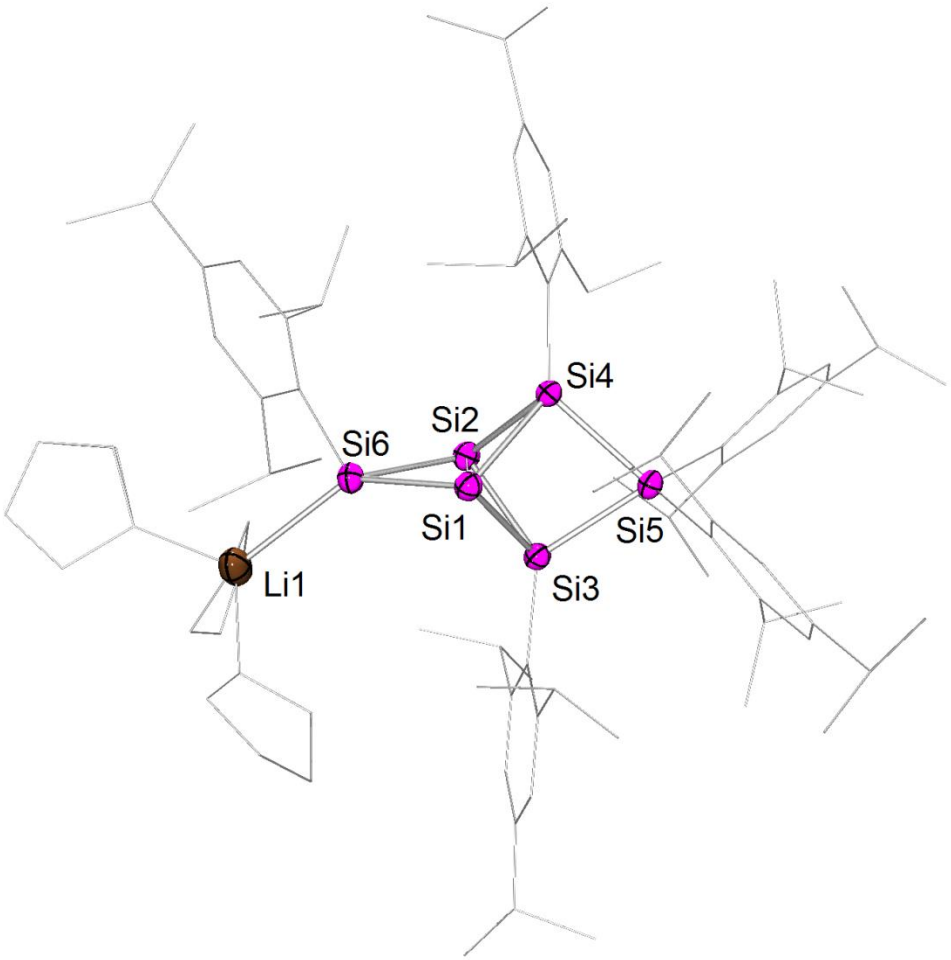

Figure 83. Molecular structure of **195** in the solid state (thermal ellipsoids at 50%, H atoms, disordered Tip-^{i}Pr-groups and - thf molecules omitted). Selected bond lengths [Å] and angles [°]: Si(1)-Si(2) 2.5563(10), Si(2)-Si(6) 2.3651(9), Si(1)-Si(6) 2.4297(10), Si(1)-Si(3) 2.3357(9), Si(1)-Si(4) 2.3630(9), Si(2)-Si(3) 2.3507(9), Si(3)-Si(5) 2.3628(9), Si(6)-Li(1) 2.699(5), Si1-Si3-Si2 66.11(3), Si1-Si4-Si2 65.983, Si1-Si6-Si2 64.42(3), Si(6)-Si(1)-Si(2) 56.57(3), Si(4)-Si(1)-Si(6) 102.61(3), Si(1)-Si(3)-Si(5) 96.15(3), Si(3)-Si(5)-Si(4) 75.97(3).

The bridgehead bond distance in **195** (Si(1)-Si(2) 2.5563(10) Å) is comparable to that in anionic siliconoid **133** (2.5506(9) Å) and thus significantly shorter than in all-Tip substituted siliconoid **125** and the functionalized derivatives **181**, **182**, **184**, **186** and **194** (2.620(1)-2.7076(8) Å, *cf.* section 3.4.7). Equally, we attribute this shortening to delocalization of the lone-pair on silicon into cluster bonding orbitals. As reflected by the angle between the two bridged “propeller blades”, the steric congestion around these particular blades in **195** (Si1-Si2-Si3/Si1-Si2-Si4: 95.760°) is much closer to what has been reported for **125** (96.7°) than to the corresponding blades in anionic siliconoid **133** (107.618°). The release of steric strain on one side of the “Si1-Si2-Si6 propeller blade” by the elimination of one Tip-group from Si6 results in a widened angle between this “blade” and one bridged “propeller blade” (Si1-Si2-Si4/Si1-Si2-

Si6: 138.808°) and a more-acute angle (Si1-Si2-Si3/Si1-Si2-Si6: 125.432°) to the other one (**125**: 131.648°).

UV/vis spectroscopy of **195** in hexane solution (Figure 133) revealed the longest wavelength absorption at λ_{max} = 468 nm (ε = 600 $M^{-1}cm^{-1}$, Figure 134), which is in good agreement with that observed for the bridged propellane derivatives discussed before and thus it is assigned to the HOMO-LUMO vertical singlet excitation.[165] A second absorption band is observed at λ = 368 nm (ε = 6400 $M^{-1}cm^{-1}$, Figure 135). Comparable absorption bands were found for anionic siliconoid **133** (λ = 364 nm, ε = 7449 $M^{-1}cm^{-1}$) and the neutral derivatives (*vide supra*).

Upon melting, a uniform rearrangement of the cluster scaffold of **195** is observed (Scheme 119).

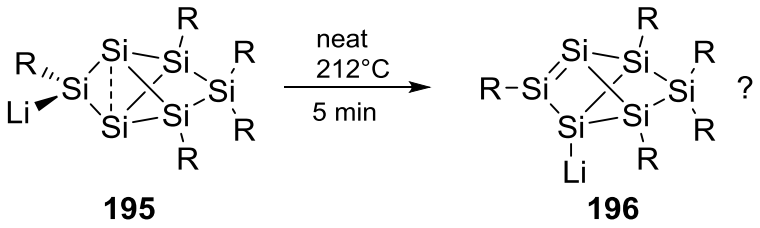

195 **196**

Scheme 119. Possible rearrangement product of **195** upon melting (R = Tip).

For the rearrangement product six resonances are detected in the ^{29}Si NMR spectrum at δ = 54.5, 10.9, −68.9, −83.5, −248.3 and −275.8 ppm (Figure 84). For the bridged propellane skeleton usually a distinct high-field shift is observed for the unsubstituted silicon vertices whereas the neighboring $SiTip_2$-unit is strongly deshielded (>150 ppm).

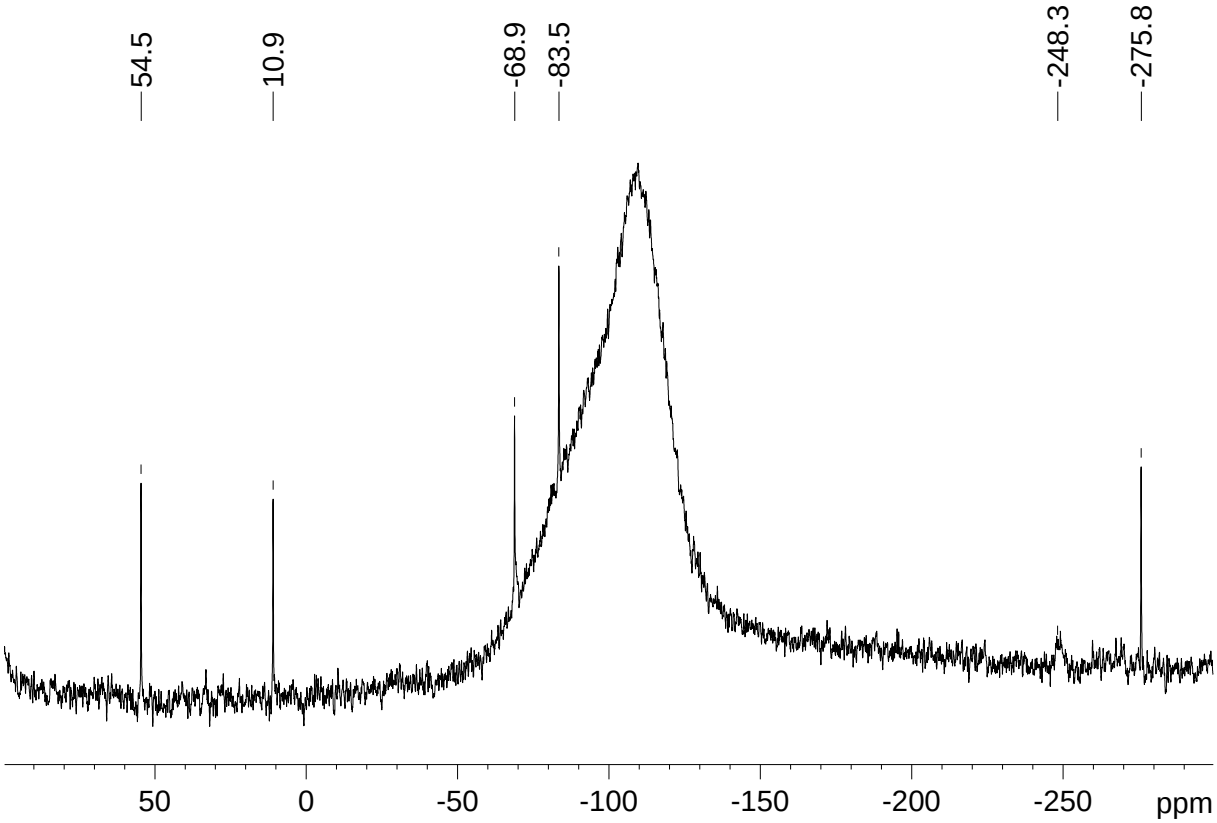

Figure 84. $^{29}Si\{^{1}H\}$ NMR spectrum of proposed rearrangement product **196**.

While the two high-field ^{29}Si NMR resonances in the rearrangement product are indeed in accord with two “naked” silicon vertices, the most down-field shifted resonance is recorded at δ = 54.5 ppm, which speaks strongly against an intact bridged propellane skeleton. Furthermore, two additional ^{29}Si NMR resonances at rather high field are observed (δ = −68.9 and −83.5 ppm). Notably, the resonance at δ = −248.3 ppm is significantly broadened and can thus be attributed to a *Si*-Li unit. The presence of a lithio silane moiety is further confirmed by coordinated thf observed in the ^{1}H NMR spectrum at δ = 3.48 and 1.32 ppm. Probably the lithium atom migrates to one flanking unsubstituted silicon vertex under Si=Si bond formation to yield cluster **196**.

The resonance ^{29}Si NMR resonance at δ = 54.5 ppm could be attributed to the doubly bonded SiTip silicon. In accord with the signal at δ = −275.8 ppm a strongly distorted geometry would be expected for the silicon atom on the other side of the double bond. However, to date no single crystalline material was obtained to elucidate the structure by an X-ray diffraction study and consequently these assumptions remain highly speculative.

3.4.9. Sequestering the Lithium Cation in Anionic Siliconoid 195

In analogy to **133**, separation of the lithium counter cation in **195**·(thf)$_2$ by a sequestering agent was investigated. Yannic Heider participated in the execution of this experiment during a research lab course in our group.[235] A "naked" silyl anion at this particular cluster position should have interesting effects on the bonding situation. When anionic siliconoid **195**·(thf)$_2$ was treated with two equivalents 12-crown-4, the orange solution turned instantly red. ^{29}Si NMR spectroscopy of the reaction mixture revealed that indeed **195**·(12-crown-4)$_2$ has formed as the major product (Scheme 120).

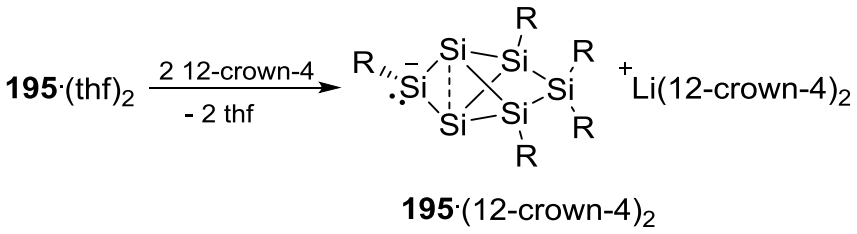

Scheme 120. Synthesis of **195**·(12-crown-4)$_2$ (R = Tip).

The anionic silicon atom in **195**·(12-crown-4)$_2$ is subject to an even stronger deshielding than in **195**·(thf)$_2$ (δ = 267.9 ppm): passing the 300 ppm benchmark the resonance for this silicon atom is detected at δ = 304.1 in the ^{29}Si NMR spectrum (Figure 85). A significant sharpening of the low-field resonance is in accord with a fully sequestered lithium cation. The considerably stronger deshielding of the anionic silicon atom further confirms that the lone pair at this position has an effect on the cluster current in the molecule. In **195**·(12-crown-4)$_2$ the lone pair on silicon is certainly better available for efficient delocalization. The remaining resonances in **195**·(12-crown-4)$_2$ (δ = 117.3, 8.8, −53.7, −212.0 and −230.2 ppm, Figure 85) are rather similar to those in **195**·(thf)$_2$ (δ = 100.2, 15.3, −43.8, −222.2 and −231.4 ppm).

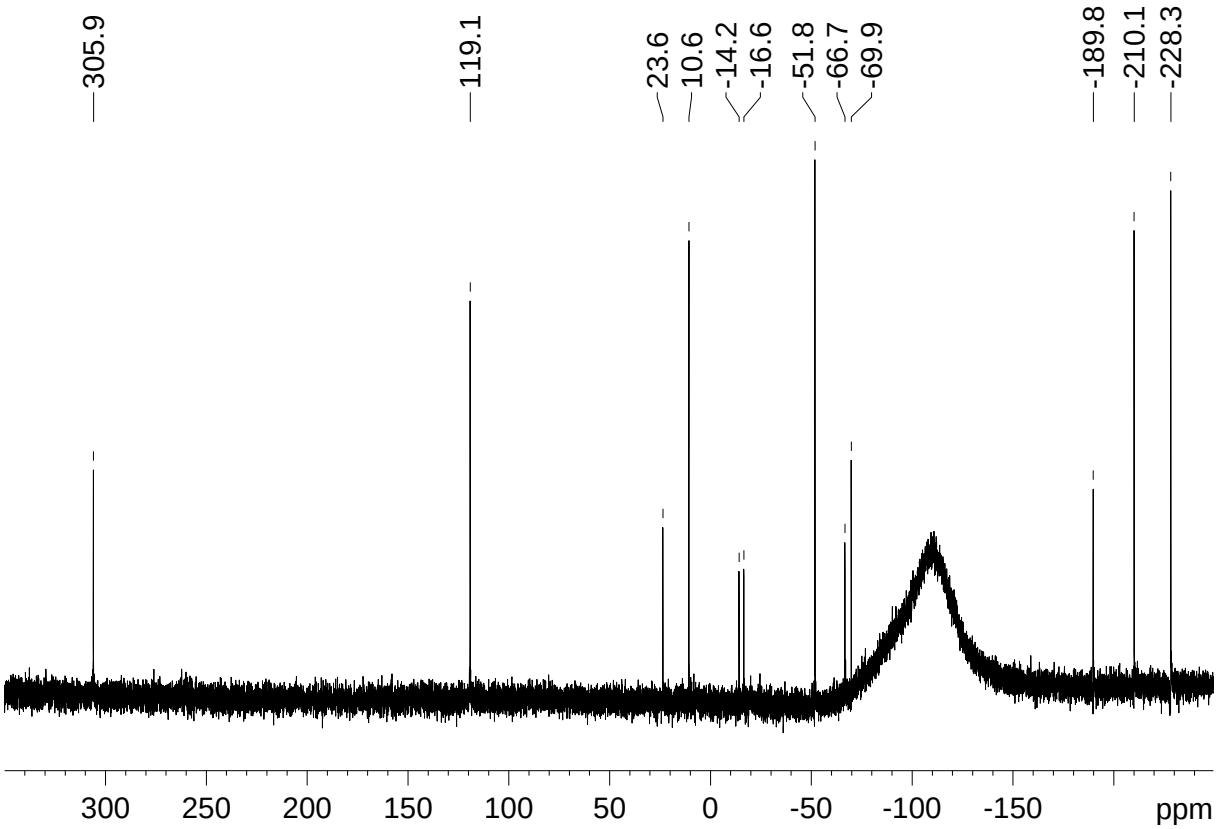

Figure 85. $^{29}Si\{^{1}H\}$ NMR spectrum from the reaction of **195**·$(thf)_2$ with two equivalents 12-crown-4.

Additionally, 15% of a Si_6 side product are observed in the ^{29}Si NMR spectrum at δ = 1.7, −16.1, −18.4, −68.6, −71.7 and −191.7 ppm (Figure 85). From the reaction it was as yet not possible to obtain single crystalline material. Consequently, we are neither able to give any evidence for the constitution of the by-product or discuss the structural details of **195**·$(12\text{-crown-4})_2$ in more detail.

3.4.10. Synthesis of Silyl Substituted Siliconoid 197

Obviously, we were interested in investigating whether in analogy to **133** anionic siliconoid **195** can be applied to transfer the intact bridged propellane motif to electrophiles. The introduction of functional groups on the silicon atom neighboring the naked vertices would be of distinct interest. A proof-of-concept reaction was carried out during this project. Yannic Heider participated in the execution of this experiment during a research lab course in our group.[235]

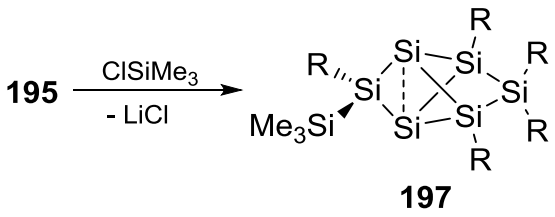

Scheme 121. Synthesis of silyl substituted siliconoid **197** (R = Tip).

Anionic siliconoid **195** was dissolved in toluene and one equivalent trimethylchloro silane was added by microsyringe (Scheme 121).

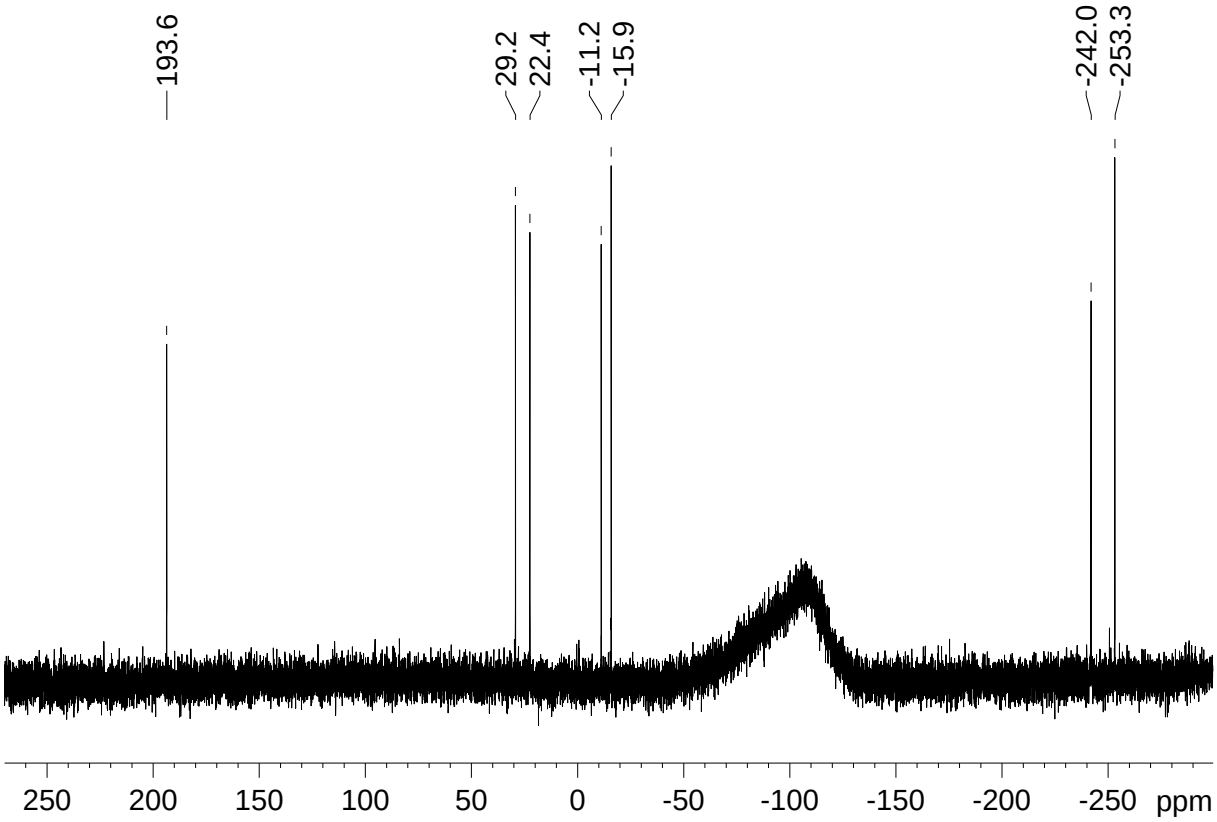

Figure 86. $^{29}Si\{^{1}H\}$ NMR spectrum of silyl substituted siliconoid **197**.

Seven resonances in the ^{29}Si NMR spectrum observed at δ = 193.6, 29.2, 22.4, −11.2, −15.9, −242.0 and −253.3 ppm are in accord with uniform formation of silyl substituted siliconoid **197** (Figure 86). In the ^{1}H NMR spectrum the trimethyl silyl protons are found at δ = −0.15 ppm. On the basis of a two-dimensional Si/H correlation NMR experiment the signal at δ = −11.2 ppm can be assigned to the trimethyl silyl group (Figure 87). Additionally, a less intense cross-peak to the low-field resonance at δ = 193.6 ppm can be assigned to the $SiMe_3$-protons further confirming the constitution of **197**.

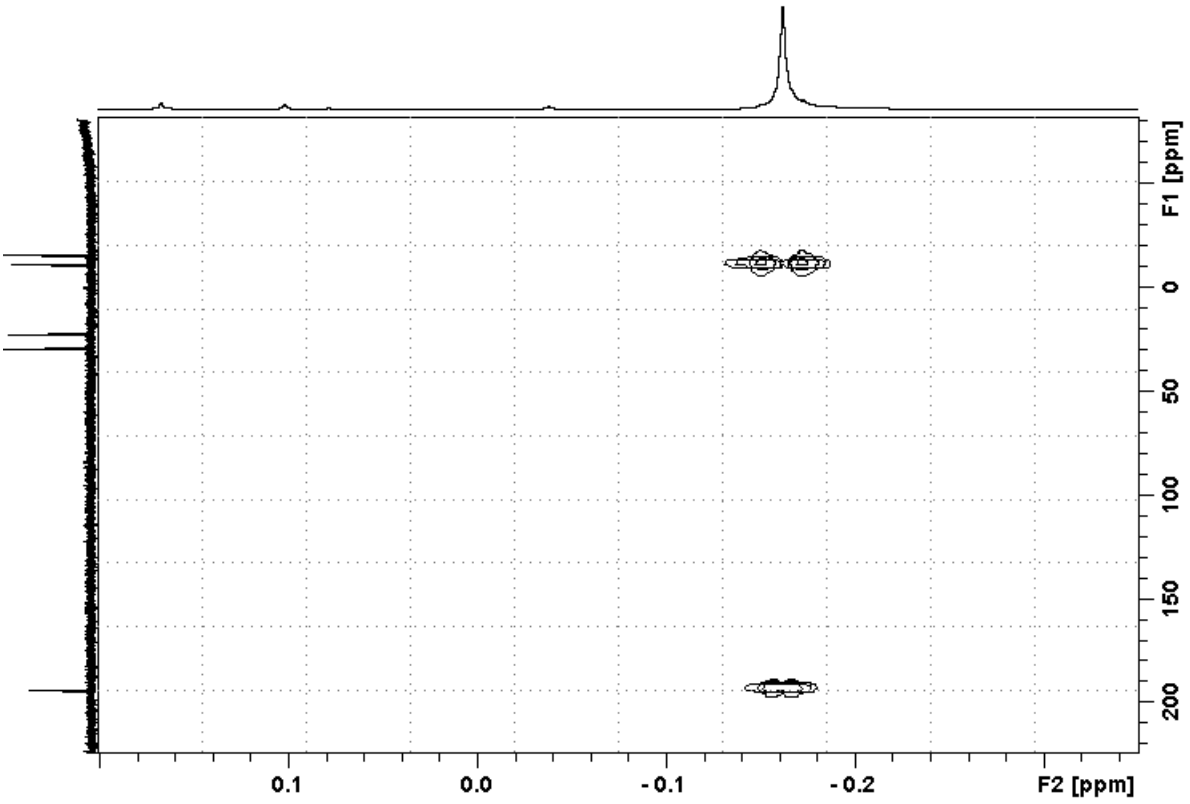

Figure 87. Relevant region of the $^{29}Si/^{1}H$ correlation 2D NMR spectrum of **197**.

In anionic siliconoid **195** a significant downfield shift was observed for the SiTipLi unit (δ = 267.9 ppm) *versus* δ = 175.4-152.2 ppm for the corresponding vertex in the other bridged propellanes (*cf*. Chapter 3.4.7, Table 2). This was attributed to effects of the lone-pair on silicon on the cluster current in **195**. Notably, also in **197** a similar trend is apparent even though less pronounced. These findings are in accordance with some degree of donation of electron density into the cluster core due to the σ-donating $SiMe_3$-moiety.

Orange single crystals of **197** (M. p. 193°C) were obtained from a concentrated hexane solution in 66% yield and an X-ray diffraction study confirmed the expected structure (Figure 88).

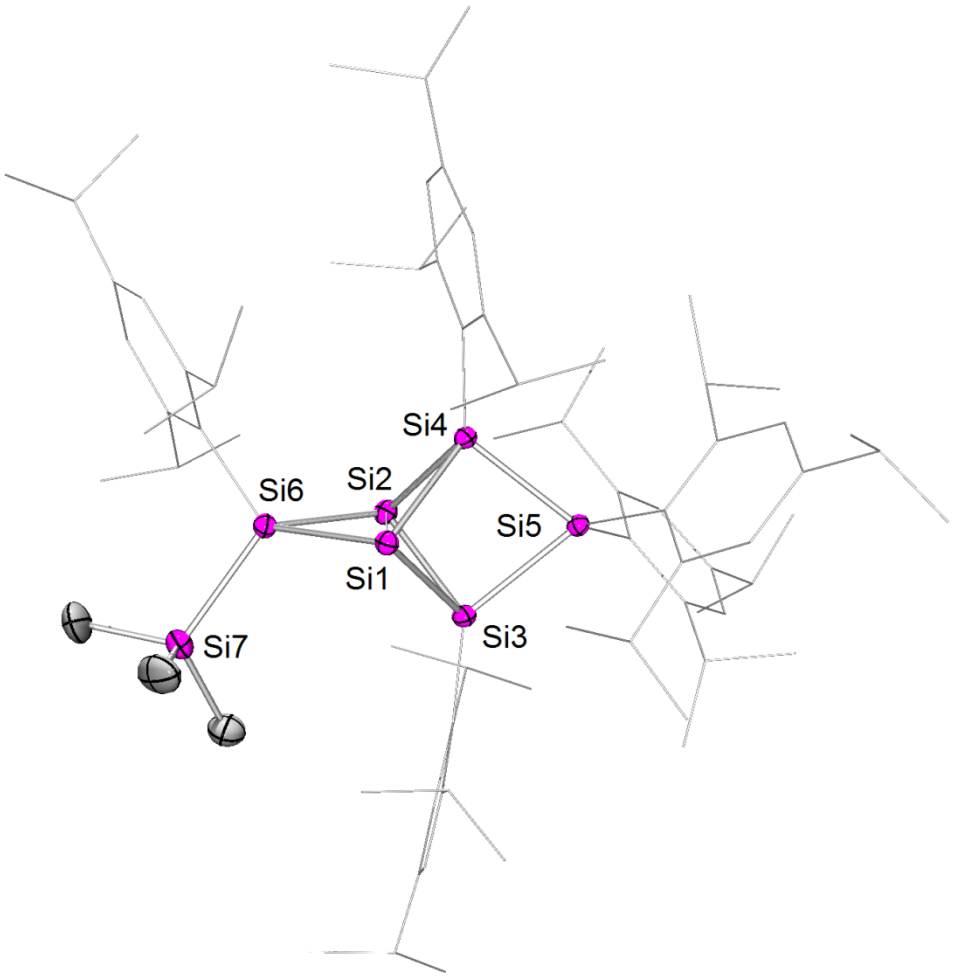

Figure 88. Molecular structure of **197** in the solid state (thermal ellipsoids at 50%, H atoms and co-crystallized solvent omitted). Selected bond lengths [Å] and angles [°]: Si(1)-Si(2) 2.6118(6), Si(2)-Si(6) 2.3319(7), Si(1)-Si(6) 2.3932(6), Si(1)-Si(3) 2.3354(6), Si(1)-Si(4) 2.3628(6), Si(2)-Si(3) 2.3547(6), Si(3)-Si(5) 2.3749(6), Si(6)-Si(7) 2.3696(7), Si(2)-Si(6)-Si(1) 67.10(2), Si(6)-Si(1)-Si(2) 55.329(18), Si(4)-Si(1)-Si(6) 96.97(2), Si(1)-Si(3)-Si(5) 94.99(2), Si(3)-Si(5)-Si(4) 76.70(2).

The bridgehead bond in **197** (Si(1)-Si(2) : 2.6118(6) Å) is longer than in anionic siliconoids **133** and **195** (2.5563(10) and 2.5506(9) Å), but slightly shortened compared to the other bridged propellanes (2.620(1)-2.7076(8) Å, *cf.* Chapter 3.4.7, Table 2), functionalized at Si2. These finding is in accord with the aforementioned σ-donating effect that also accounts for the stronger deshielding of the substituted silicon atom. Expectably, the angle between the two bridged “propeller blades” (Si1-Si2-Si3/Si1-Si2-Si4: 98.277°) is comparable to **195**, all-Tip substituted siliconoid **125** and bridged propellanes substituted with bulky substituents such as **195** or **197** (95.760°-97.798°). In contrast to what was found in **195**, both angles between the untethered “propeller blade” and the bridged blades are approximately the same (Si1-Si2-Si3/Si1-Si2-Si6: 131.025° and Si1-Si2-Si4/Si1-Si2-Si6: 130.698°). This can

be explained by the considerably more bulky trimethylsilyl group compared to the lithio substitution.

In the UV/vis spectrum of **197** (Figure 136) a bathochromic shift of the longest wavelength absorption (λ_{max} = 496 nm) was found compared to all other bridged propellane derivatives (λ_{max} = 468-475 nm). The intensity of this absorption is at the lower end (ε = 400 $M^{-1}cm^{-1}$, Figure 137) compared to the other derivatives (ε = 200-1200 $M^{-1}cm^{-1}$). Comparable to what was observed for the siliconoid derivatives discussed before, the UV/vis spectrum of **197** revealed an additional absorption band at λ = 359 nm (ε = 5500 $M^{-1}cm^{-1}$, Figure 138).

3.4.11. Oxidation of Siliconoid 195

In principle the lone–pair on silicon in anionic siliconoids is not only of interest concerning substitution reactions but should also allow for oxidative chemistry. We decided to investigate the reactivity of anionic siliconoid **195** towards silver perfluorotetraphenyl borate as oxidation agent. Treatment of **195** with one equivalent might afford a radical species **198**. Successful two-electron reduction would afford cationic siliconoid **199** (Scheme 122).

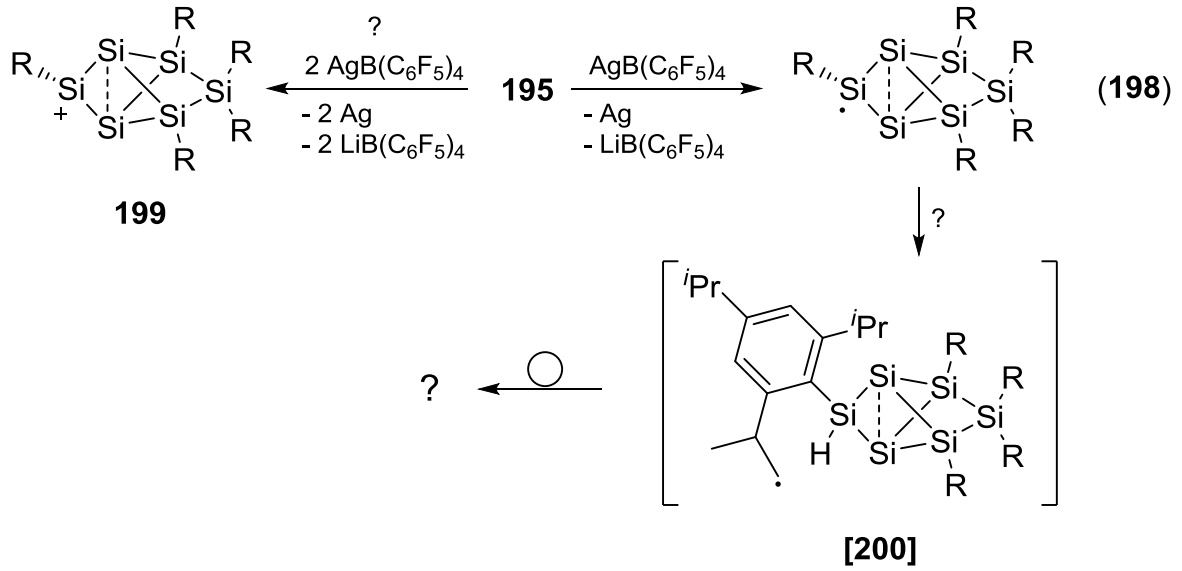

Scheme 122. Possible reaction pathways of an one or two electron reduction of anionic siliconoid **195** (R = Tip).

One equivalent $AgB(C_6F_6)_4$ was combined with anionic siliconoid **195** in diethyl ether at −80°C. Only minutes after addition the orange solution discolored to a pale yellow.

In the ^{29}Si NMR spectrum six sharp resonances are observed at δ = 8.3, −15.8, −24.4, −76.6, −90.1, −91.6 ppm (Figure 89) making the presence of a paramagnetic radical species unlikely.

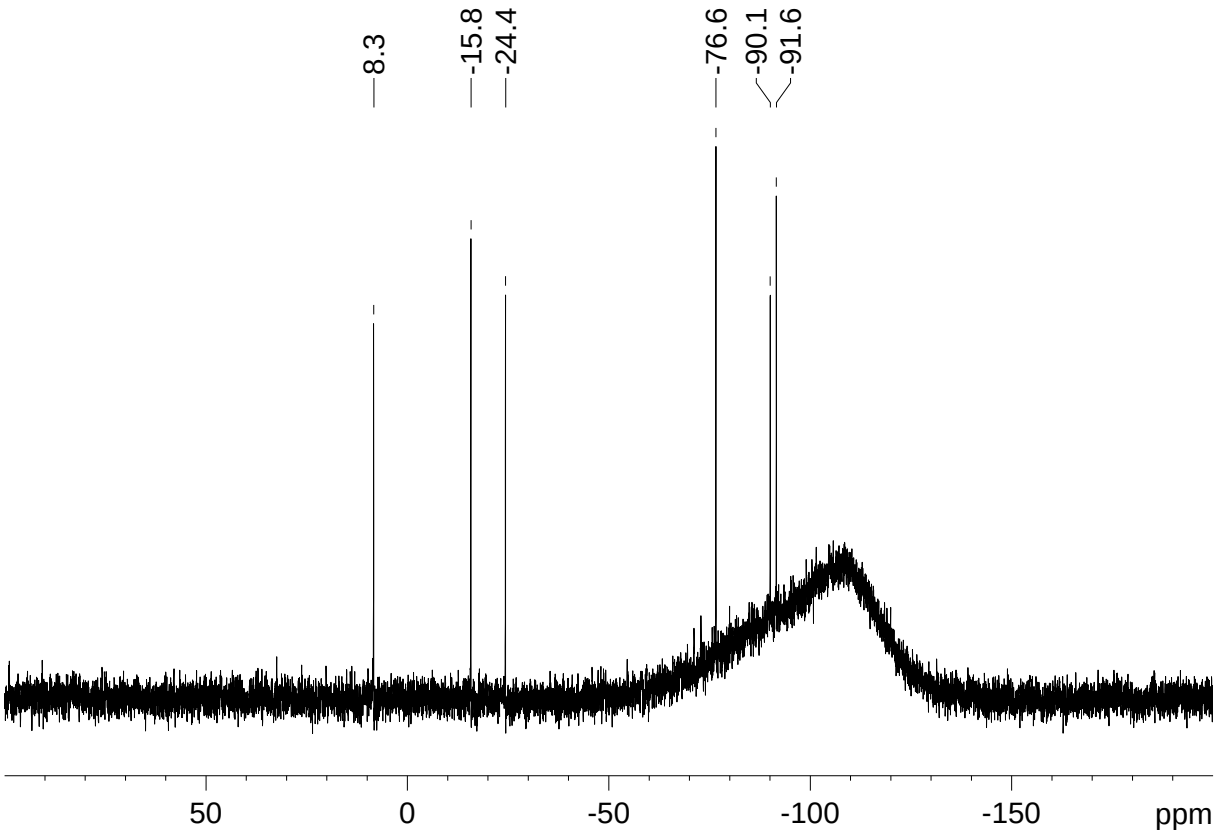

Figure 89. ^{29}Si{^{1}H} NMR spectrum from the reaction of anionic siliconoid **195** with one equivalent $AgB(C_6F_6)_4$.

The distribution of ^{29}Si NMR signals indicates a polycyclic saturated compound rather than a siliconoid cluster and excludes an uncompromised bridged propellane skeleton. $LiB(C_6F_6)_4$ as the expected by-product upon formation of **198** is detected in the ^{11}B NMR (δ = −16.0 ppm) and ^{19}F NMR (−132.5 (br d), −162.2 (tr, $^{3}J_{F\text{-}F}$ = 20.9 Hz) and −166.5 (tr, $^{3}J_{F\text{-}F}$ = 20.9 Hz)) spectra. A ^{29}Si/^{1}H correlation 2D NMR experiment (Figure 90) revealed two *Si*-H signals at δ = 6.02 (s) and 4.32 (d, $J_{H\text{-}H}$ = 12.0 Hz) ppm.

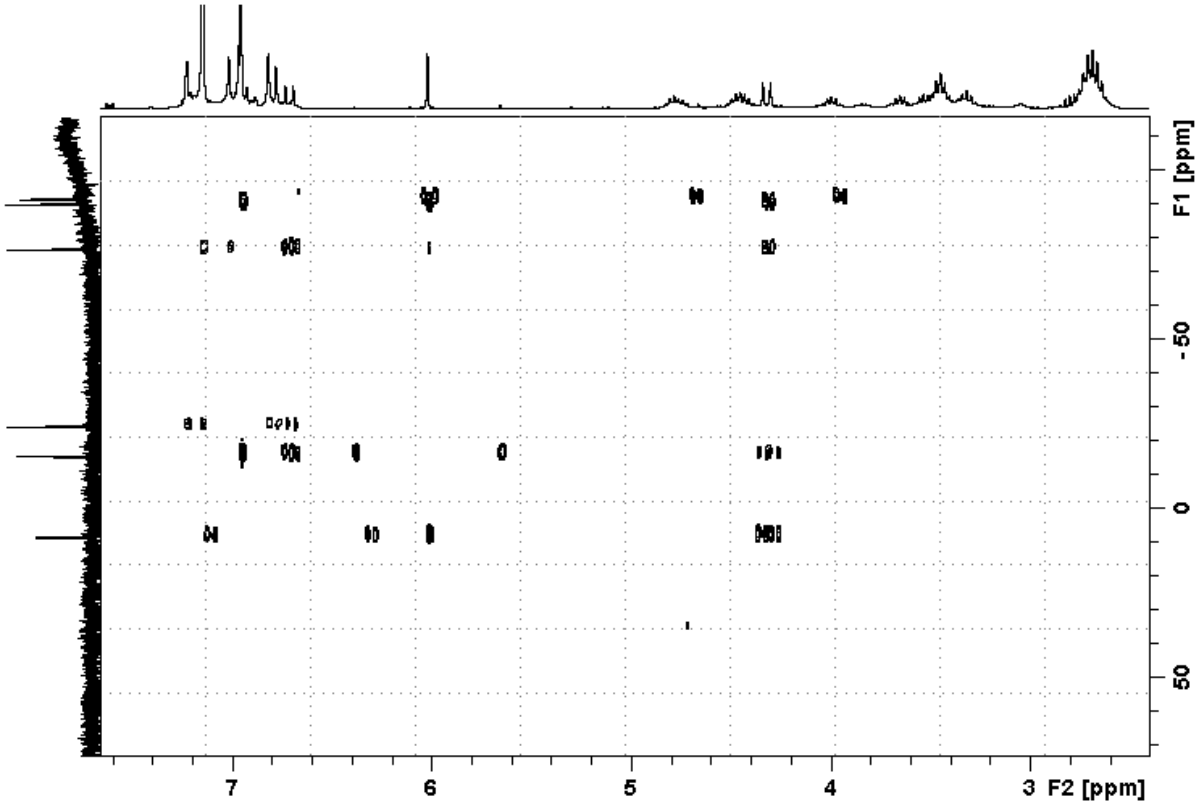

Figure 90. Selected region of the $^{29}Si/^{1}H$ correlation 2D NMR spectrum from the reaction of **195** with one equivalent $AgB(C_6F_6)_4$.

In an H/H-cosy 2D NMR experiment a cross peak of the doublet at δ = 4.32 ppm to the aromatic Tip-protons is observed. The ^{13}C NMR spectrum recorded in dept135 mode (Figure 91) indicated three CH_2-units as confirmed by three negative signals (δ = 31.8, 30.0 and 22.9 ppm).

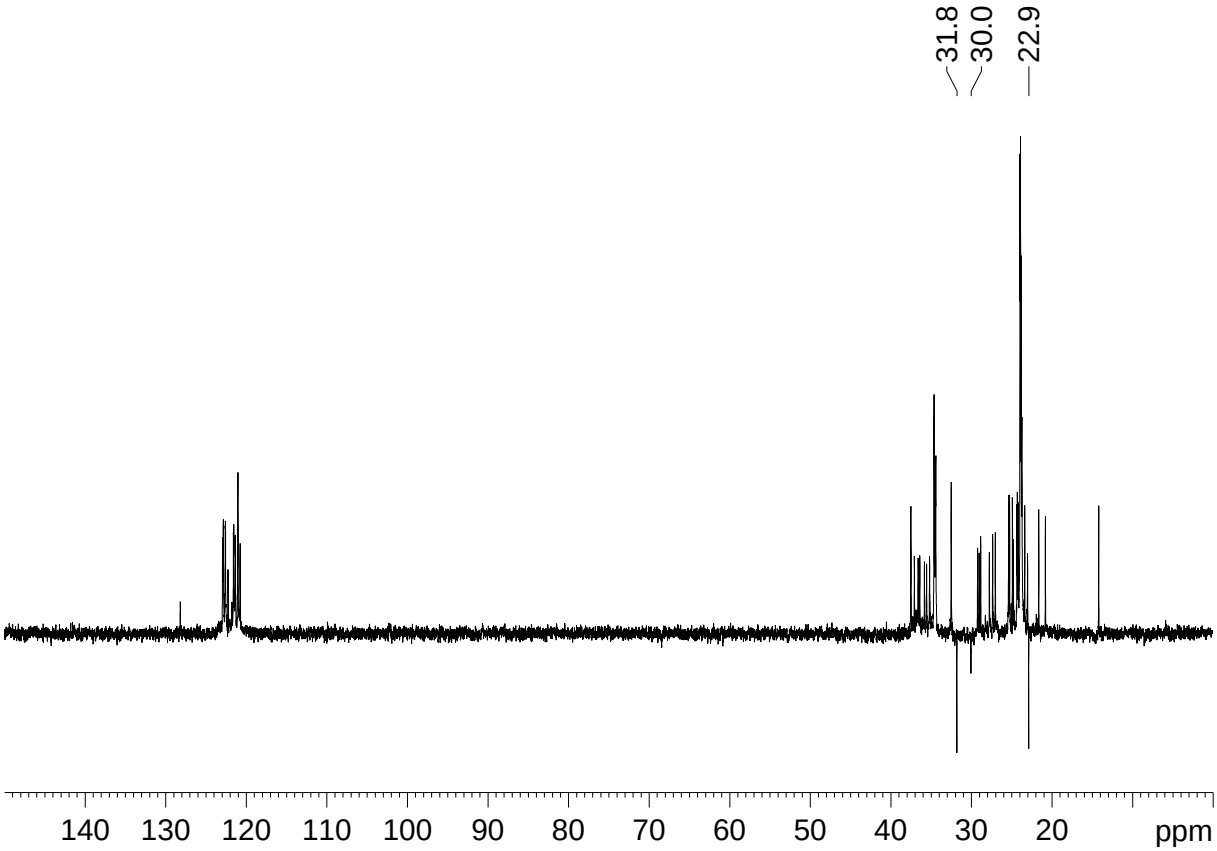

Figure 91. Dept135 ^{13}C NMR spectrum from the reaction of anionic siliconoid **195** with one equivalent $AgB(C_6F_6)_4$.

It can be reasoned that **198** is initially formed and subsequently a CH_3-proton is transferred to the radicalic silicon atom to afford **[200]**. This species further rearranges and without X-ray structure analysis the determination of the constitution of the final product appears impossible. Unfortunately, single crystalline material was as yet not obtained. The fact that no significant amounts of byproducts are observed in the reaction mixture indicates that the rearrangement of **198** is very rapid compared to the oxidation step. Consequently, a two electron reduction with an additional equivalent of $AgB(C_6F_6)_4$ to obtain cationic **199** is not promising.

To summarize, while the reaction of dismutaional isomer **122** with two equivalents lithium/naphthalene affords anionic siliconoid **133** functionalized at Si4, in Chapter 3.4 it was demonstrated that the reduction of the global minimum isomer **125** under similar conditions affords siliconoid **195** lithiated at Si6. Proof-of concept that **195** is an equally useful synthon for further functionalization at Si6 has been provided by the synthesis of silyl substituted derivative **197**. In stark contrast to substituents at Si4, the functional groups at Si6 have a strong influence on the ^{29}Si NMR chemical shifts. The Si6-atom in **195** and **197** is subjected a considerably stronger deshielding than in

125 or the derivatives functionalized at Si4. The trend that electron donating substituents induce a shortening of the bridge-head bond is both positions in common.

Position	Compound	Functional Group	^{29}Si Si1/Si2 [ppm]	^{29}Si Si6 [ppm]	Si1-Si2 [Å]
Si3	**133**	Li	−230.9 −232.6	152.2	2.5506(9)
	181	$SiCl_3$	−252.3 −264.2	175.4	2.635(1)
	182	C(O)^{t}Bu	−264.7 −271.1	171.8	2.6430(6)
	184	$P(NMe_2)_2$	−256.0 −261.4	168.7	2.6231(5)
	186	P(NHC)	−252.5, −261.4	167.7	2.6412(6)
	194	BH_3	−257.3 −265.0	161.2	2.620(1)
Si6	**195**	Li	−222.2 −231.4	267.9	2.5563(10)
	197	$SiMe_3$	−242.0 −253.3	193.6	2.6118(6)
	125	Tip[a]	−274.2[a]	174.6[a]	2.7076(8)[a]

Table 3. Pertinent analytical data of siliconoids functionalized at Si4 and Si6 (data for homoleptic siliconoid **125**[165] included for comparison); NHC = 1,3-diisopropyl-4,5-dimethylimidazol-2-ylidene; [a] atom numbering differing in **125**.

3.5. Synthesis of Dianionic Si_5-Cluster 201

Our findings described in Chapter 3.4 demonstrate that Tip-substituents can be cleaved reductively from siliconoids to afford anionic derivatives. Upon reduction of dismutational isomer **122** with two equivalents lithium/ naphthalene an initially formed anionic species isomerizes to the assumed global minimum structure and bridged propellanide **133** can be isolated. In contrast, when all-Tip substituted bridged propellane is directly reduced under similar conditions, a Tip-group is cleaved at a different position to yield bridged propellanide **195**. These findings that the negative charge can in principle be localized at two positions of the bridged propellane motif prompted us to investigate whether dianionic species are equally accessible.

When hexasilabenzene isomer **122** was treated with four equivalents lithium/ naphthalene uniform conversion to **133** was observed. Obviously, anionic siliconoid

133 is inert against an additional equivalent of reducing agent. In a next attempt siliconoid **125** was treated with four equivalents lithium/naphthalene at −80°C. Upon warming to room temperature, the solution turned very dark nearly black. Subsequently all volatiles were removed in vacuo, the residue digested with hexane and filtered. As confirmed by ^{1}H NMR spectroscopy, the mother liquor contained large quantities of TipH indeed indicating the cleavage of Tip-substituents. The ^{29}Si NMR spectrum showed a very bad signal to noise ratio further indicating only small amounts of silicon containing species. Two main signals adumbrate at δ = 55.7 and −90.1 ppm. Resonances of minor intensity are observed at δ = 19.7 and −7.4 ppm (Figure 92).

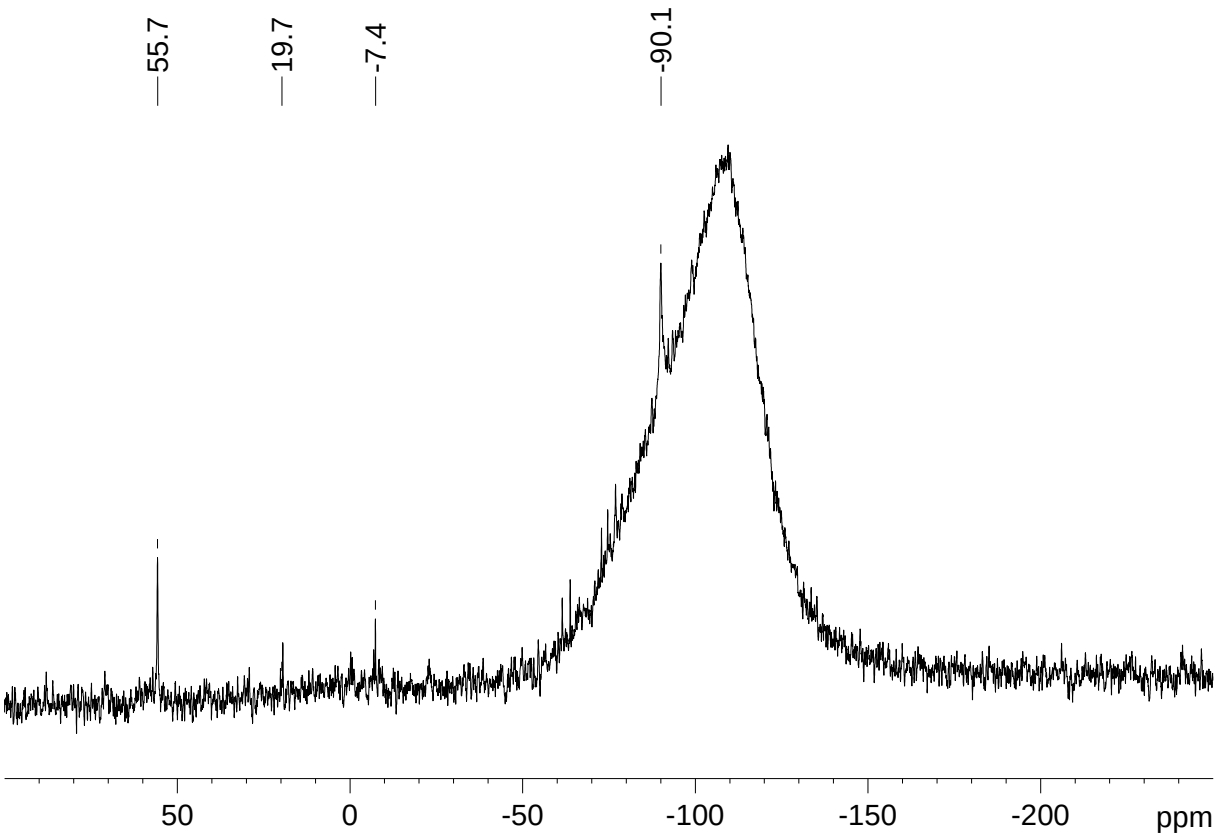

Figure 92. ^{29}Si{^{1}H} NMR spectrum from the reaction mixture after treatment of siliconoid **125** with four equivalents naphthalene/lithium.

A very small amount of pale yellow single crystals just enough for ^{1}H NMR spectroscopy was obtained from the concentrated mother liquor. An X-ray diffraction study despite heavy disorder revealed the constitution of dianionic Si_5Tip_4-cluster **201** (Figure 93, Scheme 123).

Scheme 123. Synthesis of dianionic Si_5-cluster **201** (R = Tip).

Formally the $SiTip_2$-moiety that is usually observed at low-field in the ^{29}Si NMR spectrum has been cleaved reductively from the bridged propellane skeleton. An analoguous product (potassium instead of lithium counter cations) was isolated by Dr. Kai Abersfelder during his PhD-studies upon reduction of siliconoid **125** in with potassium naphthalene. Surprisingly, in this case potassium hydroxide was found as impurity in the X-ray structure of the product.[236]

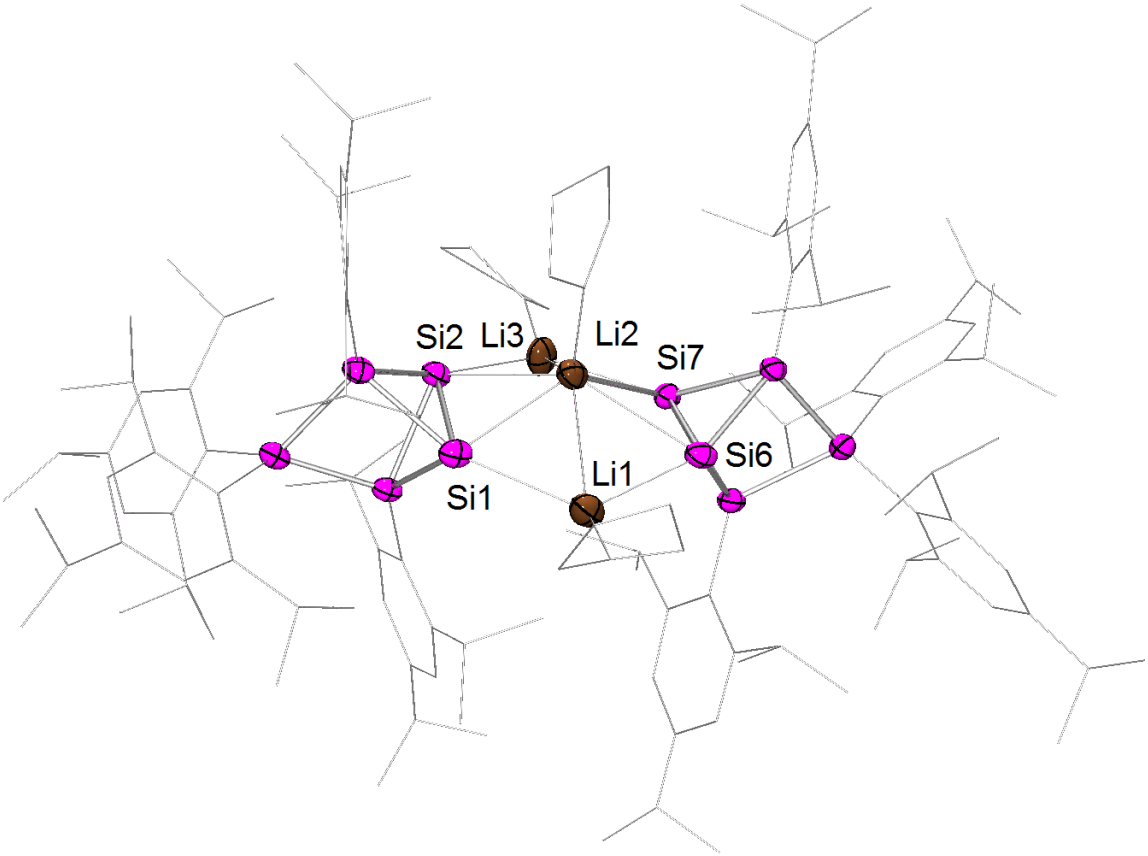

Figure 93. Molecular structure of **201** in the solid state (thermal ellipsoids at 50%, H atoms, disordered ^{i}Pr-groups, disordered thf, one completely sequestered lithium cation (as $Li(thf)_3$) and co-crystallized solvent omitted). Selected bond lengths [Å]: Si1-Si2 2.5279(14), Si6-Si7 2.5238(14).

Due to the low quality of the data obtained from the X-ray analysis of **201** a detailed discussion of the bonding situation will be excluded here. Most prominent feature is

the length of the Si1-Si2 (2.5279(14) Å) and Si6-Si7 (2.5238(14) Å) bonds that can be considered the “former bridge-head bonds” in **125**. They are significantly shorter than the bridge-head bonds in all-Tip siliconoid **125** (2.7076(8) Å) but longer than normal Si-Si single bonds (2.3-2.4 Å). The bond distance is comparable to the corresponding distances in the anionic siliconoids **133** and **195**. It should be mentioned, however, that these similarity is coincidental and assigned to entirely different effects: **201** is an electron precise system and the lengthening of the Si1-Si2 and Si6-Si7 bonds compared to normal silanes can be attributed to repulsive interactions between the two anionic silicon atoms. In contrast, the shortening in anionic siliconoids **133** and **195** compared to the neutral derivatives is assigned to delocalization of the lone-pair of electrons on silicon into cluster bonding orbitals. It was neither possible to obtain better quality single crystals of **201** nor to synthesize larger amounts for a full characterization in the time frame of this project. The reaction is currently investigated in our laboratory in order to optimize the experimental procedure.

3.6. Disilenes for Gold Surface Modifications

3.6.1. Self-assembled Monolayers (SAMs)

Surfaces are the interface between all solid substances and their environment. The properties of materials largely depend on the nature of their surface. Therefor surface modifications are of significant interest in material chemistry.[237] Self-assembled monolayers (SAMs) are molecular assemblies formed spontaneously on surfaces. They are widely applied to modify properties of certain surfaces. A SAM generally consists of a terminal functional group, a spacer and a head (or anchoring) group (Figure 94).[238]

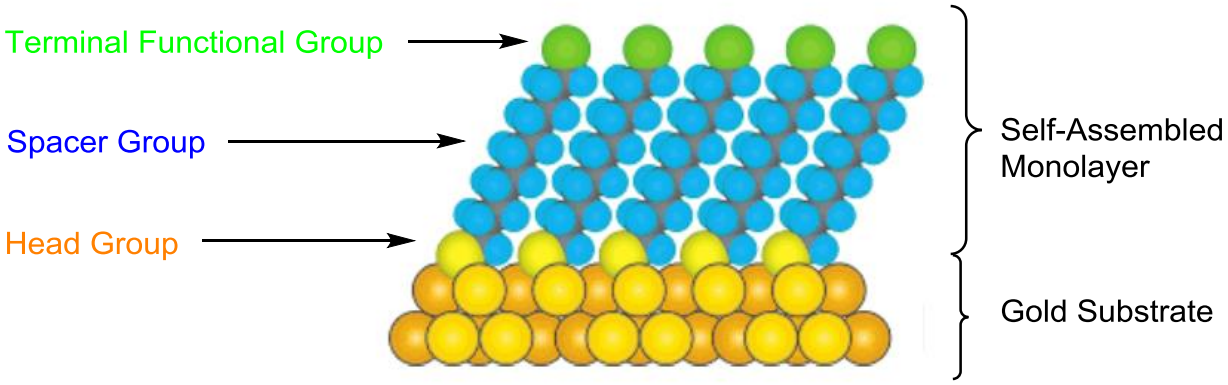

Figure 94: Schematic representation of a self-assembled monolayer (SAM) on a gold substrate (graphic reproduced from T. Büttner, Bachelor thesis).[239]

The terminal functional group basically defines the SAM surface primarily determining its properties such as wetting, adhesion or friction.[237] Reported functional groups in SAMs can vary from simple alkyl moieties to very complex species such as nanoparticles or proteins.[237]

The spacer connects the terminal functional group and the anchoring group. Furthermore, it provides a certain distance between the terminal functional group and the surface to prevent steric repulsion. Generally, it can be distinguished between two different types of spacer groups. Alkyl chains for example prevent interactions between the head and the terminal functional group and thus isolate the target group from the surface.[240] On the other hand aromatic or olefinic spacers such as biphenyl,[241] terphenyl or phenylene ethylene[242] allow for communication between the surface and the terminal functional group which can affect the properties of the monolayer.

The head (or anchoring) group is a functional group that shows a high affinity to the substrate and connects the monolayer to the surface. In this respect, sulphur-based groups are widely applied due to their high affinity to gold, silver, copper,[243] palladium,[244] platinum[245] or mercury.[246] For gold surfaces thiols are known to form very robust monolayer presumably due to the formation of covalent bonds.[244] Comparable bonds are formed with disulfides upon reductive cleavage of the S-S bond.[247] Sulfides also have been reported as anchoring groups for gold surfaces. The bonding to the surface, however, is probably much better described as dative interactions resulting in less robust monolayers.[243]

3.6.2. Synthesis of Methylsulfide Substituted Disilenes

The reactions discussed in this chapter were partially performed together with Thomas Büttner during his Bachelor studies.[239]

The introduction of functionalization to unsaturated silicon compounds is crucial for further manipulations such as embedding into extended systems.[34] Equally, in order to apply low-valent silicon compounds in material chemistry, *e. g.* for surface modifications, suitably functionalized derivatives are required. While Baines *et al.* reported disilenes as mimics for silicon surfaces,[170] the attachment of disilenes to surfaces has not been reported yet. Saturated silicon precursors such as polysilanes have been functionalized with sulfide groups and linked to gold surfaces.[248]

As outlined in Chapter 1.1.4.2 disilenide **16** is a useful synthon to transfer the disilene moiety to a variety of organic and inorganic substrates. Notably, the Scheschkewitz group demonstrated that rare examples of remotely functionalized disilenes are equally accessible starting from **16**. During the reaction of disilenide with one equivalent 1,4-dihalo benzene derivatives the residual halogen functionality is readily tolerated to afford *para*-substituted phenyl disilenes **202a-d** (Scheme 124).[249]

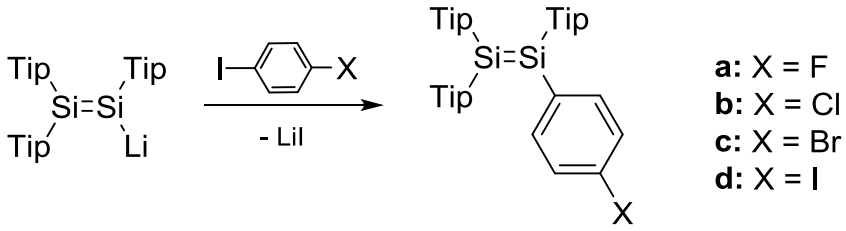

16 **202a-d**

Scheme 124. Synthesis of *para*-functionalized phenyl disilenes **202a-d** reported by Scheschkewitz *et al*.[249]

We considered an analogous strategy by reacting disilenide **16** with halogenated species and probe whether residual functionality that can in principle act as anchoring group for gold surfaces is tolerated.

Initially it was tested whether **16** reacts with *p*-bromo thiophenol under substitution to afford thiol substituted disilene **203** (Scheme 125).

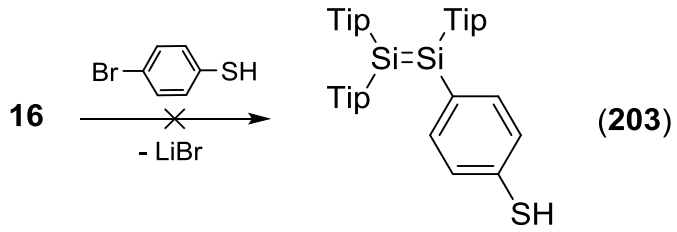

Scheme 125. Attempted synthesis of *para*-thiol substituted phenyl disilene **203**.

However, a complex mixture was obtained without any indications on an intact Si=Si bond according to ^{29}Si NMR spectroscopy. In the ^{1}H NMR spectrum several resonances are found in the typical area for *Si*-H resonances (δ = 5.5 -6.5 ppm). Unsurprisingly, the thiol functionality is too acidic to tolerate substitution reactions in *para* position.

A methyl sulfide functionality should be more compatible during the reaction with **16**. Disilenide **16** and one equivalent *p*-bromo thioanisol were thus combined in toluene at −80°C. Upon warming to rt the deep orange solution slightly changed its color to a brighter orange. The ^{29}Si NMR spectrum of the reaction mixture revealed uniform conversion to a new product with two resonances (δ = 71.3 and 55.1 ppm) in the typical range for disilenes suggesting the formation of **204a** (Scheme 126).[27]

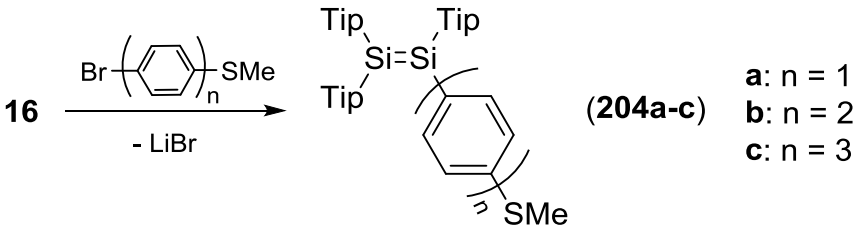

Scheme 126. Synthesis of remotely sulfide functionalized disilenes **204a-c**.

In the ^{1}H NMR spectrum the SMe group can be readily identified at δ = 1.85 ppm further indicating that a methylsulfide functionality is perfectly tolerated. Yellow single crystals were obtained from pentane and an X-ray structure analysis confirmed the constitution of *para*-methyl sulfide phenyl disilene **204a**. The *para*-thioanisol-functionalized disilene **204a** represents the first example for the simultaneous presence of sulphur and a disilene moiety in the same molecule.

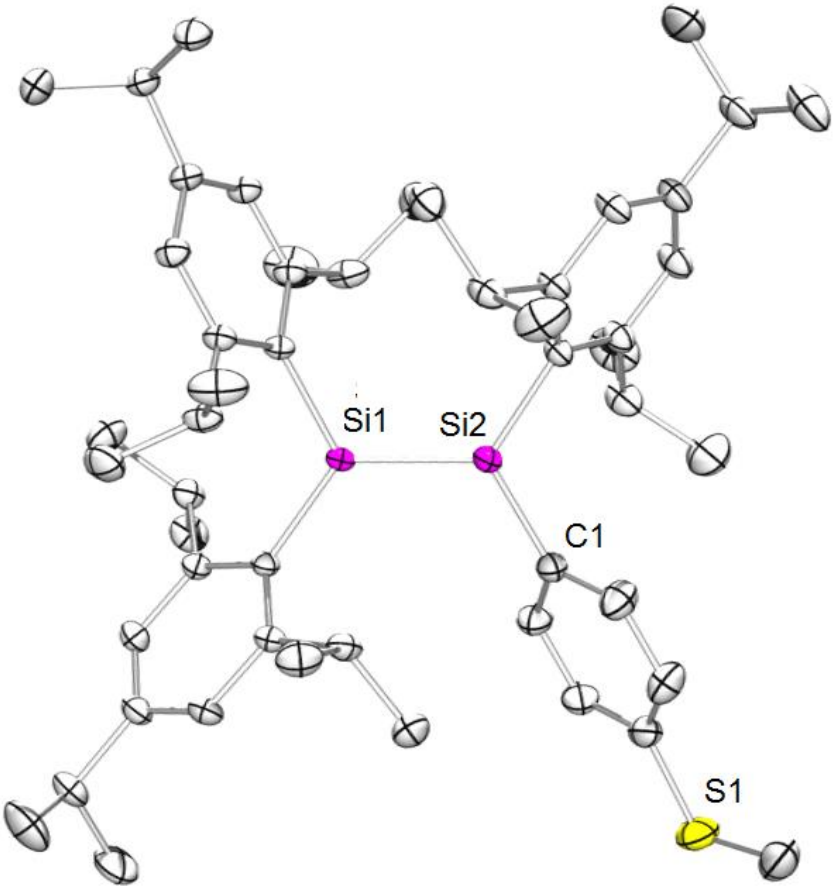

Figure 95. Molecular structure of **204a** in the solid state (thermal ellipsoids at 50%, H atoms and co-crystallized solvent omitted). Selected bond lengths [Å]: Si1-Si2 2.1565(4); Si2-C1 1.8639(12).

Even though both ends of the Si-Si double bond show a considerable degree of *trans*-bending (Si1: 12.1°, Si2: 19.2°), the Si=Si bond length (Si1-Si2 2.1565(4) Å) is at the shorter end of the range reported for disilenes and significantly shorter than in strongly *trans*-bent phenyl disilene **30** (θ_{Si1} = 23.6 and θ_{Si2} = 22.3°).[77] A minimal twisting of the Si1-Si2 bond (τ = 4.0°) is observed for **204a**.

Surprisingly, despite less pronounced *trans*-bending a red-shift is found for the longest wavelength absorption (λ_{max} = 447 nm, ε = 14824 $M^{-1}cm^{-1}$) in the UV/vis spectrum of **204a** compared to **30** (λ_{max} = 439 nm). This absorption is assigned to the π-π*-transition.[77]

Comparable values for longest wavelength absorptions have been reported for *para*-functionalized phenyl disilenes **202c,d** (λ_{max} = 445 and 447 nm). However, these derivatives equally feature a higher degree of *trans*-bending (**202c**: θ_{Si1} = 15.8 and θ_{Si2} = 23.8°, **202d**: θ_{Si1} = 16.2 and θ_{Si2} = 24.5°).[249] These findings have to be attributed

to the methylsulfide substituent in the *para*-position of the phenyl substituent. The lone-pairs at sulphur are available for delocalization over the phenyl bridge. The bond distance between the silicon atom and the *ipso*-C atom of the corresponding phenyl ring in **204a** (Si2-C1 1.8639(12) Å), however, is only slightly smaller than in phenyl disilene **30** (1.873(3) Å).[77]

A second absorption band in the UV/vis spectrum of **204a** is located at λ = 278 nm (ε = 17818 $M^{-1}cm^{-1}$) and assigned to the phenylene linking group (pure thioanisole: λ = 290 nm).[250]

As outlined in Chapter 3.6.1 the linking unit is *inter alia* important to provide sufficient space between the terminal functional group and the surface. While with the synthesis of **204a** it was demonstrated that a methylsulfide functionality is tolerated in the reaction of disilenide **16** with aryl halides, it appears unlikely that the phenyl group will provide the required distance between the bulky disilenyl unit and the surface. Consequently, for future investigations concerning SAMs of disilenes on gold surfaces larger spacers would be desirable.

In analogy to the procedure for **204a** disilenes **204b,c** were synthesized *via* the reactions of disilenide **16** with one equivalent 4′-bromo-4-methylthiobiphenyl and 4´´-bromo-4-methylthioterphenyl, respectively (Scheme 126). The ^{29}Si NMR spectra are very similar to what is found for **204a** (**204b**: δ = 70.9 and 56.1 ppm, Figure 96; **204c**: δ = 70.7 and 56.2 ppm, Figure 97).

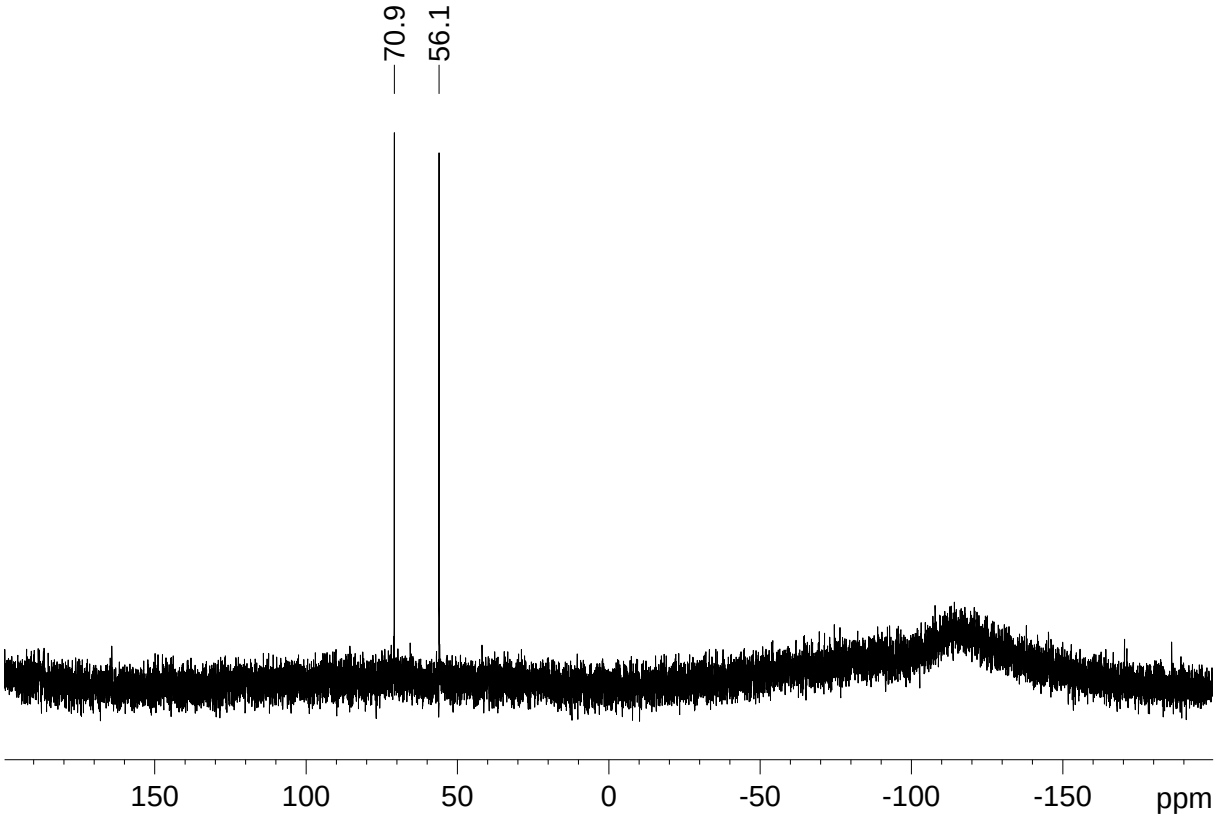

Figure 96. $^{29}Si\{^{1}H\}$ NMR of *para*-methylsulfide biphenyl disilene **204b**.

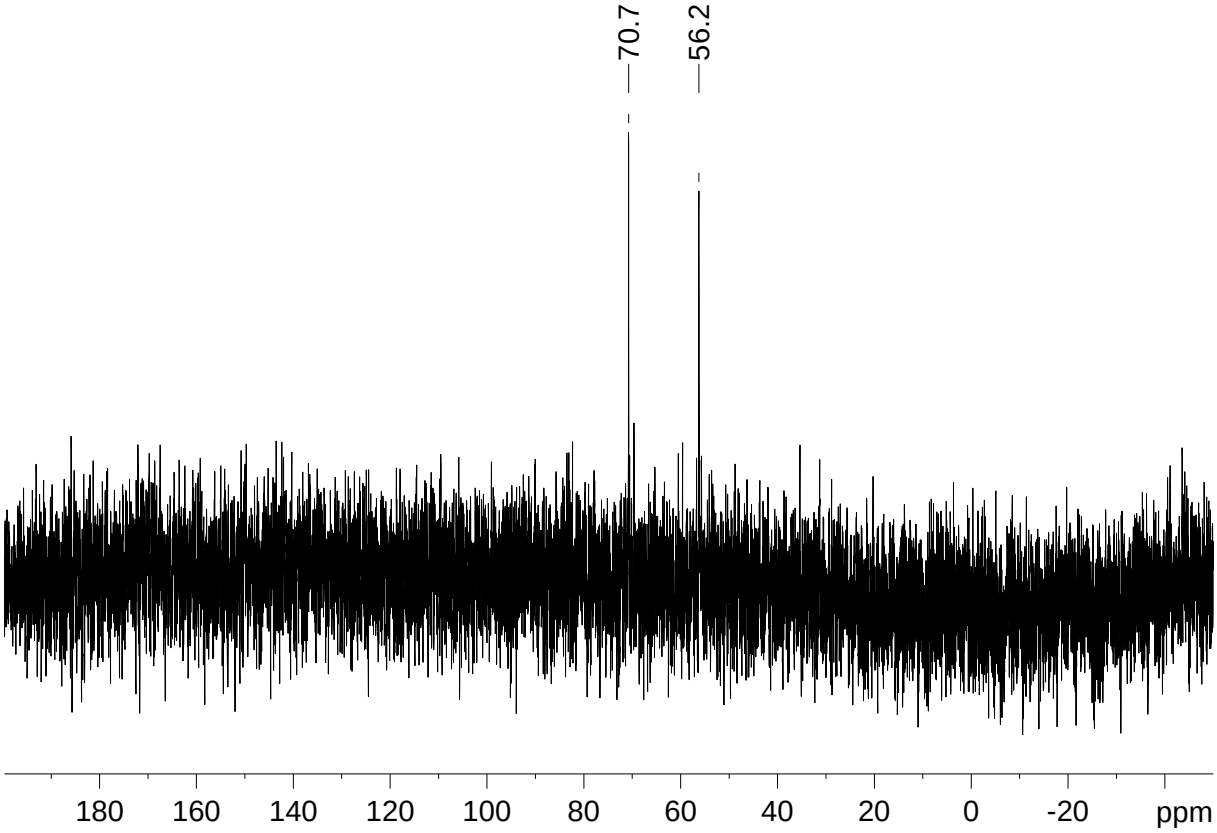

Figure 97. $^{29}Si\{^{1}H\}$ NMR of *para*-methylsulfide terphenyl disilene **204c**.

The methylsulfide moieties are observed at δ = 1.99 (**204b**) and 2.36 (**204c**) ppm in the ^{1}H NMR spectra. Even though the reactions occur without formation of large amounts of side-products, single crystals to finally confirm the constitutions of disilenes **204b,c** with an X-ray diffraction study were as yet not obtained.

UV/vis spectroscopy with crude **204b** revealed the longest wavelength absorption at λ_{max} = 456 nm (Figure 142), which is slightly red-shifted compared to **204a** (λ_{max} = 447 nm). This red-shift can either be assigned to the extended conjugated system or to a more pronounced *trans*-bending induced by the sterically more demanding biphenyl linker and cannot be specified without X-ray structure analysis. The intensity of the longest wavelength absorption of **204b** (ε = 10601 $M^{-1}cm^{-1}$, Figure 143) is smaller compared to **204a** (ε = 14824 $M^{-1}cm^{-1}$).

The absorption band of **204b** assigned to the linker is found at λ = 295 nm, which is red-shifted compared to **204a** (λ = 278 nm) and in accord with the extended π-system going from phenyl to biphenyl. Also the intensity of the absorption attributed to the linker is significantly larger for **204b** (ε = 27065 $M^{-1}cm^{-1}$, Figure 144).

The longest wavelength absorption observed in the UV/vis spectrum of **204c** (Figure 145) is similar to what was observed for **204b** (λ_{max} = 456 nm). Curiously, the intensity of this absorption band (ε = 5032 $M^{-1}cm^{-1}$, Figure 146) is again significantly smaller than that in **204b** (ε = 10601 $M^{-1}cm^{-1}$). The trend that the intensity of the longest wavelength absorption decreases with the number of phenyl bridges cannot be explained at present. An analogy to what is found for **204a,b**, an additional absorption band that is assigned to the linker unit appears in the UV/vis spectrum of **204c**. In accord with the extended π-system this band is red-shifted (λ = 303 nm) compared to **204a,b** (λ = 278 and 295 nm). Furthermore, its intensity is larger (ε = 33887 $M^{-1}cm^{-1}$) than that of the corresponding absorption bands in **204a,b** (17818 and 27065 $M^{-1}cm^{-1}$).

As decribed in Chapter 3.6.1, interactions between the head group and the surface can have a distinct effect on the properties of the monolayer. The phenyl bridges in **204a-c** should in principle allow for those interactions. For deposition experiments a sulfide substituted disilene with a linker unit preventing surface-head group interactions appeared desirable for comparison. Consequently, the synthesis of a sulfide substituted alkyl disilene was attempted. In analogy to the syntheses of

disilenes **204a-c** (*vide supra*), disilenide **16** was treated with one equivalent 8-methylthiooctyl bromide.

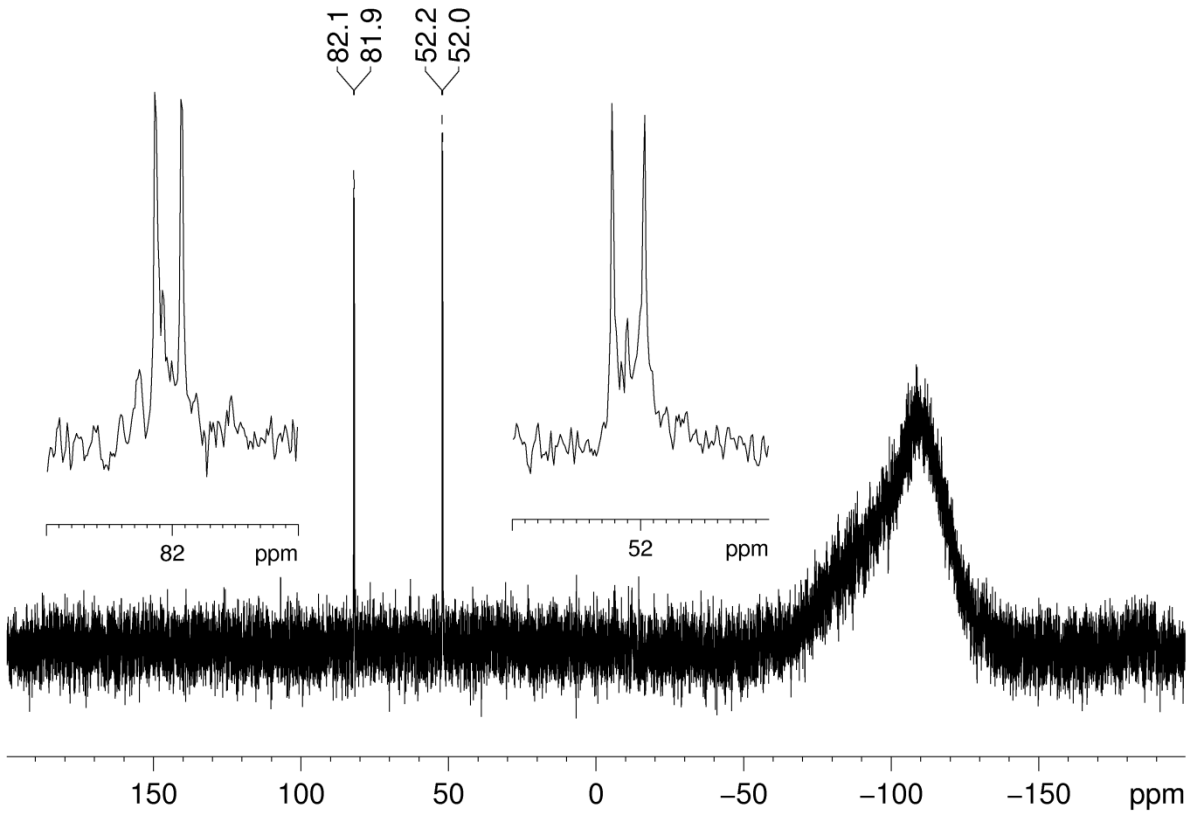

Figure 98. ^{29}Si{H} NMR spectrum of dimethyl sulfide substituted disilene **205**.

The ^{29}Si NMR spectrum of the reaction mixture revealed four resonances in the typical range for disilenes at δ = 82.1, 81.9, 52.2 and 52.0 ppm (Figure 98). Each two of the signals show very similar chemical shifts and consequently can be assigned to stereo isomers. One plausible explanation would be that disilene **205** is formed and exists as two rotamers due to the presence of the octyl chain (Figure 99).

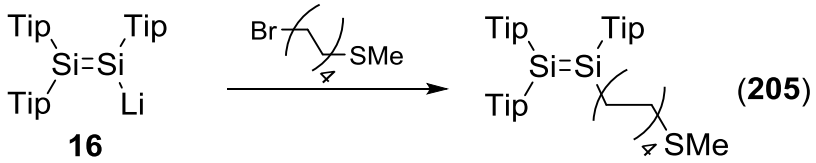

Figure 99. Synthesis of methyl sulfide substituted octyl disilene **205**.

To date it was not possible to grow single crystals of **205** to finally confirm its constitution.

In the UV/vis spectrum two absorption bands are observed at λ = 407 (Figure 148) and 357 nm. Each is assigned to the π-π*-transition one of the proposed rotamers of **205**.

The hypsochromic shift compared to the longest wavelength absorptions of **204a-c** (λ = 447 and 456 nm) can either be attributed to a less pronounced *trans*-bending or the absence of conjugation of the Si=Si-bond with the phenylene moieties, which cannot be clarified in the absence of X-ray diffraction data. No additional absorption is found around 300 nm, which lends the assignment of these bands in **204a-c** to the linker unit significant support.

Finally, we considered the synthesis of a disilenyl substituted disulfide **206** (Scheme 127). As mentioned above, disulfides are known to form monolayers of higher robustness compared to sulfides.

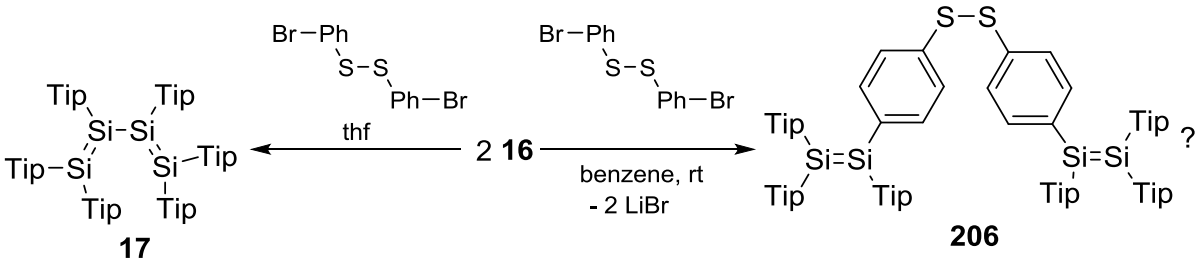

Scheme 127. Reactivity of disilenide **16** towards bis(4-bromophenyl)disulfide.

The reaction of disilenide with half an equivalent bis(4-bromophenyl)disulfide in analogy to the synthesis of **204a-c** and **205** (toluene, −80°C), however, resulted in a complex mixture. Afterwards, the optimization of the reaction conditions was attempted. While in thf mainly oxidation of **16** to tetrasilabutadiene **17** was observed, the best result was obtained in benzene at room temperature. Two very broad resonances are observed in the ^{29}Si NMR spectrum at δ = 71.3 and 55.1 ppm that are in accord with formation of **206**. The pronounced broadening of the signals can be explained with hindered rotation of the disilenyl moieties about the disulfide bridge. Unfortunately, also in this case side products are detected in the ^{29}Si NMR spectrum. A broad resonance of comparable intensity is observed at δ = −12.8 ppm. Additionally, signals of minor intensity are found at δ = 90.8, −3.9, −32.3 and −60.1 ppm. As yet it was not possible to separate the mixture by crystallization.

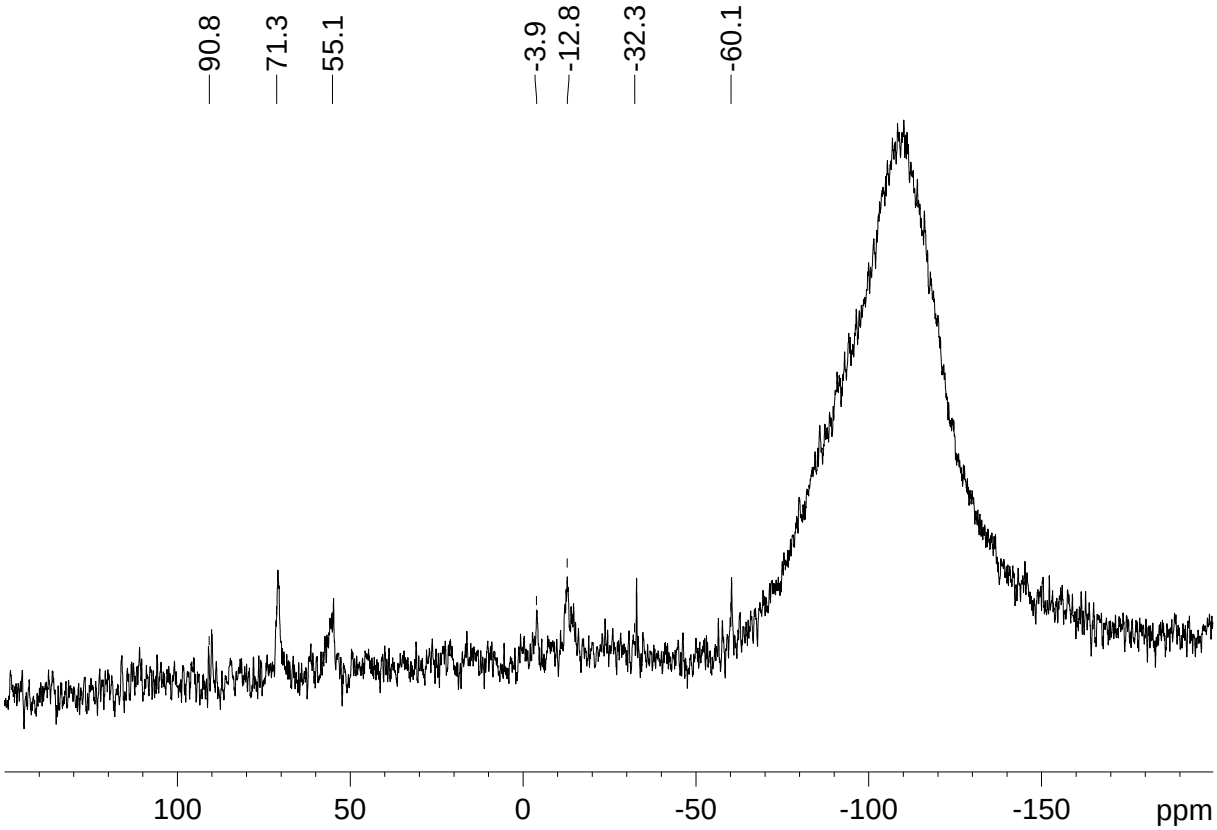

Figure 100. ^{29}Si NMR spectrum from the reaction of disilenide **16** with bis(4-bromophenyl)disulfide.

Initial attempts to deposit **204a-c** and **205** on gold surfaces and characterize the samples by atomic force microscopy were carried out and documented by Thomas Büttner in his Bachelor thesis.[239]

4. Conclusion and Outlook

The study of heavier low-valent main group compounds is still one of the major themes in inorganic chemistry.[26] Especially unsaturated compounds of silicon, carbons heavier congener, are of continuous interest.[27] During the last decade, the introduction of peripheral functionality has moved into focus. The presence of functional groups offers possibilities for further manipulations of the low-valent systems and their incorporation into extended systems.[34]

Disilenides, disila analogues of vinyl lithium, allow for the transfer of the disilenyl unit to various electrophiles.[66] During my Master project I had demonstrated that the reaction of disilenide **16** with $ClP(NMe_2)_2$ affords the first example of a *P*-amino substituted phosphasilene **108a,** presumably upon 1,3-migration of one amino group in an intermediate phosphino disilene. Upon addition of *tert.*-butyl isonitrile to **108a** the amino group on phosphorus is shifted to the neighboring silicon atom yielding 1-aza-3-phosphaallene **109a**.[130]

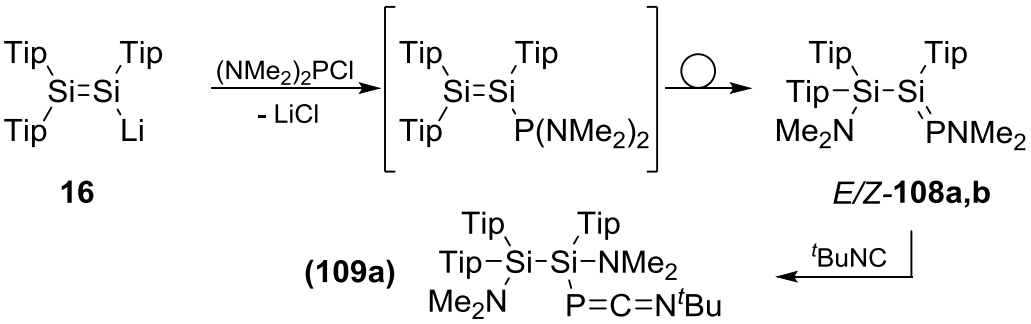

Scheme 128. Synthesis of *P*-amino substituted phosphasilenes **108a,b** and 1-aza-3-phosphaallene **109a**.[130]

Due to the apparent mobility of the *P*-amino functionality in **108a**, the reactivity of **108a** towards anionic nucleophiles was further investigated as part of this PhD thesis. While in disilene chemistry electrophilic derivatives have been reported,[34] electrophilic phosphasilenes were previously unknown. Treatment of **108a** with mesityl lithium indeed affords phosphasilene **144** providing the first example for nucleophilic substitution reactions on a Si=P bond (Scheme 129). Notably, the double bond remains unperturbed during this reaction. In contrast, the reaction of **108a** with disilenide **16** as more elaborate nucleophile may afford the initial substitution product, trisilaphosphabutadiene derivative **[145]**, only as transient intermediate. Most likely,

subsequent silylene extrusion results in **[148]** that readily isomerizes to the isolated bicycle[1.1.0]butane derivative **146** (Scheme 129).

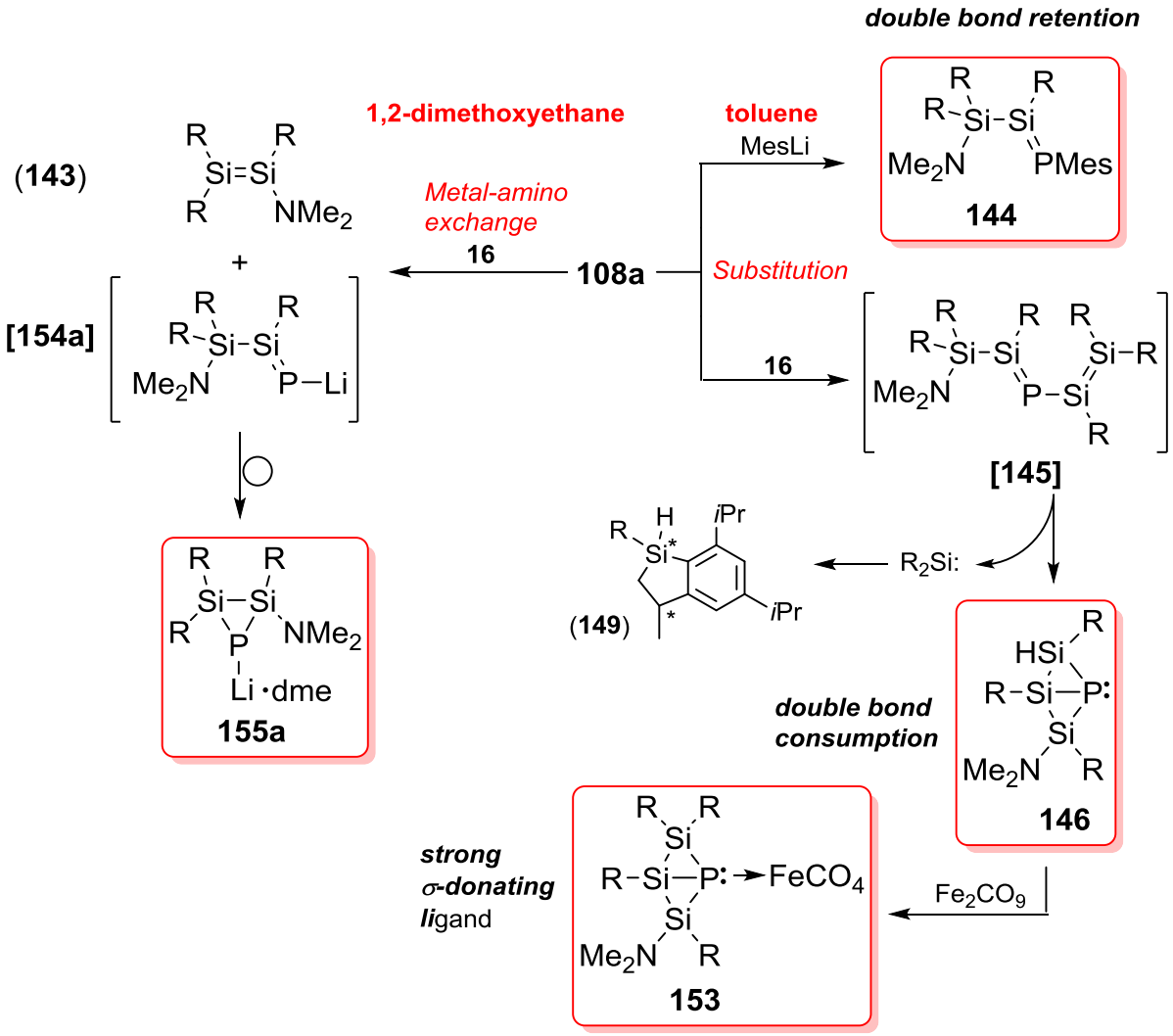

Scheme 129. Diverse reactivity of electrophilic phosphasilene **108a** towards anionic nucleophiles: substitution (under retention and consumption of the Si=P-bond) *vs*. metal-amino exchange (R = Tip).

In case the reaction of phosphasilene **108a** with disilenide **16** is carried out in the donor solvent dme, an unprecedented metal-amino exchange reaction occurs to afford amino disilene **143** and disilaphosphiranide **155a**, a rare example of a Si_2P-ring[177,178] and the first isolable disilaphosphiranide. Presumably, **155a** is formed by cyclization of an intermediate *P*-lithio phsophasilene **154a** (Scheme 129). In view of the fact that metal exchange reactions are widely applied for halogenated species,[198] these findings lend additional support for the pronounced leaving group character of the amino functionality at phosphorus in **108a**.

The inherent strong pyramidalization of the phosphorus atom (214°) should confer excellent σ-donor properties to the trisilaphospha[1.1.0]bicylobutane derivative **146**. Indeed, treatment of **146** with diiron nonacarbonyl leads to quantitative conversion to complex **153**. According to the IR spectrum of **153**, the ligand **153** is a somewhat stronger σ-donor than common phosphanes and of similar strength as N-heterocyclic carbenes.

The experiments in Scheme 129 unambiguously reveal a certain pseudo-halogenide behavior of the amino functionality at phosphorus. Consequently, the reactivity of **108a** towards reducing agents was explored since halogenated species have proven valuable reduction precursors in Group 14 and Group 15 chemistry (*cf.* Chapter 1). As confirmed by the isolation of disiladiphosphabutadiene radical anion **159** and diphosphide **160**, it is indeed possible to cleave the amino group at phosphorus reductively with lithium powder in dme (Scheme 130). Unfortunately, these reactions suffer from low yields and have so far been unreproducible. When potassium graphite was applied as milder reducing agent, uniform reaction to a compound for which we propose the constitution of *P*-potassio phosphasilene **154b** is observed (Scheme 130). The compound rearranges in apolar solvents and unfortunately it was not possible to determine the structure of any of the products by X-ray diffraction studies. For future investigations, attempts to trap alleged **154b** by the derivation with electrophiles in order to confirm the constitution might be rewarding.

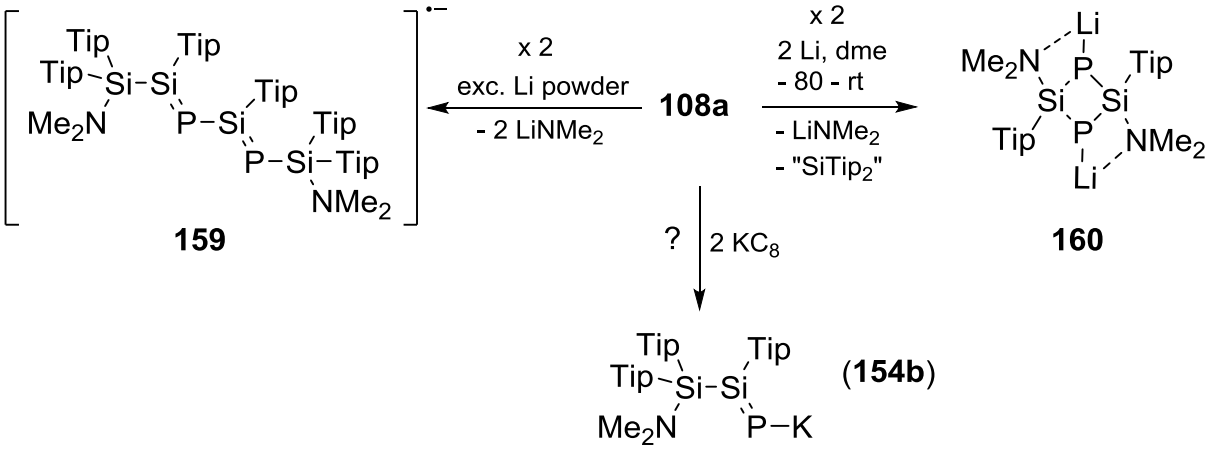

Scheme 130. Reduction attempts of phosphasilene **108a** with lithium powder and potassium graphite, respectively.

Another central aim of the present work was to investigate the reactivity of disilenide **16** towards various phosphorus- and boron-centered electrophiles with with a focus on retaining functionalization on the thus obtained unsaturated/cyclic systems. When **16** was treated with dichloro(diphenylamino)phosphane, the formation of β-chloro *P*-amino substituted phosphasilene **161** was unambiguously confirmed by NMR spectroscopy. The compound slowly rearranges to an unprecedented silaazaphosphaindane derivative **162** (Scheme 131).

From the reaction **16** with the analogous boron electrophile, (chloroboryl) disilene **176** could be isolated. X-ray and UV/vis data clearly reveal conjugation between the formal two double bonds as depicted in resonance formulae **176´** (Scheme 131). While in reported boryl dislenes very bulky donor substituents are attached to boron,[80,101,102] the residual chloro functionality in **176** provides a reactive side in the molecule. Although initial attempts to reductively cleave the chlorine substituent failed, substitution reactions in allylic position in analogy to what has been reported for trisilaallyl dichlorides could be investigated in future studies.[251]

An unexpected reactivity of **16** towards boron trifluoride diethyl etherate was observed. During the reaction a Lewis acid induced ether cleavage of coordinated dme occurs and uniform formation of methyl disilene **173** was confirmed by NMR spectroscopy and X-ray structure analysis (Scheme 131). Notably, **173** is not accessible from the reaction of **16** with methyl iodide.

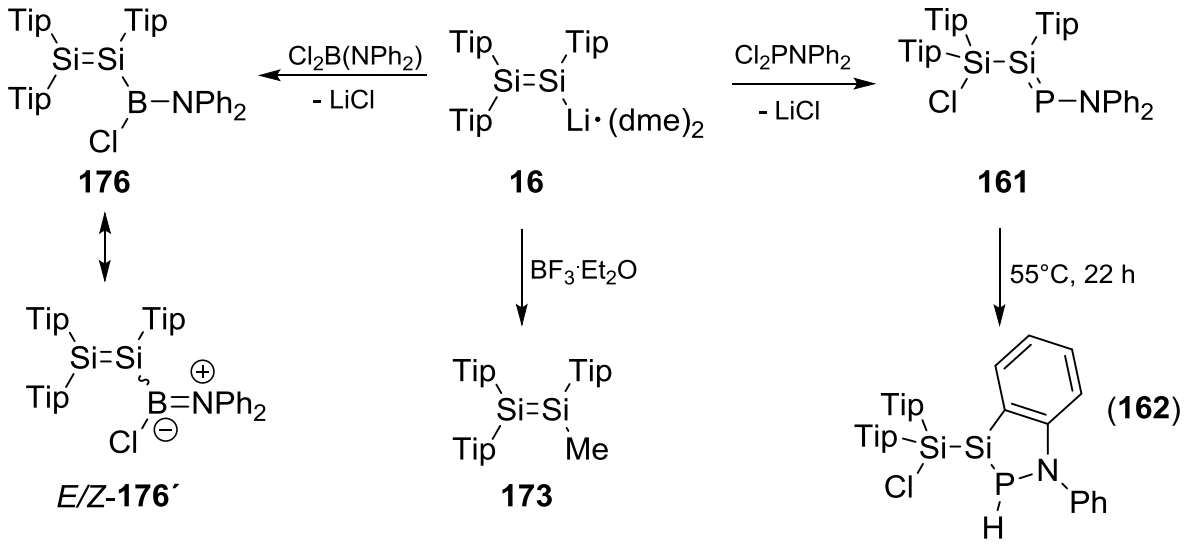

Scheme 131. Synthesis of silaazaphosphaindane derivative **162**, methyl disilene **173** and (chloroboryl) disilene **176**.

When disilenide **16** was treated with borane dimethylsulfide adduct an unobserved but plausible intermediate disilenylborate **[177]** readily cyclizes to disilaboriranide **178** (Scheme 132). Due to its limited stability single crystalline material of **178** could not be obtained but its constitution is strongly supported by multinuclear NMR spectroscopic findings. Analogous to reports for stannyl disilenes,[85] the cyclization step is less favored and open chained system **180** was isolated from the reaction of **16** with *tert.*-butyl borane. The combination of unsaturated silicon compounds and boron is generally very rare, and with isolation of **180** the first structural evidence for a disilenyl borate was obtained (Scheme 132). B-H functionalities are of considerable interest regarding hydroboration reactions. While so far all attempts to convert **178** into the neutral species failed, hydride abstraction from **180** might afford a reagent capable of transferring the disilenyl unit *via* hydroboration.

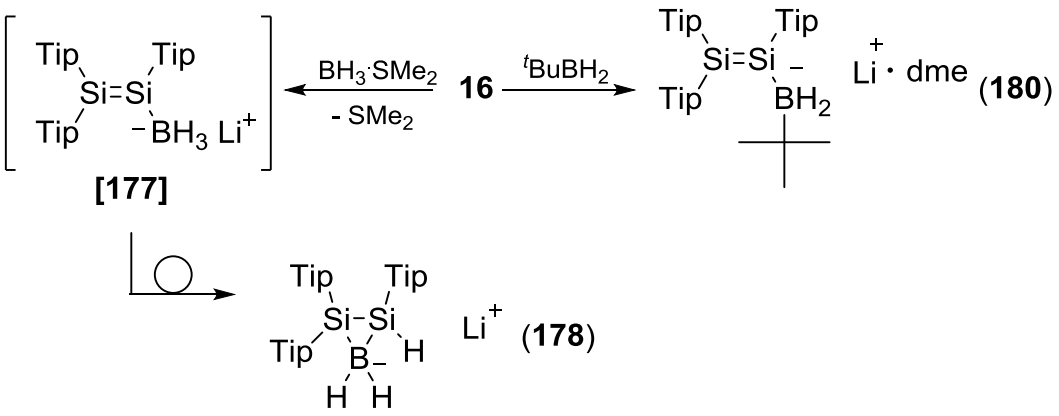

Scheme 132. Synthesis of disilaboriranide **178** and disilenyl borate **180**.

Recently, we reported in collaboration with the Jutzi group that treatment of silylium Cp*Si$^+$ **123** affords Cp*-substituted cyclotrisilene **124** (*cf.* Chapter 1.2.2).[163,164] Another objective of this PhD project was to investigate whether analogous compounds are accessible from the reaction of **16** with P(I) cations (Scheme 133). Indeed, after reaction of **16** with phosphenium cation **164b**[BPh_4] the first example of a base stabilized disilaphosphacyclopropene **166** was isolated. Subsequently, **166** was coordinated to the $Fe(CO)_4$ fragment to afford complex **168**, that isomerizes to unprecedented disilaferraphopsha[1.1.0] bicyclobutane derivative **169** upon heating (Scheme 133). Attempts to synthesize **166** without isolating the P(I) cation by treating a mixture of **164b**[Cl] and 2-chloro-1,3-diisopropyl-4,5-dimethylimidazolium chloride with disilenide **16** resulted in the formation of ylide **167**. Apparently, the Si-Si σ-bond

in **166** is chlorinated by the imidazolium chloride in the course of the reaction (Scheme 133).

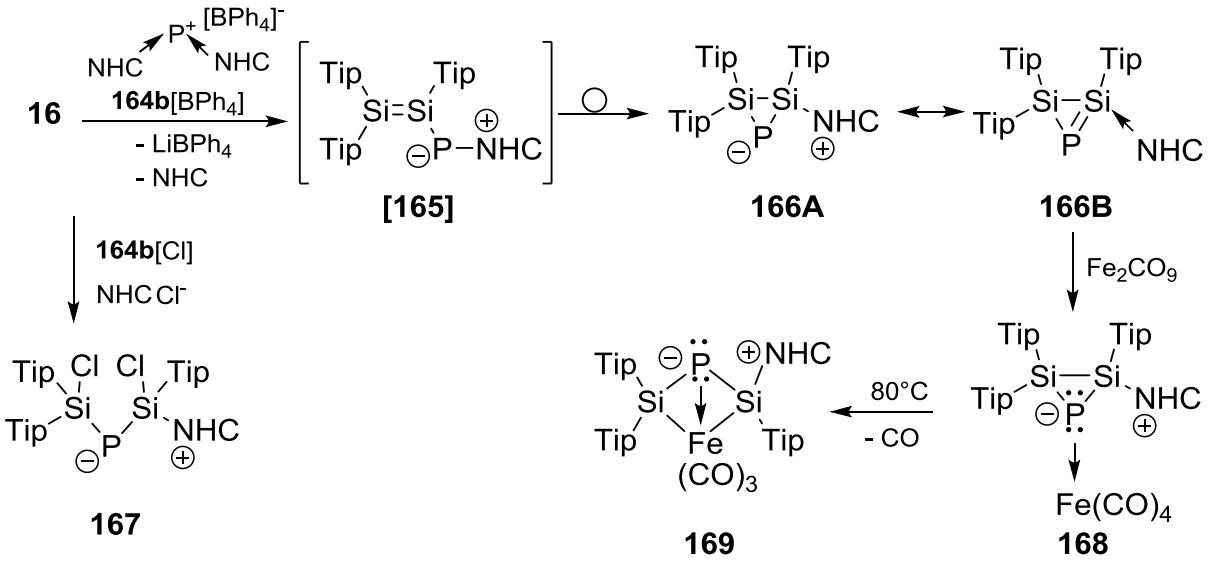

Scheme 133. Synthesis of ylide **16**7, NHC-stabilized cyclic phosphasilene **166**, tetracarbnyl iron complex **168** and rearrangement of **168** to disilaferraphosphabicyclobutane **169** (NHC = 1,3-diisopropyl-4,5-dimethylimidazol-2-ylidene).

The targeted (bottom-up) synthesis of siliconoids is ideally placed to study properties and reactivity of unsaturated cluster compounds that arise during gas phase processes of silanes.[153,154] The pronounced electronic anisotropy of molecular siliconoids – as manifest in an unprecedentedly wide distribution of ^{29}Si NMR chemical shifts – would be an attractive feature for the construction of structures in the subnano regime.[160,165] Evidently, functionalized vertices are a prerequisite for the embedding of siliconoids in extended supramolecular assemblies. However, only unfunctionalized siliconoids have been reported so far, severely limiting further developments in this direction. During his studies in the Scheschkewitz group, Dr. Kai Abersfelder found that bridged propellanide **133** is obtained if an excess of reducing agent is used in the reduction of cyclotrisilane **121**. In this project it was demonstrated that reduction of dismutational isomer **122** with two equivalents lithium/naphthalene equally affords **133** providing the first example of an anionic siliconoid. A major target of this PhD project was to investigate the reactivity of **133** and it was shown that **133** is a useful synthon to transfer the intact Si_6-core to various electrophiles. By this means siliconoids functionalized with substituents from Group 13-15 were synthesized (Scheme 134). A silyl (**181**)[168] as well as an organic substitutent (**182**) were introduced to the siliconoid backbone. Furthermore,

siliconoids functionalized with dopant atoms such as phosphorus (**184** and **186**) and boron (**194**) were isolated. Notably, remaining functionalization on the newly introduced substituents is readily tolerated by the siliconoid skeleton in principle allowing for further manipulations. The linking of functionalized substituents to the siliconoid backbone can be regarded as first step in the selective expansion of the cluster.

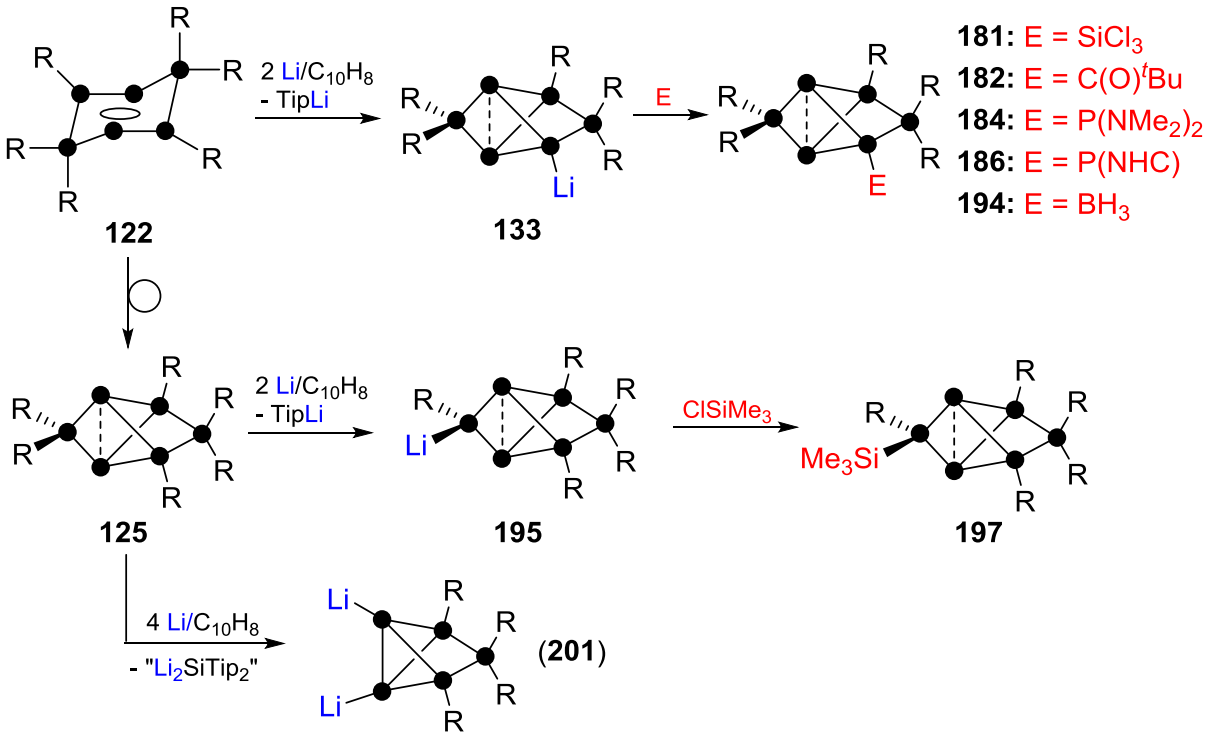

Scheme 134. Synthesis of anionic siliconoid **133**, siliconoids functionalized at Si4 **181**-**194**, anionic siliconoid **195,** silyl substituted siliconoid **197** and dianionic Si_5-cluster (R = Tip, NHC = 1,3-diisopropyl-4,5-dimethylimidazol-2-ylidene).

Thus it was demonstrated that the N-heterocyclic carbene can be removed from phosphorus in siliconoid **186** presumably resulting in the incorporation of the “naked” phosphinidene into the cluster.

Investigations concerning the reduction of the global minimum isomer **125** have been performed during this thesis. Surprisingly, the reaction of **125** with two equivalents lithium/naphthalene yields bridged propellanide **195** bearing the anionic charge at Si6. Remarkably, the lithio silane moiety is found at δ = 267.9 ppm in the ^{29}Si NMR spectrum providing by far the most deshielded silyl anion that has been reported up to now. The proof of concept that **195** can be applied to further functionalize the siliconoid skeleton on this cluster vertex was provided by the synthesis of silyl substituted derivative **197** (Scheme 134). Reduction of **125** with four equivalents of

reducing agent under similar conditions resulted in the cleavage of one “propeller blade” affording dianionic Si_5-cluster **201**, unfortunately in very low yields (Scheme 134). However, **201** might be a suitable precursor to prepare heteroatom-bridged propellanes by treatment with difunctional electrophiles. Optimization of the procedure for **201** is currently investigated.

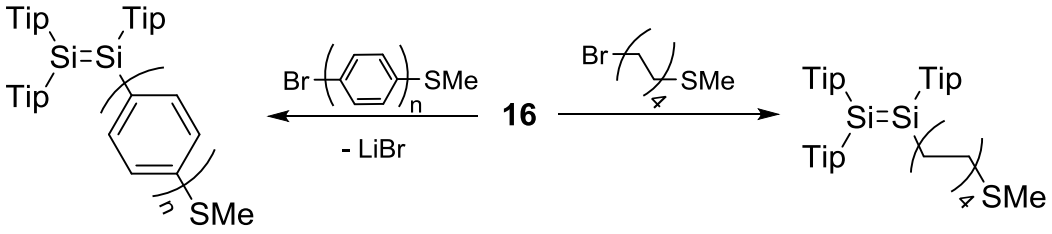

204a-c **205**

Scheme 135. Synthesis of sulfide functionalized disilenes **204a-c** and **205**.

As final part of this thesis, disilenes remotely functionalized with anchor groups that should allow for their linking to gold surfaces in self-assembled monolayers were prepared. Methyl sulfide functionalized disilenes **204a-c** with aromatic linking units of different size are accessible from the reactions of disilenide **16** with the corresponding bromo-substituted arylsulfides (Scheme 135). By the same strategy disilene **205** was prepared. In this case, the disilenyl moiety is isolated from the dimethyl sulfide functionality *via* an alkyl linker (Scheme 135).

5. Experimental

5.1. General

5.1.1. Experimental Conditions

All manipulations were carried out under a protective atmosphere of argon using standard Schlenk techniques or a glovebox. The protection gas used was Argon 5.0 supplied by PraxAir and was used without further purification.
All glassware was cleaned in a KOH/ isopropanol bath, neutralized and kept in a drying oven at 120°C overnight prior to use. All setups were evacuated and purged with argon three times. The high vacuum was generated with a slide vane rotary vacuum pump RZ 6 from Vakuubrand.

5.1.2. Purification of Solvents

Diethyl ether (Et_2O), tetrahydrofuran (thf), 1,2-dimethoxyethane (dme), benzene and toluene were refluxed over sodium/benzophenone; hexane over sodium/benzophenone/tetra(ethylene glycol)dimethyl ether (tetraglyme); deuterated benzene and toluene over sodium or potassium.
All solvents were distilled and stored under argon. The dry solvents were transferred with cannulas of stainless steel or PTFE into the reaction flasks under a protective atmosphere.

5.1.3. Methods of Analyses and Measurement

NMR spectra were recorded on a Bruker Avance III 300 spectrometer (1H, 300.13 MHZ, 11B, 96.3 MHz, 31P, 121.5 MHz, 29Si, 59.6 MHz). Chemical shifts are reported relative to $SiMe_4$ (^1H, ^{13}C, ^{29}Si) and H_3PO_4, 85 % (^{31}P, external). ^1H and ^{13}C NMR spectra were referenced to the peaks of the residual protons of deuterated solvents or the deuterated solvent itself ($CDCl_3$: δH: 7.26 ppm; C_6D_6: δC: 7.16 ppm, δC: 128.06 ppm; toluene-d_8: δH: 2.08 ppm, δC: 20.04 ppm; THF-d_8: δH: 1.72 ppm, δC: 25.31 ppm. All chemical shifts are reported in parts per million (ppm). Coupling constants are reported in Hertz (Hz) and are given in the usual notion that $^nJ(X,Y)$ means a coupling of nucleus X over n bonds with nucleus Y. Coupling constants are determined by observing satellite signals next to main signal. The multiplicity and shape of the observed signals are given as s = singlet, d = doublet, t = triplet, hept. = septet, m = multiplet or convoluted signals, br = broad signal.
UV/vis spectra are recorded on a PerkinElmer Lamda 35 UV/vis spectrometer.
Infrared spectra were recorded on a Varian 2000 FT-IR spectrometer.

Melting points were determined under argon in closed NMR tubes and are uncorrected. Without exception NMR spectra were run directly afterwards on a solution of the cooled down melt.
Elemental analysis was carried out with an elemental analyzer Leco CHN-900.

5.1.4. Computational Details

Computations have been performed by Dr. Cem B. Yildiz, Aksaray University, Turkey.
The compound **146**-**Dip** and its $Fe(CO)_4$ complex form **153-**Dip were investigated by DFT using Dip (2,6-diisopropylphenyl) groups instead of Tip (2,4,6-triisopropylphenyl) groups in the Gaussian 09 program package.[252] Full geometry optimizations were performed at B3LYP/6-31+G(d,p) level of theory. Wiberg bond indices (WBO) as a criterion to estimate the bond orders of chemical structures were calculated by natural bond orbital (NBO) analysis for **146**-**Dip** and **153-Dip**.[253] ^{29}Si and ^{31}P NMR chemical shifts were calculated by the GIAO method in solution (benzene) at B3LYP/6-311+2df level of theory. The electronic absorption spectrum was predicted using the optimized geometry by the time-dependent density functional theory (TD-DFT) method in heptane solution.[254] The solvation effects have been included to NMR and UV/vis calculations by the conductor-like polarizable continuum model CPCM.[255] Additionally, frontier molecular orbitals of the title compounds were investigated. The proposed mechanism and intermediates for the formation of **146** were calculated at B3LYP/6-31+G(d,p) level of theory using simplified model system with methyl groups instead of Tip substituents and NH_2 instead of $N(CH_3)_2$ (**146**-**Me**). Frequency analyses were performed to determine the character of optimized structures as minima or transition states. The relative Gibbs free energies are given in kcal/mol. GaussView 5.0 program was employed for visualization of the final geometries and frontier molecular orbitals of the optimized structures.

5.2. Starting Materials

5.2.1. General Starting Materials

Deuterated solvents were purchased from Sigma-Aldrich and were dried if necessary after the procedures mentioned above. bis(dimethyltrimethylsilyl)amine, bis(diphenylphosphino)ethane, (dppe), $BH_3{\cdot}SMe_2$, *p*-Bromoiodobenzene, *p*-Bromothioanisol, *p*-Bromothiophenol, $CuBr{\cdot}SMe_2$, CuCl, CuI, Copper(II) nitrate trihydrate, 1,8-Dibromooctane, diiron nonacarbonyl, diphenylamine, lithium granules, Magnesium shavings, $PdCl_2$, PI_3, *tert*.-butyisonitrile, Tetrakis(triphenylphosphine)-palladium(0), Tip-H, tris(dimethylamino)borane, xylyl isonitrile were purchased from Sigma-Aldrich or Acros Organics and used as received. Cylohexene was purchased from Sigma-Aldrich, distilled and stored over molar sieve (4 Å). PCl_3, PBr_3 and

Me_3SiCl were bought from Sigma-Aldrich or Acros Organics and distilled prior to use. Silicon tetrachloride was distilled from magnesium turnings. Pyridine was distilled from potassium hydroxide. 1,3-diisopropyl-4,5-dimethylimidazol-2-ylidene and 1,3,4,5-tetramethylimidazol-2-ylidene were taken from group supply.

5.2.2. Synthesis of 1-Bromo-2,4,6-triisopropylbenzene (TipBr)

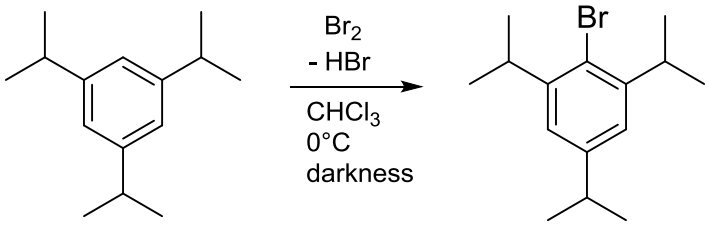

$C_{15}H_{24}$	Br_2	$C_{15}H_{23}Br$
204.35 g/mol	159.81 g/mol	283.25 g/mol

On the basis of existing publications,[256] a modified procedure is carried out. To a stirred and light protected solution of 2.45 mol of 2,4,6-triisopropylbenzene in 1 L of $CHCl_3$, 371.34 g (2.33 mol) of Br_2 are added dropwise over 4 h at 0°C. The HBr gas generated is neutralized by passing through a 2N aqueous solution of 122 g (2.5 mol) NaOH in a wash bottle. The use of a second wash bottle in between the first one and the reaction vessel is recommended as prevention of a back-lash due to decreasing pressure in the reaction vessel. After the Br_2 addition is finished, the reaction mixture is allowed to warm up slowly to room temperature in thawing ice-bath and stirring is continued for 12 h. Aqueous 2 N NaOH solution is slowly added to the reaction mixture until all remaining HBr is neutralized and the reaction mixture is basic. The organic layer is separated off and washed three times with water until it is neutral. After drying over Na_2SO_4 the organic layer is concentrated on a rotavap by removing the $CHCl_3$. The remaining residue is distilled in vacuum to give 550.28 g (79 %) Tip-Br: bp 80°C (high vacuum).

^{1}H NMR (300.13 MHZ, $CDCl_3$, 300 K): δ = 6.99 (s, 2H, Tip-*H*), 3.49 (hept., $^3J_{H\text{-}H}$ = 6.9 Hz, 2H, ^{i}Pr-C*H*), 2.88 (hept., $^3J_{H\text{-}H}$ = 6.9 Hz, 1H, ^{i}Pr-C*H*), 1.25 (d, $3J_{H\text{-}H}$ = 6.9 Hz, altogether 18H, ^{i}Pr-CH_3).

5.2.3. Synthesis of Dichlorobis(2,4,6-triisopropylphenyl)silane (Tip_2SiCl_2)

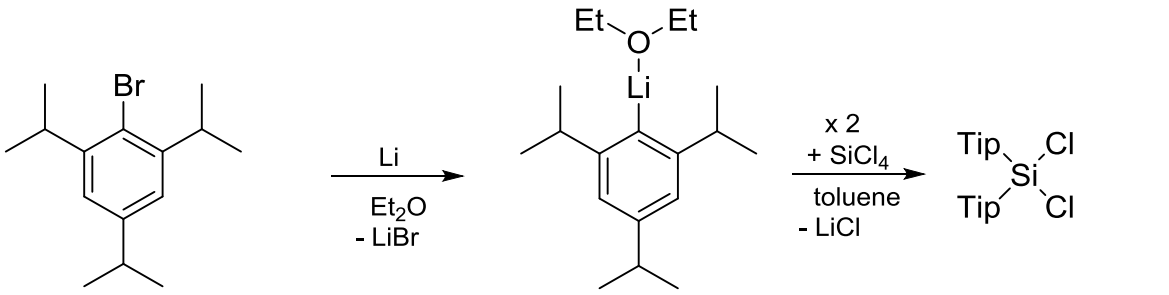

$C_{15}H_{23}Br$	Br_2	$C_{15}H_{23}Br$	Cl_4Si	$C_{30}H_{46}Cl_2Si$
283.25 g/mol	159.81 g/mol	283.25 g/mol	169.90 g/mol	505.68 g/mol

Tip_2SiCl_2 is prepared according to a modified literature procedure.[257] To a suspension of 16.83 g (2.42 mol) Li granules in 600 mL of dry Et_2O, TipBr (200 g, 0.71 mol) is added dropwise at room temperature. As soon as the reaction started (heat generation!), the mixture is slightly cooled with a water bath. Another 1000 mL of Et_2O are added to the remaining TipBr in order to allow for a diluted addition to avoid excessive heat generation. After the addition is finished stirring is continued overnight. NMR spectroscopy with a hydrolyzed aliquot showed quantitative conversion of TipBr to TipLi. Remaining Li is filtered off under argon atmosphere and Et_2O is thoroughly removed under vacuum. To the remaining TipLi 1200 mL of dry toluene is added and the mixture is cooled in an ice bath. 54.37 g (0.32 mol) $SiCl_4$ are added dropwise and after addition the reaction mixture is stirred overnight in the thawing ice bath. Stirring is continued for another two days to complete the reaction. From now on no protection atmosphere is needed as the product is almost fully stable towards air and moisture. All insoluble components are removed by filtration. The filtrate is reduced using a rotary evaporator to remove the toluene. The remaining residue is dissolved in pentane (4 mL/g) and kept at −78°C overnight. The crystallized product is further purified by second and third crystallization from pentane yielding 93.34 g (63%) of pure Tip_2SiCl_2.

^{1}H NMR (300.13 MHz, $CDCl_3$, 300 K): δ = 6.97 (s, 4H, Tip-*H*), 3.66 (hept., $^3J_{H\text{-}H}$ = 6.7 Hz, 4H, ^{i}Pr-C*H*), 2.83 (hept., $^3J_{H\text{-}H}$ = 6.9 Hz, 2H, ^{i}Pr-C*H*), 1.19 (d, $^3J_{H\text{-}H}$ = 6.9 Hz, 12H, ^{i}Pr-CH_3), 1.02 (d, $^3J_{H\text{-}H}$ = 6.7 Hz, 24H, ^{i}Pr-CH_3).

5.2.4. Preparation of Lithium Naphthalene ($Li/C_{10}H_8$)

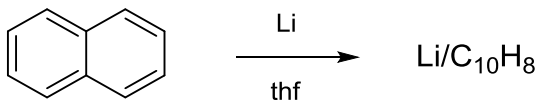

$C_{10}H_8$		
128.17 g/mol	6.94 g/mol	135.11 g/mol

Lithum granules (138 mg, 20 mmol), 3.08 g naphthalene (24 mmol) and a stirrer bar are placed in a Schlenk flask. Thf (40 mL) is added to vigorously stirred mixture mixture *via* syringe. Within five minutes the suspension turns dark green and it is stirred for additional 12 h. The exact concentration (~0.5 mol/L) is determined by titration of a hydrolyzed aliquot with aqueous hydrochloric acid against phenolphthalein.

5.2.5. Preparation of Lithium Powder

In a conical flask 100 mL paraffin oil and 50.00 g lithium rods are heated to 200°C under a constant argon flow over the surface of paraffin oil through rubber tubing. The molten lithium is thoroughly treated with a disperser. The dispersion of lithium in paraffin oil is allowed to cool down to rt . The dispersion is filtered with a filter fritte and the lithium powder washed with hexane and dried in vacuum.

5.2.6. Synthesis of 1,2,2-Tris(2,4,6-triisopropylphenyl)-disilenyl-lithium 16

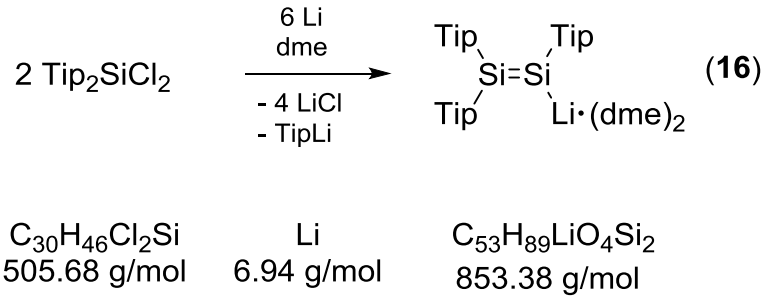

Disilenide **16** is prepared according to a modified published procedure.[69] Dry dme (300 mL) is added under ice cooling to a mixture of 60 g (118.65 mol) Tip_2SiCl_2 and 3.69 g (532.5 mmol) lithium powder. After stirring overnight the reaction mixture turned deep red and the solvent is distilled off under reduced pressure. The residue is digested in 300 mL hexane and all precipitate is filtered off at 50°C. The dark red filtrate is kept at r.t overnight. Pure disilenide **16** crystallizes in 48 % yield (29.4 g).
^{1}H NMR (300.13 MHz, C_6D_6, 300 K): δ = 7.13, 7.09, 7.07 (each br, each 2H, Tip-*H*), 4.79 (m, 4H, ^{i}Pr-C*H*), 4.27 (br, 2H, ^{i}Pr-C*H*), 2.92 (s, 12H, dme-CH_3), 2.85 (s, 8H, dme-CH_2), 2.90-2.74 (m, 3H, ^{i}Pr-C*H*), 1.42, 1.41, 1.33, 1.26, 1.21, 1.20, 1.14 (each d, altogether 54H, ^{i}Pr-CH_3).

5.2.7. Synthesis of 1,1,2-Trichlorocyclotrisilane 121

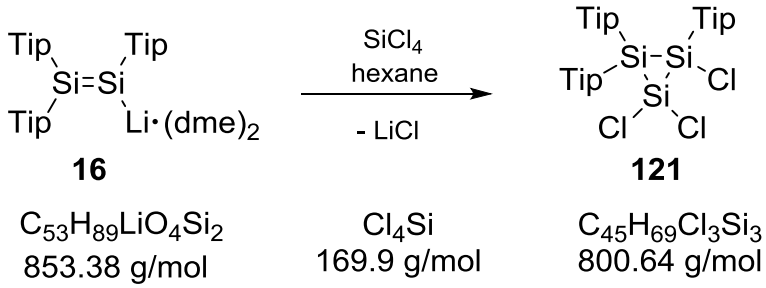

16 **121**

$C_{53}H_{89}LiO_4Si_2$ 853.38 g/mol | Cl_4Si 169.9 g/mol | $C_{45}H_{69}Cl_3Si_3$ 800.64 g/mol

1,1,2-Trichlorocyclotrisilane **121** is prepared according to the published procedure.[160] 13.6 mL (118.5 mmol) of silicon tetrachloride are rapidly added to a suspension of 20.24 g (23.7 mmol) disilenide **16** in 300 mL of hexane at room temperature. The reaction mixture turns orange and stirring is continued overnight. All insoluble materials are filtered off at 45°C. After the filtrate is reduced to dryness in vacuum, the crude product is redissolved in 60 mL of hexane and crystallized at 4°C to yield 12.1 g (64% yield) of **122** as pale yellow crystals.

^{1}H NMR (300.13 MHZ, C_6D_6, 300 K): δ = 7.21 (d, 1H, Tip-*H*), 7.16 (br, 2H, Tip-*H*), 7.03, 6.98, 6.97 (each d, each 1H, Tip-*H*), 4.24 (br, 1H, ^{i}Pr-C*H*), 4.09 (sept., 1H, ^{i}Pr-C*H*), 3.71 (br, 2H, ^{i}Pr-C*H*), 3.39 (sept., 1H, ^{i}Pr-C*H*), 3.20 (br, 1H, ^{i}Pr-C*H*), 2.69 (m, 3H, ^{i}Pr-C*H*), 1.58 (d, 3H, ^{i}Pr-CH_3), 1.38 (m, 21H, ^{i}Pr-CH_3), 1.31 (m, 24H, ^{i}Pr-CH_3), 0.54 (br, 6H, ^{i}Pr-CH_3).

5.2.8. Synthesis of Hexasilabenzene Isomer 122

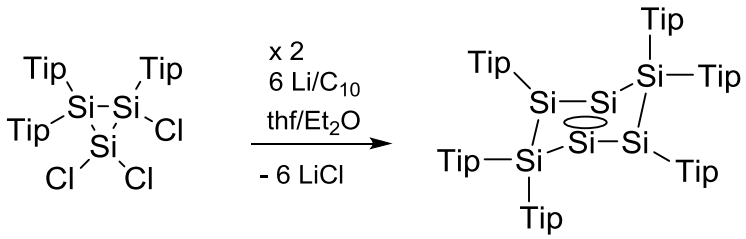

121 **122**

$C_{45}H_{69}Cl_3Si_3$ 800.64 g/mol | $C_{90}H_{138}Si_6$ 800.64 g/mol

Hexasilabenzene isomer **122** is prepared according to the published procedure.[160] A solution of 12.1 g (15.1 mmol) of 1,1,2-trichlorocyclotrisilane **121** in 120 mL of diethylether (Et_2O) is cooled to −80°C and 67 mL of lithium/naphthalene solution in thf (0.75M, 50.3 mmol, 3.3 eq.) are added dropwise within 15 minutes. The reaction mixture is allowed to slowly warm to room temperature overnight. After all volatiles are removed in vacuum at room temperature, residual naphthalene is sublimed out at 80°C under reduced pressure (10^{-3} mbar) within 4 hours. The solid residue is digested with 120 mL of benzene and filtered. The resulting solution is reduced to

approximately half of the volume. Little amounts of precipitated product are redissolved by gentle warming (35°C). Standing at room temperature overnight affords 6.5g (59% yield) of **122**·C_6H_6 as dark green blocks.

1H NMR (300.13 MHz, C_6D_6, 300 K): δ = 7.23, 7.14, 7.11, 6.90, 6.79, 6.71 (each s, each 2H, Tip-*H*), 4.73, 4.50 (each hept., each 2H, ^{i}Pr-C*H*), 4.03 (m, 4H, ^{i}Pr-C*H*), 3.66, 3.53 (each hept., each 2H, ^{i}Pr-C*H*), 1.84, 1.79, 1.75, 1.62, 1.54, 1.19, 1.17, 1.15, 1.14, 1.13, 1.12, 1.01, 0.77, 0.74, 0.65, 0.61, 0.60 (each d, altogether 108H, ^{i}Pr-CH_3).

5.2.9. Synthesis of Bridged Propellane 125

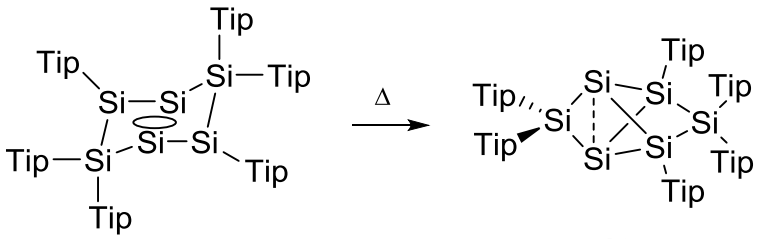

122

$C_{90}H_{138}Si_6$

1388.57 g/mol

125

$C_{90}H_{138}Si_6$

1388.57 g/mol

Following the published procedure,[165] 6.5 g of neat **122** (4.43 mmol) are heated to about 300°C using a heat gun. The temperature is maintained until all green solid was liquefied to an oily red suspension (10 min). Upon cooling to ambient temperature the intense red crude product solidifies again. 50 mL of hexane are added to the residue and the resulting suspension is filtered at 70°C. The filtrate is reduced to approximately half of the volume and standing at room temperature overnight affords 4.51 g (3.24 mmol) of **125** as red orange crystalline blocks. A second crystallization from the mother liquor yields another 670 mg (0.48 mmol; overall yield: 84%) of **125**.

^{1}H NMR (300.13 MHZ, C_6D_6, 300 K): δ = 7.21, 7.02, 6.97, 6.95, 6.81, 6.79 (each d, each 2H, Tip-*H*), 4.94 (sept., 2H, ^{i}Pr-C*H*), 4.43 (sept., 2H, ^{i}Pr-C*H*), 3.70 (m, 4H, ^{i}Pr-C*H*), 3.34 (sept., 2H, ^{i}Pr-C*H*), 3.02 (sept., 2H, ^{i}Pr-C*H*), 2.65 (m, 6H, ^{i}Pr-C*H*), 2.08, 1.70 (each d, each 6H, ^{i}Pr-CH_3), 1.52 (m, 18H, ^{i}Pr-CH_3), 1.38 (d, 6H, ^{i}Pr-CH_3), 1.16 (m, 24H, ^{i}Pr-CH_3), 1.03 (t, 12H, ^{i}Pr-CH_3), 0.77, 0.64, 0.55, 0.37 (each d, each 6H, ^{i}Pr-CH_3), 0.12 (t, 12H, ^{i}Pr-CH_3).

5.2.10. Synthesis of Bis(dimethylamino)chlorophosphane

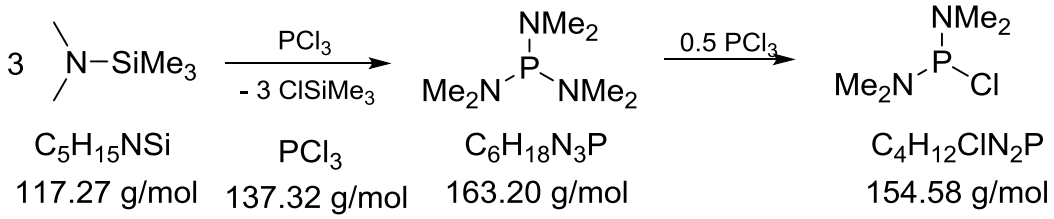

$C_5H_{15}NSi$	PCl_3	$C_6H_{18}N_3P$	$C_4H_{12}ClN_2P$
117.27 g/mol	137.32 g/mol	163.20 g/mol	154.58 g/mol

Tris(dimethylamino)phosphane is prepared according to the published procedure.[258] 25 g N,N-dimethyltrimethylsilyl amine (172 mmol) are dissolved in 100 mL diethyl ether and cooled to 0°C. A solution of phosphorus trichloride (5.93 g, 43 mmol) in 100 mL diethyl ether is added under vigorous stirring. After 12 h the reaction mixture is filtered and the solvent removed in vacuum to obtain a yellowish oil. The crude product is distilled in high vacuum (bp: 50-56°C, 5 x 10^{-2} mbar) to yield 6.75 g (41 mmol, 77 %) pure tris(dimethylamino)phosphane as colorless liquid.

^{1}H NMR (300.13 MHZ, C_6D_6, 300 K): δ = 2.47 (d, $^3J_{P\text{-}H}$ = 9.2 Hz), **^{31}P{^{1}H} NMR** (121.5 MHz, C_6D_6, 300 K): δ = 122.4.

According to a procedure from Dellinger,[259] neat tris(dimethylamino)phosphane (2.92 g, 17.7 mmol) is added to 1.44 g (8.85 mmol) PCl_3 at 0°C. After stirring for 60 minutes the crude product (slight yellow oil) is destilled at rt in high vacuum (5 x 10^{-2} mbar) and a colorless liquid is condensed in a flask cooled to −80°C (yield: 0.99 g, 93%).

^{1}H NMR (300.13 MHz, C_6D_6, 300 K): δ = 2.37 (d, $^3J_{P\text{-}H}$ = 12.1 Hz), **^{31}P{^{1}H} NMR** (121.5 MHz, C_6D_6, 300 K): δ = 158.6.

5.2.11. Synthesis of Bis(diethylamino)chlorophosphane

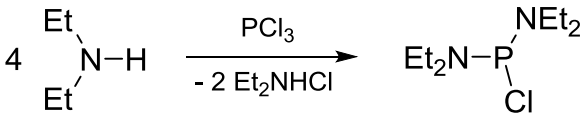

$C_4H_{11}N$		$C_8H_{20}ClN_2P$
73.14 g/mol	137.32 g/mol	210.69 g/mol

According to the published procedure,[258] a solution of diethylamine (23.7 mL, 228.90 mmol) in diethylether (70 mL) is added dropwise to a solution of PCl_3 (5 mL, 57.20 mmol) in diethyl ether (400 mL) at -20°C. The reaction mixture is allowed to warm up to room temperature and stirred for additional12 h. The suspension obtained is filtered over celite to remove $Et_2NH{\cdot}HCl$, and the solvent is evaporated. The resulting yellow liquid is distilled under high vacuum (2 x 10^{-2} mbar, 61°C) to obtain to obtain product**)** as colorless oil in 90 % yield.

^{1}H-NMR (300.13 MHZ, C_6D_6, 300 K): δ = 0.93 (tr, $^3J_{H\text{-}H}$ = 7 Hz, 12H, -C*H*$_3$), 3.00 (m, 8H, -C*H*$_2$-), **^{31}P{^{1}H}-NMR** (121.5 MHz, C_6D_6, 300 K): δ = 168.8.

5.2.12. Synthesis of Dichlorodiphenylamino Phosphane

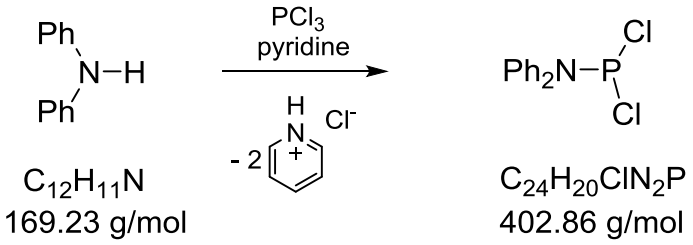

Dichlorodiphenylaminophosphane is synthesized according to a modified published procedure.[260] A solution of 4 mL (46 mMol) PCl_3 and 5.5 mL (0.069 mmol) pyridine are dissolved in 50 mL benzene and placed in a water bath. A solution of diphenylamine (7.78 g, 46 mmol) in 50 mL benzene is added with a cannula. Afterwards, the water bath is removed and the reaction mixture is refluxed for 2 h. All insoluble parts are removed by filtration and the solvent is removed in vacuum. The residue is dissolved in 100 mL diethyl ether and filtered over Al_2O_3 (neutral). After the solvent was removed in vacuum the crude product is distilled in high vacuum (bp. 110°C, 5 x 10^{-2} mbar) to yield 8.91 g (33 mmol, 72%) pure product.
^{1}H NMR (300.13 MHz, C_6D_6, 300 K): δ = 7.13 (m, 2H), 7.00 (m, 2H), 6.90 (m, 1 H), **^{31}P{^{1}H} NMR** (121.5 MHz, C_6D_6, 300 K): δ = 149.5.

5.2.13. Synthesis of 163[I]

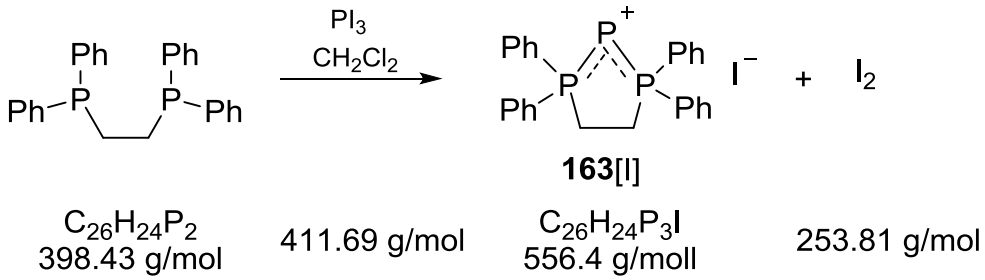

According to the procedure decribed in literature,[201] 3.87 g (9.72 mmo) dppe are dissolved in 40 mL dichloromethane and cooled to 0°C. A solution of PI_3 (4g, 9.72 mmol) in 100 mL dichloromethane is added under vigorous stirring to afford a burgundy suspension. After two hours of stirring, all volatiles are removed in vacuum and the residue is washed with diethyl ether (2 x 100 mL), pentane (2 x 100 mL) and filtered from dichloromethane. After removal of the solvent in vacuum, a deep red foam is obtained. It is not possible to wash the residue (diethylether, thf, pentane) colorless and thus remove all iodine from the product.
^{31}P{^{1}H} NMR (121.5 MHz, $CDCl_3$, 300 K): δ = 63.6 (d, 2P, $^{1}J_{P\text{-}P}$ = 454.7 Hz), −234.3 (tr, 1P, $^{1}J_{P\text{-}P}$ = 454.7 Hz).

5.2.14. Synthesis of 163[Br]

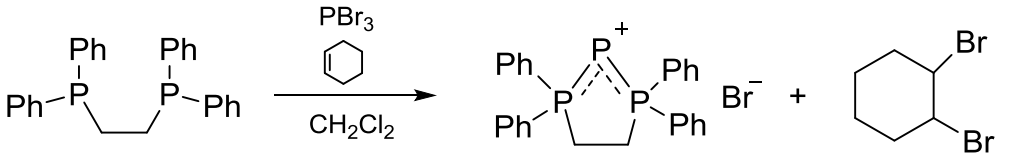

163[Br]

PBr_3	$C_{26}H_{24}P_2$	C_6H_{10}	$C_{26}H_{24}BrP_3$	$C_{10}H_{10}Br_2$
270.69 g/mol	398.43 g/mol	82.15 g/mol	509.30 g/mol	241.95 g/mol

According to the literature known procedure,[202] to a solution of PBr_3 (5.63 g, 20.8 mmol) and cyclohexene (6.6 mL, 64.69 mmol) in 350 mL dichloromethane as solution of 17.4 g (43.70 mmol) dppe in 200 mL dichloromethane is added. The colorless solution is stirred at room temperature overnight, after which the white precipitate is filtered and volatile components are removed under reduced pressure. To the colorless residue thf (350 mL) is added and the heterogeneous mixture is sonicated for 1 h at room temperature. The residue is then washed with thf (3 x 250 mL) and dried in vacuo. Standing at −20°C overnight affords 8.7 g **163**[Br] as white precipitate (17.10 mmol, 82%).

^{1}H NMR (300.13 MHZ, $CDCl_3$, 300 K): δ = 7.82-7.75 (m, 8H, Ph-*H*), 7.59-7.43 (m, 12H, Ph-*H*), 3.63 (d, $^{3}J_{P\text{-}H}$ = 16.3 Hz, 4H, C*H*$_2$), **^{31}P{^{1}H} NMR** (121.5 MHz, $CDCl_3$, 300 K): δ = 30.7 (d, 2P, $^{1}J_{P\text{-}P}$ = 450.3 Hz), −263.3 (tr, 1P, $^{1}J_{P\text{-}P}$ = 450.3 Hz).

5.2.15. Synthesis of 163[BPh_4]

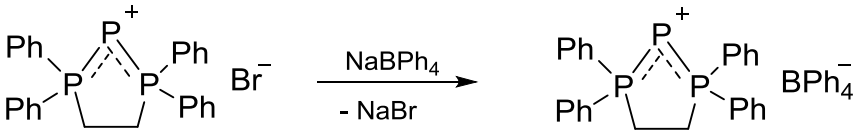

163[Br] **163**[BPh_4]

$C_{26}H_{24}BrP_3$	$C_{24}H_{20}BNa$	$C_{50}H_{44}BP_3$
509.30 g/mol	342.22 g/mol	748.63 g/mol

According to the literature known procedure,[201] 8.7 g (17.10 mmol) **163**[Br] are mixed with 7.2 g (21 mmol) $NaBPh_4$ and 250 mL dichloromethane are added and the reaction mixture is stirred overnight. After filtration, the solvent is removed in vacuo to afford 12.73 g **163**[BPh_4] as white foam (17.0 mmol, 99%).

^{1}H NMR (300.13 MHZ, $CDCl_3$, 300 K): δ = 7.59-7.50 (br m, 4H, Ph-*H*), 7.49-7.32 (br m, 16H, Ph-*H*), 7.32-7.20 (br m, 8H, Ph-*H*), 6.82-6.62 (m, 12H, Ph-*H*), **^{11}B{^{1}H} NMR** (96.3 MHZ, $CDCl_3$, 300 K): δ = −6.6, **^{31}P{^{1}H} NMR** (121.5 MHz, $CDCl_3$, 300 K): δ = 75.71 (d, 2P, $^{1}J_{P\text{-}P}$ = 439.8 Hz), −222.6 (tr, 1P, $^{1}J_{P\text{-}P}$ = 439.8 Hz).

5.2.16. Synthesis of 164b[BPh_4]

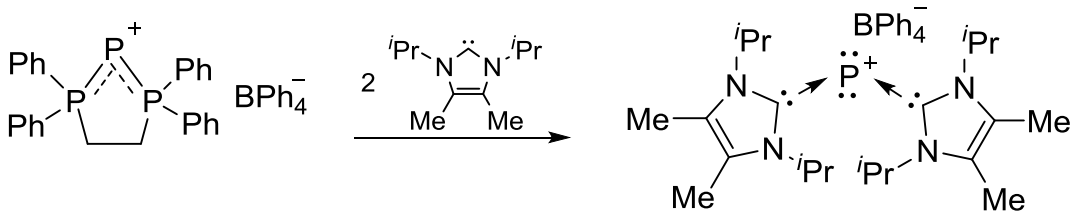

163[BPh_4] | | **164b**[BPh_4]
$C_{50}H_{44}BP_3$ | $C_{11}H_{20}N_2$ | $C_{46}H_{60}BN_4P$
748.63 g/mol | 180.30 mol/L | 710.80 g/mol

P(I) cation **164b**[BPh_4] was prepared according to the procedure published by Macdonald.[203] A solution of 1,3-diisopropyl-4,5-dimethylimidazol-2-ylidene (3.86 g; 21.43 mmol) in 250 mL of thf is slowly added *via* cannula to a solution of **163**[BPh_4] (8 g; 10.19 mmol) in 250 mL of thf. The solution immediately becomes intensely yellow-colored and is allowed to stir for 30 min. The solvent is removed in vacuo, followed by washing with toluene (3 x 400 mL) to remove the free dppe. Yield: 7.13 g (10.00 mmol, 98%).

^{1}H NMR (300.13 MHz, $CDCl_3$, 300 K): δ = 7.36-7.29 (br m, 8H, Ph-*H*), 6.97-6.91 (br m, 8H, Ph-*H*), 6.82-6.75 (br m, 4H, Ph-*H*), 5.24 (br, 4H, ^{i}Pr-C*H*), 2.10 (s, 12H, Me-*H*), 1.20 (d, 24H, ^{i}Pr-CH_3), **^{11}B{^{1}H} NMR** (96.3 MHz, $CDCl_3$, 300 K): δ = −6.5, **^{31}P{^{1}H} NMR** (121.5 MHz, $CDCl_3$, 300 K): δ = − 157.7 (br).

5.2.17. Synthesis of 164[Cl]

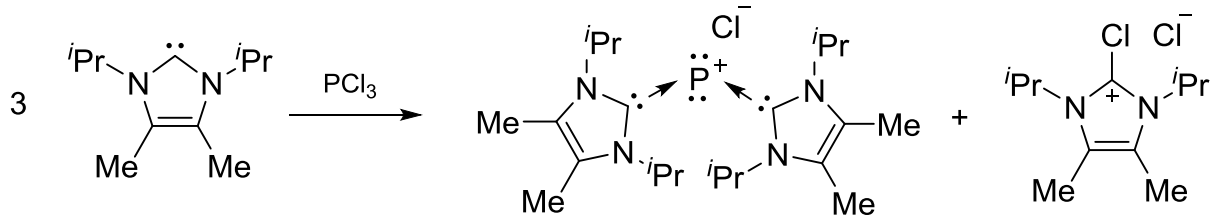

164b[Cl]
$C_{11}H_{20}N_2$ | Cl_3P | $C_{22}H_{40}ClN_4P$ | $C_{11}H_{20}Cl_2N_2$
180.30 mol/L | 137.32 g/mol | 427.01 g/mol | 251.20 g/mol

A mixture of **164b**[Cl] and 1,3-diisopropyl-4,5-dimethylimidazolium chloride is synthesized according to the literature known procedure.[203] 2.19 mmol PCl_3 (192 μL) are dissolved in 20 mL thf and a solution of three equivalents (1.19 g) 1,3-diisopropyl-4,5-dimethylimidazol-2-ylidene in 50 mL thf is added *via* cannula. After stirring for 30 minutes at room temperature, a mixture of **164b**[Cl] and 2-chloro-1,3-diisopropyl-4,5-dimethylimidazolium chloride is obtained as yellow suspension.

5.2.18. Synthesis of bis(dimethylamino)chloroborane

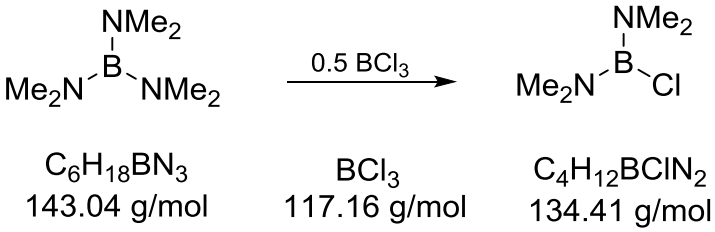

$C_6H_{18}BN_3$	BCl_3	$C_4H_{12}BClN_2$
143.04 g/mol	117.16 g/mol	134.41 g/mol

Bis(dimethylamino)chloroborane is synthesized in analogy to the procedure published for bis(dimethylamino)chlorophosphane.[259] Tris(dimethylamino)borane (2 g, 13.99 mmol) is cooled to 0°C and 0.5 equivalents (7 mL) boron trichloride solution (1 M in heptane) are added. After stirring overnight, heptane is distilled out (98-113°C) and then a fraction of pure bis(dimethylamino)chloroborane (514 mg, 19%) is collected as colorless liquid.

^{1}H NMR (300.13 MHz, C_6D_6, 300 K): δ = 2.48, **^{11}B{^{1}H} NMR** (96.3 MHz, C_6D_6, 300 K): δ = 28.1.

5.2.19. Synthesis of Dichlorodimethylaminoborane

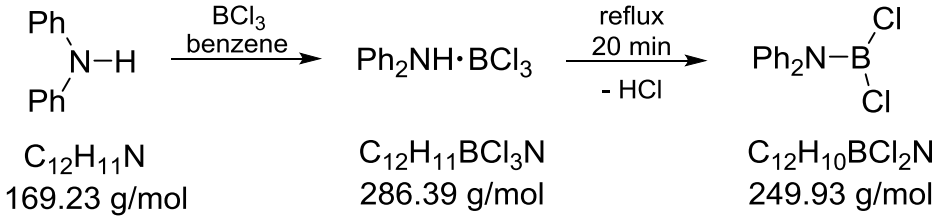

$C_{12}H_{11}N$	$C_{12}H_{11}BCl_3N$	$C_{12}H_{10}BCl_2N$
169.23 g/mol	286.39 g/mol	249.93 g/mol

Dichlorodimethylaminoborane was prepared according to the published procedure.[261] 2 g (11.80 mmol) diphenylamine are dissolved in 10 mL benzene and added dropwise to 11.8 mL boron trichloride solution (1M in heptane). After 30 min of stirring at room temperature the reaction mixture is refluxed for 20 min. All volatiles are removed in vacuo (external cold trap, HCl generation!) and the residue is distilled in high vacuum (112°C, 2.2 x 10^{-2} mbar) to afford 2.62g (89 %) colorless dichlorodimethylaminoborane that solidified upon cooling down to room temperature.

^{1}H NMR (300.13 MHz, C_6D_6, 300 K): δ = 6.98-6.82 (m, Ph-*H*), **^{11}B{^{1}H} NMR** (96.3 MHz, C_6D_6, 300 K): δ = 32.6.

5.2.20. Synthesis of Lithium *Tert*-butyltrihydroborate

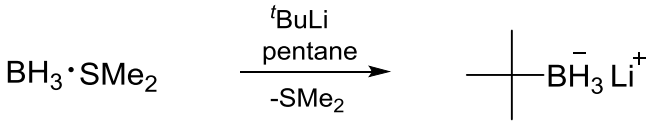

C_2H_9BS	C_4H_9Li	$C_4H_{12}BLi$
75.96 g/mol	64.06 g/mol	77.89 g/mol

According to the published procedure,[262] 4.7 mL (7.99 mmol) *tert*-butyllithium (1.7 M solution in pentane) are added to 5 mL of pentane and cooled to −78°C. A solution of 0.76 mL (7.99 mmol) of borane dimethyl sulfide adduct in 3 mL pentane is added dropwise within 1.5 hours. The reaction mixture is allowed to slowly warm to rt overnight and formation of white precipitate is observed. Filtration of the suspension is followed by washing the white solid twice with pentane. The combined filtrates are concentrated and stored at −80°C. Within 1 day, a white solid precipitates from the solution. The precipitate is filtered off, washed with cold pentane (−60°C) and dried in vacuum. Yield: 312 mg (50%).

^{1}H NMR (300.13 MHz, C_6D_6, 300 K): δ = 1.70 (s, DMS), 1.26 (s, ^{t}Bu-CH_3), **^{11}B NMR** (96.3 MHZ, C_6D_6, 300 K): δ = −19.4 ppm (q, $^1J_{B\text{-}H}$ = 60.5 Hz).

5.2.21. Synthesis of 4′-Bromo-4-methylthiobiphenyl

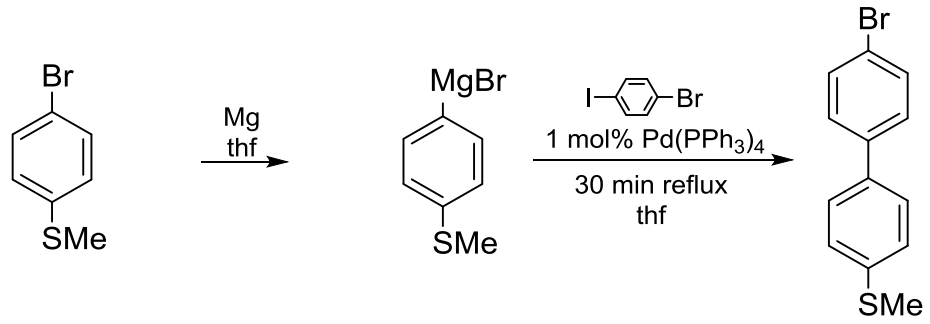

C_7H_7BrS	Mg	C_7H_7BrMgS	C_6H_4BrI	$C_{13}H_{11}BrS$
203.10 g/mol	24.31 g/mol	227.40 g/mol	282.91 g/mol	279.20 g/mol

4′-Bromo-4-methylthiobiphenyl is prepared according to a modified procedure described in literature.[263] *p*-Bromoiodobenzene (14.0 g, 49.3 mmol) and tetrakis(triphenylphosphine)palladium (0.50 g, 0.49 mmol, 0.01 eq) are dissolved in THF (60 mL) and brought to gentle reflux with stirring. A Grignard solution is prepared by stirring magnesium turnings (1.18 g, 49.3 mmol) and *p*-Bromothioanisole (10.0 g, 49.3 mmol) for 70 minutes. The Grignard solution is added dropwise to the boiling mixture of *p*-bromoiodobenzene and tetrakis(triphenylphosphine)palladium and refluxed. After the addition is complete, the reaction mixture is held under reflux for additional 30 min.

After cooling to rt, it is poured in an ice cold aqueous solution of 10% HCl. A yellow solid is filtered off and rinsed with cold water. The crude product is dissolved in dichloromethane and extracted with water (2 x) and brine (2x) and dried over $MgSO_4$. The obtained solution is reduced to dryness. A mixture of *iso*-propanol/*n*-Heptane (1:1) is added to the residue (250 mL). To this suspension dichloromethane is added dropwise until a clear solution is obtained. Standing at −25°C overnight to afford 6.57 g (23.5 mmol) of pure 4′-bromo-4-methylthiobiphenyl as beige solid. The mother liquor is concentrated to half of the volume and standing at −25°C overnight yields a second batch of pure product (4.01g, 14.4 mmol). Combined yield: 10.58 g (37.9 mmol, 77%).

^{1}H NMR: (300.13 MHz, $CDCl_3$, 300 K): δ = 7.54-7.14 (m, 8H, $(Ph)_2$-*H*), 2.46 (s, 3H, SCH_3).

5.2.22. Synthesis of 8-Methylthiooctyl Bromide

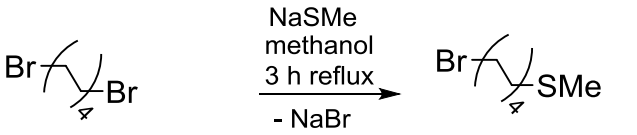

$C_8H_{16}Br_2$	CH_3NaS	$C_9H_{19}BrS$
272.02 g/mol	70.08 g/mol	239.22 g/mol

8-Methylthiooctyl bromide was prepared according to the literature known procedure.[264] Sodium thiomethoxide (1.11 g, 15.7 mmol) is dissolved in abs. methanol (30 mL). 1,8-Dibromooctane (4.29 g, 15.8 mmol) is added and the mixture is refluxed for 3 h. After cooling down to rt, the solvent is removed in vacuo. A suspension of a yellow liquid and a white solid (NaBr) is obtained. The liquid is decanted and the solid washed with diethyl ether three times. The combined organic phases are washed with water and dried over $MgSO_4$. After removing of the solvent on a rotary evaporator the crude product is distilled under reduced pressure (bp: 68 °C, 3.8 x 10^{-2} mbar) to afford pure 8-methylthiooctyl bromide (2.22 g, 9.28 mmol) as colorless oil (yield: 59%).

^{1}H NMR: (300.13 MHz, $CDCl_3$, 300 K): δ = 3.41 (t, 4H, CH_2Br and CH_2S), 2.18 (s, 3H, SCH_3), 1.86 (q, 4H, CH_2CH_2Br and CH_2CH_2S), 1.51-1.26 (m, 8H, remaining -CH_2-).

5.2.23. Synthesis of Bis(4-bromophenyl)disulfide

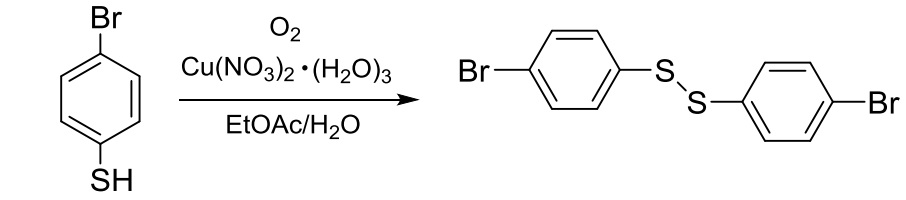

C_6H_5BrS
189.07 g/mol

$C_{12}H_8Br_2S_2$
376.12 g/mol

Bis(4-bromophenyl)disulfide was prepared according to the literature known procedure.[265] *p*-Bromothiophenol (521 mg, 2.76 mmol) is dissolved in ethyl acetate (5.5 mL). A solution of copper(II) nitrate trihydrate (673 mg, 2.79 mmol) in water (2.5 mL) is added and mixture is stirred vigorously in an open vessel at rt for 75 min. The organic layer is separated and the aqueous phase is extracted once with ethyl acetate. The combined organic layers are washed with a solution 10 % NaOH solution (2x) and with water (1x) and dried over $MgSO_4$. The solvent is removed in vacuum to obtain the product as white powder (378 mg, 73 % yield).
^{1}H NMR: (300.13 MHz, $CDCl_3$, 300 K): δ = 7.03-6.86 (m).

5.2.24. Synthesis of Phosphasilene 108a

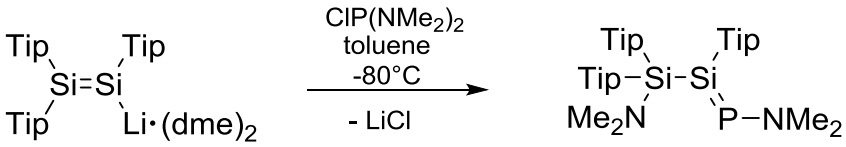

16

$C_{53}H_{89}LiO_4Si_2$
853.38 g/mol

$C_4H_{12}ClN_2P$
154.58 g/mol

108a

$C_{49}H_{81}N_2PSi_2$
785.34 g/mol

According to the procedure developed during my master thesis, a solution of disilenide **16** (8.21 g, 9.62 mmol) in toluene (150 mL) is cooled to −78°C and bis(dimethylamino)chlorophosphine (1.40 mL, 9.62 mmol) is added dropwise. The resulting red solution is allowed to warm slowly to room temperature, forming a yellow/brown suspension, which is stirred at room temperature for a further hour. All volatiles are then removed under vacuum. The yellow solid residue is dissolved in hexane (150 mL) and the resulting suspension is filtered. The filtrate is reduced to dryness to obtain bright yellow foam. Recrystallization from pentane (50 mL) at room temperature yields 97% *E*/*Z*-**108a** (7.35 g, 9.4mmol) as bright yellow crystals.
^{1}H NMR (300.13 MHz, C_6D_6, 300K): δ = 7.22-6.94 (br m, 6 H, Tip-*H*), 4.03, 3.88, 3.70, 3.57, 3.49 (each m, each 1H, ^{i}Pr-C*H*), 3.00 (br, 6 H, Si-NMe_2-*H*) 2.82, 2.75 (each m, each 2 H, ^{i}Pr-C*H*), 2.40 (d, $^3J_{H\text{-}P}$ = 6.21 Hz, 6 H, P-NMe_2-*H*), 1.82, 1.60 (each d, $^3J_{H\text{-}H}$ = 6 Hz, each 3 H, ^{i}Pr-CH_3), 1.54-1.34 (m, 18 H, ^{i}Pr-CH_3), 1.33-1.10 (m,

18 H, ^{i}Pr-CH_3), 1.00, 0.95, 0.39, 0.33 (each d, $^3J_{H\text{-}P}$ = 6.21 Hz, each 3 H, ^{i}Pr-CH_3), **^{31}P{^{1}H} NMR** (121.5 MHz, C_6D_6, 300K): δ = 344.8 ($^1J_{P\text{-}Si}$ = 186.5 Hz, $^2J_{P\text{-}Si}$ = 40.8 Hz, *E*-isomer), 336.2 (*Z*-isomer).

5.2.25. Synthesis of Phosphasilene 108b

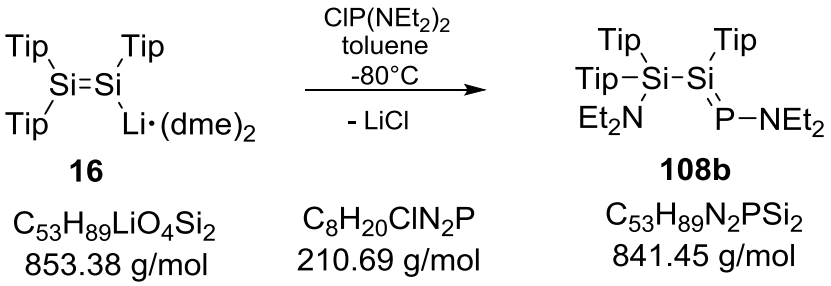

16 **108b**

$C_{53}H_{89}LiO_4Si_2$ 853.38 g/mol

$C_8H_{20}ClN_2P$ 210.69 g/mol

$C_{53}H_{89}N_2PSi_2$ 841.45 g/mol

According to the preocedure developed during my master thesis, a solution of disilenide **16** (0.5 g, 0.59 mmol) in toluene (25 mL) is cooled to −78°C and bis(diethylamino)chlorophosphane (0.125 mL, 0.59 mmol) is added dropwise. The resulting orange solution is allowed to warm slowly to room temperature, forming an orange suspension, which is stirred at room temperature for an additional 12 h. All volatiles are removed under vacuum. The orange solid residue is dissolved in hexane (30 mL) and the resulting suspension is filtered. The filtrate was reduced to dryness to obtain 80% (0.4 g, 0.83 mmol) of *E*/*Z*-**108b** as bright orange foam.
^{1}H NMR (300.13 MHz, C_6D_6, 300 K): δ = 7.14-6.83 (br m, 6H, Tip-*H*), 4.20-2.95 (br m, 9H, ^{i}Pr-C*H*), 2.75 (m, 8H, Si-N(CH_2-CH_3)$_2$, P-N((CH_2-CH_3)$_2$), 1.87-0.00 (m, 66H, ^{i}Pr-CH_3, Si-N(CH_2-CH_3)$_2$, P-N(CH_2-CH_3)$_2$), **^{31}P{^{1}H} NMR** (121.5 MHz, C_6D_6, 300 K): δ = 344.8 ($^1J_{P\text{-}Si}$ = 186.8 Hz), 336.7.

5.3. Reactivity Studies of Phosphasilene 108a

5.3.1. Reaction of Phosphasilene 108a with Xylyl-isonitril

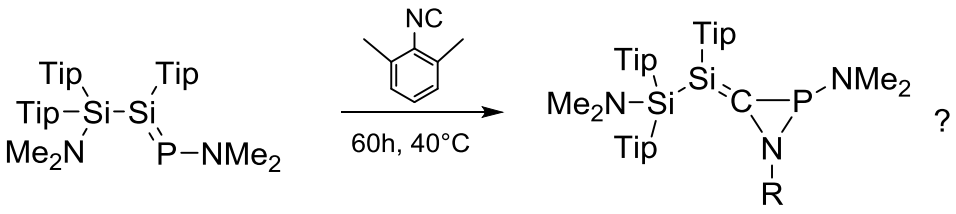

108a *E/Z*-**140**

$C_{49}H_{81}N_2PSi_2$ 785.34 g/mol

C_9H_9N 131.18 g/mol

$C_{57}H_{88}N_3PSi_2$ 902.50 g/mol

a) Phosphasilene **108a** (100 mg, 0.127 mmol) and one equivalent xyly-isonitrile (17 mg) were combined in an NMR tube and 0.5 mL C_6D_6 added. After two hours at rt the yellow solution became orange and 30% conversion to the presumed initial product **133** was observed. **^{29}Si{H} NMR** (59.6 MHZ, C_6D_6, 300 K): δ = −7.0, −10.6, −80.6 (d, $^1J_{Si\text{-}P}$ = 27 Hz), −81.4 ($^1J_{Si\text{-}P}$ = 42 Hz), **^{31}P{H} NMR** (121.5 MHz, C_6D_6, 300 K): δ = 141.6 ($^1J_{Si\text{-}P}$ = 27 Hz), 136.8 ($^1J_{Si\text{-}P}$ = 42 Hz), ratio 1:2. After another 16 h at rt the solution turned more red and formation of formation of presumed second product **134** was detected (17%). **^{29}Si{H} NMR** (59.6 MHZ, C_6D_6, 300 K): δ = −2.0 ($^1J_{Si\text{-}P}$ = 89.5 Hz), −8.2 ($^2J_{Si\text{-}P}$ = 34.5 Hz) ppm, **^{31}P{H} NMR** (121.5 MHz, C_6D_6, 300 K): δ = −212.0, −226.5 ($^1J_{Si\text{-}P}$ = 89.5 Hz, $^2J_{Si\text{-}P}$ = 34.5 Hz) ppm ratio 6:94. Upon heating to 40°C for additional 60 h complete conversion to the proposed final product **135** was observed. **^{13}C{H} NMR** (75.5 MHz, C_6D_6, 300 K): *selected resonances* δ = 202.5 ($^2J_{C\text{-}P}$ = 65.7 Hz), 175.1 ($^1J_{C\text{-}P}$ = 54.4 Hz), **^{29}Si{H} NMR** (59.6 MHZ, C_6D_6, 300 K): δ = 39.6 ($^2J_{Si\text{-}P}$ = 66.9 Hz), 11.1 ($^2J_{Si\text{-}P}$ = 51.2 Hz), −2.9 ($^3J_{Si\text{-}P}$ = 11.6 Hz) and −4.7 ($^3J_{Si\text{-}P}$ = 57.0 Hz), **^{31}P{H} NMR** (121.5 MHz, C_6D_6, 300 K): δ = −50.8, −64.8 ppm (ratio 1.7 : 1).
b) Phosphasilene **108a** (500 mg, 0.637 mmol) and one equivalent xylyl-isonitrile (85 mg) were combined in 2.5 mL toluene and the reaction mixture was kept at 40°C for 60 hours. Clean conversion to proposed final product **135** was confirmed by NMR spectroscopy. The clear red solution was concentrated to approximately 0.5 mL. No single crystalline material could be obtained even at −20°C. The solvent was exchanged for pentane. It was not possible to grow single crystals at any temperature.

5.3.2. Reaction of Phosphasilene 108a with Duryl-bisisonitrile

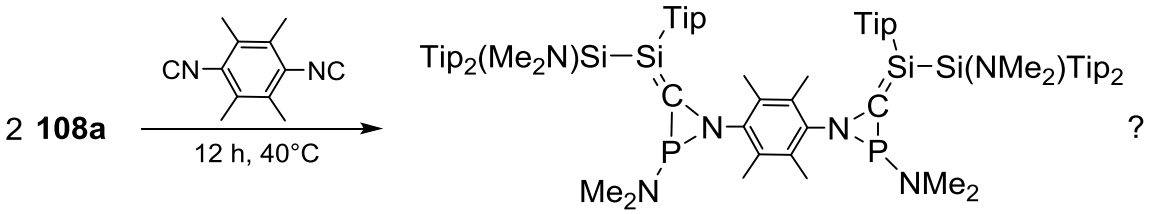

141

$C_{12}H_{12}N_2$
184.24 g/mol

$C_{110}H_{174}N_6P_2Si_4$
1754.93 g/mol

100 mg Phosphasilene **108a** (0.127 mmol) and 0.5 equivalents duryl-bisisonitrile (11.7 mg) were combined in an NMR tube and 0.5 mL C_6D_6 added. After 30 minutes at 40°C 16% conversion was observed. **^{31}P{H} NMR** (121.5 MHz, C_6D_6, 300 K): δ = 145.5 (2%), 137.2 (10%), −227.4 (4%) ppm. Upon heating for another 12 h at 40°C two additional resonances arose in the **^{31}P{H} NMR** (121.5 MHz, C_6D_6, 300 K): δ = −49.0 and −66.8 (ratio 1:0.8) and the beginning formation of various by-products was detected. Continued heating the mixture to 40°C increasingly lead to decomposition.

5.3.3. Reaction of Phosphasilene 108a with Methyl Lithium

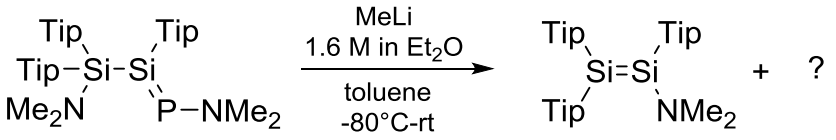

108a **143**

$C_{48}H_{81}N_2PSi_2$	CH_3Li	$C_{47}H_{75}NSi_2$
785.34 g/mol	21.98 g/mol	710.29 g/mol

500 mg (0.635 mmol) phosphasilene **108a** were dissolved in 10 mL toluene. One equivalent (0.4 mL) methyl lithium (1.6 M solution in diethyl ether) was added dropwise at room temperature. The resulting red solution was stirred at rt overnight and the solvent removed in vacuo. 10 mL of hexane were added to the residue and the mixture was filtered. The filtrate was concentrated to dryness and 1 mL of pentane was added. No single crystalline material was obtained at any temperature. **^{29}Si{H} NMR** (59.6 MHZ, C_6D_6, 300 K): δ = 95.5, 26.3, −0.5 (d, $^1J_{P\text{-}Si}$ = 33.3 Hz), −24.5, −25.1, **^{31}P{H} NMR** (121.5 MHz, C_6D_6, 300 K): −106.5 ($^1J_{P\text{-}Si}$ = 33.3 Hz).

5.3.4. Reaction of Phosphasilene 108a with *tert.*-Butyl Lithium

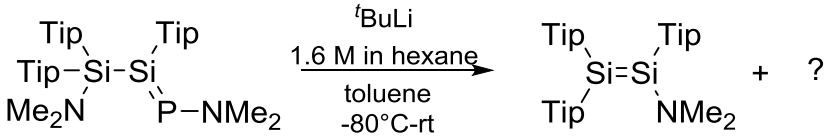

108a **143**

	C_4H_9Li	$C_{47}H_{75}NSi_2$
	64.06 g/mol	710.29 g/mol

500 mg phosphasilene **108a** (0.637 mmol) were dissolved in 40 mL toluene and cooled to −80°C. One equivalent (0.4mL) *tert.*-butyl lithium (1.6 M solution in hexane) was added dropwise. The reaction mixture was allowed to warm up to room temperature and the yellow solution turned red. After stirring for additional three hours all volatiles were removed in vacuo. The residue was digested with 20 mL pentane and filtered. Concentration of the filtrate to approximately 1 mL in volume did not afford single crystalline material at any temperature.
^{29}Si{H} NMR (59.6 MHZ, C_6D_6, 300 K): δ = 95.5, 26.2, −21.5 and −25.1, **^{31}P{H} NMR** (121.5 MHz, C_6D_6, 300 K): δ = 294.6 (65%), 282.2 (21%), 19.5 (10%), 11.9 (4%).

5.3.5. Synthesis of *P*-Mesityl Phosphasilene *E/Z*-144

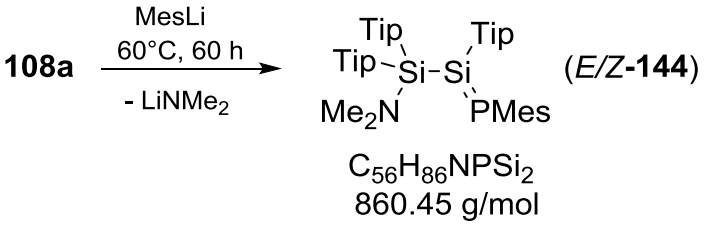

A solution of 500 mg (0.637 mmol) **108a** and 110 mg MesLi·0.1 Et_2O (0.83 mmol) in toluene (5 ml) are kept at 60°C for 60 h. All volatiles are removed in vacuum, the residue was digested with hexane (30 mL) and filtered. The filtrate was concentrated to 5 mL affording *E*-**144** as yellow crystals (0.35 g, 64%) after 24 h at rt. **m.p**. 208°C (dec).

^{1}H NMR (300.13 MHz, thf-d8, 300 K): δ = 7.09 (br, 2H, Tip-C*H*, 6.96 (br, 1H, Tip-C*H*), 6.92 (br, 2H, Tip-C*H*), 6.81 (br, 1H, Tip-C*H*), 6.64 (br, 2H, Mes-C*H*), 3.74 (sept, $^3J_{H-H}$ = 6.6 Hz, 1H, Tip-*i*Pr-C*H*), 3.29 (br m, 4H, Tip-^{i}Pr-C*H*), 3.04 (br m, 3H, Tip-^{i}Pr-C*H*), 2.90-2.53 (br m, 7H, Tip-^{i}Pr-C*H* (1H) overlapping with NMe_2-CH_3 (6H), 2.28, 2.20, 2.12, 2.07 (each s, overall 9H, *ortho*/*para E*/*Z* Mes-CH_3), 1.60 (d, $^3J_{H-H}$ = 5.4 Hz, 2H, Tip-^{i}Pr-CH_3), 1.52-1.02 (br m, overall 38H, Tip-^{i}Pr-CH_3), 0.74 (d, $^3J_{H-H}$ = 5.9 Hz, 2H, Tip-^{i}Pr-C*H*), 0.62 (d, $^3J_{H-H}$ = 5.9 Hz, 2H, Tip-^{i}Pr-CH_3), 0.49 (d, $^3J_{H-H}$ = 6.3 Hz, 1H, Tip-^{i}Pr-CH_3), 0.38 (d, $^3J_{H-H}$ = 6.1 Hz, 2H, Tip-^{i}Pr-CH_3), 0.22-0.01 (br m, 6H, Tip-^{i}Pr-CH_3), −0.13 ($^3J_{H-H}$ = 6.1 Hz, 1H, Tip-^{i}Pr-CH_3), **^{13}C{H} NMR** (75.47 MHz, thf-d8, 300 K): δ = 155.8, 155.6, 153.7, 153.1, 151.1, 150.1, 149.5, 139.5, 139.4, 139.1, 138.3, 135.3, 135.2, 135.0, 134.5, 127.6, 122.8, 122.2, 121.8, 121.5 (Ar-*C*), 42.1 (NMe_2-*C*), 38.4, 36.0, 35.4, 34.5, 34.2, 34.1, 34.0, 33.7, 33.3, 29.9, 26.9, 26.6, 23.5, 23.3, 23.2, 22.7, 22.2, 19.9 (some br, Tip-^{i}Pr-*C*H and Tip-^{i}Pr-*C*H_3), **^{29}Si{H} NMR** (59.62 MHz, 300 K, thf-d8): δ = 192.4 (d, $^1J_{Si-P}$ = 193.9 Hz), −6.6 (d, $^2J_{Si-P}$ = 46.6 Hz), **^{31}P{H} NMR** (121.5 MHz, thf-d8, 300 K): δ = 234.4 ($^1J_{Si-P}$ = 193.9 Hz, $^2J_{Si-P}$ = 46.6 Hz, *E*-**144**), 217.9 ($^1J_{Si-P}$ = 189.0 Hz, $^2J_{Si-P}$ = 25.0 Hz, *Z*-**144**); **UV/vis** (hexane): λ = 374 nm (ε = 7672 $M^{-1}cm^{-1}$), λ = 270 nm (ε = 24095 $M^{-1}cm^{-1}$); **elemental analysis** calcd (%) for $C_{56}H_{86}NPSi_2$: C 78.17, H 10.07, N 1.63; found: C 78.14, H 9.91, N 1.58.

5.3.6. Synthesis of Trisilaphospha[1.1.0]bicyclobutane 146

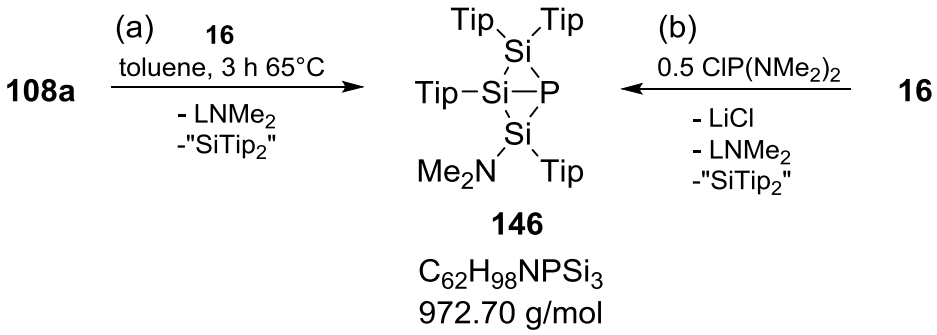

a) A solution of 2.32 g (2.72 mmol) **16** and 2.13 g **108a** (2.72 mmol) in 25 mL of toluene is stirred at 65°C for 3 h during which the orange solution turns dark red. After cooling to rt, two equivalents of Me_3SiCl are added and stirring is continued for 3 h in order to quench any unreacted anionic components. Volatiles are removed in vacuum and the residue digested with 40 mL hexane. Insoluble material is separated by filtration and the filtrate reduced to dryness. Upon dissolving in 10 mL of pentane storage at –25°C overnight affords 910 mg (34%) of **146** as colorless crystals.
b) At −80°C 0.498 mL (3.52 mmol) $(Me_2N)_2PCl$ is added *via* syringe to a solution of 6.00 g (7.03 mmol) **16** in 60 mL of toluene. The mixture is allowed to warm to rt and after 30 min heated to 65°C for 3 h. Two equivalents of Me_3SiCl are added and stirring is continued for 3 h in order to quench any unreacted anionic components. All volatiles are removed in vacuum and the resulting foam is digested with 80 mL hexane. After separation of insoluble components by filtration, the solution is reduced to dryness. The residue is dissolved in 10 mL of pentane and kept at −25°C overnight yielding 0.95 g (0.98 mmol, 28%) of **146** as colorless crystals.
^{1}H NMR (300.13 MHz, C_6D_6, 300 K): δ = 7.22 (br, 1H, Tip-C*H*), 7.16 (br, 1H, Tip-C*H*), 7.10 (d, $^4J_{H\text{-}H}$ = 1.6 Hz, 1H, Tip-C*H*), 7.09 (br, 2H, Tip-C*H*), 7.04 (d, $^4J_{HH}$ = 1.6 Hz, 1H, Tip-C*H*), 7.02 (br, 1H, Tip-C*H*), 6.81 (d, $^4J_{H\text{-}H}$ = 1.6 Hz, 1H, Tip-C*H*), 4.91 (sept, $^3J_{HH}$ = 6.4 Hz, 2H, Tip-^{i}Pr-C*H*), 4.60-4.29 (br m, 4H, Tip-^{i}Pr-C*H*), 3.89 (sept, $^3J_{H\text{-}H}$ = 6.6 Hz, 1H, Tip-*i*Pr-C*H)*, 3.47 (sept, $^3J_{H\text{-}H}$ = 6.6 Hz, 1H, Tip-*i*Pr-C*H*), 2.80-2.64 (m, 4H, Tip-*i*Pr-C*H*), 1.91 (s, 6H, NMe_2-CH_3), 1.79 (d, $^3J_{H\text{-}H}$ = 6.6 Hz, 3H, Tip-*i*Pr-CH_3), 1.72-1.55 (m, 12H, Tip-*i*Pr-CH_3), 1.44 (d, $^3J_{H\text{-}H}$ = 6.7 Hz, Tip-*i*Pr-CH_3), 1.33 (d, $^3J_{H\text{-}H}$ = 6.7 Hz, Tip-*i*Pr-CH_3), 1.27-1.09 (br m, 42H, Tip-*i*Pr-CH_3), 0.69 (d, $^3J_{H\text{-}H}$ = 6.9 Hz, 3H, Tip-*i*Pr-CH_3), 0.53 (d, $^3J_{H\text{-}H}$ = 6.7 Hz, 6H, Tip-*i*Pr-CH_3) ppm, **^{13}C{H} NMR** (75.47 MHz, C_6D_6, 300 K): δ = 157.28, 156.5, 156.3, 155.9, 154.6, 154.0, 150.8, 150.7, 150.1, 134.6, 133.8 (d, $^2J_{CP}$ = 10.1 Hz), 132.5 (d, $^3J_{CP}$ = 9.4 Hz), 126.6 (d, $^2J_{CP}$ = 4.3 Hz), 126.5, 122.7, 122.5, 122.2, 121.4, 121.1 (Ar-*C*), 38.9 (NMe_2-*C*), 37.4, 37.1, 36.2, 36.1, 35.9, 34.9, 34.8, 34.7, 34.6, 34.4, 33.5, 33.4, 26.7, 26.2, 26.0, 25.7, 25.6, 25.2, 24.8, 24.6, 24.2, 24.1, 24.0, 23.8, 22.8, 22.7 ppm, **^{29}Si{H} NMR** (59.62 MHz, C_6D_6, 300 K): δ = −5.1 (d, $^1J_{Si\text{-}P}$ = 84.7 Hz), −39.5 (d, $^1J_{Si\text{-}P}$ = 84.7 Hz), −119.8 (d, $^1J_{Si\text{-}P}$ = 5.2 Hz) ppm, **^{31}P{H} NMR** (121.5 MHz, C_6D_6, 300 K): δ = −212.3 ($^1J_{Si\text{-}P}$ = 84.7 Hz) ppm; **elemental analysis** calcd (%) for $C_{62}H_{98}NPSi_3$: C 76.56, H 10.16, N 1.44; found: C 76.16, H 10.25, N 1.52.

5.3.7. Reaction of 146 with $PdCl_2$

In an NMR tube 110 mg (0.113 mmol) **146** and 26 mg (0.147 mmol) $PdCl_2$ were combined in thf-d8 and heated at 70°C overnight. A metallic layer was observed on the wall of the NMR tube and the reaction mixture was filtered to afford a pale yellow solution. **^{31}P{^{1}H} NMR** (121.5 MHz, thf-d8, 300 K): main products: δ = −142.3 (br), −168.4 ($^1J_{P\text{-}Si}$ = 45.2, 31.8 Hz), −179.0 (br) ppm (ratio1:2:1).

5.3.8. Reaction of 146 with CuBr·(SMe_2)

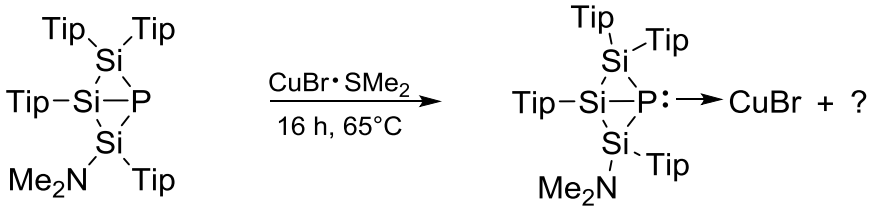

146 **152**

$C_{62}H_{98}NPSi_3$ C_2H_6BrCuS $C_{62}H_{98}NPSi_3CuBr$

972.70 g/mol 205.58 g/mol 1116.15 g/mol

100 mg (0.103 mmol) **146** and 125 mg (0.142 mmol) CuBr·SMe_2 were combined in an NMR tube and 0.5 mL C_6D_6 were added. After the mixture was kept at 65°C for 16 h, all volatiles were removed in vacuo. The residue was digested with hexane and filtered. No product could be isolated by crystallization. **^{29}Si{^{1}H} NMR** (59.62 MHz, C_6D_6, 300 K): δ = −1.4 (v br), −6.9 ($^1J_{P\text{-}Si}$ = 100.7 Hz), −6.8 ($^1J_{P\text{-}Si}$ = 27.5 Hz), −14.8, −18.3, −26.8, −39.8 ($^1J_{P\text{-}Si}$ = 76.5 Hz), −125.3 ($^1J_{P\text{-}Si}$ = 3.3 Hz), −162.4 (v br), **^{31}P{^{1}H} NMR** (121.5 MHz, C_6D_6, 300 K): δ = −222.8 (br) and −230.4 ($^1J_{P\text{-}Si}$ = 100.7, 76.5 Hz).

5.3.9. Synthesis of Complex 153

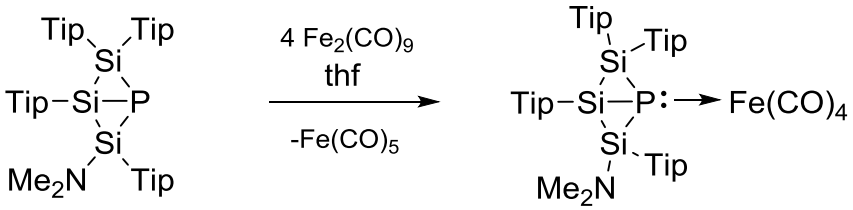

146 **153**

$C_{62}H_{98}NPSi_3$ $C_9Fe_2O_9$ $C_{66}H_{98}NPSi_3FeO_4$

972.70 g/mol 363.78 g/mol 1140.59 g/mol

After 220 mg (0.226 mmol) **146** and 400 mg (1.1 mmol) diiron nonacarbonyl are dissolved in thf and stirred for 48 hours a dark red solution is obtained. All volatiles are removed under vacuum and the residue is filtered from hexane over a small layer of celite. After the filtrate is reduced to dryness, the crude product is dissolved in pentane (1mL) and stored at room temperature. After one week, **153** is obtained as orange bocks (184 mg, 71%). **M.p.** 93°C (dec).

^{1}H NMR (300.13 MHz, C_6D_6, 300 K): δ = 7.36 (d, $^4J_{H\text{-}H}$ = 1.1 Hz, 1H, Tip-C*H*), 7.23 (d, $^4J_{H\text{-}H}$ = 1.3 Hz, 1H, Tip-C*H*), 7.18 (d, $^4J_{H\text{-}H}$ = 1.6 Hz, 1H, Tip-C*H*), 7.11 (d, $^4J_{H\text{-}H}$ = 1.5 Hz, 1H, Tip-C*H*), 7.06 (br, 2H, Tip-C*H*), 7.00 (br, 1H, Tip-C*H*), 6.91 (d, $^4J_{H\text{-}H}$ = 1.0 Hz, 1H, Tip-C*H*), 4.46 (sept, $^3J_{H\text{-}H}$ = 6.7 Hz, 1H, Tip-^{i}Pr-C*H*), 4.14 (sept, $^3J_{H\text{-}H}$ = 6.6 Hz, 2H, Tip-^{i}PrC*H*), 3.98 (sept, $^3J_{H\text{-}H}$ = 6.6 Hz, 1H, Tip-^{i}PrC*H*), 3.86 (sept, $^3J_{H\text{-}H}$ = 6.3 Hz, 2H, Tip-^{i}PrC*H*), 3.76 (sept, $^3J_{H\text{-}H}$ = 6.6 Hz, 2H, Tip-^{i}PrC*H*), 3.48 (sept, $^3J_{H\text{-}H}$ = 6.6 Hz, 1H, Tip-^{i}PrC*H*), 3.67 (sept, $^3J_{H\text{-}H}$ = 6.6 Hz, 1H, Tip-^{i}PrC*H*), 2.76 (m, 4H, Tip-^{i}PrC*H*),

2.13 (d, $^3J_{H\text{-}H}$ = 6.4 Hz, 3H, Tip-^{i}PrCH_3), 1.88 (br, NMe_2-CH_3 overlapping with d, $^3J_{H\text{-}H}$ = 6.6 Hz, Tip-^{i}PrCH_3, overall 9H), 1.70 (d, $^3J_{HH}$ = 6.3 Hz, 3H, Tip-^{i}PrCH_3), 1.62 (d, $^3J_{H\text{-}H}$ = 6.3 Hz, 3H, Tip-^{i}PrCH_3), 1.51 (d, $^3J_{H\text{-}H}$ = 6.3 Hz, 3H, Tip-^{i}PrCH_3), 1.47-1.38 (m, 6H, Tip-^{i}PrCH_3), 1.35-1.27 (m, 6H, Tip-^{i}PrCH_3), 1.26-1.16 (m, 18H, Tip-^{i}PrCH_3), 1.15 (d, $^3J_{H\text{-}H}$ = 2.0 Hz, 3H, Tip-^{i}PrCH_3), 1.13 (d, $^3J_{H\text{-}H}$ = 2.0 Hz, 3H, Tip-^{i}PrCH_3), 1.10 (d, $^3J_{H\text{-}H}$ = 2.0 Hz, 3H, Tip-^{i}PrCH_3), 0.92-0.85 (m, 6H, Tip-^{i}PrCH_3), 0.66 (d, $^3J_{H\text{-}H}$ = 6.1 Hz, 3H, Tip-^{i}PrCH_3), 0.62 (d, $^3J_{H\text{-}H}$ = 6.5 Hz, 6H, Tip-^{i}PrCH_3), 0.58 (d, $^3J_{H\text{-}H}$ = 6.5 Hz, 3H, Tip-^{i}PrCH_3), **^{13}C{^{1}H} NMR** (75.47 MHz, C_6D_6, 300 K): δ = 214.6 (d, $^2J_{CP}$ = 14.3 Hz, *C*=O), 158.7, 158.2, 156.7, 155.8, 155.2, 154.7, 154.5, 154.4, 152.7, 151.9, 151.4, 151.3, 132.6 (d, $^2J_{C\text{-}P}$ = 5.0 Hz), 130.1 (d, $^2J_{C\text{-}P}$ = 2.2 Hz), 129.4, 129.2, 124.9, 123.6, 123.5, 122.7, 122.6, 121.2, 121.1, 120.7 (Ar-*C*), 40.5 (br, NMe_2-*C*), 38.1, 38.0, 37.3, 36.5, 36.0, 35.9, 34.7, 34.3, 34.2, 33.1, 33.0, 28.1, 27.4, 27.1, 26.6, 26.5, 25.8, 25.7, 25.4, 25.3, 25.0, 24.9, 24.5, 24.2, 23.9, 23.7, 23.6, 20.9, **^{29}Si{^{1}H} NMR** (59.62 MHz, C_6D_6, 300 K): δ = −20.7 (d, $^1J_{Si\text{-}P}$ = 85.9 Hz), −68.8 (d, $^1J_{Si\text{-}P}$ = 37.4 Hz), −118.2 (d, $^1J_{Si\text{-}P}$ = 45.8 Hz) ppm, **^{31}P{^{1}H} NMR** (121.5 MHz, C_6D_6, 300 K): δ = −92.5 ($^1J_{Si\text{-}P}$ = 85.9, 45.8, 37.4 Hz) ppm; **UV/vis** (hexane): λ = 450 -300 nm (v br shoulder); **elemental analysis** calcd (%) for $C_{62}H_{98}NPSi_3$: C 69.50, H 8.66, N 1.23; found: C 69.11, H 8.33, N 1.44; **IR** (powder, cm^{-1}): 2036, 1960, 1944, 1926.

5.3.10. Synthesis of Disilaphosphiranide 155a

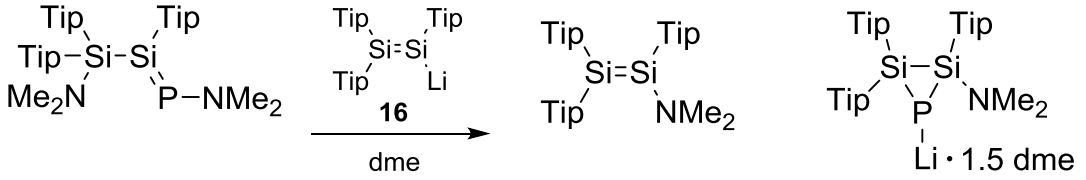

108a		**143**	**155a**
$C_{48}H_{81}N_2PSi_2$	$C_{53}H_{89}LiO_4Si_2$	$C_{47}H_{75}NSi_2$	$C_{53}H_{91}LiNO_3PSi_2$
785.34 g/mol	853.38 g/mol	710.29 g/mol	884.40 g/mol

A mixture of 2.026 g (2.37 mmol) disilenide **16** and 1.865 g (2.37 mmol) phosphasilene **108a** in 50 mL of dme is stirred at rt for 48 h. All volatiles are removed in vacuum. Repeated crystallization from pentane (containing a few drops of dme) at −20°C affords colorless single crystals of **155a** (yield: 579 mg, 22%). **M.p.** 151°C (dec).

^{1}H NMR (300.13 MHz, C_6D_6, 300 K): δ = 7.25 (d, $^4J_{H\text{-}H}$ = 1.5 Hz, 1H, Tip-C*H*), 7.17 (d, $^4J_{H\text{-}H}$ = 1.5 Hz 1H, Tip-C*H*), 7.07 (d, $^4J_{H\text{-}H}$ = 1.6 Hz, 1H, Tip-C*H*), 7.00 (br, 2H, Tip-C*H*), 6.98 (d, $^4J_{H\text{-}H}$ = 1.6 Hz, 1H, Tip-C*H*), 4.96 (sept, $^3J_{HH}$ = 7.2 Hz, 2H, Tip-^{i}Pr-C*H*), 4.25 (sept, $^3J_{H\text{-}H}$ = 6.8 Hz, 2H, Tip-^{i}PrC*H*), 4.15-3.67 (br m, 1H, Tip-^{i}PrC*H*), 2.89-2.74 br m, 4H, Tip-^{i}PrC*H*) overlapping with 2.86 (s, 9H, 3 x OCH_3), 2.82 (s, 6H, 1.5 x OC_2H_4O), 2.78 (s, 6H, NMe_2-CH_3), 1.68 (d, $^3J_{H\text{-}H}$ = 6.6 Hz, 3H, Tip-^{i}PrCH_3), 1.56-1.36 (m, 18H, Tip-^{i}PrCH_3), 1.31-1-10 (m, 22 H, Tip-^{i}PrCH_3), 0.99-0.83 (m, 11H, Tip-^{i}PrCH_3), **^{7}Li NMR** (116.6 MHZ, C_6D_6, 300 K): δ = −0.19, **^{13}C{^{1}H} NMR** (75.47 MHz,

C_6D_6, 300 K): δ = 155.6, 155.4, 153.6, 152.3, 148.2, 147.8, 147.6, 145.7 (d, $^2J_{C\text{-}P}$ = 4.0 Hz), 138.5 (d, $^2J_{C\text{-}P}$ = 4.8 Hz), 138.0 (d, $^2J_{C\text{-}P}$ = 6.6 Hz), 121.6, 121.3, 121.1, 120.9, 120.6 (Ar-*C*), 70.3 (O*C*$_2$H$_4$O), 58.9 (O*C*H$_3$), 41.2 (NMe-*C*H$_3$), 35.9, 35.3, 34.6, 34.5, 34.1, 34.0, 33.5, 33.4, 27.7, 27.3, 26.2, 26.1, 25.4, 24.3, 24.2, 24.1, 23.9, 23.7, 23.6, 22.5, 14.1(^{i}Pr-*C*H, ^{i}Pr-*C*H$_3$), **^{29}Si{^{1}H} NMR** (59.62 MHz, C_6D_6, 300 K): δ = −33.8 ($^1J_{P\text{-}Si}$ = 74.2 Hz, *Si*-NMe$_2$) and −68.1 ($^1J_{P\text{-}Si}$ = 67.4 Hz, *Si*Tip$_2$), **^{31}P{^{1}H} NMR** (121.5 MHz, C_6D_6, 300 K): δ = −249.1 (br); **elemental analysis** calcd (%) for $C_{106}H_{180}Li_2N_2O_6P_2Si_4$: C 72.06, H 10.27, N 1.59; found: C 71.20, H 10.28, N 1.43.
Small amounts of protonated **155b** are observed in the **^{31}P{^{1}H} NMR** (121.5 MHz, C_6D_6, 300 K): δ = −246.1 (7.4%), −255.3 (1.8%).

5.3.11. Synthesis of Disilaphosphirane 155b

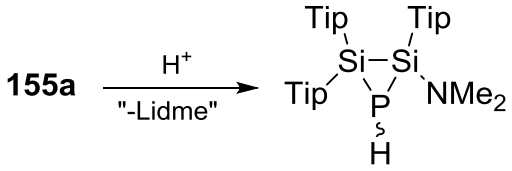

155b

$C_{47}H_{76}NPSi_2$
742.28 g/mol

In solution, **155a** is completely protonated to an *E/Z*-mixture of **155b** (ratio 2:1; no assignment of stereoisomers) after several weeks at room temperature.
^{1}H NMR (300.13 MHz, C_6D_6, 300 K): δ = 7.22 (m), 7.11 (br), 7.10 (br), 7.07 (br), 7.02 (br), 6.98 (br), 6.92 (br, each Tip-C*H*), 4.87 (m), 4.56 (sept, $^3J_{H\text{-}H}$ = 6.3 Hz, Tip-*i*Pr-C*H)*, 4.13 (sept, $^3J_{H\text{-}H}$ = 6.6 Hz, Tip-*i*Pr-C*H*), 3.97 (sept, $^3J_{H\text{-}H}$ = 6.8 Hz, Tip-*i*Pr-C*H*), 3.84 (sept, $^3J_{H\text{-}H}$ = 6.1 Hz, Tip-*i*Pr-C*H*), 3.60 (br m), 2.77 (m, Tip-*i*Pr-C*H*), 2.61 (s, 3H, N(Me$_2$)-C*H*$_3$), 2.39 (s, 6H, N(Me$_2$)-C*H*$_3$), 1.63 (d, $^3J_{H\text{-}H}$ = 6.3 Hz, Tip-*i*Pr-C*H*$_3$), 1.55 (d, $^3J_{H\text{-}H}$ = 6.3 Hz, Tip-*i*Pr-C*H*$_3$), 1.53-1.12 (br m, Tip-*i*Pr-C*H*$_3$), 0.92 (br, Tip-*i*Pr-C*H*$_3$), 0.75 (br, Tip-*i*Pr-C*H*$_3$), 0.69 (br, Tip-*i*Pr-C*H*$_3$), 0.67 (br, Tip-*i*Pr-C*H*$_3$), 0.64 (d, $^3J_{H\text{-}H}$ = 6.3 Hz, Tip-*i*Pr-C*H*$_3$), 0.59 (d, $^3J_{H\text{-}H}$ = 6.6 Hz, Tip-*i*Pr-C*H*$_3$), 0.32 (br, Tip-*i*Pr-C*H*$_3$), exact integration difficult due to partially overlapping resonances of two isomers (ratio 2:1); **13C{^{1}H} NMR** (75.47 MHz, C_6D_6, 300 K): δ = 157.8,157.2, 156.1, 155.9, 155.6, 155.41, 155.37, 155.2, 155.0, 154.9, 152.7, 152.2, 151.3, 150.2, 150.1 (Tip-*C*), 137.9, 134.9 (d, $^2J_{CP}$ = 1.6 Hz), 131.7 (d, $^2J_{C\text{-}P}$ = 4.0 Hz), 130.5 (d, $^2J_{CP}$ = 5.0 Hz), 129.8 (d, $^2J_{CP}$ = 1.5 Hz) 129.2 (d, $^2J_{C\text{-}P}$ = 7.3 Hz, Tip-*ipso-C*), 122.9, 122.7, 122.5, 122.3-121.6 (br), 122.3, 121.84, 121.76, 121.5, 121.3, 120.8, 119.8 (Tip-*C*H), 40.6, 40.4(NMe$_2$-*C*), 37.5, 37.1, 36.0, 35.8, 35.7, 34.7, 34.5, 34.3, 33.3, 33.2, 32.4, 32.1, 30.0, 29.0, 27.3, 27.1, 26.6, 25.7, 25.6, 24.8, 24.6, 24.3, 23.9, 23.0, 22.9, 22.6 (Tip-*i*Pr-*C*H, Tip-*i*Pr-*C*H$_3$) ppm ; **^{29}Si{^{1}H} NMR** (59.62 MHz, C_6D_6, 300 K): δ = −42.1 (d, $^1J_{Si\text{-}P}$ = 30.9 Hz, Tip*Si*NMe$_2$), −74.1 (d, $^1J_{Si\text{-}P}$ = 25.1 Hz, SiTip$_2$, major isomer), −35.9

(d, $^{1}J_{Si\text{-}P}$ = 38.4 Hz, Tip*Si*NMe$_2$), −67.7 (d, $^{1}J_{Si\text{-}P}$ = 15.3 Hz, *Si*Tip$_2$, minor isomer) **^{31}P{^{1}H} NMR** (121.5 MHz, C_6D_6, 300 K): δ = −246.2, −255.3 (ratio 2:1) ppm.

5.3.12. Synthesis of Amino Disilene 143

The mother liquor of the first crystallization of **155a** is removed *via* cannula. Subsequently, the deep red solution is reduced to dryness to afford crude **143.**
^{1}H NMR (300.13 MHz, C_6D_6, 300 K): δ = 7.13 (br, 2H, Tip-C*H*), 7.12 (br, 2H, Tip-C*H*), 7.01 (br, 2H, Tip-C*H*), 4.30 (m, 4H, Tip-*i*Pr-C*H*), 3.79 (sept, $^{3}J_{H\text{-}H}$ = 6.6 Hz, 2H, Tip-*i*Pr-C*H)*, 2.76 (m, Tip-*i*Pr-C*H* overlapping with residual dme), 2.29 (s, 6H, N(Me$_2$)-C*H*$_3$), 1.39-1.04 (m, Tip-*i*Pr-C*H*$_3$), **^{13}C{^{1}H} NMR** (75.47 MHz, C_6D_6, 300 K): δ = 155.7, 155.4, 153.6, 151.7, 150.4, 149.0 (Tip-C), 136.9, 136.1, 132.4 (Tip-ipso-*C*), 121.43, 121.36, 121.1 (Tip-*C*H) 41.3 (NMe$_2$-*C*), 38.5, 38.2, 37.0, 34.8, 34.6, 34.4 (Tip-*i*Pr-*C*H), 25.3, 24.9, 24.5, 24.4, 24.1, 24.0 (some br, Tip-*i*Pr-CH$_3$) ppm, **^{29}Si{^{1}H} NMR** (59.62 MHz, C_6D_6, 300 K): δ = 95.5 (Tip*Si*NMe$_2$), 26.2 (*Si*Tip$_2$).

5.3.13. Synthesis of 159

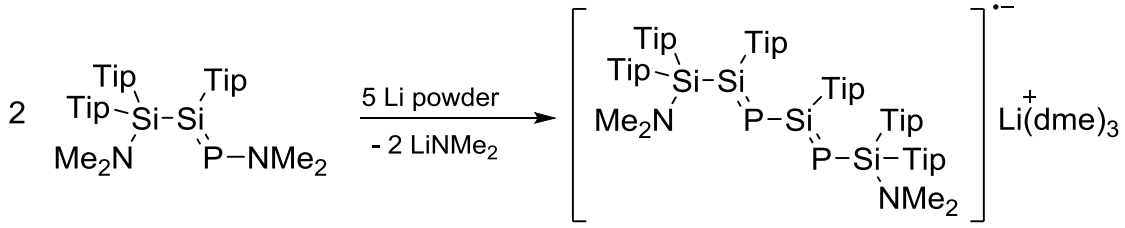

108a **159**

$C_{48}H_{81}N_2PSi_2$ Li $C_{106}H_{180}LiN_2O_6P_2Si_4$
785.34 g/mol 6.94 g/mol Molecular Weight: 1759,84

500 mg (0.637 mmol) **108a** was dissolved in 25 mL dme in transferred quickly *via* cannula to a vigorously stirred suspension of 25 mg (5 equivalents) lithium powder in dme. The suspension turned deep red-brown. After stirring overnight, all volatiles were removed in vacuo. **^{31}P{^{1}H} NMR** (121.5 MHz, C_6D_6, 300 K): more than 20 resonances observed, main products: δ = −134.2 (br), −156.0 (d, $J_{P\text{-}P}$ = 33.0 Hz), −174.2 (br), −187.6 (d, $J_{P\text{-}P}$ = 33.0 Hz), −206.3 ppm, −220.2, −231.8. The residue was digested with hexane and filtered. The red-brown solution was concentrated to 1 mL and standing overnight afforded orange single crystals as small plates. The synthesis is unreproducible and the crystals were very sensitive and unstable. Decomposition to an oily residue was observed several days after X-ray structure analysis was done to reveal the constitution of **159**.

5.3.14. Synthesis of 160

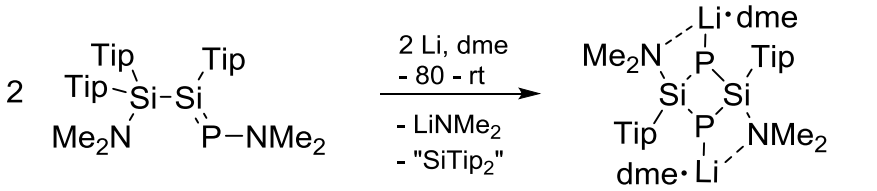

108a **160**

$C_{48}H_{81}N_2PSi_2$	Li	$C_{42}H_{78}Li_2N_2O_4P_2Si_2$
785.34 g/mol	6.94 g/mol	807.09 g/mol

A suspension of 8.7 mg lithium powder (1.26 mmol) in 20 mL dme was stirred at −80°C. 500 mg (0.637 mmol) **108a** were dissolved in 20 mL dme, cooled to −80°C and added quickly *via* cannula to the lithium powder/dme suspension. Upon warming to rt, the yellow suspension turned red slowly (−80-5°C). At 5°C the suspension turned deep green suddenly. After rt was reached, an intense red color was observed again. The solvent was removed under reduced pressure and the dark residue digested with hexane. All insoluble parts (*i. a.* lithium powder) were filtered off and a red solution was obtained. **$^{31}P\{^1H\}$ NMR** (121.5 MHz, C_6D_6, 300 K): main resonances : −178.0 (br), −188.4, −207.1, −232.5, −254.9 (v br), −260.3 (br). The solution was concentrated to 1 mL and standing overnight afforded black precipitate and a small amount of colorless crystals. An X-ray diffraction study showed the constitution of **160**.

5.3.15. Reaction of 108a with Potassium Graphite

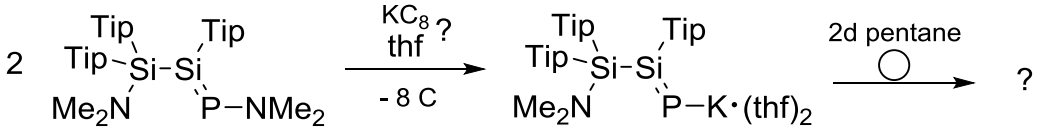

108a **154b**

$C_{48}H_{81}N_2PSi_2$	C_8K	$C_{55}H_{91}KNO_2PSi_2$
785.34 g/mol	135.19 g/mol	924.58 g/mol

1.5 g (1.905 mmol) **108a** are dissolved in 20 mL thf and added *via* cannula to a vigorously stirred suspension of two equivalents KC_8 in 20 mL thf. The suspension turns deep orange immediately and formation of black precipitate is observed. After stirring for one hour at room temperature, the reaction mixture is filtered and all volatiles are removed in vacuum to afford an orange foam.
$^{29}Si\{^1H\}$ NMR (59.62 MHz, thf-d_8, 300 K): δ = 1.1 ($^2J_{P\text{-}Si}$ = 44.7 Hz), −25.1, −56.2 ($^1J_{P\text{-}Si}$ = 139.8 Hz) ppm, **$^{31}P\{^1H\}$ NM**R (121.5 MHz, thf-d_8, 300 K): δ = 152.5 ($^1J_{P\text{-}Si}$ = 139.8 Hz, $^2J_{P\text{-}Si}$ = 44.7 Hz).

The residue is dissolved in hexane and allowed to stand at room temperature for 24 h.

^{1}H NMR (300.13 MHz, C_6D_6, 300 K): *selected resonances*: δ = 2.57 (d, $^{3}J_{P\text{-}H}$ = 9.4 Hz, PN(C*H*$_3$)$_2$), 2.41 (d, $^{3}J_{P\text{-}H}$ = 9.6 Hz, P(NC*H*$_3$)$_2$), **^{13}C{^{1}H} NMR** (75.47 MHz, C_6D_6, 300 K): *selected resonances*: δ = 46.3 (d, $^{2}J_{P\text{-}C}$ = 13.2 Hz, PN(*C*H$_3$)$_2$), 45.6 (d, $^{2}J_{P\text{-}C}$ = 10.5 Hz, PN(*C*H$_3$)$_2$), **^{29}Si{^{1}H} NMR** (59.62 MHz, C_6D_6, 300 K): δ = −8.3 ($^{1\text{ or }2}J_{P\text{-}Si}$ = 33.0 Hz), −25.1, −59.5 ($^{1}J_{P\text{-}Si}$ = 74.6 Hz). **^{31}P{^{1}H} NMR** (121.5 MHz, C_6D_6, 300 K): δ = 106.9 ($^{1}J_{P\text{-}Si}$ = 74.6 Hz, $^{1\text{ or }2}J_{P\text{-}Si}$ = 33.0 Hz).

5.4. Synthesis of Phosphasilaindoline 162

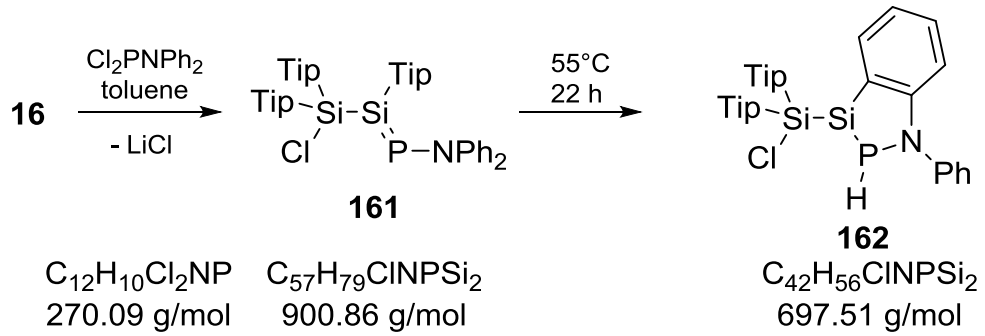

$C_{12}H_{10}Cl_2NP$ 270.09 g/mol

$C_{57}H_{79}ClNPSi_2$ 900.86 g/mol

$C_{42}H_{56}ClNPSi_2$ 697.51 g/mol

500 mg disilenide (0.585 mmol) are dissolved in 20 mL toluene and cooled to −80°C. The solution is transferred quickly *via* cannula to a −80°C cold solution of Cl_2PNPh_2 in 15 mL toluene. Upon on warming to room temperature, the orange solution becomes a red suspension and quantitative formation of β-chloro *P*-amino phosphasilene **161** is observed.

^{1}H NMR (300.13 MHz, C_6D_6, 300 K): δ = 7.04 (br, 4 H, Ar-C*H*), 6.96 (br, = 3 H, Ar-C*H*), , 6.93, 6.90, 6.88 (each br, each 2H, Ar-C*H*), 6.85 (br, 1H, Ar-C*H*), 6.72 (br, 2H, Ar-CH), 3.71 (sept, $^{3}J_{H\text{-}H}$ = 6.7 Hz, 4H, Tip-^{i}PrC*H*), 3.56 (sept, $^{3}J_{H\text{-}H}$ = 6.7 Hz, 2H, Tip-^{i}PrC*H*), 1.23-1.02 (m, 48H, Tip-^{i}PrC*H*$_3$), 0.84 (br, 6H, Tip-^{i}PrC*H*$_3$), **^{13}C{H} NMR** (75.47 MHz, C_6D_6, 300 K): δ = 155.2, 154.3, 152.9, 151.5 (br), 151.3, 133.6, 131.2, 131.0, 129.1, 123.8 (br), 123.7, 122.8, 122.2, 121.8 (Ar-*C*H), 38.2 (br), 35.2 (br), 34.7, 34.4, 25.2 (br), 25.1, 24.9, 24.2, 24.0, 23.8, 23.7 (Tip-*C*H and Tip-*C*H$_3$), **^{29}Si{H} NMR** (59.62 MHz, C_6D_6, 300 K): δ = 204.4 ppm ($^{1}J_{P\text{-}Si}$ = 217.3 Hz), −5.7 ppm ($^{2}J_{P\text{-}Si}$ = 23.0 Hz, **^{31}P{H} NMR** (121.5 MHz, C_6D_6, 300 K): δ = 315.6 (br).

The solution of **161** is filtered and accordingly kept at −78°C, however, attempts to obtain single crystals of **161** are not successful as yet.

The protocol described for **161** is repeated exactly. After the reaction mixture has reached room temperature, it is heated to 55°C for 22 h. The color changes to pale green-yellow. All volatiles are removed in vacuum, and the residue is digested with pentane (25 mL). The mixture is filtered over a small layer of celite and the volume of the filtrate is reduced to approximately 1 mL in vacuum. Standing at rt overnight affords 310 g (yield: 59%) **162** as very pale yellow crystals. **M. p.** 152-156°C (dec.).

^{1}H NMR (300.13 MHz, C_6D_6, 300 K): δ = 8.83 (dd, $^{3}J_{H\text{-}H}$ = 8.0 Hz, $^{4}J_{H\text{-}H}$ = 1.6 Hz, 1H, SiCC*H*), 6.96 (br, = 3 H, Ar-C*H*), 7.12-6.68 (m, 15H, Ar-C*H*), δ = 6.38 (d, $^{1}J_{P\text{-}H}$ = 158.7 Hz, 1H, P*H*), 4.39 (sept, $^{3}J_{H\text{-}H}$ = 6.3 Hz, 1H, Tip-^{i}PrC*H*), 4.00 (sept, $^{3}J_{H\text{-}H}$ = 6.6 Hz, 2H, Tip-^{i}PrC*H*), 3.19 (br, 1H, Tip-^{i}PrC*H*), 2,67 m, 3H, Tip-^{i}PrC*H*), 1.56-1.04 (br m, Tip-^{i}PrCH_3), 0.78 (d, $^{3}J_{H\text{-}H}$ = 6.6 Hz, 3H, Tip-^{i}PrCH_3), 0.48 (d, $^{3}J_{H\text{-}H}$ = 6.6 Hz, 3H, Tip-^{i}PrCH_3), 0.41 (d, $^{3}J_{H\text{-}H}$ = 6.6 Hz, 6H, Tip-^{i}PrCH_3), 0.31 (d, $^{3}J_{H\text{-}H}$ = 6.6 Hz, 3H, Tip-^{i}PrCH_3), 0.20 (d, $^{3}J_{H\text{-}H}$ = 6.6 Hz, 3H, Tip-^{i}PrCH_3), **^{13}C{^{1}H} NMR** (75.47 MHz, C_6D_6, 300 K): δ = 155.7, 155.6, 153.1, 152.1, 151.1, 151.0, 150.9, 149.3, 138.7, 136.8, 132.0, 130.3, 129.5, 128.6, 126.5, 126.4, 124.6, 124.1 (Ar-*C*H), 38.3 (br), 36.9, 34.5, 34.2, 34.1, 32.3, 26.5, 26.4, 25.4, 25.3, 23.9, 23.6, 23.5, 22.2 (Tip-*C*H and Tip-*C*H_3), **^{29}Si{^{1}H} NMR** (59.62 MHz, C_6D_6, 300 K): δ = −0.5, −21.0 (d, $^{1}J_{P\text{-}Si}$ = 30.0 Hz), **^{31}P{^{1}H} NMR** (121.5 MHz, C_6D_6, 300 K): δ = −29.1 ($^{1}J_{P\text{-}Si}$ = 30.0 Hz); **elemental analysis** calcd (%) for $C_{57}H_{79}ClNPSi_2$: C 76.00, H 8.84, N 1.55; found: C 75.59, H 8.82, N 1.43.

5.5. An NHC-stabilized Cyclic Phosphasilene

5.5.1. Reaction of Disilenide 16 with 149[BPh$_4$]

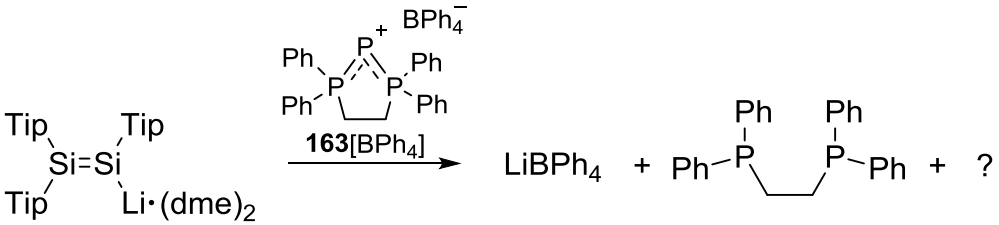

$C_{53}H_{89}LiO_4Si_2$ 853.38 g/mol | $C_{50}H_{44}BP_3$ 748.63 g/mol | $C_{24}H_{20}BLi$ 326.17 g/mol | $C_{26}H_{24}P_2$ 398.43 g/mol

438 mg (0.585 mmol) **149**[BPh_4] were dissolved in 30 mL of thf and cooled to −80°C. A solution of one equivalent disilenide **16** (500 mg) was cooled to −80°C and added to the stirred solution of **149**[BPh_4] within three minutes. Formation of an intense green solution was observed immediately. The reaction mixture was allowed to warm up to room temperature in the thawing cold bath. Subsequently all volatiles were removed in vacuum. In the hetero nuclear NMR spectra formation of lithium tetraphenylborate and free dppe could be observed exclusively. **^{11}B NMR** (96.3 MHz, C_6D_6, 25°C): δ = −6.5, **^{31}P{H} NMR** (121.5 MHz, C_6D_6, 300 K): −12.8. The dark green residue digested with hexane. The suspension was filtered and dried to afford a green foam.

5.5.2. Synthesis of 166

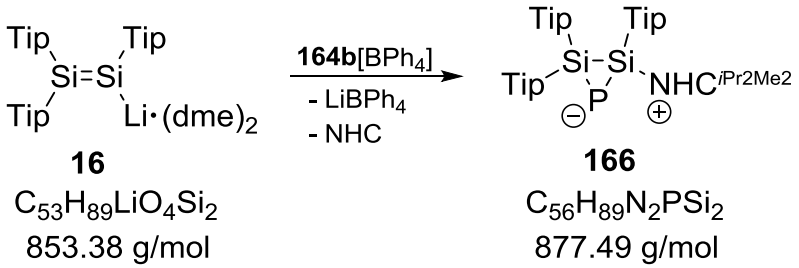

16
$C_{53}H_{89}LiO_4Si_2$
853.38 g/mol

166
$C_{56}H_{89}N_2PSi_2$
877.49 g/mol

A solution of 1.2 g (1.40 mmol) disilenide **108** in 30 mL thf is cooled to −80°C and added *via* cannula to −80°C cold solution of 1.0 g (1.40 mmol) **164b**[BPh_4] in 50 mL thf. The orange reaction mixture is allowed to warm up to room temperature within 4 hours. Subsequently, all volatiles are removed in vacuum. One equivalent free 1,3-diisopropyl-4,5-dimethylimidazol-2-ylidene formed in the course of the reaction is sublimed out in high vacuum (12 h, $2x10^{-2}$ mbar, rt). The residue is digested with hexane and filtered. After the filtrate is reduced to dryness, the crude product is dissolved in 3 mL pentane. Standing overnight at room temperature affords 0.58 g **166** as yellow crystals. **M. p.** 200-205°C (dec). Concentration of the motherliquor to half of the volume affords another batch of microcrystalline powder (0.51g) of 166. Overall yield: 89 %.

^{1}H NMR (300.13 MHz, C_6D_6, 300 K): δ = 8.61 (hept, $^3J_{H-H}$ = 6.5 Hz, 1H, NHC-^{i}Pr-C*H*), 7.21 (br, 1H, Tip-*H*), 7.11 (br, 3H, Tip-*H*), 7.09 (br, 1H, Tip-*H*), 7.03 (br, 3H, Tip-*H*), 7.01 (br, 1H, Tip-*H*), 6.98 (br, 3H, Tip-*H*), 6.68 (br hept, 1H, Tip-^{i}Pr-C*H*), 6.41 (hept, $^3J_{H-H}$ = 6.5 Hz, 1H, Tip-^{i}Pr-C*H*), 6.23 (br hept, 2H, Tip-^{i}Pr-C*H* overlapping with NHC-^{i}Pr-C*H*), 5.36 (hept, $^3J_{H-H}$ = 6.5 Hz, 1H, NHC-^{i}Pr-C*H*), 5.14 (hept, $^3J_{H-H}$ = 6.9 Hz, 1H, NHC-^{i}Pr-C*H*), 4.92 (hept, $^3J_{H-H}$ = 6.7 Hz, 1H, Tip-^{i}Pr-C*H*), 4.61 (hept, $^3J_{H-H}$ = 6.2 Hz, 1H, Tip-^{i}Pr-C*H*), 4.46 (hept, $^3J_{H-H}$ = 6.2 Hz, 1H, Tip-^{i}Pr-C*H*), 4.16 (hept, $^3J_{H-H}$ = 6.2 Hz, 1H, Tip-^{i}Pr-C*H*), 3.87 (m, 6H, hept, Tip-^{i}Pr-C*H* overlapping with NHC-^{i}Pr-C*H*), 2.81 (m, 8H, Tip-^{i}Pr-C*H*), 1.82 (d, $^3J_{H-H}$ = 6.2 Hz, 1H, Tip-^{i}Pr-CH_3), 1.63-1.13 (br 0.62 (br m, 8H, Tip-^{i}Pr-CH_3), 0.58-0.49 (br m, 13H, Tip-^{i}Pr-CH_3), 0.45 (d, $^3J_{H-H}$ = 6.9 Hz, 1H, Tip-^{i}Pr-CH_3), 0.31 (d, $^3J_{H-H}$ = 6.5 Hz, 1H, Tip-^{i}Pr-CH_3), **^{13}C{^{1}H} NMR** (75.47 MHz, C_6D_6, 300 K): δ = 162.2 (d, $^2J_{C-P}$ = 9.4 Hz, N*C*N), 159.1, 158.1, 157.5, 156.9 (d, $^2J_{C-P}$ = 9.4 Hz, N*C*N), 156.1, 155.7, 155.5, 155.2, 155.0, 154.1, 151.4, 149.8, 149.1, 148.8, 148.6, 147.5, 147.4 (Tip-*C*), 144.7 (d, $^2J_{C-P}$ = 6.6 Hz), 142.9 (d, $^2J_{C-P}$ = 6.6 Hz), 138.7 (d, $^2J_{C-P}$ = 7.7 Hz), 137.4 (d, $^2J_{C-P}$ = 4.6 Hz), 135.7 (d, $^2J_{C-P}$ = 4.6 Hz), 132.8 (d, $^2J_{C-P}$ = 6.2 Hz) (Tip-*ipso*-C), 128.6, 126.3, 124.3, 123.8 (br), 122.3, 122.1, 121.8, 121.7, 121.5, 121.3, 120.4 (br) 120.1, (Tip-*C*H), 53.3, 53.1, 52.8, 49.4 (br), 48.5, 48.2 (NHC-^{i}Pr-*C*H), 36.4, 35.7, 35.6, 35.4, 35.2, 35.1, 34.8, 34.6, 34.5, 34.4, 34.3, 31.8, 31.1, 29.5, 29.3, 29.2, 29.1, 28.8, 28.5, 27.9, 21.2, 26.4, 25.9, 25.7, 25.6, 25.5, 25.4, 25.3, 25.2, 25.1, 24.8, 24.7, 24.6, 24.5, 24.3, 24.1, 24.0, 23.9, 23.8, 23.5, 22.8, 21.3, 21.1, 20.9, 20.8, 20.6, 20.5, 20.1, 19.9 (Tip-^{i}Pr-*C*H, Tip-^{i}Pr-*C*H_3, NHC-^{i}Pr-*C*H_3), 14.2, 10.2, 10.0, 9.9, 9.7, 8.5 (NC(*C*H_3)=C(*C*H_3)N, **^{29}Si{^{1}H} NMR** (59.62 MHz, 300 K, C_6D_6): δ = −68.7 ($^1J_{P-Si}$ = 91.8 Hz), −68.9 ($^1J_{P-Si}$ = 107.4 Hz), −69.9 ($^1J_{P-Si}$ = 105.3 Hz), −73.6 ($^1J_{P-Si}$ = 97.4Hz); **^{31}P{^{1}H} NMR** (121.5 MHz, C_6D_6, 300 K): δ = −252.2,

−267.9 ppm (ratio 1 : 0.9); **Solid state $^{31}P\{^{1}H\}$ NMR:** −255.8, −270.5 (ratio 1:0.9), even though the ^{29}Si and ^{31}P NMR spectra indicate very pure material, the ^{1}H and ^{13}C NMR data hint towards formation of a NHC-related side product that cannot be removed by crystallization. However, exact integration/assignment appeared to be difficult due to partially overlapping resonances of the two stereo isomers in the ratio 1:0.9; **UV/vis** (hexane): λ = 336 nm (ε = 8700 $M^{-1}cm^{-1}$); **elemental analysis** calcd (%) for $C_{56}H_{86}NPSi_2$: C 76.65, H 10.22, N 3.19; found: C 76.27, H 10.03, N 2.50.

5.5.3. Synthesis of 167

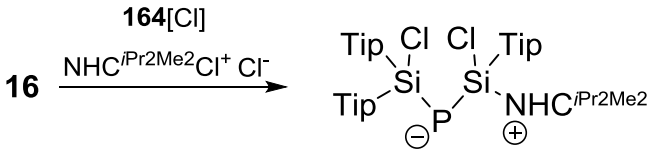

167

$C_{56}H_{89}N_2Cl_2PSi_2$

948.39 g/mol

A mixture of **164b**[Cl] (2.19 mmol) and 1,3-diisopropyl-4,5-dimethylimidazolium chloride (protocol comp. 5.2.17) in thf is cooled to −80°C and a solution of one equivalent disilenide **16** (1.88 g) in 70 mL thf cooled to −80°C is added rapidly *via* cannula. The reaction mixture is stirred overnight in the thawing cold bath and turns orange. Subsequently, all volatiles are removed in vacuum and the residue is digested with 70 mL hexane. Insoluble materials are removed by filtration. To the motherliquor 1.5 equivalents $ZnCl_2$ are added to trap free NHC and stirred overnight. Precipitated $ZnCl_2$·NHC is removed by filtration and the filtrate concentrated to dryness to afford a pale orange foam. Pentane (3 mL) is added and standing for two weeks affords 440 mg single crystals of **167** (21.5 %) that were used for an X-ray diffraction study. However, this batch of crystals contained small amounts of impurities (5% according to ^{31}P NMR spectroscopy). Recrystallization from 1 mL of pentane afforded 113 mg (6 %) pure material. **M. p.** 232-235°C (dec).
^{1}H NMR (300.13 MHz, C_6D_6, 300 K): δ = 7.10-6.99 (br, 6 H, Tip-C*H*), 5.95 (hept, $^{3}J_{H-H}$ = 7.2 Hz, 1H, NHC-^{i}Pr-C*H*), 5.67-3.64 (v br, NHC-^{i}Pr-C*H*, Tip-^{i}Pr-C*H*), 2.87-2.67 (m, 6H, ^{i}Pr-C*H*), 1.69-0.84 (v br m, NHC-^{i}Pr-CH_3, Tip-^{i}Pr-CH_3), **$^{13}C\{H\}$ NMR** (75.47 MHz, C_6D_6, 300 K): δ = 155.4, 154.2, 153.8, 150.1, 148.8, 148.7, 140.2, 135.8, 127.1, 125.3, 122.4 (most br, N*C*N, NHC-N*C*(CH_3)=*C*(CH_3)N, Tip-C*H*), 52.4 (NHC-^{i}Pr-*C*H), 34.7, 34.6, 33.2 (v br), 26.1-24.7 (v br), 24.3, 24.1, 22.2, 20.6 (br), 10.2 (NHC-NC(*C*H_3)=C(*C*H_3)N, **$^{29}Si\{H\}$ NMR** (59.62 MHz, C_6D_6, 300 K): δ = 10.1, 7.7 (each v br), **$^{31}P\{H\}$ NMR** (121.5 MHz, C_6D_6, 300 K): δ = −203.3 (br); **elemental analysis** calcd (%) for $C_{58}H_{88}FeN_2O_3PSi_2$: C 70.36, H 9.48, N 2.99; found: C 70.65, H 9.38, N 2.43.

5.5.4. Attempted Reaction of 166 with Phenylacetylene

In an NMR tube, 100 mg (0.12 mmol) **166** were dissolved in C_6D_6 and one equivalent phenylacetylene (13 μL) added *via* micro syringe. After 12 h at 80°C, only starting material was detected.

5.5.5. Attempted Reactions of 166 with Isonitriles

a) In an NMR tube, 80 mg (0.09 mmol) **166** were dissolved in C_6D_6 and 10 μL (0.09 mmol) *tert*.-butyl isonitrile were added *via* micro syringe. After 12 h of heating to 60°C the NMR spectra revealed just unchanged **166**.
b) In an NMR tube, 100 mg (0.12 mmol) **166** were dissolved in C_6D_6 and 13.1 mg (0.12 mmol) xylyl isonitrile were added *via* micro syringe. After 12 h of heating to 60°C the NMR spectra revealed just unchanged **166**.

5.5.6. Attempted Reactions of 166 with Triphenylborane

In an NMR tube, 95 mg (0.11 mmol) **166** was dissolved in C_6D_6 and three equivalents of triphenylborane (70 mg) were added. No reaction occurred, even after heating to 80°C overnight.

5.5.7. Attempted Reactions of 166 with ^{Me4}NHC

In an NMR tube, 100 mg (0.12 mmol) **166** were dissolved in C_6D_6 and one equivalent (15 mg) 1,3,4,5-tetramethylimidazol-2-ylidene were added. After 12 h of heating to 80°C the NMR spectra revealed just unchanged **166.**

5.5.8. Synthesis of Tetracarbonyliron Complex 168

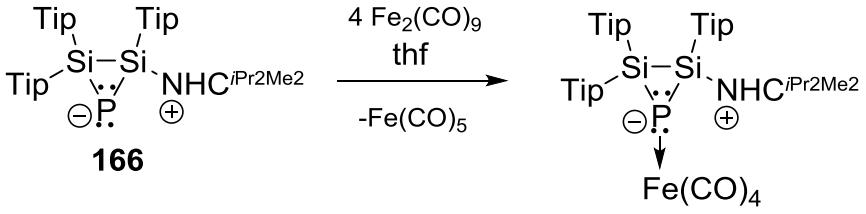

$C_{56}H_{89}N_2PSi_2$	$C_9Fe_2O_9$	$C_{60}H_{89}N_2O_4PSi_2Fe$
877.49 g/mol	363.78 g/mol	1045.37 g/mol

205 mg (0.23 mmol) **166** and 100.5 mg diiron nonacarbonyl (0.29 mmol) are mixed and 1.5 mL toluene is added. After 15 minutes of stirring at rt, the yellow-orange suspension turns deep red. Stirring is continued for 12 h. Subsequently, all volatiles

are removed in vacuo and 30 mL of toluene added to the mixture. The red solution is filtered and the filtrate reduced to approximately 0.5 mL in vacuo. Standing overnight at room temperature affords 220 g (yield: 91%) **168** as orange blocks. **M.p.** 153°C (dec).

^{1}H NMR (300.13 MHz, C_6D_6 , 300 K): , δ = 7.28 (br, 1H, Ar-C*H*), 7.21 (br, 1H, Ar-C*H*), 7.05 (br, 1H, Ar-C*H*), 7.03 (br, 1H, Ar-C*H*), 6.98 (br, 2H, Ar-C*H*), 5.30 (br, 1H, NHC-^{i}Pr-C*H*), 5.15 (br, 1H, NHC-^{i}Pr-C*H*), 4.70 (br, 1H, Tip-^{i}Pr-C*H*), 3.93 (br, 1H, Tip-^{i}Pr-C*H*), 3.82 (br, 1H, Tip-^{i}Pr-C*H*), 3.44 (br, 1H, Tip-^{i}Pr-C*H*), 3.31 (br, 1H, Tip-^{i}Pr-C*H*), 2.91-2.60 (br, 4H, Tip-^{i}Pr-C*H*), 1.85-1.06 (v br m, 42H, Tip-^{i}Pr-CH_3 and NHC-^{i}Pr-CH_3), 0.73 (d, $^{3}J_{H\text{-}H}$ = 5.0 Hz, Tip-^{i}Pr-CH_3), 0.52 (br, 9H, Tip-^{i}Pr-CH_3), 0.33 (br, 6H, Tip-^{i}Pr-CH_3), **^{13}C{H} NMR** (75.47 MHz, C_6D_6, 300 K): δ = 221.9 (d, $^{2}J_{C\text{-}P}$ = 11.3 Hz, Fe-*C*O), 158.3 (Ar-*C*) 157.9 (d, $^{2}J_{C\text{-}P}$ = 17.5 Hz, N*C*N) 157.3, 156.5, 154.9, 154.0, 153.5, 151.9, 151.4, 150.1, 149.1, 149.0 (Ar-*C* and N*C*(CH_3)=*C*(CH_3)N) 137.9 (d, $^{2}J_{C\text{-}P}$ = 10.3 Hz), 136.3 (d, $^{2}J_{C\text{-}P}$ = 7.7 Hz), 132.8 (Ar-ipso-*C*), 125.0, 122.6, 122.4, 121.9, 121.1, 120.9 (Ar-ipso-*C*), 53.6, 53.2 (NHC-^{i}Pr-*C*H), 37.3, 36.3, 36.1, 35.6, 34.8, 34.7, 34.6, 34.4, 33.2, 32.9, 32.8, 28.7, 28.0, 26.7, 26.4, 26.2, 25.6, 25.2, 25.1, 24.5, 24.2, 24.1, 24.0, 22.5, 21.6, 21.5, 21.0, 19.9 (^{i}Pr-*C*H and ^{i}Pr-*C*H_3), 10.4, 10.2 (NC(*C*H_3)=C(*C*H_3)N), **^{29}Si{H} NMR** (59.62 MHz, C_6D_6, 300 K): δ = −59.5 ($^{1}J_{P\text{-}Si}$ = 74.9 Hz), −62.2 ($^{1}J_{P\text{-}Si}$ = 62.0 Hz), **^{31}P{H} NMR** (121.5 MHz, C_6D_6, 300 K): δ = −245.9, −267.7 (ratio 89:11); **UV/vis** (hexane): λ = 460-340 (br shoulder); **elemental analysis** calcd (%) for $C_{60}H_{89}N_2O_4PSi_2$: C 68.94, H 8.58, N 2.68; found: C 68.57, H 8.63, N 2.44. **IR** (powder): ν(CO) = 2025, 1930, 1907 and 1890 cm^{-1}.

5.5.9. Rearrangement of 168 to Disilaferraphospha[1.1.0]bicyclobutane Derivative 169

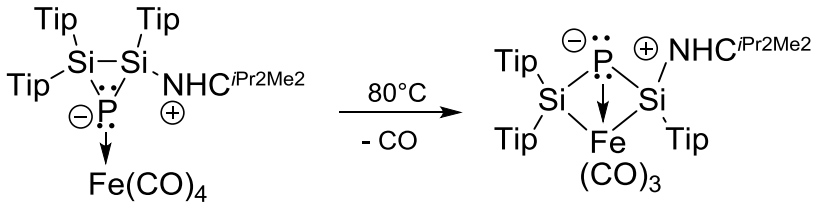

168 $C_{60}H_{89}N_2O_4PSi_2Fe$ 1045.37 g/mol

169 $C_{59}H_{89}N_2O_3PSi_2Fe$ 1017.36 g/mol

220 g (0.21 mmol) **168** are dissolved in 5 mL toluene and the solution is heated to 80°C for 17 h. All volatiles are removed in vacuo and subsequently 30 mL of toluene are added to the residue. The mixture is filtered and the filtrate reduced to approximately 2 mL. Standing at rt for three days affords 50 mg of **169** as orange blocks. The mother liquor is concentrated to half of the volume and standing at rt for several days yields another batch of microcrystalline precipitate (55 mg) of **169**. Overall yield: 48 %. **M.p.** 163°C (dec).

^{1}H NMR (300.13 MHz, thf-d_8, 300 K): δ = 7.08 (br, 1H, Tip-C*H*), 6.89 (br, 1H, Tip-C*H*), 6.86 (br, 2H, Tip-C*H*), 6.78 (br, 1H, Tip-C*H*), 6.77 (br, 1H, Tip-C*H*), 5.80 (v br, 2H, NHC-^{i}Pr-C*H*), 4.52 (hept, $^{3}J_{H-H}$ = 6.8 Hz, Tip-^{i}Pr-C*H*) partially overlapping with 4.44-4.21 (br, Tip-^{i}Pr-C*H*, overall 3H), 4.14 (hept, $^{3}J_{H-H}$ = 6.0 Hz, 1H, Tip-^{i}Pr-C*H*), 3.58 (hept, $^{3}J_{H-H}$ = 6.8 Hz, Tip-^{i}Pr-C*H* overlapping with thf-d_8), 2.74 (m, 3H, Tip-^{i}Pr-C*H*), 2.29 (s, 6H, NC(CH_3)=C(CH_3)N), 1.30 (br d, $^{3}J_{H-H}$ = 6.6 Hz, 6H, Tip-^{i}Pr-CH_3), 1.22 (br, 3H, Tip-^{i}Pr-CH_3), 1.20 (br, 4H, Tip-^{i}Pr-CH_3), 1.18 (br, 4H, Tip-^{i}Pr-CH_3), 1.17 (br, 4H, Tip-^{i}Pr-CH_3), 1.16 (br, 3H, Tip-^{i}Pr-CH_3), 1.15 (br, 3H, Tip-^{i}Pr-CH_3), 1.12, 1.10, 1.09, 1.08 (each br, each 3H, each Tip-^{i}Pr-CH_3), 1.00 (d, $^{3}J_{H-H}$ = 6.2 Hz), 0.81-0.73 (v br, 3H, Tip-^{i}Pr-CH_3), 0.44 (d, $^{3}J_{H-H}$ = 6.4 Hz, 3H, Tip-^{i}Pr-CH_3), 0.36 (d, $^{3}J_{H-H}$ = 5.5 Hz, 3H, Tip-^{i}Pr-CH_3), 0.05 (d, $^{3}J_{H-H}$ = 5.5 Hz, 3H, Tip-^{i}Pr-CH_3), **^{13}C{H} NMR** (75.47 MHz, thf-d_8, 300 K): δ = 219.9 (Fe-*C*O), 158.8 (d, $^{2}J_{C-P}$ = 20.8 Hz, N*C*N), 156.3, 155.7, 154.7, 154.3, 154.1, 151.8, 148.9, 148.4 (Tip-*C*), 142.8 (d, $^{2}J_{C-P}$ = 7.3 Hz, ipso-Tip-*C*), 137.0 (br, ipso-Tip-*C*), 133.6 (d, $^{2}J_{C-P}$ = 4.6 Hz, *ipso*-Tip-*C*), 130.7 (N*C*(CH_3)=*C*(CH_3)N), 129.5, 128.7, 123.4, 123.3, 122.2, 122.1 (Tip-*C*H), 52.0, 51.8 (NHC-^{i}Pr*C*H), 35.8, 35.5 (br), 35.2, 34.8, 34.7, 34.6 (br), 33.6 (Tip-^{i}Pr-*C*H_3), 26.3, 26.1, 24.8, 24,7, 24.4, 24.2, 24.1, 24.03, 24.00, 23.95, 23.87, 23.3 (br), 22.6, 22.0 (Tip-^{i}Pr-*C*H_3), 11.1 (NC(*C*H_3)=C(*C*H_3)N), **^{29}Si{H} NMR** (59.62 MHz, thf-d_8, 300 K): δ = 30.8 (br d, $^{1}J_{P-Si}$ = 113.6 Hz), 26.4 (d, $^{1}J_{P-Si}$ = 138.8 Hz), **^{31}P{H} NMR** (121.5 MHz, thf-d_8, 300 K): δ = −378.6 (br); **UV/vis** (thf): λ = 500-350(br shoulder); **elemental analysis** calcd (%) for $C_{58}H_{88}FeN_2O_3PSi_2$: C 69.59, H 8.91, N 2.75; found: C 69.40, H 8.73, N 2.62.

5.6. Reactivity of Disilenide towards Boron Containing Electrophiles

5.6.1. Synthesis of Methyldisilene 173

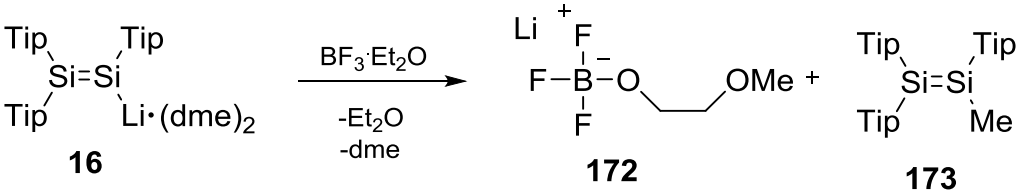

$C_{53}H_{89}LiO_4Si_2$	$C_4H_{10}BF_3O$	$C_2H_4BF_3LiO_2$	$C_{46}H_{72}Si_2$
853.38 g/mol	141.93 g/mol	134.80 g/mol	681.25 g/mol

1.2 mL (1.12 mmol) $BF_3{\cdot}Et_2O$ are added *via* surringe to a solution of 1.02 g (1.195 mmol) disilenide **16** in 25 mL toluene at −80°C. The reaction mixture is allowed to warm up to room temperature and all volatiles are removed in vacuum. The residue is digested with hexane and filtered. The solvent is removed under reduced pressure to afford a bright yellow foam. **^{11}B NMR** (96.3 MHZ, C_6D_6, 300 K): δ **=** −5.3 ppm, **^{19}F NMR** (282.2, C_6D_6, 300 K): δ = −58.8, −156.7, **^{29}Si{H} NMR** (59.6 MHZ, C_6D_6, 300 K): δ = 77.2, 54.1. Pentane (1 mL) is added and the solution was kept at 0°C for one

week. Disilene **173** was obtained as yellow crystals in 21% yield. **UV/vis** (hexane) λ_{max} = 426 nm (ε = 2900 $M^{-1}cm^{-1}$).

5.6.2. Reaction of Disilenide 16 with Methyl Iodide

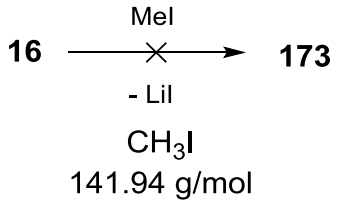

100 mg (0.117 mmol) disilenide **16** were dissolved in 2 mL toluene and cooled to 0°C. One equivalent methyl iodide (7.3 μL) was added to the solution *via* syringe. The reaction mixture turned pale yellow. All volatiles were removed in vacuo and a pale yellow residue was obtained. **^{1}H NMR** (300.13 MHZ, C_6D_6, 300 K): *selected resonances*: δ = 6.24 (d, *J* = 4.6 Hz), 6.17 (d, *J* = 8.1 Hz), 5.77 (d, *J* = 4.6 Hz), 5.7 (s), 5.63 (d, *J* = 8.1 Hz), **^{29}Si{H} NMR** (59.6 MHZ, C_6D_6, 300 K): 6.1, −14.4, −15.3, −26.3, −60.6, −61.9.

5.6.3. Synthesis of Bis(dimethylamino)boryl Disilene 174

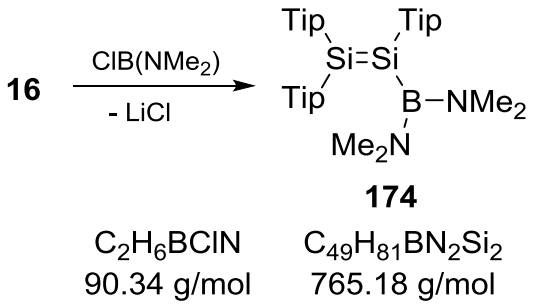

To a solution of 1.1 g (1.29 mmol) disilenide **16** in in 20 mL toluene one equivalent bis(dimethylamino)chloroborane is added at −80°C. The reaction mixture is allowed to warm up to room temperature in the thawing cold bath and stirred overnight. After all volatiles were removed under vacuum, the residue is digested with hexane and filtered. The solvent is removed in vacuum and an orange foam is obtained. **^{1}H NMR** (300.13 MHz, C_6D_6, 300 K): δ = 7.25 (d, $^{4}J_{H\text{-}H}$ = 1.3 Hz), 7.12 (d, $^{4}J_{H\text{-}H}$ = 1.5 Hz), 7.06 (d, $^{4}J_{H\text{-}H}$ = 1.6 Hz), 7.04 (d, $^{4}J_{H\text{-}H}$ = 1.5 Hz), 6.99 (d, $^{4}J_{H\text{-}H}$ = 1.7 Hz), 6.97 (d, $^{4}J_{H\text{-}H}$ = 1.6 Hz, each 1H, each Tip-C*H*), 4.90 (d, $^{3}J_{H\text{-}H}$ = 6.6 Hz, 1H, Tip-^{i}Pr-C*H*), 4.56 (sept, $^{3}J_{H\text{-}H}$ = 6.6 Hz, 1H, Tip-^{i}Pr-C*H*), 4.39 (sept, $^{3}J_{H\text{-}H}$ = 6.8 Hz, 1H, Tip-^{i}Pr-C*H*), 4.13 (sept, $^{3}J_{H\text{-}H}$ = 6.8 Hz, 1H, Tip-^{i}Pr-C*H*), 3.77 (sept, 2H, Tip-^{i}Pr-C*H*), 2.75 (m, 2H, Tip-^{i}Pr-C*H*), 2.63, 2.57 (each s, each 6H, each N(CH_3)$_2$), 1.55 (d, $^{3}J_{H\text{-}H}$ = 6.3 Hz, 3H, Tip-^{i}Pr-CH_3), 1.50 (d, $^{3}J_{H\text{-}H}$ = 6.3 Hz, 6H, Tip-^{i}Pr-CH_3), 1.46 (d, $^{3}J_{H\text{-}H}$ = 6.3 Hz, 3H, Tip-^{i}Pr-CH_3), 1.40 (br m, 3H, Tip-^{i}Pr-CH_3), 1.33 (d, $^{3}J_{H\text{-}H}$ = 6.7 Hz, 6H, Tip-^{i}Pr-CH_3), 1.28 (d,

$^3J_{H\text{-}H}$ = 6.9 Hz, 3H, Tip-^{i}Pr-CH_3), 1.23-1.12 (m, 18H, Tip-^{i}Pr-CH_3), 0.82 (d, $^3J_{H\text{-}H}$ = 6.9 Hz, 3H, Tip-^{i}Pr-CH_3), 0.77 (d, $^3J_{H\text{-}H}$ = 6.6 Hz, 3H, Tip-^{i}Pr-CH_3), 0.69 (d, $^3J_{H\text{-}H}$ = 6.6 Hz, 3H, Tip-^{i}Pr-CH_3), 0.52 (d, $^3J_{H\text{-}H}$ = 6.6 Hz, 3H, Tip-^{i}Pr-CH_3), **^{11}B NMR** (96.3 MHz, C_6D_6, 300 K): δ = 38.2 (v br), **^{13}C{H} NMR** (75.47 MHz, C_6D_6, 300 K): δ = 155.6 (br), 155.3, 154.7, 154.6, 150.7, 150.3, 149.8, 135.9, 134.9, 133.5 (Tip-*C*), 135.8, 134.9, 133.5 (Tip-*ipso*-*C*), 122.6, 122.3, 122.0, 121.3, 121.1, 120.9 (Tip-C*H*), 42.3 (N(*C*H_3)$_2$), 38.5, 37.8, 37.7, 37.6, 37.4, 35.8, 34.8, 34.7, 34.6 (Tip-^{i}Pr-*C*H), 26.1, 25.5, 25.4, 25.1, 24.9, 24.8 (br), 24.6, 24.5, 24.3, 24.2, 24.1, 23.0, 22.9 (Tip-^{i}Pr-*C*H_3), **^{29}Si{H} NMR** (59.62 MHz, 300 K, C_6D_6): δ = 85.8, 51.3 (br).

5.6.4. Synthesis of (Chloroboryl) Disilene 176

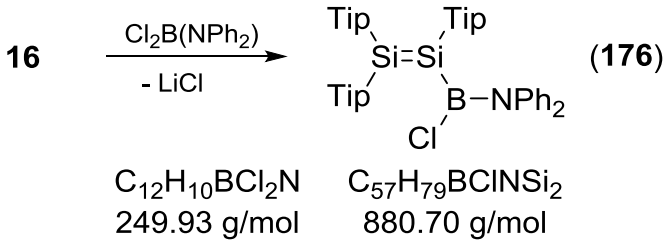

2 g (2.34 mmol) disilenide **16** are dissolved in 20 mL toluene and added to a solution of one equivalent (585.9 mg) $Cl_2B(NPh_2)$ in 20 mL toluene at −80°C. The red reaction mixture is allowed to warm up to room temperature and is stirred overnight. Subsequently all volatiles are removed in vacuum and the residue is digested with hexane. The suspension is filtered and the filtrate reduced to dryness to afford an orange foam. Crystallization from pentane (5 mL) affords 1.43 g **176** as yellow needles. Concentration of the mother liquor yields a second batch of crystals (250 mg. Overall yield: 81%. **M. p.** 123-128°C (dec.).

^{1}H NMR (300.13 MHz, tol-d_8, 223 K): δ = 7.35, 7.32, 7.25, 7.20, 7.17, 7.10, 7.09 (each br s (Ar-C*H*), 7.12-6.53 (br m, Ar-C*H* overlapping with tol-d_8), 5.08 (sept, $^3J_{H\text{-}H}$ = 6.2 Hz, Tip-^{i}Pr-C*H*), 5.00 (sept, $^3J_{H\text{-}H}$ = 6.2 Hz, Tip-^{i}Pr-C*H*), 4.51 (br, Tip-^{i}Pr-C*H*), 4.33 (sept, $^3J_{H\text{-}H}$ = 6.7 Hz, Tip-^{i}Pr-C*H*), 4.26 (sept, $^3J_{H\text{-}H}$ = 6.7 Hz, Tip-^{i}Pr-C*H*), 3.94-3.70 (m, Tip-^{i}Pr-C*H*), 3.69-3.49 (m, Tip-^{i}Pr-C*H*), 2.88-2.54 (m, sept, Tip-^{i}Pr-C*H*), 1.87 (d, $^3J_{H\text{-}H}$ = 6.3 Hz, Tip-^{i}Pr-CH_3), 1.72 (d, $^3J_{H\text{-}H}$ = 6.9 Hz, Tip-^{i}Pr-CH_3), 1.63-1.33 (m, Tip-^{i}Pr-CH_3), 1.31-1.06 (m, Tip-^{i}Pr-CH_3), 1.03 (d, $^3J_{H\text{-}H}$ = 6.3 Hz, Tip-^{i}Pr-CH_3), 0.84-0.64 (mTip-^{i}Pr-CH_3), 0.60 (d, $^3J_{H\text{-}H}$ = 6.3 Hz, Tip-^{i}Pr-CH_3), 0.51 (d, $^3J_{H\text{-}H}$ = 6.3 Hz, Tip-^{i}Pr-CH_3), 0.43 (d, $^3J_{H\text{-}H}$ = 6.3 Hz, Tip-^{i}Pr-CH_3), 0.33 (d, $^3J_{H\text{-}H}$ = 6.9 Hz, Tip-^{i}Pr-CH_3), 0.28 (br, Tip-^{i}Pr-CH_3), **^{11}B NMR** (96.3 MHz, C_6D_6, 300 K): δ = no resonance could be detected, even at 223 K, presumably due to pronounced broadening of the signal, **^{13}C{H} NMR** (75.47 MHz, C_6D_6, 300 K): δ = 157.9, 155.3, 154.4, 151.2, 150.9, 150.3, 148.8, 148.2, 135.6, 134.0, 131.1, 129.2, 126.0 (mostly broad), 123.4-121-4 (v br), 121.2, (Ar-C*H*), 38.6, 38.2, 37.7, 37.2, 36.7, 34.7 35.6 (each br, Tip-*C*H), 27.3, 26.4, 26.0 (each br), 25.3-23.9 (overlapping, mostly v br, Tip-^{i}Pr-*C*H_3), **^{29}Si{H} NMR** (59.62 MHz, 300 K, tol-d8): δ = 101.8, 71.2, 47.7 (v br), 223 K : 101.4, 69.6, 48.1 (br), 46.4

(br); **UV/vis** (hexane): λ = 457 nm (ε = 14200 $M^{-1}cm^{-1}$), 380 nm (ε = 5900 $M^{-1}cm^{-1}$); **elemental analysis** calcd (%) for $C_{57}H_{79}BClSi_2N$: C 77.74, H 9.04, N 1.59; found: C 77.08, H 9.02, N 1.50.

5.6.5. Reaction of 176 with KC_8

96.8 mg (0.114 mmol) **176** were dissolved in 0.25 mL thf and added to a suspension of two equivalents KC_8 (30.7 mg) in 0.25 mL thf. Formation of black precipitate was observed and the suspension was filtered. The pale yellow filtrate was reduced to dryness.
^{11}B NMR (96.3 MHz, C_6D_6, 300 K): δ = no resonance could be detected, **^{29}Si{H} NMR** (59.62 MHz, 300 K, C_6D_6): δ = 2.5.

5.6.6. Reaction of 176 with Naphthalene/Lithium

To a solution of 300 mg (0.341 mmol) **176** in 10 mL diethylether two equivalents of naphthalene/lithium (3 mL, 0.254 M in thf) were added dropwise at −80°C. Upon warming to room temperature, the reaction mixture turned red. Even after stirring at rt overnight, only starting material and a small amount of a mixture of products was observed by NMR spectroscopy.

5.6.7. Reaction of 176 with $^{i}Pr_2Me_2NHC$

A solution of 1,3-diisopropyl-4,5-dimethylimidazol-2-ylidene (44 mg, 0.244 mmol) in 2.5 mL toluene was added to a solution of one equivalent (215 mg) **176** in 1.5 mL toluene at −80°C. The reaction mixture was allowed to warm up to room temperature and turned red-brown. All volatiles were removed in vacuo, the residue was digested with 20 mL hexane and filtered. The filtrate was reduced to dryness to afford a red-brown solid. **^{1}H** and **^{13}C** NMR spectroscopy indicate a complex mixture. **^{11}B NMR** (96.3 MHz, C_6D_6, 300 K): δ = 40.2 – 20.6 ppm (v br), **^{29}Si{H} NMR** (59.62 MHz, 300 K, C_6D_6): δ = 4.8.

5.6.8. Synthesis of Disilaboriranide 178

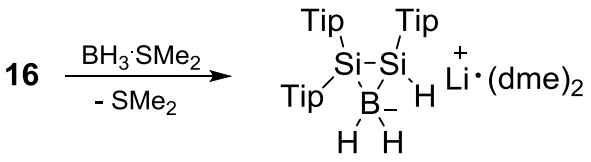

178

C_2H_9BS 75.96 g/mol

$C_{53}H_{92}BLiO_4Si_2$ 867.24 g/mol

503.6 mg (0.59 mmol) of **16** are dissolved in 2.5 mL toluene and 56 µL (0.59 mmol) of $BH_3{\cdot}SMe_2$ are added dropwise to the vigorous stirred solution of **16**. A change in color from orange to yellow-brownish is observed immediately. Stirring is continued for another 30 minutes. All volatiles are removed in vacuum to yield bright yellow foam of **178**.

^{1}H NMR (300.13 MHZ, C_6D_6, 300 K): δ = 7.20, 7.13, 7.00 (each s, each 2H, Tip-*H*), 4.83 (m, 4H, ^{i}Pr-C*H*), 4.29 (m, 2H, ^{i}Pr-C*H*), 3.97 (br, 1H, Si-*H*), 2.95 (s, 10H, dme), 2.93 (s, 15H, dme), 2.87 (m, 3H, ^{i}Pr-C*H*), 1.50, 1.48, 1.34, 1.31, 1.28, 1.26, 1.21, 1.91, 0.83 (each d, altogether 54H, ^{i}Pr-CH_3), 1.17 (br, 2H, BH_2), **^{7}Li NMR** (116.6 MHZ, C_6D_6, 300 K): δ = −0.20. **^{11}B NMR** (96.3 MHZ, C_6D_6, 300 K): δ = −38.4 (t, $^{1}J_{B\text{-}H}$ = 96.1 Hz, BH_2), **^{29}Si{H} NMR** (59.6 MHZ, C_6D_6, 300 K): δ = −81.5 (br), −99.3 (br).

5.6.9. Reaction of 16 with 2 Equivalents of Borane Dimethyl Sulfide Adduct

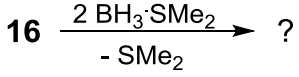

C_2H_9BS
75.96 g/mol

30 µL (0.32 mmol) of borane dimethyl sulfide adduct were added to a solution of 137 mg (0.16 mmol) of **16** in benzene. A change in color from red to brownish was immediately observed.

^{11}B NMR (96.3 MHZ, C_6D_6, 300 K): δ = −32.3 (m), −42.3 (t, $^{1}J_{B\text{-}H}$ = 80.4 Hz), −47.0 (t, $^{1}J_{B\text{-}H}$ = 80.4 Hz), **^{29}Si{H} NMR** (59.6 MHZ, C_6D_6, 300 K): δ = −38.6 (br), −59.3 (br).

5.6.10. Reaction of 178 with Methyl Iodide

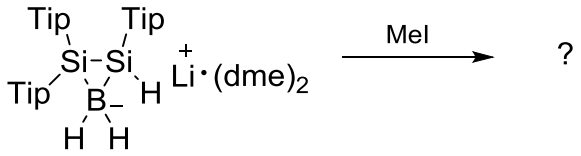

178

$C_{53}H_{92}BLiO_4Si_2$ — 867.24 g/mol

CH_3I — 141.94 g/mol

In a NMR tube **178** was prepared according to the procedure described in Chapter 5.6.8 starting from 107 mg (0.125 mmol) of **16** and 11.9 µL of $BH_3{\cdot}SMe_2$. 7.8 µL of methyl iodide were added and a change in color from bright red to dark red-brownish was observed immediately.

^{11}B NMR (96.3 MHZ, C_6D_6, 300 K): δ = −30.9 to −33.1 (m), −38.2 to −46.6 (m), **^{29}Si{H} NMR** (59.6 MHZ, C_6D_6, 300 K): δ = −50.5, −61.8, −65.9, −73.5, −75.0, −78.5.

5.6.11. Reaction of 178 with Trityl Tetrafluoroborate

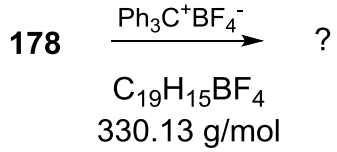

178 was prepared according to the procedure described in Chapter 5.6.8 starting from 201.4 mg (0.24 mmol) of **16** and 22 µL (0.23 mmol) of. **178** was dissolved in 5 mL of toluene and cooled to -78°C. A solution of 77.3 mg (0.23 mmol) trityl tetrafluoroborate in 5 mL thf was prepared and cooled to −78°C. Subsequently, **178** was rapidly cannulated to the cooled trityl tetrafluoroborate solution and the resulting reaction mixture was allowed to warm to rt. After all volatiles were removed in vacuum, the crude product was digested in hexane and filtered. The filtrate was reduced to dryness and red-brownish solid was obtained.
^{11}B NMR (96.3 MHZ, C_6D_6, 300 K): δ = −25.2 (br), −33.2 (t, $^1J_{B\text{-}H}$ = 74.7 Hz), −40.5 (t, $^1J_{B\text{-}H}$ = 85.6 Hz), − 45.2 (t, $^1J_{B\text{-}H}$ = 85.6 Hz), **^{29}Si{H} NMR** (59.6 MHZ, C_6D_6, 300 K): δ = −61.8, −65.9, −73.5, −78.6.

5.6.12. Reaction of 178 with Trimethylsilyl Chloride

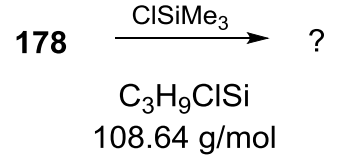

178 is prepared according to the described procedure in Chapter 5.6.8 from 535 mg (0.63 mmol) of **16** and 60 µL (0.63 mmol) of $BH_3{\cdot}SMe_2$. **178** is dissolved in toluene and cooled to 0°C. Trimethylsilyl chloride is added dropwise and the resulting solution is stirred for another 10 minutes at 0°C. The ice bath is removed and the reaction mixture is allowed to warm up to rt within 20 minutes. All volatiles are removed in vacuum, the residue digested with hexane and filtered. The filtrate was then reduced to dryness in vacuum to yield a red-brownish solid.
^{11}B NMR (96.3 MHZ, C_6D_6, 300 K): main signal at δ = −39.1 (br), **^{29}Si{H} NMR** (59.6 MHZ, C_6D_6, 300 K): δ = −12.4, −76.6, −79.2.

5.6.13. Synthesis of Disilenyl Borate 180

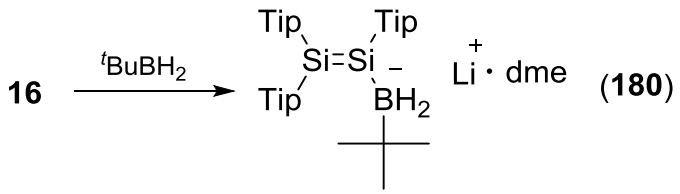

$C_4H_{11}B$ 69.94 g/mol

$C_{53}H_{90}BLiO_2Si_2$ 833.22 g/mol

127 mg (1.63 mmol) of lithium *tert*-butyltrihydroborate are dissolved in 2.5 mL of Et_2O and stirred vigorously. To generate the corresponding *tert*-butylborane, 0.81 mL (1.62 mmol) of hydrogen chloride (2M solution in Et_2O) are added. A white solid precipitates instantaneously and gas development is observed. Stirring is continued for another 45 minutes. 1.22 mg (1.41 mmol) of disilenide 16 are dissolved in 6 mL of Et_2O and added to the stirred solution of *tert*-butylborane. The reaction mixture is stirred for one hour and the color changes from orange to greenish yellow. After evaporating the solvent, the crude product is digested with hexane and filtered. Crystallization from hexane (3 mL) yielded 610 mg (58%) **180** as yellow crystals. **M. p.** 151°C (dec).

^{1}H NMR (300.13 MHZ, C_6D_6, 300 K): δ = 7.14 - 7.00 (m, 6H, Tip-*H*), 4.64 - 3.81 (br, 5H, ^{i}Pr-*H*), 2.86 (s, 6H, dme-C*H*$_3$), 2.77 (m, 4H, ^{i}Pr-*H*), 2.52 (s, 4H, dme- dme-C*H*$_2$), 1.58 (br, 9H, ^{i}Pr-C*H*$_3$), 1.41 (s, 9H, ^{t}Bu-C*H*$_3$), 1.25, 1.22, 1.20, 1.18, 1.17, 1.15 (each s, altogether 45 H, ^{i}Pr-C*H*$_3$, **^{7}Li NMR** (116.6 MHZ, C_6D_6, 300 K): δ = −0.79 (s), **^{11}B NMR** (96.3 MHZ, C_6D_6, 300 K): δ = −19.9 (t, $^1J_{B\text{-}H}$ = 64.9 Hz, *B*H$_2$), **^{13}C{H} NMR** (75.5 MHZ, C_6D_6, 300 K): δ = 155.3, 154.8, 149.1, 149.0, 148.5, 138.3, 137.9, 137.4 (Tip-*C*), 121.8, 121.7, 121.4 (Tip-*C*H), 69.4 (dme-*C*H$_3$), 59.2 (dme-*C*H$_2$), 36.5 (^{t}Bu-*C*) 35.5, 34.6, 34.5, 34.4 (^{i}Pr-*C*H), 26.2, 25.1, 24.0 (^{i}Pr-*C*H$_3$), 24.1 (^{t}Bu-*C*H$_3$), **^{29}Si{H} NMR** (59.6 MHZ, C_6D_6, 300 K): δ = 95.3 (v br, *Si*B), 72.7 (*Si*Tip$_2$); **UV/vis** (hexane) λ_{max} = 410 nm (ε = 3700 $M^{-1}cm^{-1}$); **Elemental Analyses** calculated for $C_{53}H_{90}BLiO_2Si_2$: C, 76.40, H, 10.89, Found: C, 74.47, H, 10.99.

5.7. Functionalization and Transfer of Siliconoids

5.7.1. Synthesis of Aninionic Siliconoid 133

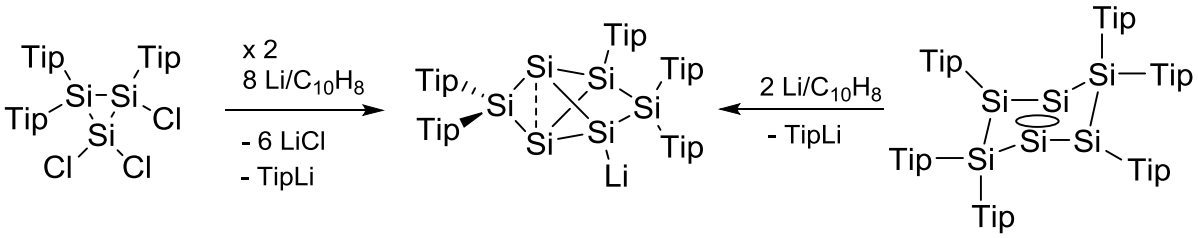

121 **133** **122**

$C_{45}H_{69}Cl_3Si_3$ 800.64 g/mol

$C_{75}H_{115}LiSi_6$ 1192.20 g/mol

$C_{90}H_{138}Si_6$ 800.64 g/mol

(a) At −80 °C 4.5 equivalents lithium/naphthalene (solution in thf, 0.515 M) are added to a solution of 3.02 g (3.77 mmol) 1,1,2-trichloro-2,3,3-tris(2',4',6'triisopropyl-phenyl)cyclotrisilane in 25 mL diethylether over a period of 5 min. The reaction mixture is allowed to warm to ambient temperature slowly in the thawing cooling bath (within 6 h) and turns deep orange. After 12 h of stirring, all volatiles are removed at rt under reduced pressure (10^{-3} mbar). The solid residue is digested with benzene (50 mL) and filtered. The solvent is evaporated and the residue dissolved in 5 mL hexane. Standing overnight affords 1.6 g **133**·4.7thf·1.1Naph as orange blocks (25%yield).

(b) 2.1 equivalents of lithium/naphthalene solution (0.30 M in thf) are added dropwise within 5 min to a solution of 0.436 g (0.314 mmol) 2,3,3,5,6,6-hexakis(2',4',6'triisopropylphenyl)-tricyclo[3.1.0.0.^{2,4}]hexasilan-1,4-diyl in 5 mL diethylether cooled to −80 °C. The reaction mixture is allowed to warm to ambient temperature slowly in the thawing cooling bath (within 6 h) and turns deep orange. After 12 h of stirring, all volatiles are removed at rt under reduced pressure (10^{-3} mbar). The solid residue is digested with benzene (10 mL) and filtered. The solvent is evaporated and the residue dissolved in 1.5 mL hexane. Standing overnight affords 0.3 g **133**·3thf·1.1Naph as orange blocks (62% yield).

^{1}H NMR (300.13 MHz, 300 K, C_6D_6): δ = 7.27 (d, 1H, Tip-C*H*), 7.08 (br, 2H, Tip-C*H*), 7.04 (br, 1H, Tip-C*H*), 6.94 (br, 2H, Tip-C*H*), 6.92, 6.87, 6.81, 6.76 (each: br, 1H, Tip-C*H*), 5.77, 5.34, 4.95, 4.83, 4.31 (each: sept, $^3J_{H\text{-}H}$ = 6.6 Hz, 1H, Tip-^{i}Pr-C*H*Me$_2$), 3.96, 3.86 (br, overlapping, 3H, Tip-^{i}Pr-C*H*Me$_2$), 3.64 (sept, $^3J_{H\text{-}H}$ = 6.6 Hz, 1H, Tip-^{i}Pr-C*H*Me$_2$), 2.82, 2.70, 2.63 (mult, overlapping, together 6H, Tip-^{i}Pr-C*H*Me$_2$), 2.12 (br, 6H, Tip-^{i}Pr-C*H*$_3$), 1.83 (d, 3H, Tip-^{i}Pr-C*H*$_3$), 1.58, 1.53 (br, together 18H, Tip-^{i}Pr-C*H*$_3$), 1.45-1.02 (mult, overlapping with thf, together 42H Tip-^{i}Pr-C*H*$_3$), 0.94, 0.81, 0.77 (each: d, 3H, Tip-^{i}Pr-C*H*$_3$), 0.37 (br, 9 H, Tip-^{i}Pr-C*H*$_3$), 0.24 (d, 3H, Tip-^{i}Pr-C*H*$_3$); 7.61 (mult, 1.1 x 4H, Naph), 7.23 (mult, 1.1 x 4H, Naph); 3.37 (t, 4.7 x 4H, thf-C*H*$_2$O), 1.35 (overlapping, 4.7 x 4H, thf-C*H*$_2$CH$_2$O). Ratio **133**:thf:Naph = 1:4.7: 1.1, **^{7}Li NMR** (116.64 MHz, 300 K, C_6D_6): δ = 0.66, **^{13}C{^{1}H} NMR** (75.46 MHz, 300 K, C_6D_6): δ = 155.35, 154.13, 153.58, 153.54, 153.00, 152.71, 152.67, 152.44, 149.33, 148.94,

148.77, 148.42, 147.76, 146.93, 145.05, 142.59, 140.73, 140.13, 137.88 (Ar-*C*), 133.89, 128.05, 125.88 (Naph-*C*), 122.50, 122.23, 122.10, 121.68, 121.47, 120.97, 120.48 (Ar-*C*H), 68.20 (thf), 36.36, 35.24, 34.66, 34.51, 34.34, 34.24, 34.00, 33.54, 28.97, 28.20, 27.98, 27.84, 27.38, 27.07 (Tip-^{i}Pr-*C*H and Tip-^{i}Pr-*C*H_3), 25.35 (thf), 24.82, 24.58, 24.36, 24.27, 24.12, 23.82, 23.63, 23.42, 23.15, 22.63, 22.44 (Tip-^{i}Pr-*C*H and Tip-^{i}Pr-*C*H_3), **^{29}Si{H} NMR** (59.62 MHz, 300 K, C_6D_6): δ = 159.59 (s, Tip_2*Si*), 27.60 (s, Tip*Si*), 12.83 (s, Tip_2*Si*), −66.82 (br, *Si*-Li), −237.29 (s, *Si*Si_3), −238.15 (s, *Si*Si_3).

Depending on the batch and crystallization conditions different ratios **133**:thf:Naph were observed. Surprisingly, both THF and naphthalene seem to be strongly bonded in the crystals and cannot be removed under vacuum ($1\cdot10^{-3}$ mbar). Consequently, for the further investigation we used **133** containing the amount of THF and naphthalene as received after crystallization.

5.7.2. Synthesis of Silyl Substituted Siliconoid 181

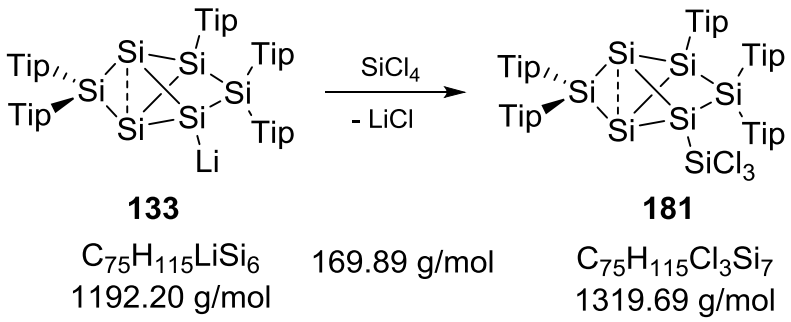

133 **181**

$C_{75}H_{115}LiSi_6$ 1192.20 g/mol — 169.89 g/mol — $C_{75}H_{115}Cl_3Si_7$ 1319.69 g/mol

This procedure was developed by Dr. Kai Abersfelder. Characterization of **181** was done during this project. Siliconoid **133**·5.4THF·1.1 Naph (4.41 g, 2.56 mmol) is dissolved in 40 mL toluene. *Via* syringe 0.48 g (2.82 mmol) $SiCl_4$ are added at rt and the reaction mixture is stirred for 12 h. All volatiles are removed in vacuum (10^{-3} mbar) and the solid residue is digested with hexane. After filtration the filtrate is reduced to 15 mL in volume and the precipitated solid is redissolved by gentle heating. Standing overnight at rt yielded 0.56 g orange blocks of **181**·0.5Naph (mp. 185 °C, decomp.). Upon reduction of the volume of the mother liquor to 10 mL another 1.95 g product could be isolated (overall yield 68%).

^{1}H NMR (300.13 MHz, 300 K, C_6D_6): δ = 6.91 (br, 10H, Tip-C*H*), 5.48 – 2.85 (very br, 10H, Tip-^{i}Pr-C*H*), 2.62 (m, 5H, Tip-^{i}Pr-C*H*), 2.28- −0.11 (very broad, overlapping with m, overall 90H, Tip-^{i}Pr-CH_3); 7.61, 7.23 (m, 0.25 x 4H, Naph-*H*), **^{13}C{H} NMR** (75.46 MHz, 300 K, C_6D_6): δ = 155.80, 153.99, 151.81, 151.55, 151.34, 150.33, 137.60, 137.10, 136.78, 129.71, 126.40, 123.50, 123.27, 122.35 (Ar-*C*), 37.12, 36.24, 35.35, 35.06, 35.05, 34.87, 34.58, 32.32, 28.13, 24.83, 24.34, 24.08, 23.40, 14.73, **^{29}Si{^{1}H} NMR** (59.62 MHz, 300 K, C_6D_6): δ = 175.40 (Tip_2*Si*), 26.16 (Tip_2*Si*), 14.10 (Tip*Si*), 12.98 (Si_2*Si*$SiCl_3$), −38.30 (*Si*Cl_3), −252.33, −264.27 (br, *Si*Si_3); **UV/vis** (hexane)**:**

$\lambda_{max}(\varepsilon)$ = 469 nm (400 $M^{-1}cm^{-1}$), 359 nm (5500 $M^{-1}cm^{-1}$); **Elemental analysis** calculated for $C_{75}H_{115}Cl_3Si_7$: C, 68.26; H, 8.78; N, 0. Found: C, 68.61; H, 8.98.

5.7.3. Synthesis of Pivaloyl Substituted Siliconoid 182

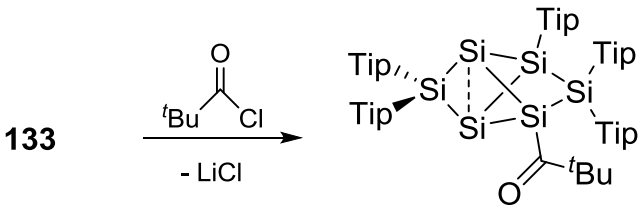

182

C_5H_9ClO
120.58 g/mol

$C_{80}H_{124}OSi_6$
1270.38 g/mol

Trimethylacetyl chloride (54 µL, 0.44 mmol) is added to a stirred solution of 735 mg (0.43 mmol) **133**·5.4thf·1.1naph in toluene at rt. The reaction mixture is stirred for additional 60 minutes and the color changes from orange to deep red. After evaporation of the solvent, the crude product is digested with hexane and filtered. The filtrate is reduced to dryness in vacuum and kept under reduced pressure (10^{-3} mbar) overnight to sublime out remaining naphthalene. Crystallization from pentane (2 mL) at rt yields 207 mg (38%) of **182** as red crystals. **M. p**. 187°C (rearrangement). **^{1}H NMR** (300.13 MHz, 300 K, C_6D_6): δ = 7.22 (br, 1H, Tip-C*H*), 7.19 (br, 1H, Tip C*H*), 6.99 (br, 1H, Tip-C*H*), 6.96 (br, 1H, Tip-C*H*), 6.95 (br, 2H, Tip-C*H*), 6.90 (br, 2H, Tip-C*H*), 6.82 (br, 1H, Tip-C*H*), 6.81 (br, 1H, Tip-C*H*), 5.14 (sept, $^3J_{H-H}$ = 6 Hz, 1H, Tip-^{i}Pr-C*H*), 4.68 (sept, $^3J_{H-H}$ = 6 Hz, 2H, Tip-^{i}Pr-C*H*Me_2), 4.23, 3.92 (each sept, $^3J_{H-H}$ = 6 Hz, each 1H, Tip-^{i}Pr-C*H*), 3.79 (br, 1H, Tip-^{i}Pr-C*H*) 3.47 (sept, $^3J_{H-H}$ = 6 Hz, 2H, Tip-^{i}Pr-C*H*), 3.18 (sept, $^3J_{H-H}$ = 6 Hz, 2H, Tip-^{i}Pr-C*H*), 3.02 (sept, $^3J_{H-H}$ = 6 Hz, 2H, Tip-^{i}Pr-C*H*), 2.65 (m, 5H, Tip-^{i}Pr-C*H*), 2.16 (d, $^3J_{H-H}$ = 6 Hz, 3H, Tip-^{i}Pr-CH_3), 1.90 (d, $^3J_{H-H}$ = 6 Hz, 3H, Tip-^{i}Pr-CH_3), 1.63 (d, $^3J_{H-H}$ = 6 Hz, 3H, Tip-^{i}Pr-CH_3), 1.56-1.29 (m, 27H, Tip-^{i}Pr-CH_3), 1.24-0.99 (m, 36H, Tip-^{i}Pr-CH_3), 0.82 (d, $^3J_{H-H}$ = 6 Hz, 3H, Tip-^{i}Pr-CH_3), 0.75 (s, 9H, C(CH_3)$_3$), 0.64 (m, 6H, Tip-^{i}Pr-CH_3), 0.46 (d, $^3J_{H-H}$ = 6 Hz, 3H, Tip-^{i}Pr-CH_3), 0.26 (m, 6H, Tip-^{i}Pr-CH_3), **^{13}C{H} NMR** (75.46 MHz, 300 K, C_6D_6): δ = 239.01 (s, 1 C, *C*=O), 156.22-154.68 (br, 2 C, Ar-*C*), 155.55 155.37, 155.14, 154.23 153.51 (each s, each 1 C, Ar-*C*), 152.17 (s, 2 C, Ar-*C*), 151.35, 151.02, 150.98, 149.98, 149.78 (each s, each 1 C, Ar-*C*), 138.13, 137.65, 137.53, 137.01, 126.40 (each s, each 1 C, Ar-*ipso*-*C*), 124.45, (s, 1 C, Ar-*C*H), 123.93-123.33 (br, 4 C, Ar-*C*H), 122.55 (br, 3 C, Ar-*C*H), 121.88, 121.80 (s, 1 C, Ar-*C*H), 50.36 (s, 1 C, *C*(CMe_3)), 38.55, 37.37, 37.12, 36.92, 36.68, 36.17 (each s, each 1 C, Tip-iPr-*C*H), 35.95, 35.06 (each br, each 3 C, Tip-iPr-*C*H) 34.89, 34.73, 34.61 (each s, each 1 C, Tip-iPr-*C*H), 29.56, 29.29, 28.77, 28.07, 27.26 (s, some br, Tip-iPr-*C*H_3), 26.13 (s, 3 C, C(*C*H_3), 25.87, 25.52, 25.28, 25.07, 25.03, 24.77, 24.66, 24.56, 24.49, 24.42, 24.33, 24.27, 24.18, 24.01, 22.90 (s, some br, Tip-iPr-*C*H_3), **^{29}Si{H} NMR** (59.62 MHz, 300 K, C_6D_6): δ = 171.76 (s, *Si*Tip$_2$), 13.55 (s, *Si*Tip$_2$), 10.12 (s, *Si*Tip), −27.39

(s, *Si*CO), −264.67, −271.07 (*Si*Si_3); **UV/vis** (hexane) λ_{max} (ε) = 475 nm (ε = 545 $M^{-1}cm^{-1}$), 349 nm (ε = 8980 $M^{-1}cm^{-1}$); **Elemental Analyses** calculated for $C_{80}H_{124}OSi_6$: C, 75.64, H, 9.84, N, 0.00. Found: C, 75.51, H, 9.97, N, 0.00; **IR** (powder): ν(CO) = 1637 cm^{-1}, 1602 cm^{-1}.

5.7.4. Reaarangement of 182 upon Melting

Oivaloyl substituted siliconoid **182** (100 mg, 0.08 mmol) is placed in an NMR tube and kept at 190°C for five minutes. **^{29}Si{H} NMR** (59.62 MHz, 300 K, C_6D_6): main resonances: δ = 56.5, −6.4, −13.3, −66.6, −156.7, −172.6, minor resonances: δ = 157.7, 106.4, 0.2, −35.8, −94.5 and −200.1.

5.7.5. Synthesis of Phosphino Substituted Siliconoid 184

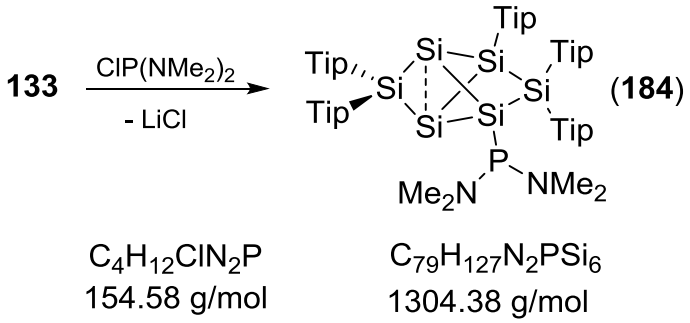

$C_4H_{12}ClN_2P$ 154.58 g/mol

$C_{79}H_{127}N_2PSi_6$ 1304.38 g/mol

At −80°C neat bis(dimethylamino)chlorophosphine (55 μL, 0.38 mmol) is added slowly to a solution of 650 mg (0.38 mmol) **133**·5.4thf·1.1 Naph in 25 mL toluene. The reaction mixture turns deep red and is allowed to warm up to room temperature in the thawing cold bath. After stirring for additional 20 min, all volatiles are removed in vacuum and remaining naphthalene is sublimed out at rt (10^{-3} mbar). The residue is digested with pentane (25 mL) and filtered. After concentrating the filtrate to 4 mL, standing at room temperature for 12 h affords 250 mg orange crystals (mp > 220°C, dec.) of **184**·0.5C_5H_{12}. The mother liquor is concentrated to 1 mL yielding a second batch of crystals (200 mg) of **184**·0.5C_5H_{12} (overall yield 91 %).
^{1}H NMR (300.13 MHz, 300 K, C_6D_6): δ = 7.19 (br, 2H, Tip CH), 7.06 (br, 1 H, Tip-C*H*), 6.95 (br, 4 H, Tip-C*H*), 6.88 (br 1H, Tip-C*H*), 6.81 (br, 1H, Tip-C*H*), 6.77 (br, 1H, Tip-C*H*), 5.35 (br, 1H, Tip-^{i}Pr-C*H*Me_2), 4.80 (br, 1H, Tip-^{i}Pr-C*H*Me_2), 4.56 (br, 1H, Tip-iPr-C*H*Me_2), 4.39 (br, 1H, Tip-^{i}Pr-C*H*Me_2), 3.91 (hept, $^3J_{H\text{-}H}$ = 6.6 Hz, 2H, Tip-^{i}Pr-C*H*Me_2), 3.51 (br, 1H, Tip-^{i}Pr-C*H*Me_2), 3.23 (br, 2H, Tip-iPr-C*H*Me_2), 2.78 - 2.54 (m, 5 H, Tip-^{i}Pr-C*H*Me_2 resonances), 2.33 (br, 12H N-CH_3) 2.15 (d, 3H, $^3J_{HH}$ = 5 Hz, Tip-iPr-CH_3), 1.9 (d, 3 H, $^3J_{HH}$ = 5 Hz, Tip-iPr-CH_3), 1.66 (d, 3 H, $^3J_{H\text{-}H}$ = 5 Hz, Tip-^{i}Pr-CH_3), 1.61 – 0.9 (br m, altogether 63H ,Tip-^{i}Pr-CH_3, pentane-CH_2), 0.86 (tr, 3H, $^3J_{H\text{-}H}$ = 7.15 Hz, pentane-CH_3) 0.61 (br, 6H, Tip-^{i}Pr-CH_3), 0.45 (br 9H, Tip-^{i}Pr-CH_3), 0.30 (d, $^3J_{H\text{-}H}$ = 5 Hz, 3H, Tip-^{i}Pr-CH_3), 0.25 (d, $^3J_{H\text{-}H}$ = 5 Hz, 3H, Tip-^{i}Pr-CH_3), **^{13}C{H} NMR**

(75.46 MHz, 300 K, C_6D_6): δ = 156.58, 155.18, 154.51, 153.85, 153.29, 152.80, 152.15, 151.92, 150.50, 149.94, 149.17, 148.97 (Ar-*C*), 139.49, 138.74, 137.87 (d, $^3J_{CP}$ = 1.94 Hz), 137.14, 130.49 (d, $^3J_{CP}$ = 1.94 Hz, Ar-*ipso*-*C*), 123.99, 122.91, 122.53, 122.71, 122.10, 121.17, 120.70 (Ar-*C*H), 42.96 (d, $^2J_{C\text{-}P}$ = 12.35 Hz), 41.95 (d, 2 C, $^2J_{CP}$ = 15.15 Hz, N(*C*H$_3$)$_2$), 38.25, 36.52, 36.13, 35.61, 35.20, 35.02, 34.54 (Tip-^{i}Pr-*C*H and Tip-^{i}Pr-*C*H$_3$), 34.45 (pentane-*C*H$_2$), 34.28, 34.07, 28.57, 28.10 (Tip-iPr-*C*H and Tip-iPr-*C*H$_3$), 27.72 (pentane-*C*H$_2$), 26.90, 25.04, 24.81, 24.65, 24.37, 23.94, 23.51, 22.72, 22.55 (Tip-^{i}Pr-*C*H and Tip-^{i}Pr-*C*H$_3$), 14.11 (pentane-*C*H$_3$), **^{29}Si{H} NMR** (59.62 MHz, 300 K, C_6D_6): δ = 168.70 (s, Tip$_2$*Si*), 18.24 (d, $^2J_{Si\text{-}P}$ = 16.2 Hz, Tip$_2$*Si*), 14.39 (d, $^3J_{Si\text{-}P}$ = 14.0 Hz, Tip*Si*), −33.80 ($^1J_{Si\text{-}P}$ = 186.6 Hz, P-*Si*), −255.99 ($^2J_{Si\text{-}P}$ = 7.6 Hz, *Si*Si$_3$), −261.37 ($^2J_{Si\text{-}P}$ = 7.6 Hz, *Si*Si$_3$), **^{31}P{H} NMR** (121.5 MHz, 300K, C_6D_6): δ = 148.00 (s, $^1J_{P\text{-}Si}$ = 186.6 Hz); **UV/vis** (hexane): $\lambda_{max}(\varepsilon)$ = 475 nm (1200 $M^{-1}cm^{-1}$), 354 nm (16500 $M^{-1}cm^{-1}$); **Elemental analysis:** calculated for $C_{81.5}H_{133}N_2Si_6P$: C, 73.03; H, 10.00; N, 2.09. Found: C, 72.54; H, 9.80; N, 1.73.

5.7.6. Reaction of 133 with Cl_2PNPh_2

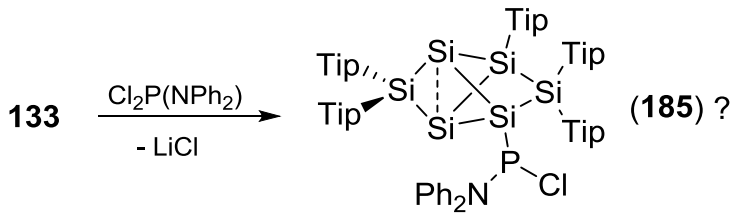

$C_{12}H_{10}Cl_2NP$
270.09 g/mol

$C_{87}H_{125}ClNPSi_6$
1419.90 g/mol

Anionic siliconoid **133**·5.4thf·1.1 Naph (0.082 mmol, 130 mg) and one equivalent dichlorodiphenylamino phosphane were combined in C_6D_6. Subsequently the orange solution turned dark red.
^{31}P{H} NMR (121.5 MHz, 300K, C_6D_6): δ = 152.9 ($^1J_{P\text{-}Si}$ = 179.6 Hz), 149.5, 139.6.
Decomposition to a complex mixture is observed with time.

5.7.7. Synthesis of Phosphinidenyl Substituted Siliconoid 186

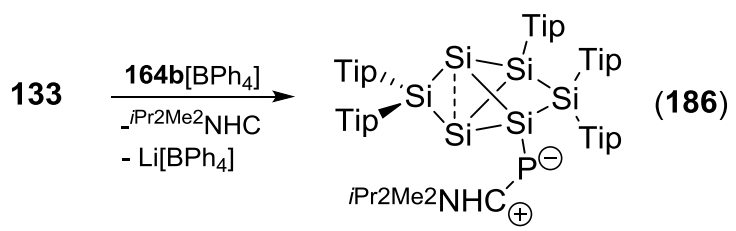

$C_{86}H_{135}N_2PSi_6$
1396.52 g/mol

Anionic siliconoid **133**·5.4thf·1.1Naph (500 mg, 0.295 mmol) and one equivalent (210.28 mg) **164b**[BPh_4] are mixed and 2.5 mL thf are added. The reaction mixture is stirred for 3 h at 75°C and turns deep green. After the mixture is allowed to cool down to rt, all volatiles are removed in vacuum. Remaining naphthalene as well as liberated NHC are sublimed out in high vacuum (12 h 3 x 10^{-2} mbar, rt). Subsequently, the residue is digested with hexane (40 mL) and all insoluble materials are removed by filtration. The intense green filtrate is reduced to approximately 5 mL in volume and standing at rt overnight affords 206 mg (yield: 50 %) **186** as green needles. **M.p.** 205°C (dec).

^{1}H NMR (300.13 MHZ, C_6D_6, 300 K): δ = 7.03 (br, 2H, Tip-*H*), 7.00 (br, 4H, Tip-*H*), 6.90 (br, 4H, Tip-*H*), 5.63 (br, 2H, NHC-^{i}Pr-C*H*), 4.15-3.44(v br, 6H, ^{i}Pr-C*H*), 2.7 (br, 9H, ^{i}Pr-C*H*), 1.53 (s, NHC-Me-CH_3), 1.8-0.16 (br m, ^{i}Pr-CH_3, NHC-^{i}Pr-CH_3), **^{13}C{H} NMR** (75.46 MHz, 300 K, C_6D_6): δ = 166.7 (d, $^{1}J_{C\text{-}P}$ = 134.4 Hz, N*C*N), 155.5-153.1 (br), 150.3, 149.7, 159.5, 148.8 (br), 140.2, 139.6, 139.4, 137.9, 136.2, 134.1, 130.4, 123.8-121.5 (br, Ar-C, NC(CH_3)*C*=*C*(CH_3)N), 51.0, 50.8 (NHC-^{i}Pr-*C*H), 36.3, 35.6 (br), 34.9, 34.7, 34.4, 34.3, 27.5 (br), 25.8-23.4 (br), 10.5 (NC(CH_3)*C*=*C*(CH_3)N), **^{29}Si{H} NMR** (59.62 MHz, 300 K, C_6D_6): δ = 167.70 (s, Tip$_2$*Si*), 8.46 (d, $^{3}J_{Si\text{-}iP}$ = 16.0 Hz, Tip*Si*), 7.21 (d, $^{1}J_{Si\text{-}P}$ = 220.0 Hz, *Si*P), −9.31 ($^{2}J_{Si\text{-}P}$ = 25.6 Hz, *Si*Tip$_2$), −252.5, −261.37 (each br, each *Si*Si$_3$), **^{31}P{H} NMR** (121.5 MHz, 300K, C_6D_6): δ = −163.8 (br, $^{1}J_{S\text{-}iP}$ = 223.7 Hz); **UV/vis (hexane):** $\lambda_{max}(\varepsilon)$ = 589 nm (400 $M^{-1}cm^{-1}$), 464 nm (1400 $M^{-1}cm^{-1}$); **Elemental analysis:** calculated for $C_{86}H_{135}N_2Si_6P$: C, 73.97; H, 9.74; N, 2.01. Found: C, 71.92; H, 9.52; N, 1.43.

5.7.8. Reaction of Siliconoid 186 with BPh_3

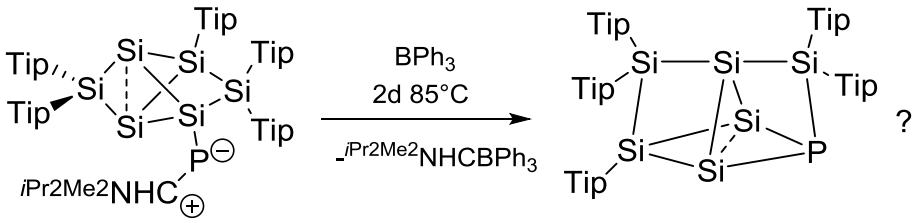

186 $C_{86}H_{135}N_2PSi_6$ 1396.52 g/mol

$C_{18}H_{15}B$ 242.13 g/mol

188 $C_{75}H_{115}PSi_6$ 1216.23 g/mol

Sliconoid **186** (29 mg, 0.02 mmol) was dissolved in C_6D_6 and 10 mg trophenylborane were added. After the reaction mixture was kept at 85°C for two days, the green solution turned deep red. **^{31}P{H} NMR** (121.5 MHz, 300K, C_6D_6): major resonance: δ = −278.9 (^{1}J = 120.4, 61.3, 48.3 Hz, 83 %), minor resonances: δ = −160.9 (9 %), −162.2 (8 %).

5.7.9. Reaction of 133 with ClB(NMe$_2$)

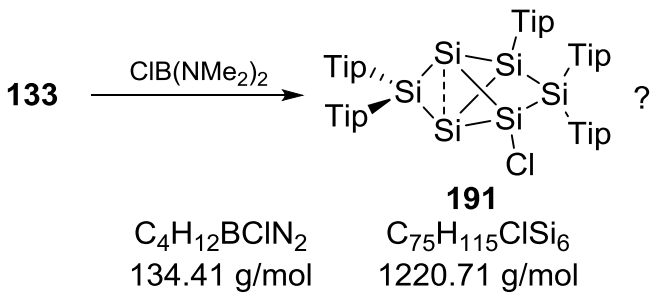

154 mg (0.097 mmol) were placed in an NMR tube and dissolved in 0.5 mL C_6D_6. One equivalent (50 μL) ClB(NMe$_2$) were added and the deep orange solution turned bright red. Upon heating to 50°C for 30 minutes approximately still 50% of the starting materials were observed. **^{11}B NMR** (96.3 MHz, C_6D_6, 300 K): δ = 28.0, 25.3 (br), **^{29}Si{H} NMR** (59.6 MHz, C_6D_6, 300 K): δ = 169.2, 11.9, 5.9, 3.7, −266.1, −278.0.

5.7.10. Reaction of 133 with Cl$_2$BNPh$_2$

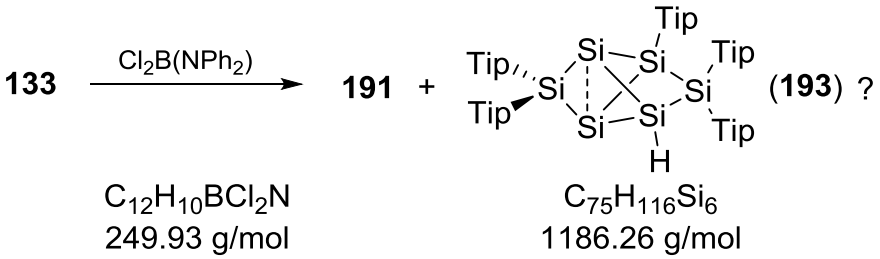

650 mg (0.41 mmol) **133**·5.4THF·1.1naph were dissolved in 30 mL toluene and cooled to −80°C. A solution of one equivalent BCl_2NPh_2 (102 mg) in 15 mL toluene was added. Upon warming to room temperature the orange reaction mixture turned red. All volatiles were removed in vacuum and the residue digested with hexane. The red suspension was filtered and the filtrate reduced to dryness. A red foam was obtained. **^{11}B NMR** (96.3 MHz, 300 K, C_6D_6): δ = 40.0, 26.6, −2.5, −40 (each br, overlapping), **^{29}Si{H} NMR** (59.62 MHz, 300 K, C_6D_6): major resonances: δ = 169.2, 12.5, 6.0, 2.6, −266.1, −278.0, minor resonances: δ = 174.0, 19.7, 5.2 and −38.2.

5.7.11. Synthesis of Borate Substituted Siliconoid 194

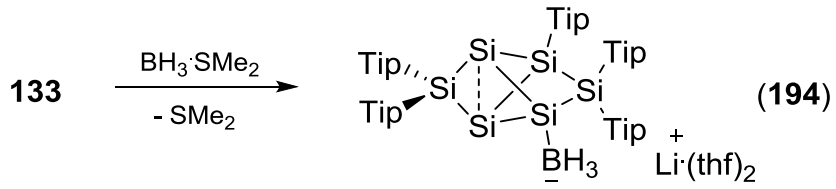

C_2H_9BS
75.96 g/mol

$C_{83}H_{134}BLiO_2Si_6$
1350.24 g/mol

A solution of 1.00 g **133**·5.4thf·1.1naph (0.58 mmol) in 10 mL toluene is cooled to −78°C. Borane dimethyl sulfide adduct (0.58 mmol, 55 µL) is added dropwise and the color of the reaction mixture changes from orange to dark red-brownish. The reaction mixture is allowed to warm up to room temperature in the thawing cold bath and stirred for additional 20 min. Evaporating the solvent is followed by sublimation of remaining naphthalene under reduced pressure (10^{-3} mbar) at rt. Crystallization from toluene yields 446 mg (60% yield) of bright yellow crystals of **194**. **M. p.** > 220°C, dec).

^{1}H NMR (300.13 MHz, 300 K, C_6D_6): δ = 7.06-6.87 (br, 10H, Tip-C*H*), 5.42 (br, 1H, Tip-^{i}Pr-C*H*), 5.27 (br, 1H, Tip-^{i}Pr-C*H*), 4.92 (br, 1 H, Tip-iPr-C*H*), 4.52 (br, 1H, Tip-^{i}Pr-C*H*), 4.03 (br, 4H, Tip-^{i}Pr-C*H*), 3.35 (m, thf, CH_2O) 2.85-2.54 (br, 7H, Tip-^{i}Pr-C*H*), 3.51 (br, 1H, Tip-^{i}Pr-C*H*), 2.33-0.00 (br m, altogether 93 H ,Tip-^{i}Pr-CH_3, BH_3, 1.38 (m, thf, CH_2). **^{7}Li NMR** (116.64 MHz, 300 K, C_6D_6): δ = −0.66, **^{11}B NMR** (96.3 MHz, 300 K, C_6D_6): δ = −41.27 (q, $^1J_{B\text{-}H}$ = 75 Hz), **^{13}C{H} NMR** (75.46 MHz, 300 K, C_6D_6): δ = 153.69 (br, 7 C, Ar-*C*), 149.51, 149.08 (each s, each 1 C, Ar-*C*), 147.78 (s, 3 C, Ar-*C*), 141.23, 139.93, 139.12, 133.27 (each s, each 1 C, Ar-*C*), 123.47-120.10 (br, 14 C, Ar-*C*), 68.15 (s, thf, *C*H_2O) 35.55, 34.66, 34.48, 34.24, 34.18, 27.94, 24.06, 24.01, 23.91 (s, some br, Tip-^{i}Pr-*C*H and Tip-^{i}Pr-*C*H_3), 25.34 (s, thf, *C*H_2), **^{29}Si{H} NMR** (59.62 MHz, 300 K, C_6D_6): δ = 161.22 (s, *Si*Tip$_2$), 12.15 (s, *Si*Tip$_2$), 7.07 (s, *Si*Tip), −4.78 (br, *Si*BH_3), −257.26, −264.95 (*Si*Si_3); **UV/vis (hexane):** $\lambda_{max}(\varepsilon)$ = 475 nm (220 $M^{-1}cm^{-1}$), 360 nm (3960 $M^{-1}cm^{-1}$); **Elemental Analyses** calculated for $C_{79}H_{126}BLiOSi_6$: C, 74.24, H, 9.94, N, 0.00. Found: C, 72.61, H, 9.65, N, 0.00.

5.7.12. Synthesis of Anionic Siliconoid 195

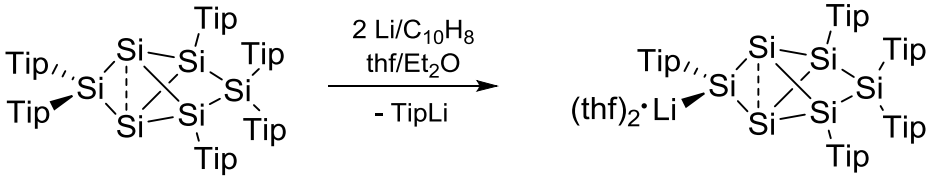

$C_{90}H_{138}Si_6$
1388.57 g/mol

$C_{83}H_{131}LiO_2Si_6$
1336.41 g/mol

A solution of 4.5 g of siliconoid **125** (3.2 mmol) in 10 mL of Et_2O is cooled to −78°C and 14.5 mL of a lithium/naphthalene solution in thf (0.5 M, 7.25 mmol) are added. The reaction mixture is allowed to slowly warm to room temperature in the thawing cold bath. After stirring at rt overnight all volatiles are removed in vacuum and the residue is digested with 160 mL of hexane. Pure **195**·$(thf)_2$ is filtered off as pale orange microcrystalline residue (1.31 g; 31% yield) at 35°C. **M. p.** 208-212°C (rearrangement). Single crystalline material was obtained from a toluene solution containing a few drops of thf as **195**·$(thf)_3$.
^{1}H NMR (300.13 MHZ, C_6D_6, 300 K): δ = 7.27 (d, 1H, Tip-*H*), 7.26 (d, 1H, Tip-*H*), 7.05 (d, 1H, Tip-*H*), 6.98 (s, 2H, Tip-*H*), 6.94 (d, 1H, Tip-*H*), 6.91 (s, 1H, Tip-*H*), 6.83, 6.81 (each d, each 1H, Tip-*H*), 5.44 (hept, 1H, ^{i}Pr-C*H*), 5.06 (m, 2H, ^{i}Pr-C*H*), 4.56 (hept, 1H, ^{i}Pr-C*H*), 4.43 (hept, 1H, ^{i}Pr-C*H*), 4.16 (hept, 2H, ^{i}Pr-C*H*), 3.62 (hept, 1H, ^{i}Pr-C*H*), 3.36 (m, 2H, ^{i}Pr-C*H*), 3.03 (t, 8H, thf-CH_2OCH_2), 2.75 (m, 5H, ^{i}Pr-C*H*), 2.14 (m, 6H, ^{i}Pr-CH_3), 1.61 (m, 28H, ^{i}Pr-CH_3), 1.22 (br, 8H, thf-CH_2CH_2OCH_2CH_2), 1.19 (m, 29H, ^{i}Pr-CH_3), 0.93 (d, 6H, ^{i}Pr-CH_3), 0.67 (m, 15H, ^{i}Pr-CH_3), 0.34 (m, 6H, ^{i}Pr-CH_3), **^{7}Li NMR** (116.6 MHZ, C_6D_6, 300 K): δ = 0.31 (s), **^{13}C{H} NMR** (75.5 MHZ, C_6D_6, 300 K): δ = 158.3, 156.4, 156.1, 156.0, 153.8, 153.5, 152.5, 152.4, 151.0, 149.3, 148.8, 148.4, 148.3, 147.5, 146.2, 140.9, 139.8, 131.6, 131.5 (Ar-*C*), 123.0, 122.6, 122.4, 122.2, 121.4, 121.3, 120.9, 120.1, 119.8 (Ar-*C*H), 68.5 (thf-*C*H_2O*C*H_2), 36.8, 36.7, 36.5, 36.3, 36.1, 36.0, 35.1, 34.9, 34.8, 34.7, 34.6, 30.2, 28.1, 27.8, 27.5, 27.1, 26.7, 25.6 (Tip-^{i}Pr-*C*H and Tip-^{i}Pr-*C*H_3), 25.3 (thf-*C*H_2CH_2OCH_2*C*H_2), 25.2, 24.9, 24.8, 24.7, 24.6, 24.5, 24.3, 24.2, 23.6, 22.6, 21.9 (Tip-^{i}Pr-*C*H and Tip-^{i}Pr-*C*H_3), **^{29}Si{H} NMR** (59.6 MHZ, C_6D_6, 300 K): δ = 267.9 (br), 100.2, 15.3, −43.8, −222.2, −231.4; **UV/vis** (hexane): $\lambda_{max}(\varepsilon)$ = 468 nm (600 $M^{-1}cm^{-1}$), 368 nm (6400 $M^{-1}cm^{-1}$); **Elemental analysis:** calculated for $C_{83}H_{131}LiO_2Si_6$: C, 74.60; H, 9.88. Found: C, 72.68; H, 9.51.

5.7.13. Rearrangement of 195 upon Melting

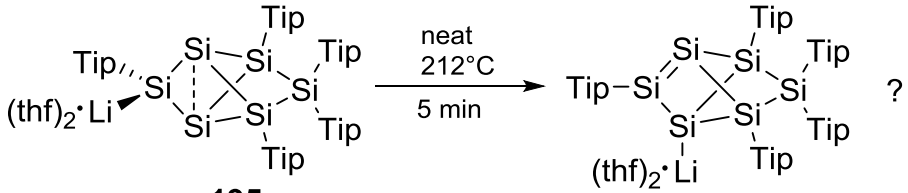

195
$C_{83}H_{131}LiO_2Si_6$
1336.41 g/mol

196
$C_{83}H_{131}LiO_2Si_6$
1336.41 g/mol

100 mg **195** are placed in an NMR tube, molten and kept at 212°C for two minutes. **^{7}Li NMR** (116.6 MHZ, C_6D_6, 300 K): δ = 1.93, 0.78 (br), **^{29}Si{H} NMR** (59.6 MHZ, C_6D_6, 300 K): δ = 54.5, 10.9, −68.9, −83.5, −248.3 (br), −275.8.

5.7.14. Reaction of 195 with 12-crown-4

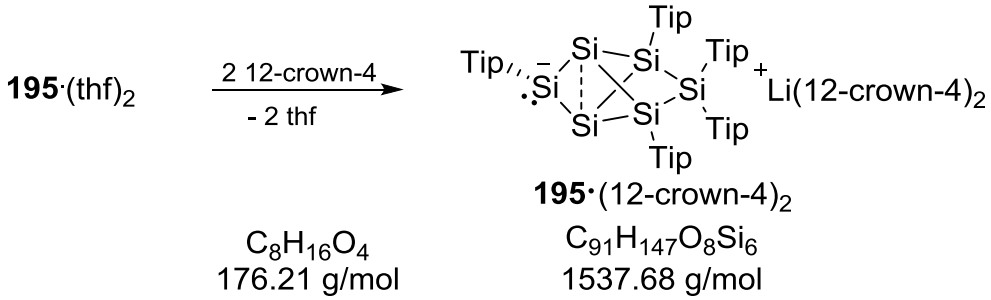

$C_8H_{16}O_4$
176.21 g/mol

$C_{91}H_{147}O_8Si_6$
1537.68 g/mol

12-crown-4 (0.17 mmol, 27 μL) was added o a solution of 110 mg anionic siliconoid **195** (0.082 mmol) in 2.5 mL thf. The resulting mixture was stirred for one hour and subsequently all volatiles were removed in vacuum.

^{1}H NMR (300.13 MHZ, thf-d_8, 300K): δ = 7.03 (s, 2H, Tip-*H*), 6.92 (s, 1H, Tip-*H*), 6.75, 6.69, 6.59 (each m, overall 6H, Tip-*H*), 6.51 (s, 1H, Tip-*H*), 5.38 (m, 1H, ^{i}Pr-C*H*), 4.91 (m, 2H, ^{i}Pr-C*H*), 4.35 (m, 2H, ^{i}Pr-C*H*), 3.63 (s, 34H 12-crown-4-CH_2), 3.35, 3.12, 2.71 (each m, overall 10H, ^{i}Pr-C*H*), 1.80, 1.53, 1.40, 1.30, 1.24, 1.25 (each br, overall 62H, ^{i}Pr-CH_3), 0.68, 0.34, 0.01 (each m, overall 28 H, ^{i}Pr-CH_3). **^{29}Si{H} NMR** (59.6 MHZ, thf-d_8, 300 K): δ = 304.1, 117.3, 8.8, −53.7, −212.0, −230.2, *15% side product*: 21.7, −16.1, −18.4, −68.6, −71.7, −191.7.

5.7.15. Synthesis of Silyl Substituted Siliconoid 197

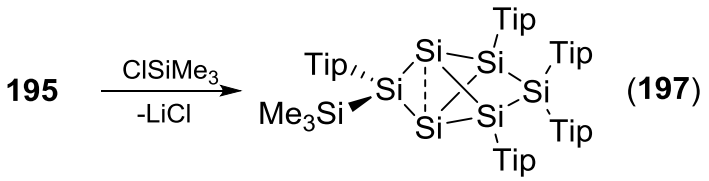

C_3H_9ClSi
108.64 g/mol

$C_{78}H_{124}Si_7$
1258.45 g/mol

To a solution of 104 mg of anionic siliconoid **195** (0.078 mmol) in 2 mL of toluene 11 μL of trimethylsilyl chloride (0.086 mmol) are added *via* micro syringe. The reaction mixture is stirred for 2.5 h at ambient temperature. Subsequently all volatiles are removed in vacuum. The residue is digested with hexane and filtered. Concentration of the mother liquor affords 65 mg (yield: 66%) of trimethylsilyl substituted siliconoid **197** as orange crystals (m. p. 193°C).

^{1}H NMR (300.13 MHZ, C_6D_6, 300 K): δ = 7.27 (d, 2H, Tip-*H*), 7.07, 7.01, 6.97, 6.91, 6.83 (each d, each 1H, Tip-*H*), 6.80 (d, 2H, Tip-*H*), 6.75 (d, 1H, Tip-*H*), 4.93 (m, 2H, ^{i}Pr-C*H*), 4.37 (sept., 1H, ^{i}Pr-C*H*), 4.06 (sept., 2H, ^{i}Pr-C*H*), 3.74, 3.63 (each m, each 1H, ^{i}Pr-C*H*), 3.57 (t, 10H, THF), 3.37 (m, 2H, ^{i}Pr-C*H*), 2.71 (m, 6H, ^{i}Pr-C*H*), 2.14 (d, 3H, ^{i}Pr-CH_3), 2.05 (d, 3H, ^{i}Pr-CH_3), 1.82 (d, 3H, ^{i}Pr-CH_3), 1.67 (m, 7H, ^{i}Pr-CH_3), 1.57 (m, 14H, ^{i}Pr-CH_3), 1.43 (br, 10H, THF), 1.24, 1.21, 1.20, 1.18, 1.17, 1.16, 1.15, 1.13,

1.11, 1.08 (each d, overall 36H, ^{i}Pr-CH_3), 0.79 (d, 3H, ^{i}Pr-CH_3), 0.67 (t, 6H, ^{i}Pr-CH_3), 0.51 (m, 6H, ^{i}Pr-CH_3), 0.40, 0.38 (each d, overall 6H, ^{i}Pr-CH_3), 0.29 (d, 3H, ^{i}Pr-CH_3), −0.15 (s, 9H, Si(CH_3)$_3$), **^{29}Si{H} NMR** (59.6 MHZ, C_6D_6, 300 K): δ = 193.6 (s), 29.2 (s), 22.4 (s), −11.2 (s), −15.9 (s), −242.0 (s), −253.3 (s), **^{13}C NMR** (75.5 MHZ, C_6D_6, 300 K): δ = 157.1, 156.9, 156.6, 156.1, 153.7, 153.2, 152.6, 152.0, 150.7, 150.2, 149.9, 149.4, 149.2, 138.7, 138.3, 134.8, 129.1, 126.9, 123.7 (Ar-*C*), 123.1, 122.8, 122.6, 122.4, 122.2, 122.1, 121.7, 121.6, 121.3, 121.0 (Ar-*C*H), 37.7, 37.6, 37.3, 36.9, 36.7, 36.4, 35.1, 35.0, 34.8, 34.7, 34.6, 34.5, 27.8, 27.6, 27.4, 27.1, 27.0, 26.5, 26.4, 26.2, 25.7, 25.4, 25.3, 25.1, 25.0, 24.9, 24.6, 24.4, 24.3, 24.1, 24.0, 23.9, 22.6 (Tip-^{i}Pr-*C*H and Tip-^{i}Pr-*C*H$_3$), 1.5 (Si(*C*H$_3$)$_3$; **UV/vis** (hexane): $\lambda_{max}(\varepsilon)$ = 468 nm (600 $M^{-1}cm^{-1}$), 368 nm (6400 $M^{-1}cm^{-1}$); **Elemental analysis:** calculated for $C_{78}H_{124}Si_7$: C, 74.45; H, 9.93. Found: C, 71.65; H, 9.83.

5.7.16. Oxidation of 195 with Silver (Perfluorotetraphenyl)borate

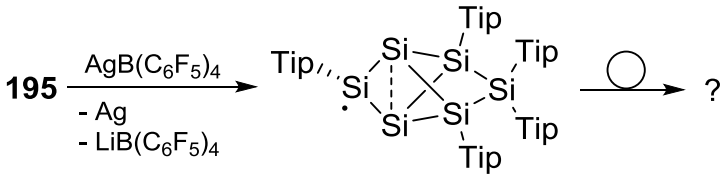

198

$C_{24}AgBF_{20}$
786.91 g/mol

$C_{75}H_{115}Si_6$
1185.26 g/mol

58.6 mg (0.075 mmol) silver (perfluorotetraphenyl)borate were dissolved in 5 mL diethyl ether and cooled to −80°C. A solution one equivalent **195** (100 mg) in 5 mL diethyl ether cooled to −80°C was added to the vigorously stirred borate solution *via* cannula. The reaction mixture was allowed to warm up to room temperature within 3 h and turned very pale yellow. All volatiles were removed in vacuum, the colorless residue digested with hexane and filtered. The filtrate was reduced to dryness and a colorless solid was obtained. **^{1}H NMR** (300.13 MHZ, C_6D_6, 300 K): *selected resonance*: δ = 6.02 (s, Si-*H*), **^{29}Si{H} NMR** (59.6 MHZ, C_6D_6, 300 K): 8.3, −15.8, −24.4, −76.6, −90.1, −91.6.

5.8. Synthesis of Dianionic Si_5-Cluster 201

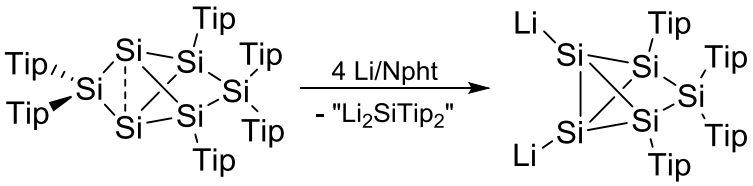

125

$C_{90}H_{138}Si_6$
1388.57 g/mol

201

$C_{60}H_{92}Li_2Si_5$
967.70 g/mol

A solution of 670 mg of siliconoid **125** (3.2 mmol) in 10 mL of Et_2O was cooled to −78°C and 4.4 mL of a lithium/naphthalene solution in thf (0.5 M, 4.4 equivalents) was added. The reaction mixture was allowed to slowly warm to room temperature in the thawing cold bath. After stirring at rt overnight all volatiles were removed in vacuum and the residue was digested with hexane. After filtration, the filtrate was reduced to dryness. **^{7}Li NMR** (116.6 MHZ, C_6D_6, 300 K): δ = 3.71, 0.96 (br), **^{29}Si{H} NMR** (59.6 MHZ, C_6D_6, 300 K): major resonances: δ = 55.7, −90.1, minor resonances: δ = 19.7, −7.4.
The residue was dissolved in toluene and standing at rt for one week afforded a small amount of single crystals of **201**·$(thf)_3$.

5.9. Synthesis of Thio-functionalized Disilenes

5.9.1. Reaction of Disilenide 16 with *p*-Bromo Thiophenol

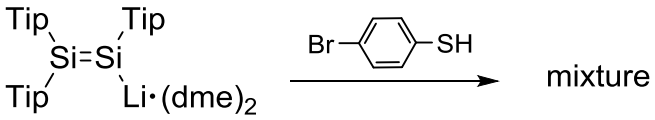

16

$C_{53}H_{89}LiO_4Si_2$
853.38 g/mol

C_6H_5BrS
189.07 g/mol

Disilenide **16** (100 mg, 0.117 mmol) was dissolved in 5 mL toluene. A solution of one equivalent (22.12 mg) *p*-bromo thiophenol in 5 mL toluene was added dropwise. The solution was stirred for 12 h. NMR spectroscopic investigation revealed a complex mixture.

5.9.2. Synthesis of Disilene 204a

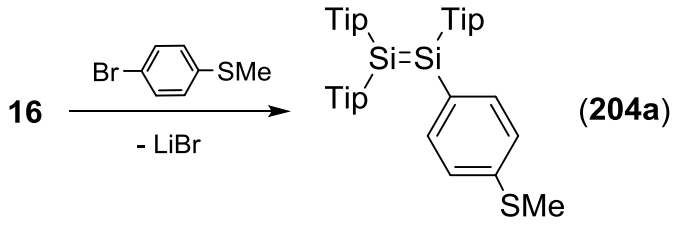

C_7H_7BrS
203.10 g/mol

$C_{52}H_{76}SSi_2$
789.41 g/mol

A solution of disilenide **16** (0.51 g, 0.52 mmol) in toluene (20 mL) is cooled to −80°C and a solution of 1.1 equivalents *p*-bromothioanisole (0.12 g) in toluene (20 mL) is added *via* cannula. The mixture is allowed to warm up to rt and stirred for additional

22 h. All volatiles are removed in vacuum and 20 mL of hexane are added. The orange suspension is filtered. Subsequently the filtrate is reduced to dryness and the crude product is dissolved in 1 mL of pentane. Standing for several weeks at room temperature affords **204a** as yellow crystals.
^{1}H NMR (300.13 MHz, C_6D_6, 300 K): δ = 7.24 (d, $^{3}J_{H\text{-}H}$ = 8.4 Hz, 2H, phenylene-*H*), 7.14, 7.11, 7.05 (each s, each 2H, Tip-*H*), 6.76 (d, $^{3}J_{H\text{-}H}$ = 8.4 Hz, 2H, phenylene-*H*), 4.30 (hept, $^{3}J_{H\text{-}H}$ = 6.7 Hz, 2H, Tip-^{i}Pr-C*H*), 4.2 (hept, $^{3}J_{H\text{-}H}$ = 6.7 Hz 2H, Tip-^{i}Pr-C*H*), 4.02 (hept, $^{3}J_{H\text{-}H}$ = 6.6 Hz, 2H, ^{i}Pr-C*H*), 2.84-1.61 (m, 3H, ^{i}Pr-C*H*), 1.85 (s, 3H, SCH_3), 1.28-1.03 (m, ^{i}Pr-CH_3), **^{29}Si{H} NMR** (59.6 MHz, C_6D_6, 300 K): δ = 71.3, 55.1; **UV/vis** (hexane): $\lambda_{max}(\varepsilon)$ = 447 nm (14800 $M^{-1}cm^{-1}$), 278 nm (17800 $M^{-1}cm^{-1}$); **Elemental analysis** calculated for $C_{52}H_{76}SSi_2$: C, 79.12; H, 9.7; S, 4.06. Found: C, 76.97; H, 9.54; S 3.30.

5.9.3. Synthesis of Disilene 204b

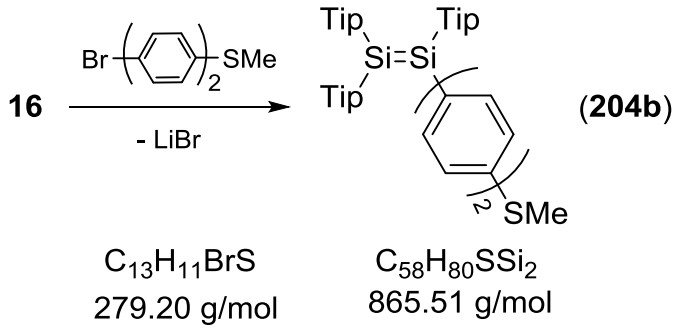

4′-Bromo-4-methylthiobiphenyl (166 mg, 0.59 mmol) is dissolved in toluene (25 mL) and cooled to −80°C. A −80°C cold solution of disilenide **16** (501 mg, 0.59 mmol) in toluene (10 mL) is added to the sulfide solution *via* cannula. The reaction mixture is allowed to warm up to rt and stirred for additional three hours. All volatiles are removed in vacuum and the residue is digested with 10 mL of hexane. The red suspension is filtered and the mother liquor reduced to dryness to afford crude **204b** as red-orange solid (217 mg, 0.25 mmol) in 43 % yield.
^{1}H NMR (300.13 MHz, C_6D_6, 300 K): δ = 7.28 (d, 2H, phenylene-*H*), 7.28-699 (m, 12H, phenylene-*H* and Tip-*H*), 4.31 (m, 3H, Tip-^{i}Pr-C*H*), 4.10 (hept, $^{3}J_{H\text{-}H}$ = 6.6 Hz, 2H, Tip-^{i}Pr-C*H*), 1.99 (s, 3H, SCH_3), 1.29-1.03 (m, ^{i}Pr-CH_3), **^{29}Si{H} NMR** (59.6 MHz, C_6D_6, 300 K): δ = 70.9, 56.1; **UV/vis** (hexane): $\lambda_{max}(\varepsilon)$ = 456 nm (10600 $M^{-1}cm^{-1}$), 295 nm (27000 $M^{-1}cm^{-1}$).

5.9.4. Synthesis of Disilene 204c

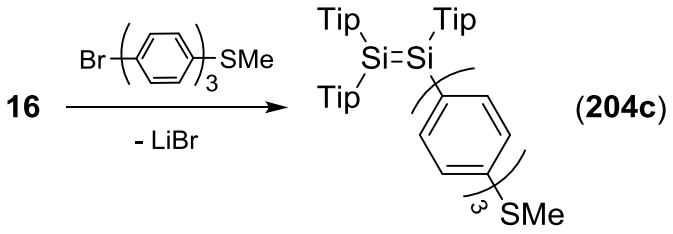

$C_{19}H_{15}BrS$ 355.29 g/mol

$C_{64}H_{84}SSi_2$ 941.61 g/mol

(4''-bromo-*p*-terphenyl-4-yl)-(methyl)sulfane (210 mg, 0.59 mmol) was dispersed in toluene (50 mL) and cooled −80 °C. Disilenide **16** (505 mg, 0.59 mmol) was dissolved in toluene (20mL) and added to the sulfide suspension *via* cannula. The mixture was allowed to warm up to rt. Subsequently, all volatiles were removed in vacuo and the residue digested with toluene (20 mL). The dark red suspension is filtered and the filtrate reduced to dryness. Crude **204c** was obtained as red solid (434 mg, 0.46 mmol, 78% yield).

^{1}H NMR (300.13 MHz, C_6D_6, 300 K): δ = 7.74 – 6.57 (m, 24H, terphenylene-*H* and Tip-*H*), 4.52 – 2.47 (m, 9H, ^{i}Pr-CH), 2.09 (s, 3H, SCH_3), 1.79-0.20 (m, ^{i}Pr-CH_3); **^{29}Si{H} NMR** (59.6 MHz, C_6D_6, 300 K): δ = 70.8, 56.3; **UV/vis** (hexane): $\lambda_{max}(\varepsilon)$ = 456 nm (5000 $M^{-1}cm^{-1}$), 303 nm (33900 $M^{-1}cm^{-1}$).

5.9.5. Synthesis of Disilene 205

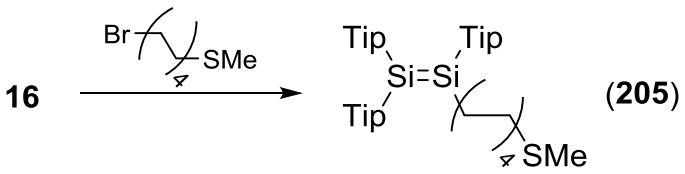

$C_9H_{19}BrS$ 239.22 g/mol

$C_{54}H_{88}SSi_2$ 825.53 g/mol

Disilenide **16** (524 mg, 0.62 mmol) was dissolved in toluene (17 mL) and cooled to −80 °C. 8-Methylthiooctyl bromide (155 mg, 0.65 mmol) was dissolved in toluene (3 mL) and transferred to the disilenide solution *via* cannula. The mixture was allowed to warm up to room temperature and stirred for additional 23 h. A color change from orange to green-yellow was observed. All volatiles were removed in vacuo and a greenish-yellow solid was obtained. Hexane was added to the residue and the suspension was filtered. The filtrate was reduced to dryness to afford crude **205** as yellow solid.

^{1}H NMR (300.13 MHz, C_6D_6, 300 K) δ = 7.32, 7.30, 7.24 (each s, each 2H, each Tip-*H*), 4.38 (sept, 3H, ^{i}Pr-C*H*), 4.17-4.05 (m, 2H, ^{i}Pr-C*H*), 3.42-3.26 (m, 2H, CH_2S),

3.02-2.77 (m, 4H, ^{i}Pr-C*H*), 2.49-2.36 (m, 2H, CH_2CH$_2$S), 2.01-1.94 (m, 3H, SCH_3), 1.83-0.98 (m, remaining aliphatic *H* and ^{i}Pr-CH_3); **^{29}Si{H} NMR** (59.6 MHz, C_6D_6, 300 K) δ= (59.6 MHz, C_6D_6, 300 K): δ = 82.1, 81.9, 52.2, 52.0; **UV/vis** (hexane): $\lambda_{max}(\varepsilon)$ = 407 nm (7900 $M^{-1}cm^{-1}$), 357 nm (5700 $M^{-1}cm^{-1}$).

5.9.6. Reaction of Disilenide 16 with Bis(4-bromophenyl)disulfide

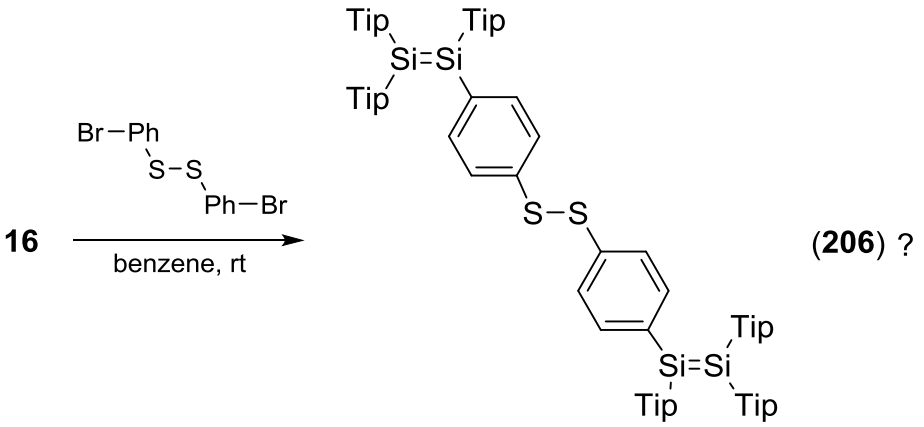

$C_{12}H_{10}Br_2S_2$ 378.14 g/mol

$C_{102}H_{146}S_2Si_4$ 1548.75 g/mol

Bis(4-bromophenyl)disulfide (112 mg, 0.30 mmol) is dissolved in benzene (130 mL) and a solution of disilenide (505 mg, 0.59 mmol) in THF (50 mL) is added dropwise for 6.5 h. After additional stirring for 15 h an intensively orange solution is received. The solvent is removed *in vacuo* and the orange solid is dissolved in hexane. The suspension is filtered and the filtrate is reduced to dryness. ^{1}H and ^{29}Si NMR spectra are measured. The remaining orange solid is dissolved in *n*-hexane to crystallize the desired product.

^{29}Si NMR: (59.6 MHz, C_6D_6, 300 K) major resonances: δ = 71.3 (br), 66.3 (br), -12.8 (br), minor resonances: 90.8, −3.9, −32.3 and −60.1.

6. References

[1] M. Schulenburg, *Bundesministerium für Bildung und Forschung (BMBF) Referat Publikationen*; Internetredaktion,11055 Berlin **2004**, Vom Sand zum Superchip.

[2] R. G. Blezard, "*The History of Calcareous Cements*" in Hewlett, C. Peter, ed. Lea's chemistry of cement and concrete. 4. ed. Amsterdam: Elsevier Butterworth-Heinemann, **2004**, 1-24.

[3] C. B. Carter, M. G. Norton, Ceramic materials: Science and engineering. *Springer* **2007**.

[4] B. H. W. S. de Jong, "Glass"; in "*Ullmann's Encyclopedia of Industrial Chemistry*"; 5th edition, *vol. A12*, VCH Publishers, Weinheim, Germany, **1989**.

[5] H.-H. Moretto, M. Schulze, G. Wagner "Silicones" in *Ullmann's Encyclopedia of Industrial Chemistry*, Wiley-VCH, Weinheim, **2000**.

[6] P. Siffert, E. F. Krimmel, *Science & Business Media,* Silicon: Evolution and future of a technology, Springer, **2004.**

[7] W. W. Emmett, Geolocigal Survey (US), *Geological Survey Professional Paper* **1975**, 870-A, A54.

[8] H. Davy, *Philosophical Transactions of the Royal Society [of London]* **1808**, *98*, 333–370, p. 353.

[9] T. Thomson, *A System of Chemistry in Four Volumes, 5th ed.* **1817**, *1*, 252.

[10] J. Brezelsius, *Kongliga Vetenskaps-Academiens Handlingar [Proceedings of the Royal Science Academy]* **1824**, *12*, 46–98.

[11] G. W. Pickard, *Patent US836531:* Means For Receiving Intelligence Communicated By Electric Waves. **1905**

[12] *Recent review:* B. L. Oliva-Chatelain, T. M. Ticich, A. R. Barron, *Nanocale* **2016**, doi: 10.1039/c5nr04978d.

[13] *For examples see:* (a) A. Höfler, T. Feudel, N. Strecker, W. Fichtner, K.-H. Stegemann, H. Syhre, G. Dallmann, *J. Appl. Phys.* **1995**, *78*, 3671–3679; (b) R. Tiwari, S. Chandra, B. R. Chakraborty, *Mat. Sci. Semicon. Proc.* **2013**, *16*, 2013–2020 and references herein.

[14] *For Aluminum:* (a) U. Landman, R. N. Barnett, A. G. Scherbakov, P. Avouris, *Phys. Rev. Lett.* **2000**, *85*, 1958−1961; *Gallium:* (b) S. W. Glunz, S. Rein, J. Knobloch, W. Wettling, T. Abe, *Prog. Photovolt: Res. Appl.* **1999**, *7*, 463–469; *Indium:* (c) S. Scalese, M. Italia, A. La Magna, G. Mannino, V. Privitera, M. Bersani, D. Giubertoni, M. Barozzi, S. Solmi, P. Pichler, J. Appl. Phys. **2003**, *93*, 9773–9782.

[15] (a) G. Feher, *Phys. Rev.* **1959**, *114*, 1219–1244; (b) A. M. Tyryshkin, S. A. Lyon, A. V. Astashkin, A. M. Raitsimring, *Phys. Rev.* **2003**, *B 68*, 193207/1–193207/4.

[16] (a) *For Arsenic:* (a) C. C. Lo, V. Lang, R. E. George, J. J. L. Morton, A. M. Tyryshkin, S. A. Lyon, J. Bokor, T. Schenkel. *Phys. Rev. Lett.* **2011**, *106*, 207601/1-207601/4; *Antimony:* (b) C. C. Lo, J. Bokor, T. Schenkel, A. M. Tyryshkin, S. A. Lyon, *Appl. Phys. Lett.* **2007**, *91*, 242106/1–242106/3; *Bismuth:* (c) G. W. Morley, M.

Warner, A. M. Stoneham, P. T. Greenland, J. van Tol, C. W. M. Kay, G. Aeppli *Nature Mater.* **2010**, *9*, 725–729.

[17] J. S Hill, *Multicrystalline Silicon Modules To Dominate Solar PV Industry In 2014*, **2012**, http://cleantechnica.com.

[18] H. Queisser, Kristallene Krisen, **1985**, S. 8, München.

[19] J. A. del Alamo, *Nature* **2011**, *479*, 317–323.

[20] W. Lu, C. M. Lieber, *Nature Mat.* **2007**, *6*, 841–850.

[21] *Unsuccessful attempts for P=P-bonds*: (a) H. Köhler, A. Michaelis, *Ber. Dtsch. Chem. Ges.* **1877**, *10*, 807−814; (b) J. J. Daly, L. Maier, *Nature*, **1964**, *203*, 1167-1168; *Si=O-bonds*: (c) F. S. Kipping, L. L. Loyed, *J. Chem. Soc., Trans.* **1901**, *79*, 449−459; *for Si=Si-bonds*: (d) F. S. Kipping, J. E. Sands, *J. Chem. Soc., Trans.* **1921**, *119*, 830−847. (e) F. S. Kipping, *J. Chem. Soc., Trans.* **1924**, *125*, 2291–2297.

[22] Although the expression “double bond rule” is often used in literature, it does not appear to exist an original citation for the initial mentioning of this rule. For early discussions see e. g.: (a) J. Goubeau, *Angew. Chem*. **1957**, *69*, 7; (b) P. Jutzi, *Angew. Chem*. **1975**, *87*, 269−283; *Angew. Chem. Int. Ed. Engl.* **1975**, *14*, 232–245.

[23] A. G. Brook, F. Abdesaken, B. Gutekunst, G. Gutekunst, R. K. Kallury, J. Chem. Soc., *Chem. Commun.* **1981**, 191–192.

[24] R. West, M. J. Fink, J. Michl, *Science*, **1981**, *214*, 1343–1344.

[25] M. Yoshifuji, I. Shima, N. Inamoto, K. Hirotsu, T. Higuchi, J. Am. Chem. Soc., **1981**, *103*, 4587–4589.

[26] *Review*: R. C. Fischer, P. P. Power, *Chem. Rev.* **2010**, *110*, 3877–3923.

[27] *Reviews*: (a) M. Weidenbruch in *The Chemistry of Organic Silicon Compounds, Vol. 3* (Eds.: Z. Rappoport, Y. Apeloig), Wiley, Chichester, UK, **2001**, Chapter 5; (b) M. Karni, Y. Apeloig, J. Kapp, von R. Schleyer in *The Chemistry of Organic Silicon Compounds, Vol. 3* (Eds.: Z. Rappoport, Y. Apeloig), John Wiley & Sons, Ltd. Chichester, **2001**, Chapter 1; (c) M. Kira, T. Iwamoto, *Adv. Organomet. Chem*. **2006**, *54*, 73–148; (d) V. Ya. Lee, A. Sekiguchi, *Organometallic Compounds of Low-coordinate Si, Ge, Sn and Pb*: *From Phantom Species to Stable Compounds,* Wiley, Chichester, UK, **2010**, Chapter 5.

[28] N. Wiberg, S. K. Vasisht, G. Fischer and P. Meyer, *Z. Anorg. Allg. Chem.* **2004**, *630*, 1823−1828.

[29] A. Sekiguchi, R. Kinjo, M. Ichinohe, *Science* **2004**, *305*, 1755−1757. (b) N. Wiberg, S. K. Vasisht, G. Fischer and P. Meyer, *Z. Anorg. Allg. Chem.* **2004**, *630*, 1823−1828.

[30] M. Faraday, *Phil. Trans. R. Soc. Lond*. **1825**, *115*, 440−466.

[31] *Review*: V. Ya. Lee, A. Sekiguchi, *Angew. Chem. Int. Ed.* **2007**, *46*, 6596−6620.

[32] (a) G. H. Spikes, J. C. Fettinger, P. P. Power, *J. Am. Chem. Soc.* **2005**, *127*, 12232−12333; (b) G. C. Welch, R. R. S. Juan, J. D. Masuda, D. W. Stephan, *Science* **2006**, *314*, 1124−1126; (c) G. D. Frey, V. Lavallo, B. Donnadieu, W. W. Schoeller, G. Bertrand, *Science* **2007**, *316*, 439−441.

[33] M. Kobayashi, T. Matsuo, T. Fukunaga, D. Hashizume, H. Fueno, K. Tanaka, K. Tamao, *J. Am. Chem. Soc.* **2010**, *132*, 15162−15163.

[34] (a) T. Iwamoto, S. Ishida in *Functional Molecular Silicon Compounds II Low Oxidation Sates* (Ed.: D. Scheschkewitz), Springer, **2015**, p. 128; (b) C. Präsang, D. Scheschkewitz, *Chem. Soc. Rev.* **2016**, *45*, 900–921.

[35] (a) D. E. Goldberg, D. H. Harris, M. F. Lappert, K. M. Thomas, *J. Chem. Soc., Chem. Commun.* **1976**, 261−262; (b) P. J. Davidson, D. H. Harris, M. F. Lappert, *J. Chem. Soc., Dalton Trans.* **1976**, 2268−2274; (c) P. B. Hitchcock, M. F. Lappert, S. J. Miles, A. J. Thorne, J*. Chem. Soc., Chem. Commun.* **1984**, 480−482.

[36] D. N. Roark, G. J. D. Peddle, *J. Am. Chem. Soc.* **1973**, *94*, 5837−5841.

[37] E. Fluck, K. Issleib, *Z. Naturforschg.* **1966**, *21b*, 736−738.

[38] K. S. Pitzer, *J. Am. Chem. Soc.* **1948**, *70*, 2140−2145.

[39] (a) R. S. Mulliken, *J. Am. Chem. Soc.* **1950**, *72*, 4493−4503; (b) R. S. Mulliken, *J. Am. Chem. Soc.* **1955**, *77*, 884−887.

[40] (a) E. A. Carter, W. A. Goddard, *J. Phys. Chem.* **1986**, *90*, 998-1001; (b) G. Trinqier, J. P. Malrieu, *J. Am. Chem. Soc.* **1987**, *109*, 5303-5315; (c) G. Trinquier, J. P. Malrieu, *J. Phys. Chem.* **1990**, *94*, 6184-6196.

[41] (a) A. R. W. McKeller, P. R. Bunker, T. J. Sears, K. M. Evenson, R. J. Saykally, S. R. Langhoff, *J. Chem. Phys.* **1983**, *79*, 5251−5264. (b) Sears, T. J.; Bunker, P. R. *J. Chem. Phys* **1983**, *79*, 5265-5271. (c) Bunker, P. R.; Jensen, P.; Kraemer, W. P.; Beardsworth, R. *J. Chem. Phys.* **1986**, *85*, 3724−3731.

[42] Experimental determinations of E_{ST} in SiH_2: (a) A. Kasden, E. Herbst, W. C. Lineberger, W. C. *J. Chem. Phys.* **1975**, *62*, 541−548; (b) J. L. Berkowitz, J. P. Green, H. Cho, R. Ruscic, *J. Chem. Phys.* **1987**, *86*, 1235−1248; Theoretical studies of E_{ST} in SiH_2: (c) T. J. Van Huis, Y. Yamaguchi, C. D. Sherrill, H. F. Schaefer III., *J. Phys. Chem.* **1997**, *101*, 6955−6963; (d) J. C. Stefens, Y. Yamaguchi, C. D. Sherrill, H. F. Schaefer, III., *J. Phys. Chem.* **1998**, *102*, 3999−4006. (e) Y. Apeloig, R. Pauncz, M. Karni, R. West, W. Steiner, D. Chapman, *Organometallics* **2003**, *22*, 3250−3256; For GeH_2: (f) J. Satgé, *Chem. Heterocycl. Compd.* **1999**, *35*, 1013−1032; (g) M. Haaf, T. A. Schmedake, R. West, *Acc. Chem. Res.* **2000**, *33*, 704−714; (h) N. Tokitoh, R. Okazaki, *Coord. Chem. Rev.* **2000**, *210*, 251−272.

[43] M. Karni, Y. Apeloig, *J. Am. Chem. Soc.* **1990**, *112*, 8589−8590.

[44] M. J. Fink, M. J. Michalczyk, K. J. Haller, R. West, J. Michl, *Organometallics*, **1984**, 793−800.

[45] M. Wind, D. R. Powell, R. West, *Organometallics* **1996**, *15*, 5772−5773.

[46] B. D. Sheherd, C. F. Campana, R. West, *Heteroat. Chem.* **1990**, *1*, 1-7.

[47] M. Kira, T. Iwamoto, *Adv. Organomet. Chem.* **2006**, *54*, 73-148.

[48] D. Scheschkewitz*, Chem. Lett.* **2011**, *40*, 2−11.

[49] A. Sekiguchi, S. Inoue, M. Ichinohe, Y. Arai, *J. Am. Chem. Soc.* **2004**, *126*, 9626–9629.

[50] S. Masamune, Y. Hanzawa, S. Murakami, T. Bally, J. F. Blount, *J. Am. Chem. Soc.* **1982**, 104, 1150−1153.

[51] A. Schaefer, M. Weidenbruch, K. Peters, H. G. Von Schnering, *Angew. Chem*. **1984**, *96*, 311-312; *Angew. Chem. Int. Ed. Engl.* **1984**, *23*, 302−303.

[52] M. Kira, T. Maruyama, C. Kabuto, K. Ebata, H. Sakurai, Angew. Chem. 1994, 106, 1575-1577; *Angew. Chem. Int. Ed. Engl.* **1994**, *33*, 1489−1491.

[53] H. Watanabe, K. Takeuchi, N. Fukawa, M. Kato, M. Goto, Y. Nagai, *Chem. Lett.* **1987**, 1341−1344.

[54] S. Masamune, Y. Eriyama, T. Kawase, *Angew. Chem.* **1987**, *99*, 601-602; *Angew. Chem. Int. Ed. Engl.* **1987**, *26*, 584−585.

[55]T. Iwamoto, J. Okita, C. Kabuto, M. Kira, *J. Am. Chem. Soc.* **2002**, *124*, 11604−11605.

[56] A. Sekiguchi, M. Ichinohe, S. Yamaguchi, *J. Am. Chem. Soc.* **1999**, *121*, 10231−10232.

[57] M. Ichinohe, Y. Arai, A. Sekiguchi, N. Takagi, S. Nagase, *Organometallics* **2001**, *20*, 4141−4143.

[58] Review: R. Okazaki, R. West, *Adv. Organomet. Chem.* **1996**, *39*, 231−273.

[59] D. J. De Young, M. J. Fink, R. West, J. Michl, *Main Group Met. Chem.* **1987**, *10*, 19−43.

[60] A. Sekiguchi, I. Maruki, H. Sakurai, *J. Am. Chem. Soc.* **1993**, 115, 11460−1 1466.

[61] S. Boomgaarden, W. Saak, M. Weidenbruch, H. Marsmann, *Z. Anorg. Allg. Chem.* **2001**, *627*, 349−352.

[62] M. Kira, T. Ishima, T. Iwamoto, M. Ichinohe, *J. Am. Chem Soc.* **2001**, *123*, 1676−1682.

[63] (a) R. West, D. J. de Young, K. J. Haller, *J. Am. Chem. Soc.* 1985, 107, 4942−4946; (b) R. P. K. Tan, G. R. Gilette, D. R. Powell, R. West, Organometallics 1991, 10, 546−551.

[64] H. B. Yokelson, A. J. Millevolte, K. J. Haller, R. West, *J. Chem. Soc. Chem. Commun.* **1987**, 1605−1606.

[65] C. E. Dixon, K. M. Baines, *Phosphorus, Sulfur, Silicon Relat. Elem*. **1997**, 124 & 125, 123-132.

[66] D. Scheschkewitz, *Chem. Eur. J.* **2009**, *15*, 2476−2485.

[67] M. Weidenbruch, S. Willms, W. Saak, G. Henkel, *Angew. Chem.* **1997**, *109*, 2612−2613; *Angew. Chem., Int. Ed. Engl.* **1997**, *36*, 2503−2504

[68] J. Park, S. A. Batcheller, S. Masamune, *J. Organomet. Chem.* **1989**, *367*, 39−45.

[69] D. Scheschkewitz, *Angew. Chem.* **2004**, *116*, 3025−3028; *Angew. Chem., Int. Ed.* **2004**, *43*, 2965−2967.

[70] M. Ichinohe, K. Sanuki, S. Inoue, A. Sekiguchi, *Organometallics* **2004**, *23*, 3088−3090.

[71] M. Ichinohe, K. Sanuki, S. Inoue, A. Sekiguchi, *Silicon Chem.* **2005**, *3*, 111−116.

[72] S. Inoue, M. Ichinohe, A. Sekiguchi, *Chem. Lett*. **2005**, *34*, 1564−1565.

[73] T. Iwamoto, M. Kobayashi, K. Uchiyama, S. Sasaki, S. Nagendram, H. Isobe, M. Kira, *J. Am. Chem. Soc.* **2009**, *131*, 3156−3157.

[74] M. J. Cowley, K. Abersfelder, A. J. P. White, M. Majumdar, D. Scheschkewitz, *Chem. Commun.* **2012**, *48*, 6595−6597.

[75] K. Abersfelder, D. Güclü, D. Scheschkewitz, *Angew. Chem.* **2006**, *118*, 1673-1675; *Angew. Chem., Int. Ed.* **2006**, *45*, 1643−1645.

[76]H. Yasuda, V. Y. Lee and A. Sekiguchi, *J. Am. Chem. Soc.* **2009**, *131*, 6352−6353.

[77] I. Bejan, D. Scheschkewitz, *Angew. Chem.* **2007**, *119*, 5885−5888; *Angew. Chem. Int. Ed.* **2007**, *46*, 5783−5786.

[78] A. Fukazawa, Y. Li, S. Yamaguchi, H. Tsuji and K. Tamao, *J. Am. Chem. Soc.* **2007**, *129*, 14164−14165.

[79] M. Majumdar, Iulia Bejan, Volker Huch, A. J. P. White, G. R. Whittell, A. Schäfer, I. Manners, D. Scheschkewitz, *Chem. Eur. J.* **2014**, *20*, 9225−9229.

[80] S. Inoue, M. Ichinohe, A. Sekiguchi, *Chem. Lett.* **2008**, *37*, 1044−1045.

[81] M. Hartmann, A. Haji-Abdi, K. Abersfelder, P. R. Haycock, A. J. P. White, D. Scheschkewitz, *Dalton Trans.* **2010**, 9288−9295.

[82] M. J. Cowley, K. Abersfelder, A. J. P. White, M. Majumdar, D. Scheschkewitz, *Chem. Commun.* **2012**, *48*, 6595−6597.

[83] T.-l. Nguyen, D. Scheschkewitz, *J. Am. Chem. Soc.* **2005**, *127*, 10174−10175.

[84] K. Abersfelder, D. Scheschkewitz, *J. Am. Chem. Soc.* **2008**, *130*, 4114−4121.

[85] K. Abersfelder, T.-l. Nguyen, D. Scheschkewitz, *Z. Anorg. Allg. Chem.* **2009**, *635*, 2093−2098.

[86] S. Inoue, M. Ichinohe, A. Sekiguchi, *Angew. Chem.* **2007**, *119*, 3410−43412; *Angew. Chem., Int. Ed.* **2007**, *46*, 3346−3348.

[87] H. Tanaka, S. Inoue, M. Ichinohe, A. Sekiguchi, *Organometallics* **2009**, *28*, 6625−6628.

[88] I. Bejan, D. Güclü, S. Inoue, M. Ichinohe, A. Sekiguchi, D. Scheschkewitz, *Angew. Chem.* **2007**, *119*, 3413−3416; *Angew. Chem., Int. Ed.* **2007**, *46*, 3349−3352.

[89] I. Bejan, S. Inoue, M. Ichinohe, A. Sekiguchi, D. Scheschkewitz, *Chem. Eur. J.* **2008**, *14*, 7119−7122.

[90] A. Jana, M. Majumdar, V. Huch, M. Zimmer, D. Scheschkewitz *Dalton Trans.* **2014**, *43*, 5175-5181.

[91] D. Nieder, C. B. Yildiz, A. Jana, M. Zimmer, V. Huch, D. Scheschkewitz, *Chem. Commun.* **2016**, *52*, 2772-2775.

[92] (a) S. P. Stanforth in *Comprehensive Organic Functional Group Transformations II*, A. R. Katritzky, R. J. K. Taylor, R, Eds.; Elsevier: Oxford **2005**, *2*, 1025−1057; (b) A. B. Dounay, L. E. Overman, *Chem. Rev.* **2003**, *103*, 2945−2964.

[93] N. Wiberg, W. Niedermayer, G. Fischer, H. Nöth, M. Suter, *Eur. J. Inorg. Chem.* **2002**, 10662−1070.

[94] T. Sasamori, K. Hironaka, Y. Sugiyama, N. Takagi, S. Nagase, Y. Hosoi, Y. Furukawa, N. Tokitoh, *J. Am. Chem. Soc.* **2008**, *130*, 13856–13857.

[95] K. Suzuki, T. Matsuo, D. Hashizume, K. Tamao, *J. Am. Chem. Soc.* **2011**, *133*, 19710–19713.

[96] Presumably better described as *bis(plumbylene*): L. Pu, B. Twamley, P. P. Power, *J. Am. Chem. Soc.* **2000**, *122*, 3524−3525.

[97] A. D. Phillips, R. J. Wright, M.M. Olmstead, P. P. Power, *J. Am. Chem. Soc.* **2002**, *124*, 5930−5931.

[98] M. Stender, A. D. Phillips, R. J. Wright, P. P. Power, *Angew. Chem.* **2002**, *114*, 1863−1865; *Angew. Chem., Int. Ed.*, **2002**, *41*, 1785−1787.

[99] Y. Murata, M. Ichinohe, A. Sekiguchi, *J. Am. Chem. Soc.* **2010**, *132*, 16768−16770.

[100] M. Asay, A. Sekiguchi, *Bull. Chem. Soc. Jpn.* **2012**, *85*, 1245−1261.

[101] K. Takeuchi, M. Ikoshi, M. Ichinohe, A. Sekiguchi, *J. Am. Chem. Soc.* **2010**, *132*, 930−931.

[102] K. Takeuchi, M. Ichinohe, A. Sekiguchi, *Organometallics* **2011**, *30*, 2044−2050.

[103] Takeuchi, M. Ikoshi, M. Ichinohe, A. Sekiguchi, *J. Organomet. Chem.* **2011**, *696*, 1156−1162.

[104] M. Driess, *Coord. Chem. Rev.* **1995**, *145*, 1−25.

[105] C.N. Smit, F.M. Lock, F. Bickelhaupt, *Tetrahedron Lett.* **1984**, *25*, 3011−3014.

[106] C.N. Smit, F. Bickelhaupt, *Organometallics* **1987**, *6*, 1156−1163.

[107] M. Driess, *Angew. Chem*. **1991**, *103*, 979–981, *Angew. Chem. Int. Ed. Engl.* **1991**, *30*, 1022–1024.

[108] E. Niecke, E. Klein, M. Nieger, *Angew. Chem.* **1989**, *101*, 792−793; *Angew. Chem. Int. Ed. Engl.* **1989**, *28*, 751−752.

[109] H. R. G. Bender, E. Niecke, M. Nieger, *J. Am. Chem. Soc.* **1993**, *115*, 3314−3315.

[110] M. Driess, S. Rell, H. Pritzkow, *J. Chem. Soc., Chem. Commun.* **1995**, 253−254.

[111] M. Driess, H. Pritzkow, S. Rell, U. Winkler, *Organometallics* **1996**, *15*, 1845−1855.

[112] M. Driess, H. Pritzkow, *Angew. Chem*. **1992**, *104*, 775−777; *Angew. Chem. Int. Ed. Engl*. **1992**, *31*, 751−753.

[113] B. Li, T. Matsuo, D. Hashizume, H. Fueno, K. Tanaka, K. Tamao, *J. Am. Chem. Soc.* **2009**, *131*, 13222−13223.

[114] B. Li, T. Matsuo, T. Fukunaga, D. Hashizume, H. Fueno, K. Tanaka, K. Tamao, *Organometallics* **2011**, *30*, 3453−3456.

[115] . Driess, H. Pritzkow, U. Winkler, *J. Organomet. Chem.* **1997**, *529*, 313−321.

[116] M. Driess, S. Block, M. Brym, M. T. Gamer, *Angew. Chem.* **2006**, *118*, 2351−2354; *Angew. Chem. Int. Ed.* **2006**, *45*, 2293 −2296.

[117] S.Yao, S. Block, M. Brym, M. Driess, *Chem. Commun*. **2007**, 3844−3846.

[118] (a) D. Himmel, A. Schnepf, I. Krossing, *Angew. Chem.* **2014**, *126*, 378−382; *Angew. Chem. Int. Ed.* **2014**, *53*, 370 – 374; (b) G. Frenking, *Angew. Chem.* **2014**, *126*, 6152−6158; *Angew. Chem. Int. Ed.* **2014**, *53*, 6040−6046.

[119] Intramolecular nitrogen-donor stabilization of a P=Si bond: R.Corriu, G. Lanneau, C. Priou, *Angew. Chem.* **1991**, *103*, 1153−1155; *Angew. Chem. Int. Ed. Engl.* **1991**, *30*, 1130−1132.

[120] S. Inoue, W. Wang, C. Praesang, M. Asay, E. Irran, M. Driess, *J. Am. Chem. Soc.* **2011**, *133*, 2868−2871.

[121] N. C. Breit, T. Szilvási, S. Inoue, *Chem. Commun.* **2015**, *51*, 11272−11275.

[122] N. C. Breit, T. Szilvási, T. Suzuki, D. Gallego, S. Inoue, *J. Am. Chem. Soc.* **2013**, *135*, 17958−17968.

[123] N. C. Breit, T. Szilvási, S. Inoue, *Chem. Eur. J.* **2014**, *20*, 9312−9318.

[124] H. Cui, J. Zhang, C. Cui, *Organometallics* **2013**, *32*, 1−4.

[125] K.Hansen, T. Szilvási, B. Blom, S. Inoue, J. Epping, M. Driess, *J. Am. Chem. Soc.* **2013**, *135*, 11795−11798.

[126] K. Hansen, T. Szilvási, B. Blom, E. Irran, M. Driess, *Chem. Eur. J.* **2014**, *20*, 1947−1956.

[127] K. Hansen, T. Szilvási, B. Blom, M. Driess, *Organometallics* **2015**, *34*, 5703−5708.

[128] K. Hansen, Tibor Szilvási, B. Blom, M. Driess, *Angew. Chem.* **2015**, *127*, 15274−15277; *Angew. Chem. Int. Ed.* **2015**, *54*, 15060−15063.

[129] V. Ya. Lee, M.Kawai, A. Sekiguchi, H. Ranaivonjatovo, J. Escudié, *Organometallics***2009**, *28*, 4262−4265.

[130] P. Willmes, *Masterthesis* **2013**, Saarland University*, Krupp-Chair of General and Inorganic Chemistry*, Scheschkewitz Group.

[131] a) I. Fleming, U. Ghosh, *J. Chem. Soc., Perkin Trans.* **1994**, 257–262; b) M. Buswell, I. Fleming, U. Ghosh, S. Mack, M. Russell, B. P. Clark, *Org. Biomol. Chem.* **2004**, *2*, 3006–3017.

[132] A. C. R. Joanis, *Acad. Sci.* **1891**, *113*, 795−798.

[133] (a) E. Zintl, A. Harder, *Z. Phys. Chem.* **1931**, *A154*, 47−92; (b) E. Zintl, W. Dullenkopf, *Z. Phys. Chem*. **1932**, *B16*, 195.

[134] a) S. Scharfe, T. F. Fässler, *Philos. Trans. R. Soc. London Ser. A* **2010**, *328*, 1265−1284; (b) S. Scharfe, T. F. Fässler, in Nanoparticles - From Theory to Application Vol. 2 (Ed.: G. Schmid), WILEY-VCH,Weinheim, **2010**, pp. 49.

[135] . Matsumoto, K. Higuchi, Y. Hoshino, H. Koike, Y. Naoi, Y. Nagai, *J. Chem. Soc., Chem. Commun.* **1988**, 1083−1084.

[136] Reviews: (a) A. Sekiguchi, H. Sakurai, *Adv. Organomet. Chem.* **1995**, *37*, 1−38; (b) N. Wiberg, P. P. Power, in Molecular Clusters of the Main Group Elements, (Ed.: M. Dries and H. Nöth), Wiley-VCH, New York, **2004**, pp. 188

[137] N. Wiberg, C. M. M. Finger, K. Polborn*, Angew. Chem.* **1993**, *105*, 1140−1142; *Angew. Chem., Int. Ed. Engl.* **1993**, *32*, 1054−1056.

[138] N. Wiberg, W. Hochmuth, H. Nöth, M. Schmidt-Amelunxen, *Angew. Chem.* **1996**, *108*, 1437−1438; *Angew. Chem., Int. Ed. Engl.* **1996**, *35,* 1333

[139] M. Ichinohe, M. Toyoshima, R. Kinjo, A. Sekiguchi, *J. Am.Chem. Soc.* **2003**, *125*, 13328–13329;

[140] Reviews: (a) A. Schnepf, *Chem. Soc. Rev*. **2007**, *36*, 745−758; (b) A. Schnepf, *New J. Chem.* **2010**, *34*, 2079−2092; for reviews concerning Zintl Ions, cage compounds, and intermetalloid Clusters of Group 14 and Group 15 Elements see: (c) S. Scharfe, F. Kraus, S. Stegmaier, A. Schier, T. F. Fässler, *Angew. Chem.* **2011**, *123*, 3712−3754; *Angew. Chem. Int. Ed.* **2011**, *50*, 3630−3670; (d) T. F. Fässler, *Struct. Bond.* 2011, *140*, 91−131.

[141] H. Schnöckel, *Dalton Trans.* **2005**, 3131−3136.

[142] K. Abersfelder, A. Russell, H. S. Rzepa, A. J. P. White, P. R. Haycock, D. Scheschkewitz, *J. Am. Chem. Soc.* **2012**, *134*, 16008−16016.

[143] (a) D. J. Chapman, S. C. Sevov, *Inorg. Chem.* **2008**, *47*, 6009−6013; (b) F. S. Kocak, P. Y. Zavalij, Y. F. Lam, B. W. Eichhorn, *Chem. Commun.* **2009**, 4197–4199.

[144] a) M. W. Hull, S. C. Sevov, *J. Am. Chem. Soc.* **2009**, *131*, 9026−9037; b) F. Li, A. MuÇoz-Castro, S. C. Sevov, *Angew. Chem.* **2012**, *124*, 8709–8712; *Angew. Chem. Int. Ed.* **2012**, *51*, 8581–8584; c) F. Li, S. C. Sevov, *J. Am. Chem. Soc.* **2014**, *136*, 12056–12063.

[145] a) S. Joseph, M. Hamberger, F. Mutzbauer, O. Härtl, M. Meier, N. Korber, *Angew. Chem. Int. Ed.* **2009**, *48*, 8770−8772; *Angew. Chem.* **2009**, *121*, 8926−8929; b) M. Waibel, F. Kraus, S. Scharfe, B. Wahl, T. F. Fässler, *Angew. Chem. Int. Ed.* **2010**, *49*, 6611−6615; *Angew. Chem*. **2010**, *122*, 6761−6765.

[146] N. Wiberg, H.-W. Lemer, S. Wagner, H. Nöth, T. Seifert, *Z. Naturforsch.* **1999**, *54b*, 877−880.

[147] B. E. Eichler, Philip P. Power, *Angew. Chem.* **2001**, *113*, 818−819; *Angew. Chem. Int. Ed.* **2001**, *40*, 796−797.

[148] J. M. Buriak, *Chem. Rev.* **2002**, *102*, 1271–1308.

[149] W. Lu, C. M. Lieber, *Nat. Mater.* **2007**, *6*, 841–850.

[150] H. N. Waltenburg, J. T. Yates, Jr., *Chem. Rev.* **1995,** *95,* 1589−1673.

[151] B. Issa, I. M. Obaidat, B. A. Albiss, Y. Haik, *Int. J. Mol. Sci.* **2013**, *14*, 21266−21305.

[152] D. K. Yu, R. Q. Zhang, S. T. Lee, *Phys. Rev. B* **2002**, *65*, 245417/1−245417/7; S. M.I. Morsy, *Int. J. Curr. Microbiol. App. Sci.* **2014**, *3*, 237−260.

[153] (a) H. Murakami, T. Kanayama, *Appl. Phys. Lett.* **1995**, *67*, 2341−2343. (b) W. M. M. Kessels, M. C. M. van de Sanden, D. C, Schram, *Appl. Phys. Lett.* **1998**, 72, 2397−2399; (c) M. T. Swihart, S. L. Girshick, *J. Phys. Chem. B.* **1999**, *103*, 64−76. (d) N. Ning, S. M. Rinaldi, H. Vach, *Thin Solid Films* **2009**, *517*, 6234−6238; (e) N. Ning, H. Vach, *Phys. Chem. A* **2010**, *114*, 3297−3305.

[154] (a) Y. S. Shcherbyna, T. V. Torchynska, *Thin Solid Films*n **2010**, *518*, 204−207; (b) T. V. Torchynska, *Superlattices Microstruct.* **2009**, *45*, 267−270.

[155] (a) X.-jun. Li, C.-ping Li, J.-cai Yang, A. F. Jalbout, *Int. J. Quant. Chem.* **2008**, *109*, 1283−1301; (b) M. Tang, C. Wang, W. Lu, K. Ho, *Phys. Rev. B.* **2006**, 74, 1−9, (c) D. Yu, R. Q. Zhang, S. T. Lee, *J. Appl. Phys.* **2002**, *92*, 7453−7458.

[156] T. Iwamoto, M. Tamura, C. Kabuto, M. Kira, *Science*, **2000**, *290*, 504−506.

[157] D. Scheschkewitz, *Angew. Chem.* **2005**, *117*, 3014−3016; *Angew. Chem. Int. Ed.* **2005**, *44*, 2954−2956.

[158] Gerd Fischer, Volker Huch, Peter Mayer, Sham Kumar Vasisht, Michael Veith, Nils Wiberg, *Angew. Chem.* **2005**, *117*, 8096−8099; *Angew. Chem. Int. Ed.* **2005**, *44*, 7884−7887.

[159] D. Nied, R. Köppe, W. Klopper, H. Schnöckel, F. Breher, *J. Am. Chem. Soc.* **2010**, *132*, 10264−10265.

[160] K. Abersfelder, A. J. P. White, H. S. Rzepa, D. Scheschkewitz, *Science* **2010**, *327*, 564−566.

[161] D. Kratzert, D. Leusser, J. J. Holstein, Birger Dittrich, K. Abersfelder, D. Scheschkewitz, D. Stalke, *Angew. Chem.* **2013**, *125*, 4574−457; *Angew. Chem. Int. Ed.* **2013**, *52*, 4478−4482.

[162] P. Jutzi, A. Mix, B. Rummel, W. W. Schoeller, B. Neumann, H.-G. Stammler, *Science* **2004**, *305*, 849−851.

[163] K. Leszczyńska, K. Abersfelder, A. Mix, B. Neumann, H.-G. Stammler, M. J. Cowley, P. Jutzi, D. Scheschkewitz, *Angew. Chem.* **2012**, *124*, 6891−6895; *Angew. Chem. Int. Ed.* **2012**, *51*, 6785−6788.

[164] Kinga Leszczyńska, K. Abersfelder, M. Majumdar, B. Neumann, H.-G. Stammler, H. S. Rzepa, P. Jutzi, D. Scheschkewitz, *Chem. Commun.* **2012**, *48*, 7820−7822.

[165] K. Abersfelder, A. J. P. White, R. J. F. Berger, H. S. Rzepa, D. Scheschkewitz, *Angew. Chem.* **2011**, *123*, 8082−8086; *Angew. Chem. Int. Ed.* **2011**, *50*, 7936−7939.

[166] A. Jana, V. Huch, M. Repisky, R. J. F. Berger, D. Scheschkewitz, *Angew. Chem.* **2014**, *126*, 3583−3588; *Angew. Chem. Int. Ed.* **2014**, *53*, 3514−3518.

[167] (a) Y. Chang, G. Li, A. Gao, H. Chen, Q.-s. Li *Theor. Chem. Acc.* **2011**, *130*, 1009−1022; (b) S. A. Fischer, C. M. Isborn, O. V. Prezhdo *Chem. Sci.* **2011**, *2*, 400−406.

[168] The experiment was carried out initially by Dr. Kai H. Abersfelder, Saarland University*, Krupp-Chair of General and Inorganic Chemistry*, Scheschkewitz Group.

[169] Reductive cleavage of aryl substituents in silicon compunds is known to generate anionic species: C. Strohmann, D. Schildbach, D. Auer, *J. Am. Chem. Soc.* **2005**, *127*, 7968–7971; compare also reference 69.

[170] N. Y. Tashkandi, F. Parsons, J. Guo, K. M. Baines, *Angew. Chem.* **2015**, *127*, 1632−1635; *Angew. Chem. Int. Ed.* **2015**, *54*, 1612-1615

[171] K. Furukawa, K. Ebata, H. Nakashima, Y. Kashimura, K. Torimitsu, *Macromolecules* **2003,** *36,* 9-11.

[172] M. Driess, S. Rell, K. Merz, *Z. Anorg. Allg. Chem.* **1999**, *625*, 1119 – 1123.

[173] (a) An early report on 1D version of 1H pulse selective NMR techniques: F.W. Dahlquist, K. J. Longmuir, R. B. du Vernet, *J. Magn. Reson.* **1975**, *17*, 406 – 410; (b) Review on 2D versions of the experiment: C. Perrin, T. J. Dwyer, *Chem. Rev*. **1990**, *90*, 935 – 967.

[174] For modeling DynaFit 3 was used, for visualizing the graphs OriginPro 2016G was used, the origin plot was performed by Y. Heider, Saarland University*, Krupp-Chair of General and Inorganic Chemistry*, Scheschkewitz Group.

[175] (a) O. Kolodiazhnyi, *Tetrahedron Lett*. **1982**, *23*, 4933−4936; (b) M. Yoshifuji, K. Toyota, K. Shibayama, N. Inamoto, *Tetrahedron Lett.* **1984**, *25*, 1809−1812; (c) R. Appel, C. Behnke, *Z. Anorg. Allg. Chem.* **1987**, *555*, 23−25; (d) M. Yoshifuji, T. Niitsu,K. Toyota, N. Inamoto, K. Hirotsu, Y. Odagaki, T. Higuchi, S.Nagase, *Polyhedron* **1988**, *7*, 2213−2216; (e) T. Niitsu, N.Inamoto, K. Toyota, M. Yoshifuji, *Bull. Chem. Soc. Jpn.* **1990**, *63*, 2736−2738; (f) T. Wegmann, M. Hafner, M. Regitz, *Chem. Ber.* **1993**, *126*, 2525−2530.

[176] (a) M. Driess, H. Pritzkow, M. Sander, *Angew. Chem.* **1993**, *105*, 273−275; *Angew. Chem., Int. Ed. Engl.* **1993**, *32*, 1439−1440; (b) M. Driess, H. Pritzkow, *J. Chem. Soc.,* Chem. Commun. **1993**, 1585−1587.

[177] M. Driess, H. Pritzkow, *Z. Anorg. Allg. Chem.* **1996**, *622*, 858.

[178] M. Driess, S. Rell, H. Pritzkow, R. Janoschek, *Angew. Chem.* **1997**, *109*, 1384–1386; *Angew Chem. Int. Ed. Engl.* **1997**, *36*, 1326–1329.

[179] Review concerning P=C and P≡C bonds: R. Appel, F. Knoll, I. Ruppert, *Angew. Chem.* **1981**, *93*, 771−784, *Angew. Chem. Int. Ed. Engl.* **1981**, *20,* 731-744.

[180] M. Majumdar, V. Huch, I. Bejan, A. Meltzer, D. Scheschkewitz, *Angew. Chem.* **2013**, *125*, 3601−3605; *Angew. Chem. Int. Ed.* **2013**, *52*, 3516−3520.

[181] Review: V. M. S. Gil, W. von Philipsborn, *Magn. Reson. Chem.* **1989**, *27*, 409−430.

[182] K. Ueba-Ohshima, T. Iwamoto, M. Kira, *Organometallics* **2008,** *27,* 320−323.

[183] M. Kira, T. Iwamoto, C. Kabuto *J. Am. Chem. Soc.* **1996,** *118,* 10303−10304.

[184] T. Iwamoto, M. Tamura, C. Kabuto, M. Kira, *Organometallics* **2003,** *22,* 2342−2344.

[185]M. Driess, A. D. Fanta, D. R. Powell, R. West, *Angew. Chem.* **1989**, *101*, 8, 1087-1088*; Angew. Chem.,Int. Ed. Engl.* **1989***, 28,* 1038-1039.

[186] R. Riedel, H.-D. Hausen, E. Fluck, *Angew. Chem.* **1985**, *97*, 1050; *Angew. Chem. Int. Ed. Engl.* **1985**, *24*, 1056–1057.

[187] A. G. Avent, D. Bonafoux, C. Eaborn, M. S. Hill, P. B. Hitchcock, J. D Smith, *J. Chem. Soc., Dalton Trans.*, **2000,** 2183−2190-

[188] (a) N. Tokitoh, H. Suzuki, and R. Okazaki, *J. Am. Chem. Soc.* **1993**,*115*, 10428–10429; (b) N. Takeda, H. Suzuki, N. Tokitoh, R. Okazakic, *J. Am. Chem. Soc.* **1997,** *119,* 1456–1457; (c) S. Tsutsui, H. Tanaka, E. Kwon, S. Matsumoto, K. Sakamoto, *Organometallics* **2004,** *23,* 5659–5661.

[189] Mechanistical studies: a) K. A. Nguyen, M. S. Gordon *J. Am. Chem. Soc.* **1995**, *117*, 3835–3847; b) J. C. Slootweg, A. W. Ehlers, K. Lammertsma *J. Mol. Model.* **2006**, *12*, 531–536.

[190] a) W. Ando, Y. Hamada, A. Sekiguchi, *J. Chem. Soc., Chem. Commun.* **1983**, 952–954; b) M. Kosa, M. Karni, Y. Apeloig, *J. Am. Chem. Soc.* **2013**, *135*, 9032−9040; c) L. Lange, B. Meyer, W. W. du Mont, *J. Organomet. Chem.* **1987**, *329*, C17; d) P. Jutzi, C. Leue, *Organometallics*, **1994**,*13*, 2898−2899. e) D. Lei, M. E. Lee, P. P. Gaspar, *Tetrahedron* **1997**, *53*, 10179−10186; f) B. Gehrhus, P. B. Hitchcock, M. F. Lappert, *Angew. Chem.* **1997**, *22*, 2624–2626, *Angew. Chem. Int. Ed.* **1997**, *36*, 2514–2516.

[191] L. Junk, *Vertiefungsarbeit* **2013**, Saarland University*, Krupp-Chair of General and Inorganic Chemistry*, Scheschkewitz Group.

[192] M. C. Simpson, D. J. Cole-Hamilton, *Coord. Chem. Rev.***1999**, 155, 163-207.

[193] N. Selander, K. J. Szabó, *Chem. Rev.* **2011**, *111*, 2048−2076.

[194] J. Won, D. Noh, J. Yun, J. Y. Lee, *J. Phys. Chem. A* **2010**, *114*, 12112−12114.

[195] A. H. Cowley, R. A. Kemp, J. C. Wilburn, *Inorg. Chem.* **1981**, *20*, 4289−4293.

[196] H.-Y. Liu, K. Eriks, A. Prock, W. P. Giering, *Organometallics* **1990**, *9***,** 1758–1766.

[197] S. Warratz, L. Postigo, B. Royo, *Organometallics* **2013**, *32*, 893–897.

[198] H. Gilman, W. Langham, A. L. Jacoby, *J. Am. Chem. Soc.* **1939**, *61*, 106−109.

[199] M. Westerhausen, T. Rotter, H. Görls, C. Birg, M. Warchhold, H. Nöth, *Z. Naturforsch.* **2005**, 60b**,** 766 – 770.

[200] P. Willmes, *Vertiefungsarbeit* **2011**, Saarland University*, Krupp-Chair of General and Inorganic Chemistry*, Scheschkewitz Group.

[201] B.D. Ellis, M. Carlesimo, C. L. B. Macdonald, *Chem. Commun.* **2003**, 1946−1947.

[202] E. L. Norton, K. L. S. Szekely, J. W. Dube, P. G. Bomben, Charles L. B. Macdonald, *Inorg. Chem.* **2008**, *47*, 1196−1203.

[203] B.D. Ellis, C. A. Dyker, A. Deckenc, C. L. B. Macdonald, *Chem. Commun.* **2005**, 1965−1967.

[204] (a) D. Martin, M. Soleilhavoup, G. Bertrand, *Chem. Sci.* **2011**, *2*, 389−399; (b) M. Asay, C. Jones, M. Driess, *Chem. Rev.* **2011**, *111*, 354−396; (c) Y. Wang G.H. Robinson, *Inorg. Chem.* **2011**, *50*, 12326−12337; (d) R. S. Ghadwal, R. Azhakar, H. W. Roesky, *Acc. Chem. Res.* **2013**, *46*, 444−456; (e) G. Prabusankar, A. Sathyanarayana, P. Suresh, C. N. Babu, K. Srinivas, B. P. R. Metla, *Coord. Chem. Rev.* **2014**, *269*, 96−133.

[205] A. Jana, V. Huch, H. S. Rzepa, D. Scheschkewitz, *Angew. Chem*. **2015**, *127*, 291−295; *Angew. Chem., Int. Ed*. **2015**, *54*, 289−292.

[206] P. A. Rupar, M. C. Jennings, K. M. Baines, Oragnometallics **2008**, *27*, 5043−5051.

[207] A. Jana, I. Omlor, V. Huch, H. S. Rzepa, D. Scheschkewitz, *Angew. Chem.* **2014**, *126*, 10112−10116; *Angew. Chem. Int. Ed. 2014*, *53*, 9953−9956.

[208] G. Magyarfalvi, P. Pulay, *Chem. Phys. Lett.* **1995**, *241*, 393−398.

[209] T. Takayama, I. Ando, T. Asakura, *Bul. Chem. Soc. Jap*. **1989**, *63*, 1233−1236.

[210] Y. Heider, *Bachelorarbeit* **2015**, Saarland University*, Krupp-Chair of General and Inorganic Chemistry*, Scheschkewitz Group.

[211] E. Zygadło-Monikowska, Z. Florjańczyk, J. Ostrowska, P. Bołtromiuk, J. Frydrych, W. Sadurski, N. Langwald*, Electrochimica Acta* **2011**, *57* 66−73.

[212] D. Ballweg, Y. Liu, I. A. Guzei, R. West, *Silicon Chemistry* **2002**, *1*, 57–60.

[213] To date, silaborene reported by Sekiguchi *et al*. remains the sole example of a Si=B bond: N. Nakata, A. Sekiguchi *J. Am. Chem. Soc.* **2006***, 128,* 422−423.

[214] For **28a** no X-ray data was obtained by the authors, however, these findings were confirmed by UV/vis spectroscopy.

[215] S. Berski, Z. Latajka, A. J. Gordon, *New J. Chem*., **2011**, *35*, 89–96 .

[216] Recent review: E. R. Burkhardt, K. Matos, *Chem. Rev.* **2006**, *106*, 2617−2650.

[217] W. Lippert, H. Nöth, W. Ponikwar, T. Seifert, *Eur. J. Inorg. Chem.* **1999**, 817−823.

[218] A. Skancke, J. F. Liebman, *J. Mol. Struct.* 1998, *445*, 29−34.

[219] K. T. Giju, A. K. Phukan, E. D. Jemmis, *Angew. Chem.* **2003**, *115*, 557-560; *Angew. Chem. Int. Ed.* **2003**, *42*, 539−542.

[220] T. E. Cole, R. K. Bakshi, M. Srebnik, B. Singaram, H. C. Brown, *Organometallics* **1986**, *5*, 2303−2307.

[221] M. Oda, T. Kajioka, T. Uehiyama, K. Nagara, T. Okujima, S. Ito, N. Morita, T. Sato, R. Miyatake, S. Kuroda, *Tetrahedron* 1999, *55*, 6081−6096.

[222] L. Pasumansky, D. Haddenham, J. W. Clary, G. B. Fisher, C. T. Goralski, B. Singaram, *J. Org. Chem.* **2008**, *73*, 1898−1905.

[223] W. Lippert, H. Nöth, W. Ponikwar, T. Seifert, *Eur. J. Inorg. Chem.* **1999**, 817−823.

[224] C. Strohmann, D. Schildbach, D. Auer, *J. Am. Chem. Soc.* **2005**, *127*, 7968−7971.

[225] **133**·(12-crown-4)$_2$ was synthesized and crystallized by Dr. Kinga Leszczyńska, Saarland University*, Krupp-Chair of General and Inorganic Chemistry*, Scheschkewitz Group.

[226] H. Stueger, B. Hasken, M. Haas, M. Rausch, R. Fischer, A. Torvisco, *Organometallics* **2014**, *33*, 231−239.

[227] T. P. Robinson, M. J. Cowley, D. Scheschkewitz, J. M. Goicoechea, *Angew. Chem.* **2015**, *127*, 2, 693−696; *Angew. Chem. Int. Ed.* **2015**, *54*, 683−686.

[228] H. Stueger, B. Hasken, M. Haas, M. Rausch, R. Fischer, A. Torvisco, *Organometallics* **2013**, *33*, 231−239.

[229] Recent review: P. A. Byrne, D. G. Gilheany, *Chem. Soc. Rev.* **2013**, *42*, 6670−6696.

[230] E. E. Nifantiev, N. S. Vyazankin, S. F. Sorokina, L. A. Vorobieva, O. A. Vyazankina, D. A. Bravo-Zhivotovsky, A. R. Bekker, *J. Organomet. Chem.* **1984**, *277*, 211−225.

[231] M. Bispinghoff, A. M. Tondreau, H. Grützmacher, C. A. Faradjib, Paul G. Pringle, *Dalton Trans.* **2016**, *45*, 5999−6003.

[232] S. Roy, P. Stollberg, R. Herbst-Irmer, D. Stalke, D. M. Andrada, G. Frenking, H. W. Roesky, *J. Am. Chem. Soc.* **2015**, *137*, 150−153.

[233] N. Poiters, *Masterarbeit* **2016**, Saarland University*, Krupp-Chair of General and Inorganic Chemistry*, Scheschkewitz Group.

[234] K.-C. Kim, C. A. Reed, D.W. Elliott, L. J. Mueller, F. Tham, L.Lin, J. B. Lambert, *Science* **2002**, *297*, 825−827.

[235] Into this experiment Y. Heider (Saarland University*, Krupp-Chair of General and Inorganic Chemistry*, Scheschkewitz Group) was involved during his V-lab course.

[236] K. Abersfelder, *PhD Thesis*, Imperial College London, Scheschkewitz group, **2012**.

[237] J. C. Love, L. A. Estroff, J. K. Kriebel, R. G. Nuzzo, G. M. Whitesides, *Chem. Rev.* **2005**, *105*, 1103−1169.

[238] I. Rubinstein, E. Sabatani, R. Maoz and J. Sagiv, Organized Monolayers on Gold Electrodes, in *Electrochemical Sensors for Biomedical Applications*, C.K.N. Li (Ed.), The Electrochemical Society **1986**, 175.

[239] T. Büttner, *Bachelorarbeit* **2015**, Saarland University*, Krupp-Chair of General and Inorganic Chemistry*, Scheschkewitz Group.

[240] J. C. Love, D. B. Wolfe, R. Haasch, M. L. Chabinyc, K. E. Paul, G. M. Whitesides, R. G. Nuzzo, *J. Am. Chem. Soc.* **2003**, *125*, 2597–609.

[241] R. Hiremath, J. a. Basile, S. W. Varney, J. a. Swift, *J. Am. Chem. Soc.* **2005**, *127*, 18321–18327.

[242] (a) T. Weidner, M. Zharnikov, J. Hoßbach, D. G. Castner, U. Siemeling, *J. Phys. Chem. C* **2010**, *114*, 14975–14982; (b) T. Kitagawa, H. Matsubara, K. Komatsu, K. Hirai, T. Okazaki, T. Hase, *Langmuir* **2013**, *29*, 4275–4282.

[243] P. E. Laibinis, G. M. Whitesides, D. L. Allara, Y. T. Tao, A. N. Parikh, R. G. Nuzzo, *J. Am. Chem. Soc.* **1991**, *113*, 7152–7167.

[244]J. C. Love, D. B. Wolfe, R. Haasch, M. L. Chabinyc, K. E. Paul, G. M. Whitesides, R. G. Nuzzo, *J. Am. Chem. Soc.* **2003**, *125*, 2597–609.

[245] Z. Li, S.-C. Chang, R. S. Williams, *Langmuir* **2003**, *19*, 6744–6749.

[246] N. Muskal, I. Turyan, D. Mandler, *J. Electroanal. Chem.* **1996**, *409*, 131–136.

[247] H. A. Biebuyck, C. D. Bain, G. M. Whitesides, *Langmuir* **1994**, *10*, 1825–1831.

[248] K. Furukawa, K. Ebata, H. Nakashima, Y. Kashimura, K. Torimitsu, *Macromolecules* **2003,** *36,* 9−11.

[249] J. Jeck, I. Bejan, A. J. P. White, D. Nied, F. Breher, David Scheschkewitz, *J. Am. Chem. Soc*. **2010**, *132*, 17306−17315.

[250] W. J. Balfour, K. S. Chandrasekhar, S. P. Kyca, *Spectrochim. Acta Part A Mol. Spectrosc.* **1986**, *42*, 39–42.

[251] K. Abersfelder, H. Zhao, A. J. P. White, C. Praesang, D. Scheschkewitz*, Z. Anorg. Allg. Chem.* **2015**, *641*, 2051–2055

[252] M. J. Frisch, G. W. Trucks, H. B. Schlegel, G. E. Scuseria, M. A. Robb, J. R. Cheeseman, G. Scalmani, V. Barone, B. Mennucci, G. A. Petersson, H. Nakatsuji, M. Caricato, X. Li, H. P. Hratchian, A. F. Izmaylov, J. Bloino, G. Zheng, J. L. Sonnenberg, M. Hada, M. Ehara, K. Toyota, R. Fukuda, J. Hasegawa, M. Ishida, T. Nakajima, Y. Honda, O. Kitao, H. Nakai, T. Vreven, J. A. Montgomery, Jr., J. E. Peralta, F. Ogliaro, M. Bearpark, J. J. Heyd, E. Brothers, K. N. Kudin, V. N. Staroverov, R. Kobayashi, J. Normand, K. Raghavachari, A. Rendell, J. C. Burant, S. S. Iyengar, J. Tomasi, M. Cossi, N. Rega, J. M. Millam, M. Klene, J. E. Knox, J. B. Cross, V. Bakken, C. Adamo, J. Jaramillo, R. Gomperts, R. E. Stratmann, O. Yazyev, A. J. Austin, R. Cammi, C. Pomelli, J. W. Ochterski, R. L. Martin, K. Morokuma, V. G. Zakrzewski, G. A. Voth, P. Salvador, J. J. Dannenberg, S. Dapprich, A. D. Daniels, Ö. Farkas, J. B. Foresman, J. V. Ortiz, J. Cioslowski, and D. J. Fox, Gaussian, Inc., Wallingford CT, Gaussian 09, Revision A.02, **2009**.

[253] K. B. Wiberg, *Tetrahedron* **1968**, 24, 1083−1096.

[254] M. Cossi, N. Rega, G. Scalmani, V. Barone, *J. Comp. Chem*. **2003**, 24, 669−681.

[255] R. Ditchfield, *Mol. Phys*., **1974**, 27, 789−807.

[256] (a) G. M. Whitesides, M. Eisenhut, W. M. Bunting, *J. Am. Chem. Soc.* **1974**, *96*, 5398−5407; (b) A. R. Miller, D. Y. Curtin, *J. Am. Chem. Soc.* **1976**, *98*, 1860−1865.

[257] C. N. Smit, F. Bickelhaupt, *Organometallics* **1987**, *6*, 1156−1163.

[258] B. Punji, J. T. Mague, M. S. Balakrishna, *Inorg. Chem.* **2007**, *46*, 10268−10275.

[259] D. J. Dellinger, D. M. Sheehan, N. K. Christensen, J. G. Lindberg, H. M. Caruthers, *J. Am. Chem. Soc.* **2003**, *125*, 940−950.

[260] H. Nöth, H.-J. Vetter, *Chem. Ber.* **1963**, *96*, 1109−1118.

[261] H. J. Becher, *Z. Allg. Anorg. Chem.* **1957**, *289*, 262−278.

[262] W. Biffar, H. Nöth, D. Sedlak, *Organometallics*, **1983**, *2*, 579−585.

[263] R. Hiremath, J. a. Basile, S. W. Varney, J. a. Swift, *J. Am. Chem. Soc.* **2005**, *127*, 18321–18327.

[264] A. J. Macleod, G. Macleod, *Phytochemistry* **1977**, *16*, 907–909.

[265] M. Soleiman-Beigi, Z. Taherinia, *Monatshefte für Chemie - Chem. Mon.* **2014**, *145*, 1151–1154.

7. Appendix

7.1. Overview of Numbered Compounds

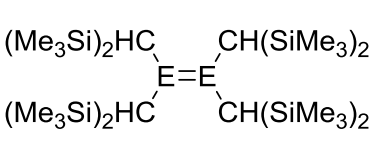

1: E = Ge, **2**: E = Sn

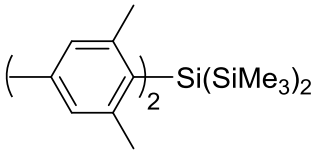

3

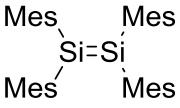

4

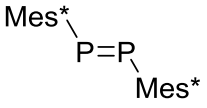

5

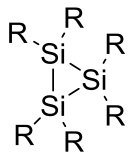

6a (R = dmp)
6b (R = ^{t}BuMe$_2$Si)

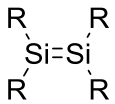

7: R = dmp
8: R = ^{t}BuMe$_2$Si

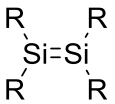

9: R = Tip
10: R = (Me$_3$Si)$_2$CH

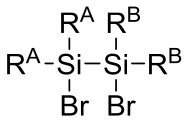

11a,b

R^{A} = ^{t}BuMe$_2$Si
11a: R^{B} = ^{i}PrMe$_2$Si
11b: R^{B} = ^{i}Pr$_3$Si

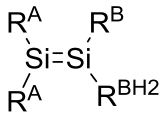

12a,b

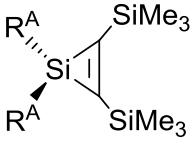

13a,b

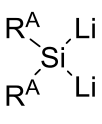

14a,b

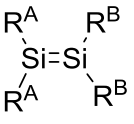

15a-d

a: R^{A} = Si^{i}Pr$_3$, R^{B} = Mes
b: R^{A} = Si^{t}Bu$_3$, R^{B} = Mes
c: R^{A} = Si^{i}Pr$_3$, R^{B} = Tip
d: R^{A} = Si^{t}Bu$_3$, R^{B} = Tip

R^{A} = ^{t}BuMe$_2$Si
12a: R^{B} = ^{i}PrMe$_2$Si
12b: R^{B} = ^{i}Pr$_3$Si

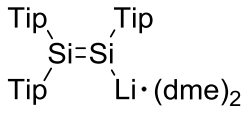

16

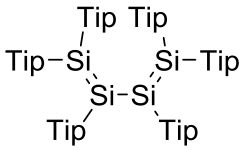

17

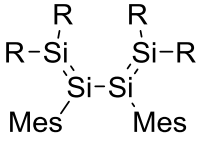

18
R = ^{t}Bu$_2$MeSi

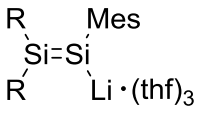

19a
R = ^{t}Bu$_2$MeSi

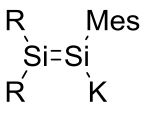

19b
R = ^{t}Bu$_2$MeSi

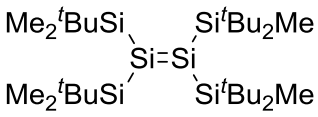

20

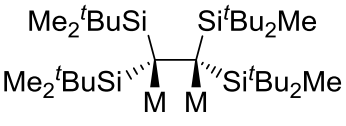

21a-c

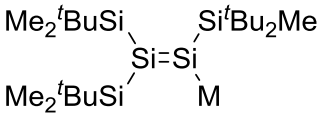

22a-c

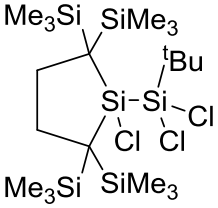

23

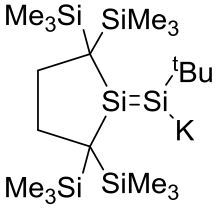

24

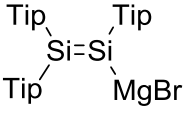

25

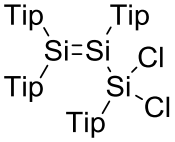

26

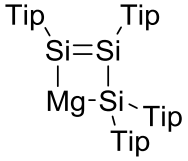

27

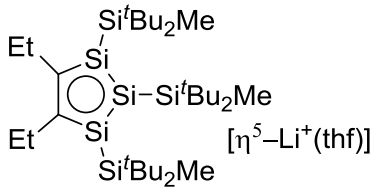

28

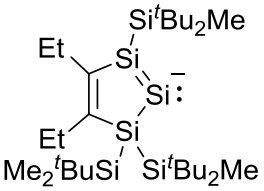

29

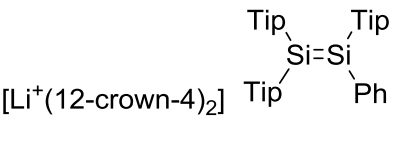

30

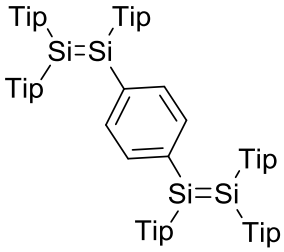

31

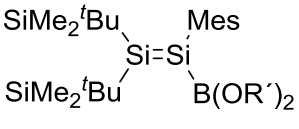

32a,b

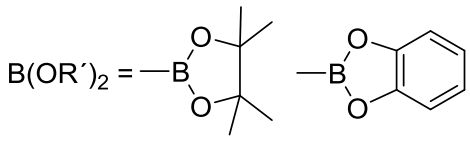

32a **32b**

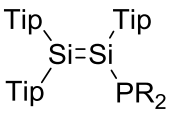

a: R = Ph
b: R = ^{i}Pr
c: R = Cy
d: R = ^{t}Bu

33a-d

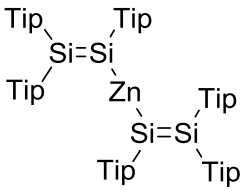

34

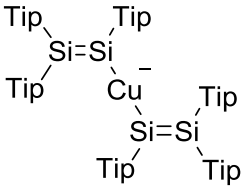

35

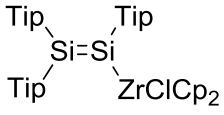

36

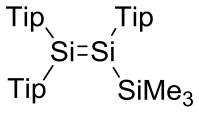

37

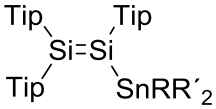

38a-d

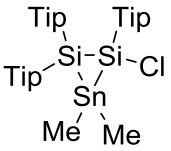

39

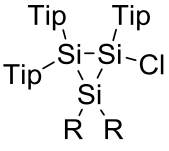

40a,b

a: R = R´ = Me
b: R = R´= Ph
c: R = R´ = ^{n}Bu
d: R = Cl, R´ = ^{t}Bu

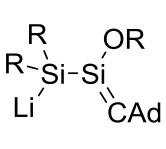

41

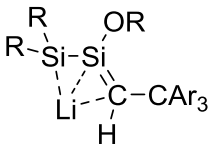

42

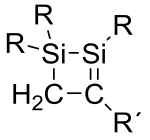

43a-e

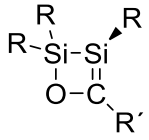

44a-c

R = SiMe^{t}Bu$_2$
Ar = 3,5-^{t}Bu$_2$C$_6$H$_3$

a: R= Tip, R´ = Ph
b: R = SiMe^{t}Bu$_2$, R´ = Ph
c: R = Tip, R´ = SiMe$_3$
d: R = SiMe^{t}Bu$_2$, R´ = SiMe$_3$
e: R = SiMe^{t}Bu$_2$, R´ = H

a: R = Tip, R´ = 1-adamantlyl
b: R = Tip, R´ = ^{t}Bu
c: R= SiMe*t*Bu$_2$, R´ = 1-adamantyl

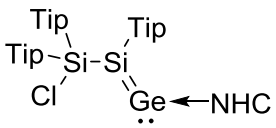

45

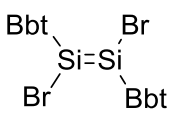

46

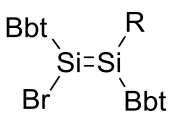

47a-d

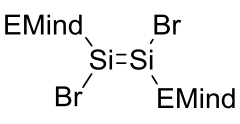

48

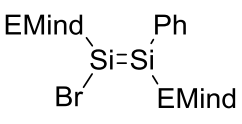

49

a: R = Me, **c**: R = ^{n}Bu,
b: R = Et, **d**: R = Ph

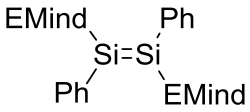

50

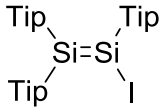

51

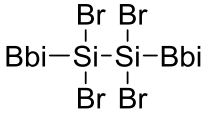

52

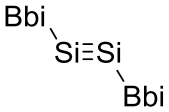

53

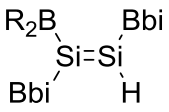

54a (R_2 = 9-BBN
54b (R_2 = catechol)

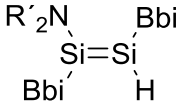

55a (R´ = Et)
55b (R´ = Ph)
55c (NR'_2 = NH^tBu)
55d (R´ = -$(CH_2)_4$-)

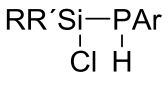

56a-e

a: R = R´ = Mes;
b: R = R´ = Es
c: R = Ph, R´ = Tip
d: R = Mes, R´ = Tip
e: R = ^{t}Bu, R´ = Tip

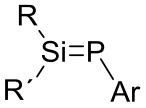

57a-e

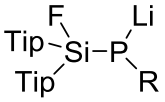

58a-c

a: R = Si^iPr_3
b: R = $SiMe_2{}^tBu$
c: R = $^tBu_2P$

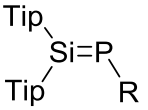

59a-c

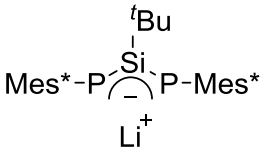

60

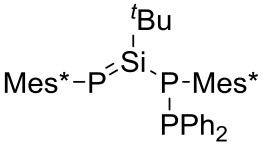

61

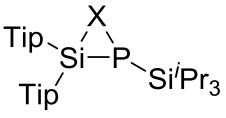

62a = S
62b = Te

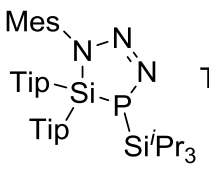

63

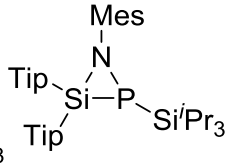

64

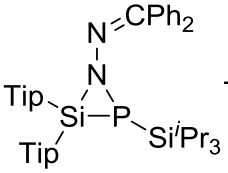

65

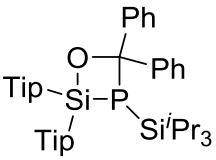

66

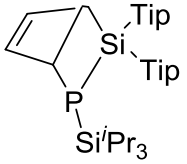

67

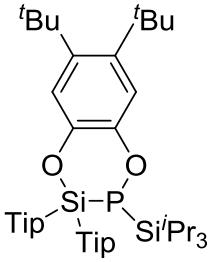

68

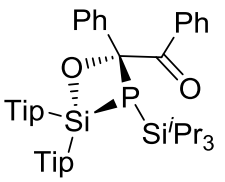

69

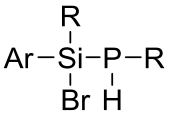

70a (Ar = phenyl)
70b (Ar = naphtyl)
70c (Ar = anthracenyl)

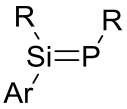

71a (Ar = phenyl)
71b (Ar = naphtyl)
71c (Ar = anthracenyl)

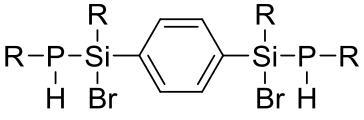

72

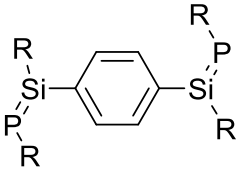

73

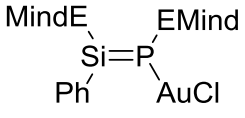

74

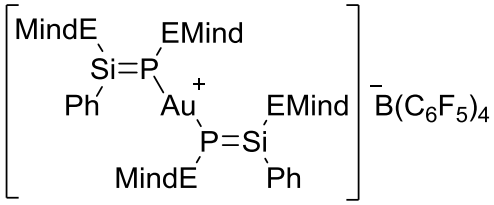

75

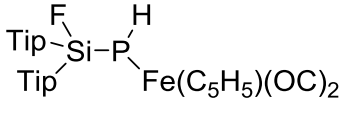

76

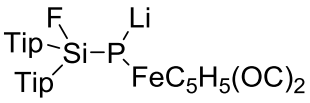

77

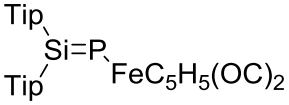

78

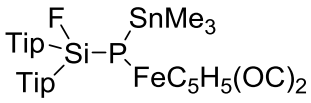

79

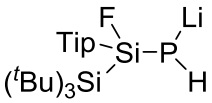

80

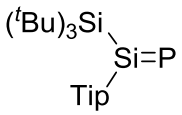

81a

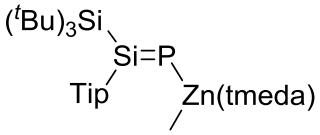

81b

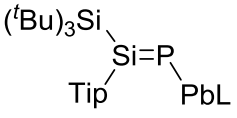

81c

L = N,N-Dip$_2$-2,4-dimethyl-β-diketiminate

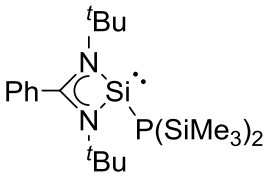

82

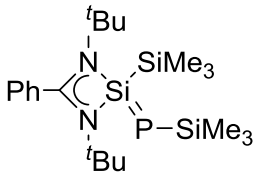

83

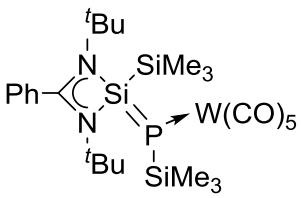

84

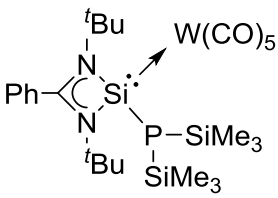

85

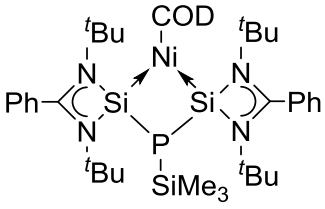

86

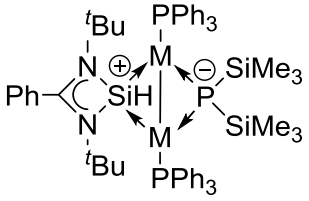

87a,b (**a**: M = Pt, **b**: M = Pd)

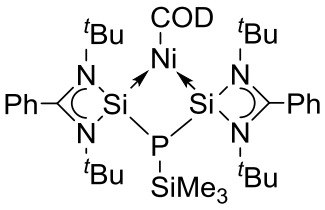

88

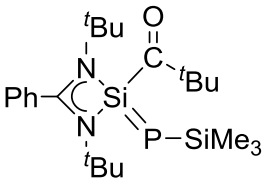

89

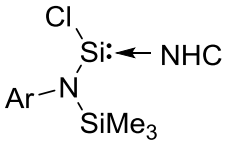

90

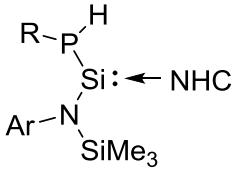

91

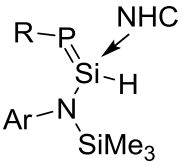

92

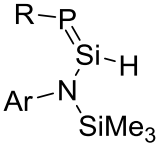

93

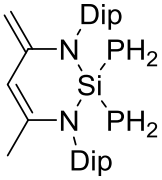

94

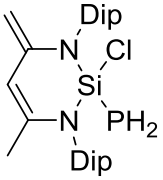

95

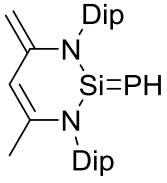

96

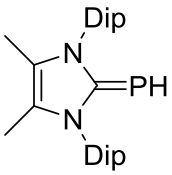

97

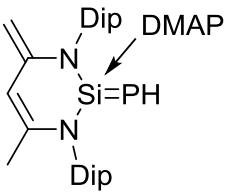

98

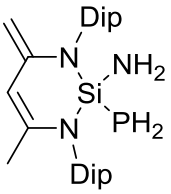

99

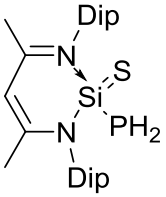

100

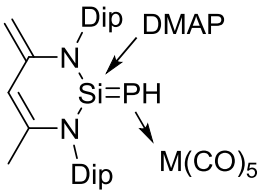

101a-c

a: M = Cr
b: M = Mo
c: M = W

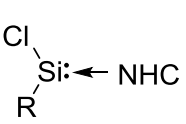

102

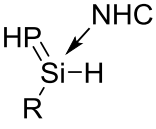

103

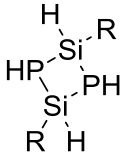

104

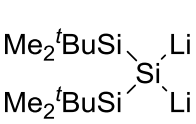

105

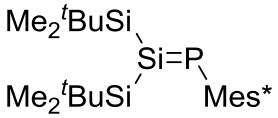

106

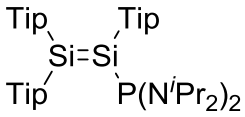

107

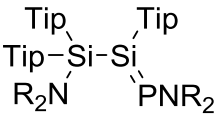

E/Z-**108a** (R = Me)
E/Z-**108b** (R = Et)

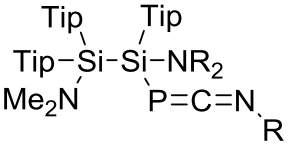

109a (R = ^{t}Bu)
109b (R = Xylyl)

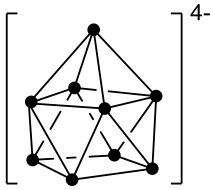

110a-d

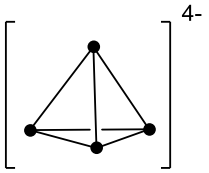

111a-d

● = E
E = Si, Ge, Sn, Pb

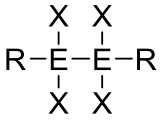

112a-c

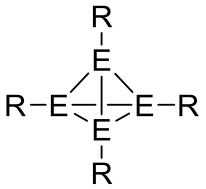

113a-c

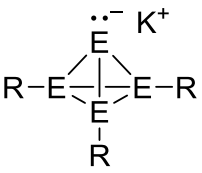

114c

a: E = Si, X = Br, R = Si^{t}Bu$_3$
b: E = Ge, X =Cl, R = Si^{t}Bu$_3$
c: E = Si, X = Br, R = Dis$_2$MeSi

E = Si
R = Dis$_2$MeSi

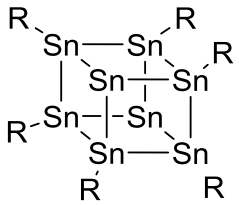

115 (R = Si^{t}Bu$_3$)

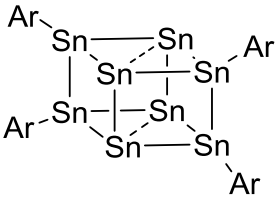

116 (Ar = 2,6-Mes-H$_3$C$_6$)

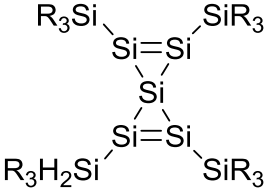

117 (R = ^{t}Bu$_2$MeSi)

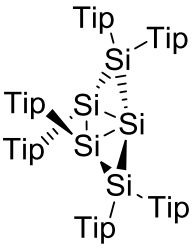

118

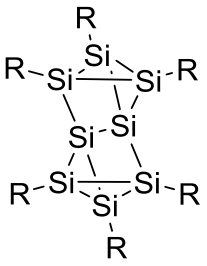

119 (R = Si^{t}Bu$_3$)

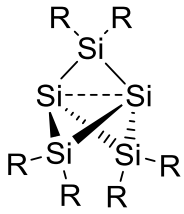

120 (R = Mes)

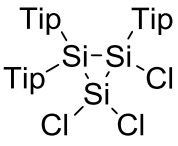

121

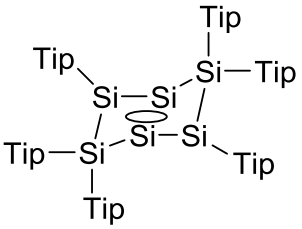

122

Cp*Si$^+$
[B(C$_6$F$_5$)$_4$]$^-$

123

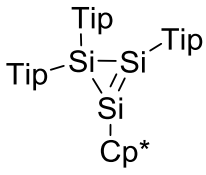

124

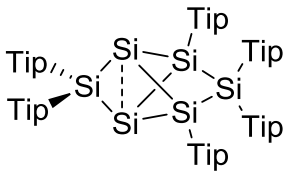

125

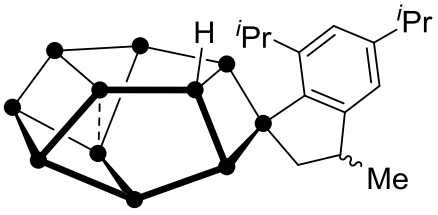

126

= SiTip$_2$ = SiTip

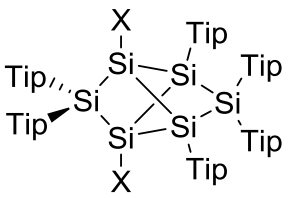

127a-c

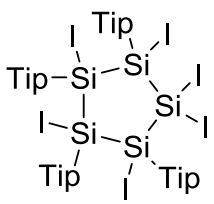

128

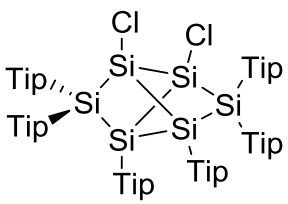

129a

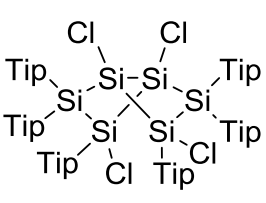

129b

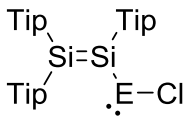

130a (E = Ge)
130b (E = Sn)

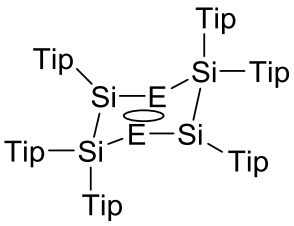

131a (E = Ge)
131b (E = Sn)

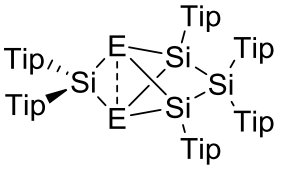

132a (E = Ge)
132b (E = Sn)

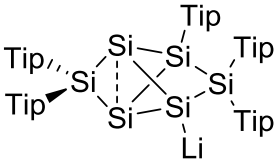

133

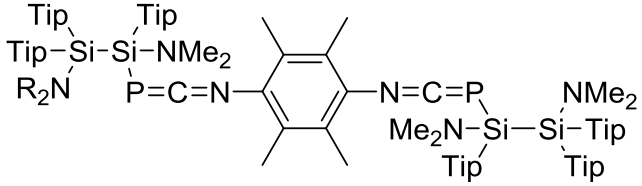

134

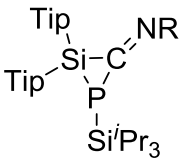

135a (R = Cy)
135b (R = Mes)

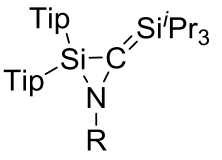

136a (R = Cy)
136b (R = Mes)

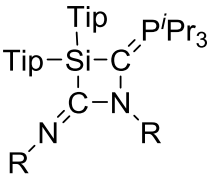

137a (R = Cy)
137b (R = Mes)

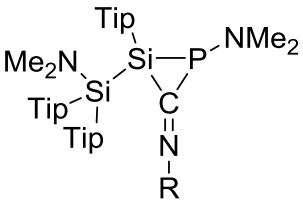

138 (R = Xylyl)

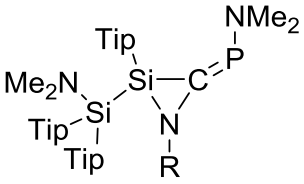

E/Z-**139** (R = Xylyl)

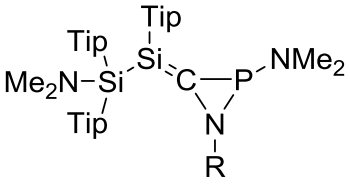

E/Z-**140** (R = Xylyl)

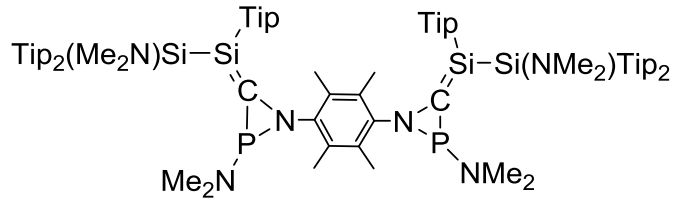

141

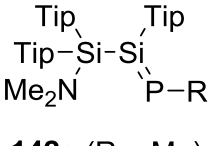

142a (R = Me)
142b (R = ^{t}Bu)

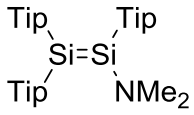

143

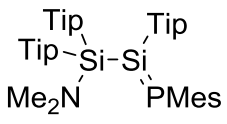

E/Z-**144**

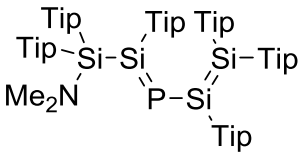

145

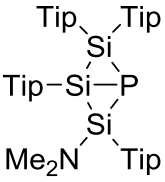

146

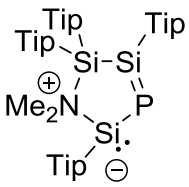

147

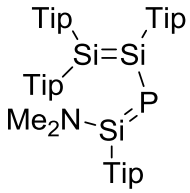

148

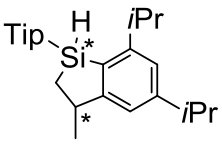

149

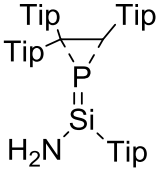

150

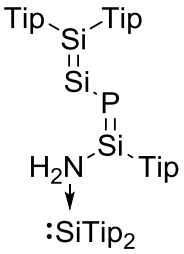

151

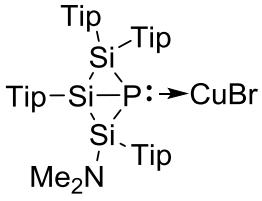

152

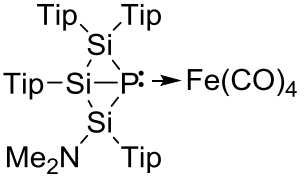

153

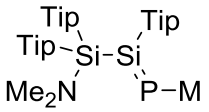

154a (R = Li)
154b (R = K)

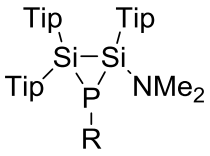

155a (R = Li)
155b (R =H)

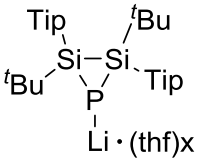

156a (R = Li)
156b (R = H)

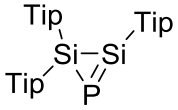

157

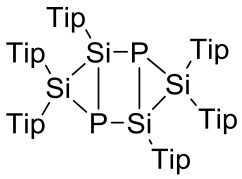

158

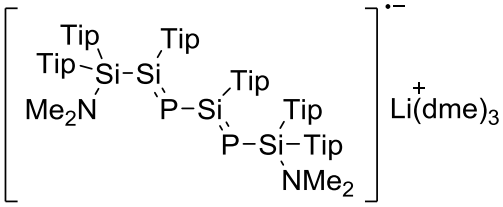

159

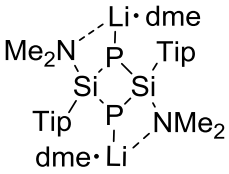

160

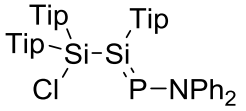

161

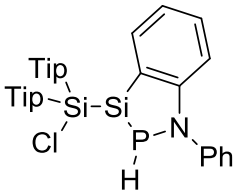

162

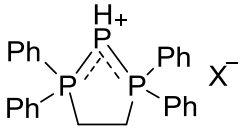

163[X]

X= Cl, Br, I, BPh_4
a: R_1 = Et, R_2 = Me
b: R_1 = ^{i}Pr, R_2 = Me
c: R_1 = Mes, R_2 = H

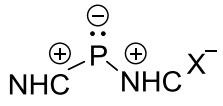

164a-c[X]

X= Cl, Br, I, BPh_4
a: R_1 = Et, R_2 = Me
b: R_1 = ^{i}Pr, R_2 = Me
c: R_1 = Mes, R_2 = H

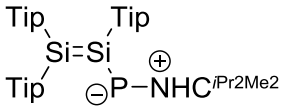

165

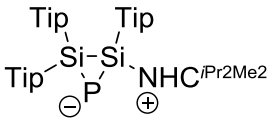

166

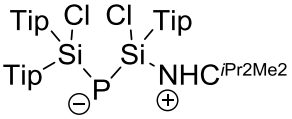

167

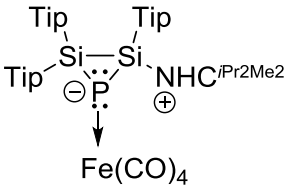

168

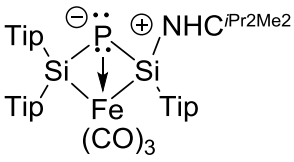

169

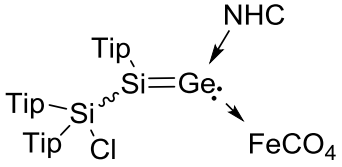

E/Z-**170**

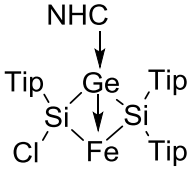

171

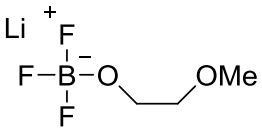

172

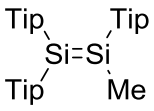

173

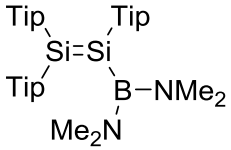

174

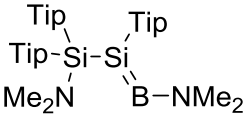

175

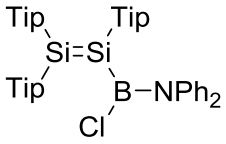

176

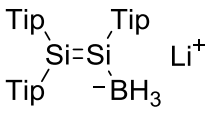

177

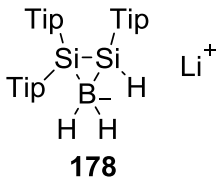

178

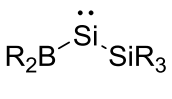

179a (R =H)
179b (R = Tip)

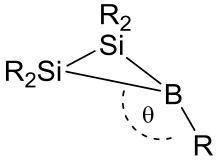

179a´ (R =H)
179b´ (R = Tip)

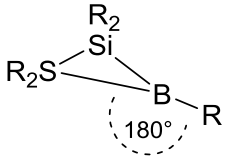

179a´´ (R =H)
179b´´ (R = Tip)

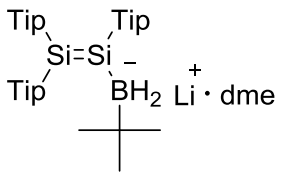

180

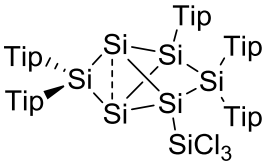

181

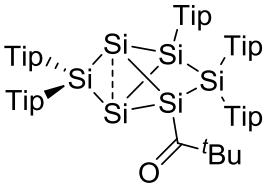

182

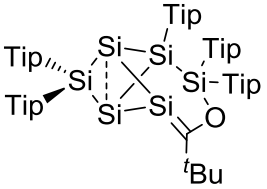

183

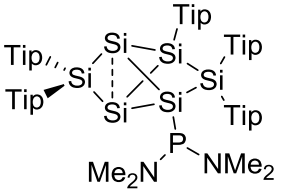

184

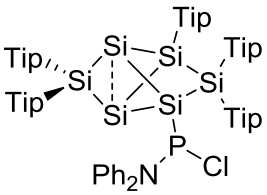

185

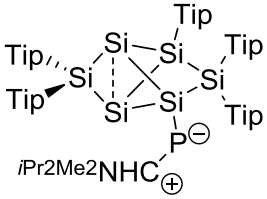

186

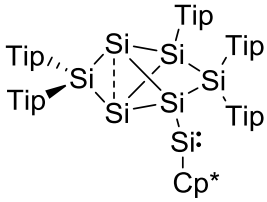

187

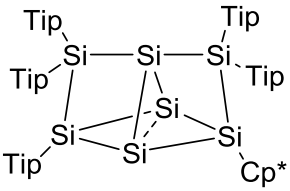

188

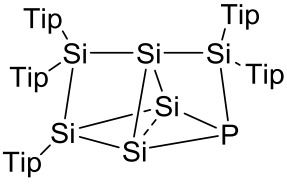

189

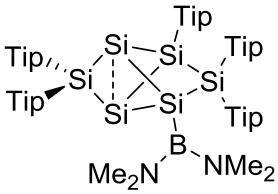

190

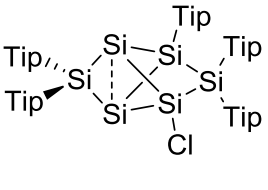

191

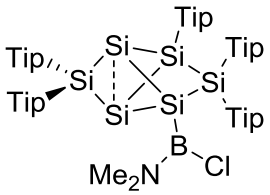

192

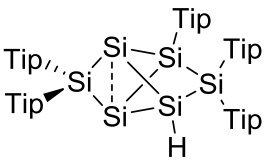

193

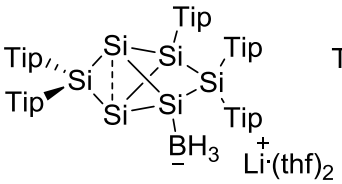

194

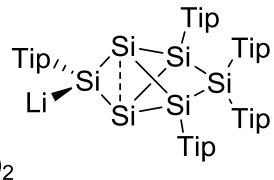

195

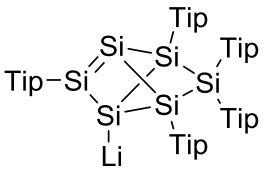

196

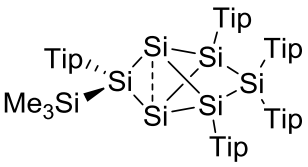

197

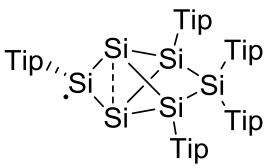

198

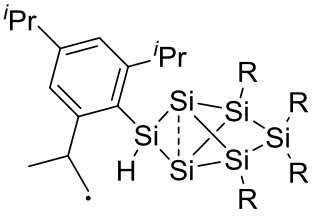

200

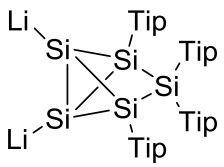

201

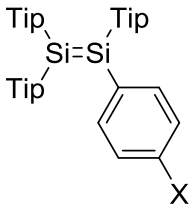

202a-d

a: X = F
b: X = Cl
c: X = Br
d: X = I

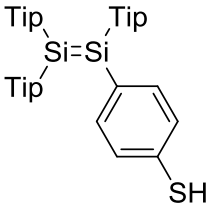

203

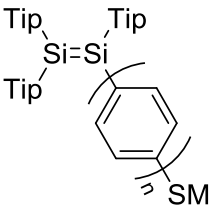

(**204a-c**)
a: n = 1
b: n = 2
c: n = 3

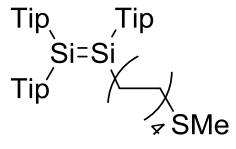

(**205**)

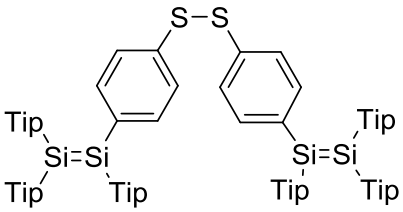

(**206**)

7.2. Determination of Activation Parameters for *Cis/Trans* Isomerization of *E/Z*-108b

***E*-108b**		***Z*-108b**	
d8 [s]	Population	d8 [s]	population
0.0	0	0	100
0.0024	9.94	0.0024	90.06
0.004	14.00	0.004	86.00
0.008	23.52	0.008	76.48
0.01	26.00	0.01	74.00
0.015	29.12	0.015	70.88
0.02	30.80	0.02	69.20
0.025	31.25	0.025	68.75
0.08	32.13	0.08	67.87
0.1	32.63	0.1	67.37
0.2	32.86	0.2	67.14

Table 4. Values for the population of *E*/*Z*-**108b** at different mixing times d8 (300 K).

***E*-108b**		***Z*-108b**	
d8 [s]	Population	d8 [s]	population
0.00	0.00	0.00	100.00
0.0024		0.0024	95.00
0.004	7.33	0.004	92.67
0.01	15.40	0.008	84.60
0.015	19.70	0.01	80.30
0.025	25.35	0.015	74.65
0.03	28.20	0.02	71.80
0.035	29.68	0.025	70.32
0.045	32.15	0.08	67.85
0.06	32.23	0.1	67.77

Table 5. Values for the population of *E*/*Z*-**108b** at different mixing times d8 (290 K).

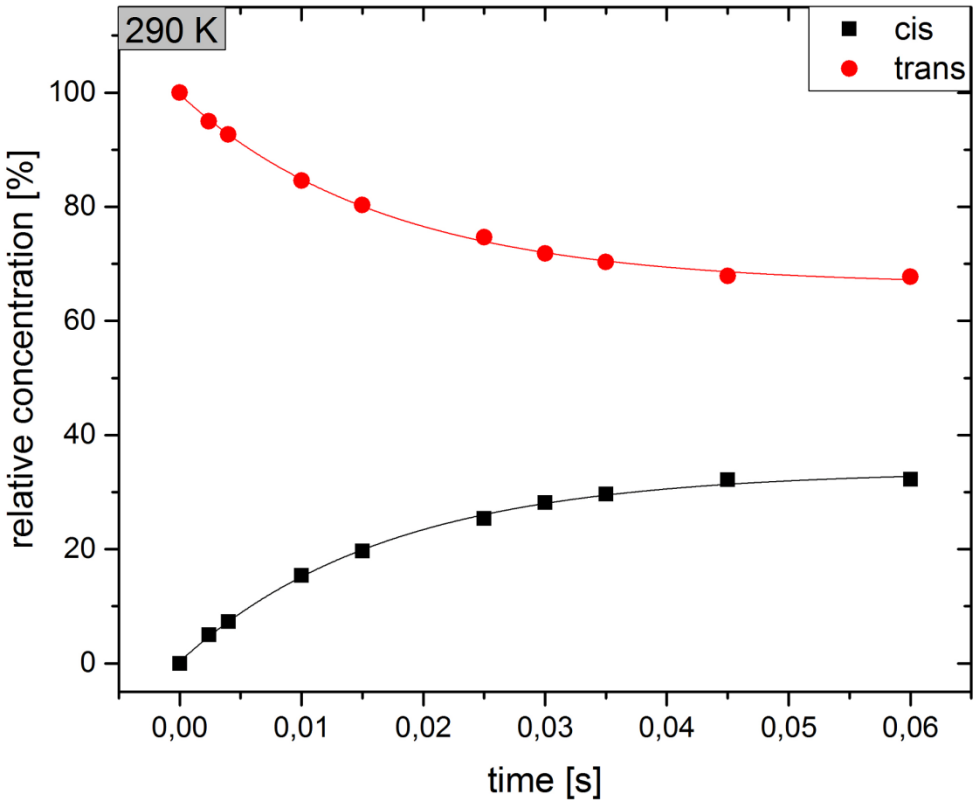

Figure 101. Plot of population of *E*/*Z*-**108b** against mixing time d8 (290 K).[174]

***E*-108b**		***Z*-108b**	
d8 [s]	Population	d8 [s]	population
0	0	0	100
0,0024	1,7	0,0024	98,3
0,01	7,51	0,01	92,49
0,02	13,09	0,02	86,91
0,035	19,36	0,035	80,64
0,05	23,81	0,05	76,19
0,1	28,7	0,1	71,3
0,2	29,66	0,2	70,34

Table 6. Values for the population of *E*/*Z*-**108b** at different mixing times d8 (280 K).

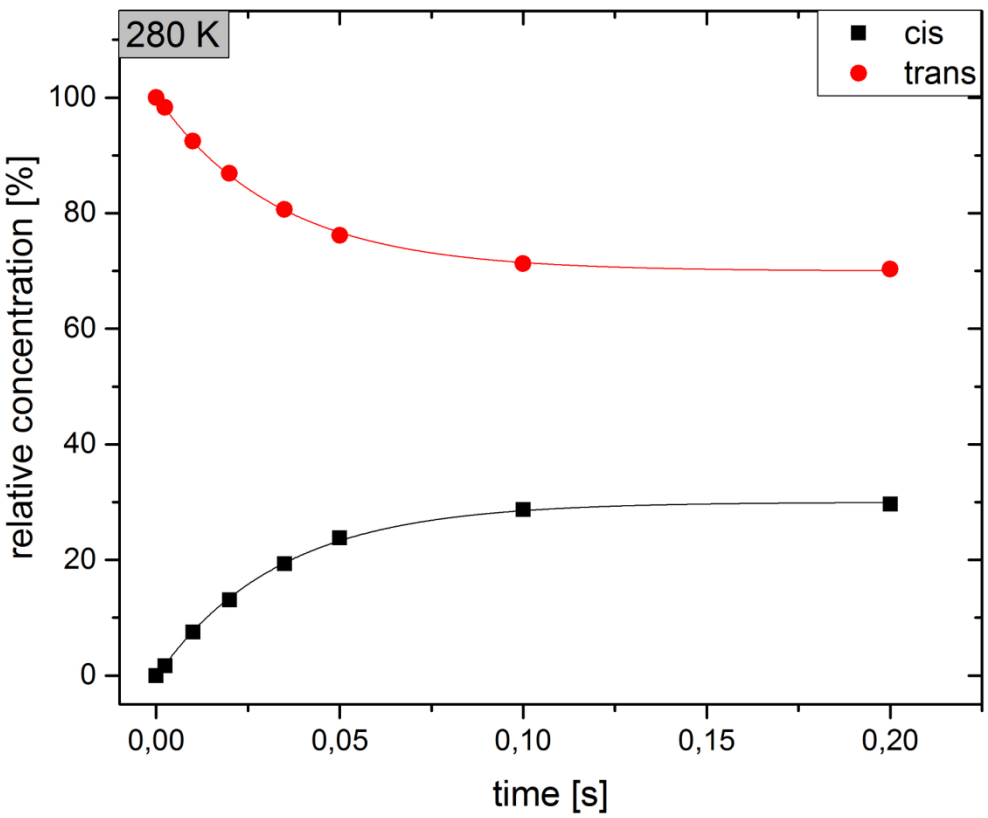

Figure 102. Plot of population of *E*/*Z*-**108b** against mixing times d8 (280 K).[174]

***E*-108b**		***Z*-108b**	
d8 [s]	Population	d8 [s]	population
0	0	0	100
0.005	1.30	0.005	98.70
0.02	5.34	0.02	94.66
0.05	11.43	0.05	88.57
0.125	22.21	0.125	77.79
0.175	25.85	0.175	74.15
0.2	27.60	0.2	72.40
0.3	28.61	0.3	71.39

Table 7. Values for the population of *E*/*Z*-**108b** at different mixing times d8 (270 K).

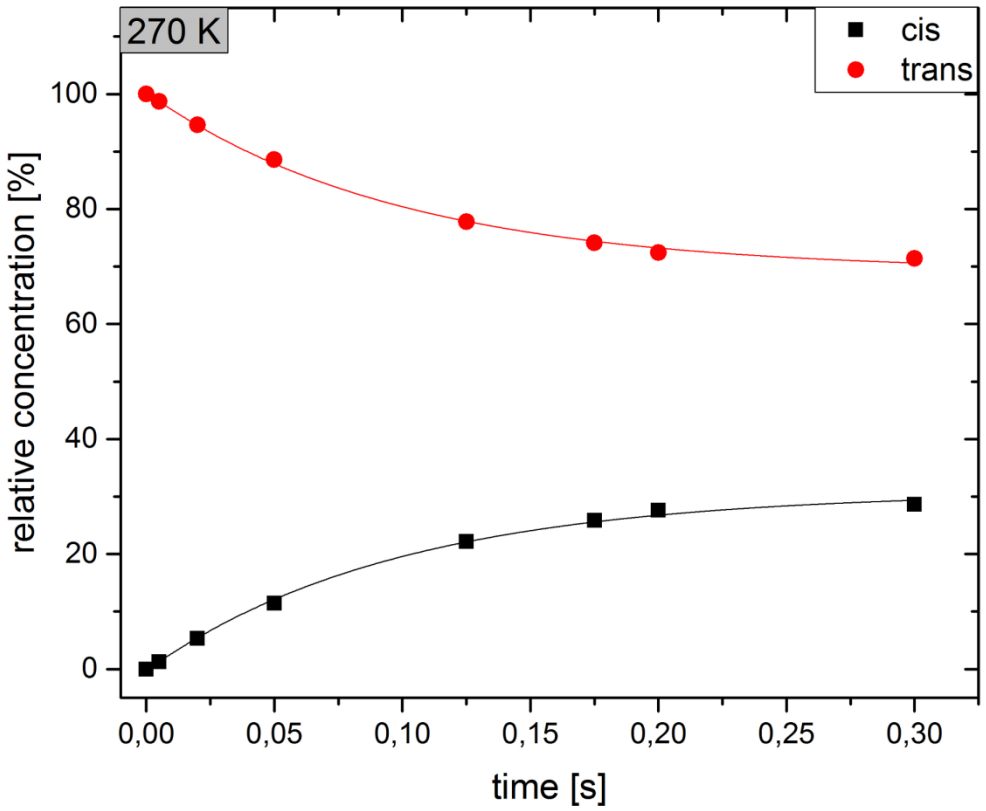

Figure 103. Plot of population of *E*/*Z*-**108b** against mixing time d8 (270 K).[174]

***E*-108b**		***Z*-108b**	
d8 [s]	Population	d8 [s]	population
0	0	0	100
0.015	1.65	0.015	98.35
0.04	4.02	0.04	95.98
0.1	9.05	0.1	90.95
0.25	17.87	0.25	82.13
0.375	18.43	0.375	81.57
0.5	24.64	0.5	75.36

Table 8. Values for the population of *E*/*Z*-**108b** at different mixing times d8 (260 K).

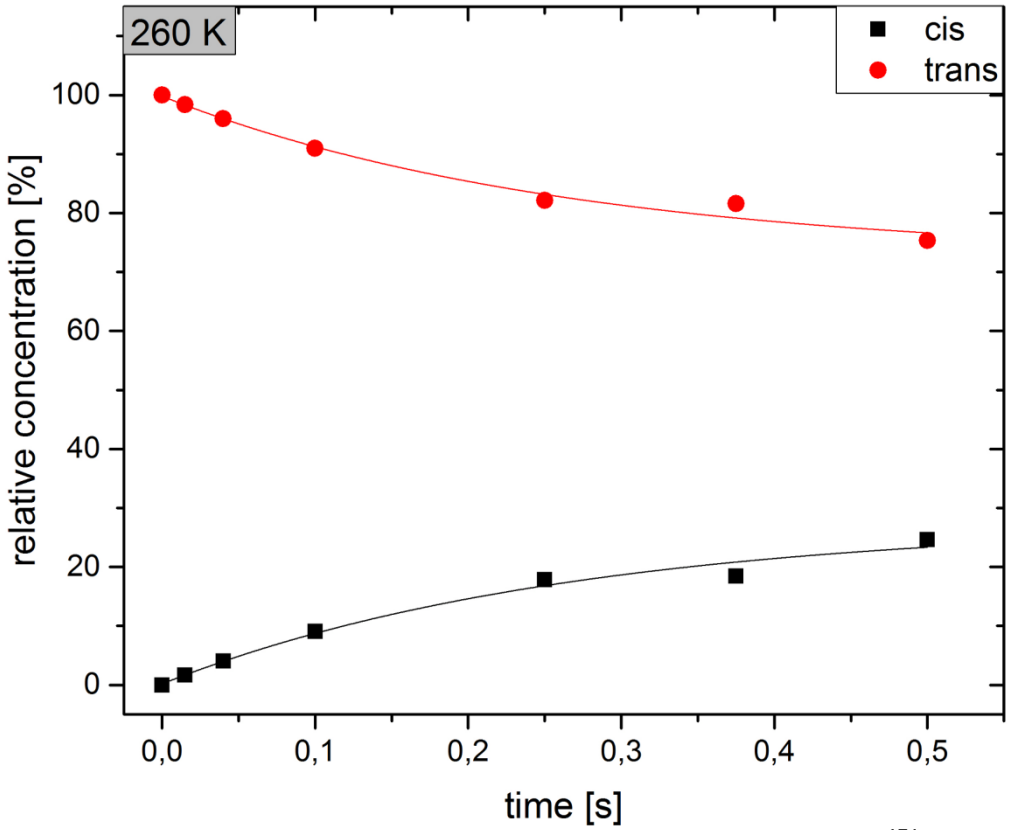

Figure 104. Plot of population of *E*/*Z*-**108b** against mixing times d8 (260 K).[174]

$\Delta H^{\#}$ and $\Delta S^{\#}$ of eac

h isomer were determined *via* Eyring Plot. The plots of $\ln(k_1/T)$ and $\ln(k_2/T)$ *versus* 1/T give straight lines with slope $m = -\Delta H^{\#}/R$ and with intercept $n = \ln(k_B/h) + \Delta S^{\#}/R$ (R = gas constant, k_B = Boltzmann constant, h = Planck´s constant). For plotting the graphs Origin 8.0 was used.

T	k_1	k_2	1/T	$\ln(k_1/T)$	$\ln(k_2/T)$
300.000	49.797	103.680	0.00333	−1.79583	−1.06247
290.000	20.171	39.820	0.00345	−2.66563	−1.98551
280.000	8.919	20.746	0.00357	−3.44661	−2.60244
270.000	3.078	6.850	0.00370	−4.47414	−3.67417
260.000	1.057	2.833	0.00385	−5.50525	−4.51935

Table 9. Values for for k_1 and k_2 at the different temperatures; values for 1/T, $\ln(k_1/T)$ and $\ln(k_2/T)$. Note: T in K; k_1, k_2 in l/(mol*s).

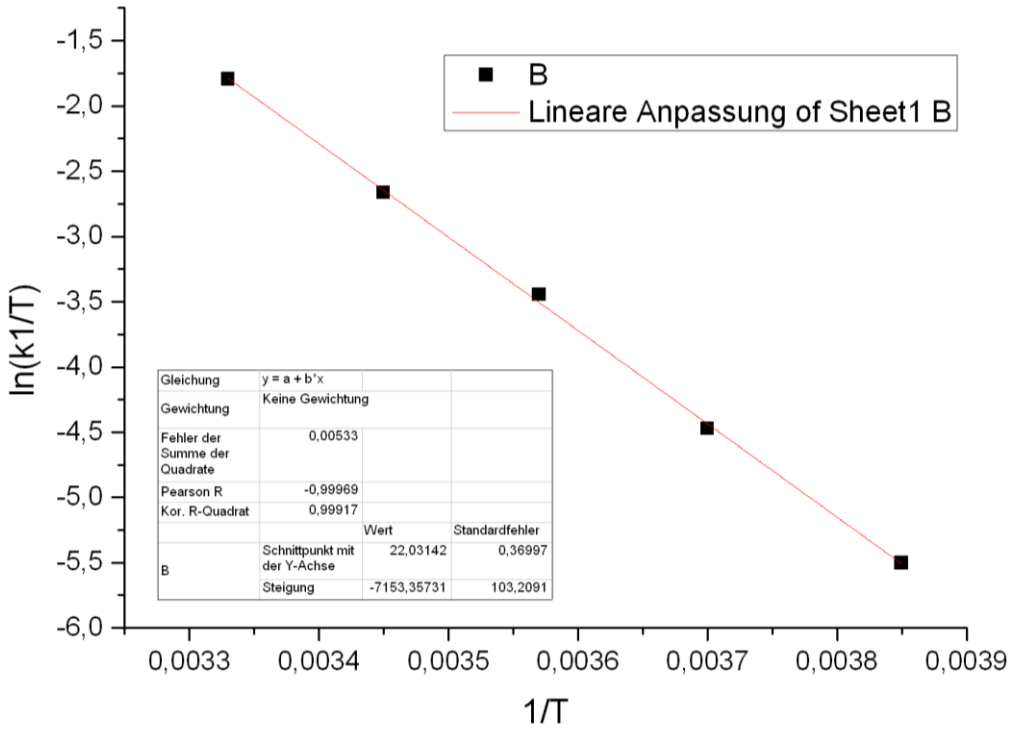

Figure 105. Plot of ln(k_1/T) *vs.*1/T.

	Slope m	Intercept n	$\Delta H^{\#}$ [J/mol]	$\Delta S^{\#}$ [J/(mol*K)]
	−7153.357	22.031	59473.035	−0.2079
Error	103.209	0.370	858.080	0.0445

Table 10. Values for slope, intercept, $\Delta H^{\#}$ and $\Delta S^{\#}$ for *E*-**5b**. $\Delta H^{\#}$ = -m*R; $\Delta S^{\#} = \frac{n-\ln(\frac{K_B}{h})}{R}$.

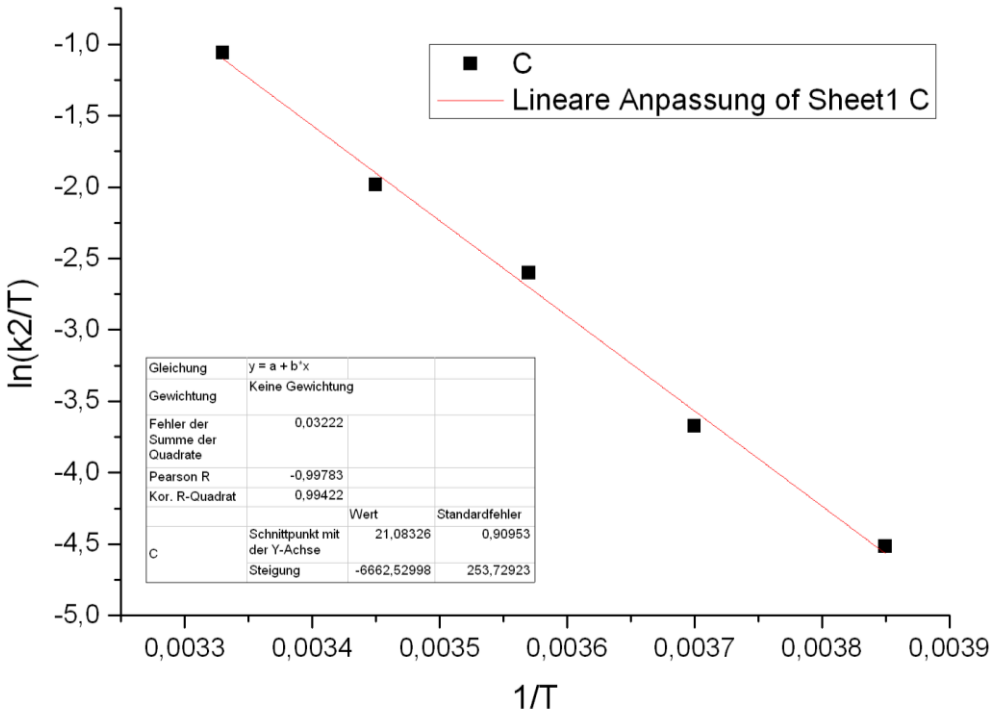

Figure 106. Plot of ln(k_2/T) *vs.* 1/T.

	Slope m	Intercept n	$\Delta H^{\#}$ [J/mol]	$\Delta S^{\#}$ [J/(mol*K)]
	−6662.523	21.083	55392.216	−0.3219
Error	253.729	0.910	2109.503	0.110

Table 11. Values for slope, intercept, $\Delta H^{\#}$ and $\Delta S^{\#}$ for *Z*-**108b**. $\Delta H^{\#}$ = -m*R; $\Delta S^{\#} = \frac{n-\ln(\frac{K_B}{h})}{R}$.

Applying the Gibb´s equation, $\Delta G^{\#} = \Delta H^{\#} - T^{*} \Delta S^{\#}$ can be calculated for both isomerisation steps:

At 300 K:

E-**108b**: $\Delta G^{\#}$ = 59.535 ± 0.844 kJ/mol

Z-**108b**: $\Delta G^{\#}$ = 55.488 ± 2.08 kJ/mol

The difference in $\Delta G^{\#}$ represents $\Delta\Delta G^{0}$ of the two isomers:

$\Delta\Delta G^{0}_{(E/Z)}$ = 4.050 ± 1.12 kJ/mo

7.3. Absorption Spectra

7.3.1. UV/vis Spectra and Determination of ε for *P*-Mesityl Phosphasilene 144

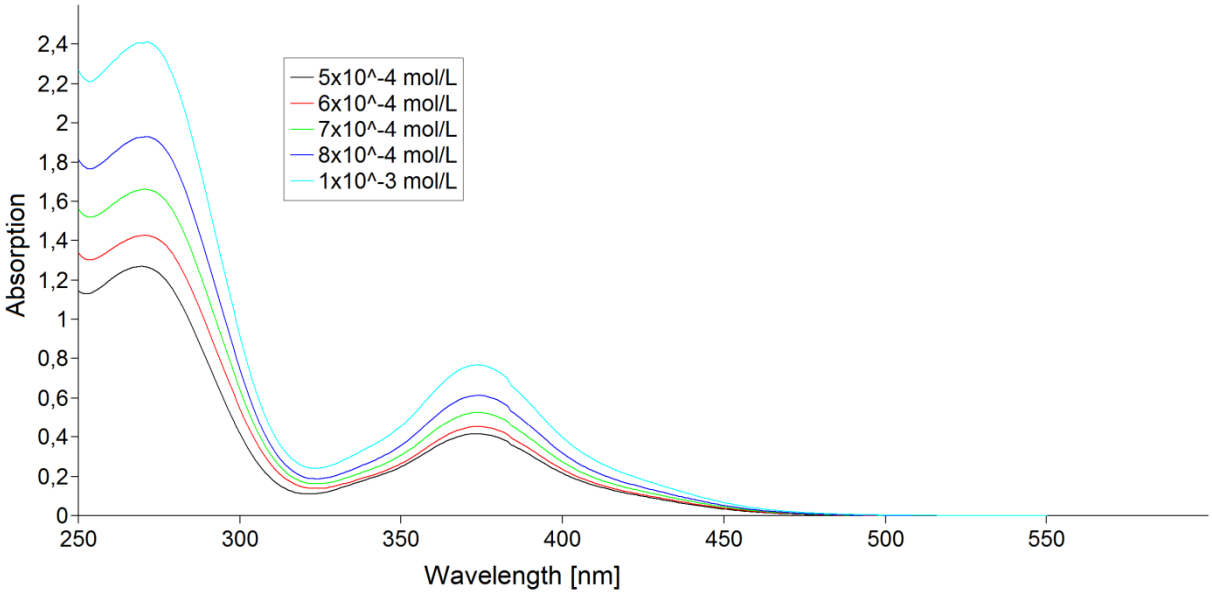

Figure 107. UV/vis spectra of **144** in hexane at different concentrations ($5 \cdot 10^{-4}$ - $1 \cdot 10^{-3}$ mol/L).

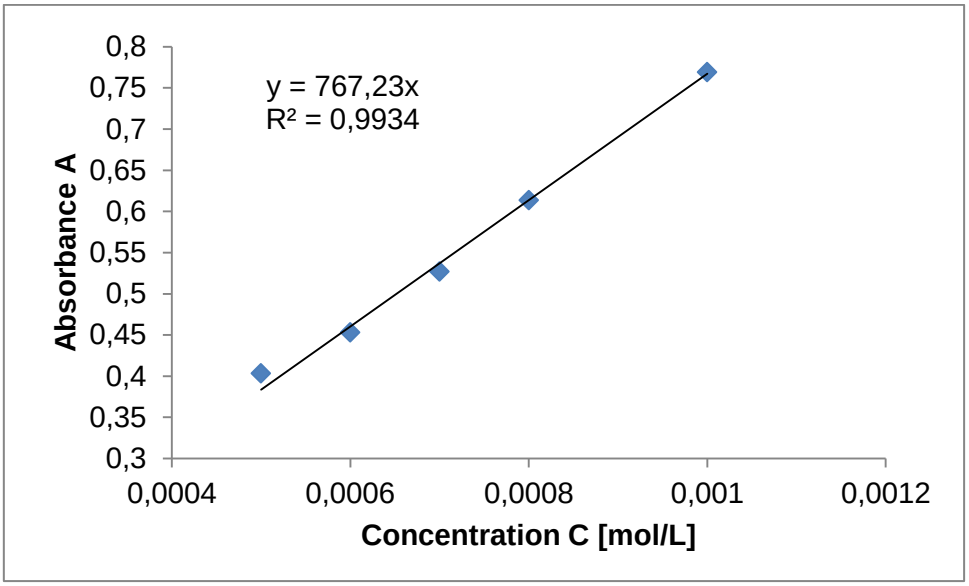

Figure 108. Determination of ε (7700 $M^{-1}cm^{-1}$) through a graphical draw of absorptions (λ = 374 nm) of **144** against their concentrations.

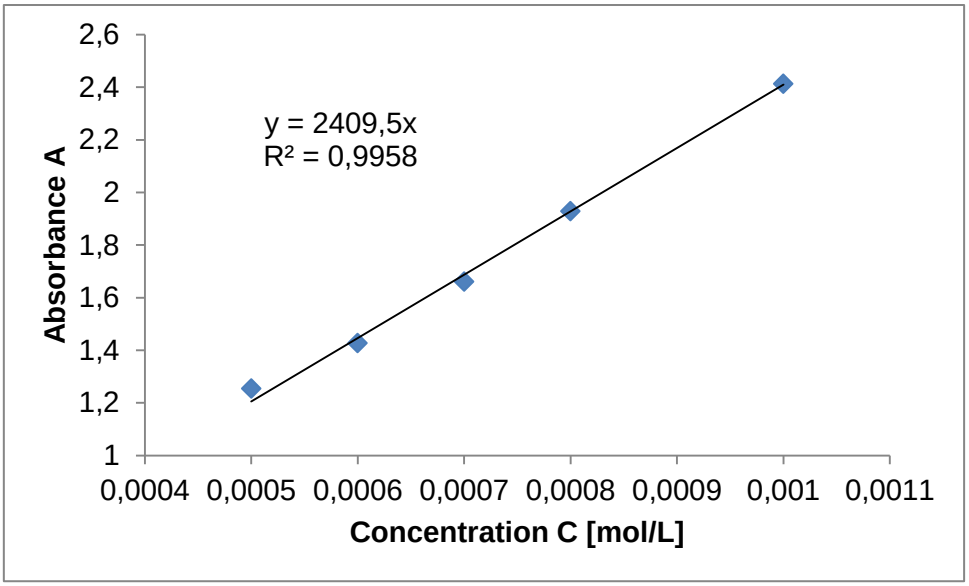

Figure 109. Determination of ε (24100 $M^{-1}cm^{-1}$) through a graphical draw of absorptions (λ = 270 nm) of **144** against their concentrations.

7.3.2. UV/vis Spectra of Trisilaphospha[1.1.0]bicyclobutane Tetracarbonyl Iron Complex 153

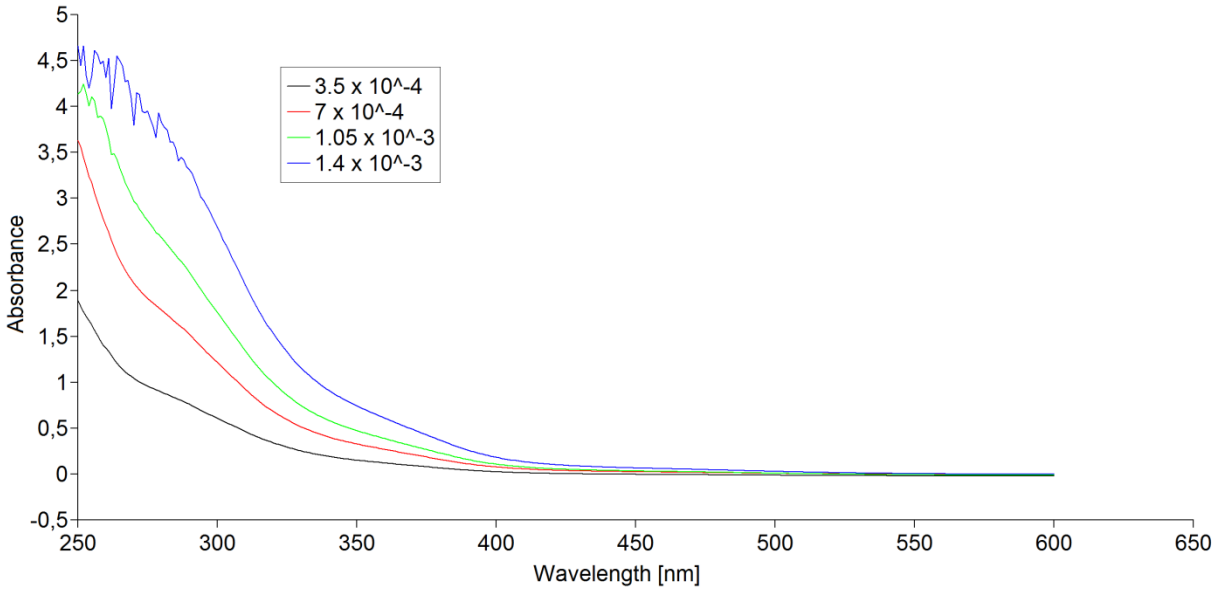

Figure 110. UV/vis spectra of **153** in hexane at different concentrations ($5 \cdot 10^{-4}$ - $1 \cdot 10^{-4}$ mol/L).

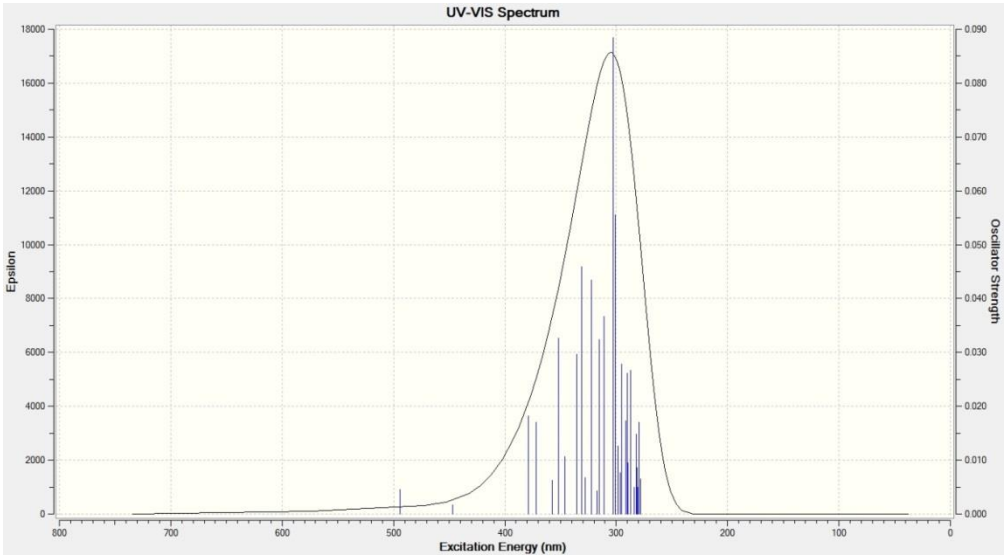

Figure 111. The calculated UV/visof **153**-Dip at B3LYP/6-31+G(d.p) level of theory (Solvent = Heptane), A = 303 nm; figure produced by Cem B. Yildiz, Aksaray University, Turkey.

7.3.3. UV/vis Spectra and Determination of ε for NHC-stabilized Cyclic Phosphasilene 166

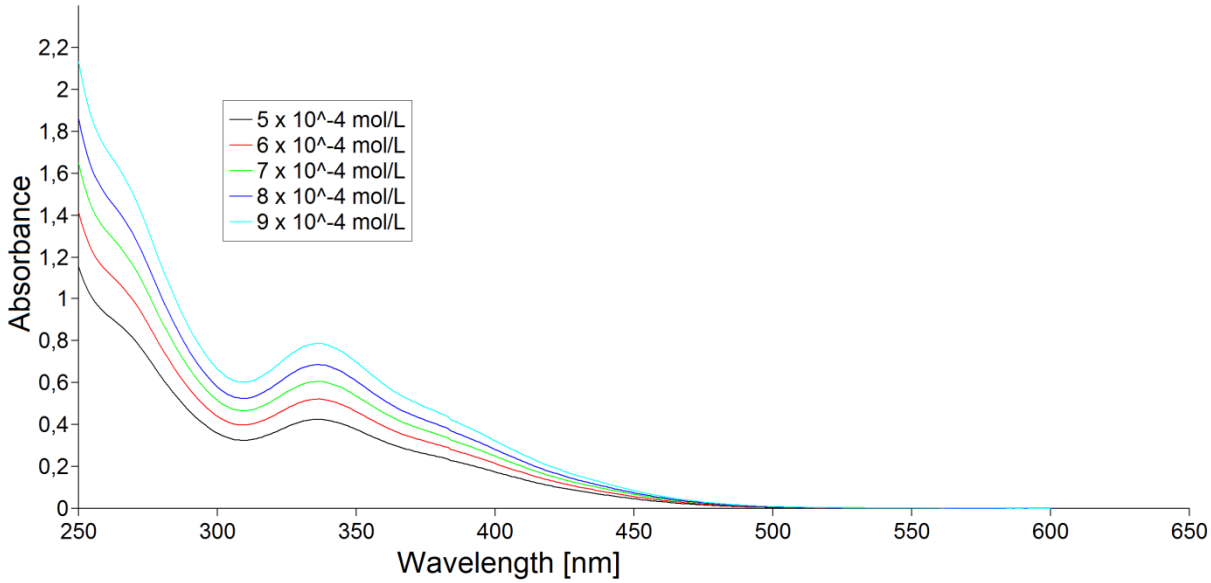

Figure 112. UV/vis spectra of **166** in hexane at different concentrations ($5 \cdot 10^{-4}$ - $9 \cdot 10^{-4}$ mol/L).

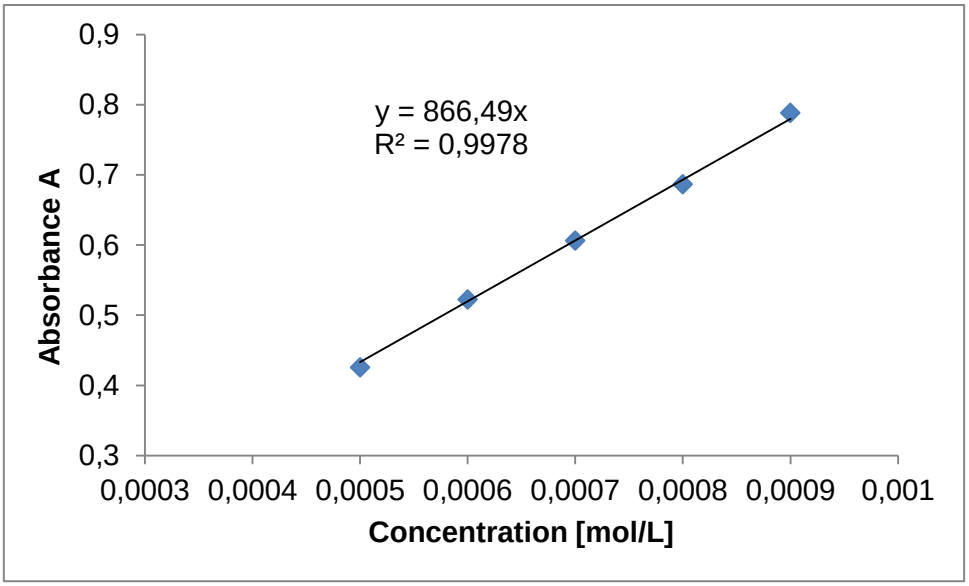

Figure 113. Determination of ε (8700 $M^{-1}cm^{-1}$) through a graphical draw of absorptions (λ= 336 nm) of **166** against their concentrations.

7.3.4. UV/vis Spectra of Tetracarbonyl Iron Complex of NHC-stabilized Cyclic Phosphasilene 170

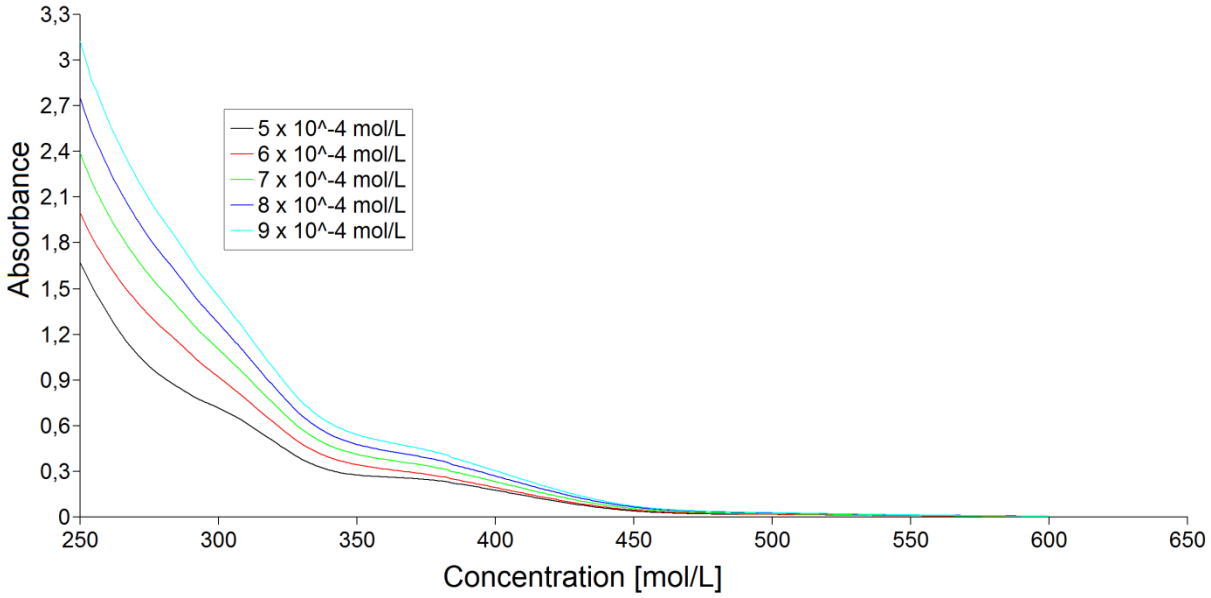

Figure 114. UV/vis spectra of **170** in hexane at different concentrations ($5 \cdot 10^{-4}$ - $9 \cdot 10^{-4}$ mol/L).

7.3.5. UV/vis Spectra of Disilaphosphaferra[1.1.0]bicyclobutane Derivative 171

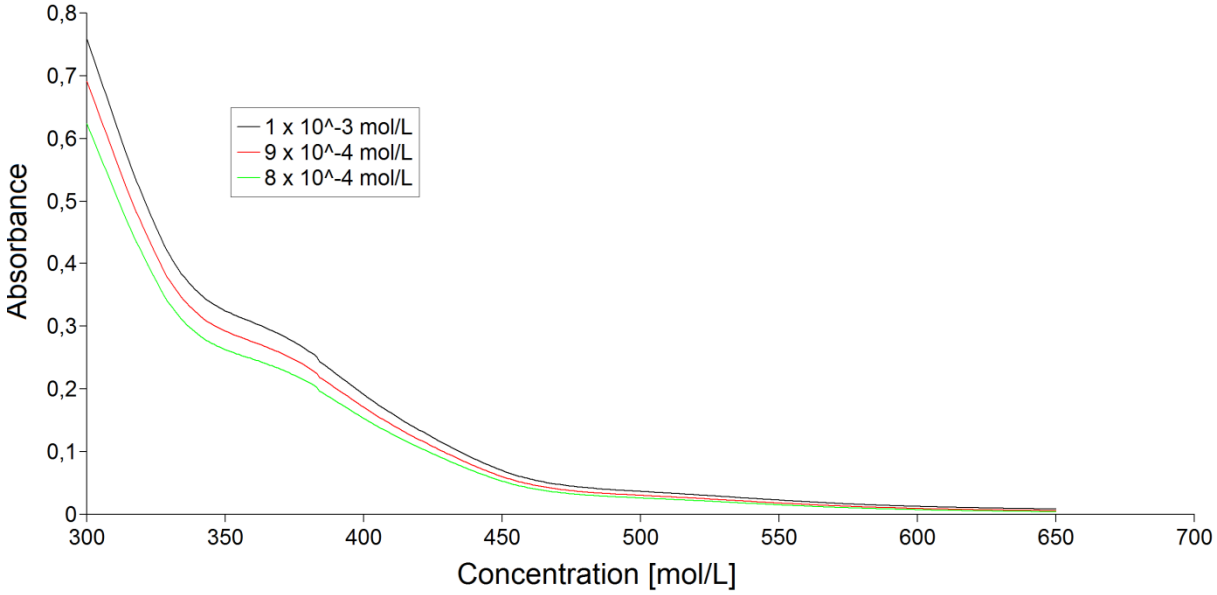

Figure 115. UV/vis spectra of **171** in hexane at different concentrations ($8 \cdot 10^{-4}$ - $1 \cdot 10^{-3}$ mol/L).

7.3.6. UV/vis Spectra and Determination of ε for Methyl Disilene 173

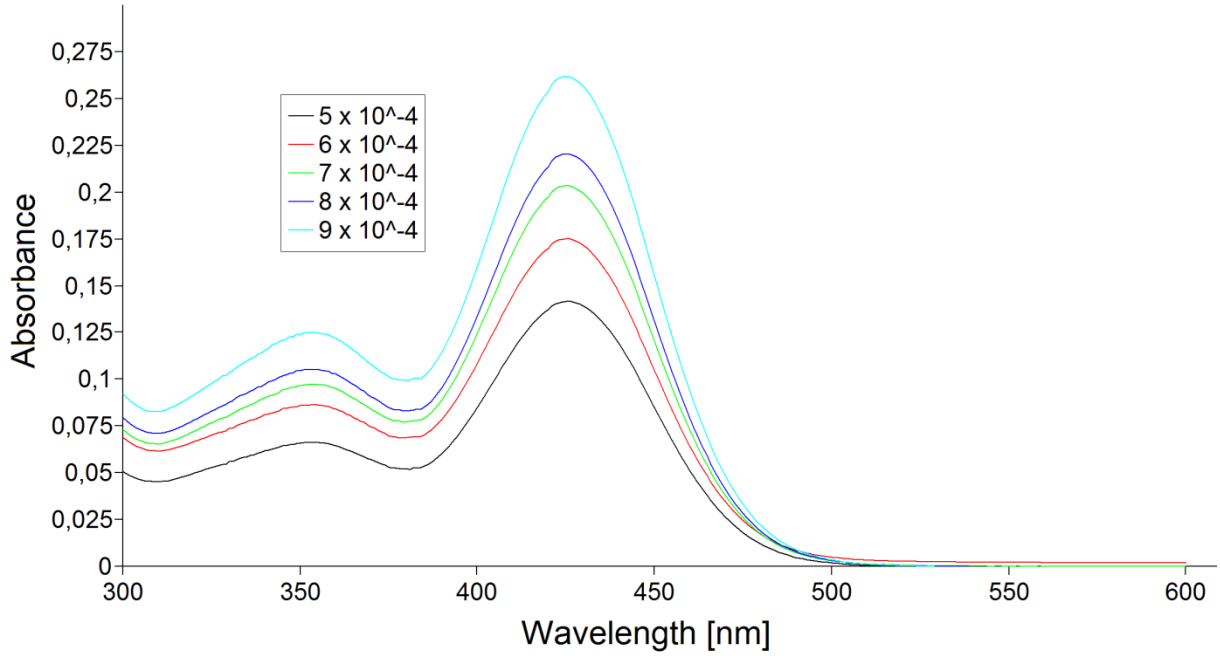

Figure 116. UV/vis spectra of **173** in hexane at different concentrations ($5 \cdot 10^{-4}$ - $9 \cdot 10^{-4}$ mol/L).

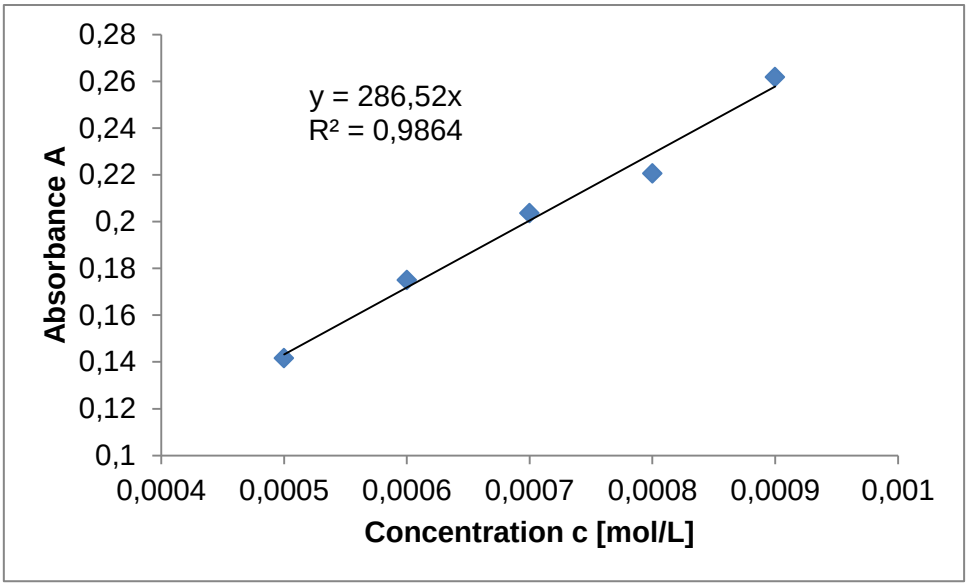

Figure 117. Determination of ε (2900 $M^{-1}cm^{-1}$) through a graphical draw of absorptions (λ = 426 nm) of **173** against their concentrations.

7.3.7. Determination of ε for Boryl Disilene 176

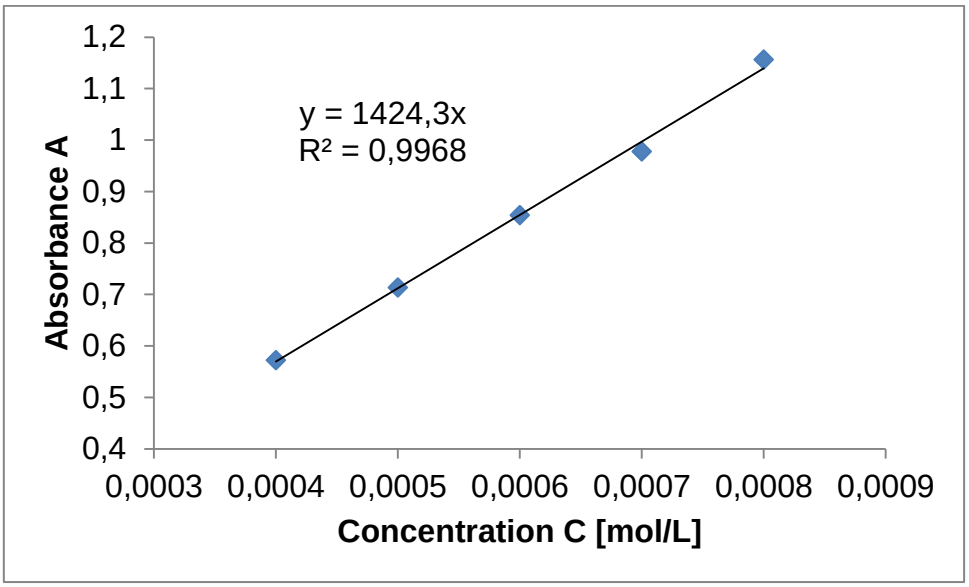

Figure 118: Determination of ε (14200 $M^{-1}cm^{-1}$) through a graphical draw of absorptions (λ = 457 nm) of **176** against their concentrations.

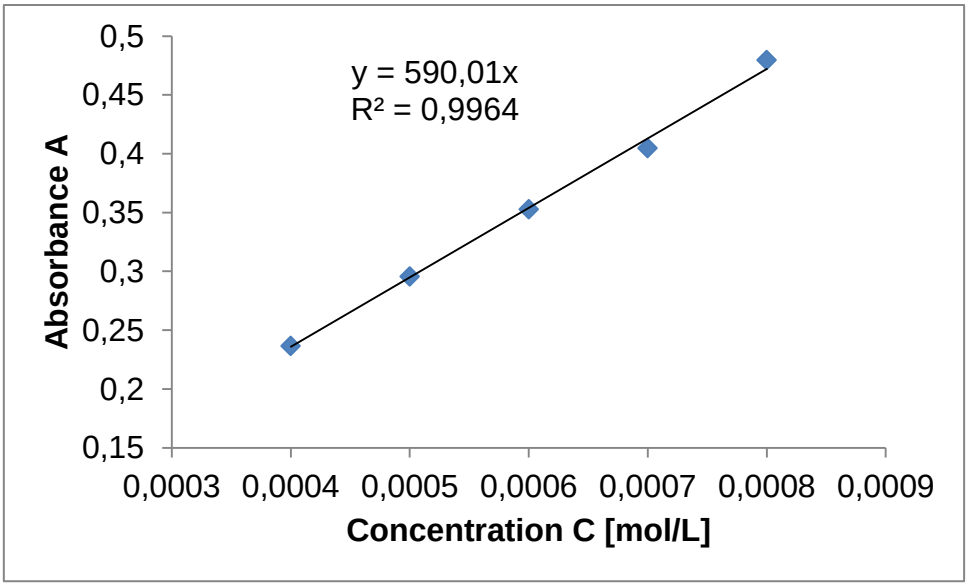

Figure 119: Determination of ε (5900 $M^{-1}cm^{-1}$) through a graphical draw of absorptions (λ = 380 nm) of **176** against their concentrations.

7.3.8. UV/vis Spectra and Determination of ε for Disilenylborate 180

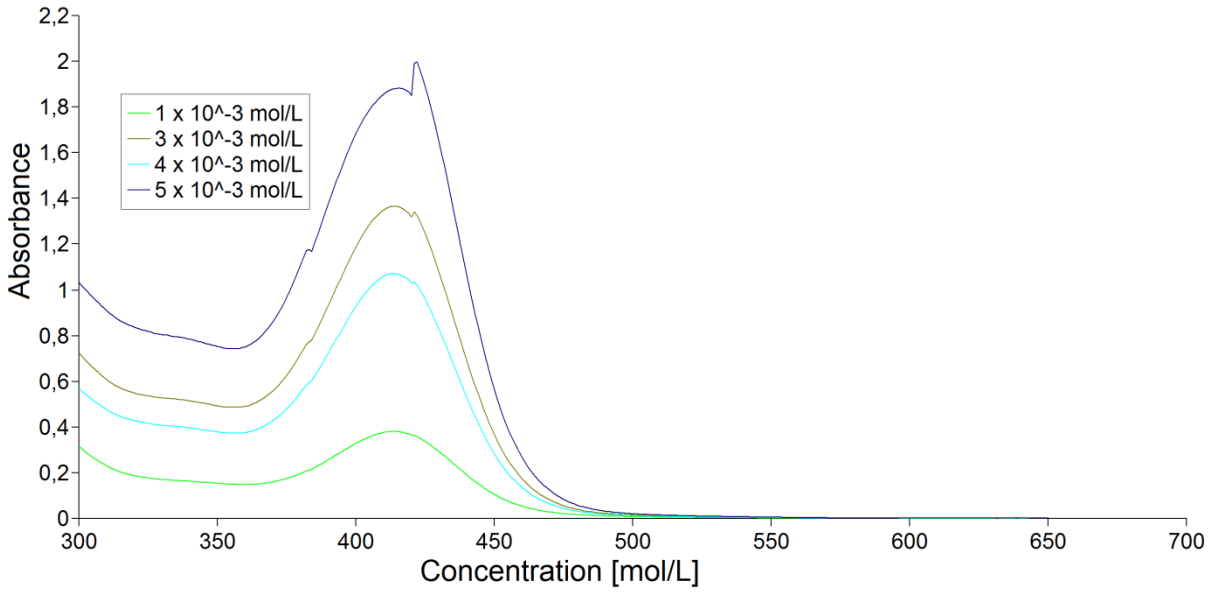

Figure 120. UV/vis spectra of **180** in hexane at different concentrations ($1 \cdot 10^{-3}$, $3 \cdot 10^{-3}$-$5 \cdot 10^{-3}$ mol/L).

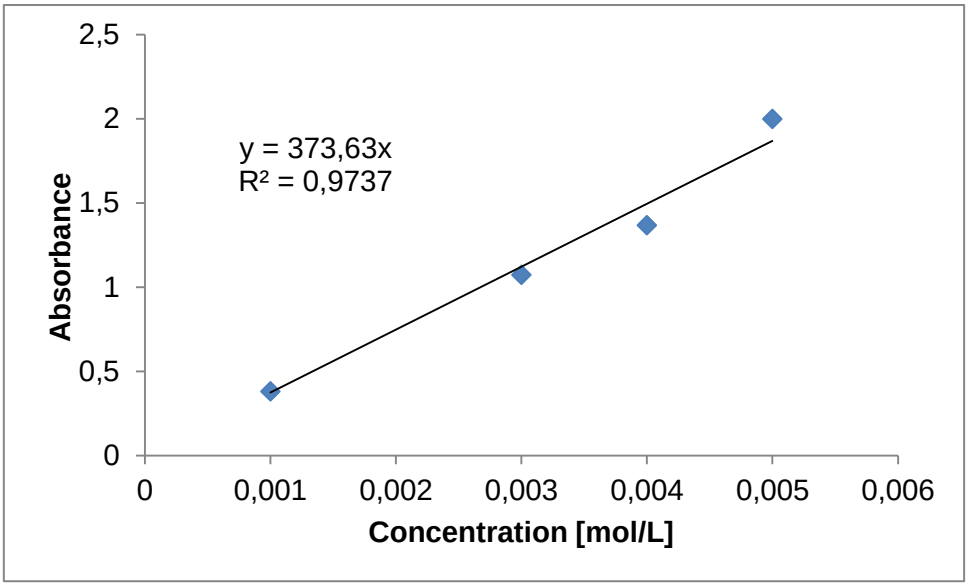

Figure 121. Determination of ε (3700 $M^{-1}cm^{-1}$) through a graphical draw of absorptions (λ = 414 nm) of **180** against their concentrations.

7.3.9. UV/vis Spectra and Determination of ε for Pivaloyl Substituted Siliconoid 182

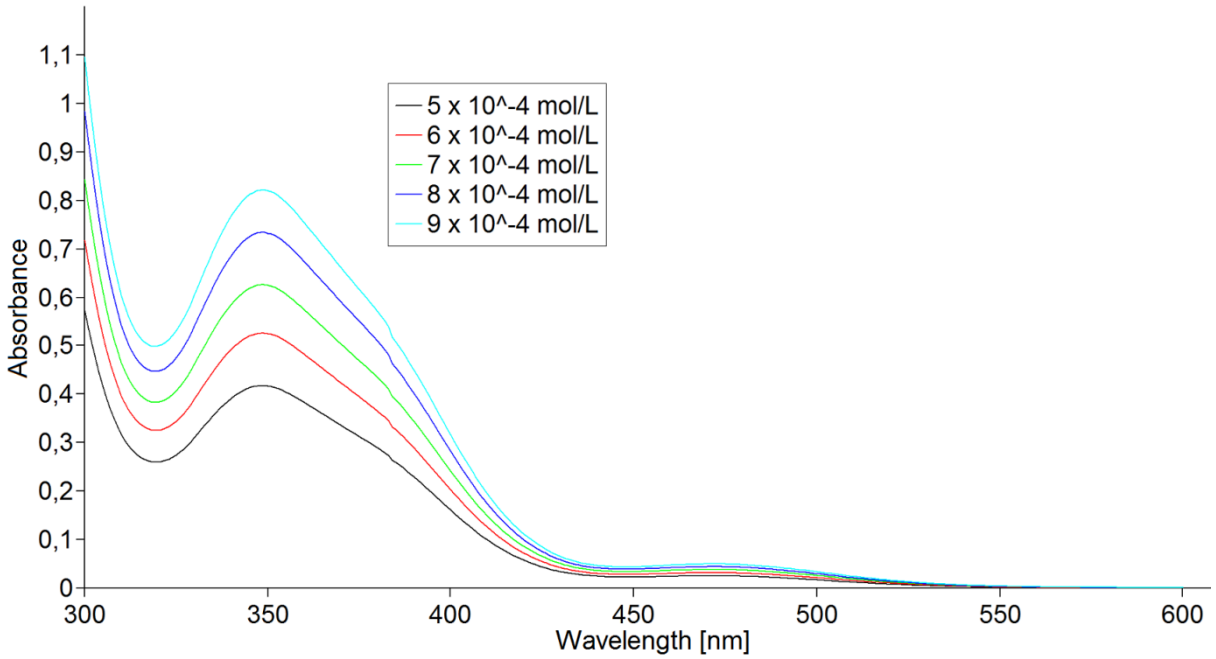

Figure 122. UV/vis spectra of **182** in hexane at different concentrations ($5 \cdot 10^{-4}$ - $9 \cdot 10^{-4}$ mol/L).

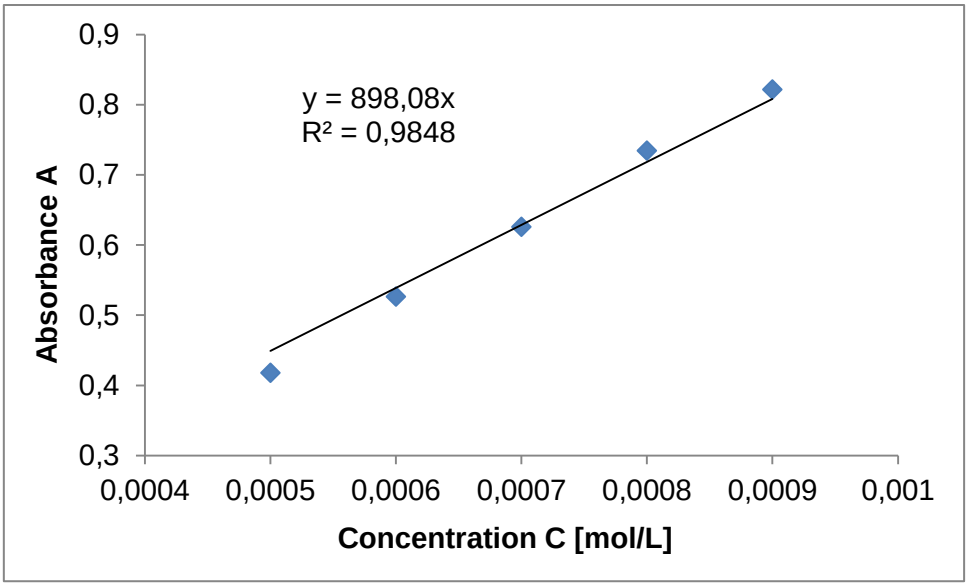

Figure 123. Determination of ε (500 $M^{-1}cm^{-1}$) through a graphical draw of absorptions (λ = 475 nm) of **182** against their concentrations.

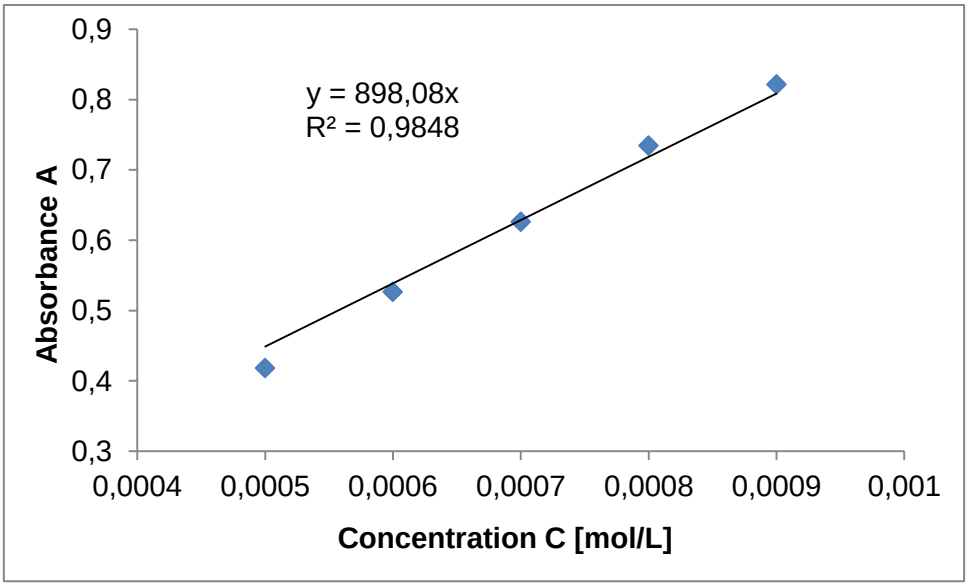

Figure 124. Determination of ε (9000 $M^{-1}cm^{-1}$) through a graphical draw of absorptions (λ = 349 nm) of **182** against their concentrations.

7.3.10. UV/vis Spectra and Determination of ε for Phosphino Substituted Siliconoid 184

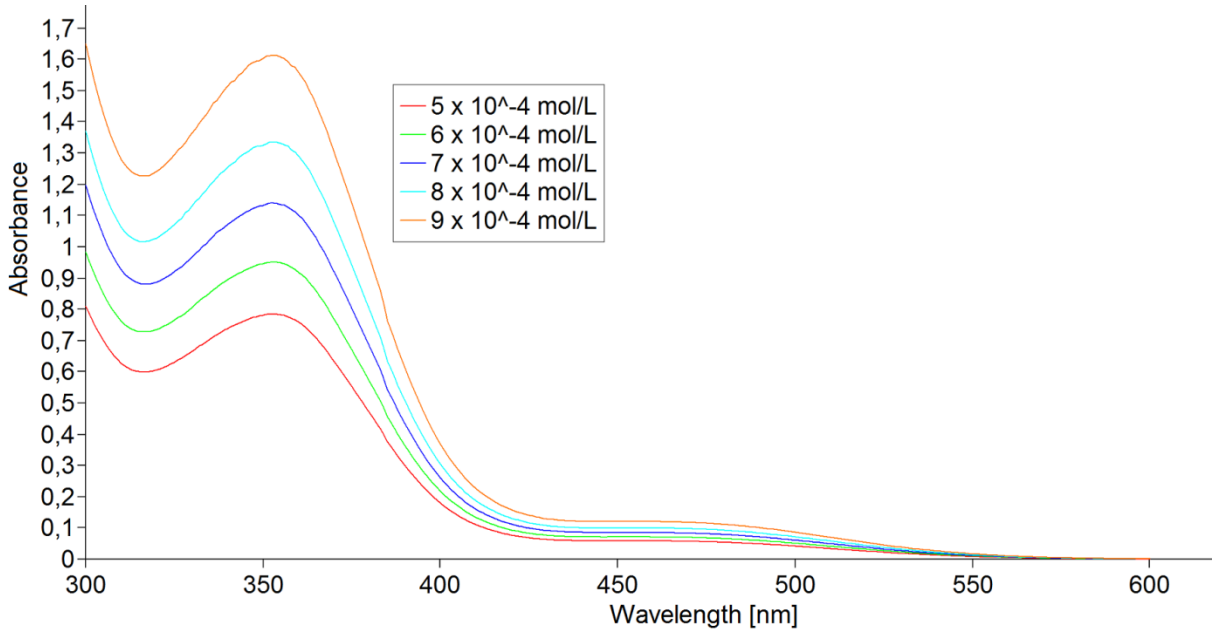

Figure 125. UV/vis spectra of **184** in hexane at different concentrations ($5 \cdot 10^{-4}$ - $9 \cdot 10^{-4}$ mol/L).

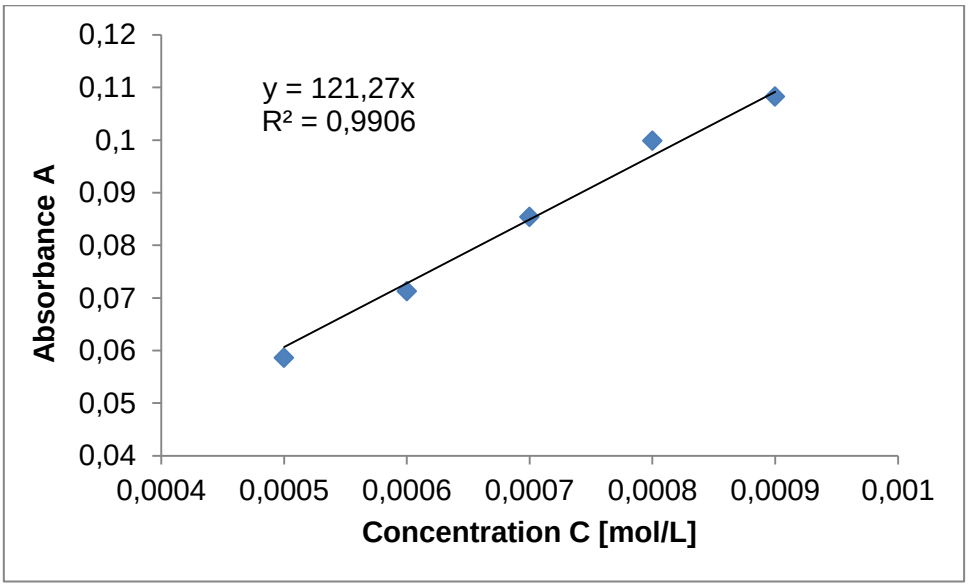

Figure 126. Determination of ε ($1200 M^{-1}cm^{-1}$) through a graphical draw of absorptions (λ = 475 nm) of **184** against their concentrations.

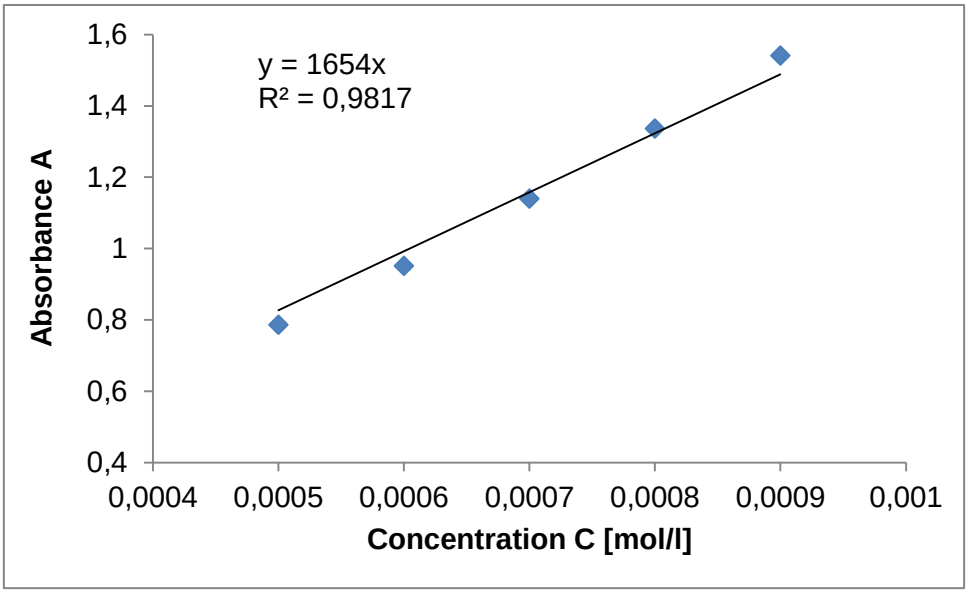

Figure 127. Determination of ε (16500 $M^{-1}cm^{-1}$) through a graphical draw of absorptions (λ = 354 nm) of **184** against their concentrations.

7.3.11. Determination of ε for Phosphinidene Substituted Siliconoid 186

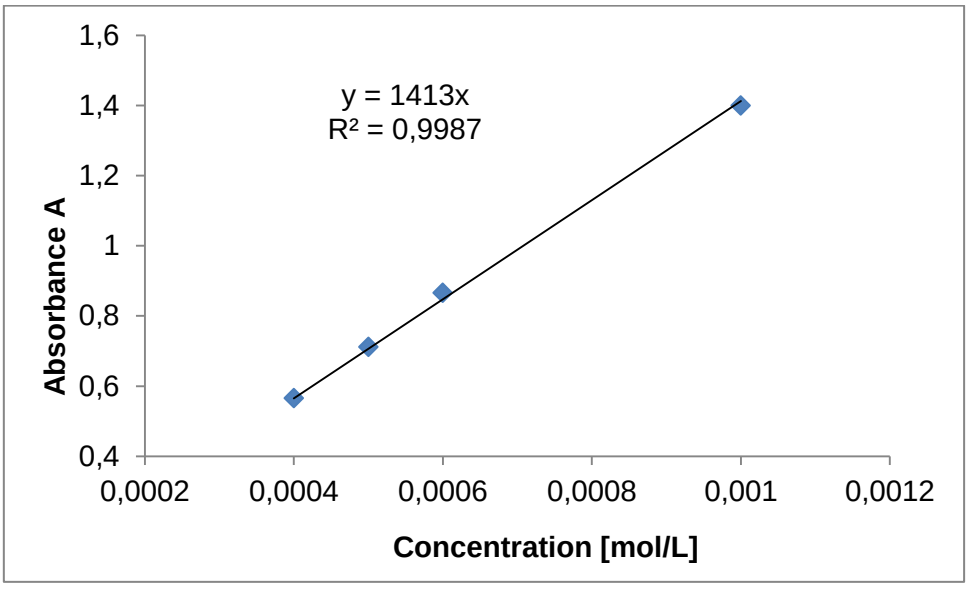

Figure 128. Determination of ε (14100 $M^{-1}cm^{-1}$) through a graphical draw of absorptions (λ = 364 nm) of **186** against their concentrations.

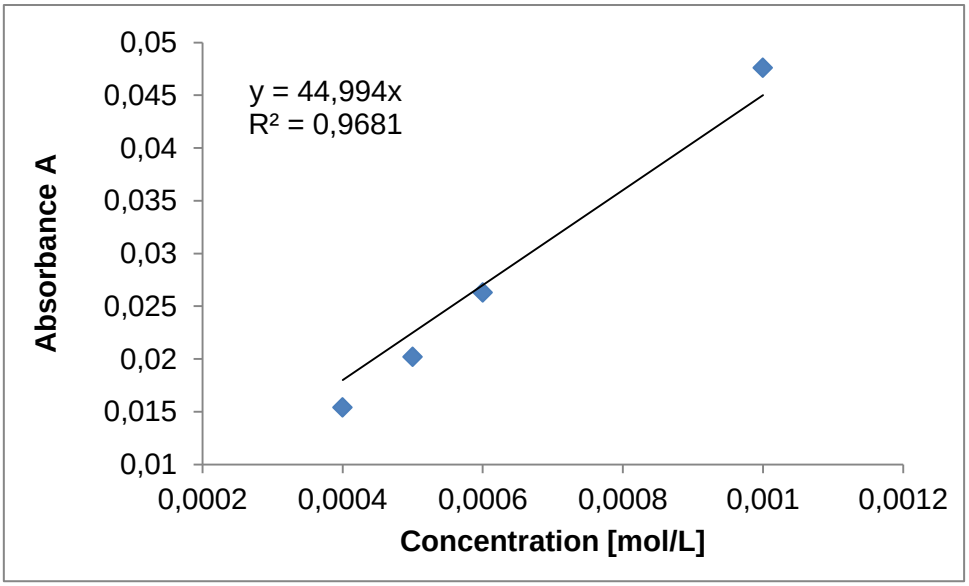

Figure 129. Determination of ε (400 $M^{-1}cm^{-1}$) through a graphical draw of absorptions (λ = 589 nm) of **186** against their concentrations.

7.3.12. UV/vis Spectra and Determination of ε for Borate Substituted Siliconoid 194

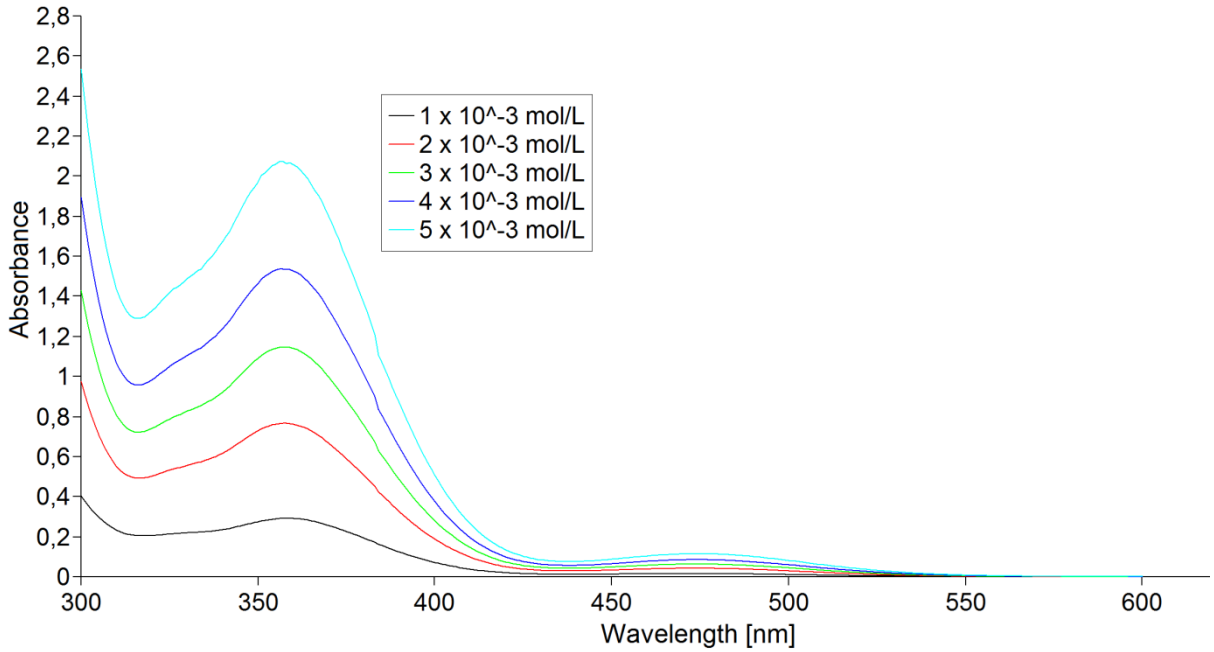

Figure 130. UV/vis spectra of **194** in hexane at different concentrations ($5 \cdot 10^{-4}$ - $1 \cdot 10^{-3}$ mol/L).

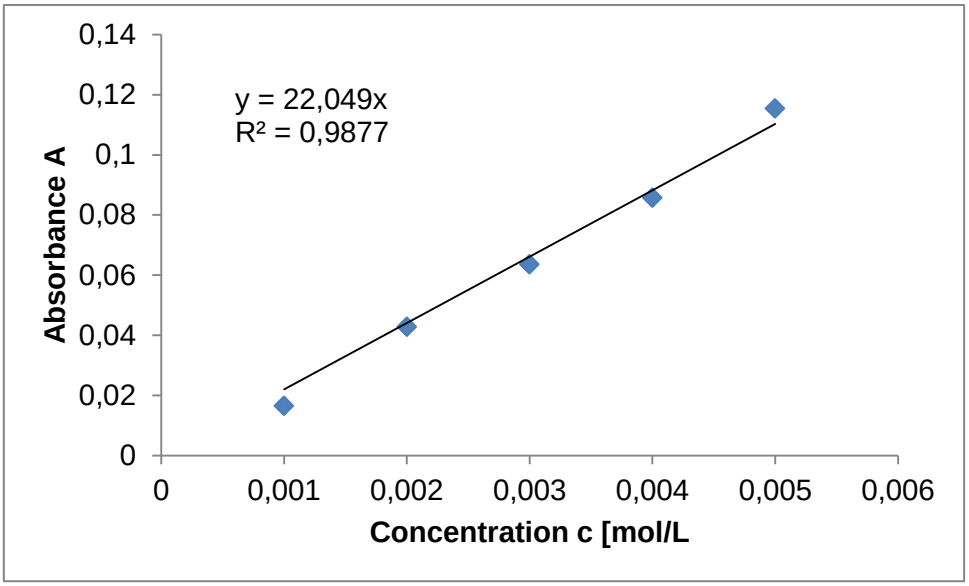

Figure 131. Determination of ε (200 $M^{-1}cm^{-1}$) through a graphical draw of absorptions (λ = 475 nm) of **194** against their concentrations.

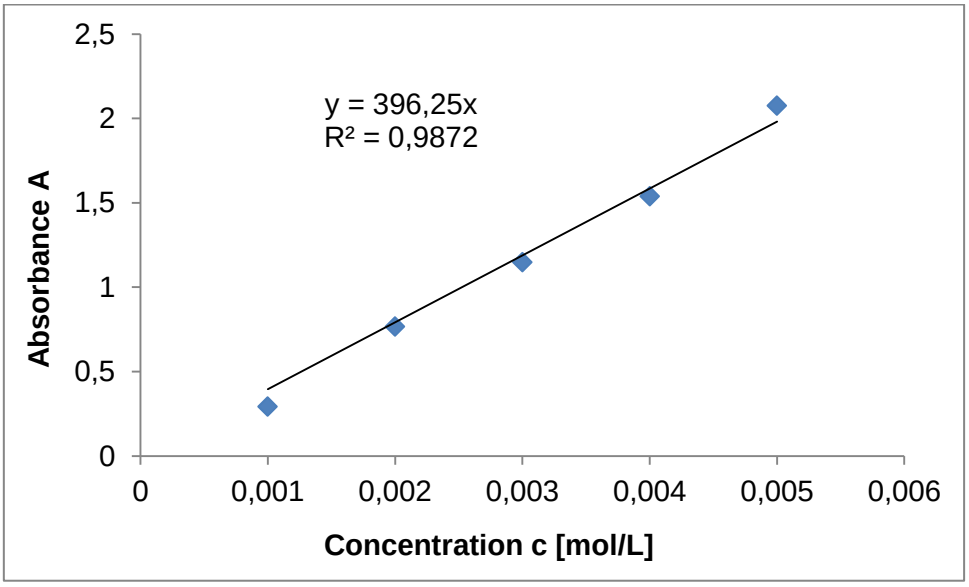

Figure 132. Determination of ε (4000 $M^{-1}cm^{-1}$) through a graphical draw of absorptions (λ = 357 nm) of **194** against their concentrations.

7.3.13. UV/vis Spectra and Determination of ε for Anionic Siliconoid 195

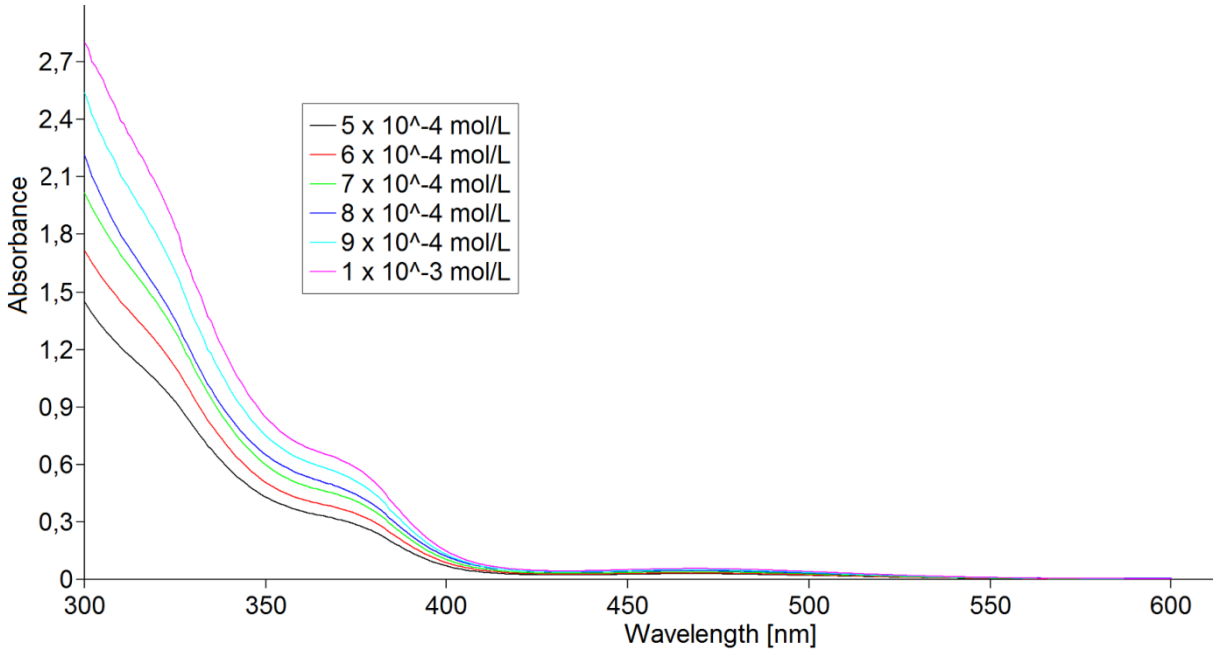

Figure 133. UV/vis spectra of **195** in hexane at different concentrations ($5 \cdot 10^{-4}$ - $1 \cdot 10^{-3}$ mol/L).

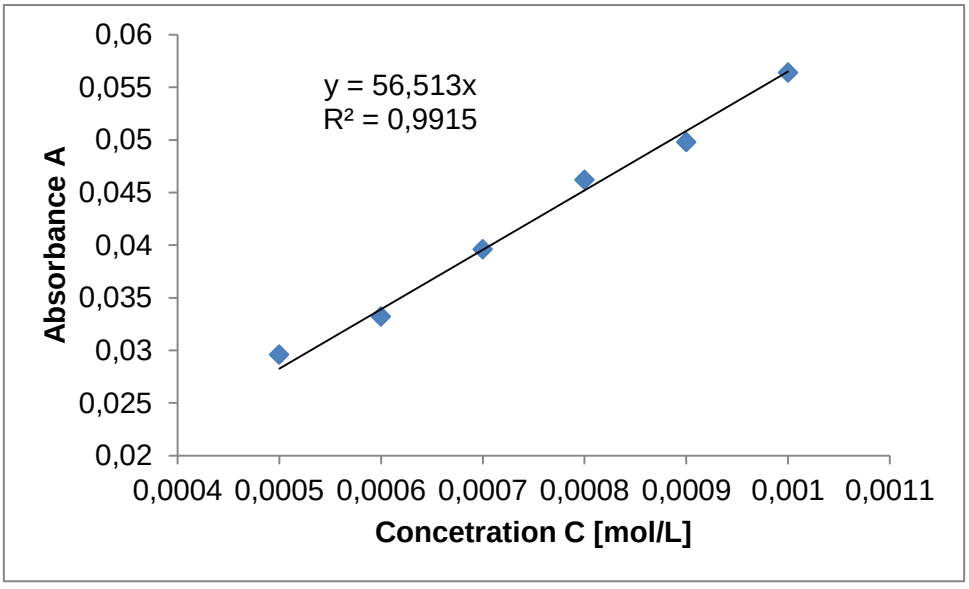

Figure 134. Determination of ε (600 $M^{-1}cm^{-1}$) through a graphical draw of absorptions (λ = 468 nm) of **195** against their concentrations.

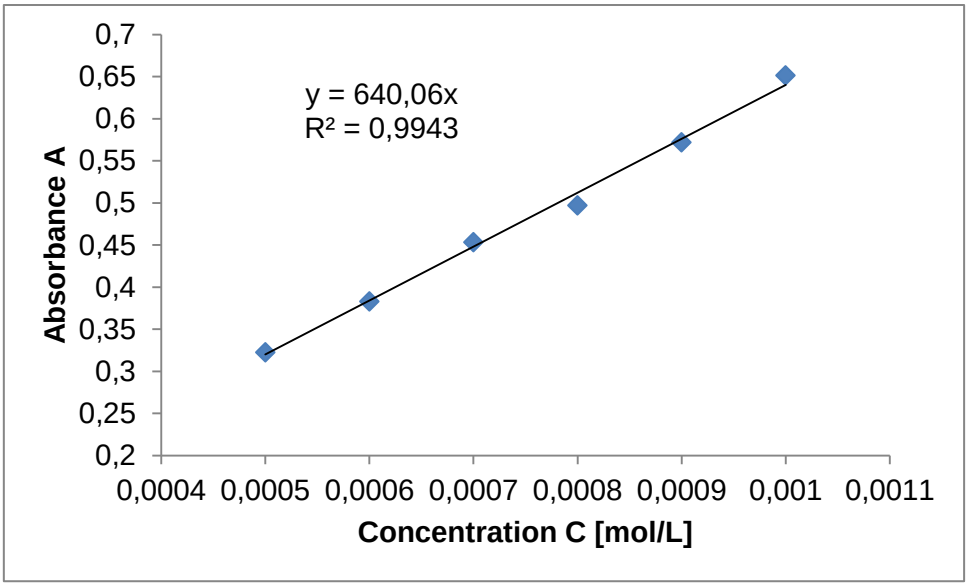

Figure 135. Determination of ε (6400 $M^{-1}cm^{-1}$) through a graphical draw of absorptions (λ = 368 nm) of **195** against their concentrations.

7.3.14. UV/vis Spectra and Determination of ε for Silyl Substituted Siliconoid 197

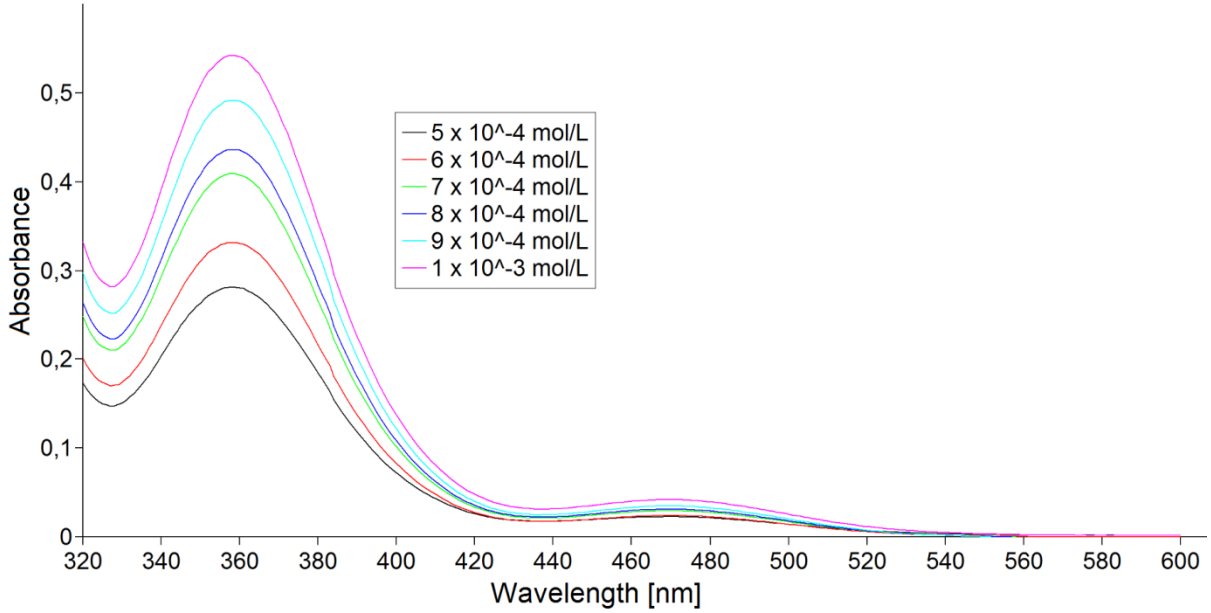

Figure 136. UV/vis spectra of silyl substituted siliconoid **197** in hexane at different concentrations ($5 \cdot 10^{-4}$ - $1 \cdot 10^{-3}$ mol/L).

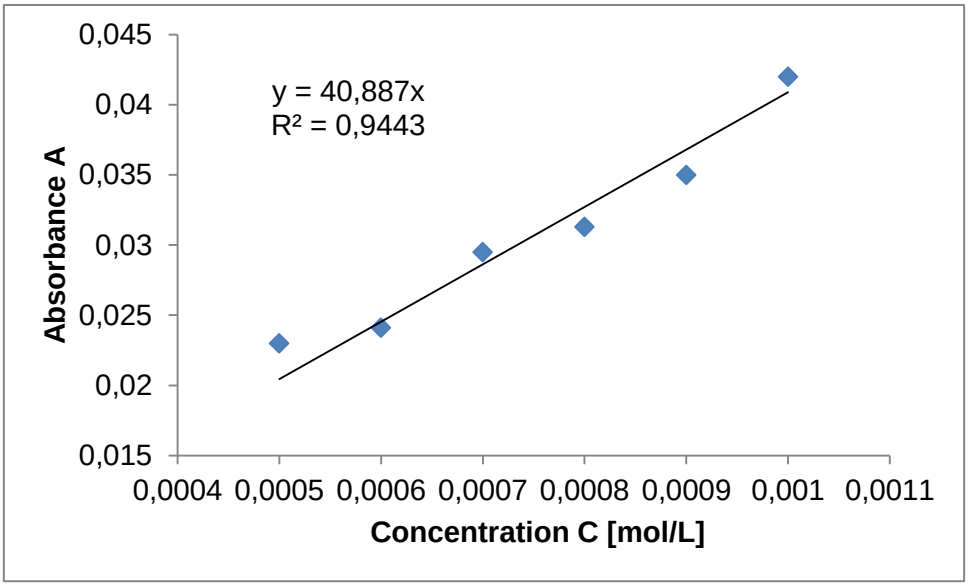

Figure 137. Determination of ε (400 $M^{-1}cm^{-1}$) through a graphical draw of absorptions (λ = 496 nm) of **197** against their concentrations.

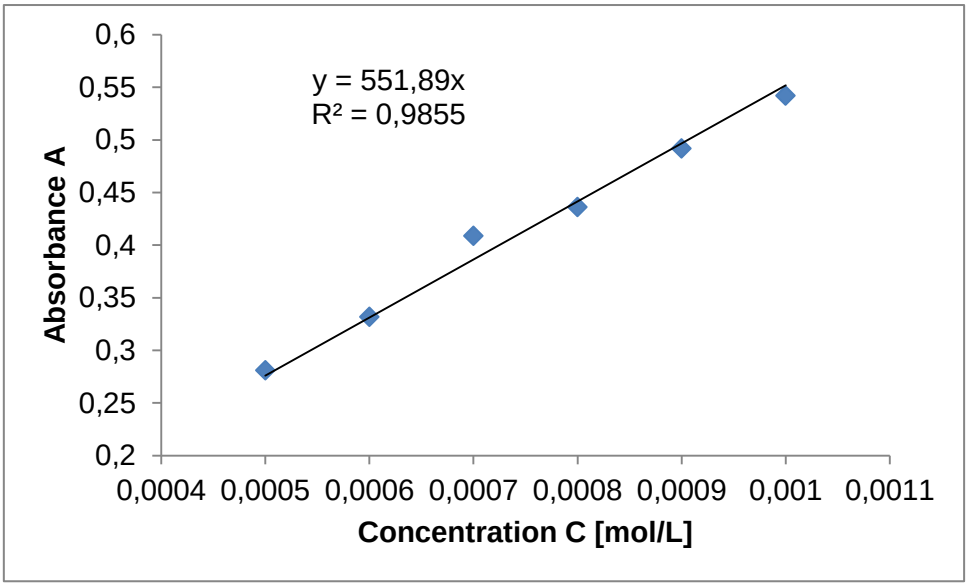

Figure 138. Determination of ε (5500$M^{-1}cm^{-1}$) through a graphical draw of absorptions (λ = 359 nm) of **197** against their concentrations.

7.3.15. UV/vis Spectra and Determination of ε for *p*-Methylsulfide Substituted Phenyl disilene 201a

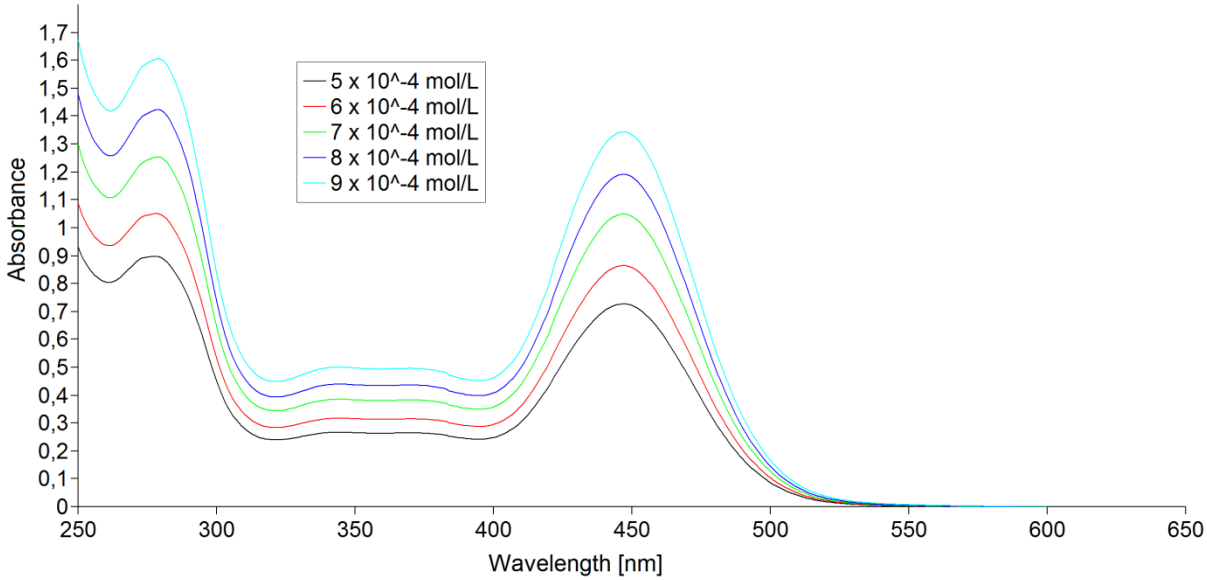

Figure 139. UV/vis spectra of **201a** in hexane at different concentrations ($5 \cdot 10^{-4}$ - $9 \cdot 10^{-4}$ mol/L).

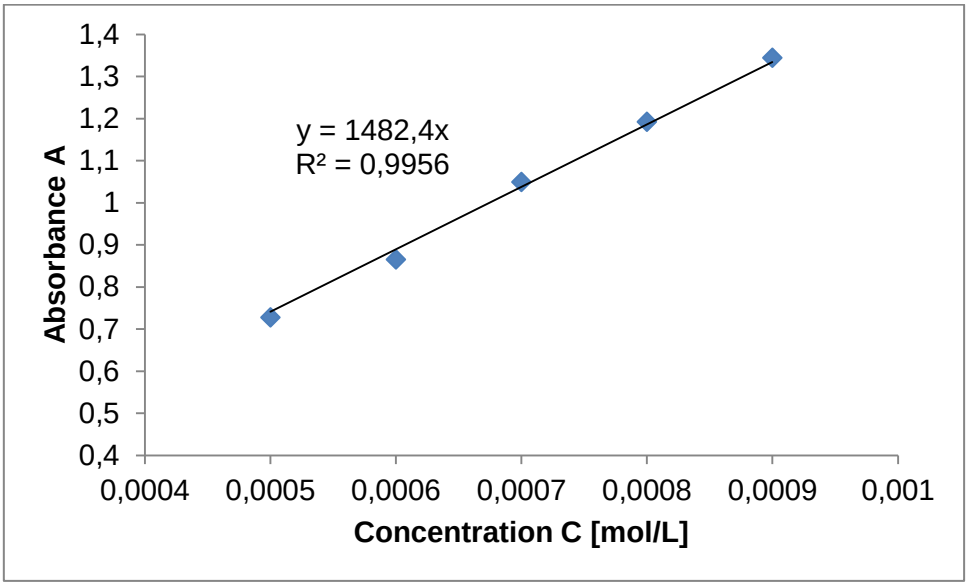

Figure 140. Determination of ε (14800 $M^{-1}cm^{-1}$) through a graphical draw of absorptions (λ = 447 nm) of **201a** against their concentrations.

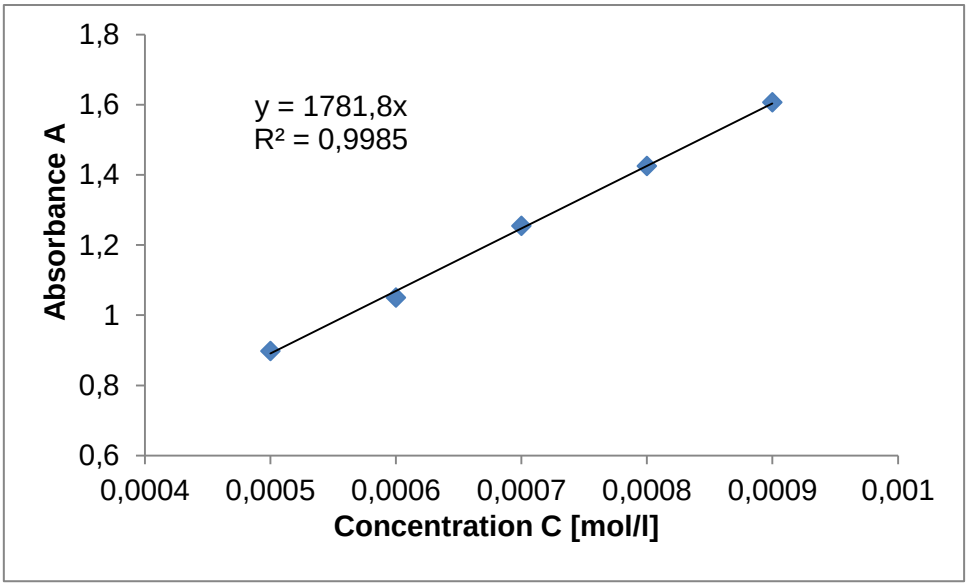

Figure 141. Determination of ε (17800 $M^{-1}cm^{-1}$) through a graphical draw of absorptions (λ = 278 nm) of **201a** against their concentrations.

7.3.16. UV/vis Spectra and Determination of ε for *p*-Methylsulfide Substituted Biphenyl disilene 201b

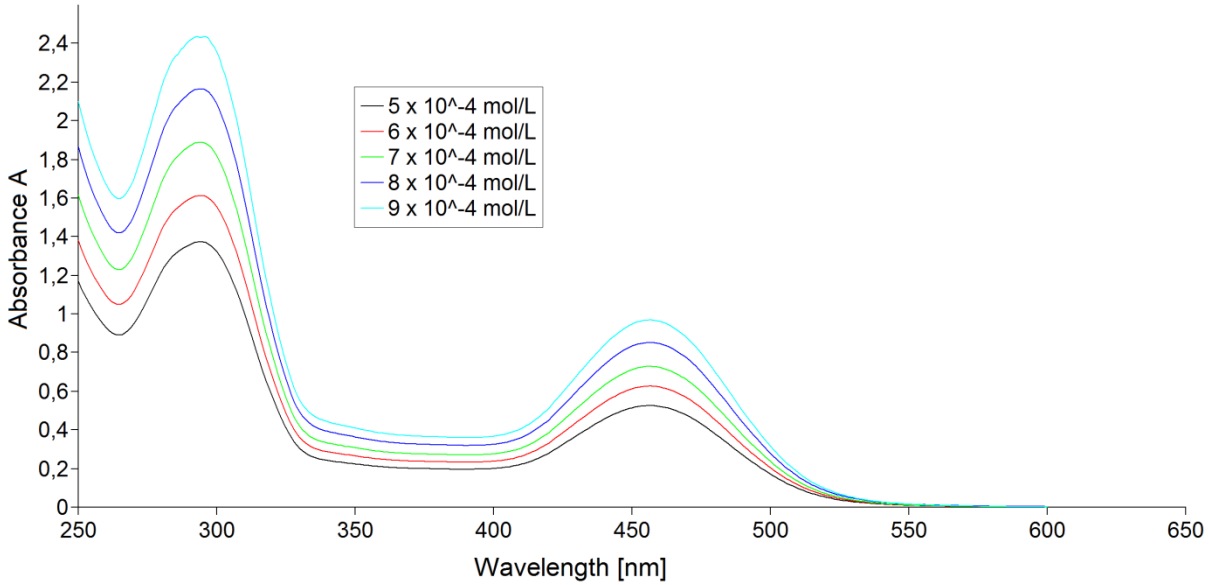

Figure 142. UV/vis spectra of **201b** in hexane at different concentrations ($5 \cdot 10^{-4}$ - $9 \cdot 10^{-4}$ mol/L).

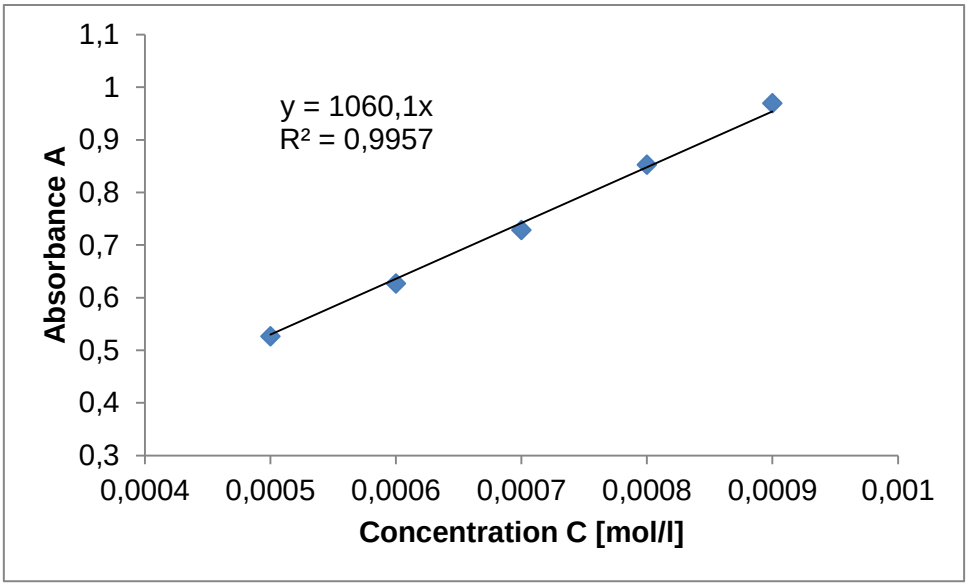

Figure 143. Determination of ε (10600 $M^{-1}cm^{-1}$) through a graphical draw of absorptions (λ = 456 nm) of **201b** against their concentrations.

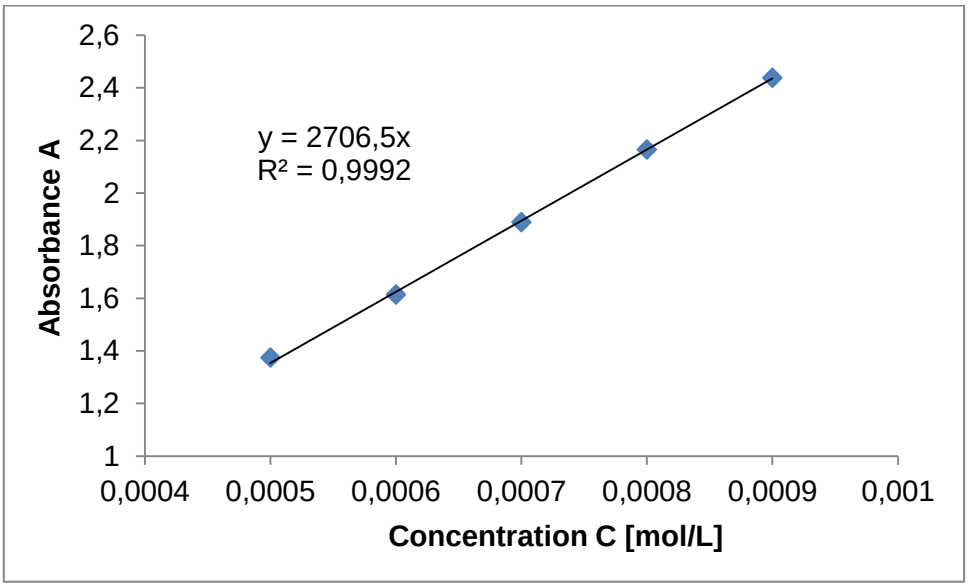

Figure 144. Determination of ε (27000 $M^{-1}cm^{-1}$) through a graphical draw of absorptions (λ = 295 nm) of **201b** against their concentrations.

7.3.17. UV/vis Spectra and Determination of ε for *p*-Methylsulfide Substituted Terphenyl disilene 201c

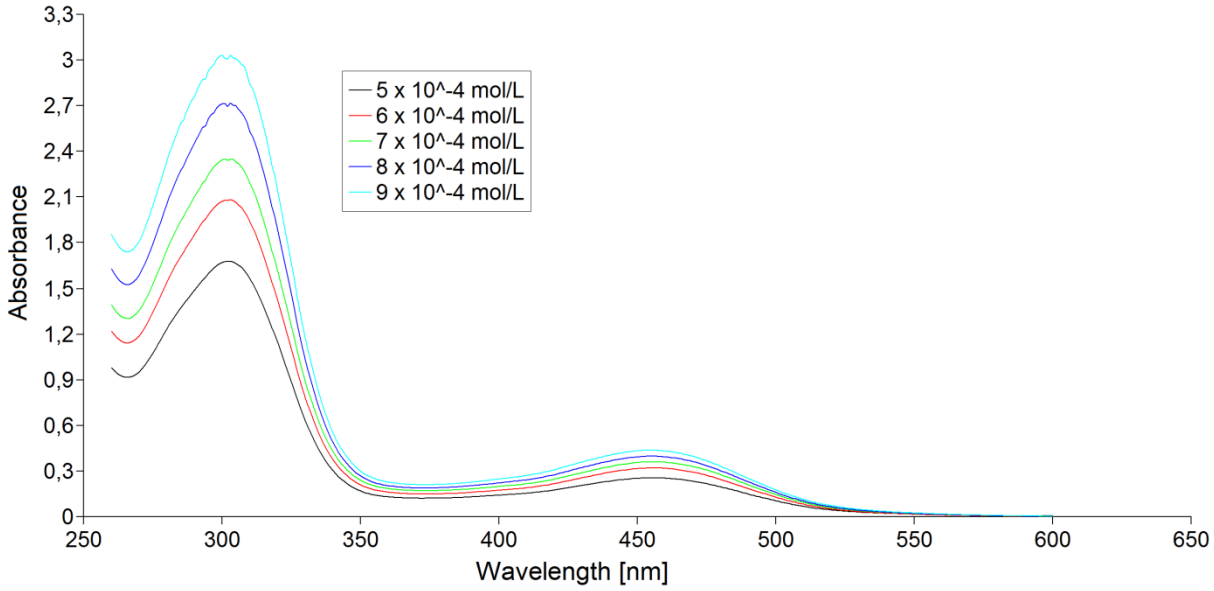

Figure 145. UV/vis spectra of **201c** in hexane at different concentrations ($5 \cdot 10^{-4}$ - $9 \cdot 10^{-4}$ mol/L).

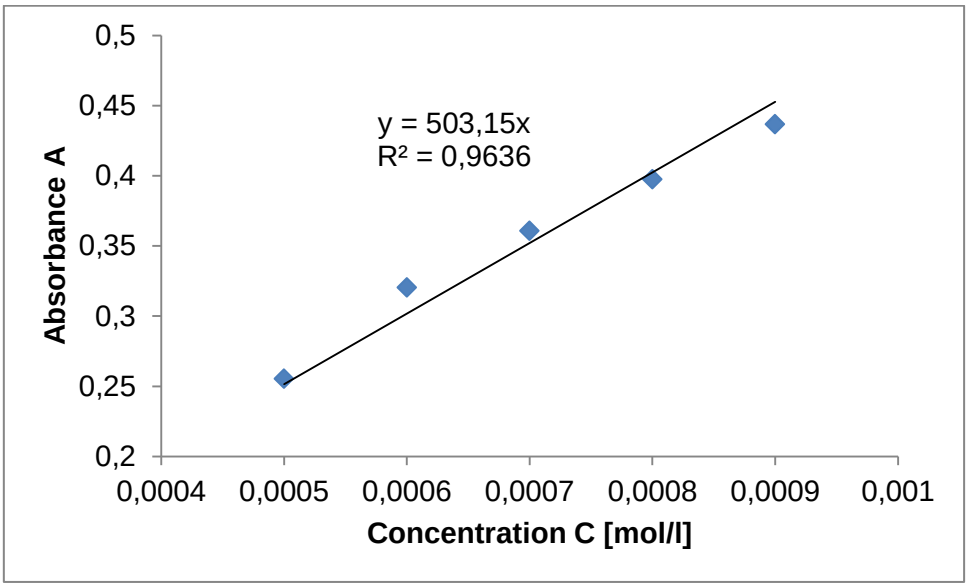

Figure 146. Determination of ε (5000 $M^{-1}cm^{-1}$) through a graphical draw of absorptions (λ = 456 nm) of **201c** against their concentrations.

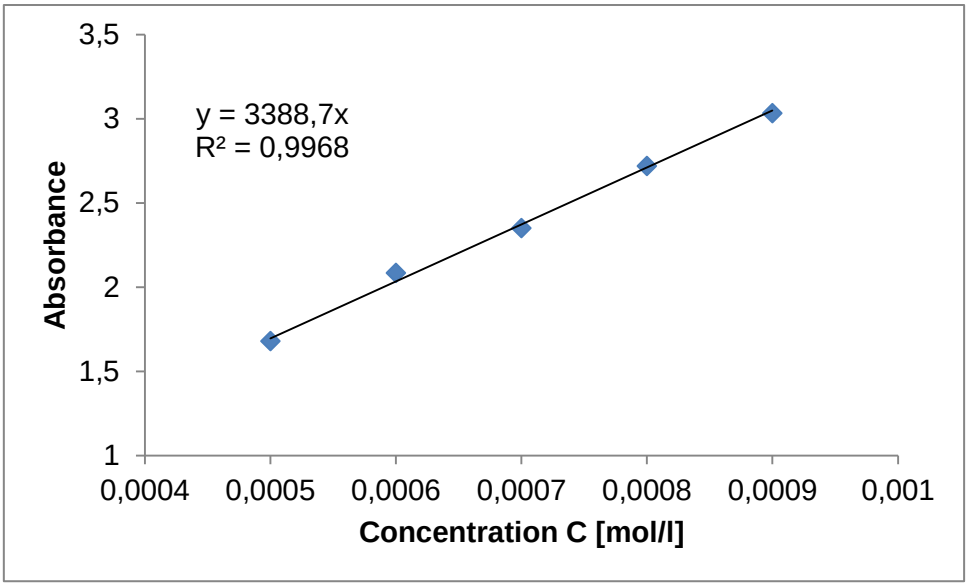

Figure 147. Determination of ε (33900 $M^{-1}cm^{-1}$) through a graphical draw of absorptions (λ = 303 nm) of **201c** against their concentrations.

7.3.18. UV/vis Spectra and Determination of ε for Octylsulfide Substituted Disilene 202

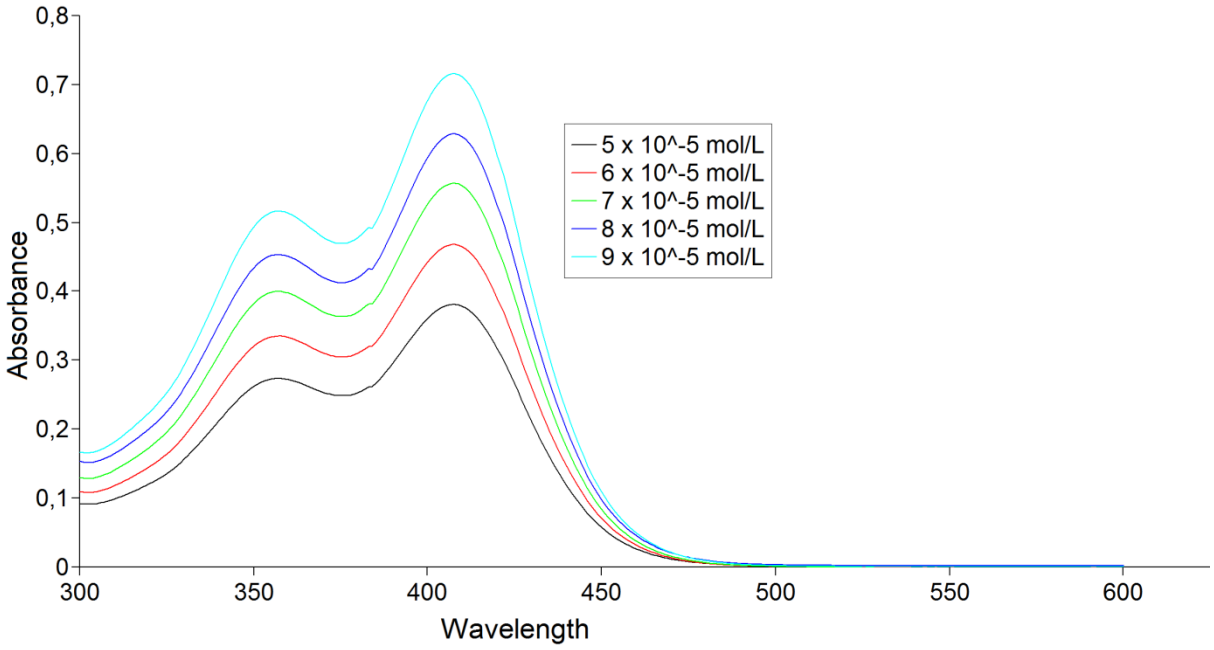

Figure 148. UV/vis spectra of **202** in hexane at different concentrations ($5 \cdot 10^{-4}$ - $9 \cdot 10^{-4}$ mol/L).

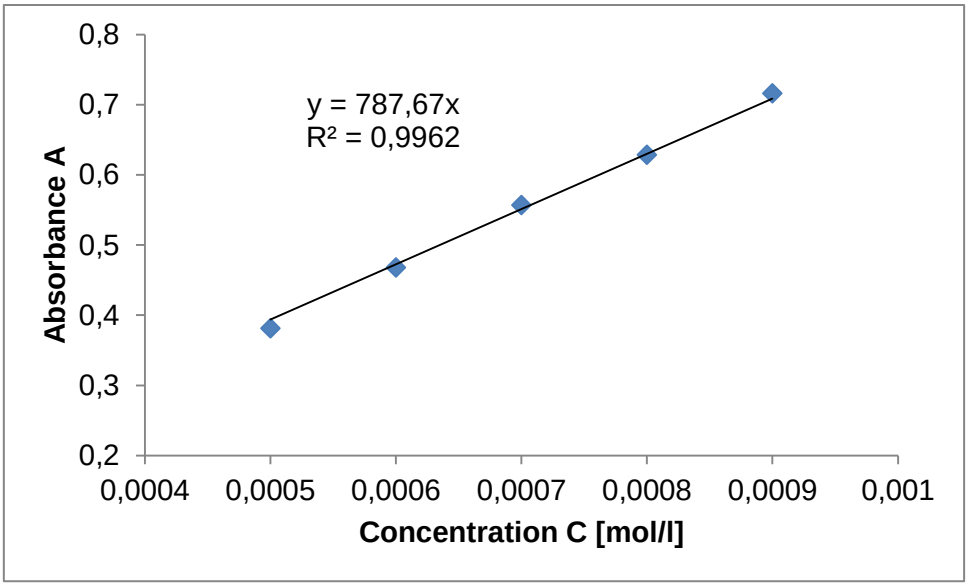

Figure 149. Determination of ε (7900 $M^{-1}cm^{-1}$) through a graphical draw of absorptions (λ = 407 nm) of **202** against their concentrations.

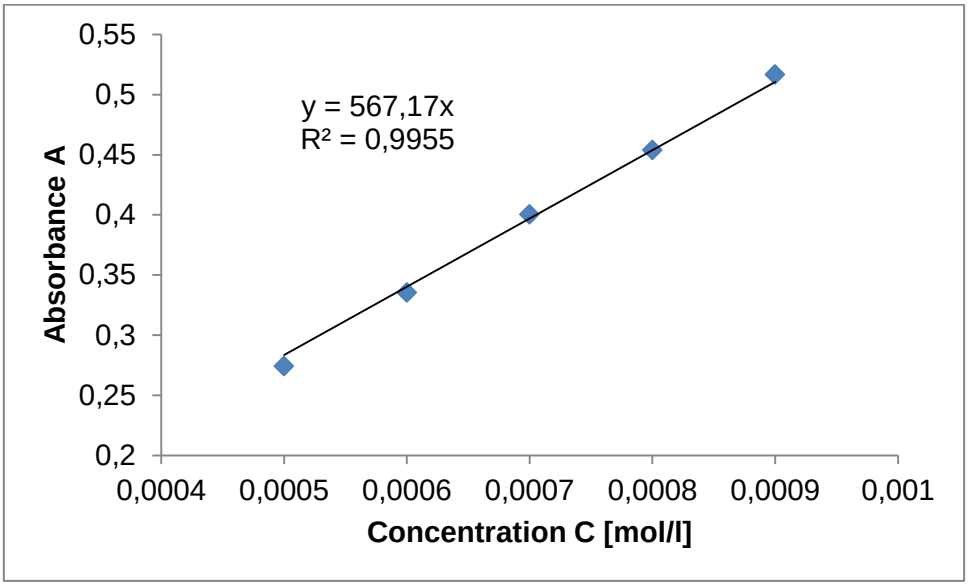

Figure 150. Determination of ε (5700 $M^{-1}cm^{-1}$) through a graphical draw of absorptions (λ = 357 nm) of **202** against their concentrations.

7.4. X-ray Structure Determination

7.4.1. Crystal Data and Structure Refinement for *E*-144

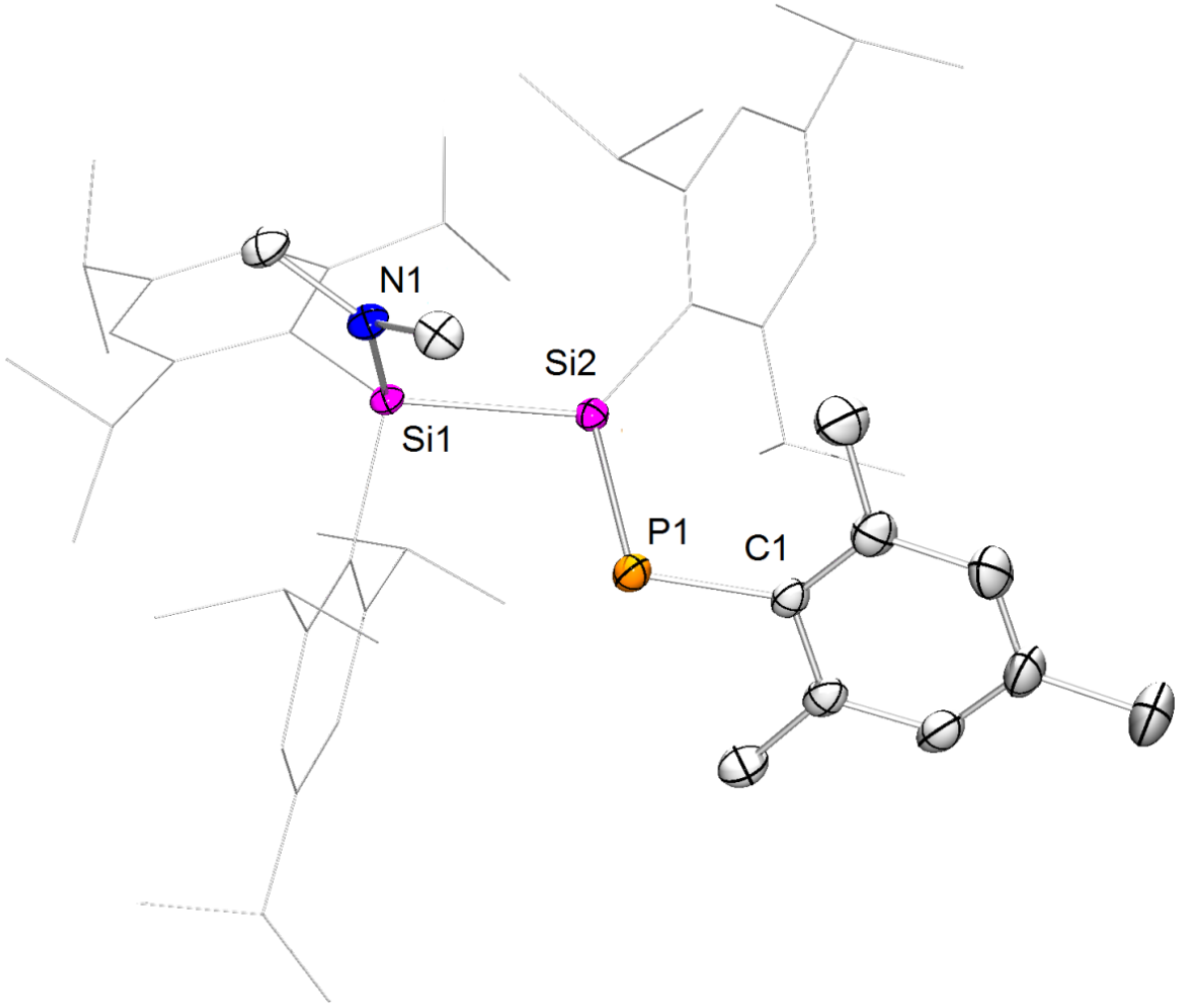

Identification code	sh3393	
Empirical formula	C56 H86 N P Si2	
Formula weight	860.40	
Temperature	153(2) K	
Wavelength	0.71073 Å	
Crystal system	Monoclinic	
Space group	$P2_1/c$	
Unit cell dimensions	a = 13.2155(3) Å	α= 90°.
	b = 20.2986(5) Å	β= 101.0180(10)°.
	c = 19.8199(5) Å	γ = 90°.
Volume	5218.8(2) $Å^3$	
Z	4	
Density (calculated)	1.095 Mg/m^3	
Absorption coefficient	0.134 mm^{-1}	
F(000)	1888	
Crystal size	0.396 x 0.391 x 0.132 mm^3	
Theta range for data collection	1.450 to 27.951°.	
Index ranges	-17<=h<=17, -25<=k<=26, -15<=l<=26	
Reflections collected	46879	
Independent reflections	12502 [R(int) = 0.0346]	
Completeness to theta = 25.242°	100.0 %	
Absorption correction	Semi-empirical from equivalents	
Max. and min. transmission	0.7456 and 0.6591	
Refinement method	Full-matrix least-squares on F^2	
Data / restraints / parameters	12502 / 206 / 865	
Goodness-of-fit on F^2	1.018	
Final R indices [I>2sigma(I)]	R1 = 0.0434, wR2 = 0.1079	
R indices (all data)	R1 = 0.0607, wR2 = 0.1185	
Extinction coefficient	n/a	
Largest diff. peak and hole	0.736 and -0.389 $e.Å^{-3}$	

7.4.2. Crystal Data and Structure Refinement for 146

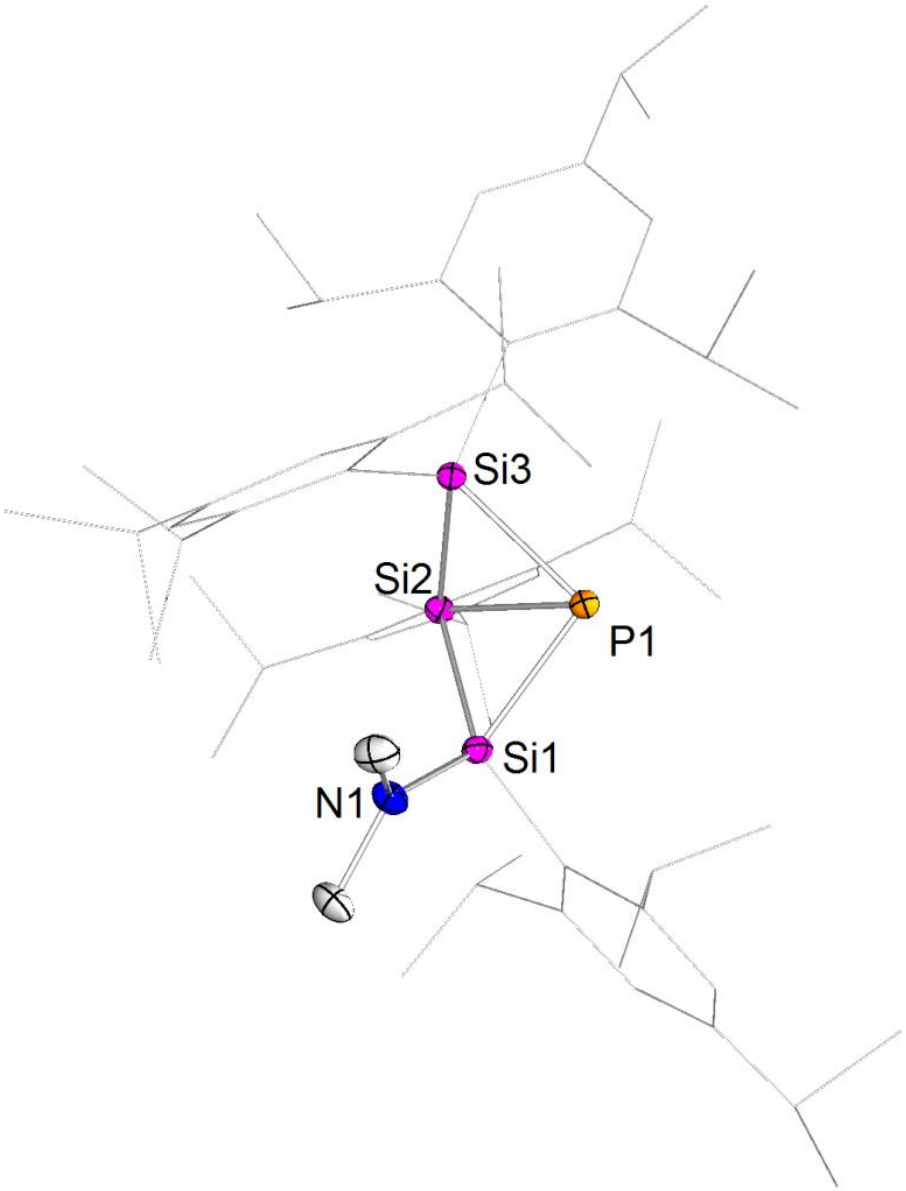

Identification code	sh3379	
Empirical formula	C62 H99 N P Si3	
Formula weight	973.66	
Temperature	133(2) K	
Wavelength	0.71073 Å	
Crystal system	Monoclinic	
Space group	C2/c	
Unit cell dimensions	a = 27.3618(12) Å	α= 90°.
	b = 24.1215(12) Å	β= 91.087(4)°.
	c = 19.0013(10) Å	γ = 90°.
Volume	12538.7(11) $Å^3$	
Z	8	
Density (calculated)	1.032 Mg/m^3	
Absorption coefficient	0.136 mm^{-1}	
F(000)	4280	
Crystal size	0.50 x 0.31 x 0.04 mm^3	
Theta range for data collection	1.13 to 26.37°.	
Index ranges	-34<=h<=33, -30<=k<=30, -23<=l<=23	
Reflections collected	99428	
Independent reflections	12822 [R(int) = 0.0675]	
Completeness to theta = 26.37°	100.0 %	
Absorption correction	Semi-empirical from equivalents	
Max. and min. transmission	0.9943 and 0.9348	
Refinement method	Full-matrix least-squares on F^2	
Data / restraints / parameters	12822 / 217 / 663	
Goodness-of-fit on F^2	1.024	
Final R indices [I>2sigma(I)]	R1 = 0.0493, wR2 = 0.1202	
R indices (all data)	R1 = 0.0758, wR2 = 0.1339	
Largest diff. peak and hole	0.702 and -0.876 $e.Å^{-3}$	

7.4.3. Crystal Data and Structure Refinement for 155a·(C_5H_{12})

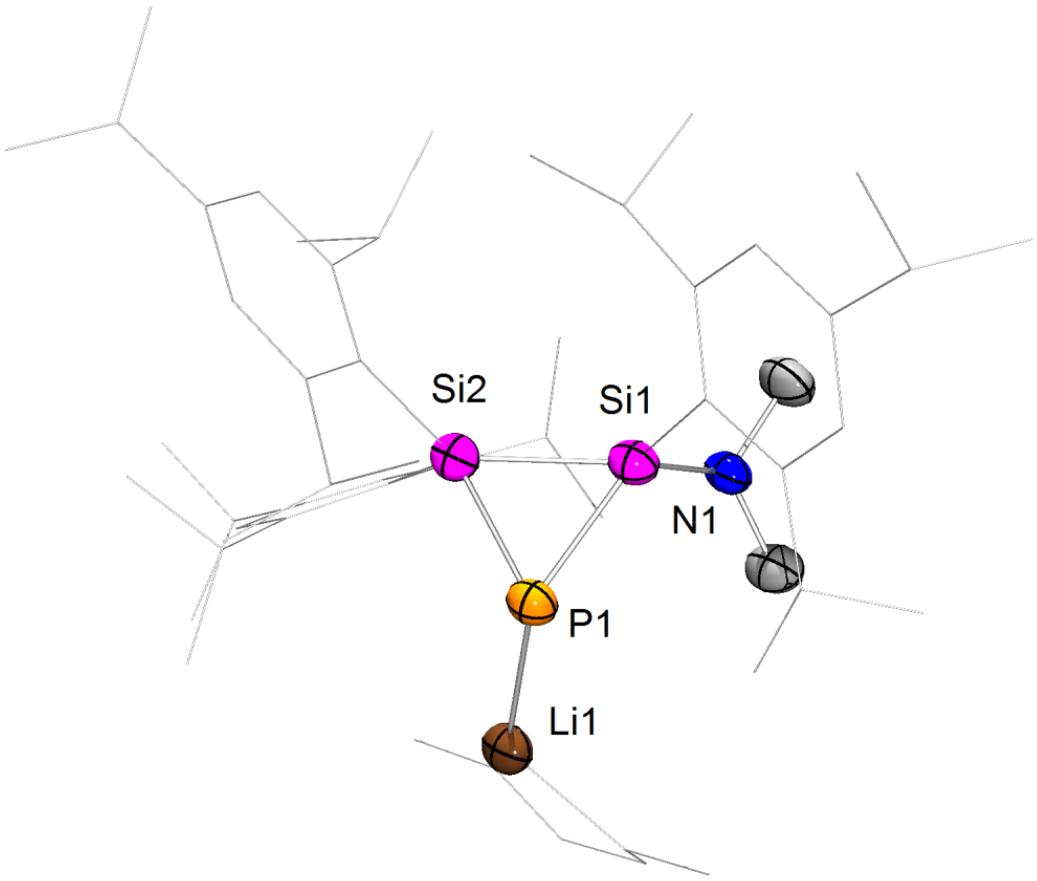

Identification code	sh3739	
Empirical formula	C106 H180 Li2 N2 O6 P2 Si4 x C5 H12	
Formula weight	1838.83	
Temperature	162(2) K	
Wavelength	0.71073 Å	
Crystal system	Monoclinic	
Space group	P2/c	
Unit cell dimensions	a = 14.6175(5) Å	α= 90°.
	b = 14.1683(4) Å	β= 93.254(2)°.
	c = 29.0041(8) Å	γ = 90°.
Volume	5997.2(3) $Å^3$	
Z	2	
Density (calculated)	1.018 Mg/m^3	
Absorption coefficient	0.123 mm^{-1}	
F(000)	2024	
Crystal size	0.575 x 0.228 x 0.224 mm^3	
Theta range for data collection	1.395 to 27.184°.	
Index ranges	-18<=h<=18, -16<=k<=18, -37<=l<=37	
Reflections collected	51547	
Independent reflections	13307 [R(int) = 0.0276]	
Completeness to theta = 25.242°	99.9 %	
Absorption correction	Semi-empirical from equivalents	
Max. and min. transmission	0.7455 and 0.7033	
Refinement method	Full-matrix least-squares on F^2	
Data / restraints / parameters	13307 / 66 / 627	
Goodness-of-fit on F^2	1.034	
Final R indices [I>2sigma(I)]	R1 = 0.0589, wR2 = 0.1518	
R indices (all data)	R1 = 0.0852, wR2 = 0.1707	
Extinction coefficient	n/a	
Largest diff. peak and hole	0.728 and -0.462 $e.Å^{-3}$	

7.4.4. Crystal Data and Structure Refinement for 159

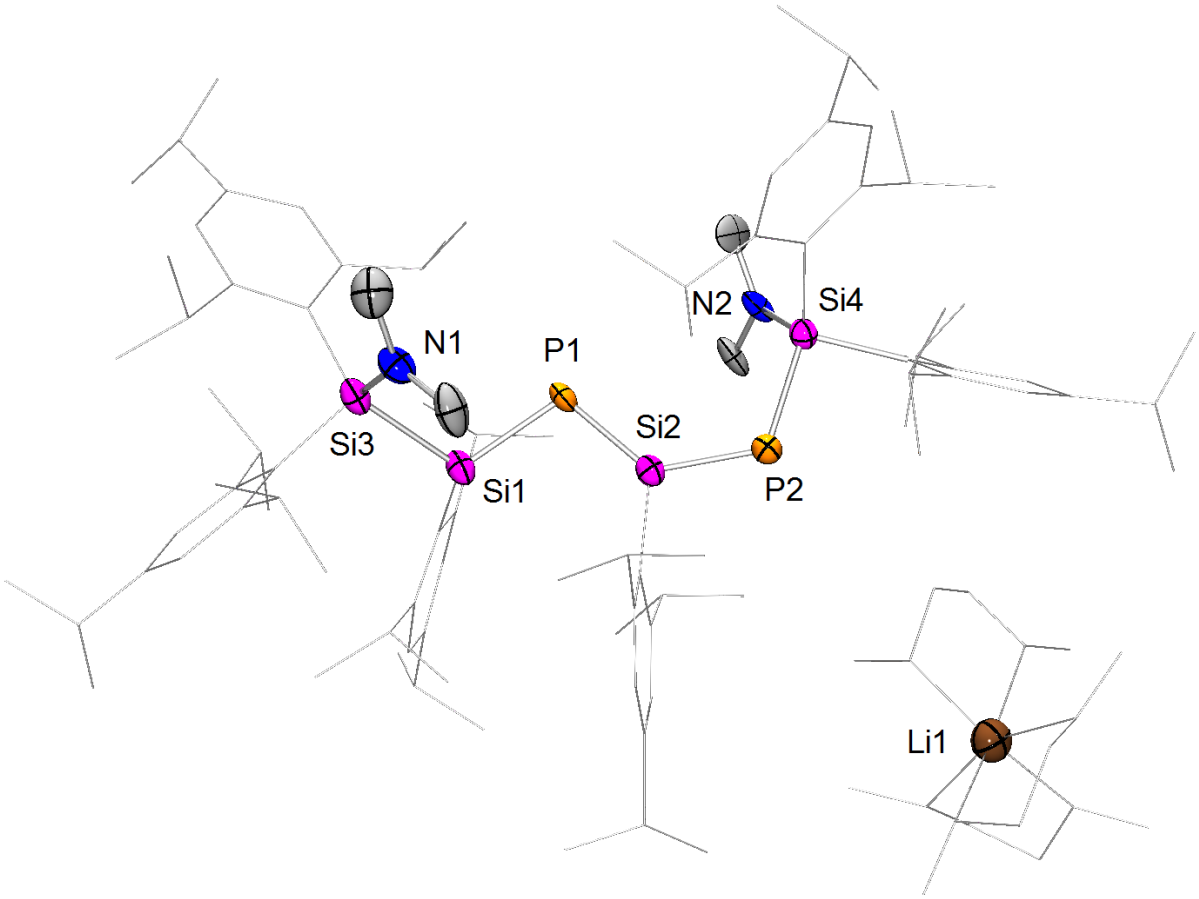

Identification code	sh3405	
Empirical formula	C57.50 H100.50 Li0.50 N O3 P Si2	
Formula weight	944.51	
Temperature	142(2) K	
Wavelength	0.71073 Å	
Crystal system	Triclinic	
Space group	P-1	
Unit cell dimensions	a = 16.291(6) Å	α= 81.144(10)°.
	b = 18.129(8) Å	β= 88.91(2)°.
	c = 22.482(11) Å	γ = 65.282(15)°.
Volume	5952(5) $Å^3$	
Z	4	
Density (calculated)	1.054 Mg/m^3	
Absorption coefficient	0.126 mm^{-1}	
F(000)	2084	
Crystal size	0.59 x 0.10 x 0.05 mm^3	
Theta range for data collection	0.92 to 26.37°.	
Index ranges	-17<=h<=12, -22<=k<=15, -28<=l<=14	
Reflections collected	13596	
Independent reflections	12419 [R(int) = 0.0452]	
Completeness to theta = 26.37°	51.0 %	
Absorption correction	Semi-empirical from equivalents	
Max. and min. transmission	0.9942 and 0.9292	
Refinement method	Full-matrix least-squares on F^2	
Data / restraints / parameters	12419 / 421 / 1234	
Goodness-of-fit on F^2	0.977	
Final R indices [I>2sigma(I)]	R1 = 0.0986, wR2 = 0.1759	
R indices (all data)	R1 = 0.3157, wR2 = 0.2593	
Largest diff. peak and hole	0.361 and -0.291 $e.Å^{-3}$	

7.4.5. Crystal Data and Structure Refinement for 160

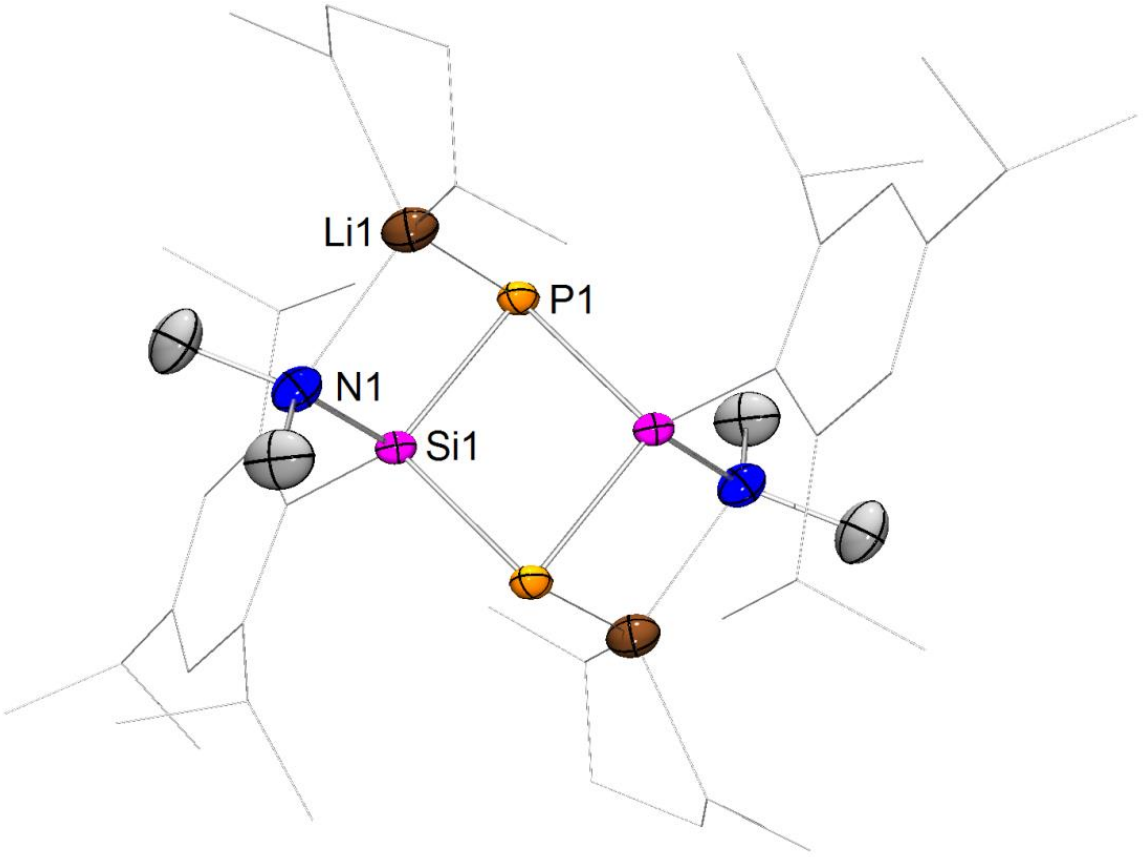

Identification code	sh3455	
Empirical formula	C42 H78 Li2 N2 O4 P2 Si2	
Formula weight	807.06	
Temperature	152(2) K	
Wavelength	0.71073 Å	
Crystal system	Monoclinic	
Space group	$P2_1/c$	
Unit cell dimensions	a = 11.6996(4) Å	α= 90°.
	b = 10.9823(3) Å	β= 98.4869(19)°.
	c = 19.4099(6) Å	γ = 90°.
Volume	2466.64(13) $Å^3$	
Z	2	
Density (calculated)	1.087 Mg/m^3	
Absorption coefficient	0.174 mm^{-1}	
F(000)	880	
Crystal size	0.450 x 0.268 x 0.128 mm^3	
Theta range for data collection	1.760 to 30.009°.	
Index ranges	-16<=h<=16, -15<=k<=15, -26<=l<=27	
Reflections collected	45321	
Independent reflections	7197 [R(int) = 0.0395]	
Completeness to theta = 25.242°	100.0 %	
Absorption correction	Semi-empirical from equivalents	
Max. and min. transmission	0.7460 and 0.6817	
Refinement method	Full-matrix least-squares on F^2	
Data / restraints / parameters	7197 / 80 / 400	
Goodness-of-fit on F^2	1.050	
Final R indices [I>2sigma(I)]	R1 = 0.0401, wR2 = 0.0993	
R indices (all data)	R1 = 0.0637, wR2 = 0.1163	
Extinction coefficient	n/a	
Largest diff. peak and hole	0.491 and -0.278 $e.Å^{-3}$	

7.4.6. Crystal Data and Structure Refinement for 162·0.5(C_5H_{10})

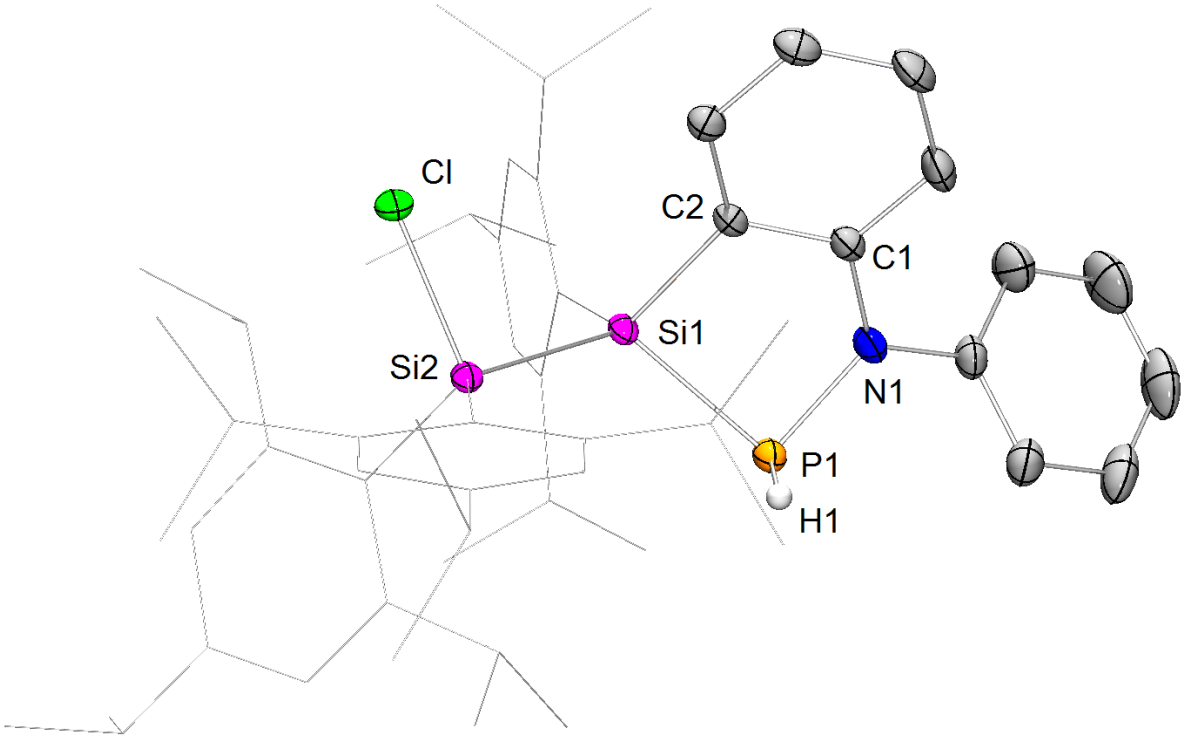

Identification code	sh3511	
Empirical formula	C57H79 Cl N P Si2 x 0.5(C5 H12)	
Formula weight	936.88	
Temperature	133(2) K	
Wavelength	0.71073 Å	
Crystal system	Triclinic	
Space group	P-1	
Unit cell dimensions	a = 9.6626(3) Å	α= 100.277(2)°.
	b = 11.7500(4) Å	β= 96.220(2)°.
	c = 25.2299(10) Å	γ = 95.351(2)°.
Volume	2783.32(17) $Å^3$	
Z	2	
Density (calculated)	1.118 Mg/m^3	
Absorption coefficient	0.177 mm^{-1}	
F(000)	1018	
Crystal size	0.462 x 0.150 x 0.092 mm^3	
Theta range for data collection	1.654 to 28.791°.	
Index ranges	-13<=h<=13, -15<=k<=15, -34<=l<=34	
Reflections collected	99145	
Independent reflections	14476 [R(int) = 0.0377]	
Completeness to theta = 25.242°	100.0 %	
Absorption correction	Semi-empirical from equivalents	
Max. and min. transmission	0.7458 and 0.7159	
Refinement method	Full-matrix least-squares on F^2	
Data / restraints / parameters	14476 / 4 / 917	
Goodness-of-fit on F^2	1.031	
Final R indices [I>2sigma(I)]	R1 = 0.0431, wR2 = 0.1038	
R indices (all data)	R1 = 0.0569, wR2 = 0.1121	
Extinction coefficient	n/a	
Largest diff. peak and hole	0.864 and -0.516 $e.Å^{-3}$	

7.4.7. Crystal Data and Structure Refinement for 166·(C_5H_{10})

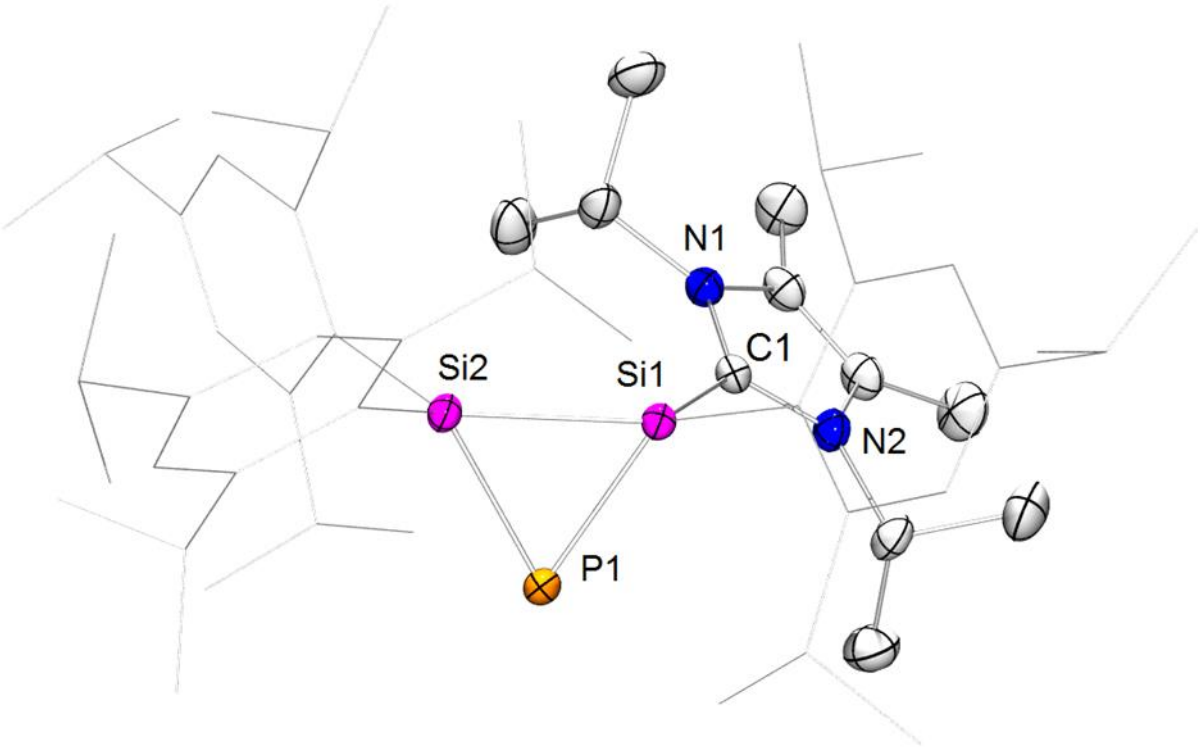

Identification code	sh3412	
Empirical formula	C56 H89 N2 P Si2 x C5 H12	
Formula weight	949.59	
Temperature	162(2) K	
Wavelength	0.71073 Å	
Crystal system	Monoclinic	
Space group	P2(1)/n	
Unit cell dimensions	a = 13.2893(3) Å	α= 90°.
	b = 17.9129(4) Å	β= 97.0720(10)°.
	c = 25.5877(8) Å	γ = 90°.
Volume	6044.8(3) $Å^3$	
Z	4	
Density (calculated)	1.043 Mg/m^3	
Absorption coefficient	0.121 mm^{-1}	
F(000)	2096	
Crystal size	0.62 x 0.42 x 0.28 mm^3	
Theta range for data collection	1.39 to 27.10°.	
Index ranges	-17<=h<=16, -22<=k<=16, -32<=l<=32	
Reflections collected	54029	
Independent reflections	13317 [R(int) = 0.0334]	
Completeness to theta = 27.10°	100.0 %	
Absorption correction	Semi-empirical from equivalents	
Max. and min. transmission	0.9673 and 0.9289	
Refinement method	Full-matrix least-squares on F^2	
Data / restraints / parameters	13317 / 43 / 973	
Goodness-of-fit on F^2	1.014	
Final R indices [I>2sigma(I)]	R1 = 0.0475, wR2 = 0.1124	
R indices (all data)	R1 = 0.0681, wR2 = 0.1242	
Largest diff. peak and hole	0.745 and -0.384 $e.Å^{-3}$	

7.4.8. Crystal Data and Structure Refinement for 167

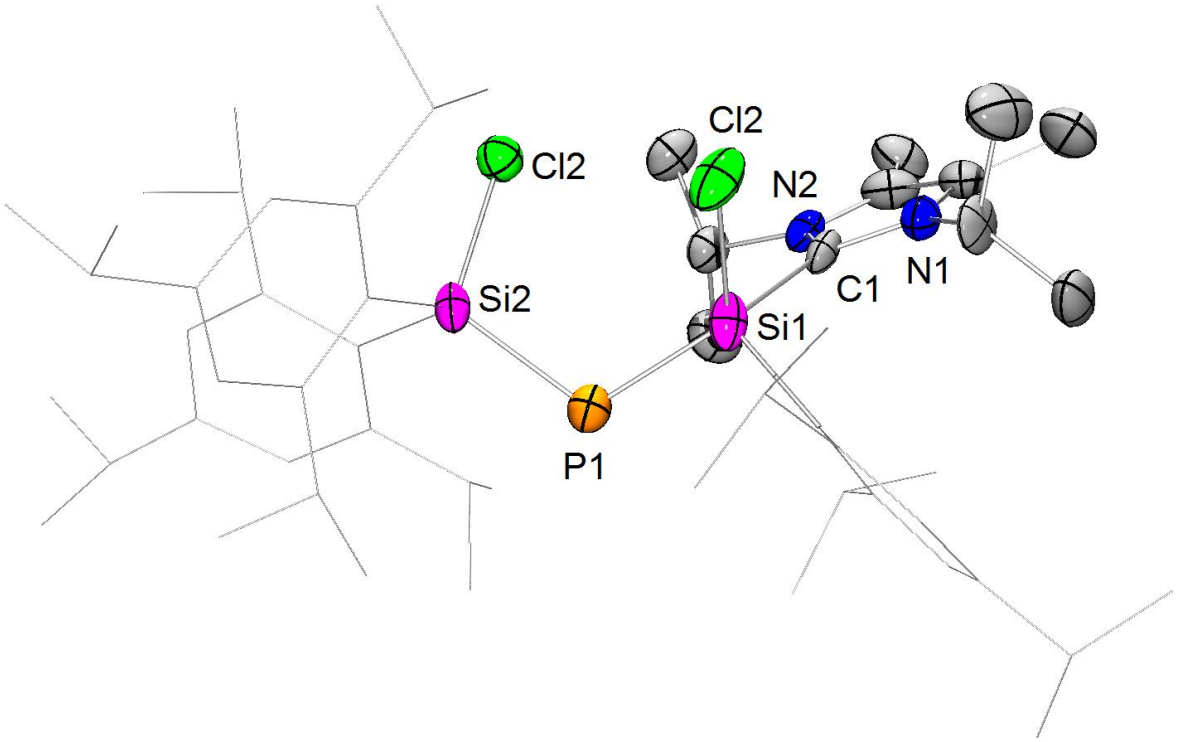

Identification code	sh3527	
Empirical formula	C56 H89 Cl2 N2 P Si2	
Formula weight	948.34	
Temperature	152(2) K	
Wavelength	0.71073 Å	
Crystal system	Monoclinic	
Space group	C2/c	
Unit cell dimensions	a = 36.386(3) Å	α= 90°.
	b = 17.2225(15) Å	β= 108.087(5)°.
	c = 19.1300(14) Å	γ = 90°.
Volume	11395.6(17) $Å^3$	
Z	8	
Density (calculated)	1.106 Mg/m^3	
Absorption coefficient	0.219 mm^{-1}	
F(000)	4128	
Crystal size	0.65 x 0.40 x 0.07 mm^3	
Theta range for data collection	1.18 to 26.54°.	
Index ranges	-45<=h<=45, -15<=k<=21, -24<=l<=24	
Reflections collected	63572	
Independent reflections	11553 [R(int) = 0.0944]	
Completeness to theta = 26.54°	97.2 %	
Absorption correction	Semi-empirical from equivalents	
Max. and min. transmission	0.9848 and 0.8711	
Refinement method	Full-matrix least-squares on F^2	
Data / restraints / parameters	11553 / 0 / 592	
Goodness-of-fit on F^2	2.007	
Final R indices [I>2sigma(I)]	R1 = 0.1263, wR2 = 0.2725	
R indices (all data)	R1 = 0.2202, wR2 = 0.3044	
Largest diff. peak and hole	2.620 and -0.693 $e.Å^{-3}$	

7.4.9. Crystal Data and Structure Refinement for 168·0.5(C_6H_6)

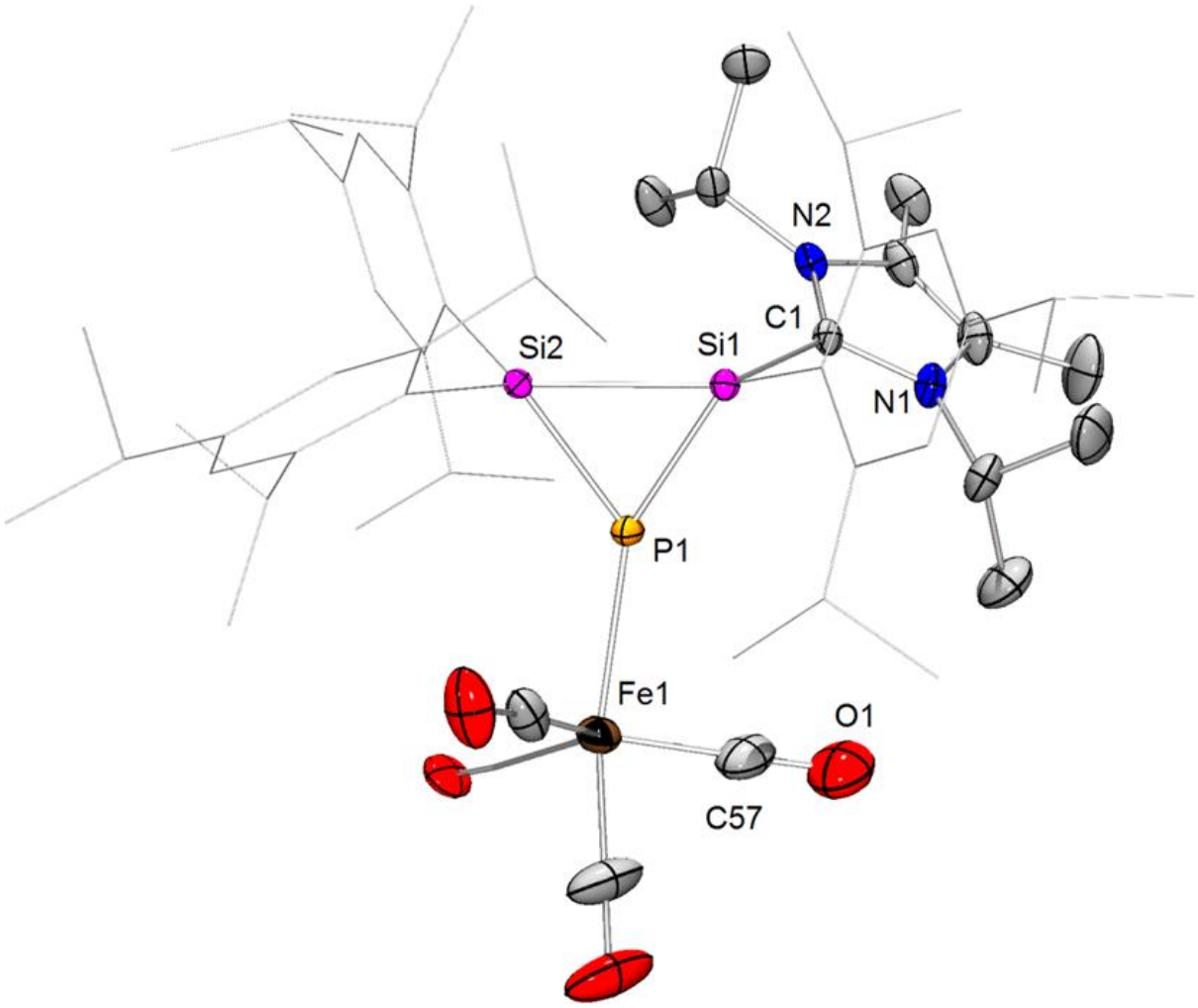

Identification code	sh3639
Empirical formula	C60 H89 Fe N2 O4 P Si2 x 0.5(C6 H6)
Formula weight	1084.38
Temperature	122(2) K
Wavelength	0.71073 Å
Crystal system	Monoclinic
Space group	$P2_1/n$
Unit cell dimensions	a = 13.7347(6) Å α= 90°. b = 21.3829(10) Å β= 100.853(3)°. c = 21.3318(10) Å γ = 90°.
Volume	6152.8(5) $Å^3$
Z	4
Density (calculated)	1.171 Mg/m^3
Absorption coefficient	0.356 mm^{-1}
F(000)	2340
Crystal size	0.755 x 0.664 x 0.204 mm^3
Theta range for data collection	1.361 to 30.209°.
Index ranges	-19<=h<=18, -30<=k<=27, -30<=l<=30
Reflections collected	74588
Independent reflections	18245 [R(int) = 0.0347]
Completeness to theta = 25.242°	100.0 %
Absorption correction	Semi-empirical from equivalents
Max. and min. transmission	0.7460 and 0.6726
Refinement method	Full-matrix least-squares on F^2
Data / restraints / parameters	18245 / 271 / 811
Goodness-of-fit on F^2	1.013
Final R indices [I>2sigma(I)]	R1 = 0.0401, wR2 = 0.0956
R indices (all data)	R1 = 0.0604, wR2 = 0.1066
Extinction coefficient	n/a
Largest diff. peak and hole	0.903 and -0.773 $e.Å^{-3}$

7.4.10. Crystal Data and Structure Refinement for 169

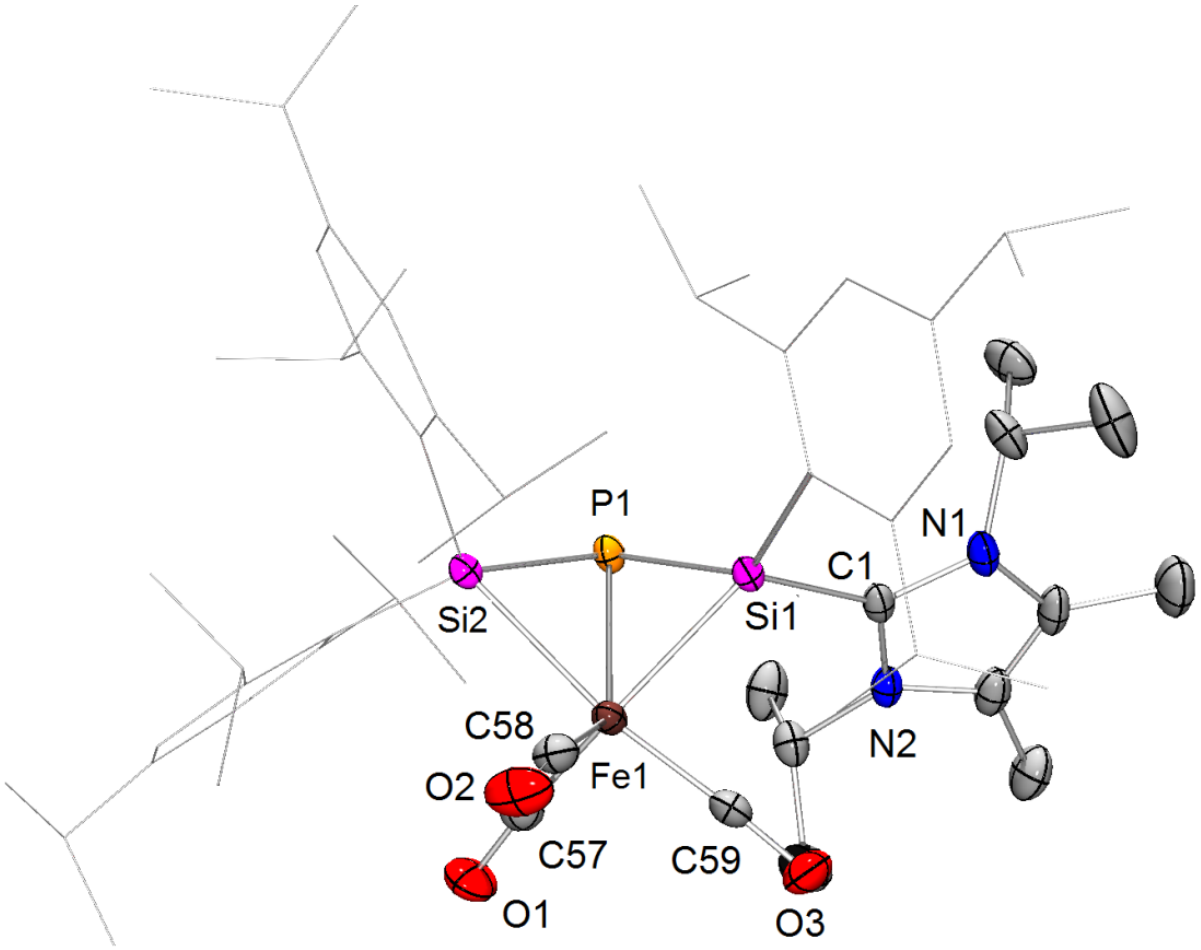

Identification code	sh3686
Empirical formula	C59 H89 Fe N2 O3 P Si2
Formula weight	1017.32
Temperature	182(2) K
Wavelength	0.71073 Å
Crystal system	Monoclinic
Space group	$P2_1/c$
Unit cell dimensions	a = 14.0996(9) Å α= 90°. b = 15.5510(10) Å β= 96.251(4)°. c = 26.4731(19) Å γ = 90°.
Volume	5770.1(7) $Å^3$
Z	4
Density (calculated)	1.171 Mg/m^3
Absorption coefficient	0.374 mm^{-1}
F(000)	2200
Crystal size	0.442 x 0.366 x 0.100 mm^3
Theta range for data collection	1.453 to 26.452°.
Index ranges	-17<=h<=17, 0<=k<=19, 0<=l<=33
Reflections collected	20005
Independent reflections	20005 [R(int) = ?]
Completeness to theta = 25.242°	94.4 %
Absorption correction	Semi-empirical from equivalents
Max. and min. transmission	0.7454 and 0.6237
Refinement method	Full-matrix least-squares on F^2
Data / restraints / parameters	20005 / 0 / 638
Goodness-of-fit on F^2	1.001
Final R indices [I>2sigma(I)]	R1 = 0.0457, wR2 = 0.1183
R indices (all data)	R1 = 0.0735, wR2 = 0.1346
Extinction coefficient	n/a
Largest diff. peak and hole	0.383 and -0.267 $e.Å^{-3}$

7.4.11. Crystal Data and Structure Refinement for 173

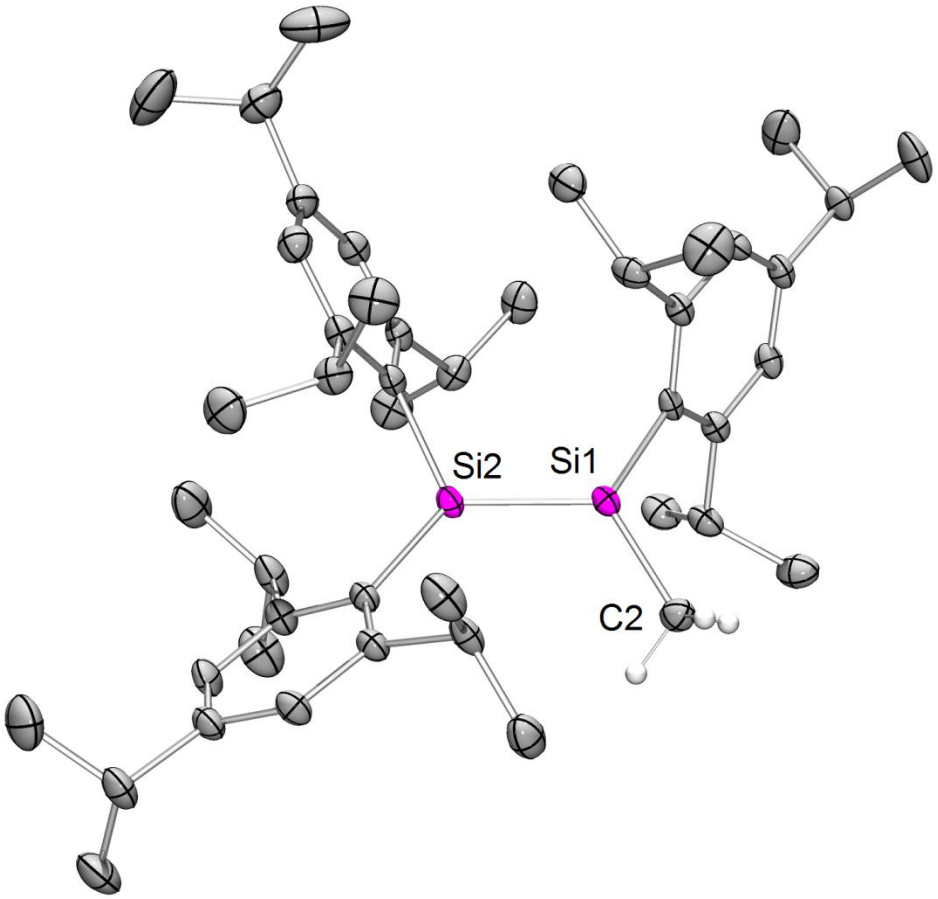

Identification code	sh3435	
Empirical formula	C46 H72 Si2	
Formula weight	681.22	
Temperature	132(2) K	
Wavelength	0.71073 Å	
Crystal system	Triclinic	
Space group	P-1	
Unit cell dimensions	a = 14.4267(4) Å	α= 111.4920(10)°.
	b = 17.3000(4) Å	β= 93.1540(10)°.
	c = 19.6441(5) Å	γ = 103.0160(10)°.
Volume	4393.25(19) $Å^3$	
Z	4	
Density (calculated)	1.030 Mg/m^3	
Absorption coefficient	0.109 mm^{-1}	
F(000)	1504	
Crystal size	0.72 x 0.53 x 0.10 mm^3	
Theta range for data collection	1.13 to 27.27°.	
Index ranges	-18<=h<=17, -21<=k<=22, -25<=l<=24	
Reflections collected	71499	
Independent reflections	19621 [R(int) = 0.0371]	
Completeness to theta = 27.27°	99.4 %	
Absorption correction	Semi-empirical from equivalents	
Max. and min. transmission	0.9894 and 0.9254	
Refinement method	Full-matrix least-squares on F^2	
Data / restraints / parameters	19621 / 0 / 925	
Goodness-of-fit on F^2	1.019	
Final R indices [I>2sigma(I)]	R1 = 0.0478, wR2 = 0.1064	
R indices (all data)	R1 = 0.0813, wR2 = 0.1215	
Largest diff. peak and hole	0.448 and -0.272 $e.Å^-$	

7.4.12. Crystal Data and Structure Refinement for 176

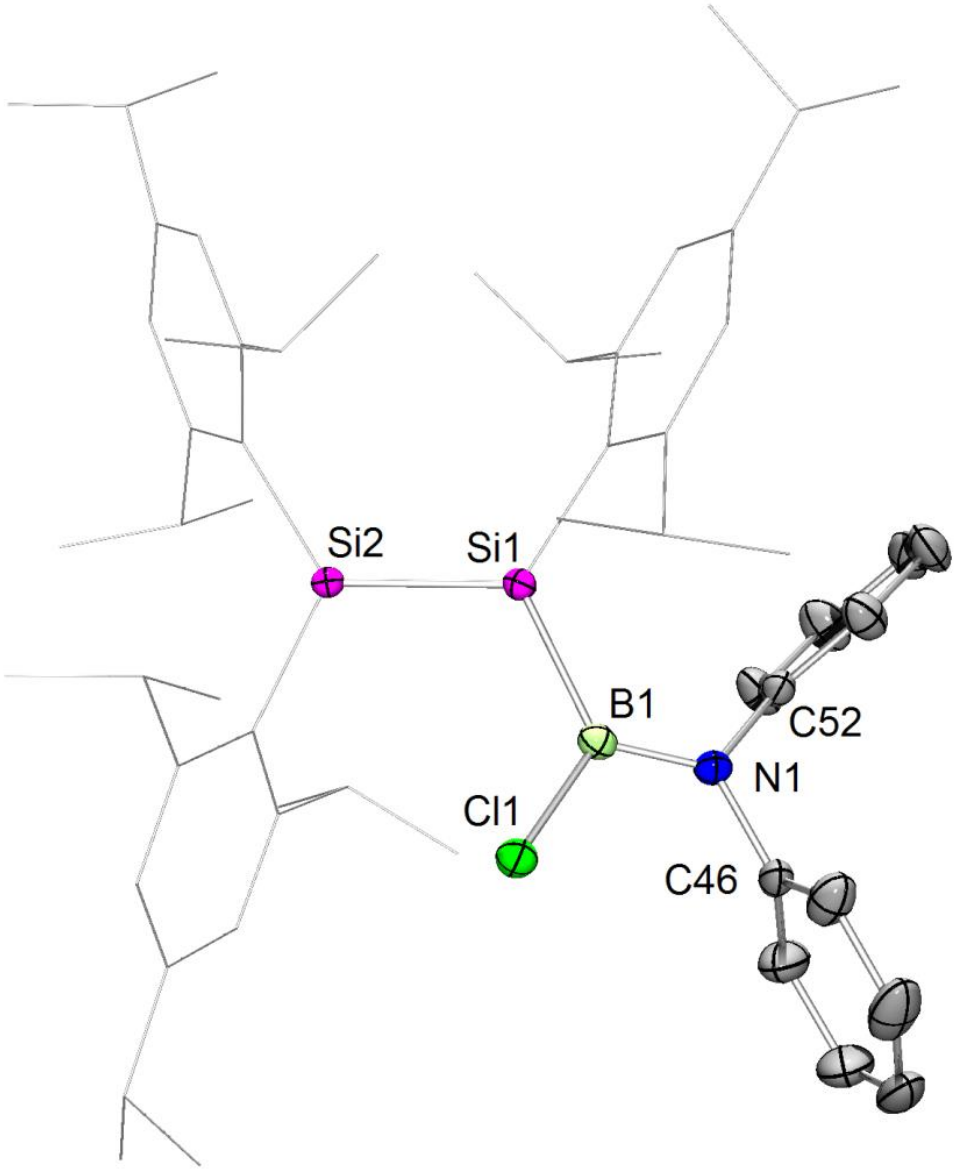

Identification code	sh3501	
Empirical formula	C57 H79 B Cl N Si2	
Formula weight	880.65	
Temperature	133(2) K	
Wavelength	0.71073 Å	
Crystal system	Monoclinic	
Space group	C 2/c	
Unit cell dimensions	a = 17.0099(5) Å	α= 90°.
	b = 16.7126(5) Å	β= 99.222(2)°.
	c = 37.8880(10) Å	γ = 90°.
Volume	10631.5(5) $Å^3$	
Z	8	
Density (calculated)	1.100 Mg/m^3	
Absorption coefficient	0.153 mm^{-1}	
F(000)	3824	
Crystal size	0.544 x 0.263 x 0.204 mm^3	
Theta range for data collection	1.089 to 26.611°.	
Index ranges	-21<=h<=21, -21<=k<=21, -47<=l<=47	
Reflections collected	82255	
Independent reflections	11131 [R(int) = 0.0363]	
Completeness to theta = 25.242°	100.0 %	
Absorption correction	Semi-empirical from equivalents	
Refinement method	Full-matrix least-squares on F^2	
Data / restraints / parameters	11131 / 0 / 875	
Goodness-of-fit on F^2	1.079	
Final R indices [I>2sigma(I)]	R1 = 0.0414, wR2 = 0.0940	
R indices (all data)	R1 = 0.0512, wR2 = 0.0987	
Extinction coefficient	n/a	
Largest diff. peak and hole	0.624 and -0.270 $e.Å^{-3}$	

7.4.13. Crystal Data and Structure Refinement for 180

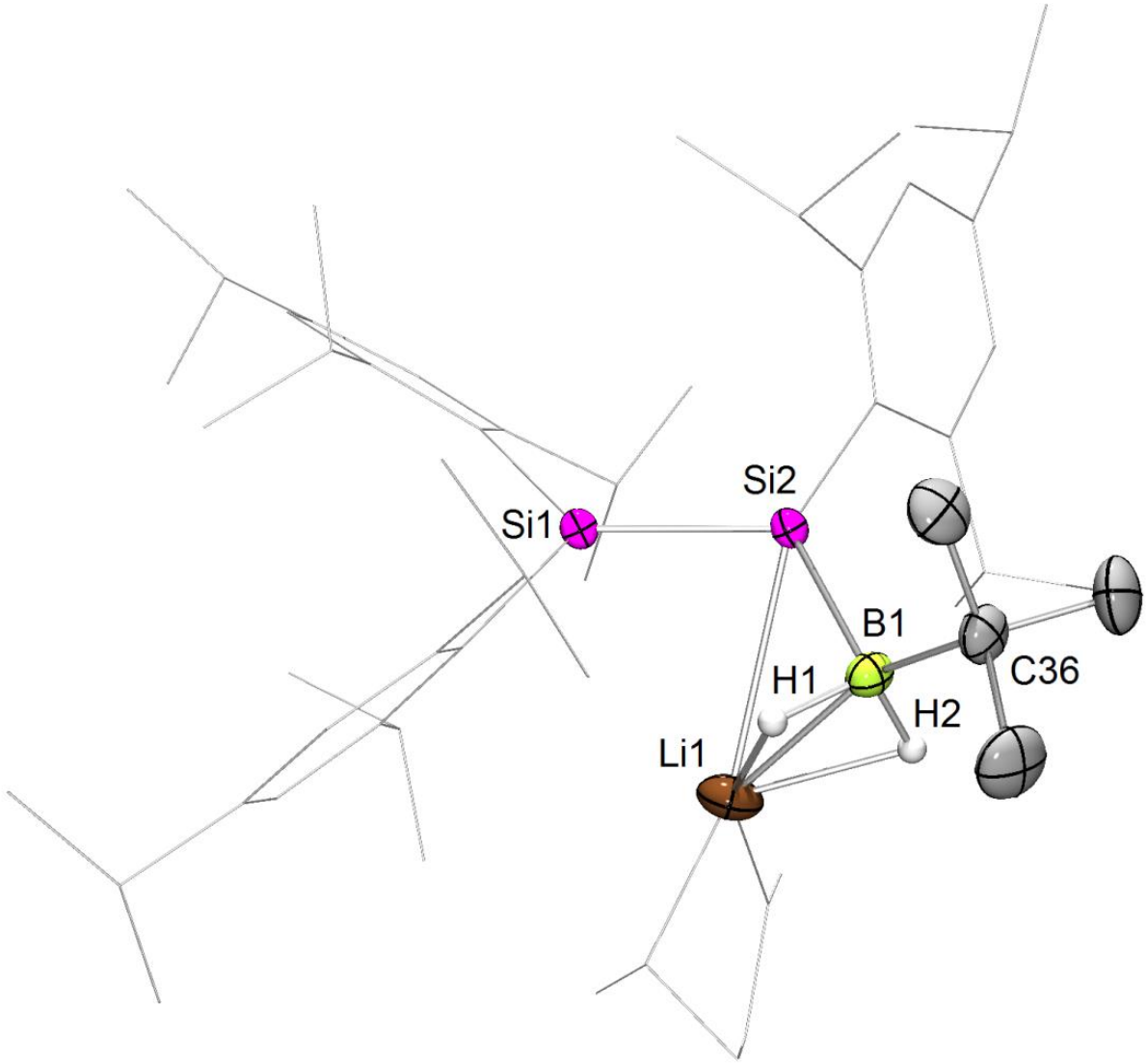

Identification code	sh3559	
Empirical formula	C53 H90 B Li O2 Si2	
Formula weight	833.17	
Temperature	172(2) K	
Wavelength	0.71073 Å	
Crystal system	Triclinic	
Space group	P-1	
Unit cell dimensions	a = 10.7245(4) Å	α= 92.7638(18)°.
	b = 11.1431(4) Å	β= 96.5598(19)°.
	c = 24.3088(9) Å	γ = 111.5565(17)°.
Volume	2671.31(17) Å^3	
Z	2	
Density (calculated)	1.036 Mg/m^3	
Absorption coefficient	0.102 mm^{-1}	
F(000)	920	
Crystal size	0.912 x 0.601 x 0.038 mm^3	
Theta range for data collection	1.695 to 28.310°.	
Index ranges	-13<=h<=14, -14<=k<=14, -32<=l<=32	
Reflections collected	48383	
Independent reflections	13247 [R(int) = 0.0364]	
Completeness to theta = 25.242°	100.0 %	
Absorption correction	Semi-empirical from equivalents	
Max. and min. transmission	0.7457 and 0.6992	
Refinement method	Full-matrix least-squares on F^2	
Data / restraints / parameters	13247 / 0 / 563	
Goodness-of-fit on F^2	1.014	
Final R indices [I>2sigma(I)]	R1 = 0.0445, wR2 = 0.1014	
R indices (all data)	R1 = 0.0658, wR2 = 0.1116	
Extinction coefficient	n/a	
Largest diff. peak and hole	0.359 and -0.267 e.Å^{-3}	

7.4.14. Crystal Data and Structure Refinement for 182·0.5(C_6H_{14})

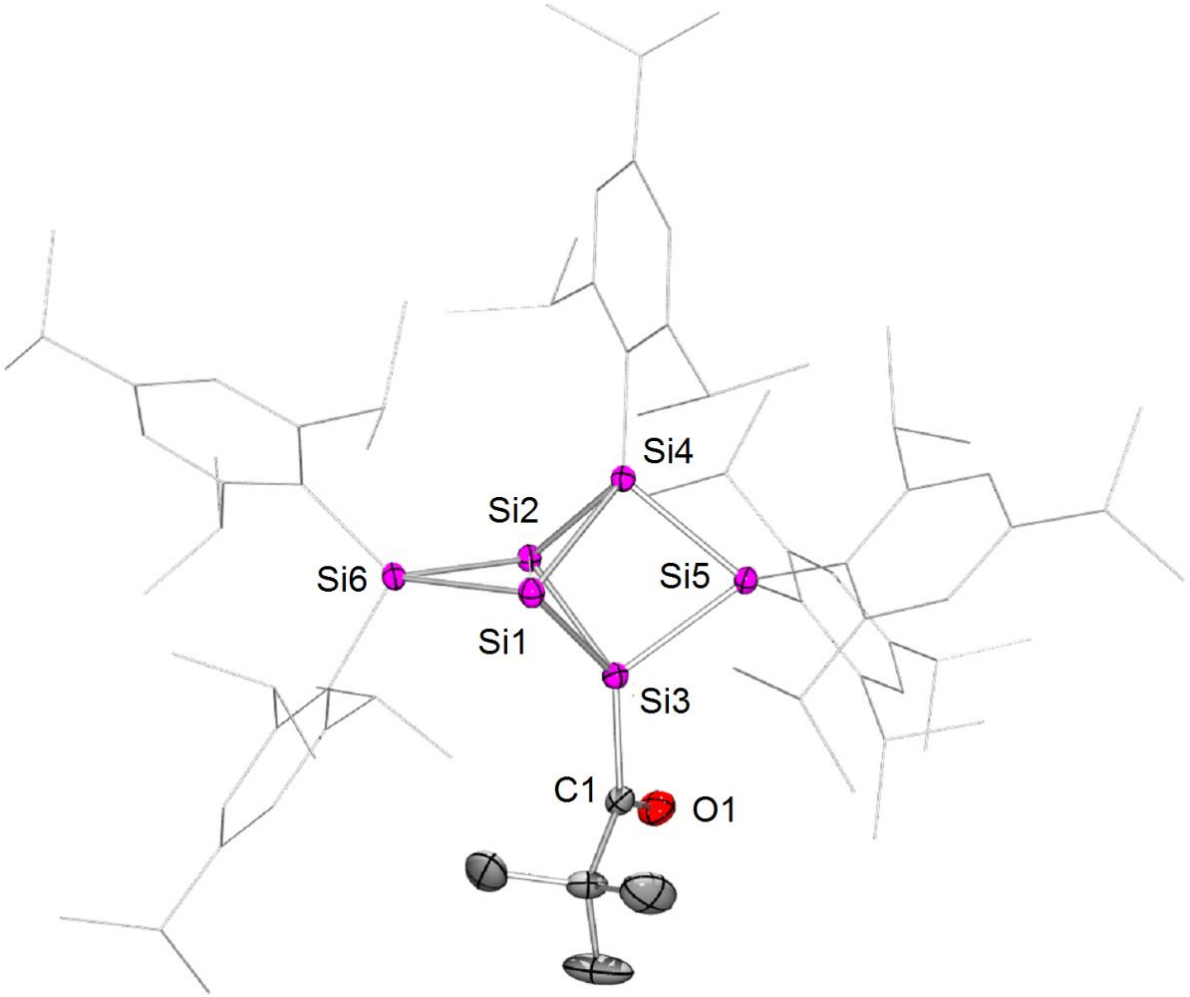

Identification code	sh3558	
Empirical formula	C83.50 H128 O Si6	
Formula weight	1316.39	
Temperature	133(2) K	
Wavelength	0.71073 Å	
Crystal system	Monoclinic	
Space group	C2/c	
Unit cell dimensions	a = 38.603(2) Å	α= 90°.
	b = 12.5277(6) Å	β= 93.822(3)°.
	c = 33.8066(15) Å	γ = 90°.
Volume	16312.9(14) $Å^3$	
Z	8	
Density (calculated)	1.072 Mg/m^3	
Absorption coefficient	0.144 mm^{-1}	
F(000)	5768	
Crystal size	0.614 x 0.506 x 0.286 mm^3	
Theta range for data collection	1.207 to 27.453°.	
Index ranges	-49<=h<=48, -16<=k<=14, -43<=l<=43	
Reflections collected	123643	
Independent reflections	18283 [R(int) = 0.0335]	
Completeness to theta = 25.242°	100.0 %	
Absorption correction	Multiscan	
Max. and min. transmission	0.7455 and 0.6970	
Refinement method	Full-matrix least-squares on F^2	
Data / restraints / parameters	18283 / 24 / 862	
Goodness-of-fit on F^2	0.992	
Final R indices [I>2sigma(I)]	R1 = 0.0435, wR2 = 0.0999	
R indices (all data)	R1 = 0.0565, wR2 = 0.1080	
Extinction coefficient	n/a	
Largest diff. peak and hole	0.414 and -0.478 $e.Å^{-3}$	

7.4.15. Crystal Data and Structure Refinement for 184·0.5(C_5H_{12})

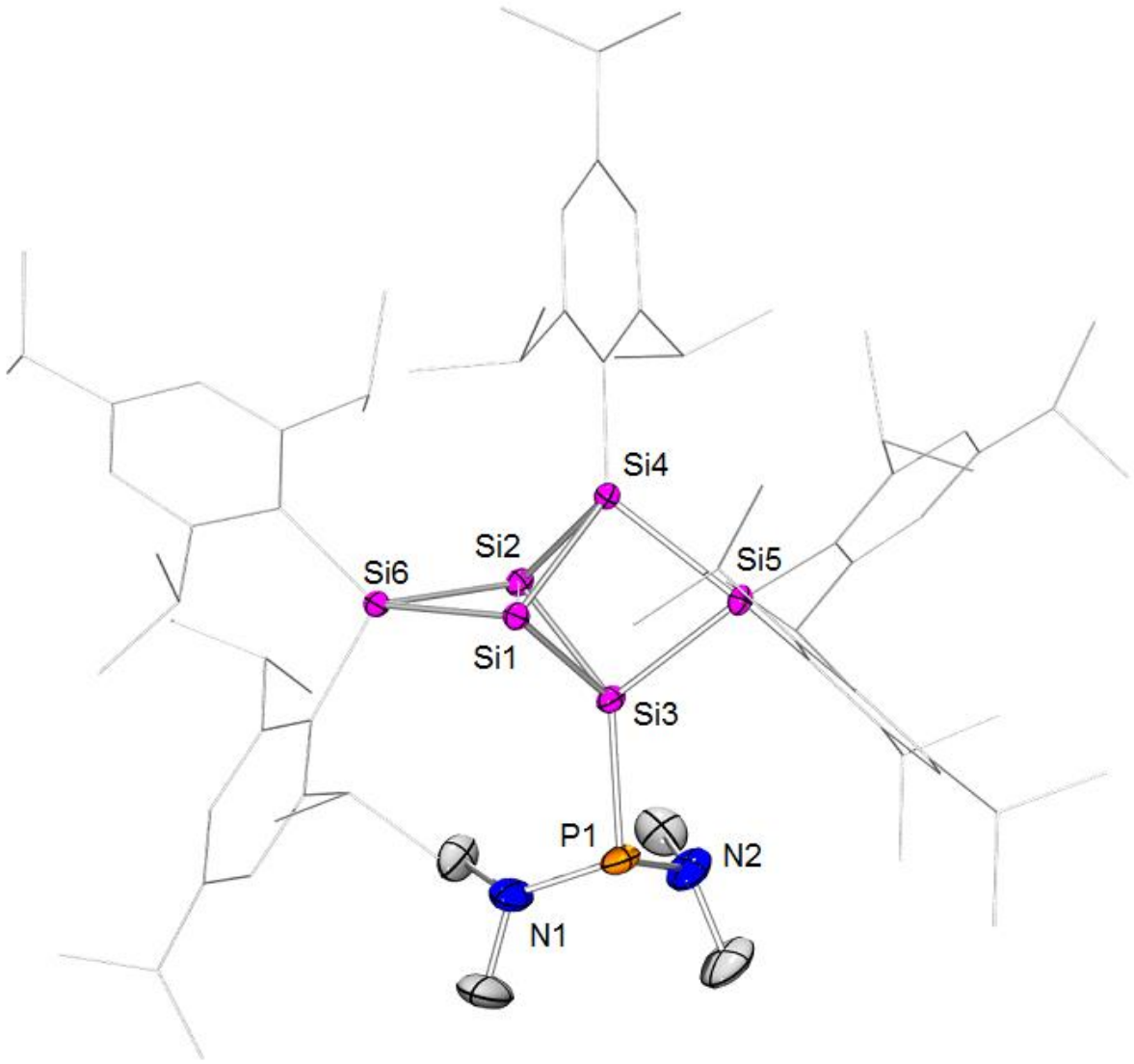

Identification code	sh3499	
Empirical formula	C81.50 H133 N2 P Si6	
Formula weight	1340.40	
Temperature	133(2) K	
Wavelength	0.71073 Å	
Crystal system	Monoclinic	
Space group	C 2/c	
Unit cell dimensions	a = 39.0433(13) Å	α= 90°.
	b = 12.5661(4) Å	β= 94.193(3)°.
	c = 33.8435(10) Å	γ = 90°.
Volume	16559.9(9) $Å^3$	
Z	8	
Density (calculated)	1.075 Mg/m^3	
Absorption coefficient	0.161 mm^{-1}	
F(000)	5880	
Crystal size	0.715 x 0.439 x 0.365 mm^3	
Theta range for data collection	1.046 to 32.120°.	
Index ranges	-58<=h<=53, -18<=k<=18, -50<=l<=50	
Reflections collected	207493	
Independent reflections	28950 [R(int) = 0.0463]	
Completeness to theta = 25.242°	100.0 %	
Absorption correction	Semi-empirical from equivalents	
Refinement method	Full-matrix least-squares on F^2	
Data / restraints / parameters	28950 / 78 / 888	
Goodness-of-fit on F^2	1.060	
Final R indices [I>2sigma(I)]	R1 = 0.0512, wR2 = 0.1191	
R indices (all data)	R1 = 0.0765, wR2 = 0.1325	
Extinction coefficient	n/a	
Largest diff. peak and hole	0.725 and -0.550 $e.Å^{-3}$	

7.4.16. Crystal Data and Structure Refinement for 186

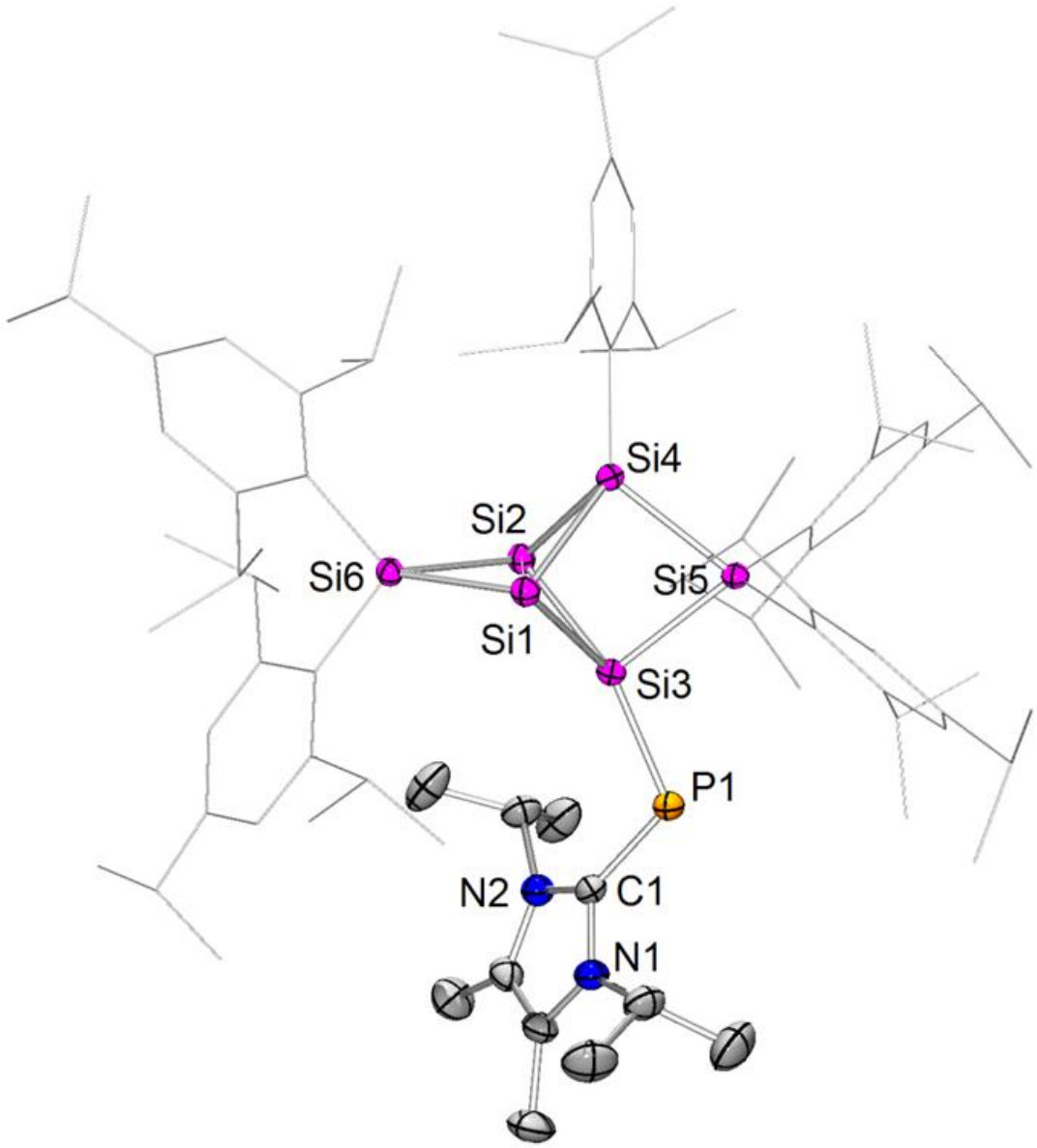

Identification code	sh3566	
Empirical formula	C86 H135 N2 P Si6	
Formula weight	1396.46	
Temperature	182(2) K	
Wavelength	0.71073 Å	
Crystal system	Triclinic	
Space group	P-1	
Unit cell dimensions	a = 16.2370(5) Å	α= 113.7570(16)°.
	b = 16.2970(6) Å	β= 90.0730(16)°.
	c = 17.5756(6) Å	γ = 98.1949(16)°.
Volume	4204.3(3) $Å^3$	
Z	2	
Density (calculated)	1.103 Mg/m^3	
Absorption coefficient	0.161 mm^{-1}	
F(000)	1528	
Crystal size	0.574 x 0.448 x 0.124 mm^3	
Theta range for data collection	1.269 to 28.818°.	
Index ranges	-15<=h<=21, -22<=k<=17, -23<=l<=23	
Reflections collected	70778	
Independent reflections	21480 [R(int) = 0.0330]	
Completeness to theta = 25.242°	99.8 %	
Absorption correction	Semi-empirical from equivalents	
Max. and min. transmission	0.7458 and 0.7009	
Refinement method	Full-matrix least-squares on F^2	
Data / restraints / parameters	21480 / 73 / 918	
Goodness-of-fit on F^2	1.031	
Final R indices [I>2sigma(I)]	R1 = 0.0447, wR2 = 0.1058	
R indices (all data)	R1 = 0.0700, wR2 = 0.1187	
Extinction coefficient	n/a	
Largest diff. peak and hole	0.515 and -0.391 $e.Å^{-3}$	

7.4.17. Crystal Data and Structure Refinement for 194

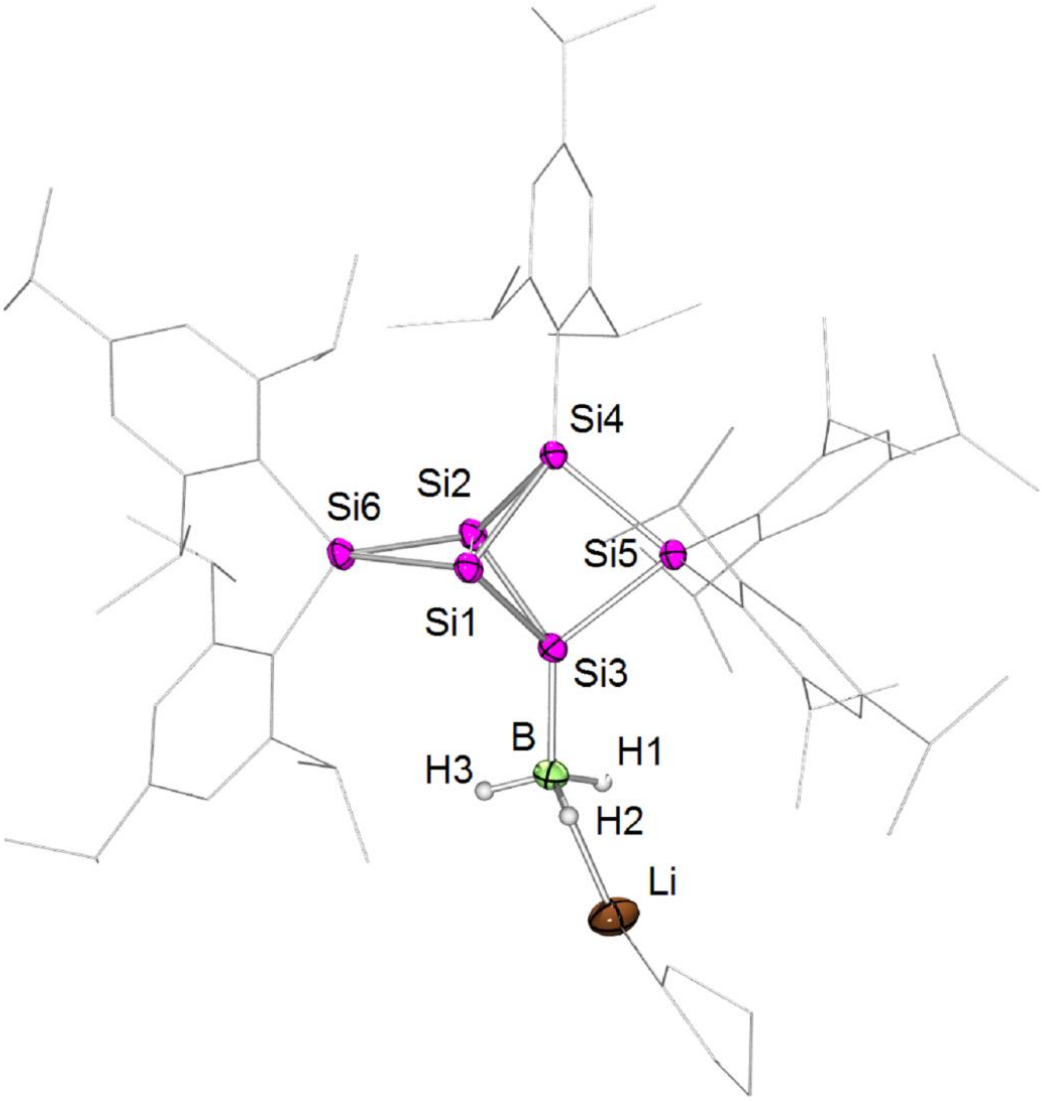

Identification code	sh3547
Empirical formula	C158 H254 B2 Li2 O2 Si12
Formula weight	2558.18
Temperature	142(2) K
Wavelength	0.71073 Å
Crystal system	Monoclinic
Space group	$P2_1/n$
Unit cell dimensions	a = 18.0893(8) Å α= 90°.
	b = 21.0995(8) Å β= 98.4877(17)°.
	c = 21.4926(9) Å γ = 90°.
Volume	8113.3(6) $Å^3$
Z	2
Density (calculated)	1.047 Mg/m^3
Absorption coefficient	0.142 mm^{-1}
F(000)	2804
Crystal size	0.334 x 0.269 x 0.172 mm^3
Theta range for data collection	1.360 to 27.531°.
Index ranges	-21<=h<=23, -23<=k<=27, -27<=l<=26
Reflections collected	65118
Independent reflections	18654 [R(int) = 0.0709]
Completeness to theta = 25.242°	100.0 %
Absorption correction	Semi-empirical from equivalents
Max. and min. transmission	0.7456 and 0.6742
Refinement method	Full-matrix least-squares on F^2
Data / restraints / parameters	18654 / 161 / 948
Goodness-of-fit on F^2	1.018
Final R indices [I>2sigma(I)]	R1 = 0.0590, wR2 = 0.1233
R indices (all data)	R1 = 0.1230, wR2 = 0.1485
Extinction coefficient	n/a
Largest diff. peak and hole	0.433 and -0.407 $e.Å^{-3}$

7.4.18. Crystal Data and Structure Refinement for 195·(thf)$_3$

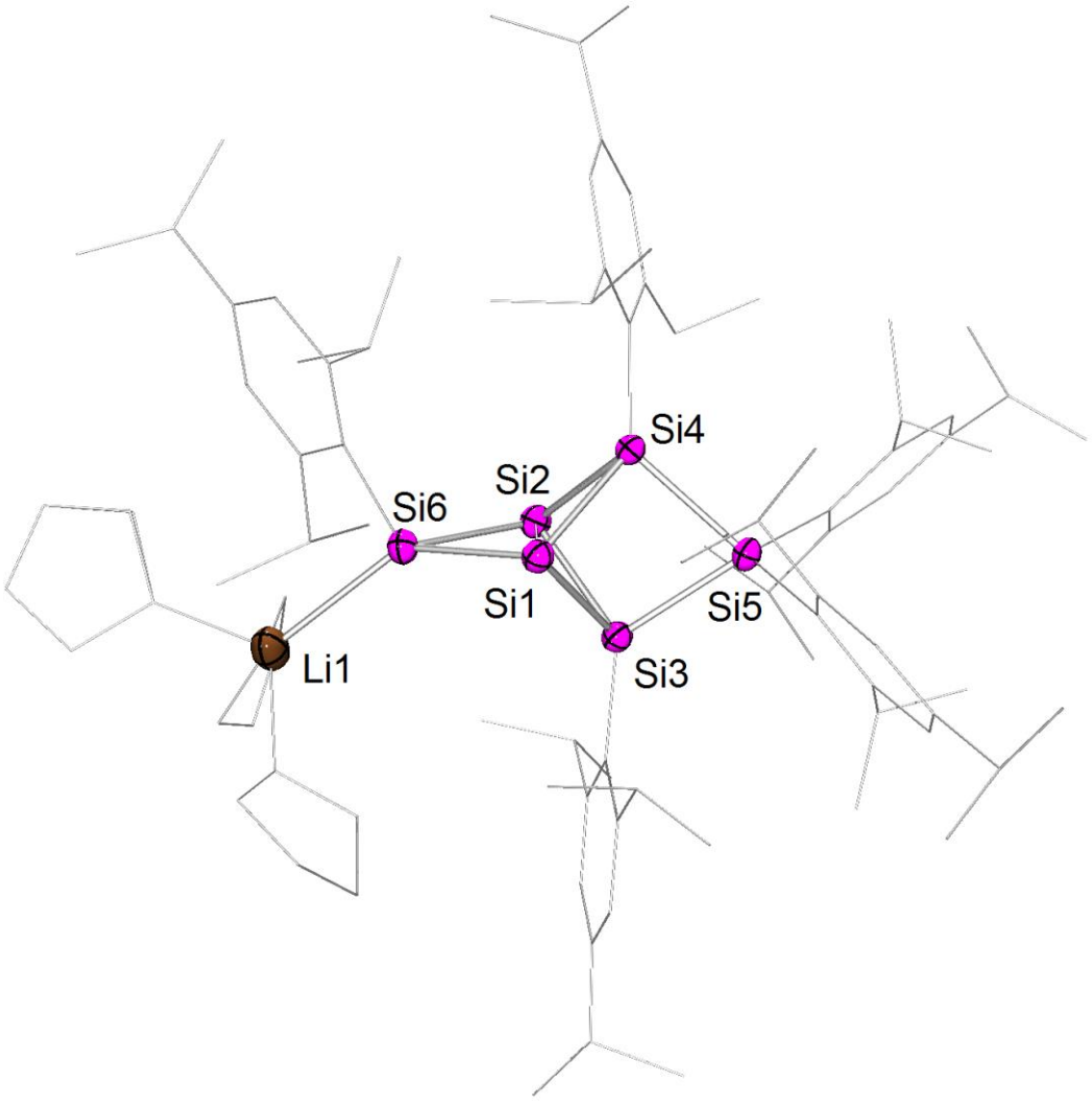

Identification code	sh3618	
Empirical formula	C87 H139 Li O3 Si6	
Formula weight	1408.45	
Temperature	175(2) K	
Wavelength	0.71073 Å	
Crystal system	Triclinic	
Space group	P-1	
Unit cell dimensions	a = 14.2918(16) Å	α= 109.652(5)°.
	b = 16.4145(18) Å	β= 104.243(4)°.
	c = 21.516(3) Å	γ = 99.970(4)°.
Volume	4422.6(9) $Å^3$	
Z	2	
Density (calculated)	1.058 Mg/m^3	
Absorption coefficient	0.138 mm^{-1}	
F(000)	1544	
Crystal size	0.696 x 0.647 x 0.466 mm^3	
Theta range for data collection	1.362 to 27.284°.	
Index ranges	-18<=h<=18, -21<=k<=20, -27<=l<=27	
Reflections collected	69055	
Independent reflections	19545 [R(int) = 0.0443]	
Completeness to theta = 25.242°	100.0 %	
Absorption correction	Semi-empirical from equivalents	
Max. and min. transmission	0.7455 and 0.6196	
Refinement method	Full-matrix least-squares on F^2	
Data / restraints / parameters	19545 / 231 / 1002	
Goodness-of-fit on F^2	1.059	
Final R indices [I>2sigma(I)]	R1 = 0.0622, wR2 = 0.1550	
R indices (all data)	R1 = 0.0945, wR2 = 0.1851	
Extinction coefficient	n/a	
Largest diff. peak and hole	1.086 and -0.401 $e.Å^{-3}$	

7.4.19. Crystal Data and Structure Refinement for 197·C_6H_{12}

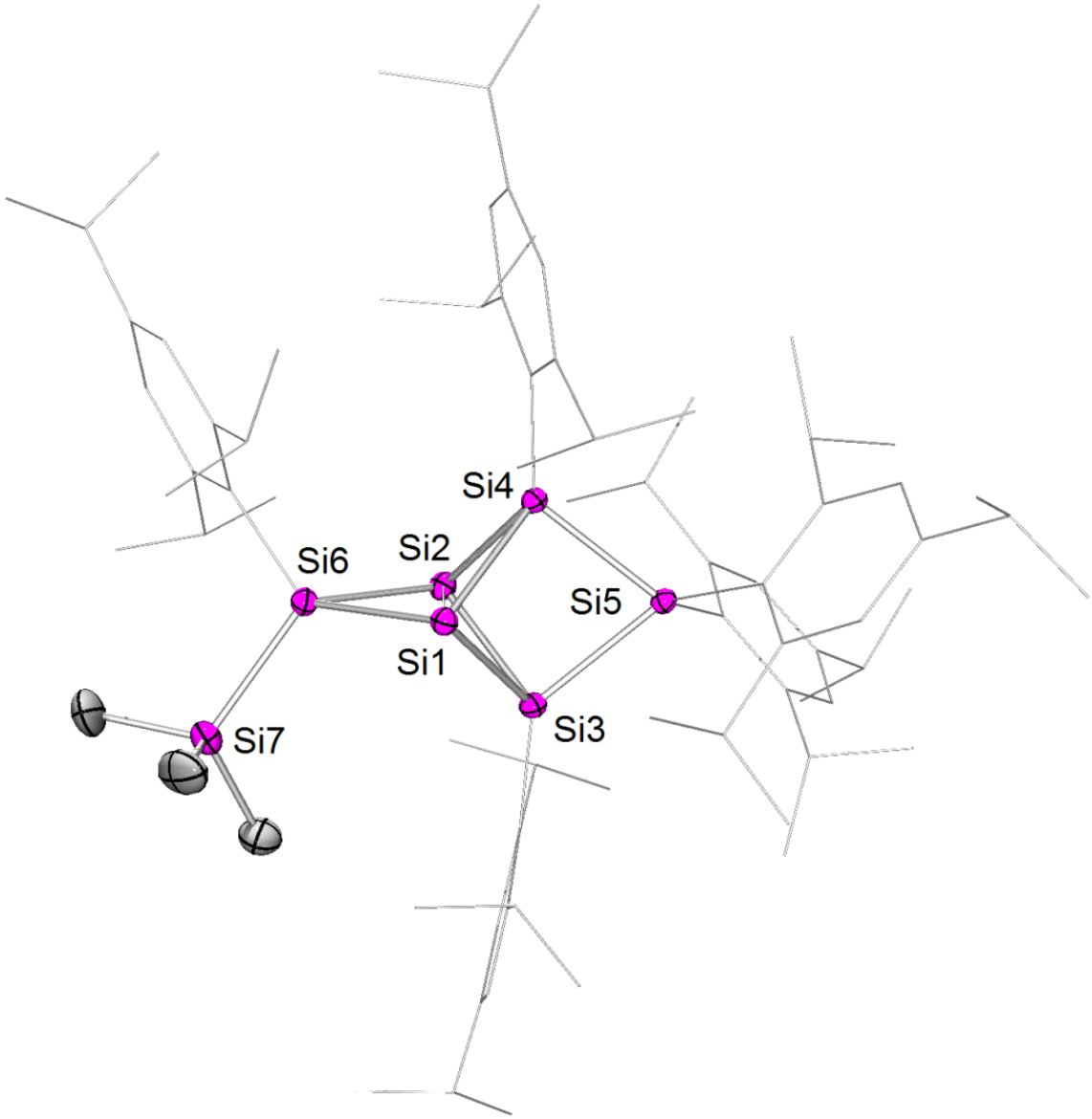

Identification code	sh3668	
Empirical formula	C84 H138 Si7	
Formula weight	1344.57	
Temperature	152(2) K	
Wavelength	0.71073 Å	
Crystal system	Monoclinic	
Space group	$P2_1/c$	
Unit cell dimensions	a = 21.0070(7) Å	α= 90°.
	b = 20.4182(7) Å	β= 95.4324(13)°.
	c = 19.9183(7) Å	γ = 90°.
Volume	8505.1(5) $Å^3$	
Z	4	
Density (calculated)	1.050 Mg/m^3	
Absorption coefficient	0.152 mm^{-1}	
F(000)	2960	
Crystal size	0.480 x 0.380 x 0.166 mm^3	
Theta range for data collection	0.974 to 28.755°.	
Index ranges	-27<=h<=28, -27<=k<=25, -24<=l<=26	
Reflections collected	68739	
Independent reflections	22100 [R(int) = 0.0376]	
Completeness to theta = 25.242°	100.0 %	
Absorption correction	Semi-empirical from equivalents	
Max. and min. transmission	0.7458 and 0.6844	
Refinement method	Full-matrix least-squares on F^2	
Data / restraints / parameters	22100 / 17 / 1278	
Goodness-of-fit on F^2	1.030	
Final R indices [I>2sigma(I)]	R1 = 0.0473, wR2 = 0.1155	
R indices (all data)	R1 = 0.0736, wR2 = 0.1317	
Extinction coefficient	n/a	
Largest diff. peak and hole	0.779 and -0.507 $e.Å^{-3}$	

7.4.20. Crystal Data and Structure Refinement for 201

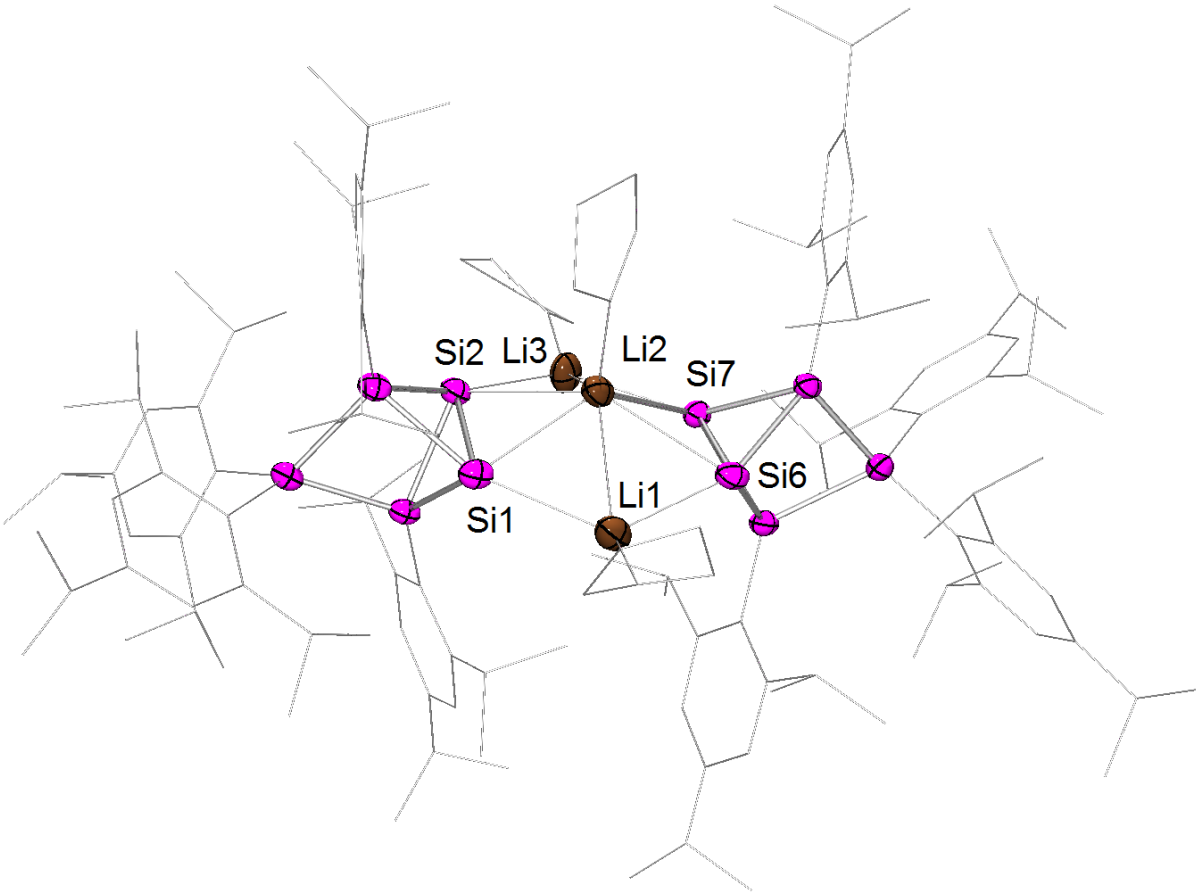

Identification code	sh3685a
Empirical formula	2(C132 H208 Li3 O3 Si10), C136 H216 Li3 O4 Si10, 2(C16 H32 O4 Li), 10(C7 H8)
Formula weight	2672.74
Temperature	152(2) K
Wavelength	0.71073 Å
Crystal system	Triclinic
Space group	P-1
Unit cell dimensions	a = 23.5887(12) Å α= 74.122(2)°. b = 23.9402(13) Å β= 82.075(2)°. c = 25.3720(13) Å γ = 73.941(2)°.
Volume	13213.6(12) $Å^3$
Z	3
Density (calculated)	1.008 Mg/m^3
Absorption coefficient	0.122 mm^{-1}
F(000)	4385
Crystal size	0.740 x 0.673 x 0.344 mm^3
Theta range for data collection	0.836 to 29.291°.
Index ranges	-32<=h<=20, -32<=k<=32, -34<=l<=34
Reflections collected	439029
Independent reflections	71759 [R(int) = 0.0598]
Completeness to theta = 25.242°	100.0 %
Absorption correction	Semi-empirical from equivalents
Max. and min. transmission	0.7458 and 0.6913
Refinement method	Full-matrix least-squares on F^2
Data / restraints / parameters	71759 / 2346 / 2595
Goodness-of-fit on F^2	2.186
Final R indices [I>2sigma(I)]	R1 = 0.1205, wR2 = 0.2919
R indices (all data)	R1 = 0.2379, wR2 = 0.3376
Extinction coefficient	n/a
Largest diff. peak and hole	1.318 and -0.821 $e.Å^{-3}$

7.4.21. Crystal Data and Structure Refinement for 204a·0.5(C_5H_{12})

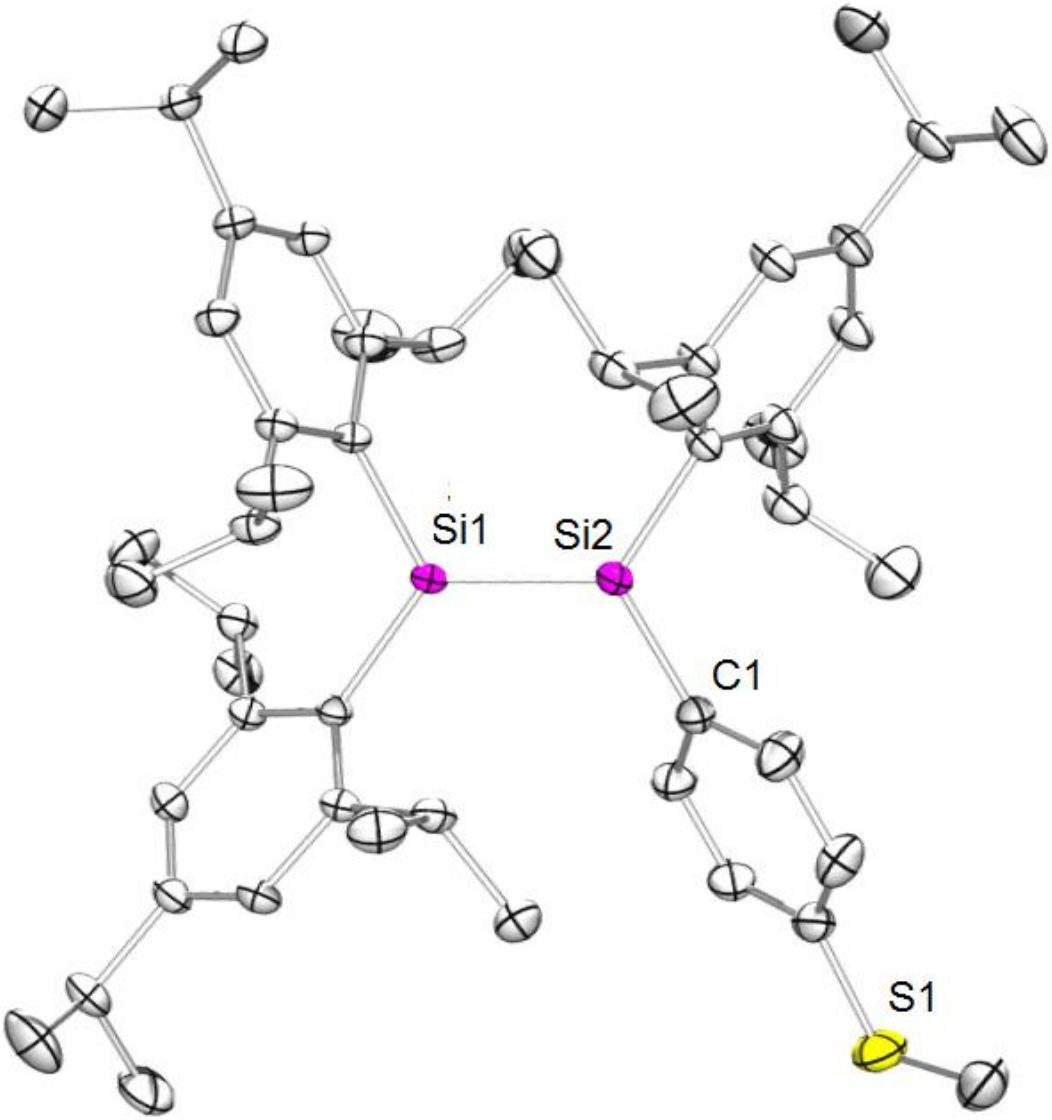

Identification code	sh3660	
Empirical formula	C52 H76 S Si2 x 0.5(C5 H12)	
Formula weight	825.44	
Temperature	172(2) K	
Wavelength	0.71073 Å	
Crystal system	Triclinic	
Space group	P-1	
Unit cell dimensions	a = 12.9835(7) Å	α= 92.6765(14)°.
	b = 14.0123(8) Å	β= 99.6756(13)°.
	c = 14.6449(8) Å	γ = 99.8640(12)°.
Volume	2579.8(2) $Å^3$	
Z	2	
Density (calculated)	1.063 Mg/m^3	
Absorption coefficient	0.142 mm^{-1}	
F(000)	906	
Crystal size	0.724 x 0.707 x 0.332 mm^3	
Theta range for data collection	1.415 to 34.040°.	
Index ranges	-20<=h<=20, -22<=k<=21, -22<=l<=22	
Reflections collected	79417	
Independent reflections	20797 [R(int) = 0.0257]	
Completeness to theta = 25.242°	99.9 %	
Absorption correction	Semi-empirical from equivalents	
Max. and min. transmission	0.7467 and 0.6991	
Refinement method	Full-matrix least-squares on F^2	
Data / restraints / parameters	20797 / 61 / 843	
Goodness-of-fit on F^2	1.076	
Final R indices [I>2sigma(I)]	R1 = 0.0520, wR2 = 0.1443	
R indices (all data)	R1 = 0.0734, wR2 = 0.1600	
Extinction coefficient	n/a	
Largest diff. peak and hole	1.255 and -0.652 $e.Å^{-3}$	